CALIFORNIA INSTITUTE OF TECHNOLOGY

SOIL MECHANICS LABORATORY

DYNAMIC CENTRIFUGE TESTING OF CANTILEVER RETAINING WALLS

by

L. Alexander Ortiz

SML 82-02

A Report on Research Conducted under a Grant from the National Science Foundation

Pasadena, California
August, 1982

This investigation was sponsored by Grant No. CME-7913822 from the National Science Foundation, Geotechnical Engineering Program, under the supervision of R.F. Scott. Any opinions findings, and conclusions or recommendations expressed in this publication are those of the author and do not necessarily reflect the views of the National Science Foundation.

DYNAMIC CENTRIFUGE TESTING
OF CANTILEVER RETAINING WALLS

Thesis by

L. Alexander Ortiz

In Partial Fulfillment of the Requirements

for the Degree of

Doctor of Philosophy

California Institute of Technology

Pasadena, California

1982

(Submitted May 24, 1982)

i.a

ABSTRACT

An investigation was made into the behavior of flexible cantilever walls retaining a cohesionless soil backfill and subjected to earthquake-type dynamic excitations using the centrifuge modelling technique. The study was motivated by the abundant observations of earth retaining structure damage and failures documented in earthquake damage reports.

The "prototype" typical walls were designed using the traditional Mononobe-Okabe dynamic lateral earth pressure theory, were properly scaled for use in the centrifuge at 50 g's, and were subjected to lateral earthquake-like motions which were considered to be of realistic levels. The walls were amply instrumented with pressure and displacement transducers, accelerometers, and strain gages. Moment, pressure, shear, and displacement distributions (static, dynamic, and residual) were obtained.

From the test data, some empirical curves for relating the upper bound responses of the retaining walls to the strong motion characteristics of the applied earthquakes were obtained.

ACKNOWLEDGMENTS

The author wishes to express his appreciation and gratitude to his research advisor, Professor Ronald F. Scott for, first of all, suggesting the research topic, and then providing guidance and suggestions during the course of the investigation. Additional thanks are owed to other faculty members and postgraduate fellows at Caltech, especially Professor Paul C. Jennings, Dr. John F. Hall and Dr. John M-M. Ting, for helpful discussions of some of the problems which were encountered.

In addition, the aid provided by Mr. John R. Lee in designing, building, and maintaining the experimental equipment is gratefully acknowledged and appreciated. Special gratitude is also owed to Mr. Raul Relles for his help in maintaining the digitizer in working order when it was most needed.

Finally the author wishes to thank Mrs. Sharon Beckenbach, Mrs. Gloria Jackson and Mrs. Beth McGrath for the expert typing of this work.

The financial support for research provided by the National Science Foundation (work performed under Grant No. CME79-13822), and the California Institute of Technology is also gratefully appreciated.

TABLE OF CONTENTS

TABLE OF CONTENTS (CONCLUDED)

CHAPTER I

INTRODUCTION

In this study, an investigation was made into the behavior of cantilever retaining walls, with a cohesionless soil backfill, subjected to earthquake-type dynamic excitations.

Interest in this problem arose from the fact that in virtually every earthquake damage report there is documentation of damage or failure of bridge abutments, sea walls, quay walls, canals, dikes, retaining walls, etc.; in other words, earth retaining structures. This is further enhanced by the fact that in most seismically active areas, there are absolutely no code provisions for some aseismic design of retaining structures. Where seismic considerations are taken into account, a design with the 60 year old pseudo-static Mononobe-Okabe theory with reduced design accelerations is usually accomplished.

Even though many experimental (model) and analytical studies have been done on the subject in the last 60 years, many have been improperly formulated, oversimplified, or simply inadequate. To this day there seems to be no general agreement as to what seismic method of design should be used or even if one should be used at all.

In recent years, the centrifuge has become a more accepted and useful tool in the modelling of soil mechanics problems. It was therefore decided to use this device in order to try to develop some empirical-type design guidelines for at least one type of retaining structure, namely cantilever retaining walls. In order to do this an "earthquake generating" mechanism, simple and light enough not to take up a substantial portion of the centrifuge payload, was developed in order to provide properly scaled earthquake-type excitations to the properly scaled and designed wall-soil system.

A series of fourteen tests was performed on two properly scaled retaining walls which were designed according to the traditional seismic theory. Since these walls are bending beams, bending moments were measured directly. This appears to be unprecedented since model studies have generally been done only on rigid walls. In addition, earth pressures behind the walls were measured and these results integrated to determine the shear forces. With the aid of accelerometers and displacement transducers, deflection shapes were also determined.

Although model tests were performed, they provided the response of a real (not idealized) retaining structure system subjected to a real earthquake excitation. This was afforded by using the artificial gravity field provided by the centrifuge.

1.1. Mononobe-Okabe Method

During the 1920's, N. Mononobe and N. Matsuo [31], and S. Okabe [39], developed an approximate method for determining the dynamic lateral earth pressure on a retaining structure. The method was based on the traditional Coulomb lateral earth pressure theory where inertial forces of the soil due to the earthquake were treated as additional static forces, through the use of horizontal and vertical accelerations. The observed failure mechanisms of gravity walls which had displaced under lateral acceleration provided a physical basis for this approach. The method, therefore, does not incorporate a calculation of the pressures which may develop between wall and soil prior to wall failure.

The Mononobe-Okabe method set a standard with which most future research in the field would be compared. Ensuing research has been concerned with refinement of the method or tests of its validity by model studies. Only a few countries have building codes that specify earthquake provisions for wall structures [17,55], but in general, when specified, these provisions are based on the Mononobe-Okabe method. Even in localities where no specific code requirements exist, it appears that the Mononobe-Okabe method is used in design when a dynamic analysis is desired.

Details of the Mononobe-Okabe method and suggestions regarding its application to design problems are given by Seed and Whitman [55].

1. The wall is assumed to displace laterally a sufficient amount to generate minimum active pressure.
2. The soil is assumed to satisfy the Mohr-Coulomb failure criterion.
3. Failure in the soil is assumed to occur along a plane surface through the toe of the wall and inclined at some angle to the horizontal.
4. The wedge of soil between the wall and the failure plane is assumed to be in equilibrium at the point of incipient failure, under gravity, earthquake, and the boundary forces along the

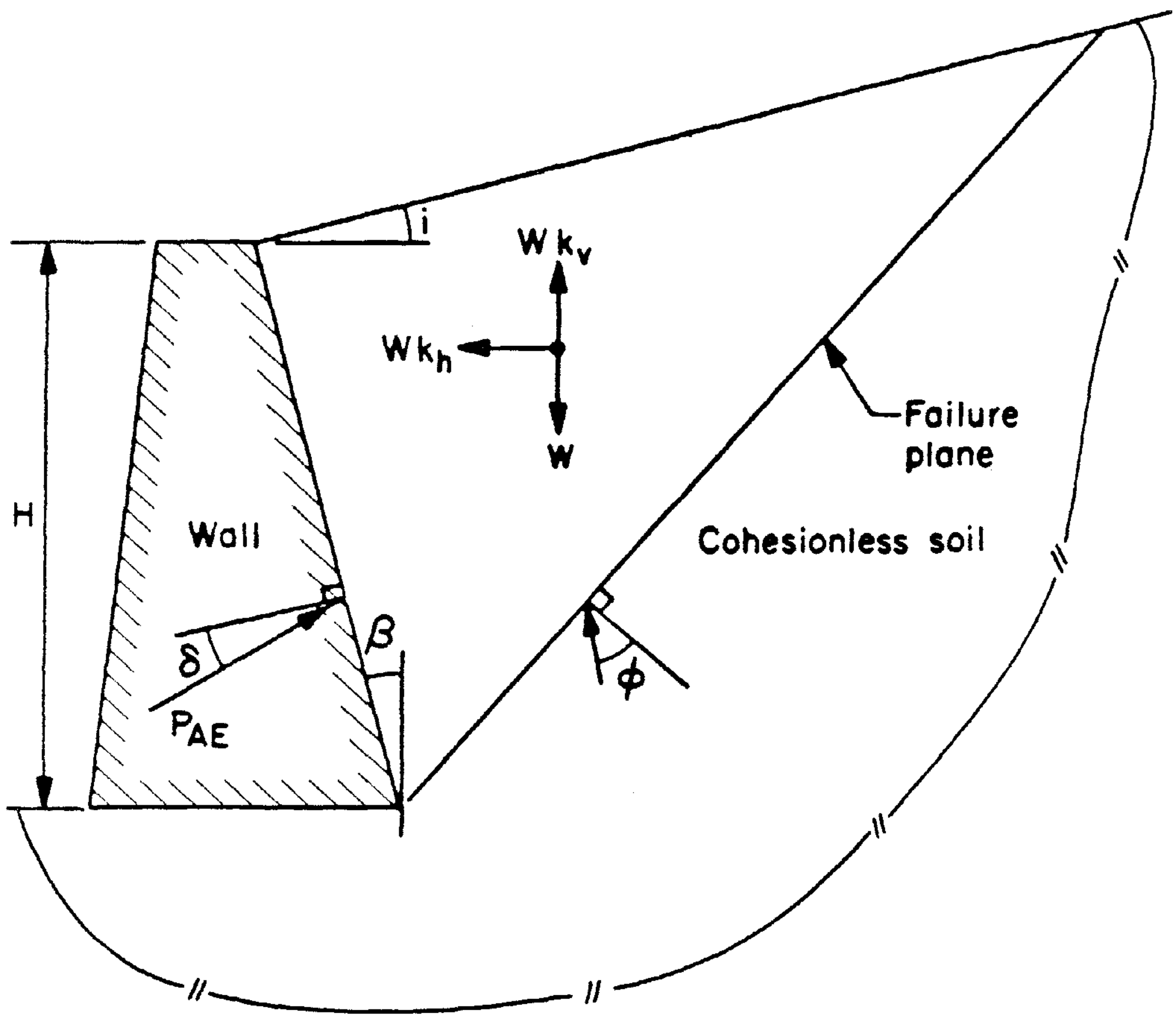

MONONOBE-OKABE ANALYSIS

FIGURE 1.1

wall and failure surface. The forces acting on the soil wedge of weight W are shown in Figure 1.1 for the case of a cohesionless soil.

5. Equivalent static horizontal and vertical forces $k_h W$ and $k_v W$, applied to the center of gravity of the wedge, represent the earthquake effect. The parameters k_h and k_v are the horizontal and vertical earthquake coefficients expressed as fractions of g, the gravitational acceleration.

6. The method gives the magnitude of the total acting force on the wall, but does not give the point of application or the pressure distribution. The method apparently was developed with the assumption that the total force acted 1/3H above the base of the wall of height H. Based on more recent refinements to the method, as well as model test results, Seed and Whitman [55] recommended that the dynamic force should be assumed to act 0.6H above the base. The total active wall force, due to gravity and earthquake, is determined by a force and moment equilibrium analysis of the soil wedge behind the wall (Figure 1.1).

As in a Coulomb analysis, the angle of the failure plane is varied to give a maximum value of the wall force per unit width P_{AE}, and under the critical condition it can be shown that

$$P_{AE} = 1/2\gamma H^2(1-k_v)K_{AE} \qquad (1.1)$$

in which:

$$K_{AE} = \frac{\cos^2(\phi-\theta-\beta)}{\cos\theta\ \cos^2\beta\ \cos(\delta+\beta+\theta)} \left[1 + \left(\frac{\sin(\phi+\delta)\sin(\phi-\theta-i)}{\cos(\delta+\beta+\theta)\cos(i-\beta)}\right)^{1/2}\right]^{-2} \quad (1.2)$$

(coefficient of lateral earth pressure)

$\theta = \tan^{-1} \dfrac{k_h}{1 - k_v}$

γ = unit weight of soil

ϕ = angle of internal friction of soil

δ = angle of wall-soil friction

i = angle of backfill slope

β = angle of wall slope

k_h = horizontal earthquake coefficient (fraction of g)

k_v = vertical earthquake coefficient (fraction of g)

Figure 1.2 illustrates the variation of K_{AE} with k_h with changes in the various soil/wall/lateral acceleration parameters. The Mononobe-Okabe method can be readily extended to encompass cohesive soils by considering the equilibrium of cohesive forces acting along the wall boundary and the failure surface.

Some limitations on the method are given by Wood [67]. A brief summary follows:

1. For full active pressure (full plastic state) to develop in the soil behind the wall, it is necessary for the top of the wall to deflect laterally about 0.5% of the wall height. This

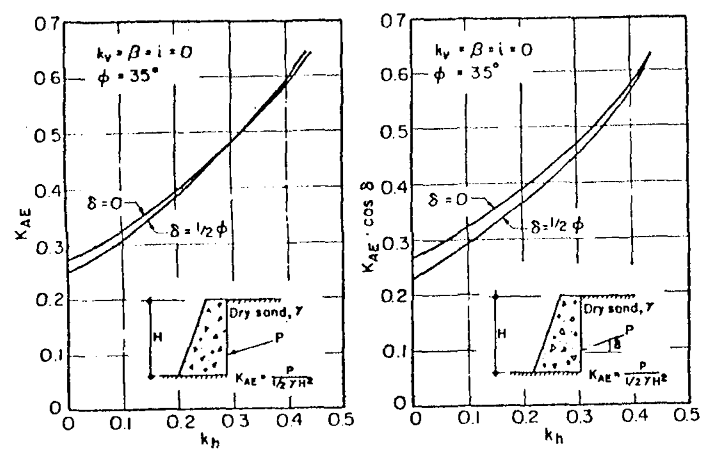

a INFLUENCE OF WALL FRICTION ON DYNAMIC LATERAL PRESSURES DETERMINED BY MONONOBE-OKABE ANALYSIS

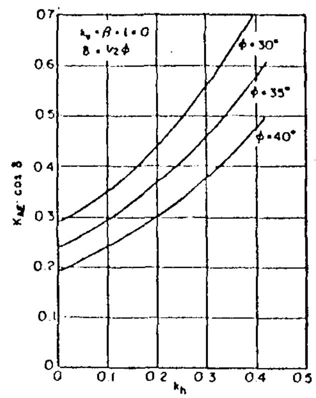

b INFLUENCE OF ANGLE OF FRICTION OF BACKFILL ON DYNAMIC LATERAL PRESSURES DETERMINED BY MONONOBE-OKABE ANALYSIS

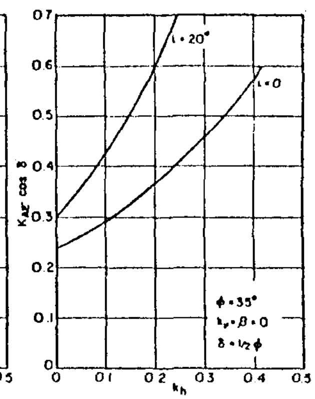

c INFLUENCE OF SLOPE OF BACKFILL ON DYNAMIC LATERAL PRESSURES DETERMINED BY MONONOBE-OKABE ANALYSIS

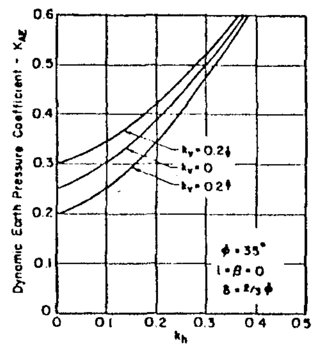

d INFLUENCE OF VERTICAL ACCELERATION ON DYNAMIC LATERAL PRESSURE COEFFICIENT DETERMINED BY MONONOBE-OKABE ANALYSIS

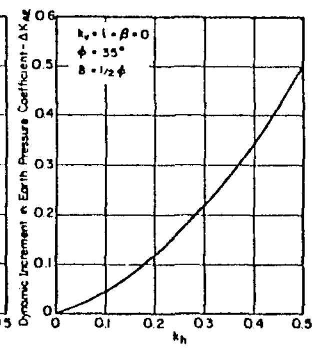

e DYNAMIC INCREMENT IN EARTH PRESSURE COEFFICIENT DETERMINED MONONOBE-OKABE ANALYSIS

FIGURE 1.2 - FROM (55)

condition probably occurs readily in gravity and cantilever walls, but may not always occur in channel sections or anchored sheet-pile walls. It was shown by Wood that for a rigid wall on a rigid foundation the earthquake force component computed by elastic theory was likely to be greater than twice the force computed by the Mononobe-Okabe method. This result was based on a static solution of identical horizontal earthquake coefficients for each case. Thus failure of a rigid structure designed using the Mononobe-Okabe criterion is a great possibility.

Unlike design procedures which allow yielding of structural members of building frames during strong earthquakes, it is generally undesirable to allow excessive yielding in retaining structures. This is because yielding of the structure generally tends to occur in only one direction away from the backfill. Unidirectional yielding may lead to excessive wall displacements with severe cracking to both wall and backfill. It is thus considered desirable to prevent yielding of the retaining structure during an earthquake.

2. Although the assumption of a plane failure surface appears reasonable, its validity has been based on a very limited number of test and field observations.

3. The Mononobe-Okabe Method is a pseudo-static method. Inertia forces are included by use of the earthquake coefficients k_h and k_v. These are generally chosen without any uniform basis

and are generally well below the values for expected peak accelerations. This is basically due to the assumption that some permanent movement of the wall due to shaking can be tolerated.

4. In the Mononobe-Okabe method no account is taken of resonance effects or the amplification of earthquake motions that might occur as a result of the propagation of the motion through the relatively soft soil behind the wall.

5. The Mononobe-Okabe method neglects the influence of the dynamic behavior of the wall structure itself on the earth pressures. Richards and Elms [43] (see section 1.3) have performed a study taking wall parameters into consideration.

1.2. Experimental Studies

In order to verify the Mononobe-Okabe theory, experiments on small-scale laboratory models subjected to sinusoidal excitation on shaking tables have been performed by a number of researchers: Mononobe and Matsuo, 1929 [31]; Jacobsen, 1939 [19]; Ishii, Arai, and Tsuchida, 1960 [18]; Matsuo and Ohara, 1960, [28]; Murphy, 1960 [33]; Niwa, 1960 [36]; Ohara, 1960 [38].

Mononobe and Matsuo used a 4 ft high, 4 ft wide, and 9 ft long sandbox which was subjected to horizontal excitations with vibration periods of 0.42 to 0.48 seconds. The end-walls of the box were hinged at the base and restrained by pressure measuring devices at the top. Total end-wall forces were measured and were found to be in reasonable agreement to those given by the Mononobe-Okabe method. Although no details were given, the wall was presumably allowed to displace sufficiently to allow full active pressure to develop.

Jacobsen performed tests on a sandbox using a shaking table and a 3 ft high layer of sand. Although no other details as to size of the box, flexibility of the wall, or type of excitation are given, it was concluded that the tests were in reasonable agreement with the Mononobe-Okabe method, and that the dynamic component of the force acted at about two thirds of the height of the sand layer above the base.

Ishii, Arai and Tsuchida performed tests with which they concluded that, in general, their results were in agreement with the Mononobe-Okabe analysis. They conducted tests on a sandbox with fixed and movable end-walls. Model gravity walls were also used in the box. A 2.3 ft depth of sand was used behind the walls. The entire box was subjected to sinusoidal excitations of approximately 3 Hz and 0.1g to 0.7g amplitude. Observations on wall displacement, sand settlement, residual earth pressures, and phase relationships between the earth pressures and base motion were made.

Matsuo and Ohara performed tests on dry and saturated sands in a shaking box 3.28 ft x 1.97 ft x 1.31 ft high. Conditions were similar to the tests of Ishii, et al. The box was subjected to 3 Hz sinusoidal excitations with an amplitude of 0.1g to 0.4g. Tests were conducted for both a fixed end-wall (essentially rigid) and a movable end-wall that was permitted to rotate about its base. Shaking was allowed to vary during the tests. For the rigid case the earth pressures were significantly higher than predicted by Mononobe-Okabe. The earth pressure distributions were also found to deviate considerably from linear.

Based on elasticity theory, Matsuo and Ohara also derived analytical expressions for pressure distributions for the fixed and rotating wall. The experimental pressures were significantly less for the rigid wall than those predicted by their theory. They attribute the discrepancies to influences of the side walls of the box and to the elasticity of the pressure cells used.

Murphy conducted tests to determine the mode of failure of wall-soil systems. A 1/64 scale wall model was placed in a shaking sand box and subjected to a 5.4 Hz excitation with a maximum acceleration of 0.25g. No pressures or displacements were recorded. It was found that failure occurred by outward rotation of the wall about the toe with a failure surface in the soil inclined at 35^{o} to the horizontal. The results were considered consistent with the failure plane in the Mononobe-Okabe method.

Niwa performed tests on a large-scale gravity-type quay wall model. The wall was 9.8 ft high and 13.1 ft wide with a 16.4 ft long sand backfill. In addition, a 6.6 ft $\times$ 6.6 ft $\times$ 13.1 ft surcharge of sand was placed right behind the wall. A large vibration generator was used. It was capable of delivering frequencies of 3 Hz to 6 Hz with a lateral force of 35 tons @ 6 Hz and a lateral acceleration of 0.3g @ 6 Hz. The generator was placed 34.8 ft behind the wall. A sizeable number of transducers were used to instrument the wall. These included pressure cells, as well as displacement, velocity and acceleration transducers.

Unfortunately, results were very sketchy. Pressures recorded were zero at the top and increased fairly linearly towards the bottom. No comparison with the Mononobe-Okabe method was given.

Ohara conducted experiments on a 12 in deep, 22 in wide and 39 in long sandbox which was harmonically forced with accelerations of up to 0.4g. The end wall was given controlled displacements and the results were found to be consistent with those predicted by the Mononobe-Okabe method.

From the shaking table experiments it is generally concluded that the Mononobe-Okabe method gives the total resultant force reasonably well, but not the pressure distribution, and hence, does not predict the point of application of the force or the magnitude of the overturning moment correctly. Overall, the results of the shaking table experiments are questionable. The tests were performed under fairly unreal conditions. They generally had externally controlled restricted displacements and rotations of the wall. The tests were performed in the laboratory at earth gravity, using scaled harmonic forcing, which was not random as seismic forcing is and may not adequately represent transient earthquake stresses. The rationale for these tests is based on the following argument (Wood[67]). A similarity condition for an elastic soil and a rigid wall under the assumption that both the model and prototype have the same Poisson's ratio is given by the dimensionless equation for the frequency of a vibrating elastic system:

$$\frac{f_p^2 \rho_p \; Hp^2}{G_p} = \frac{f_m^2 \rho_m \; H_m^2}{G_m} \tag{1.3}$$

where:

$f_{m,p}$ = frequency of vibration of model and prototype respectively.

$\rho_{m,p}$ = soil mass density

$H_{m,p}$ = height

$G_{m,p}$ = shear modulus

and both model and prototype tests are performed at the same gravitational acceleration.

The equation is usually employed to determine the frequency at which the model is to be vibrated to simulate the full-scale behavior. If the ratio of length scale in prototype to model is denoted as N, the equation can be rearranged in terms of frequency to give

$$\frac{f_m}{f_p} = \left[\left(\frac{H_p}{H_m}\right)^2 \left(\frac{G_m}{G_p}\right) \left(\frac{\rho_p}{\rho_m}\right) \right]^{1/2} \tag{1.4}$$

However, H_p/H_m = N, and, since the same soil is generally used in model and prototype, ρ_p/ρ_m is close to unity so that

$$\frac{f_m}{f_p} = N \left(\frac{G_m}{G_p}\right)^{1/2} \tag{1.5}$$

In a clay, a laboratory model can be prepared with G_m essentially any desired value, from a low level, appropriate in some way to the model dimension, to a value the same as the prototype. In sands, the shear modulus G varies with the effective stress, which depends directly on the gravitational field. As a consequence G_m in a model sand is considerably smaller over the wall depth than G_p in the full-scale domain. The choice of f_m therefore, depends on the relationship adopted between G and the effective stress in the sand. If G is taken to vary linearly with effective stress, then f_m is approximately equal to $N^{1/2}f_p$. Alternative if G is taken to vary as some power of effective stress, say 1/2 (Seed and Idriss [54]), f_m would be given as $N^{3/4}f_p$.

Given this uncertainty about the variation of G with effective stress, no clear approach is indicated, nor do the experiments clarify the effect on the dynamic pressure distributions obtained by the use of different model exciting frequencies. It can be concluded that it is difficult or impossible to achieve a pressure distribution in a (one g) model on a shaking table similar to that found in the full-scale field situation. Therefore, true modelling of the prototype soil cannot be attained in a (one g) shaking table experiment.

1.3. Analytical Studies

In addition to the experimental research, analytical models have been proposed to describe the dynamic earth pressures acting on walls: Tajimi, 1969-73 [59-61]; Prakash and Basavanna, 1969 [42]; Scott, 1973 [50]; Wood, 1973 [67]; Richards and Elms, 1977 [43]; Chang and Chen, 1981 [6,7].

Tajimi obtained the solution for earthquake-induced soil pressures on a cylindrical structure embedded in an elastic soil. He also obtained the solution for a harmonically forced rigid wall of finite height at the corner of a quarter-infinite elastic medium (Figure 1.3). The analysis was based on elastic wave propagation theory. Although the boundary conditions are not very realistic, the solution can be used as an approximation for some dynamic problems.

Prakash and Basavanna computed an approximate wall pressure distribution on a wall under similar assumptions to those of the Mononobe-Okabe method. It was determined that the pressure distribution was essentially parabolic although the resultant was virtually of the same magnitude as give by Mononobe-Okabe. The resultant, however, acts at a height above the base H_a given by:

$$H_a = C_a H/3 \tag{1.6}$$

where C_a is a very complicated expression dependent on all the Mononobe-Okabe wall-soil parameters. H is the height of the wall. C_a is greater than one. For $k_h = 0.3$, H_a is approximately midheight and continues to rise with higher lateral acceleration.

Scott performed an analysis on a simple yet useful model (Figure 1.4). It basically consists of a rigid wall with the soil modelled as a simple shear beam on a Winkler foundation. He also performed an analysis where a wall flexibility was included. Closed form solutions were obtained for various cases that include variations of the elastic constants with depth and certain types of wall

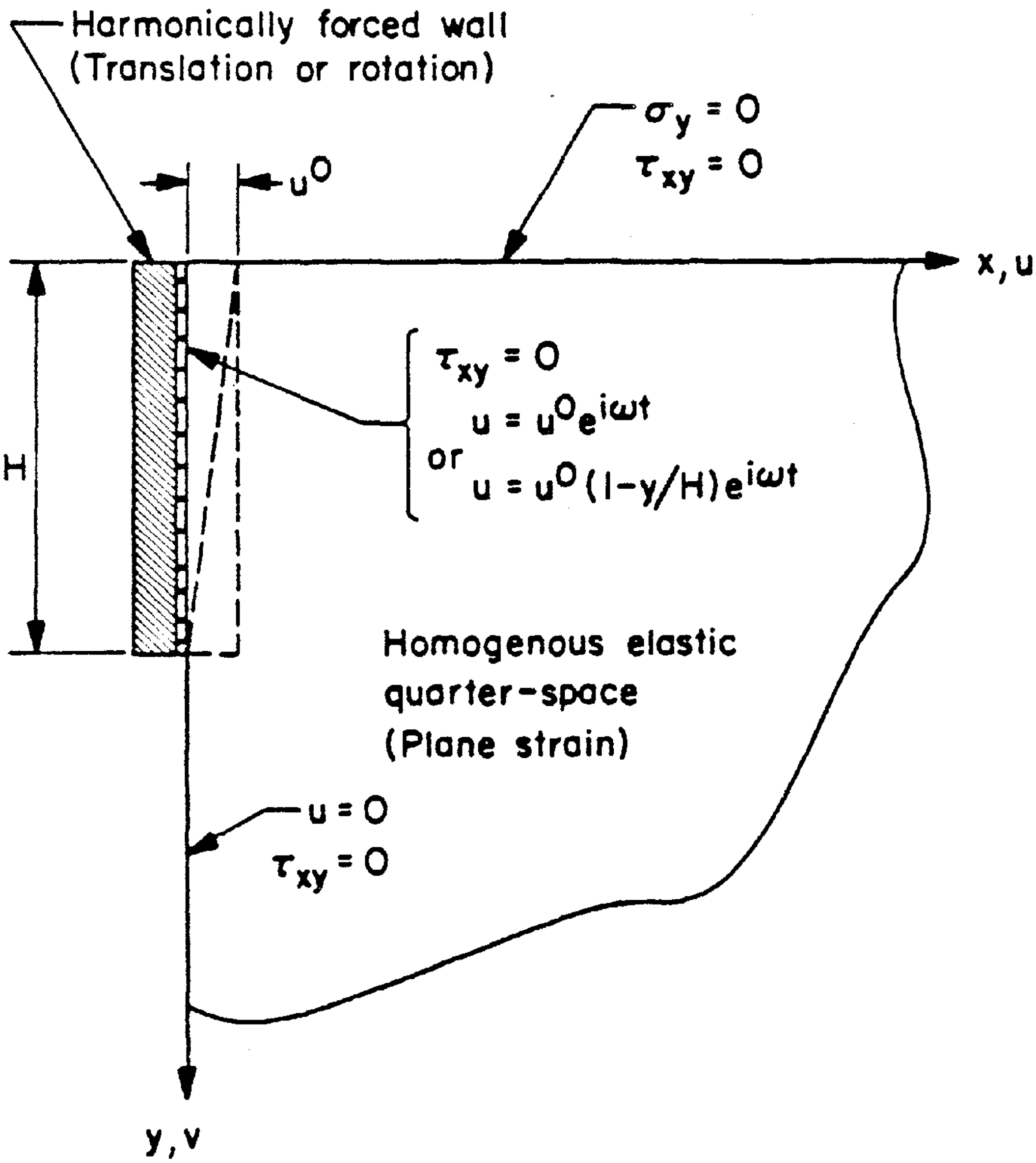

TAJIMI'S PROBLEM

FIGURE 1.3

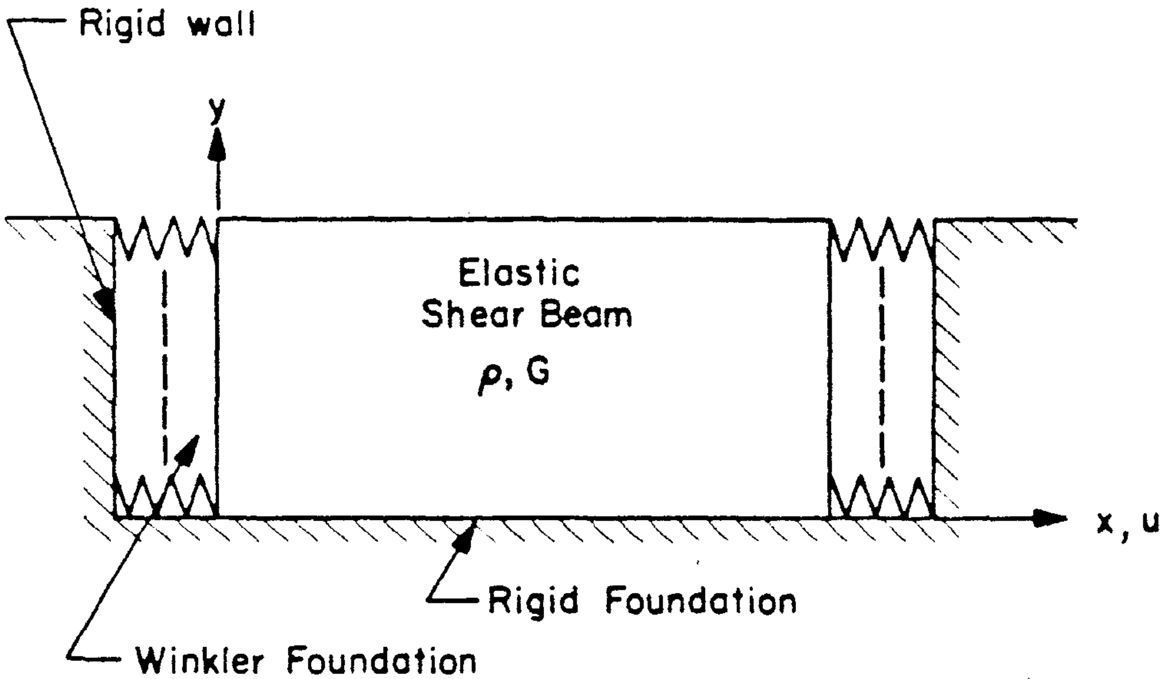

SCOTT'S MODEL

FIGURE 1.4

deformations. Because of simplicity the solutions are quite useful in preliminary design applications. Scott concluded that what happens in an earthquake to a wall designed by the Mononobe-Okabe method is that "elastic", transient forces much higher than those predicted by Mononobe-Okabe act on the wall, causing it to displace and rotate. When the wall reaches a displacement of 1/2% or so of the height, the soil reaches failure. The wall continues to displace and rotate due to inertia and when it stops what is observed is the failure (Mononobe-Okabe) mechanism - not the stresses that caused failure. This is why all the experiments involving failure end up by concluding that Mononobe-Okabe is the right analysis. If the earthquake force only reached Mononobe-Okabe levels of stress, then the wall designed to M-O should not fail.

Wood, using elastic and elastic wave propagation theories developed solutions for an elastic soil stratum of finite or infinite length and finite depth on a rigid base with a rigid wall under various and forcing conditions. For a perfectly rigid wall (Figure 1.5), supporting a relatively long layer of soil, he determined that the earthquake force component computed was likely to be greater than twice that estimated by the Mononobe-Okabe method (Figure 1.6). Identical horizontal earthquake coefficients k_n were used in the comparison. It was thus recommended that for a rigid wall embedded in rock or very firm soil, restrained by piles or deeply buried, an elastic analysis should be used in lieu of the Mononobe-Okabe method.

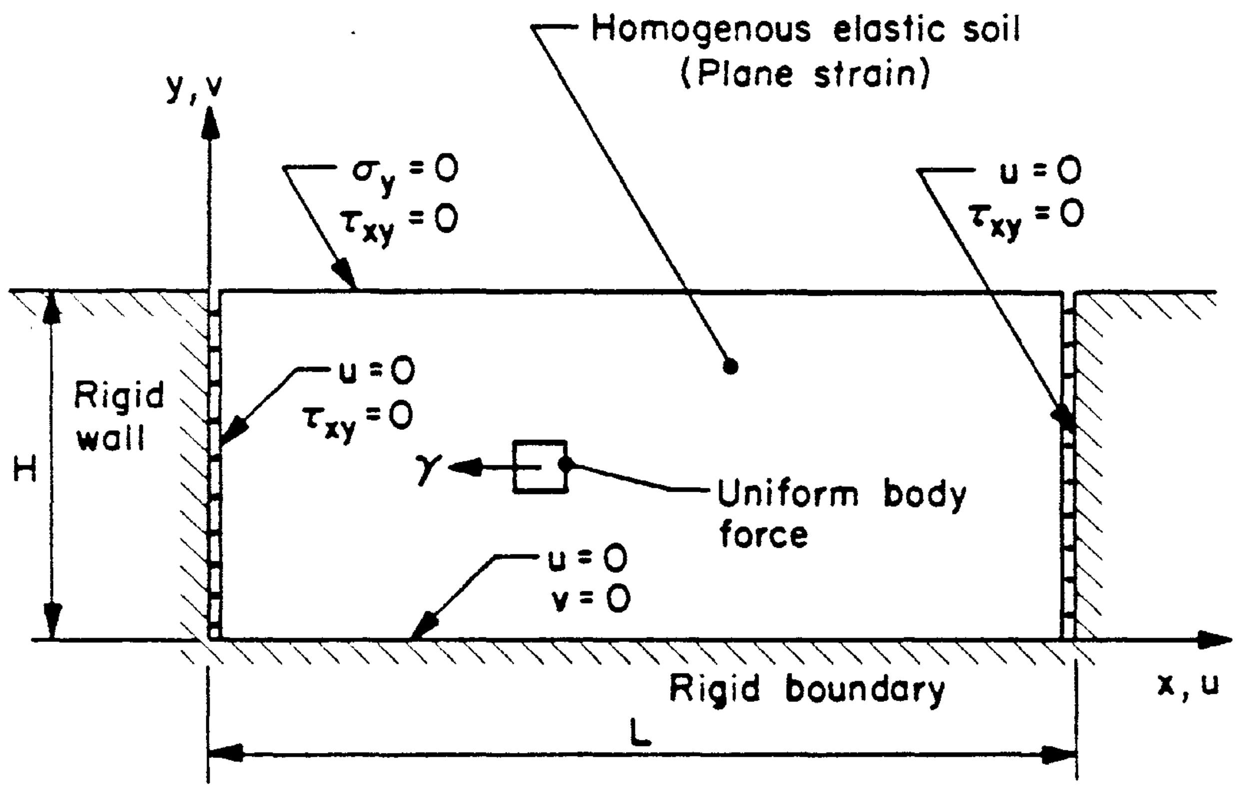

WOOD'S RIGID WALL PROBLEM

FIGURE 1.5

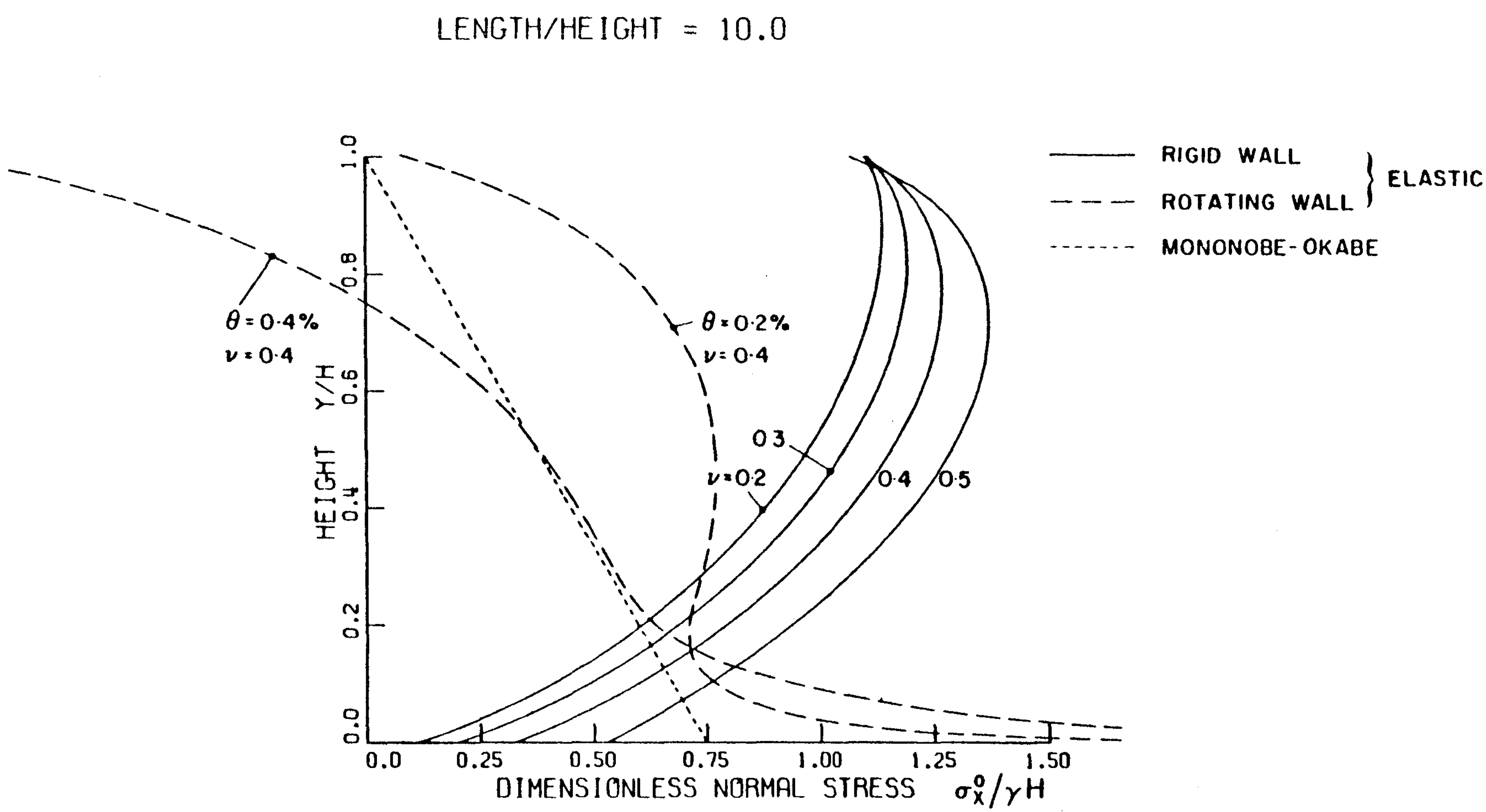

Pressure distributions for one-g static horizontal body force. Comparison between elastic theory and Mononobe-Okabe method.

FIGURE 1.6 – FROM (67)

Richards and Elms extended the Mononobe-Okabe method to include the influence of the dynamic behavior of the wall structure itself (Figure 1.7). It was concluded that for gravity retaining walls the Mononobe-Okabe analysis is satisfactory provided that the inertia of the wall is taken into consideration. In addition, Richards and Elms give a description of the significance of each of the Mononobe-Okabe parameters which is useful in a further understanding of the method.

Chang and Chen developed an upper bound technique of limit analysis and then applied it the earthquake problem. It is basically an approach similar to Mononobe-Okabe with the main difference being that more refined failure surfaces (Figure 1.8) are used. The seismic coefficient of active earth pressure K_{AE} was found to be practically the same as that obtained by a Mononobe-Okabe analysis.

1.4. Earthquake Damage to Retaining Structures

Failures in retaining structures due to earthquakes occur very frequently. These are documented in virtually every earthquake-damage report. It should be noted that in most reports, unless failures are dramatic, retaining-structure damage is given secondary importance. This is generally due to the fact that failure of these structures does not entail severe loss of life and limb. The damage done by the earthquake can, however, be very costly in terms of repair and replacement as well as economic setbacks to a community. A few examples of damage to retaining structures follow.

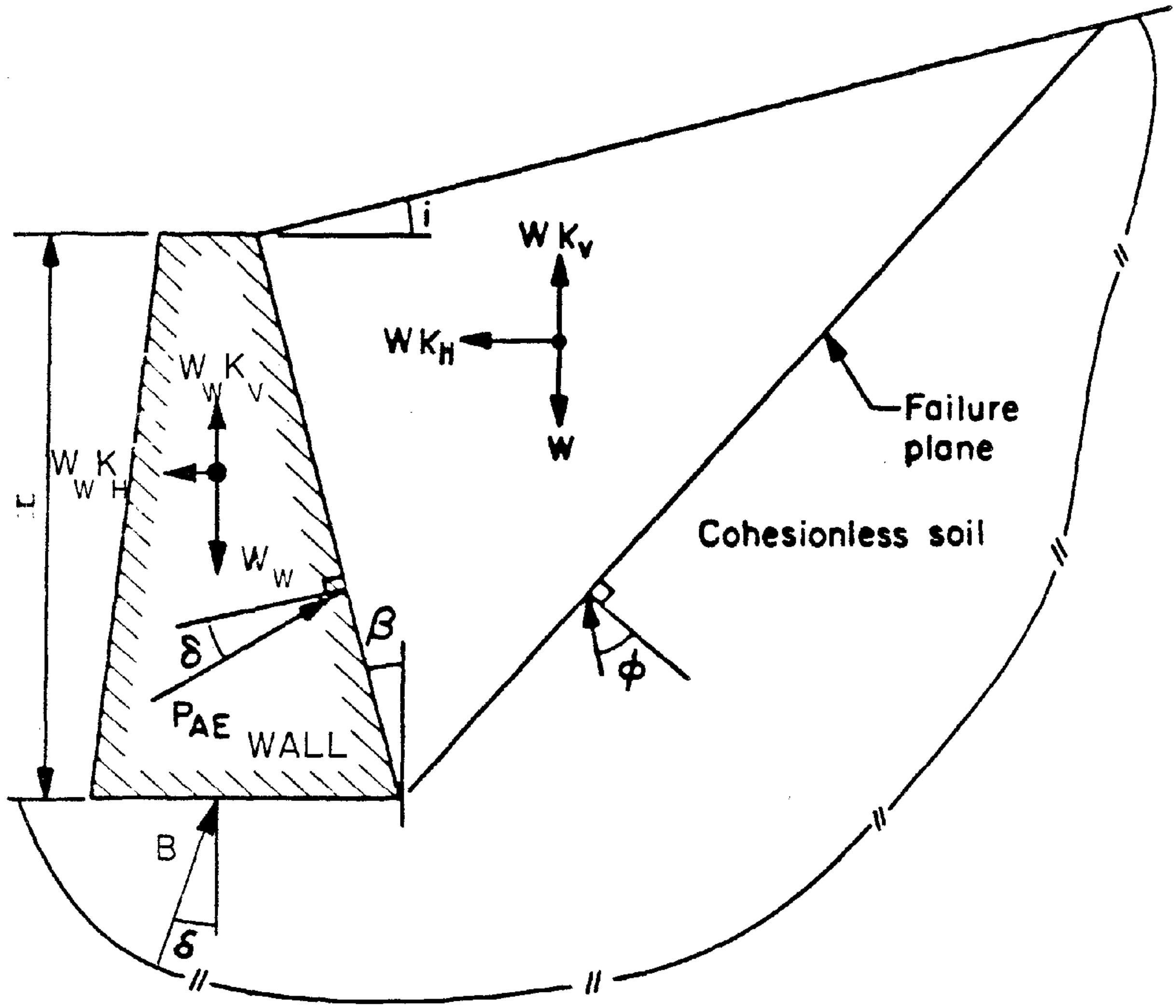

RICHARDS & ELMS ANALYSIS

FIGURE 1.7

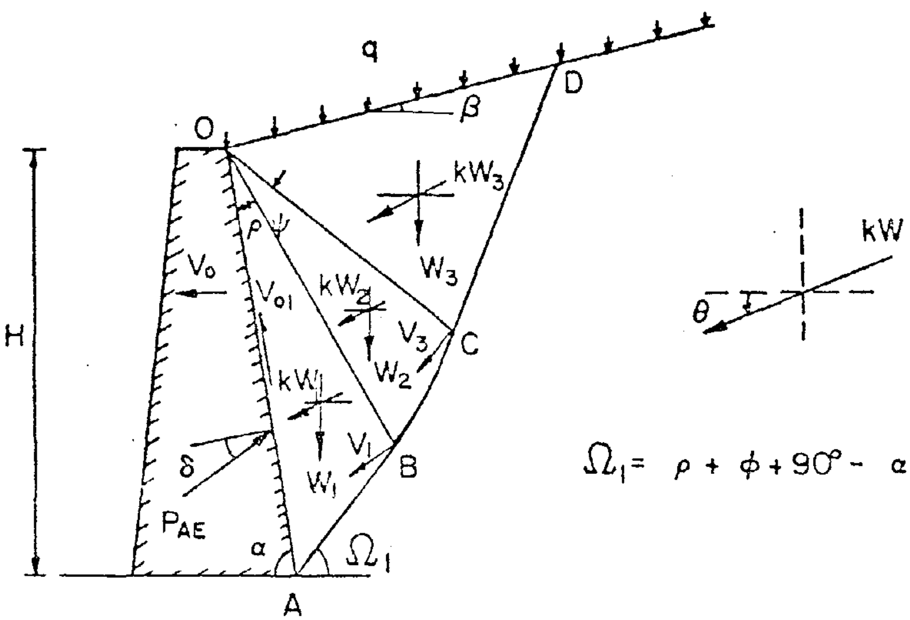

FIGURE 1.8 - FROM (7) Log-Sandwich Failure Mechanism for Seismic Active Earth Pressure Analysis

1.4.1. Chile

Duke and Leeds [11] provide an extensive account of damage to retaining structures in the 1960 Chilean Earthquakes, the most severe of which had a Richter magnitude of 8.5. At Puerto Montt (Figure 1.9), the Modified Mercalli Intensity (MMI) was estimated to be between VIII and IX. There was essentially total failure of the harbor gravity-type quay walls (Figs. 1.10, 1.11, 1.12, 1.13). Both walls completely overturned. Sheet pile sea walls (Figs. 1.11, 1.14) were severely damaged. The piles had approximately 5" x 15" hat-shaped cross-sections with 5/16" thick webs and were made in Germany. Since the walls were about 30 years old at the time of the earthquake, failure principally occurred when the corroded rods broke due to the added tension resulting from the added soil pressure.

Most of the above-mentioned structures were founded on fill consisting of gravel, sand, silt, some masonry fragments, and organic matter. In general, it was placed by dumping although some was placed hydrodynamically by dredging from the harbor bottom. The disastrous damage to structures retaining this material was largely due to liquefaction as a result of earthquake motion.

Figure 1.15 shows distortion of the Isla Teja bridge in Valdivia (MMI X) due to the added soil pressure on the abutment whose excessive movement caused damage to the bridge superstructure. Unlike the Puerto Montt failures, damage to this structure was not due to liquefaction, but solely to the added inertia from the shaking.

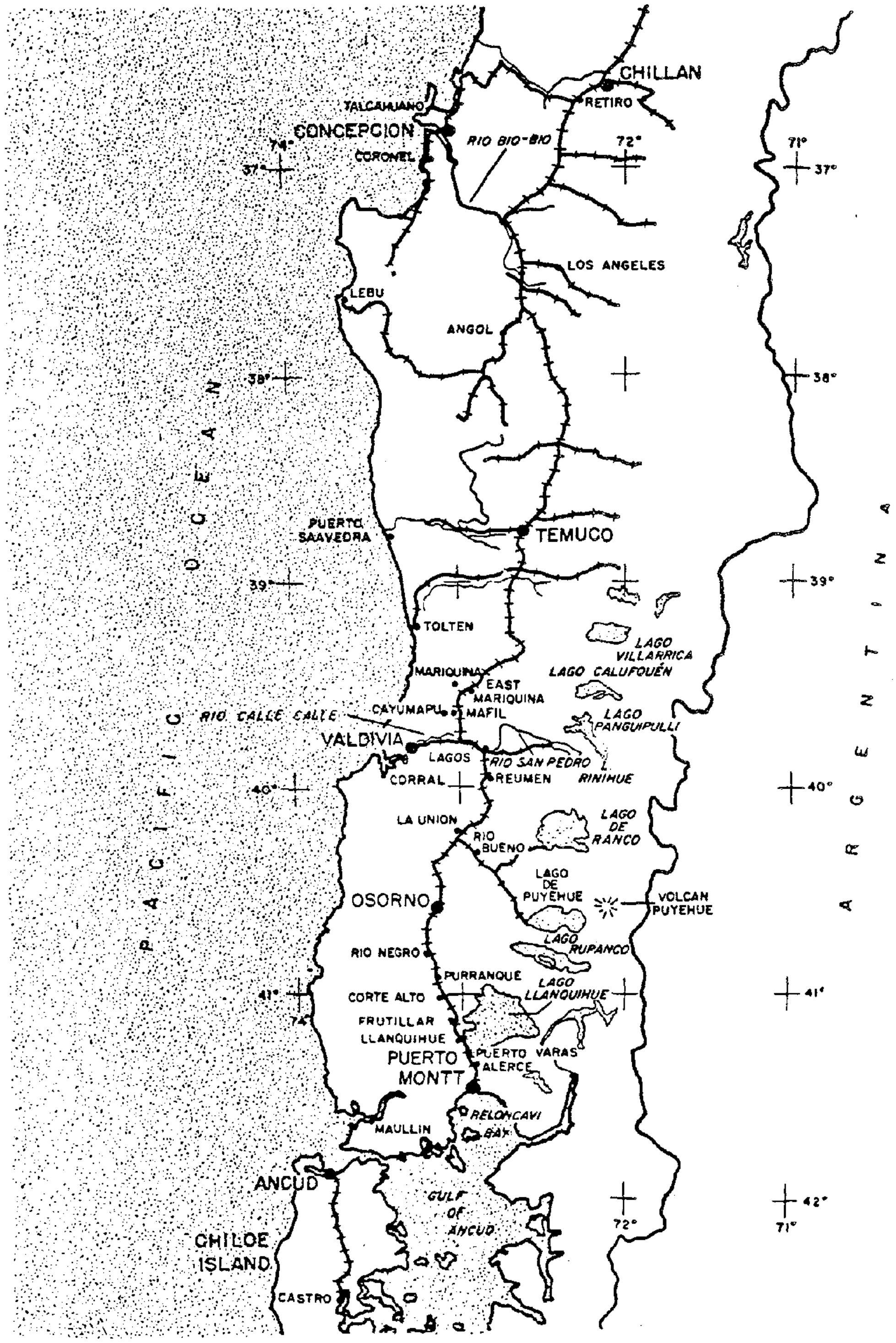

Region affected by the Chile Earthquakes of May 1960.

FIGURE 1.9 – FROM (11)

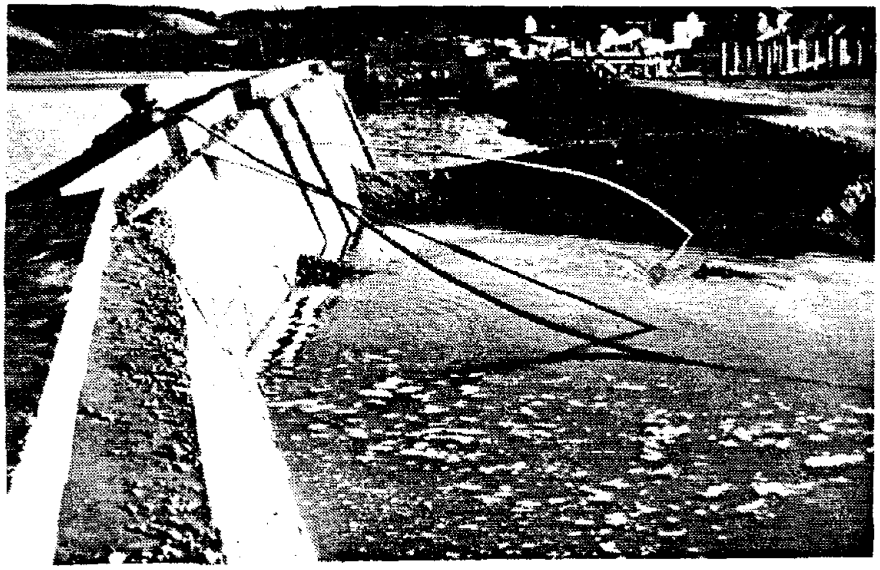

FIGURE 1.10 - FAILURE OF QUAY WALL AT PUERTO MONTT - FROM (55)

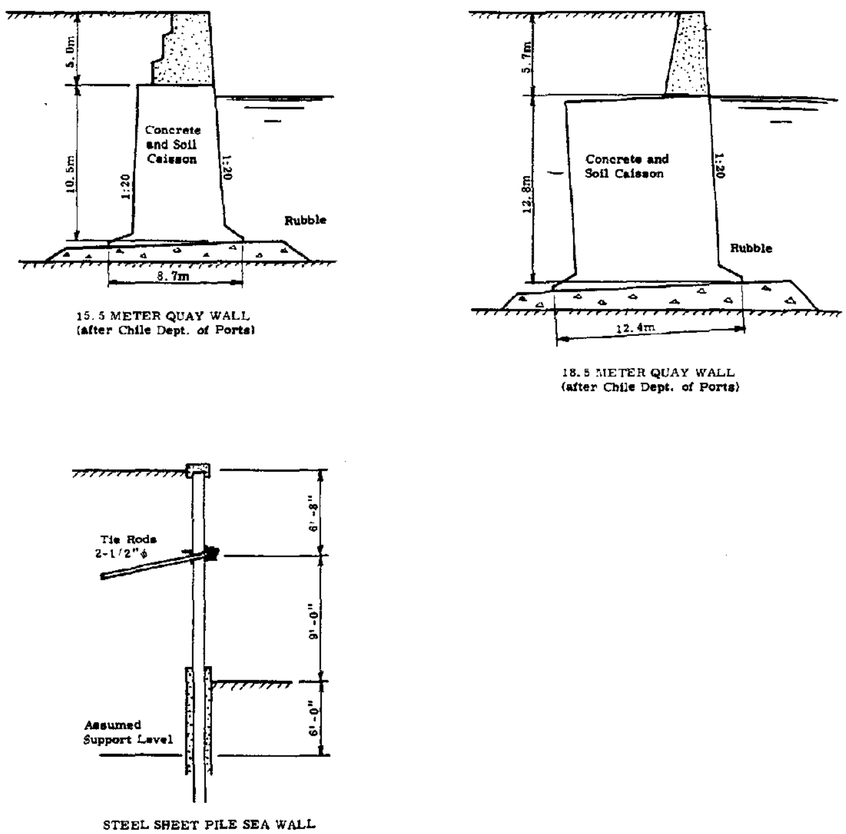

FIGURE 1.11 - PUERTO MONTT, WATERFRONT WALLS, DESIGN FEATURES - FROM (11)

FIGURE 1.12 – FAILURE OF GRAVITY WALL AT PUERTO MONTT – FROM (11)

FIGURE 1.13 – PUERTO MONTT, GRAVITY WALL FAILURE – FROM (11)

FIGURE 1.14 - FAILURE OF SHEET-PILE SEA WALL AT PUERTO MONTT - FROM (11)

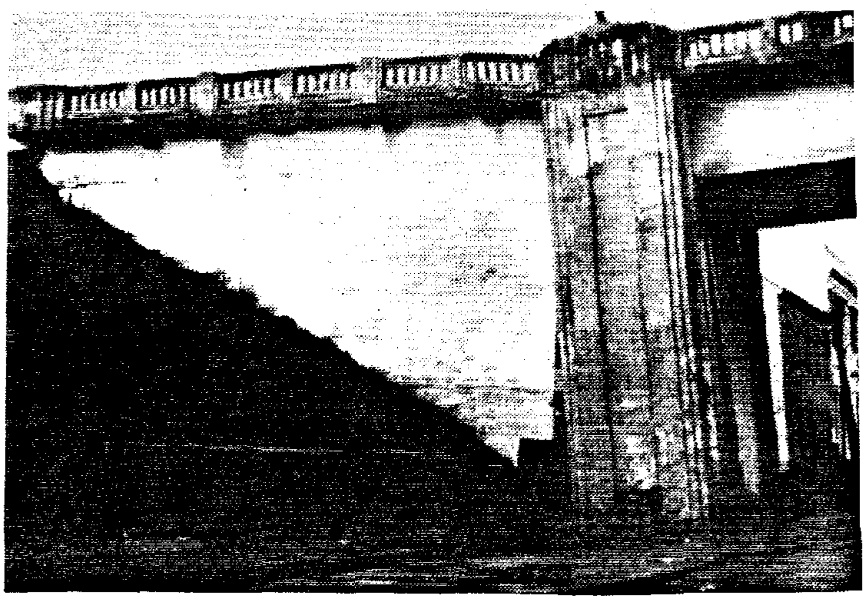

FIGURE 1.15 - DISTORTION OF ISLA TEJA BRIDGE DUE TO SOIL PRESSURE ON ABUTMENT - FROM (55)

Seed and Whitman [55] also report on a gravity retaining wall failure at Frutillar (MMI VIII) where dry material was encountered (Fig. 1.16).

1.4.2. Alaska

Ross, Seed, and Migliaccio [45] report on extensive bridge damage due to the 8.4 magnitude Alaska earthquake of 1964. Most of the bridges which suffered damage were 50 to 80 miles away from the cone of major energy release. The most severe damage occurred on the Seward, Sterling, and Copper River Highways (Fig. 1.17). Table 1.1 gives a foundation damage classification reduced from reports of the Alaska Department of Highways.

Most of the bridges were founded on alluvial deposits composed of granular materials which ranged anywhere from coarse gravels to fine sands and silts depending on location. The deposits ranged in depth from 50 to 150 ft and were generally underlain by clays or bedrock. A few bridges were founded on bedrock.

Damage was due completely or in part to the lateral displacement of the bridge abutments toward the channels causing tilting of piers and buckling of superstructures (Figs. 1.18, 1.19, 1.20). There was also spreading and settlement of abutment fills. The greatest concentrations of severe damage occurred in regions characterized by thick deposits of saturated cohesionless soils. There was ample evidence of liquefaction of these materials during the earthquake. This phenomenon probably played a major role in the development of foundation displacements and

FIGURE 1.16 – FRUTILLAR,RETAINING WALL FAILURE – FROM (55)

TABLE 1.1

Classification of Damage to Highway Bridge Foundations During the Alaska Earthquake (from Ross et al. [45])

114 Bridges Classified

Classification	Description	Percentage
Severe	Abutments moved streamward and/or markedly subsided; piers shifted, tilted, or settled; substructure rendered unsalvageable	28
Moderate	Distinct and measurable net displacements as in previous category, but to a lesser degree, so that substructure could perhaps be repaired and used to support a new superstructure	22
Minor	Evidence of foundation movements (such as cracked backwalls, split piles, closed expansion devices), but net displacements small and substructure serviceable.	18
Nil	No evidence of foundation displacements	32

bridge damage. Even where damage was moderate or minor, there was evidence of bridge joints closing indicating lateral displacement of the abutments.

It should be noted that where bridges were founded completely on bedrock there was virtually no damage. However, severe to moderate displacements were reported for bridges founded partly on bedrock and partly in soils.

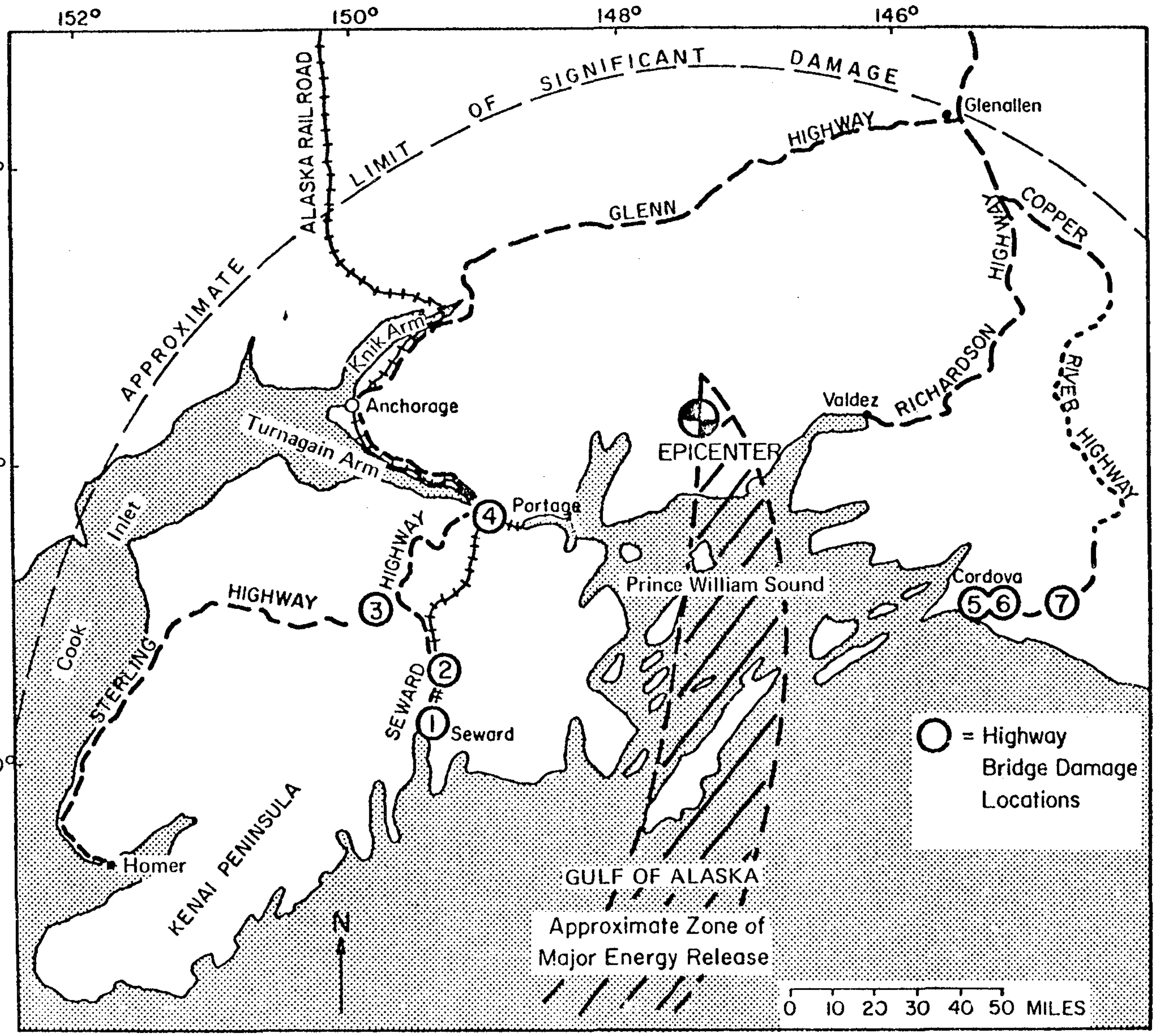

Highway routes of seven main bridge-damage locations in earthquake-damaged region, south central Alaska.
FIGURE 1.17 – FROM (45)

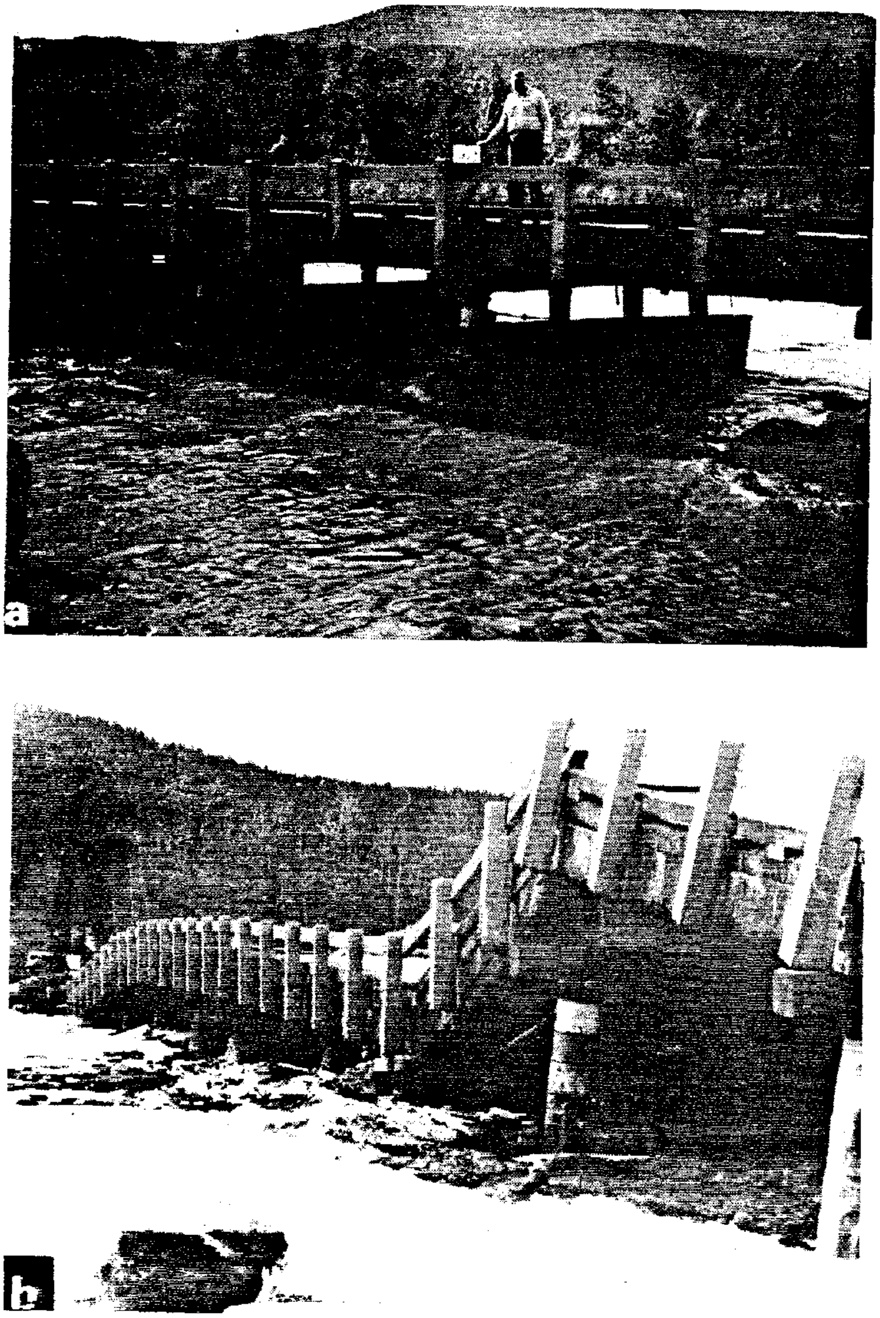

FIGURE 1.18 – SUPERSTRUCTURE BUCKLING OF SNOW RIVER BRIDGE 605 – FROM (45)

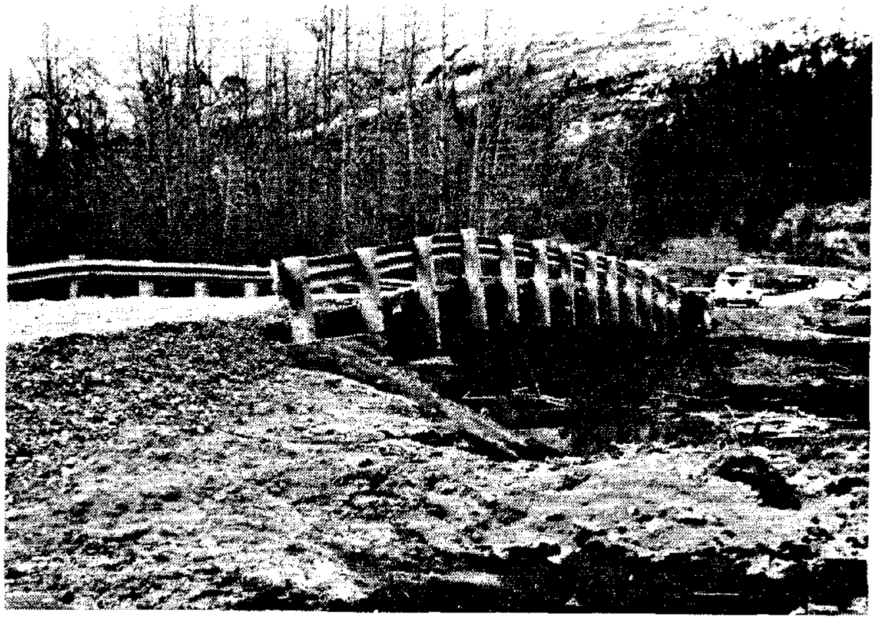

FIGURE 1.19 - SUPERSTRUCTURE BUCKLING OF SNOW RIVER BRIDGE 604 - FROM (45)

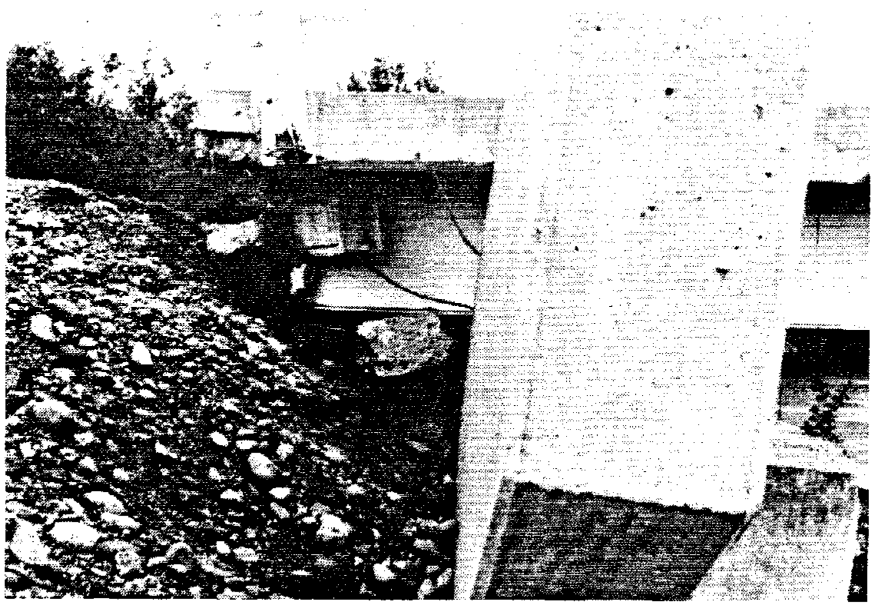

FIGURE 1.20 - SUPERSTRUCTURE DRIVEN THROUGH ABUTMENT BACKW/.LL,COPPER RIVER BRIDGE 345 - FROM (45)

1.4.3. Niigata, Japan

The 7.5 magnitude, 1964 Niigata, Japan earthquake caused severe damage to waterfront structures and virtually paralyzed operations at the port of Niigata, one of Japan's most important. Accounts of the damage are given by Hayashi, Kubo, and Nakase [14], and by Kawasumi [22].

The total length of waterfront structures including jetties and dikes at the port of Niigata was 10.25 miles. About 76% of this length was composed of earth retaining structures. Sixty-nine percent of these were steel sheetpile bulkheads, 8% were concrete sheetpile walls and 6% were concrete gravity walls. The severity of damage to harbor structures is outlined in Table 1.2.

TABLE 1.2

(from Hayashi, et al. [14])

Grade of Damage	Description	Total Length* (mi.)	Proportion to the Overall Length* (%)
4	Complete failure of whole structure	5.43 (4.43)	52.8 (57.1)
3	Failure in main part of structure	2.32 (2.32)	22.6 (30.0)
2	Appreciable Deformation to main part of structure	0.07 (0.02)	0.7 (0.3)
1	Failure in sub-part of structure	3.98 (0.39)	14.5 (5.0)
0	No damage	0.97 (0.59)	9.4 (7.6)

*Figures in parentheses refer to earth retaining structures only.

It should be noted that due to the failure of earth retaining structures, 61 warehouses and sheds, 676, 600 ft^2 in total area, fell down completely, and 92, 691, 500 ft^2, were seriously damaged (Figs. 1.21, 1.22).

Most of the sheet pile structures in Niigata Harbor underwent damage and a large number were completely destroyed or submerged. A common feature of the damage was a swelling of the backfill and inclination of the wall toward the sea. This type of damage was typically observed in bulkheads with poor anchor resistance. Tie rods were severed in some cases. In others there was a shear failure in the concrete anchor blocks due to the stress concentration created by the tie rods. The sheetpile bulkheads were designed employing a Mononobe-Okabe Analysis and a seismic coefficient of 0.10. Actual horizontal ground accelerations were around 0.2g amplitude.

The brand new Yamanoshita wharf (completed 1963) which had been Mononobe-Okabe designed with a seismic coefficient of 0.12 suffered no appreciable damage, except for local sinking of the fill behind the anchor plate.

Concrete sheetpile walls, which formed a small part of the waterfront, were completely destroyed by the earthquake.

The gravity retaining walls were generally composed of several concrete blocks stacked up on top of each other and then assumed to act as a monolithic structure. A seismic coefficient of 0.10 was used in design, but it was later found that when the seismic coefficient reaches

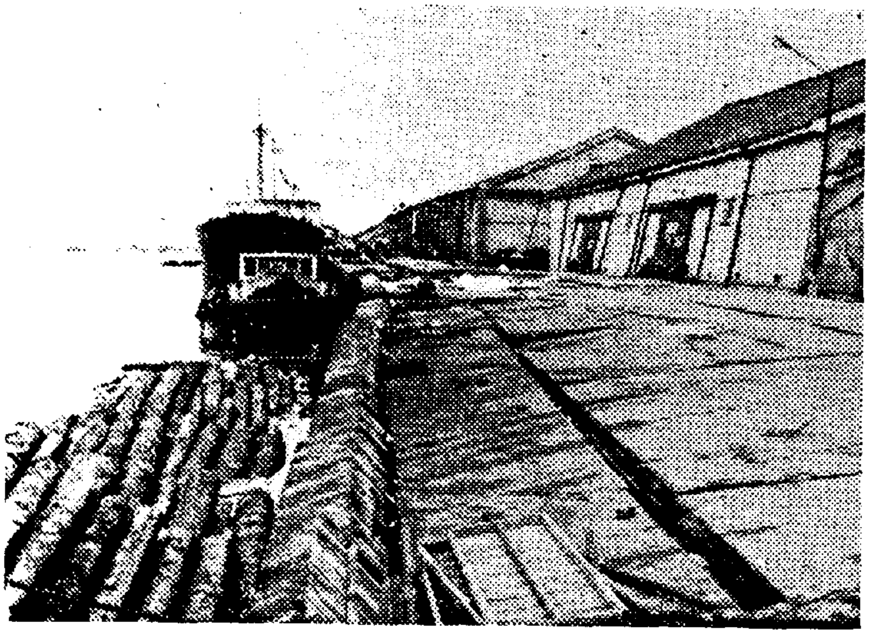

FIGURE 1.21 - SHEET-PILE BULKHEAD FAILURE,NIIGATA - FROM (14)

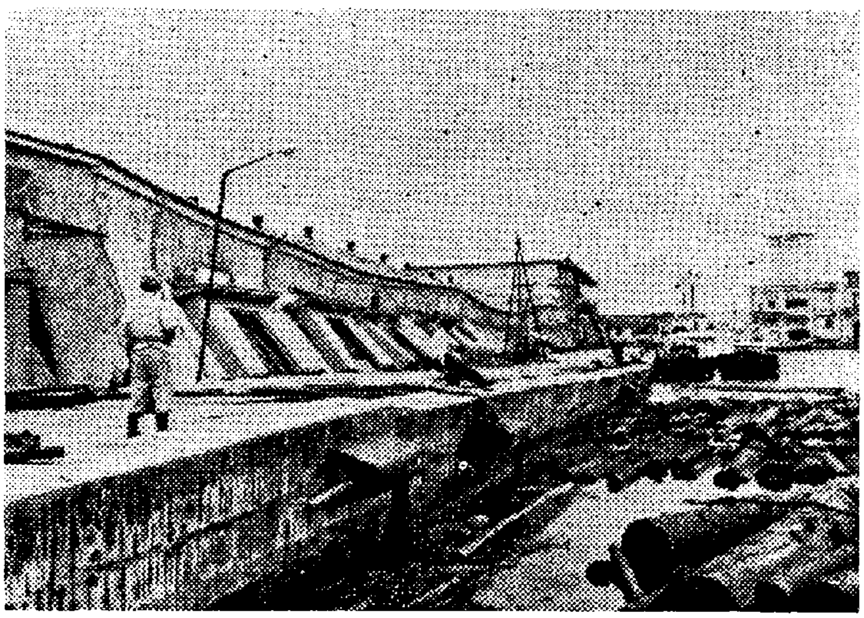

FIGURE 1.22 - WAREHOUSE COLLAPSE DUE TO SHEET-PILE BULKHEAD FAILURE,NIIGATA - FROM (14)

0.12 or 0.13 the structure cannot any longer be assumed to act monolithically. As a result, damage was characterized by blocks falling forward, slippage, and sinking of blocks, and general inclination and sliding of the structures. Damage was severe.

The general soil profile of the Niigata area consists of a layer of sand about 130 ft deep underlain by clays and containing pockets of fine silty soil in the top 60 ft. The soil was generally saturated and much of the damage was due to the occurrence of liquefaction. Before the earthquake the top 30 ft of soil was characterized by an average blowcount of from 4 to 8 using the Standard Penetration Test. Between 30 and 60 feet, it varied linearly from about 8 at 30 ft to about 30 at 60 ft. These figures were reduced by one third after the earthquake. In general, the deeper the structure was embedded in the soil the less severe the damage.

Based on the damage caused by the 1964 earthquakes, replacement structures have been designed and built based on a seismic coefficient of 0.2.

1.4.4. <u>San Fernando, California</u>

The 1971 San Fernando, California, earthquake, which had a magnitude of 6.2, severely damaged, in some cases, earth retaining structures including flood control channels, bridge abutments, and underground water storage tanks and tunnels.

Murphy [32], Scott in Reference [21], Lew, Leyendecker and Dickers [24], and Wood [67] provide descriptions of damage to the Wilson Canyon and Mansfield Street Flood Control Channels and to the Lopez Canyon Diversion Channel which were located in an area where transient lateral accelerations may have been as high as 50%g.

The Wilson Canyon Channel is partially an open, rectangular, reinforced concrete channel, with a width of about 15 feet and wall heights which vary from 9 to 11.5 feet (Figure 1.23) and partially a covered, rectangular, box section with widths varying from 15 to 22 feet and wall heights ranging from 105 to 16 feet; it is about 3 miles long.

The Lopez Canyon Diversion Channel is an open, rectangular reinforced concrete channel about 1.8 miles long, with widths varying from 12 to 16 feet and wall heights ranging from 7 to 12 feet.

All the above-mentioned structures were built in the early 1960's by the Corps of Engineers in accordance with the Chief of Engineers' design criteria with no seismic consideration. Allowable design stresses were $f_c' = 1.05$ ksi for concrete and $f_s = 20$ ksi for steel. The channels were designed as L-type retaining walls where the wall heights were less than half the channel width, and as U-type channel sections otherwise.

No significant ground displacements seem to have occurred in the vicinity of the damaged sections of the Wilson Canyon and Mansfield Street Channels so the damage can be attributed to an increase in the lateral earth pressure due to ground shaking. There were some inward displacements in the open sections which measured up to 6 inches at the top of the walls (Figs. 1.24, 1.25). Damage to the underground box sections varied from hairline cracks to major shear and moment failures in

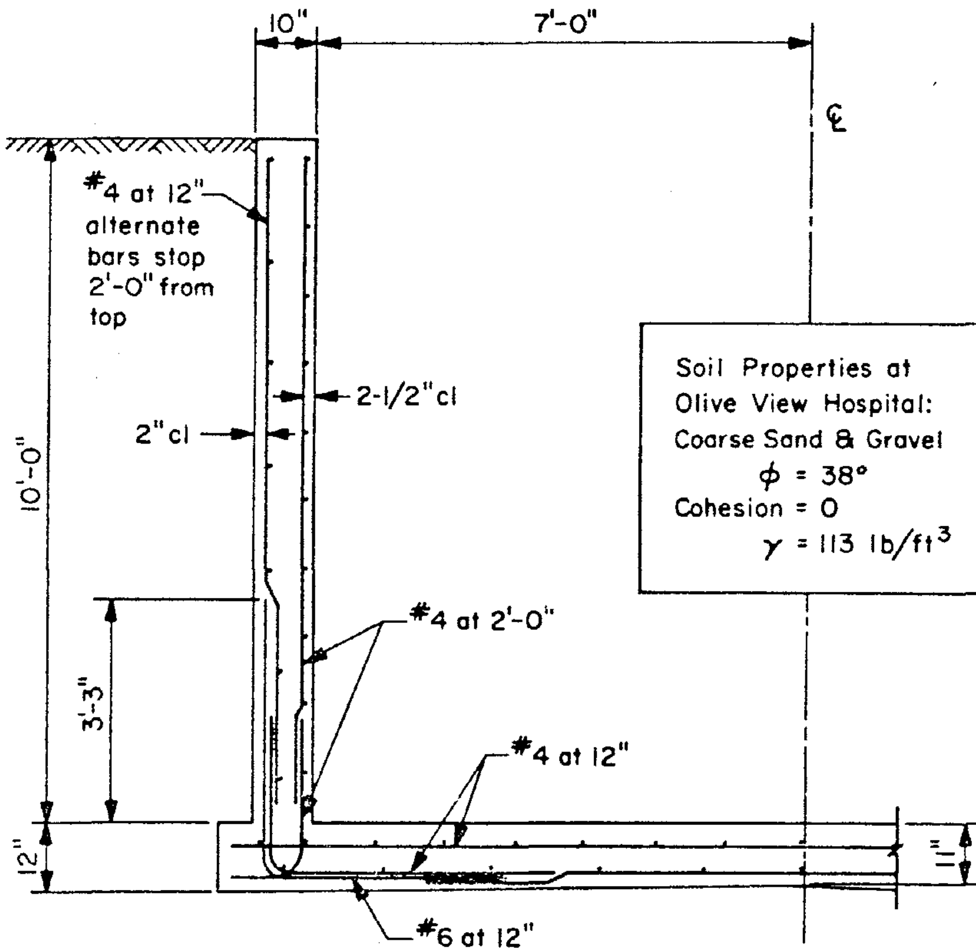

WILSON CANYON CHANNEL
Section 65' Upstream & Downstream of ℄ Olive Ave. Bridge

FIGURE 1.23 - FROM (67)

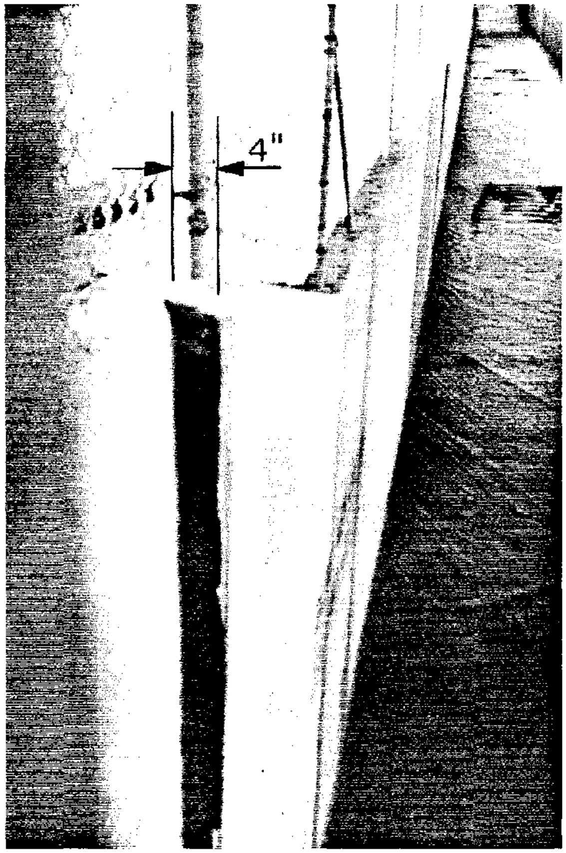

FIGURE I.24 - WILSON CANYON CHANNEL:WALL TOP DISPLACED 4" WITH RESPECT TO THE BRIDGE ABUTMENT AT LEFT - FROM (67)

FIGURE I.25 - WILSON CANYON CHANNEL:CRACKING IN SOIL AS A RESULT OF WALL DISPLACEMENT - FROM (67) walls. Inward deflections of up to 12 inches at midheight were measured at the most severely damaged sections.

Complete failure occurred in sections of the Lopez Canyon Channel, but the failed sections were close to a surface expression of the faulting associated with the earthquake and probably permanent ground displacements contributed significantly to the damage.

It should be noted that the failure of the flood control structures did not create any danger to human life and since in the Los Angeles area these carry only infrequent flood flows, a need for seismic consideration in design and construction might not be economically warranted except for replacement costs.

1.4.5. Friuli, Italy

Similar in magnitude to the San Fernando Earthquake were the 1976 Friuli, Italy earthquakes. The May main shock had a magnitude of about 6.5 while two September aftershocks had magnitudes around 6.0. There was some damage to earth retaining structures [10,57].

Along the Ledra River a retaining wall was considerably damaged during the May shock (Figs. 1.26, 1.27). There were reports of water and sand gushing and evidence of severe cracking in the backfill indicating that liquefaction had occurred. After the September shocks water and sand gushing occurred again in lines parallel to the river course, and the damaged wall completely collapsed.

After the May event damage to the Udine-Carnia-Tarvisio highway due to movement by the retaining structures below it was observed

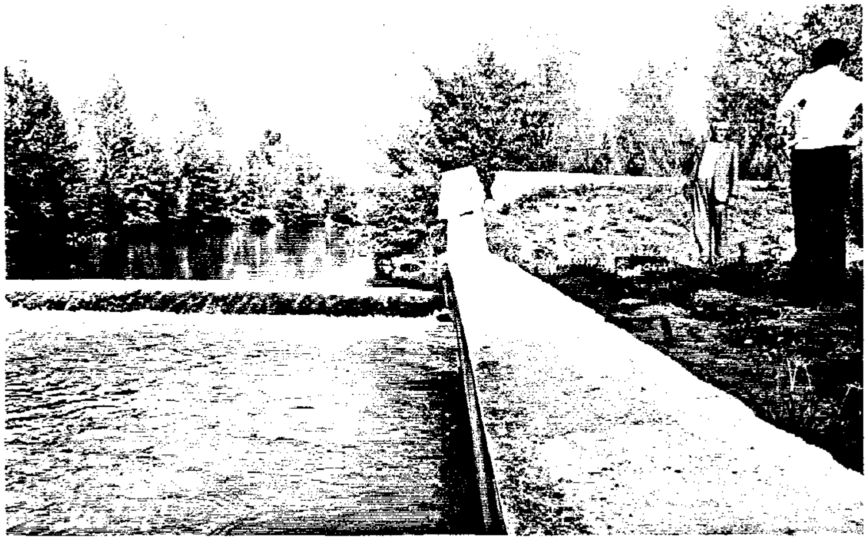

FIGURE 1.26 - WEIR ON THE LEDRA RIVER:DAMAGED RETAINING WALL - FROM (10)

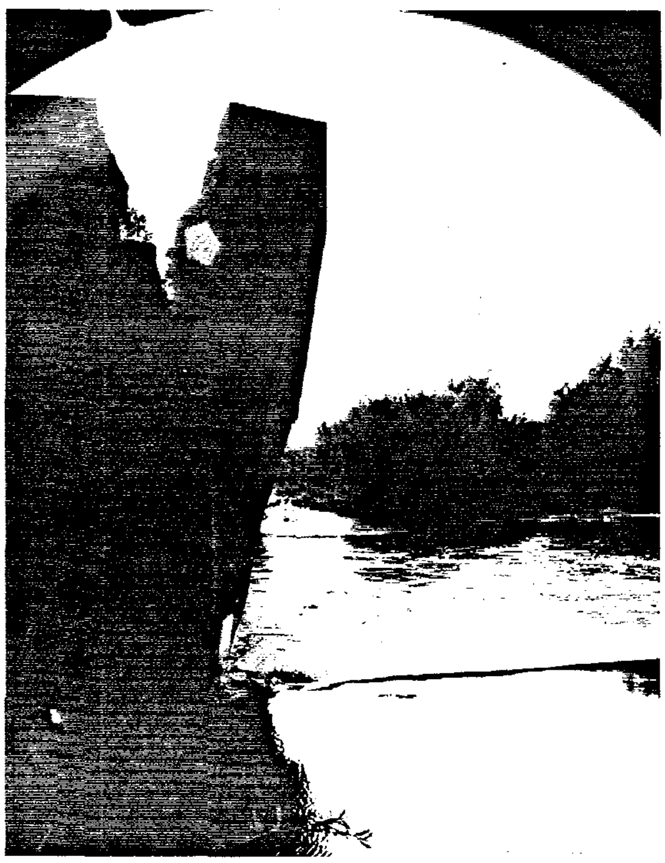

FIGURE 1.27 - WEIR ON THE LEDRA RIVER:DAMAGED RETAINING WALL - FROM (10)

(Figs. 1.28, 1.29). This is where the highway runs between a canal and a mountainside. On the canal side the embankment is retained by a 33 ft high wall built on piles. Figure 1.30 illustrating a normal section of the road axis shows the relative positions of the canal, the retaining wall, and road embankment, with a rough representation of the supporting soil profile.

Perhaps the fact that the entire embankment was underlain by an inclined rock formation contributed to the slipping of the retaining wall towards the canal and probably to the failure of the foundation piles. Vertical displacements along the 660 yards of retaining wall ranged from 1.6 to 9.5 inches while horizontal movements were between 9.1 and 19.3 inches.

As a consequence of the September aftershocks the damage described above increased.

In addition, there was also some severe damage of several autostrada (freeway) bridges in the area, but these were due mainly to impact from the moving bridge superstructures as opposed to failure due to increase in lateral earth pressure.

1.4.6. Tangshan, China

Yuxian [70] reports bridge failure during the 1976 Tangshan (People's Republic of China) earthquake which had a Richter magnitude of 7.8. The failure came from falling of superstructures to the river, or more usually, from sliding and tilting of the abutments. Lateral movement of abutments is blamed for buckling in bridge decks which would

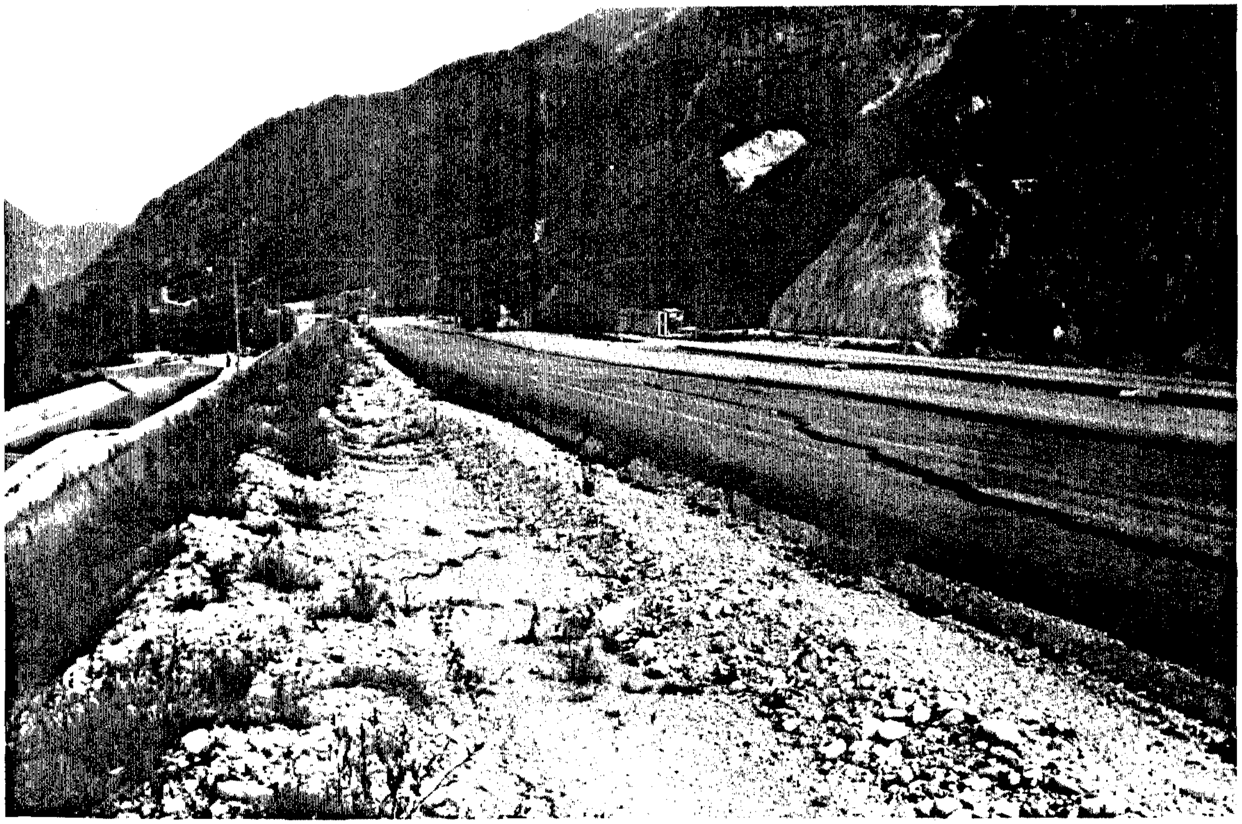

FIGURE I.28 – UDINE–CARNIA–TARVISIO HIGHWAY,ROAD CRACKING DUE TO EMBANKMENT WALL DAMAGE – FROM (10)

FIGURE I.29 - DAMAGE TO EMBANKMENT RETAINING WALL AND CANAL,UDINE-CARNIA-TARVISIO HIGHWAY - FROM (10)

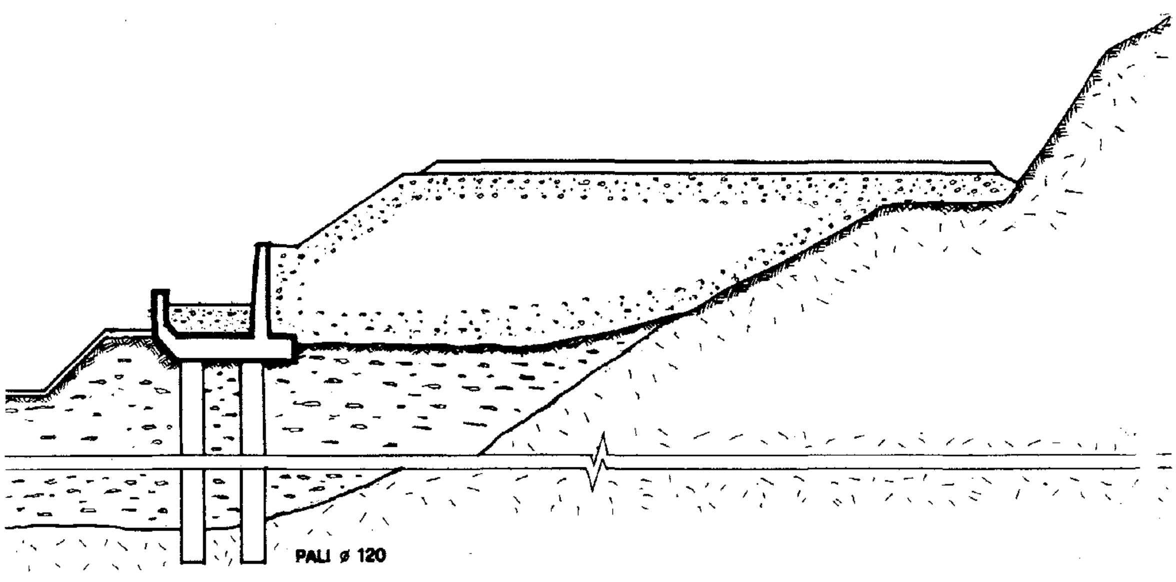

FIGURE I.30 - UDINE-CARNIA-TARVISIO HIGHWAY,SECTION THROUGH EMBANKMENT RETAINING STRUCTURE ADJACENT TO CANAL -FROM (10) have otherwise remained standing. No details were given on design criteria or construction methods.

1.4.7. Miyagi-Ken-Oki, Japan

The 7.4 magnitude Miyagi-Ken-Oki, Japan earthquake of 1978 caused failures in several sites where earth retaining structures were in place due mainly to soil liquefaction (Yanev [6] and Ellingwood [12]). A dike along the Natori River was contained by a concrete retaining wall. A section of wall several hundred yards long moved about one foot toward the river (Figure 1.31). Longitudinal fissures opened in the dike behind the wall and in some concrete pavement along part of the dike. The dike also settled as much as one foot. The site, which is at the mouth of the river, is underlain by at least 65 feet of sand.

In the port of Ishinomaki, a fine-sand fill liquefied, causing severe damage to anchored sheet-pile bulkheads. The fill material had been dredged from the seafloor and placed hydraulically with no compaction. It was placed next to old beach deposits, and the boundary of the liquefaction damage followed the contact very closely; the beach deposits were not involved in the liquefaction.

In addition, there were reports of cracking and settlements of bridge abutments. A comparison was made between the Japanese and American criteria for bridge design under earthquake conditions. According to the 1971 Japan Road Association (JRA) bridge design code a provision is made for the inclusion of a design force for lateral seismic earth pressure, whereas the 1977 American Association of State

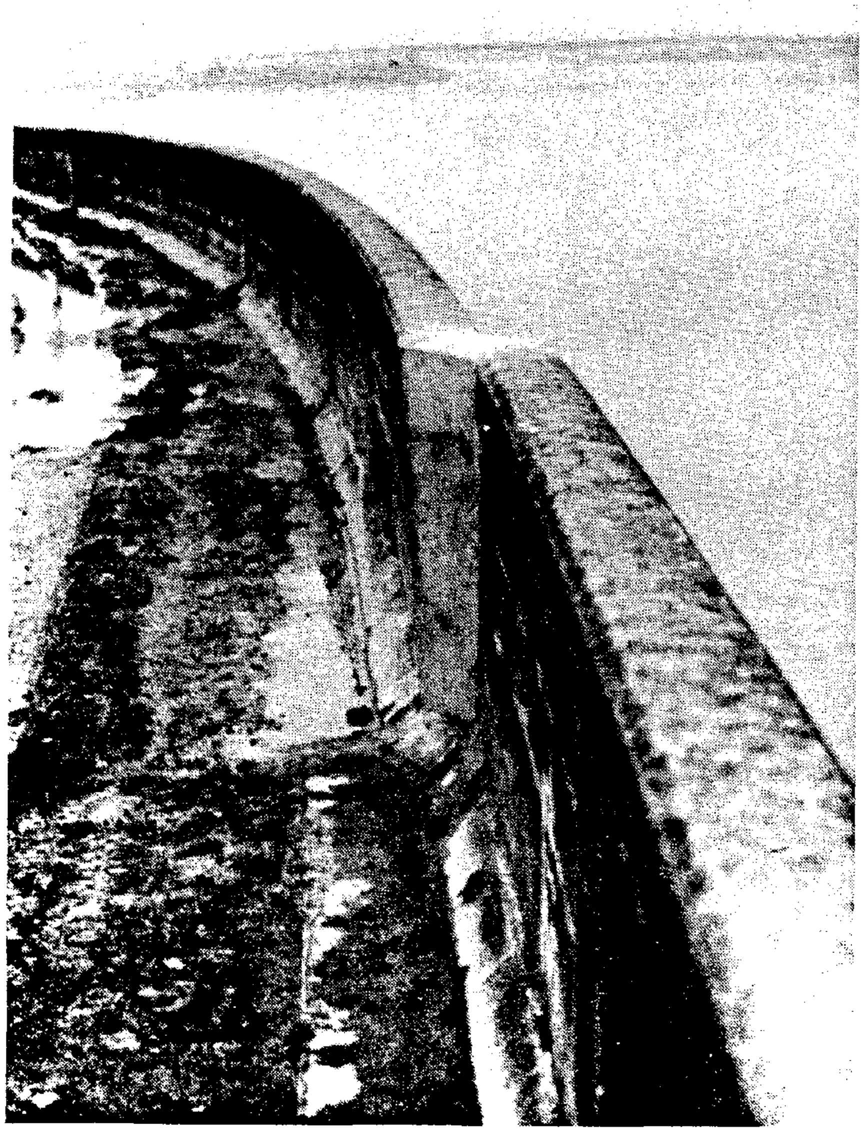

FIGURE 1.31 - REPAIRED PORTION OF DIKE, NATORI RIVER - FROM (12)

Highway and Transportation Officials (AASHTO) criteria, which is an adaptation of the criteria developed by the California Department of Transportation in 1973, does not. From the earthquake damage descriptions above, it seems clear that even the seismic design criteria for earth retaining structures are inadequate. No country, whether wealthy or poor, where there is seismic activity seems to be immune from this type of damage.

CHAPTER II

CENTRIFUGE MODEL TESTING

In recent years, the centrifuge has become a more accepted and useful tool in the modelling of soil mechanics problems. Most soil properties are generally dependent on continuum stresses which are generally gravity-induced. Thus, it is very difficult and inconvenient, if not impossible, to find a model material which will exhibit correctly scaled properties if a test is to be performed at the same gravitational acceleration as the prototype. It would be convenient to use prototype material, but as demonstrated in Chapter I, it would obviously not behave in an appropriate manner at the reduced confining stresses in the model. In such a model, in order to develop the same stresses as in the prototype, it is necessary to increase the gravitational acceleration by the lineal scale factor. Thus, if a 1/50th scale model, made of the same material as the prototype is subjected to a gravitational acceleration 50 times that of the prototype, the confining stresses, and thus the properties and behavior of the model are the same as in the prototype (an analytical description of scaling relations is found in Appendix A). A centrifuge is a machine that can provide model gravity as desired.

It must be realized that the model structure must be properly scaled to provide accurate results. The ratio of the accelerations in model and prototype structures is inversely proportional to the ratio of their lineal dimensions. If the ratio of linear prototype dimensions to those of the centrifuge model is N, then the ratio of area is N^2 and volumes N^3. The scaling relations indicate that the forces in the prototype are N^2 times those in the model and moments N^3 times while the stresses (force per unit area) are unchanged. Deformation in the prototype is N times larger than in the model, but strains (deformation per unit length) are the same. Thus, the pressure of the same material in both prototype and model results in identical stresses and strains at homologous points.

In the experiments, it was necessary to model the reinforced concrete walls by means of aluminum due to the difficulty in properly scaling down both the reinforcement bars and concrete to a small scale (see Chapter 3). Therefore, the model wall was designed to a similar stiffness per unit width, EI with the stiffness in the prototype being N^3 times that in the model.

Where dynamic problems are involved, it turns out that the prototype time scale is N times that in the model. As a consequence, model frequencies are higher by the factor N. Table 2.1 lists the relations between prototype and model (centrifuge) parameters when the centrifuge is employed [15,46].

In the experiments described here, N was chosen to be 50, so that the model was 1/50 of the prototype linear dimension, and the model acceleration employed was 50 times normal terrestrial gravity. It was also considered desirable to subject the retaining wall and associated

TABLE 2.1

Scaling Relations

Parameter	Full Scale (Prototype)	Centrifugal Model at Ng's
Acceleration	1	N
Velocity	1	1
Linear Dimension	1	1/N
Area	1	$1/N^2$
Volume	1	$1/N^3$
Stress	1	1
Strain	1	1
Force	1	$1/N^2$
Mass	1	$1/N^3$
Mass Density	1	1
Weight Density (Unit Weight)	1	N
Time (dynamic)	1	1/N
Time (consolidation)	1	$1/N^2$
Frequency	1	N
Unit stiffness, EI	1	$1/N^3$

soil mass as a passive system to essentially random, earthquake-like excitations at levels equivalent to strong earthquake motions.

As previously described by Scott [52], the attractiveness of the centrifugal method is that the stresses and strains in the model are identical to those in the prototype so that it avoids problems associated with testing, at earth gravity, small soil models involving material with strongly nonlinear behavior. The disadvantages are associated with performing the tests on models which are rotating at rates of 100 to 500 rpm in a centrifuge. Power and signals have to be passed in and out through electric and hydraulic sliprings. There are problems associated with the addition of electrical noise in recording transducer output. The noise comes from ambient sources, the electric motor driving the centrifuge, as well as mundane sources such as local radio stations. Most noise can be effectively taken care of by proper amplification and filtering of output signals as well as numerical smoothing of the digitized data.

In initiating a program of centrifuge testing several questions must be asked concerning the proof or the accuracy of the technique. How well does a model test predict a prototype behavior? Do the scaling relations tell the whole story? In addition, particularly when models of particularly small dimensions such as retaining walls are considered for testing, there is a problem in deciding at what soil grain scale the applicability of continuum constitutive laws to both model and prototype soils breaks down. For very fine grained soils, such as clays, there will be many particles per unit width in both model and prototype retaining wall; on the other hand, in a coarse sand, with grains one twentieth of an inch or so in diameter, there will be relatively few grains per model retaining wall unit width. It is likely that gravity scaling will apply to the constitutive laws, but not to the grain dimensions in the first example. In the second example, it seems possible that the stress-strain relations of model and prototype may not be the relevant factors, but that the individual grains in the model represent the behavior of boulders in the prototype. Thus, a model retaining wall in coarse sand may not represent the behavior of a prototype retaining wall in the same coarse sand, but that of a retaining wall with a backfill composed of boulders.

The use of the centrifuge in geomechanics dates back to the early 1930's when Bucky [4] first used one in the study of some simple mining problems. The use of a soil mechanics centrifuge was also reported in the Soviet Union around the same time [52]. The use of the centrifuge technique, however, has not been extensively practiced since then, although in the past 15 or 20 years it has been gaining in popularity.

At present, a number of centrifuges have been built and used for soil testing. There are three in the United Kingdom, two at Cambridge and one at Manchester, with radii up to 16 ft and acceleration capabilities up to 200g. It has been reported that "several dozen" centrifuges for soil testing purposes are in use in the Soviet Union [41]. In addition, centrifuges are currently used for geotechnical research in Sweden, Denmark, France, and Japan. Surprisingly, in the United States, where the technique originated, there are only a handful of small centrifuges currently in use. There is one at Princeton, one at Colorado, and one is being developed at the Ames Research Center by the University of California at Davis, in addition to the one at Caltech. The reasons for their limited usage have not been determined.

A compilation of references on centrifugal testing, worldwide, extends to more than 150 papers and a number of books.

With the number of centrifuges built and operational, and the number of tests performed, it might well be thought that the questions above would have been satisfactorily answered by this time; that many comparisons would have been made between models and prototypes. Study of the accessible literature does not show this to be the case in the quantitative sense, although a fair number of studies show qualitatively similar behavior and mechanisms. The particular type of testing involved in this case, the dynamic centrifuge testing of flexible retaining walls, however, has, as far as known, no precedent.

CHAPTER III

EQUIPMENT AND INSTRUMENTATION

3.1. The Centrifuge

The centrifuge (Figure 3.1) used is a Model A1030 Genisco G-accelerator", which consists of an 80-inch diameter aluminum-alloy arm which rotates in the horizontal plane and is rated at 10,000 g-pounds payload capacity. At each end of the arm is located an 18 X 22 inch magnesium mounting frame (Figure 3.2) capable of carrying a 200-pound payload to 50g or 60 pounds to 175g. The acceleration range at the approximately 40-inch radius of the basket is from 1 to 175g.

The machine is driven by means of a Sabina Electric and Engineering Type RG 2600 Single phase Full Wave Regenerative Static D.C. Drive with a 5 HP, 1725 rpm, 230v, 3-phase, constant torque, double-ended electric drive motor. For accurate determination of the rotational speed, there is located on the main drive shaft a 600 tooth gear wheel, which via a magnetic pickoff produces 600 pulses per revolution. The pulses are read by an electronic counter which converts them to an LED display of RPM accurate to 0.1 rpm. The drift and wow of the system at any given setting is 0.05%. The acceleration arm is housed in an extruded aluminum enclosure, with all the controls and instrumentation, in the interests of safety, located remotely.

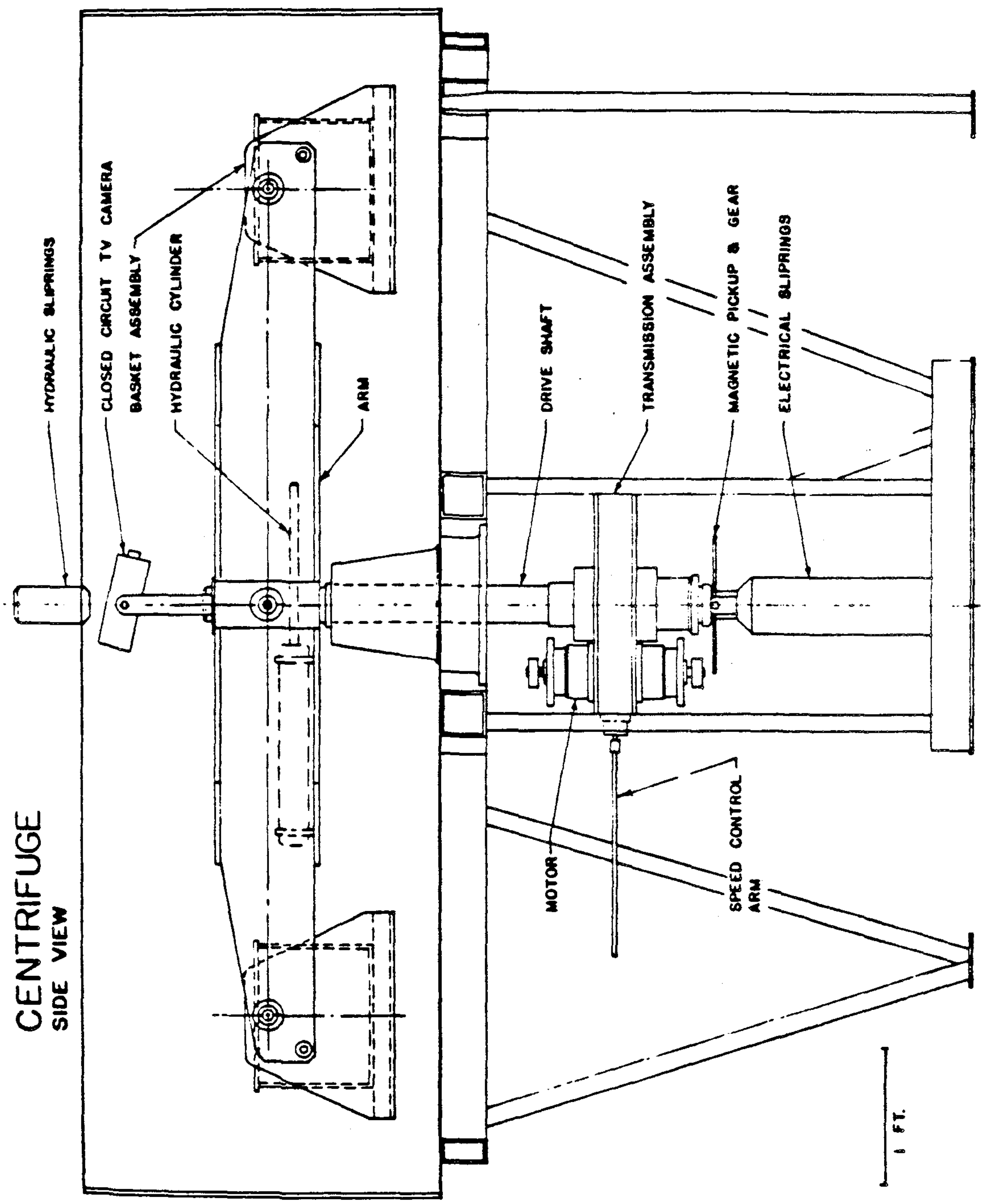

FIGURE 3.1 – SIDE VIEW OF CALTECH CENTRIFUGE AT REST

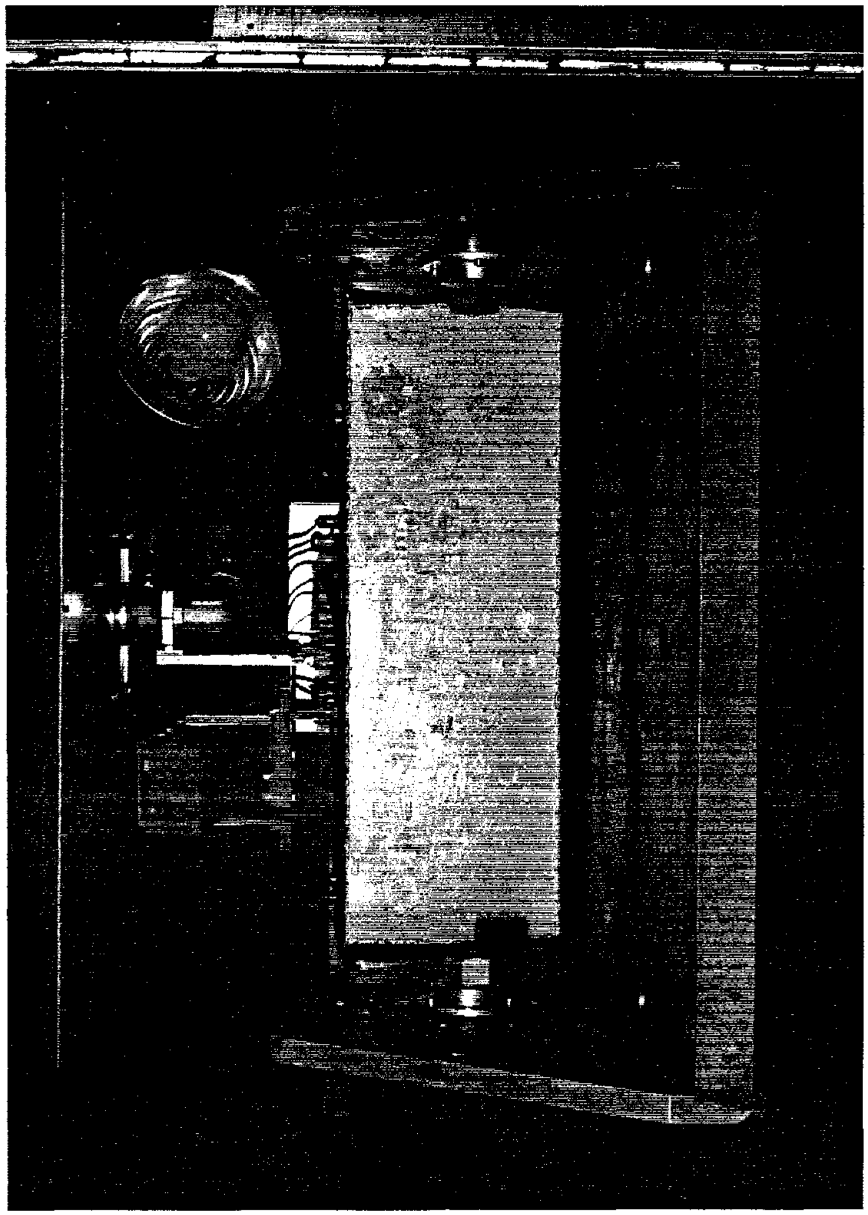

FIGURE 3.2 – CENTRIFUGE FRAME

Electrical power and signals to and from the rotating arm or frame are conducted through 44 sliprings of various capacities in the 10 to 30 amp range. Hydraulic pressure is externally generated with a Haskell Engineering and Supply Co. Model DEN.PR51 pump unit with a line capacity of 3000 psi and is transmitted through either two or four lines by means of rotary unions (hydraulic sliprings). Operations on the centrifuge can be observed by means of a television camera mounted on the arm close to the axis; its signal is conveyed either through the rings mentioned above or through coaxial cable and related, separate sliprings to a monitor TV in the instrumentation room.

3.2. The "Earthquake Generating" Mechanism

As mentioned previously the centrifuge is rated at 10,000 g-pounds payload capacity. The load ("payload") of model structure, soil, and containment that it can sustain is limited to 200 lbs (taken up to 50g). Consequently, the need for a method of creating an earthquake-like motion in the centrifuge without taking up a substantial amount of the payload was imperative and was developed with the aid of John Lee.

The "earthquake-generating" mechanism (Figures 3.3, 3.4) consists of a 14.6" X 11.6"X 10" reinforced aluminum container mounted on a bed of ball bearings which lie in horizontal parallel grooves in a steel plate attached to the swinging magnesium centrifuge frame. The bearings were separated with a perforated teflon sheet which allowed equal spacing between them and thus an even pressure distribution throughout (Figure 3.5). At one end, between the bucket and the frame is a spring

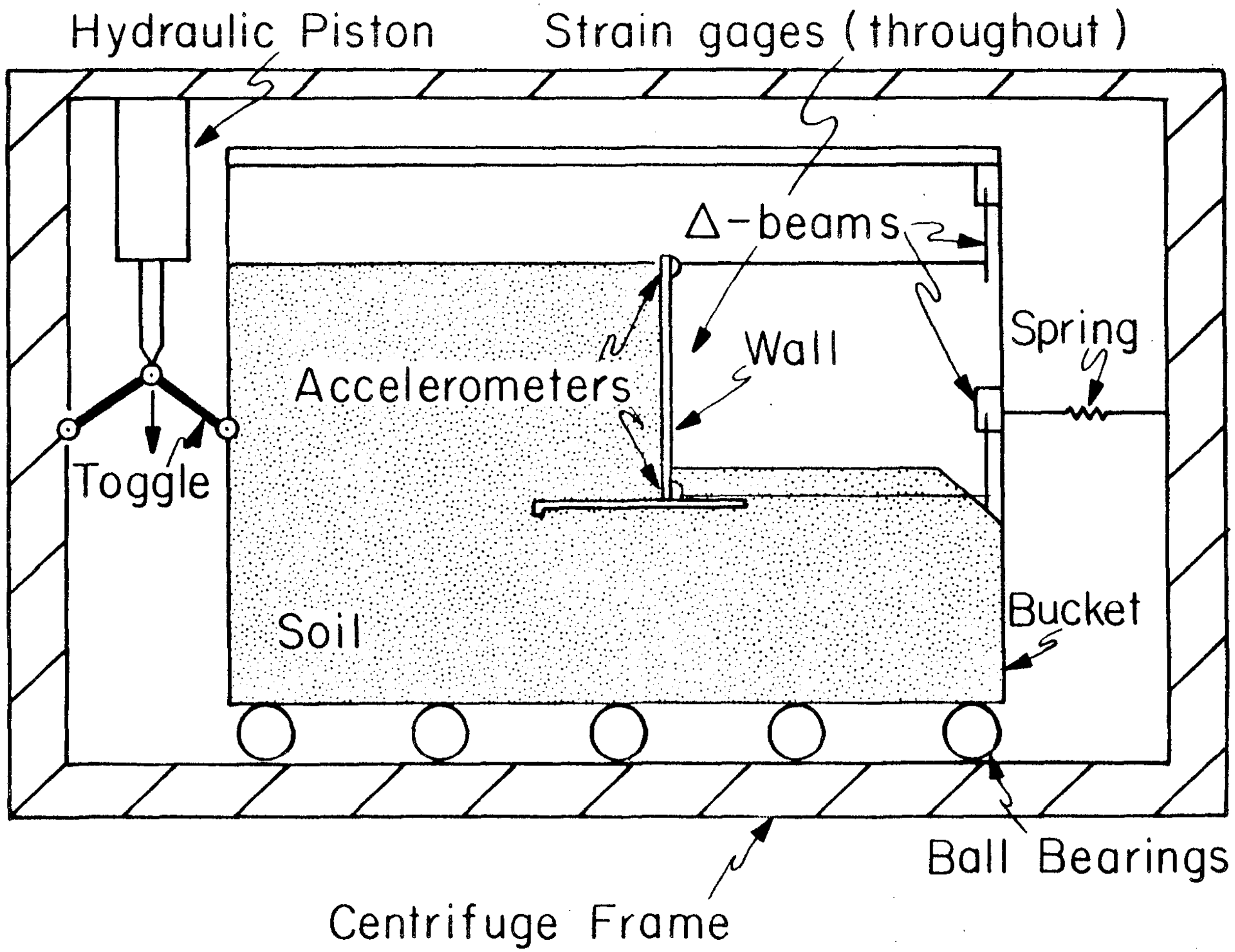

FIGURE 3.3 – SCHEMATIC OF EXPERIMENT

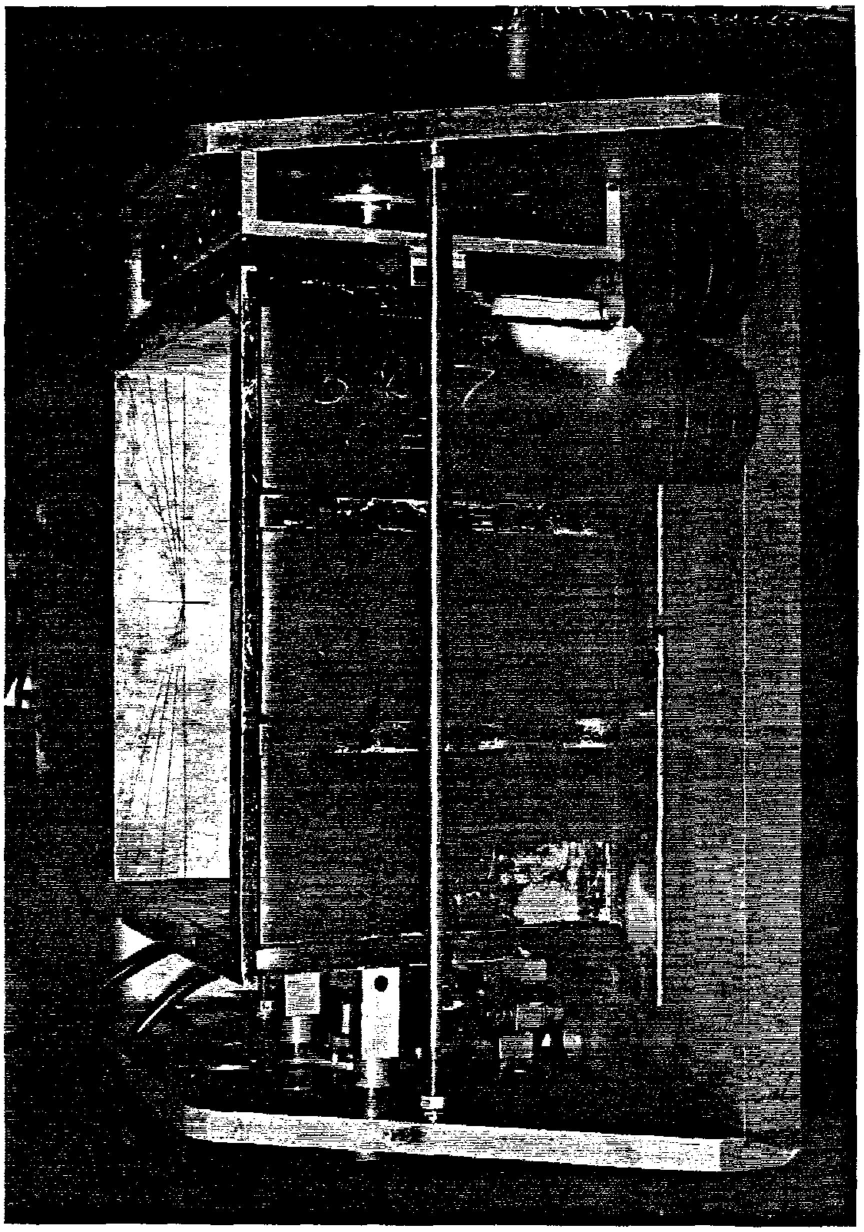

FIGURE 3.4 - EARTHQUAKE GENERATING MECHANISM

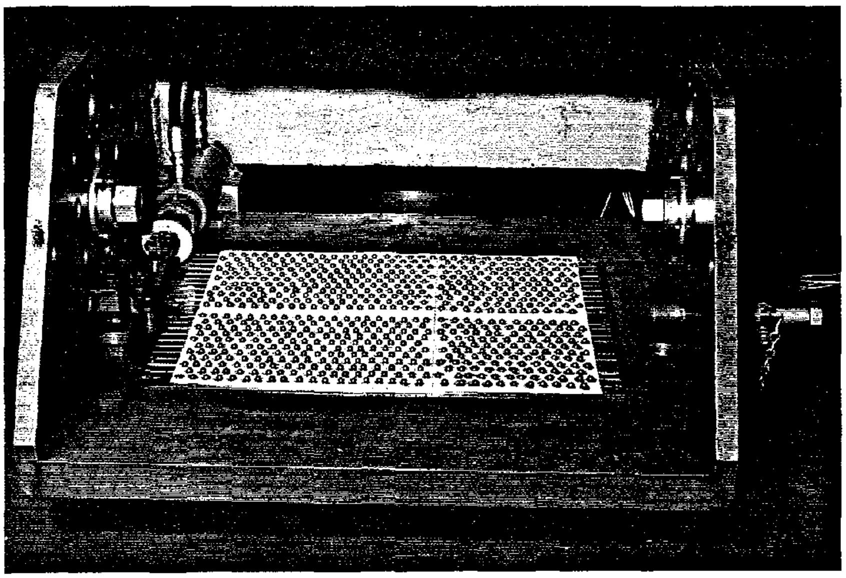

FIGURE 3.5 – BALL BEARINGS SEPARATED BY TEFLON SHEET

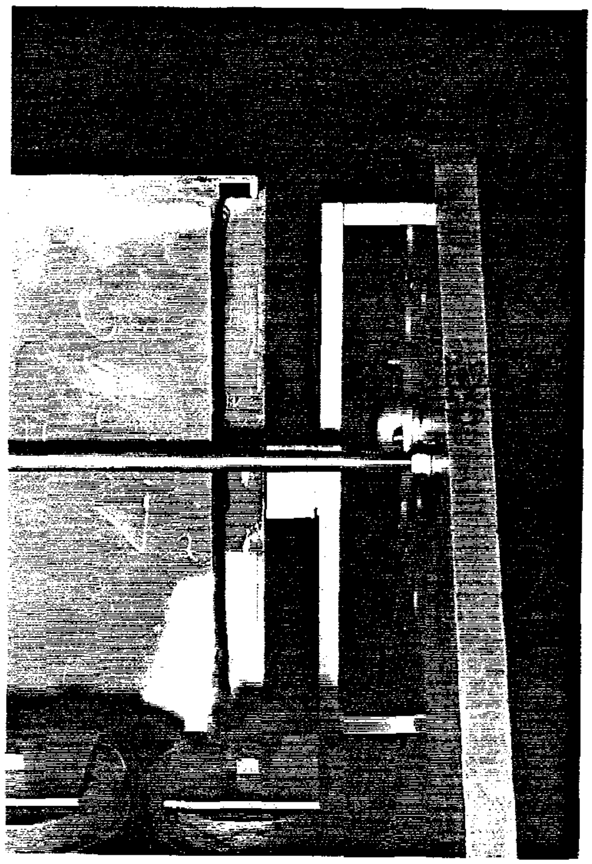

FIGURE 3.6 – REACTION SPRING

(spring constant = 75 kips/in) (Figure 3.6). At the other end is a toggle mechanism connected to a hydraulic piston (Figures 3.7,3.8). Under control the piston displaces the center of the toggle, spreading the ends, and thus forcing the bucket to move, deforming the spring at the other end. When the toggle goes over center, it snaps through, driven by the sudden energy release of the spring, and the soil container snaps back until it hits, stops and rebounds. This happens a number of times for one model "earthquake" event. The bucket thus moves back and forth for a couple of tenths of a second in a relatively random motion which resembles that of a short but intense earthquake. The comparison of the model earthquakes with that of one component of a record of the 1966 Parkfield, California earthquake is done in Section 5.2. Because of the simplicity of the "earthquake generating" mechanism, the motion attained resembles that which would occur near a short fault rupture. The production of prolonged earthquake motions typical of sites at intermediate distances from a long fault rupture (a "great" earthquake) would require another (probably more complicated and thus heavier) mechanism.

3.3. Model Retaining Walls

Ideally, a model retaining wall made of (properly scaled) reinforced concrete similar to one described in the design example of Section 12.7 of Wang and Salmon's Reinforced Concrete Design [64] would be desirable for centrifuge testing, but as can be seen from the design sketch (Figure 3.9) of a prototype, it would be very difficult to scale

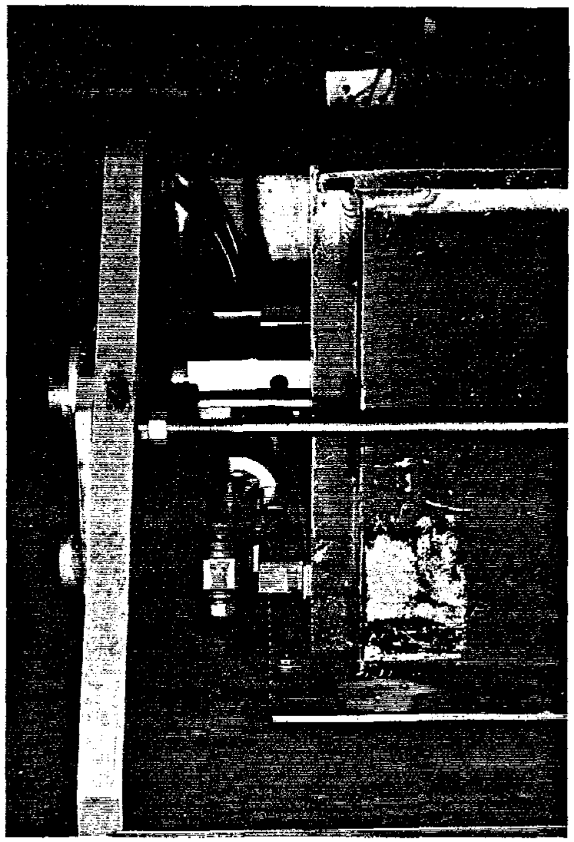

FIGURE 3.7 – PISTON,TOGGLE,AND BUMPER (FRONT VIEW)

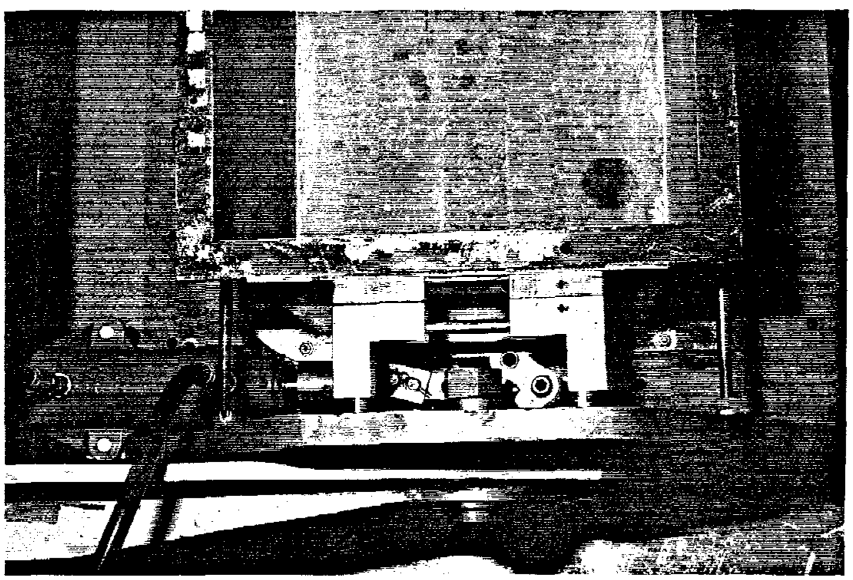

FIGURE 3.8 – PISTON,TOGGLE,AND BUMPER (TOP VIEW)

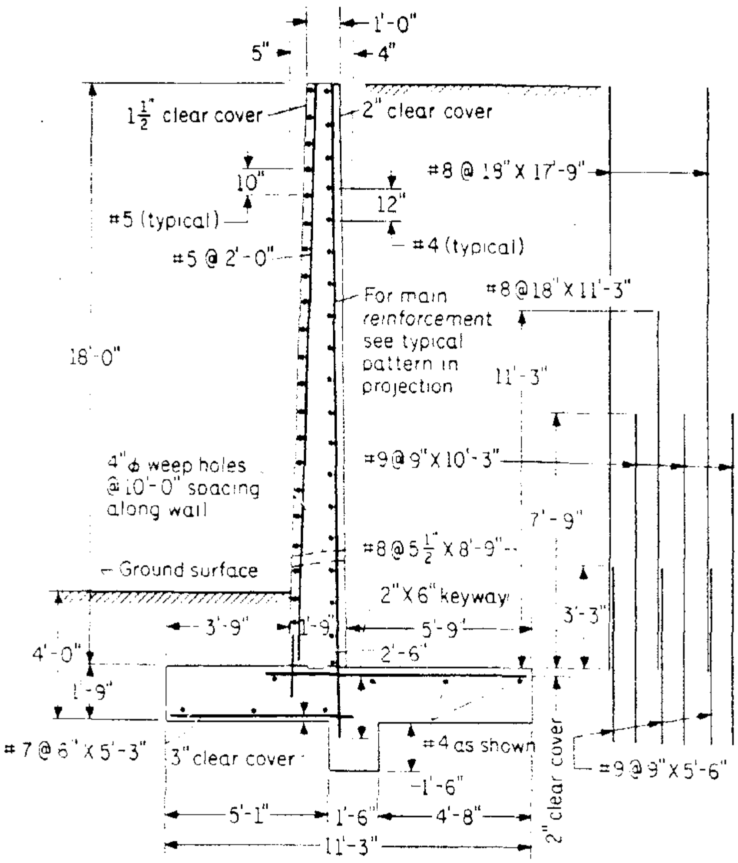

Design sketch for cantilever retaining wall.

FIGURE 3.9 – FROM (64)

down all the components of the wall to 1/50th the size shown. Because of the ease of modelling, it was decided to design a retaining wall made of aluminum instead, and then scale it down. The procedure is similar to the procedure used in the design of a regular reinforced concrete cantilever retaining wall.

3.3.1. Design of the Retaining Walls

It is required to design a prototype, aluminum cantilever retaining wall to support a backfill of earth 16 ft high above the final level of earth at the toe of the wall. The backfill is to be level. A lateral earthquake acceleration of 0.25g is expected for design purposes (in actuality, it doesn't occur though). The following data is given for design:

soil density γ = 92 pcf (Nevada 120 sand @ medium density)

Elastic Strength of 6061-T6 Aluminum $f_A = 48{,}000$ psi

Elastic Modulus $E_A = 10 \times 10^6$ psi

First of all, it is necessary for the wall-soil system to be in a state of equilibrium. A Mononobe-Okabe analysis (see Section 1.1) with $k_H = 0.25$ will be used.

The Mononobe-Okabe parameters are:

$$\theta = \tan^{-1}(0.25) = 14^\circ \qquad \delta = 0^\circ$$

$$\gamma = 0.092\text{kcf} \qquad i = 0^\circ$$

$$\phi = 35^\circ \qquad \beta = 0^\circ$$

Therefore:

$$K_{AE}=0.43$$

and the total force P_{AE} is thus

$$P_{AE} = 1/2\gamma h^2(1-k_v)K_{AE} \tag{3.1}$$

or

$$P_{AE} = (1/2)(0.092)(18.3)^2(0.43) = 6.6\text{kips/ft.}$$

This is the total lateral force acting on the wall. As recommended by Seed and Whitman [55], the force increment on the wall, ΔP_{AE}, due to the earthquake load should be assumed to act 0.6 h or so above the base. Thus, it is necessary to find the static force P_A and place the forces on the wall as shown in Figure 3.10.

From the Rankine static lateral earth pressure theory P_A is given by:

$$P_A = 1/2\gamma h^2 K_A \tag{3.2}$$

where:

$$K_A = \frac{1-\sin\phi}{1+\sin\phi} \tag{3.3}$$

For the soil involved $K_A = 0.27$ so:

$$P_A = (1/2)(0.092)(18.3)^2(0.27) = 4.2\text{kips/ft.}$$

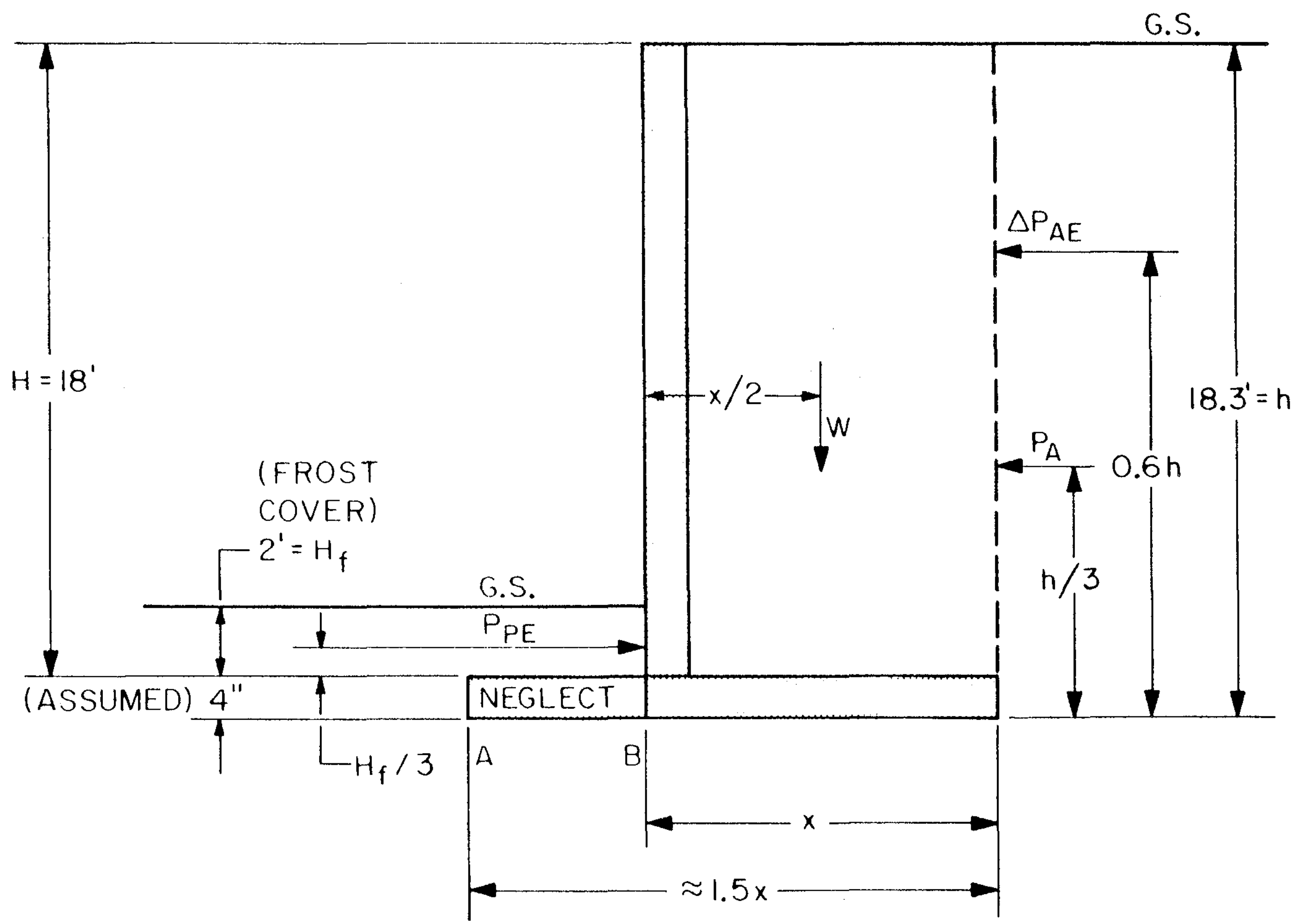

FIGURE 3.10 – PRELIMINARY PROPORTIONING OF PROTOTYPE CANTILEVER RETAINING WALL

which acts at h/3 above the base of the wall. Thus:

$$\Delta P_{AE} = P_{AE} - P_A = 6.6-4.2 = 2.4\text{kips/ft}$$

which acts at 0.6 h above the base.

The weight of the backfill, W, is:

$$W = \gamma Hx = (0.092)(18)X = 1.6x\text{kips/ft.}$$

Summing moments about point B. $\left(\sum M_b = 0 \right)$

$$\frac{Wx}{2} = \frac{P_A h}{3} + 0.6\Delta P_{AE} h = h(1/3P_A + 0.6\ \Delta P_{AE})$$

Consequently:

$$\frac{1.6x^2}{2} = (18.3)[(1/3)(4.2) + (0.6)(2.4)]$$

Therefore:

$$x = \left[\frac{(2)(18.3)[(1/3)(4.2) + (0.6)(2.4)]}{1.6}\right]^{1/2} = 8.1 \text{ ft.}$$

The entire base length is recommended by Wang and Salmon to be approximately:

$$\text{Base length} \simeq 1.5x = (1.5)(8.1) = 12.2\text{ft.}$$

The base length was thus decided upon to be 15.25 feet long (3.66 in long in the 1/50 scale model) which gives about an extra 25% or so of length for safety. A check must now be made for safety against overturning. Recalling that the design base length is 15.25 ft, the design x (Figure 3.10) is thus 2/3 of this or 10.2 ft. (10 ft,2 in). Thus the weight W of the backfill is, from above:

$$W = 1.6x = (1.6)(10.2) = 16.3 \text{kips/ft.}$$

Taking moments about point A of the base and neglecting the weight of the wall, the resisting moment is:

$$M_R = (10.2)(16.3) = 166.3 \text{ ft k/ft}$$

The overturning moment is:

$$M_o = h(1/3P_A + 0.6\Delta P_{AE})$$

Thus:

$$M_o = (18.3)[(1/3)(4.2) + (0.6)(2.4)] = 52.0 \text{ft-k/ft}$$

Therefore, the factor of safety against overturning is:

$$\text{F.S.} = \frac{M_R}{M_o} = \frac{166.3}{52.0} = 3.2$$

which is greater than the traditional value of 2.0. This factor of safety does not even include the weight of the wall itself which would provide additional resistance to overturning.

The stem of the wall must now be designed to resist the bending moment M given by:

$$M = H(1/3P_A + 0.6\Delta P_{AE}) - 1/3P_{PE}H_f$$

where P_{PE} is the resultant of the passive force provided by the frost cover of depth H_f (Figure 3.10).

The coefficient of passive earth pressure, K_{PE}, for a Mononobe-Okabe analysis is given by

$$K_{PE} = \frac{\cos^2(\phi-\theta+\beta)}{\cos\theta\cos^2\beta\cos(\beta-\delta-\theta)\left(1-\sqrt{\frac{\sin(\phi+\delta)\sin(\phi-\theta+i)}{\cos(\beta-\delta-\theta)\cos(\beta-i)}}\right)^2} \tag{3.4}$$

and:

$$P_{PE} = 1/2\gamma H_f^2(1-k_v)K_{PE} \tag{3.5}$$

Therefore:

$$K_{PE} = 3.18$$

Therefore:

$$P_{PE} = (1/2)(0.092)(4)(3.18) = 0.6 \text{ kips}$$

Thus:

$$M = 18[(1/3)(4.2) + (0.6)(2.4)] - (1/3)(0.6)(2) = 50.7 \text{ ft k/ft}$$

With a bending factor of safety of 1.7, the design moment is:

$$M_D = 86.1 \text{ ft k/ft}$$

The thickness of the stem is determined by the use of the bending formula for a beam:

$$\sigma = M/S \tag{3.6}$$

Where:

σ = stress of the material

S = unit section modulus of cross section

For a rectangular cross section, the unit section modulus is:

$$S = \frac{d^2}{6} \tag{3.7}$$

Where d is the thickness of the section. Taking the elastic strength of the aluminum f_A as σ, the stem thickness is determined:

$$d = \left(\frac{6M}{\sigma}\right)^{1/2} = \left(\frac{6M_o}{f_A}\right)^{1/2} = \left[\frac{(6)(86.1)}{48}\right]^{1/2} = 3.28 \text{ in.}$$

This corresponds to a thickness of 0.065 inches in the model wall, at 1/50 scale.

Two models of the 16 ft high cantilever retaining wall were built (Figure 3.11). They were made of two aluminum 6061-T6 plates dip-brazed together by Precision Dipbraze, Inc. of Van Nuys, CA. The base of both walls is made of 0.063 inch plate while the stems are 0.063 inches thick in wall No. 1 and 0.050 in wall No. 2. The thicknesses stated are standard aluminum plate sizes. The 0.063 inch thickness of wall No. 1 is approximately the correct size for the design conditions imposed with the appropriate safety factors. Wall No. 2 has no safety factor (F.S. = 1.0) at all. (Its prototype wall would have a moment capacity of 50.0 ft-k/ft versus the calculated acting moment of 52.0 ft-k/ft).

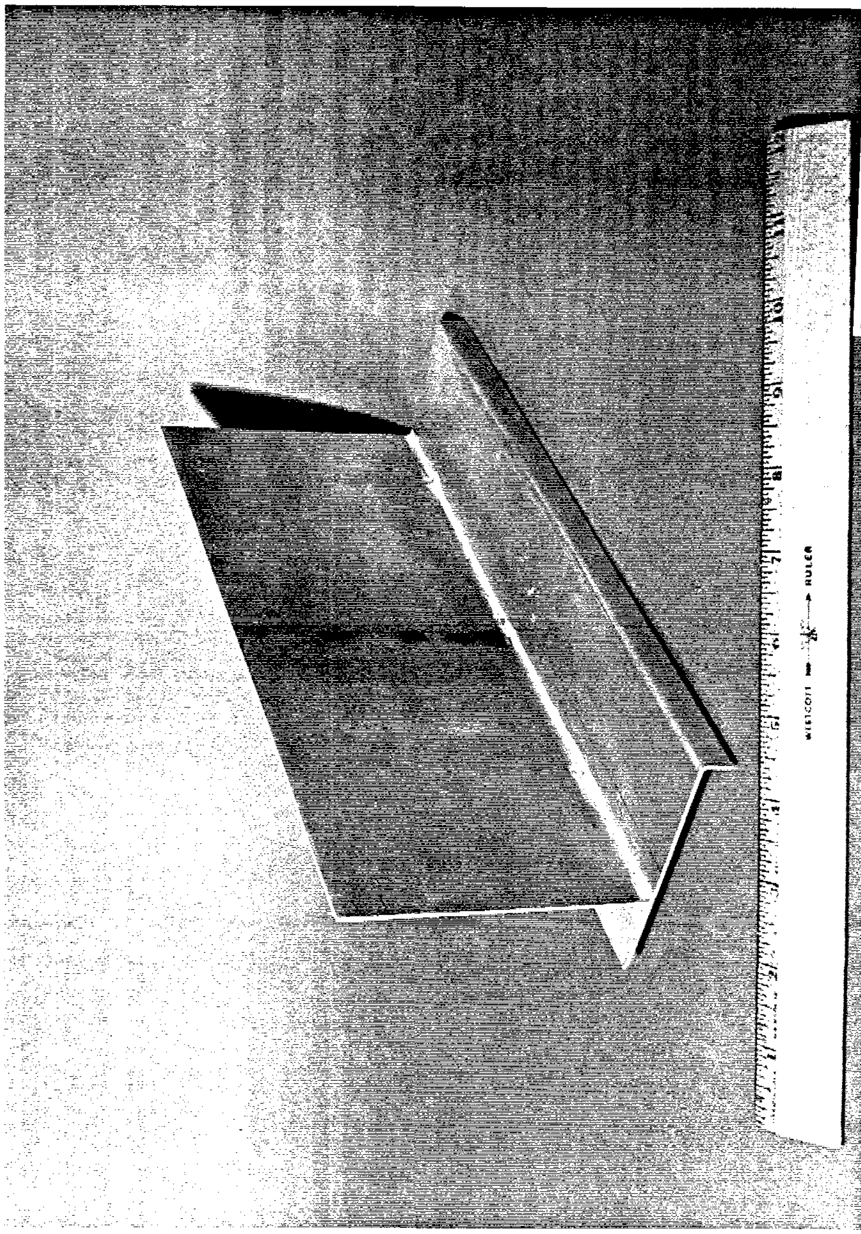

FIGURE 3.11 – MODEL RETAINING WALL

It should be noted that it is generally agreed upon in practice that the Mononabe-Okabe method gives a conservative design (i.e., calls for larger walls than "necessary"), and in most cases is not even used (nor is any other method) when a seismic design is in order.

3.3.2. Determination of Actual EI of Walls

In order to determine the true stiffness (EI) of the retaining walls, the Young's Modulus E of the aluminum used had to be measured. To do this a rectangular piece of the same 0.063" thick plate used to make the walls 6.555" long and 1.493" wide was cut. The piece was then clamped and held horizontal so that it formed a cantilever beam 5.026" long. Weights of 0, 0.220, 0.441, 0.661 and 0.772 lbs (0, 100, 200, 300, and 350 grams) were then hung from the free end. The end deflection was measured with a Federal dial gage accurate to 0.0001 inches. Recalling that the end (maximum) deflection y_{MAX} of a cantilever beam with an end point load is:

$$y_{MAX} = \frac{Pl^3}{3EI} \tag{3.8}$$

where P is the load, l the beam length, and I the bending moment of inertia it follows that:

$$E = \frac{Pl^3}{3Iy_{MAX}} \tag{3.9}$$

The average E then determined from the measurements was found to be 9.699×10^6 psi.

Recalling that the moment of inertia per unit width I of a rectangular cross section is $\frac{h^3}{12}$, where h is the section depth, for retaining wall No. 1 (RW1) the EI was determined as 202.1 lb in^2/in and for (RW2) as 101.0 lb in^2/in.

3.3.3. Determination of the Fundamental Frequency of the Wall-Soil System

The fundamental frequency of the wall-soil system was determined by an examination of the Fourier Amplitude Spectra of the accelerograms recorded at the top and bottom of the wall (in prototype scale) from tests 1CN0001,* 1CN0002, and 1CN1003 for RW1, and from test 2CN0011 for RW2 using the FORTRAN program IVMAIN described in Section 4.2. The accelerograms at the top of the wall indicate the output response of the system while those at the bottom are a measure of the input excitation to the system. Taking the corresponding pairs of Fourier Spectra for each test and finding where the ratio of output (top) to input (bottom) amplitude is a maximum provides an accurate determination of the system's natural frequencies.

Upon examination of the Fourier spectra (Figures 3.12 through 3.19), it was determined that the fundamental frequencies were 2.3 Hz for 1CN0001, 2.7 Hz for 1CN0002, and 2.7 Hz for 1CN1003. There was

* The following nomenclature was chosen for test numbering:

Test $\frac{a}{1}\ \frac{b}{C}\ \frac{c}{N}\ \frac{d}{00}\ \frac{e}{01}$

a = wall number; b = type of wall; c = type of sand; d = backfill angle (in degrees); e = test number; C = cantilever; N = Nevada 120.

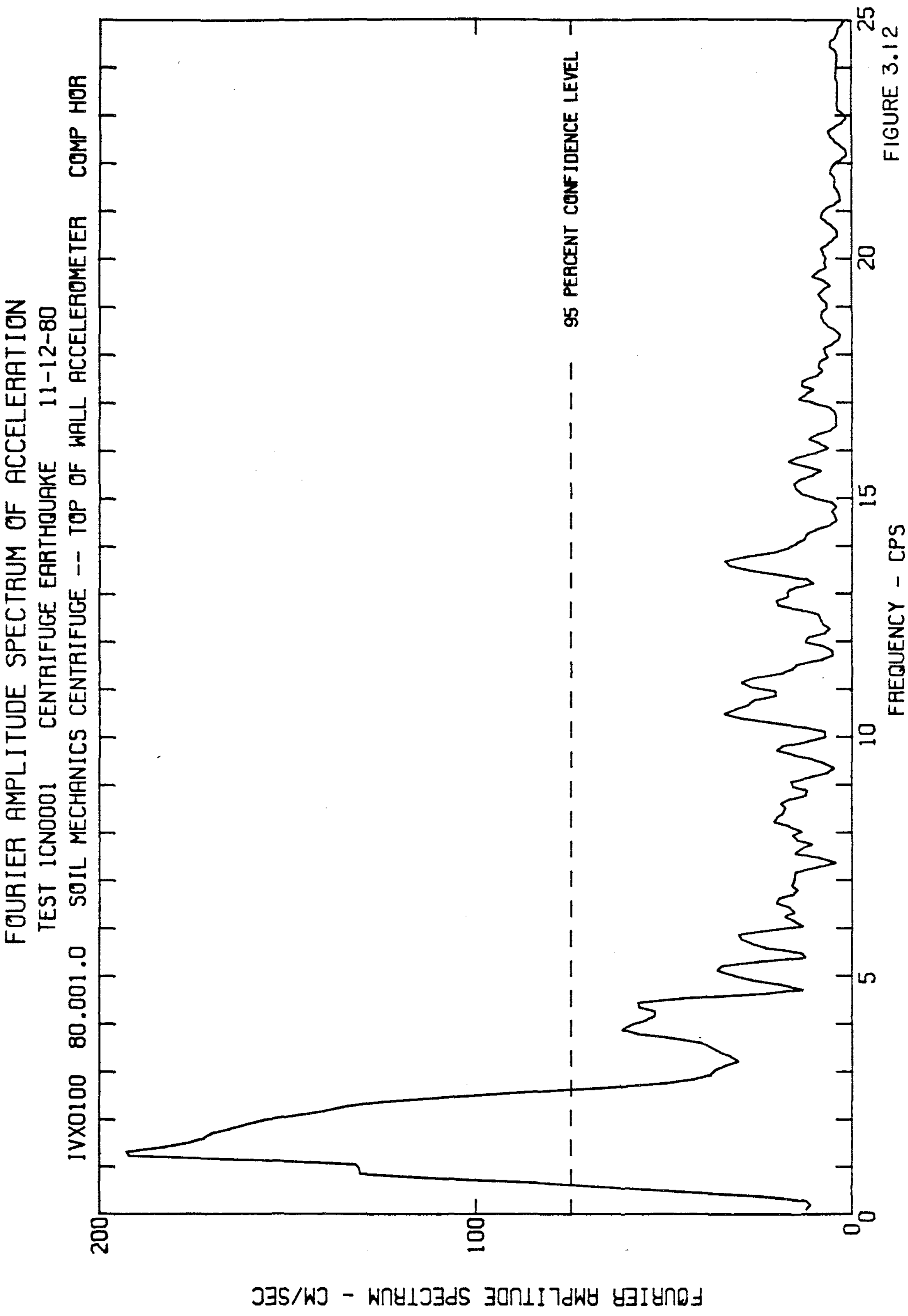
FOURIER AMPLITUDE SPECTRUM OF ACCELERATION
IVX0100 80.001.0 TEST 1CN0001 CENTRIFUGE EARTHQUAKE 11-12-80
SOIL MECHANICS CENTRIFUGE -- TOP OF WALL ACCELEROMETER COMP HOR
95 PERCENT CONFIDENCE LEVEL
FOURIER AMPLITUDE SPECTRUM - CM/SEC
0
100
200
FREQUENCY - CPS
0
5
10
15
20
25

FIGURE 3.12

FOURIER AMPLITUDE SPECTRUM OF ACCELERATION

TEST 1CN0001 CENTRIFUGE EARTHQUAKE 11-12-80

IVX0100 80.001.0 SOIL MECHANICS CENTRIFUGE-BOTTOM OF WALL ACCELEROMETER COMP HOR

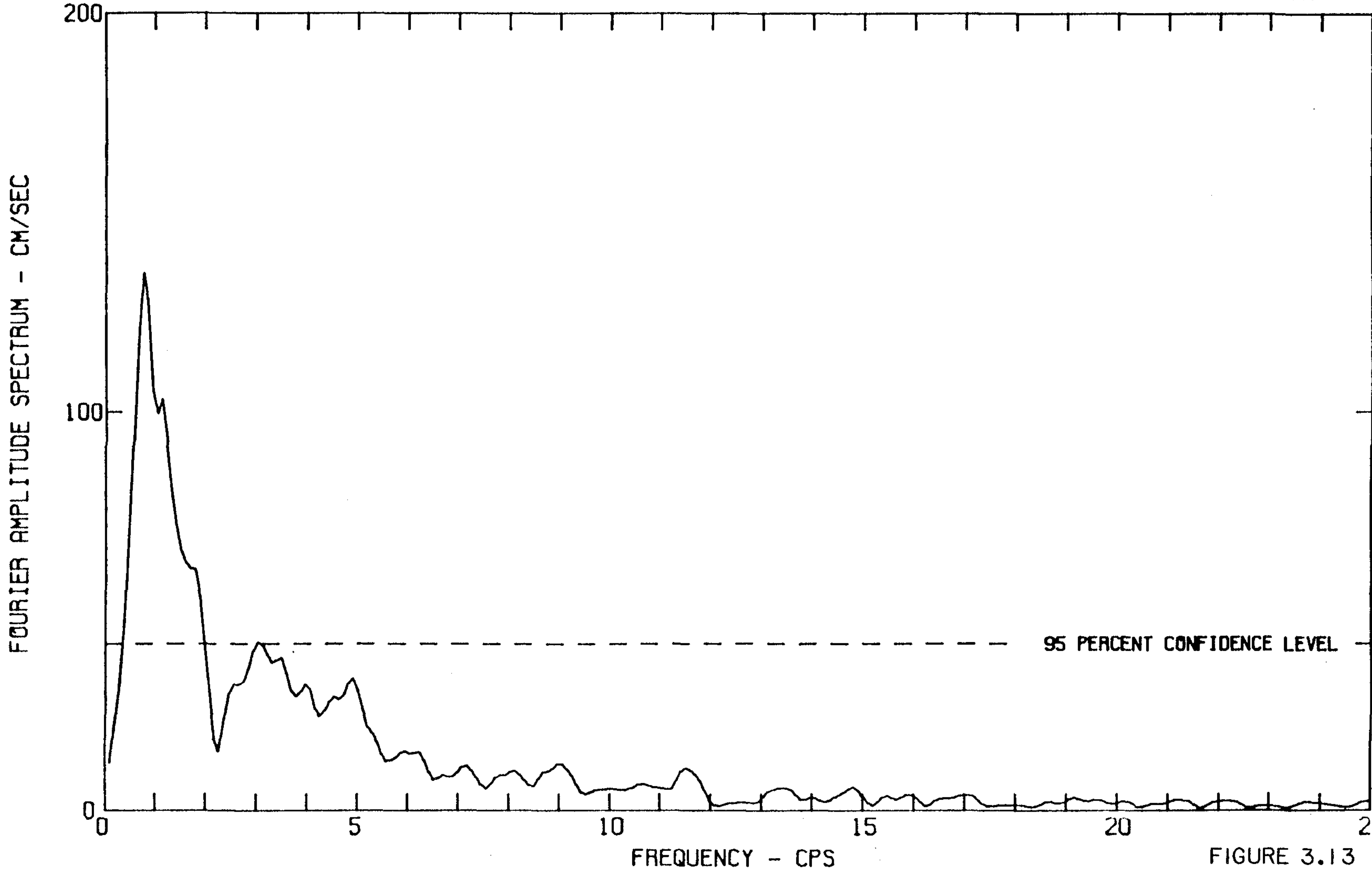

FIGURE 3.13

FOURIER AMPLITUDE SPECTRUM OF ACCELERATION

TEST 1CN0002 CENTRIFUGE EARTHQUAKE 3- 4-81

IVX0200 81.002.0 SOIL MECHANICS CENTRIFUGE -- TOP OF WALL ACCELEROMETER COMP HOR

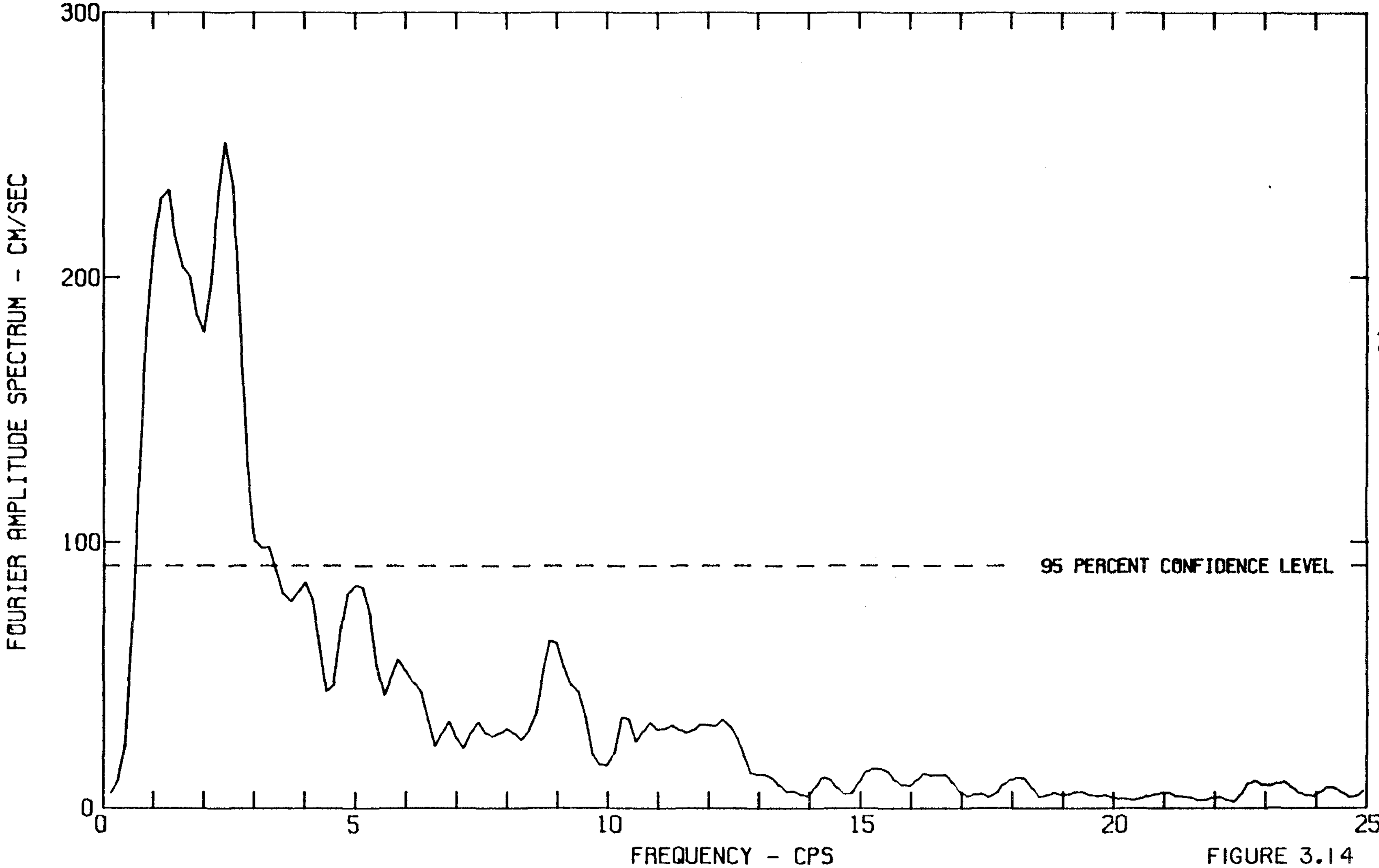

FIGURE 3.14

FOURIER AMPLITUDE SPECTRUM OF ACCELERATION

TEST 1CN0002 CENTRIFUGE EARTHQUAKE 3- 4-81

IVX0200 81.002.0 SOIL MECHANICS CENTRIFUGE-BOTTOM OF WALL ACCELEROMETER COMP HOR

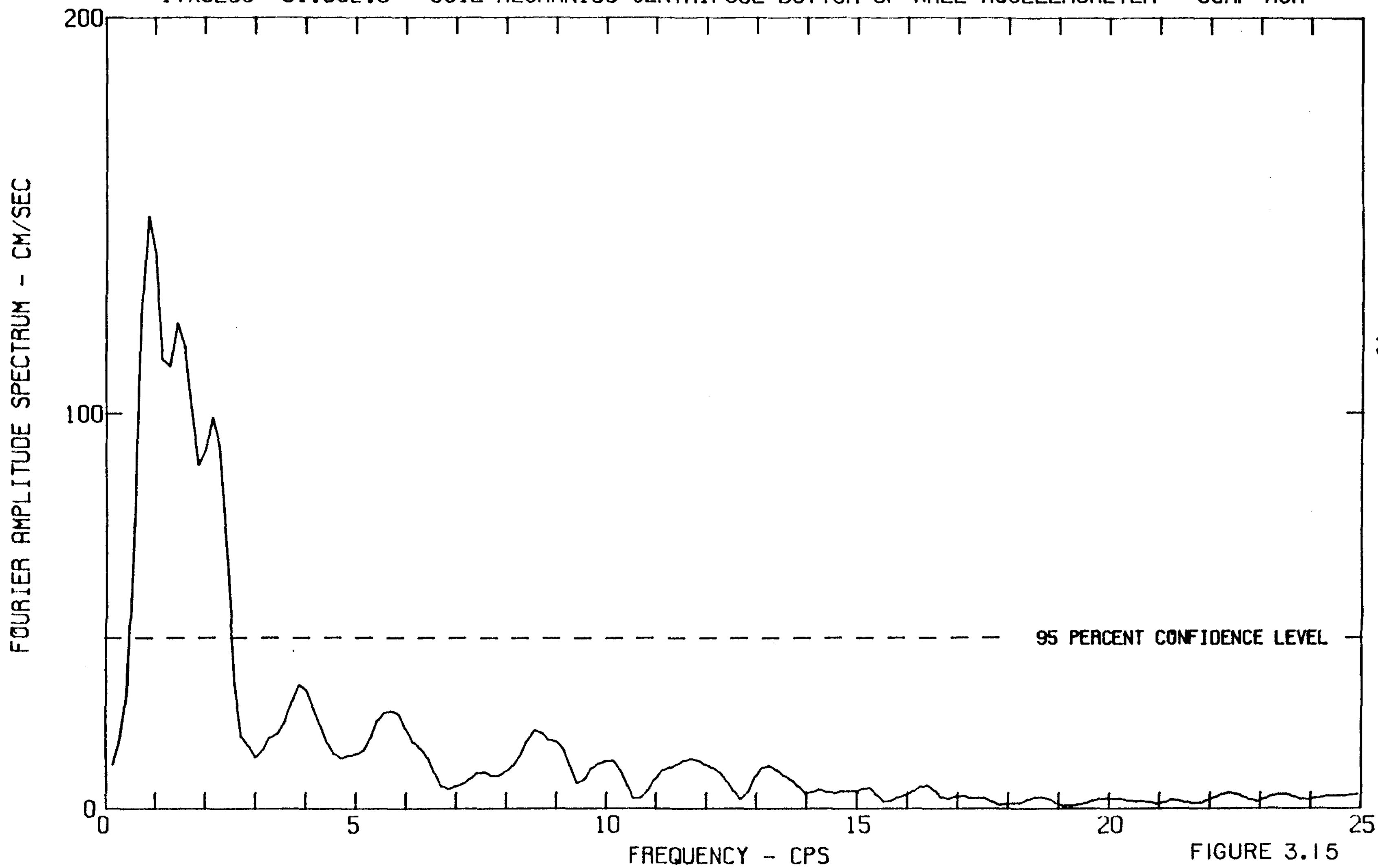

FIGURE 3.15

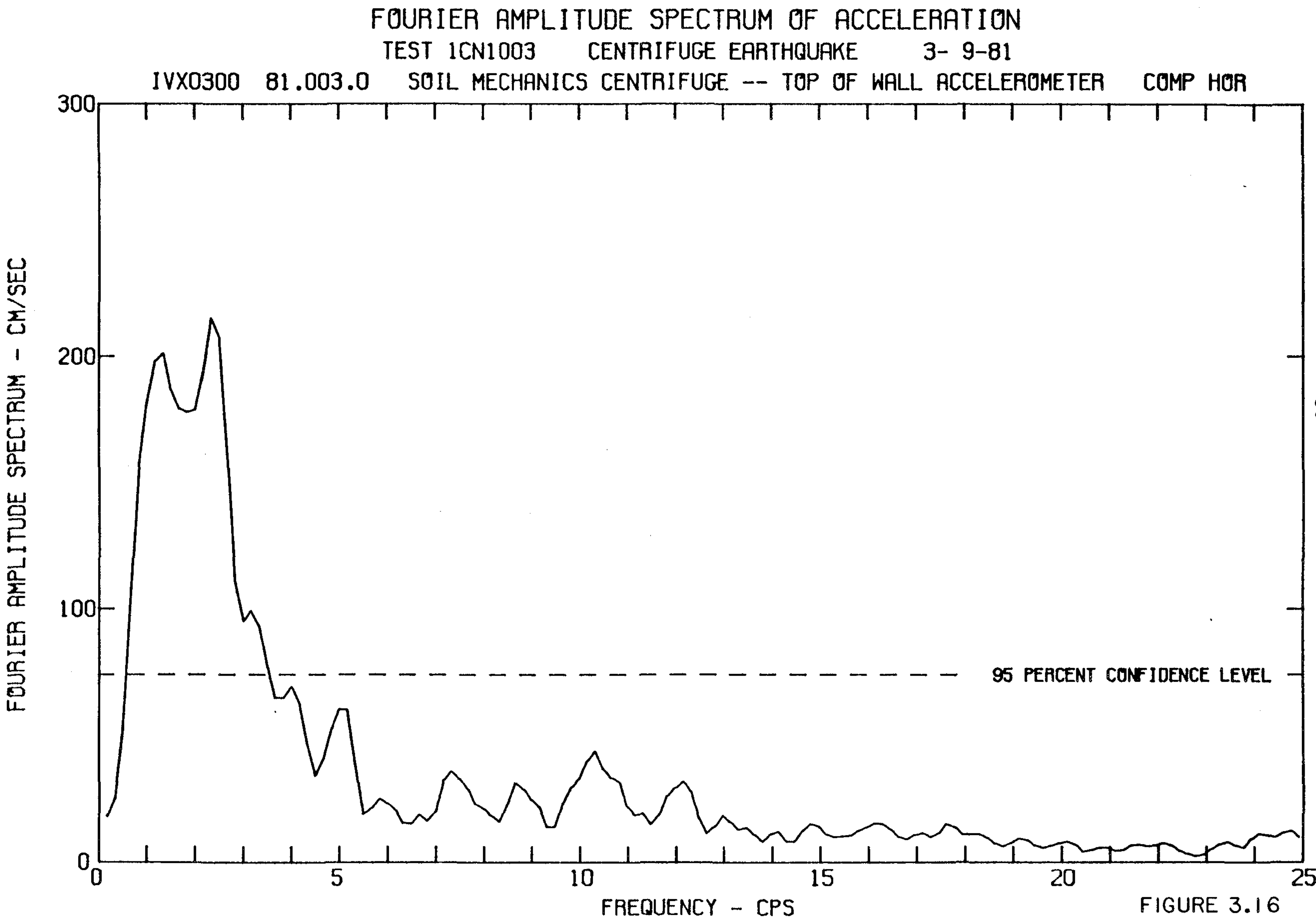
FOURIER AMPLITUDE SPECTRUM OF ACCELERATION
TEST 1CN1003 CENTRIFUGE EARTHQUAKE 3- 9-81
IVX0300 81.003.0 SOIL MECHANICS CENTRIFUGE -- TOP OF WALL ACCELEROMETER COMP HOR
FOURIER AMPLITUDE SPECTRUM - CM/SEC
300
200
100
0
95 PERCENT CONFIDENCE LEVEL
0
5
10
15
20
25
FREQUENCY - CPS

FIGURE 3.16

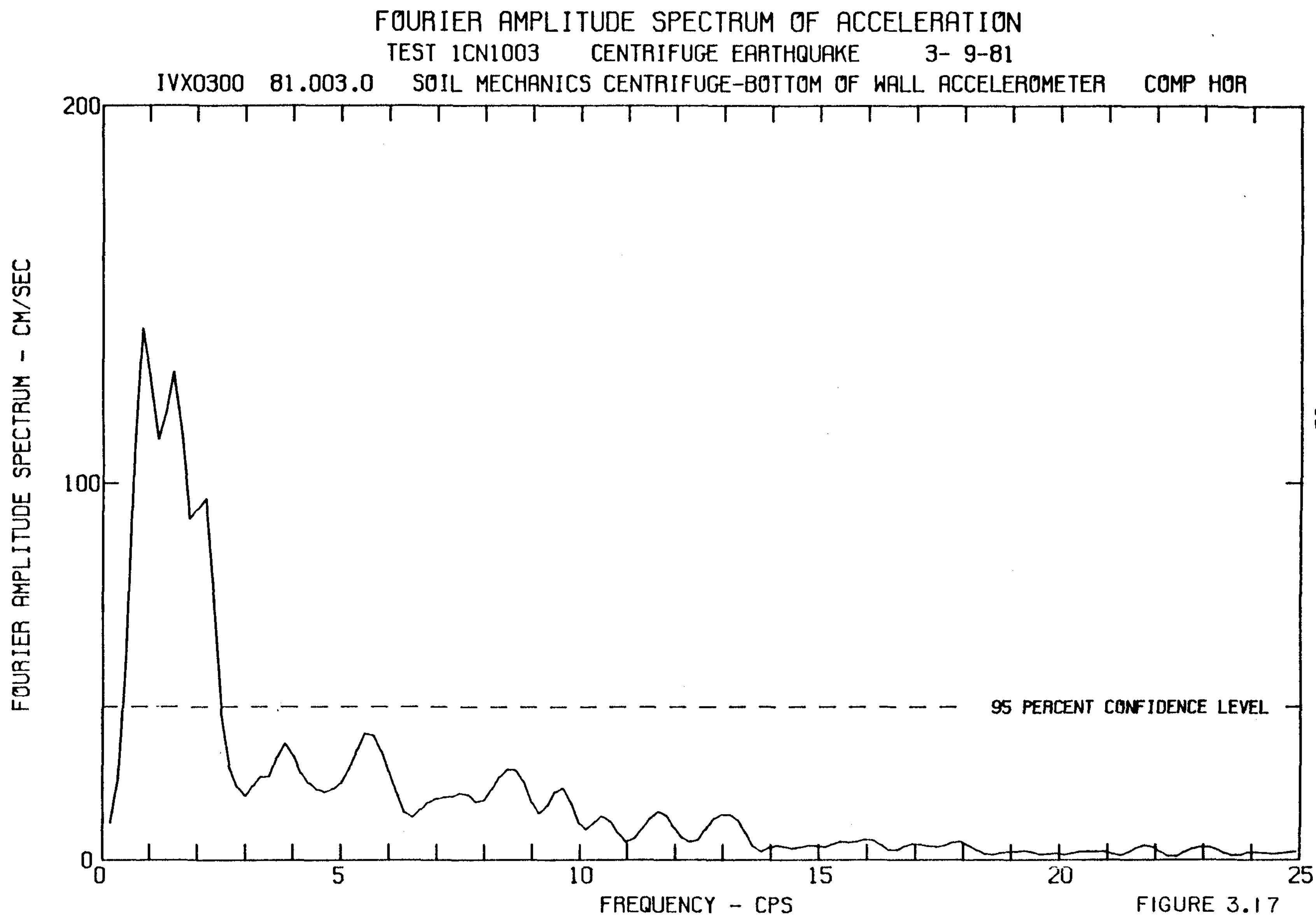
FOURIER AMPLITUDE SPECTRUM OF ACCELERATION
TEST 1CN1003 CENTRIFUGE EARTHQUAKE 3- 9-81
IVX0300 81.003.0 SOIL MECHANICS CENTRIFUGE-BOTTOM OF WALL ACCELEROMETER COMP HOR
FOURIER AMPLITUDE SPECTRUM - CM/SEC
200
100
0
95 PERCENT CONFIDENCE LEVEL
0
5
10
15
20
25
FREQUENCY - CPS

FIGURE 3.17

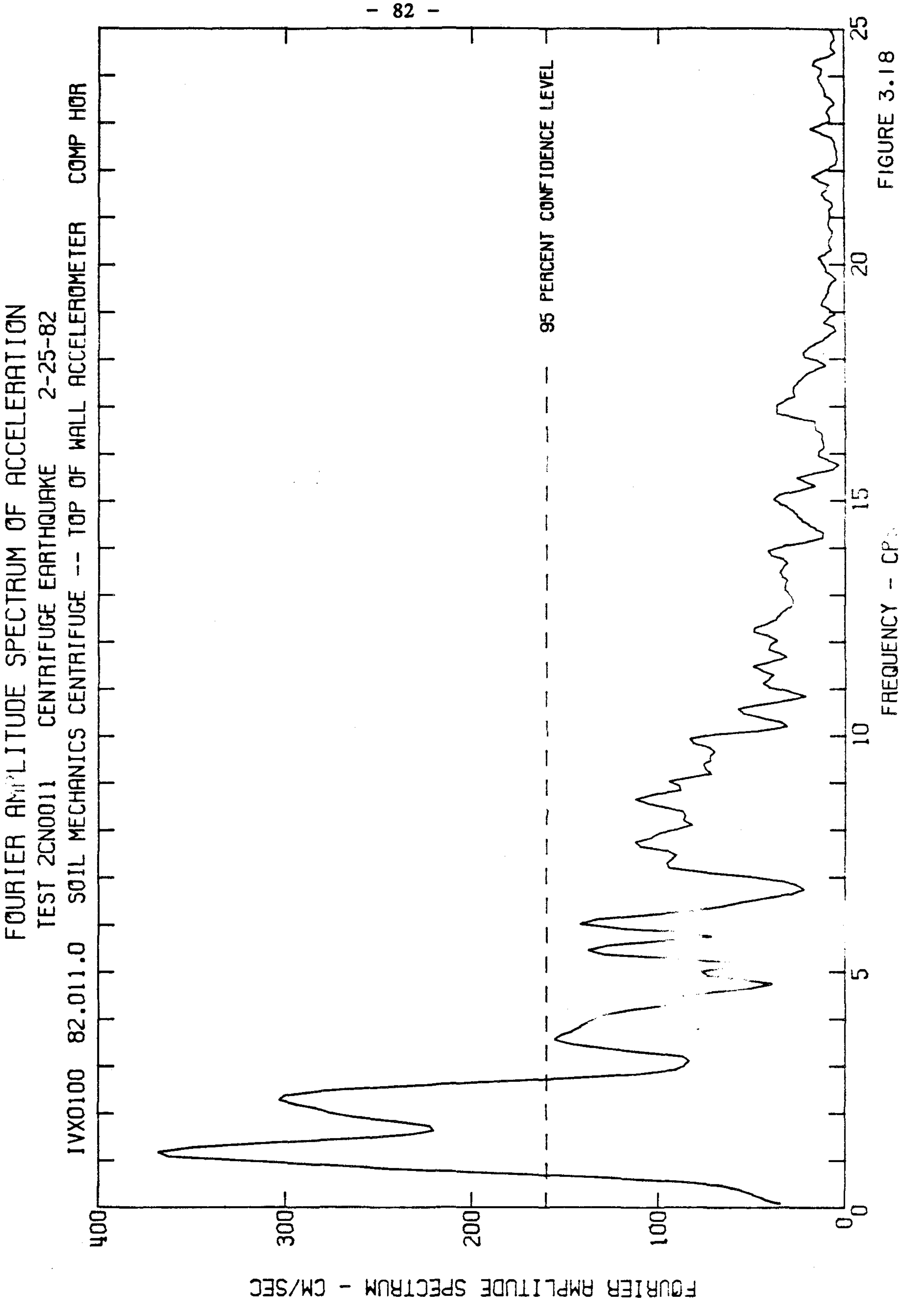
FOURIER AMPLITUDE SPECTRUM OF ACCELERATION
TEST 2CN0011 CENTRIFUGE EARTHQUAKE 2-25-82
IVX0100 82.011.0 SOIL MECHANICS CENTRIFUGE -- TOP OF WALL ACCELEROMETER COMP HOR
95 PERCENT CONFIDENCE LEVEL
FOURIER AMPLITUDE SPECTRUM - CM/SEC
400
300
200
100
0
0
5
10
15
20
25
FREQUENCY - CPS

FIGURE 3.18

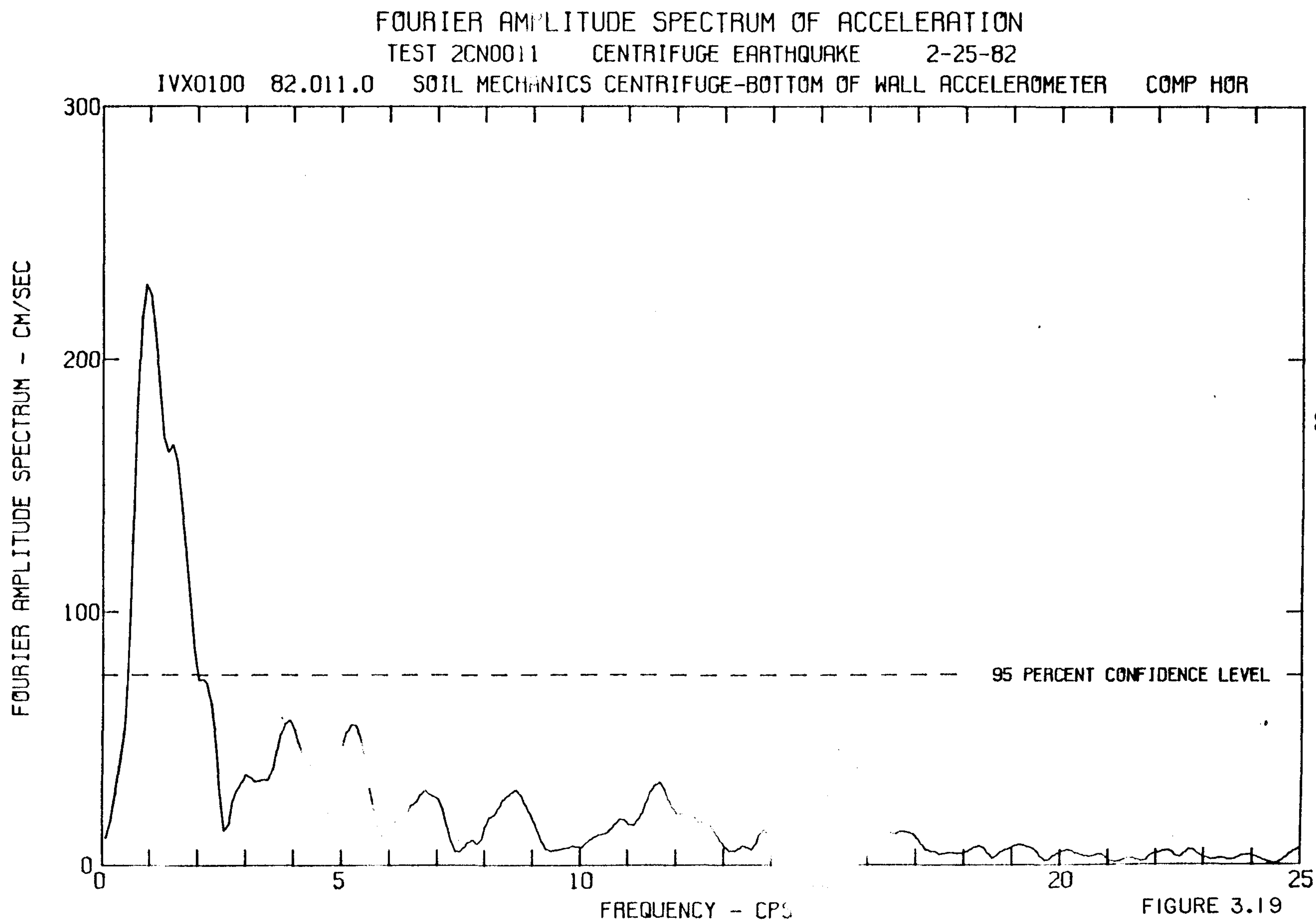
FOURIER AMPLITUDE SPECTRUM OF ACCELERATION
TEST 2CN0011 CENTRIFUGE EARTHQUAKE 2-25-82
IVX0100 82.011.0 SOIL MECHANICS CENTRIFUGE-BOTTOM OF WALL ACCELEROMETER COMP HOR
300
200
100
0
FOURIER AMPLITUDE SPECTRUM - CM/SEC
95 PERCENT CONFIDENCE LEVEL
0
5
10
20
25
FREQUENCY - CPS

FIGURE 3.19

very little relative difference between the frequencies determined from these tests, leading to the conclusion that there is little sensitivity in the system with regard to backfill slope or soil density differences for RW1. The fundamental frequency of the tests where RW1 was used was then taken to be the average of these tests, 2.6 Hz (129 Hz model). Similarly from the spectra for 2CN0011, the fundamental frequency of RW2 was taken to be 2.5 Hz (123 Hz model). This is also very close to the frequencies of tests using RW1, so there is little variation of frequency with regard to wall stiffness as well.

From examination of the Fourier spectra it can also be seen that there is only a significant contribution to the response of the systems by only one frequency, the fundamental. This is confirmed upon examination of the displacement curves presented in Chapter 5.

As will be explained in section 5.1, the fundamental frequencies of the systems are used to create dimensionless time parameters since they are a characteristic of each system.

3.4. Soil

The type of soil used was Nevada 120 Silica. This sand is a uniformly-graded, fine grained soil. A grain size distribution is shown in Figure 3.20. The soil was dry in all of the tests. It has a density range of from about 85 pcf in its loosest state to 99 pcf in its most dense. For the tests the density ranged from 91 to 99 pcf. For the medium density soil, the angle of internal friction ϕ is about 35°.

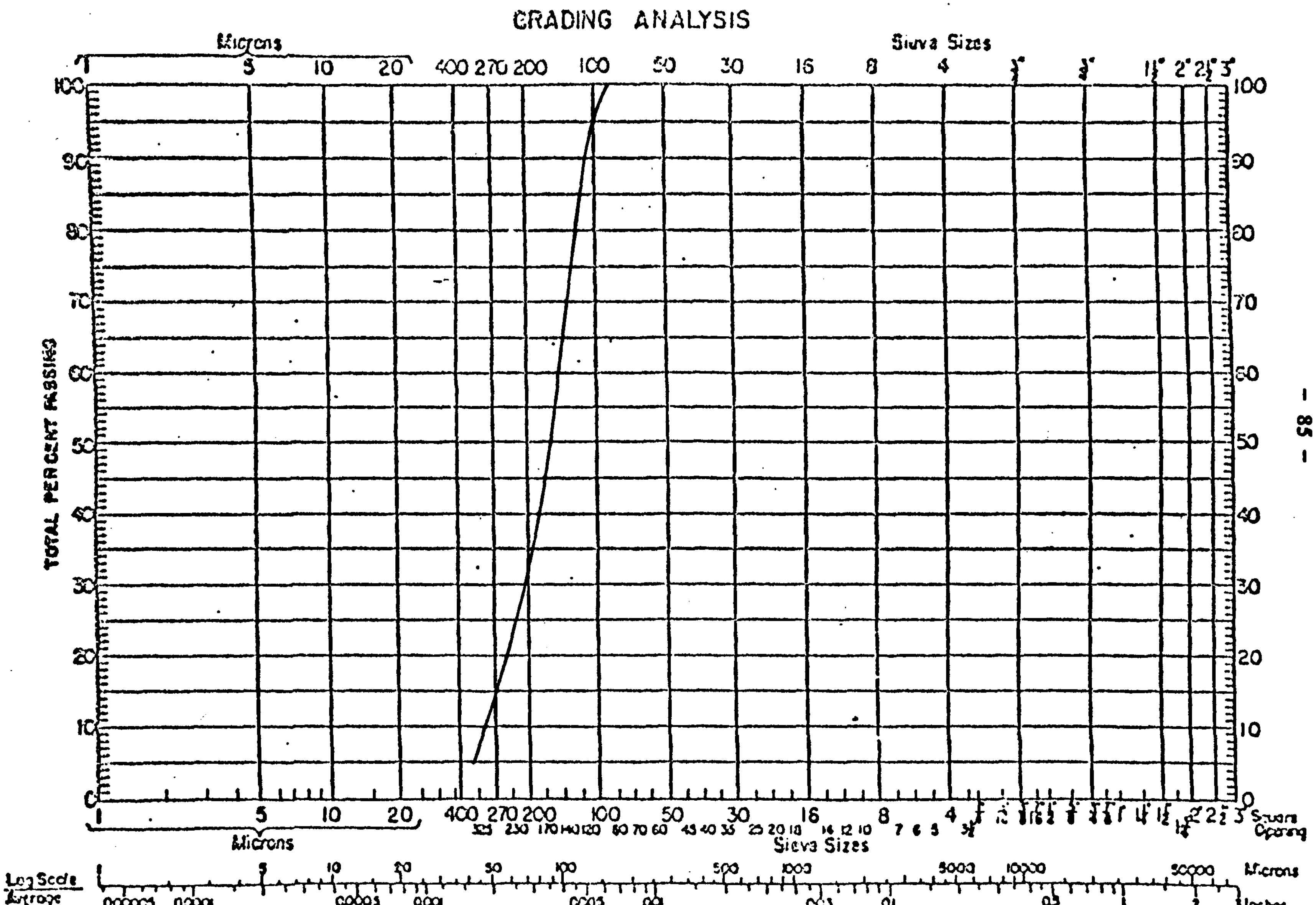

FIGURE 3.20 – GRAIN SIZE DISTRIBUTION OF NEVADA 120 SAND

The soil was chosen because of its fine grained size which is desirable when doing centrifuge work, as already mentioned in Chapter 2.

3.5. Instrumentation

A cross section of the retaining walls indicating the location of all the transducers which will be described below is shown in Figure 3.21.

3.5.1. Strain Gages

Moments on the retaining walls are measured directly by the use of strain gages which in reality measure the curvature, M/EI.

Retaining wall No. 1 (RW1) is instrumented with seven pairs of Micromeasurements Model CEA-13-062UW-350 strain gages located at distances 1.50", 2.25", 275", 3.15", 3.50", 3.75" and 4.00" from the top of the wall, and down the centerline, one strain gage of each pair on the front and one on the back at each location. Retaining wall No. 2 (RW2) is likewise instrumented with four pairs at distances from the top of 1.50", 2.75", 3.50" and 4.00" (Figure 3.22). The type of strain gage used is a universal general-purpose strain gage. These gages are polymide-encapsulated Constantan ('A' Alloy) gages featuring large, integral, copper-coated terminals. This construction provides optimum capability for direct leadwire attachment. The gage is extremely thin and flexible (0.0022"). The gage length is 0.062" and the grid width is 0.062". The resistance is 350 ± 0.3% Ω with a strain range of ± 3%.

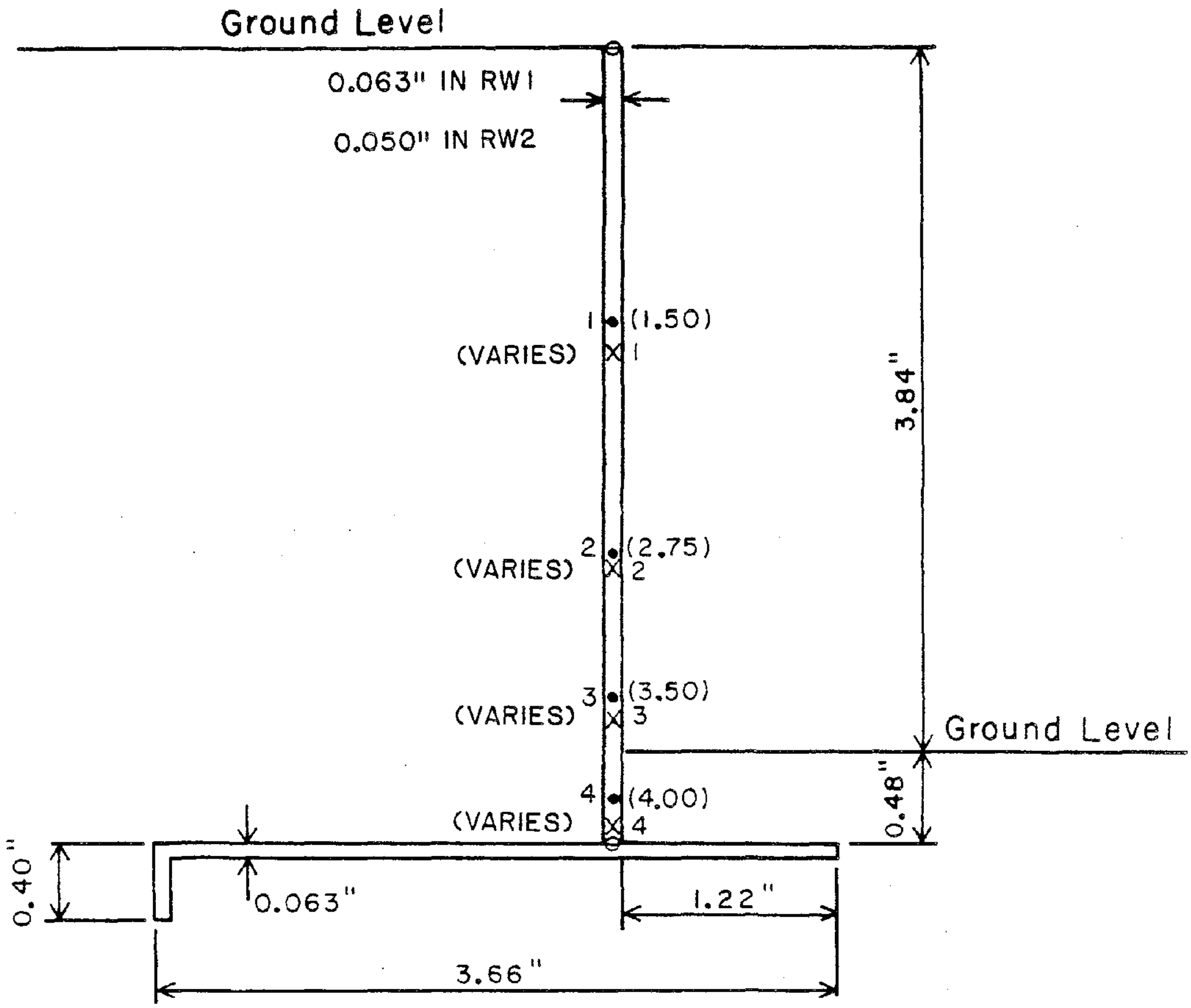

o Accelerometer and Δ- beam locations
• Strain gage locations
x Pressure transducer locations

(Parentheses indicate distance of transducer from top of wall in inches)

FIGURE 3.21 - MODEL WALL CROSS SECTION

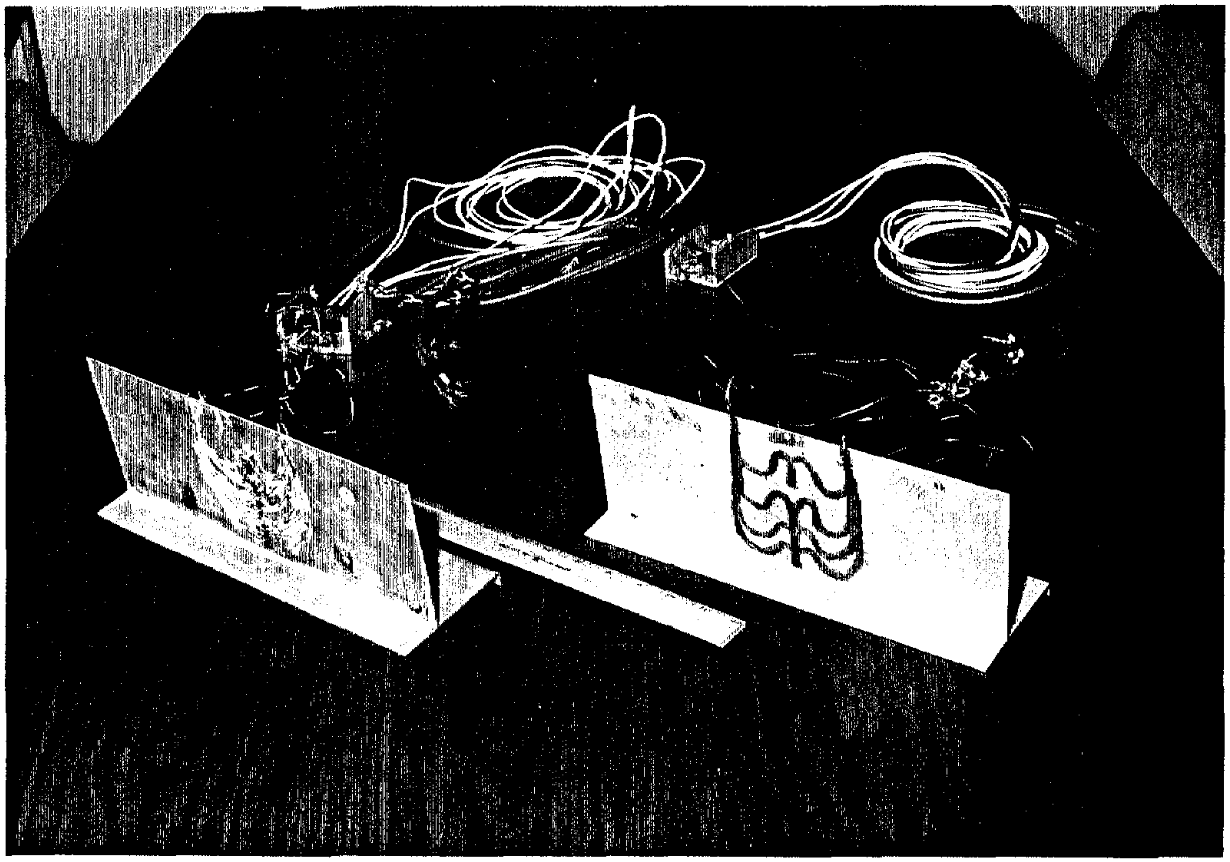

FIGURE 3.22 – MODEL RETAINING WALLS (RW1,LEFT:RW2,RIGHT) STRAIN GAGE BRIDGES IN BACKGROUND

The gages are bonded to the wall surface according to M-Line Accessories Instruction Bulletin B-130-6 (8/77) with M-Bond 600 epoxy resin adhesive. Soldered to each gage are two lengths of Belden AWG32 magnet wire. The leads were laid on the faces of the wall and coated with a flexible, impermeable protective coating (BLH Barrier J).

The strain gage circuit is arranged as a Chevron Wheatstone bridge circuit as shown in Figure 3.23. This configuration minimizes the number of balancing resistors used as well as the number of sliprings taken up since all the pairs of strain gages have but one common ground. The excitation voltage is 5V DC.

The location of the Soil Mechanics Centrifuge at Caltech is on the roof of Thomas Laboratory in close proximity to air conditioning units and elevator drive motors which make for a very noisy electrical environment. In order to minimize this noise, the signals from the strain gage bridge are amplified with one LF352 amplifier (Figure 3.24) for each pair of strain gages. This is done inside the centrifuge itself as the amplifiers are loaded on the centrifuge arm. The gain is set at 50. The amplified signals then pass through the sliprings to the control room where they are recorded on a Honeywell Model 1858 CRT Visicorder which allows inertialess recording from DC to 5 kHz. The analog signals are recorded on Kodak Type UV 1920-80330Y Visicorder Recording Paper at an amplitude of 200 mV/division (1 division = 2.5 cm). In the dynamic portions of the test, the recording takes

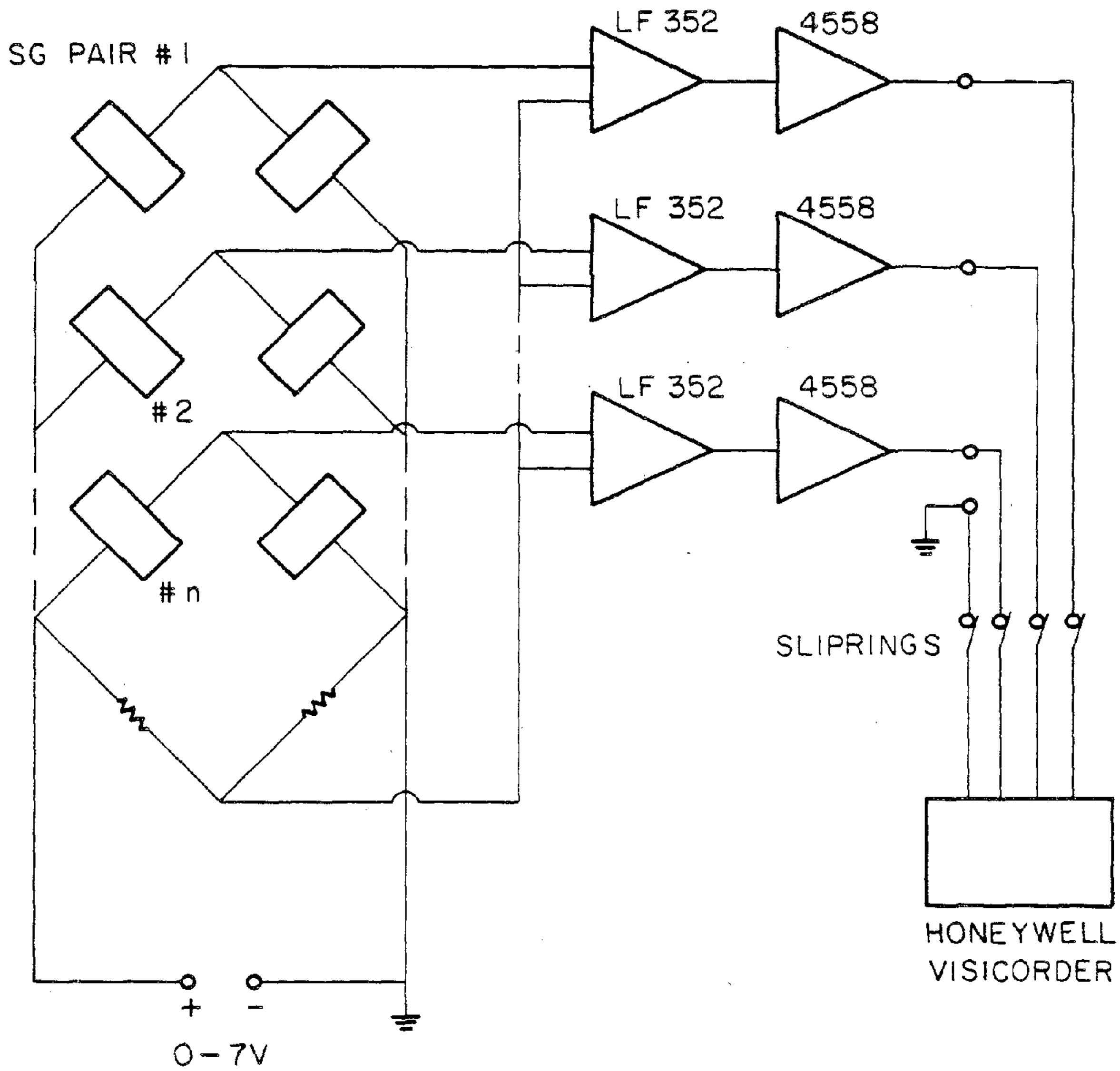

FIGURE 3.23 – STRAIN GAGE CIRCUIT

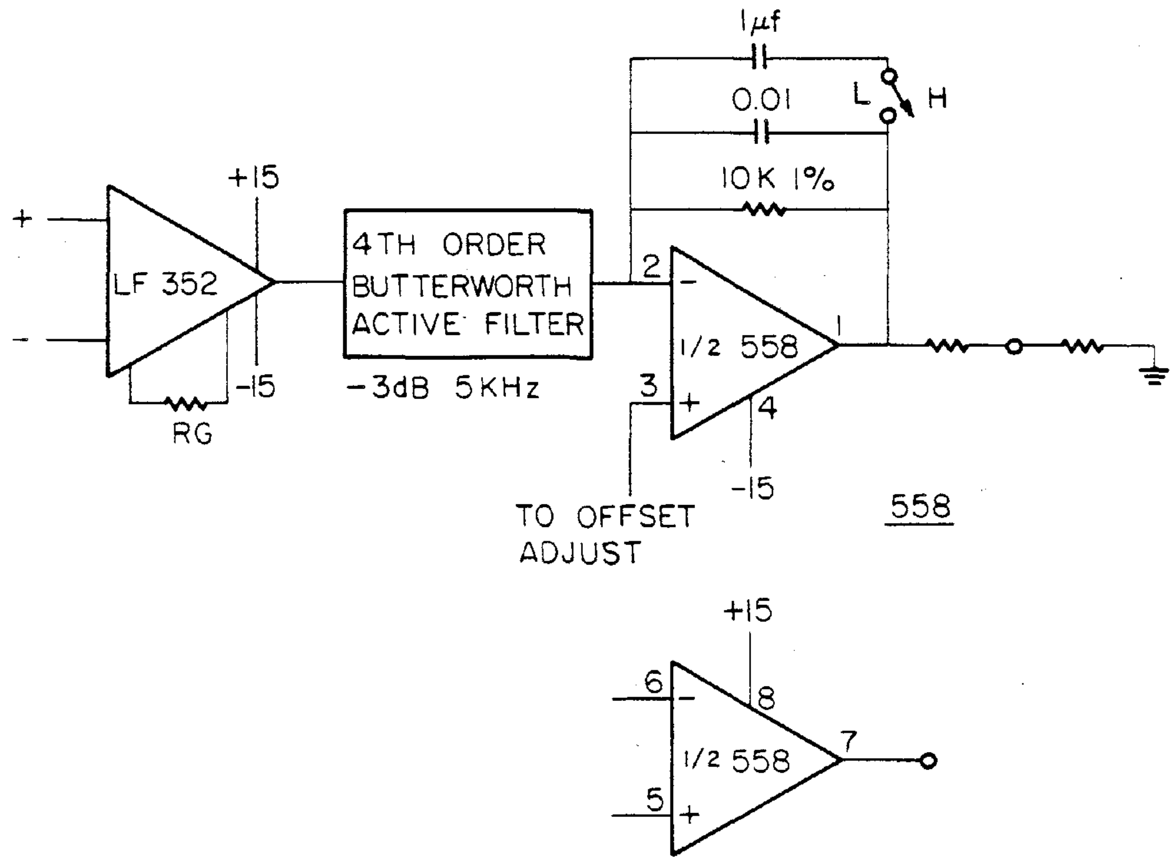

FIGURE 3.24 – AMPLIFIERS FOR STRAIN GAGES AND ACCELEROMETERS

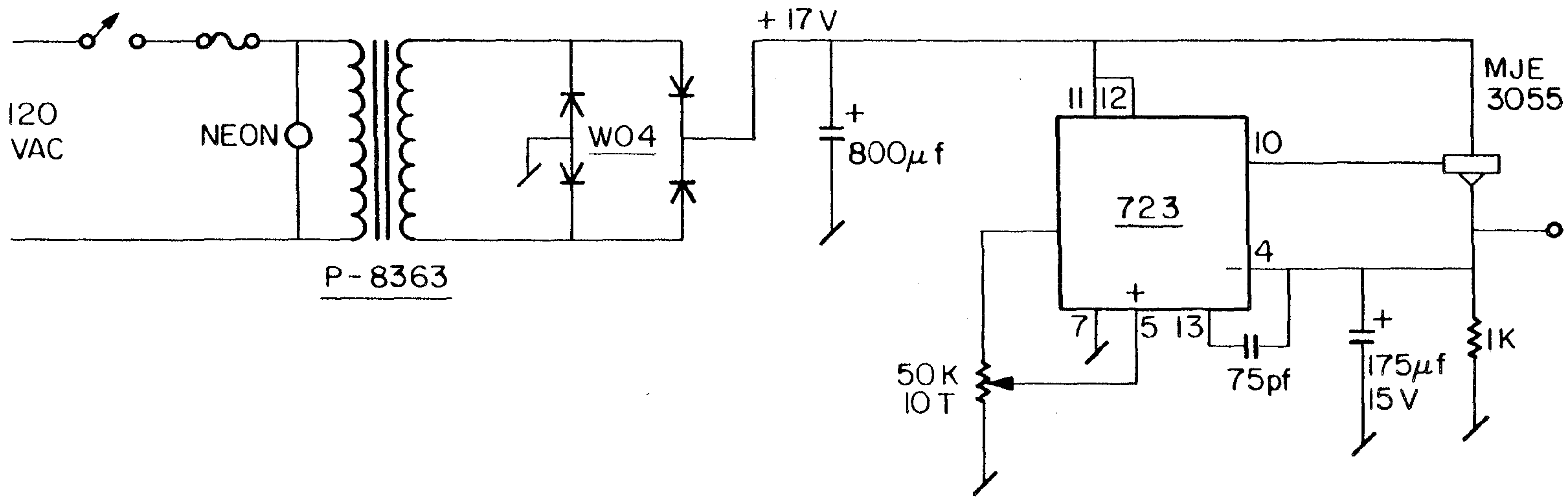

FIGURE 3.25 – CENTRIFUGE POWER SUPPLY TO DRIVE BRIDGE

place at a rate of from 50 to 80 inches per second of recording paper depending on the particular test.

3.5.2. Accelerometers

At the top and bottom of the centerline of the face of each retaining wall is mounted an Entran Devices Inc. Model EGA-125F-500D miniature accelerometer. In most tests there is an additional one located in the backfill approximately half way between the wall and the wall of the bucket and is buried near the surface.

The accelerometers employ a fully active Wheatstone Bridge consisting of semiconductor strain gages. The strain gages are bonded to a simple cantilever beam which is end-loaded with a mass (Figure 3.26). Under acceleration, a "g" force, the force on the cantilever is created by the g effect on the mass (F = ma). The accelerated mass creates a force which in turn provides a bending moment to the beam. The moment creates a strain (proportional to the acceleration) which results in a bridge unbalance. With an applied voltage, this unbalance produces a millivolt deviation at the bridge output, which is proportional to the acceleration vector.

A very attractive feature of this type of accelerometer is its very small size. The entire unit (minus the leads) weighs only 0.02 oz. The accelerometer unit is 0.270" long by 0.145" wide by 0.105" (unit weight of 525 lb/ft^3) high and is mounted on a 0.270" X 0.370" X 0.040" flange as shown in Figure 3.27. The bold-faced arrows indicate the sensitive axis. The accelerometers are attached to the model walls with

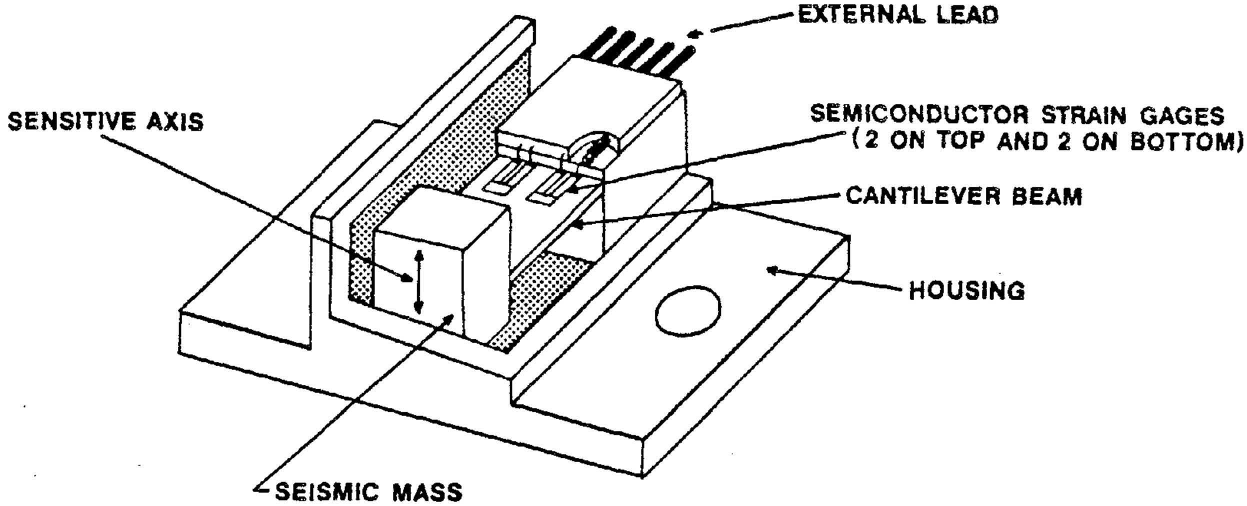

FIGURE 3.26 – ACCELEROMETER CUTAWAY (FROM ENTRAN DEVICES)

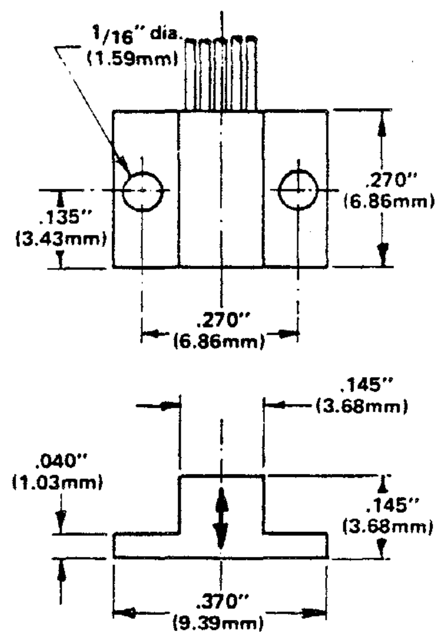

FLANGED UNIT

FIGURE 3.27 – ACCELEROMETER DIMENSIONS (FROM ENTRAN DEVICES)

two 0-80 hex screws. The model of accelerometer used has a range of $\pm$ 500g with a nominal sensitivity of about 0.5 mV/g (varies slightly from this with each particular unit), an input impedance of about 1150 Ω, an output impedance of about 550 Ω, and a resonant frequency of 3000 Hz. In addition, the unit is damped to 0.7 of critical using a viscous fluid medium. This helps to eliminate resonance and allows a useful frequency range of DC to 1000 Hz. The excitation voltage is 15 V DC.

Similarly, as with the strain gages, the output signals were suitably amplified and filtered to minimize the high frequency noise inherent with centrifuge testing. The accelerometer circuit is shown in Figure 3.28. The gain on the amplifiers was set at 10, and the analog signals recorded on the Honeywell Visicorder at an amplitude of 200 mV/division. The accelerometer signals were recorded directly alongside those of the strain gages on the recording paper.

3.5.3. Pressure Transducers

Originally, it was planned to obtain pressure distributions behind the retaining walls by means of differentiating the moment distributions twice with respect to the length coordinate x. From elementary relationships it is well known that the shear Q is:

$$Q = \frac{\partial M}{\partial x} \tag{3.10}$$

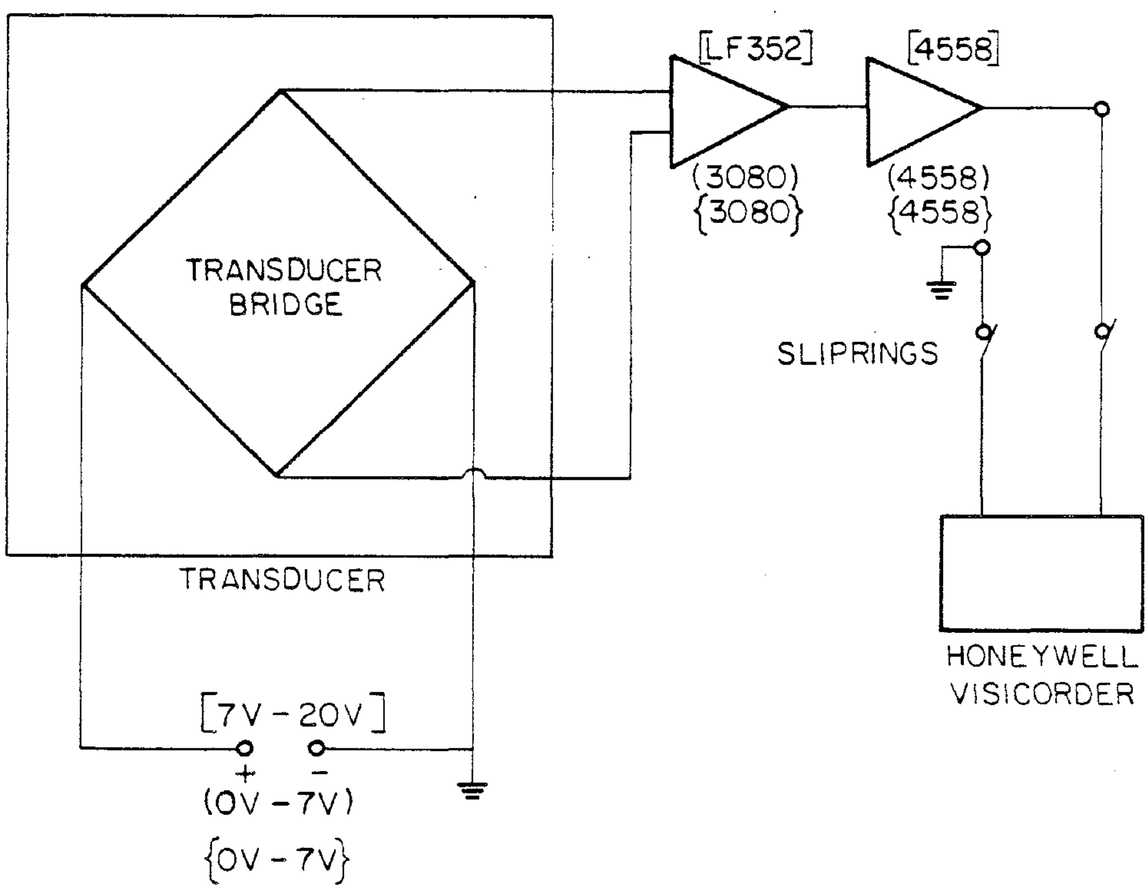

[ACCELEROMETER]

FIGURE 3.28 (PRESSURE TRANSDUCER) CIRCUIT

{DELTA-BEAM}

where M is the moment distribution. The load (pressure) distribution P is:

$$P = \frac{\partial Q}{\partial x} = \frac{\partial^2 M}{\partial x^2} \qquad (3.11)$$

Unfortunately, because of inaccuracies which develop and propagate in numerical differentiation it was found that these simple relations did not give adequate or accurate pressure distributions.

Figure 3.29 (which is fully explained in Section 5.3) shows how inaccurate the use of moment differentiation to arrive at pressure distributions is. It was thus necessary to measure pressure directly by the use of pressure transducers and then integrate the determined pressure distributions (numerical integration is much more stable and accurate than differentiation) to obtain the shear distributions.

Except for test 1CN0001, four miniature, low profile pressure transducers were placed at various locations (depending on the particular test) along the centerline of the back of the walls. In tests 1CN0002, 1CN1003, and 1CN0004, the pressure transducers were located 1.68", 2.78", 3.59", and 4.17" from the top of the wall; in tests 1CN1505, 1CN0006 at 1.79", 2.75", 3.60", 4.16", in tests 1CN0007, 1CN0508, 1CN1009, 1CN1510 at 1.86", 2.77", 3.59", 4.21", and in tests 2CN0011, 2CN0012, 2CN1013, 2CN1514 at 1.83", 2.92", 3.36", 3.91".

The pressure transducers used are Entran Devices Inc. Model EPF-200-50 Flatline Pressure Transducers. The transducer consists of a semiconductor strain gaged circular diaphragm less than 0.2" in diameter constructed of 17-4 PH stainless steel. This is a piezo resistive

FIGURE 3.29 – PRESSURE DISTRIBUTION OBTAINED FROM MOMENT DOUBLE-DIFFERENTIATON

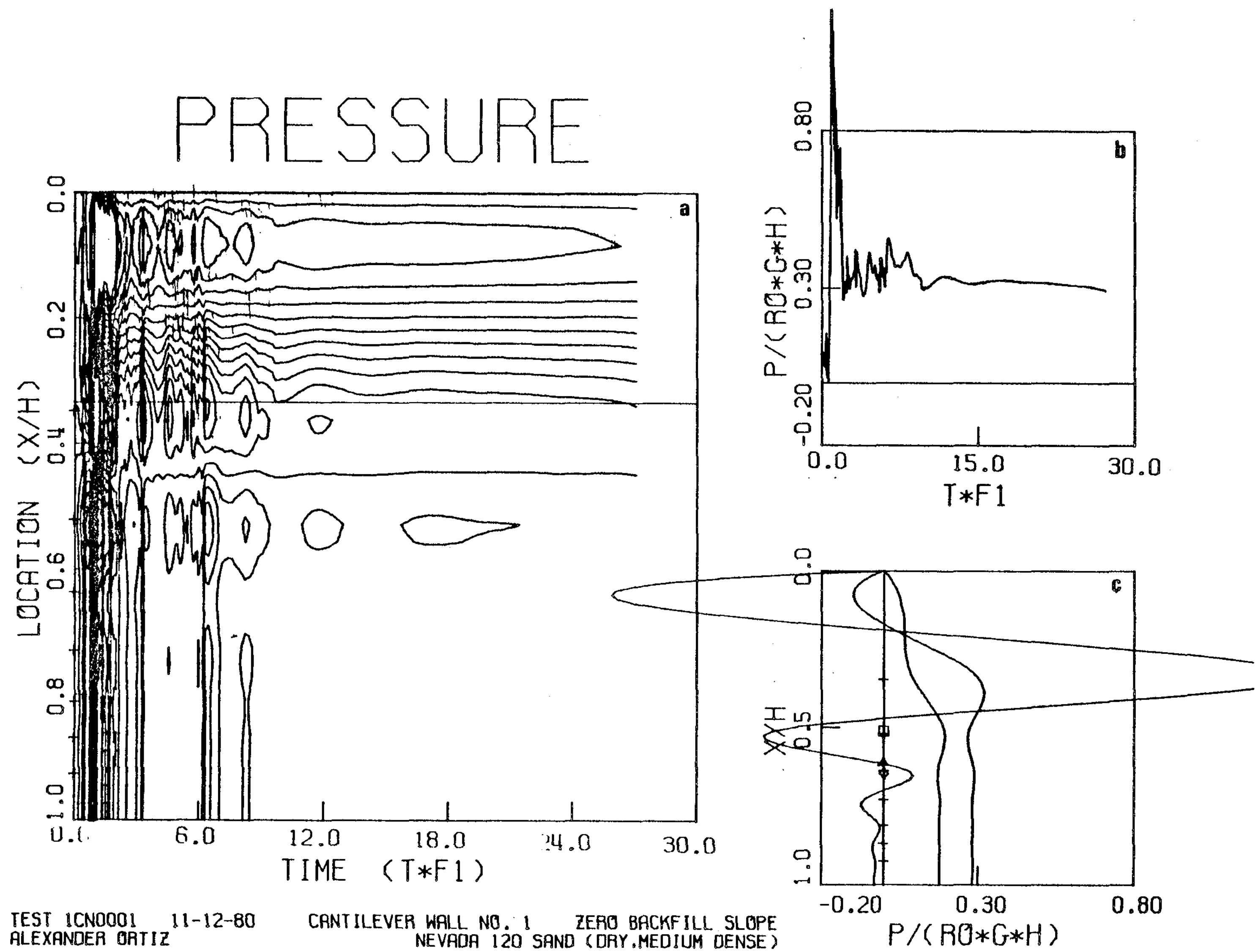

pressure transducer with a fully active semiconductor bridge. Similarly, as with the accelerometer, a load on the diaphragm will create a strain (proportional to the pressure) which results in a bridge unbalance. With an applied voltage, this unbalance produces a millivolt deviation at the bridge output, which is proportional to the pressure.

The transducer is very small (Figure 3.30) and thin being only 0.040" thick. It has a range of 0 to 50 psis with a nominal sensitivity of about 2.5 mV/psi (varies slightly from this with each particular unit), an input impedance of about 750 Ω, an output impedance of about 250 Ω and a resonant frequency of 50 kHz. The excitation voltage is 6 V DC.

As previously described with the other types of transducers, the output signal is suitably amplified and filtered. The pressure transducer circuit (Figure 3.28) is similar to that of the accelerometers with the exception that the signals are amplified with a CA3080 amplifier (Figure 3.31). The amplifier gain was 25, and the signals were recorded alongside those of the other transducers on the Honeywell Visicorder at an amplitude of 200 mV/div.

3.5.4. Displacement Transducers (Λ-beams)

In order to determine the relative displacements of the retaining walls with respect to the centrifuge bucket, the moment distribution

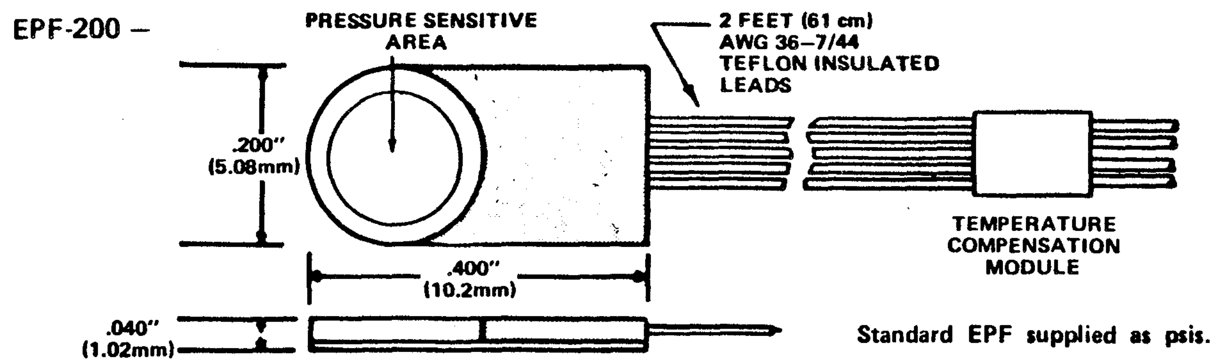

FIGURE 3.30 – PRESSURE TRANSDUCER (FROM ENTRAN DEVICES)

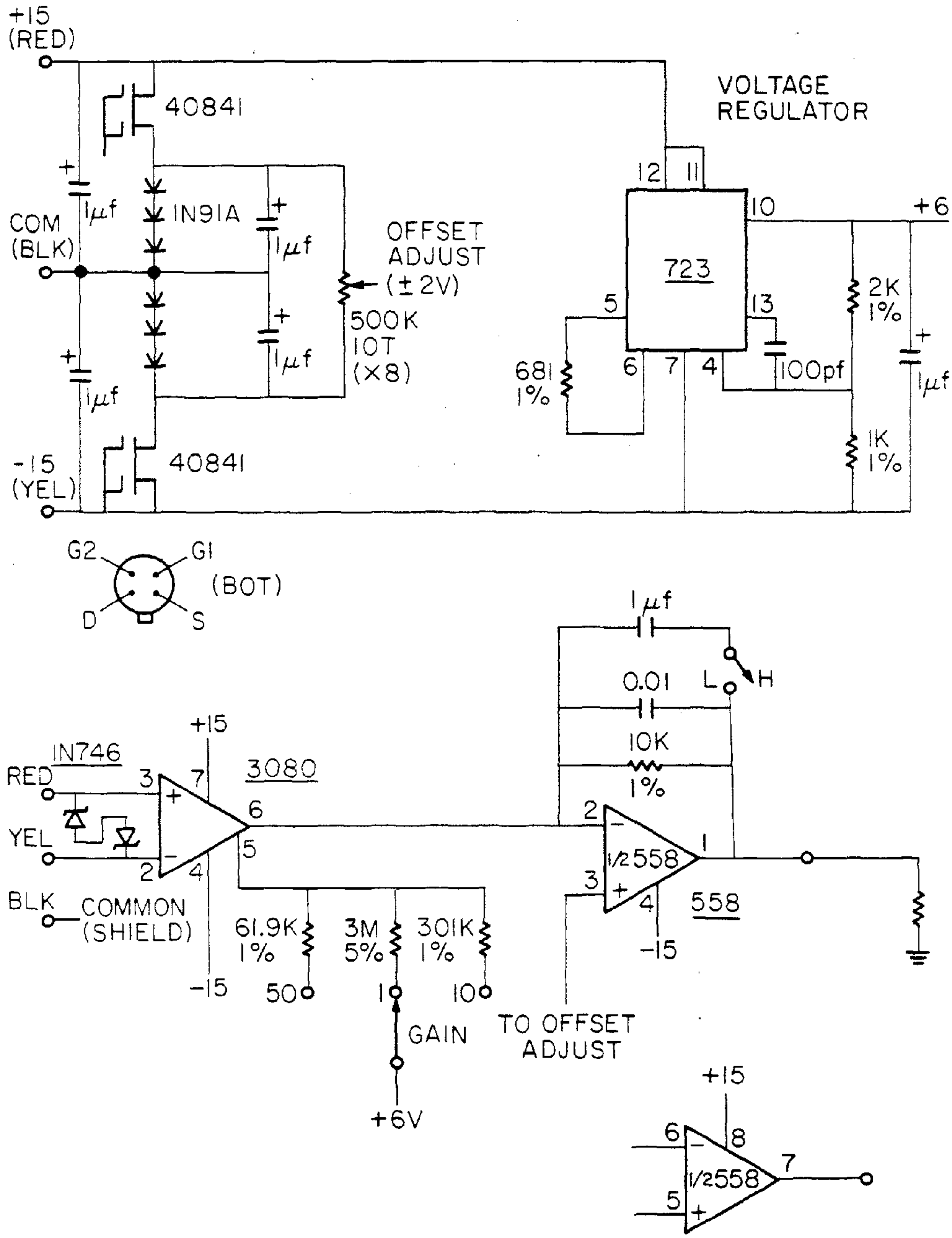

FIGURE 3.31 – AMPLIFIERS FOR PRESSURE TRANSDUCERS AND DELTA-BEAMS

along the wall must be integrated twice with respect to the length coordinate x. Recalling the equation for a the curvature of the deflected shape of a simple beam:

$$\frac{\partial^2 y}{\partial x^2} = \frac{-M}{EI} \qquad (3.12)$$

it follows that the deflected shape y is given by:

$$y = \frac{1}{EI} \int_0^H \int_0^H M dx dx + Ax + B. \qquad (3.13)$$

where A and B are constants of integration dependent on the boundary conditions of the wall. A and B can be determined knowing the displacements at the top and the bottom of the wall. The displacements at these locations can be deduced by integrating the accelerometer records twice with respect to time. This, however, requires the determination of two additional constants of integration dependent on time-imposed conditions. At each location if the initial (static), and final (static, after shaking is over) displacements are known at each of the locations, the pair of time imposed constants of integration can be determined, and thus the relative displacements between the walls and bucket can be determined at the top and bottom of the wall. Knowing this, A, B, and the full displacement curves can thus be determined.

Initial and final displacements at the top and bottom of the walls are measured by means of a pair of cantilever beams (called Δ-beams for simplicity) which are attached to the front of the bucket and connected by means of a very thin wire to the accelerometer locations on the face of the wall. These Δ-beams are very thin (0.015" thick) strips 2.25" long, 1.00" wide of spring steel attached to a rigid base and strain gaged, so that, properly calibrated, they can record displacements over a relatively wide range.

The Δ-beam circuit is similar to that of the pressure transducers (Figure 3.28). Since the frequency response is very low, the transducer signals are only recorded on the Visicorder during the static portions of the test. The circuit excitation is 5 V, the gain 25, and the Visicorder amplitude is 100 mV/div.

3.6. Calibration of Transducers

All pre-test calibrations were carried out using the entire electronic circuitry, i.e. the calibration signals were routed through those terminals, amplifier channels, filters, sliprings, and Visicorder channels which they would use during the actual testing. The excitations, gains, and recording amplitudes used in calibration were likewise the same as in the tests. The outputs recorded on the Visicorder were converted directly to parameter (moment, displacement, acceleration, etc.) measurements without the use of instrument factors. All transducers are linear and therefore require two calibration factors (slope, intercept) for each. These factors were determined using the linear least-squares function on a Hewlett-Packard 55 pocket calculator.

All calibrations were recorded on the Visicorder and the traces digitized with a Benson-Lehner 099D data reducer unit. The digitizer had a resolution of 790.8 digitizer units (du) per inch of width of recording paper and 792.0 du/inch of length. The calibration slopes were thus in units of parameter per digitizer unit and the intercepts in units of parameter. Data reduction of the tests will be discussed in Section 4.2.

3.6.1. Strain Gages

The strain gages are calibrated to measure moments directly. To accomplish this, the base of the model retaining walls is rigidly secured to the bottom of the centrifuge magnesium frame which was rotated 90° so that the stem forms as horizontal cantilever beam. Two 1" thick (each) Plexiglas beams were then clamped in sandwich fashion to the free end of the stem and weights hung from the center. The calibration arrangement is shown in Figure 3.32. The Plexiglas beams distribute the load evenly across the width of the wall. This creates in effect a cantilever beam with a concentrated load at the end, moments of which can be readily determined. Weights of 0,1,2,3,4,5,6,and 8 pounds were hung and the output recorded at the Visicorder at the other end of the system.

3.6.2. Accelerometers

In order to calibrate the accelerometers, they were placed with the sensitive axis facing downward on the upper lip of the centrifuge bucket which is at a radius of 30.5 inches from the centrifuge axis. Readings were recorded on the Visicorder with this arrangement, i.e., the accelerometers reading 1g. The centrifuge was then taken up to accelerations of 10, 20, 30, 40, 50, 60, and 70g respectively. It was

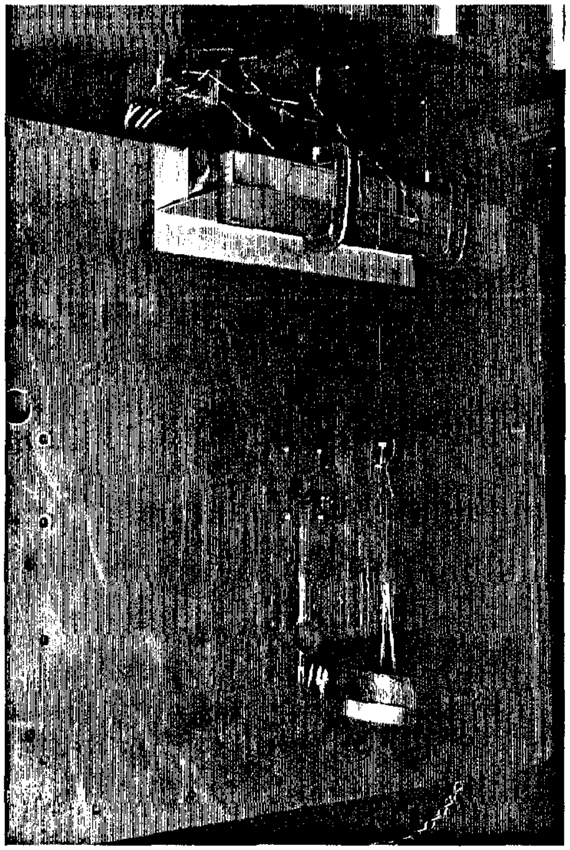

FIGURE 3.32 – STRAIN GAGE CALIBRATION

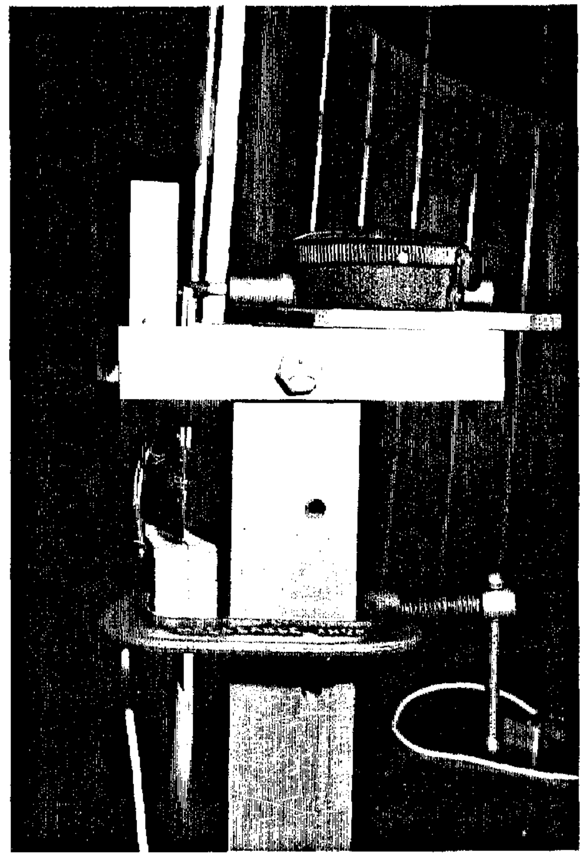

FIGURE 3.33 – DELTA-BEAM CALIBRATION

assumed that an amplitude of 0 du on the Visicorder was 1g. The calibrations were then determined in relation to this.

3.6.3. Pressure Transducers

The pressure transducers were calibrated by placing them on the bottom of the centrifuge bucket at a radius of 40.5 inches from the centrifuge axis, and placing 4.90" of Nevada 120 sand at a density of 93.3 pcf on top of them. Measurements were then taken with the centrifuge stationary (at 1g) and spinning at 10,20,30,40, and 50g. The increase in g-acceleration to N g's causes an increase in the soil unit weight by N (see Table 2.1) and thus an increase in pressure, the pressure simply being the weight density of the soil (at the particular acceleration level) times the depth (4.90"). Thus pressures of 38, 381, 762, 1143, 1524, and 1905 psf corresponded to each g level used in the calibration.

3.6.4. Δ-beams

The Δ-beams were calibrated by fixing them to a vice and measuring displacements with the aid of a Federal dial gauge accurate to 0.001 in. Displacements of 0, 0.01, 0.02, 0.03, 0.04, 0.05, and 0.10 inches were measured (Figure 3.33).

CHAPTER IV

4.1. The Experiment

In every test performed, the following sequence of experimental procedures was carried out.

To begin with, sand was placed on the centrifuge bucket to a depth of about 4 inches (Figure 4.1). If looser conditions were desired, it was just dumped in; if denser, it was tamped and/or vibrated after being placed in one to two inch lifts. Following this, one of the walls, along with all its instrumentation, was placed approximately 6 inches from the front of the bucket (leaving about 8-1/2 inches for backfill) and carefully seated on the sand layer already placed (Figure 4.2). Special care was taken to assure the wall was vertical by following guide lines drawn on the inside of the bucket. Sand was then placed on both sides of the wall following the procedure for looser or denser conditions described above (Figure 4.3). The total depth of sand (for a flat backfill) was 8 inches. For a sloping backfill, it was placed to the desired slope above the 8 inch mark on both sides. The weight of the sand placed was then totalled and, since the bucket dimensions were well known, the unit weight determined.

By placing sand on both sides of the wall and taking the container up to 50g's the transducers were thus zeroed. In this manner, the walls were subjected to no moment, lateral acceleration, or displacement and an accurate zero was recorded on the Visicorder at the test centrifuge

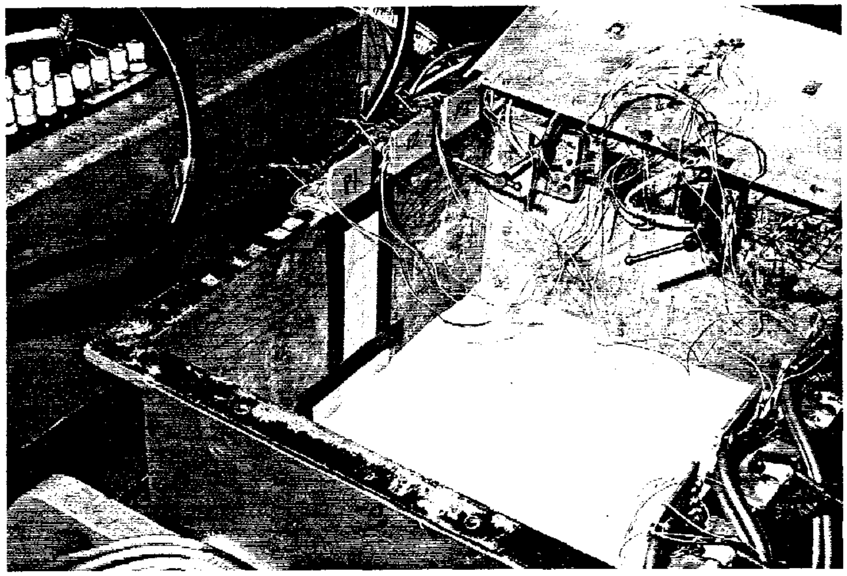

FIGURE 4.1

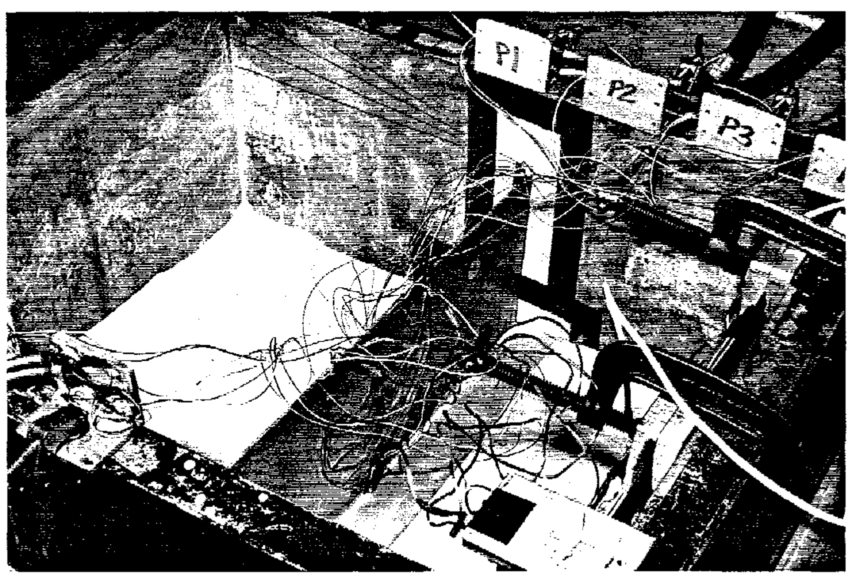

FIGURE 4.2

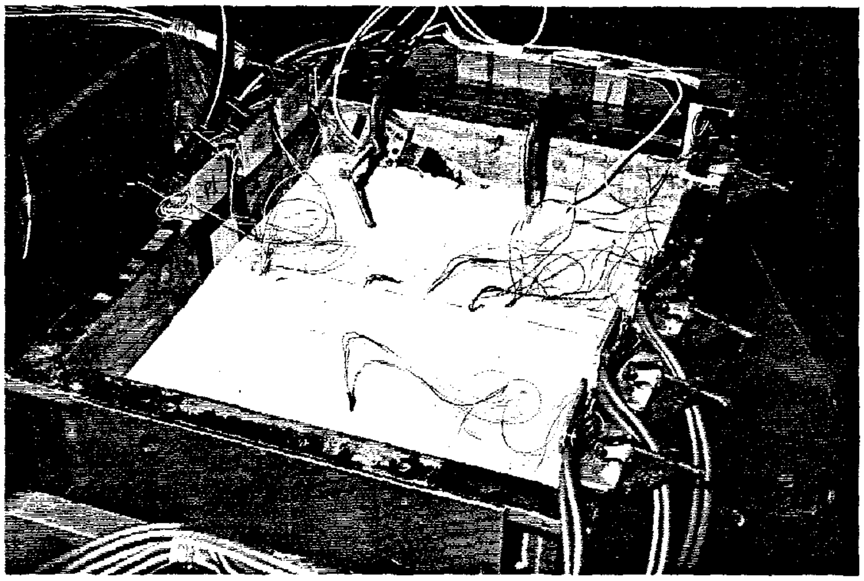

FIGURE 4.3

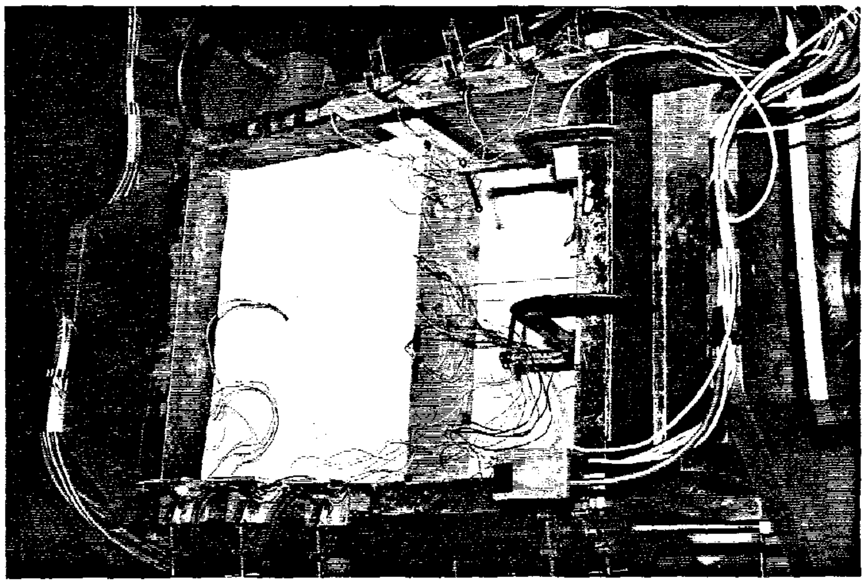

FIGURE 4.4

acceleration. The experiment was then returned to one g where the sand on the front of the walls was removed to the design height (Figure 4.4).

Table 4.1 Soil Densities

Test	Density @ 1g (pcf)	Density @ 50g (pcf)	Test	Density @ 1g (pcf)	Density @ 50g (pcf)
1CN0001	92.6	4630	1CN0508	95.9	4797
1CN0002	91.2	4561	1CN1009	97.0	4849
1CN1003	92.0	4597	1CN1510	95.3	4764
1CN0004	93.9	4695	2CN0011	98.8	4941
1CN1505	92.4	4621	2CN0012	95.8	4790
1CN0006	94.5	4726	2CN1013	97.3	4865
1CN0007	98.1	4906	2CN1514	97.7	4886

The system was next taken back up to 50g's where all the static outputs were recorded on the Visicorder. The channels which carried the signals of the Δ-beams were then turned off since, due to the poor frequency response of the Δ-beams, they were inadequate for dynamic measurements. After this, the container was subjected to the "earthquake" shaking described in Sections 3.2 and 5.2. The output signals were recorded on the Visicorder at a recording paper rate of 50 to 80 inches per second depending on the particular test. Usually there were 4 strain gage, 3 accelerometer and 4 pressure transducer outputs (11 traces total) being recorded on paper only 8 inches wide. Needless to say, there was some overlapping of traces, and a high density of analog data, but the recordings were usually clear and easy to follow when digitizing subsequently.

Figure 4.5 is an example of the traces recorded on the Visicorder during part of the dynamic portion of a typical test (2CN0012 in this case).

Following the shaking, the two Δ-beam channels were turned back on, and their outputs taken along with those from the other transducers now static once more. The system was then brought back to rest which concluded the actual experiment itself. Data reduction of the Visicorder output followed.

4.2. Data Reduction

The digitizing was performed on a Benson-Lehner 099D data reducer unit and the following procedure used. The cross hairs are manually set to successive x-y coordinates on each record trace. The coordinates are converted to digital position figures by means of a magnetic readout head, and are stored in a 6-digit accumulator system from which they are automatically read out to an IBM 29 card punch. The resolution of the system is 792.0 du/inch in the x and 790.8 du/inch in the y directions. The Visicorder paper is placed on the 24" X 16" digitizing table with the horizontal axis lined up by eye to an estimated zero axis. The lining up of the paper need not be too accurate since it will be corrected with respect to a baseline recorded on the paper. All traces are digitized without moving the record on the table.

First of all, a baseline, which will be used to make corrections for deviation from the horizontal, is digitized. Each trace on the Visicorder paper is then digitized individually as follows. The zero

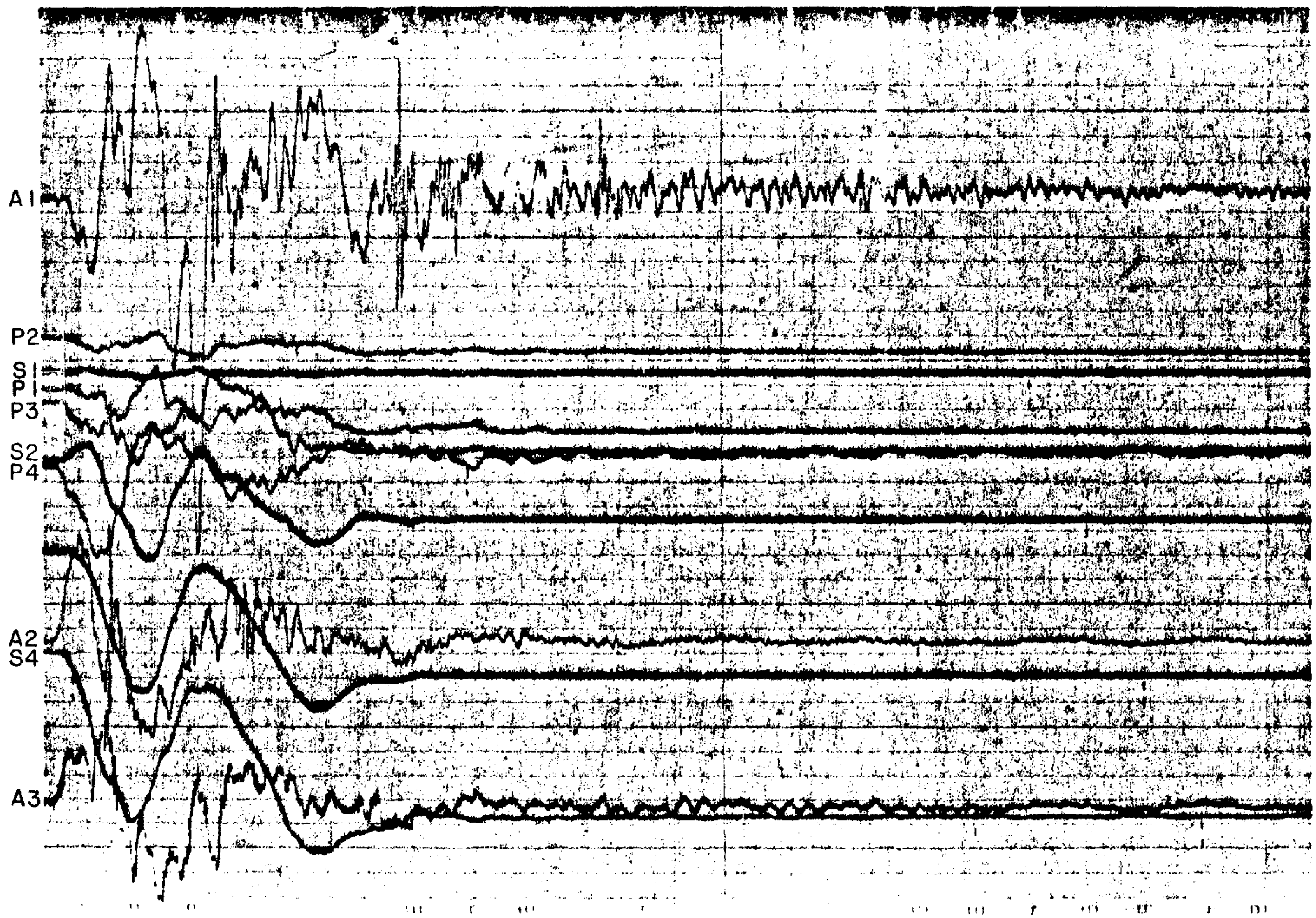

FIGURE 4.5 – TYPICAL VISICORDER RECORD (2CN0012) REDUCED TO 77% OF ORIGINAL
A = ACCELEROMETER P = PRESSURE GAGE S = STRAIN GAGE

point of the trace is first digitized. This is the point at 50g where sand is on both sides of the wall. For the pressure transducers and the Δ-beams the zero point is the reading when the centrifuge is at rest. Next the static point at 50g (normal experiment, backfill sand only) is digitized followed by the digitization of the dynamic part of the test. The records are digitized on an unequal time basis since this leads to the best definition of the trace for a given number of data points. All significant peaks, points of inflection, etc., are picked, along with as many intermediate points as are needed for an accurate definition of shape.

The digitized data are directly punched on cards which are then read into magnetic disks on a VAX 11 Wordprocessing system. Program P1CHECK (Trifunac, Lee [63]) reads the data and checks whether the time coordinates monotonically increase. It also searches for possible disproportionate jumps of the amplitude data. If any error is found, the program prints out the message. Small errors are corrected immediately. The data are then plotted to the same scale as the digitized record, and the two versions are compared to check the accuracy of digitization. Any portion that is digitized improperly has to be redigitized and replotted until the final plot agrees well with the digitized record.

The corrected digitized data is now fed into the data processing program WALL which will be described below and which is listed in Appendix B. WALL prints out static, maximum dynamic, and final static moment, pressure, shear, and displacement distributions along the wall to discrete locations; moment, pressure, shear, displacement vs. time distributions at the location of each maximum response at equal time steps; accelerometer, velocity and displacement vs. time records for each of the three accelerometer locations, as well as other data pertaining to the test, namely, centrifuge operation data, material properties, and calibration factors. In addition plots are made of the above-mentioned distributions. Contour plots of moment, pressure, shear, and displacement distributions with respect to location and time are also made. This provides a very descriptive and compact representation of the entire test.

It was sometimes desired to obtain characteristics of the motion recorded by the accelerometers in order to have a comparison with actual accelerogram characteristics of real earthquakes. For this purpose, some of the accelerometer records were given the routine computer processing of strong-motion accelerograms developed at Caltech by Trifunac and Lee [63]. Programs P1CHECK, P2SCALE, and P3TAPE form Volume I of data in which the raw data is converted into uncorrected, scaled, accelerogram data. Program IIMAIN creates Volume II which contains corrected accelerogram, velocity, and displacement data. Volume III, which gives the response spectra of the record, is created using program IIIMAIN. Program IVMAIN creates Volume IV containing the Fourier Spectra. From this volume, the fundamental frequency of the system is determined (see Section 3.3.3). As will be seen in the results, it is the only frequency which contributes significantly to the response. The standard accelerogram processing is outlined in Figure 4.6.

The results from the tests are obtained by processing the digitized data with the FORTRAN program WALL. The program is run on an IBM 370/3032 Computer System at the Booth Computing Center at Caltech.

After the raw digitized data is checked by program P1CHECK, the corrected data from the transducers is fed into WALL, along with other experimental data, namely centrifuge speed, distance from centrifuge axis to top of wall, wall/soil properties, order of polynomial desired for least-squares fit (see below), type, number, and location of transducers used, and calibration factors.

All the traces are then corrected with respect to the input baseline to avoid errors due to the slight slope which all the records inherently have because of positioning on the digitizer table. This is particularly important in the accelerometer records since double integrations can introduce errors proportional to the square of the running time with just a small initial slope present.

Following this, the data is scaled to model dimensions using the calibration factors.

Since all the separate traces are digitized individually, it is necessary to correlate them to specific, discrete time steps. This is done by smoothing the individual trace data point by point with a cubic spline and then picking off the values from the spline at particular time intervals. For convenience (see Section 5.1), it was decided to use a dimensionless time group tf_1 to express time. t is the real

STANDARD ACCELEROGRAM PROCESSING

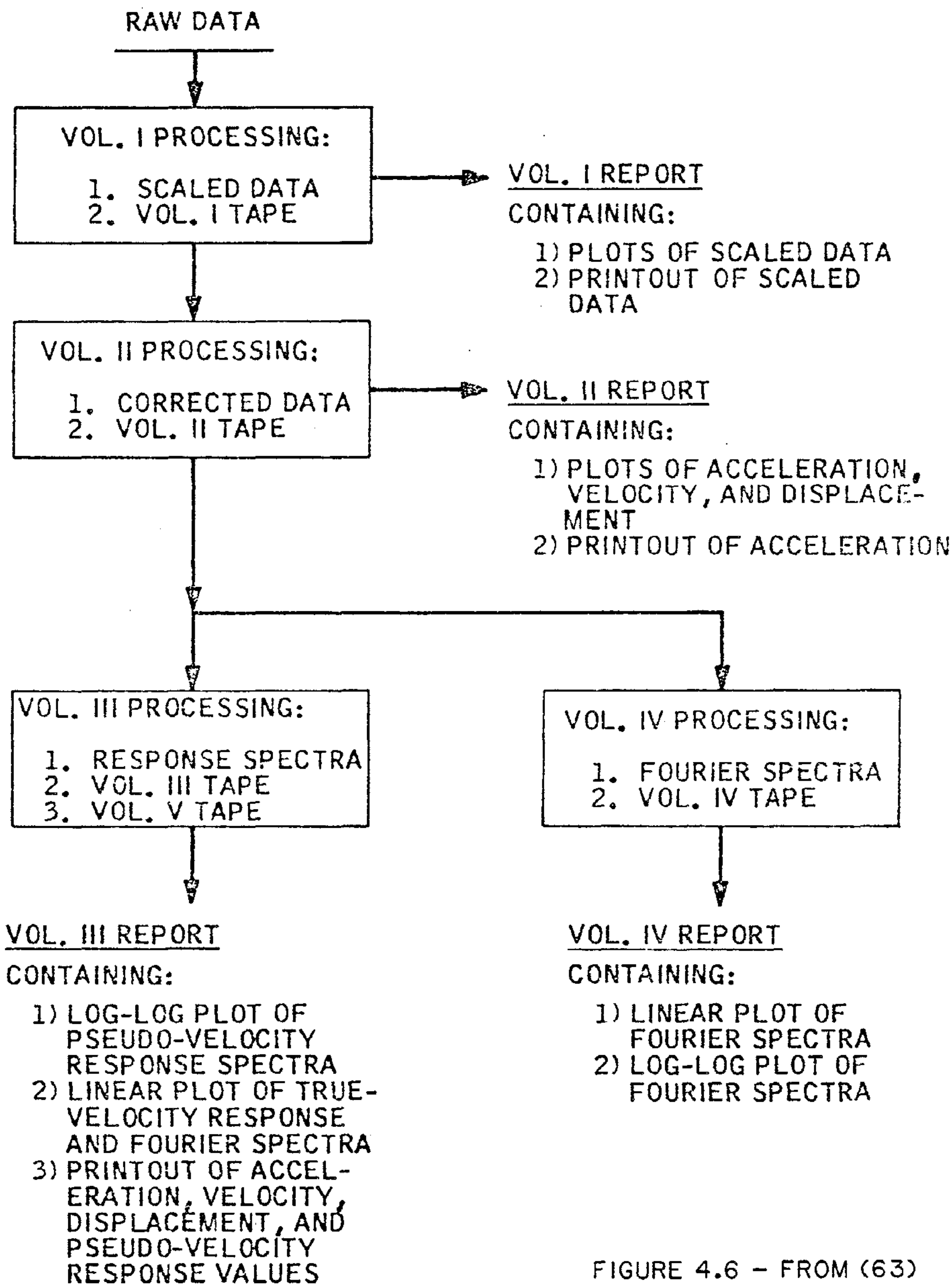

FIGURE 4.6 – FROM (63)

prototype (or model) time and f_1 is the real prototype (or model) fundamental frequency of the system. tf_1 is the same for both model and prototype. The discrete time steps are chosen at 150 per tf_1 for the first six tf_1 and 75 per tf_1 thereafter. Because of the nature of the experimental shaking, most of the critical (maximum and high frequency) response occurs when $0 \lesssim tf_1 \lesssim 6.0$.

The moments are determined from the scaled strain gage data. It is intended to use a quintic (fifth order) spline fit to the data points at each time step. The spline fitting, however, requires six boundary conditions, the moment and the first and second derivatives of the moment, at the top and base of the wall. At the top of the wall, these are known. The moment and shear (first derivative) are zero since this is the free end of a cantilever beam. The pressure (second derivative) is also zero (no load). Since the bottom-most strain gage is located at some distance from the base of the wall (Section 3.5.1), the boundary conditions at this location are thus not known. In order to estimate these a polynomial least-square fit is made of the data points at each time step. A third or fourth order fit is done and the base boundary conditions are determined from this. Once this is done, the quintic spline is fitted to the data points and the moment distribution determined from this fit at each time step.

If no pressure transducers are used, the moment distributions are numerically differentiated with a fourth order finite difference scheme, once to obtain the shears and once more to obtain pressures. (This is why a quintic-spline was used, since a cubic spline would give straight line segments in the second derivative.) However, due to the instabilities of numerical differentiation, it was determined that first derivatives were marginally satisfactory and second derivatives very inaccurate (recall Figure 3.29). This spawned the use of pressure transducers in tests.

When pressure transducers were used (all the tests except the first one) at each time step, the pressure transducer data points were polynomial fitted and a cubic spline fitted in a manner similar to the moments. An advantage of the cubic spline is that it requires no boundary conditions to be specified. The pressure distribution at each time step is thus read directly from the spline. The location of the resultants is then determined by finding the centroids of the pressure distributions. The shear distributions are obtained by direct trapezoidal rule integration of the pressure distributions. Numerical integration, as opposed to differentiation, is stable and accurate.

The following step is to determine the displacements at the top and bottom of the wall for every time step. The accelerograms are integrated twice and the Δ-beam readings are used to tie in the initial and final conditions. (In the case of the free-field accelerometer, the initial and final displacements are assumed to be zero). The displacement distributions along the wall are then determined by integrating the moments twice and using the end displacements to find the two constants of integration required (see Section 3.5.4). The velocities at the accelerometer locations are also calculated in this process.

After each parameter distribution was determined, the corresponding printing and plotting described in the previous section was done.

The data processing procedure is outlined in the flow chart of program WALL in Figure 4.7.

FLOWCHART FOR PROGRAM "WALL"

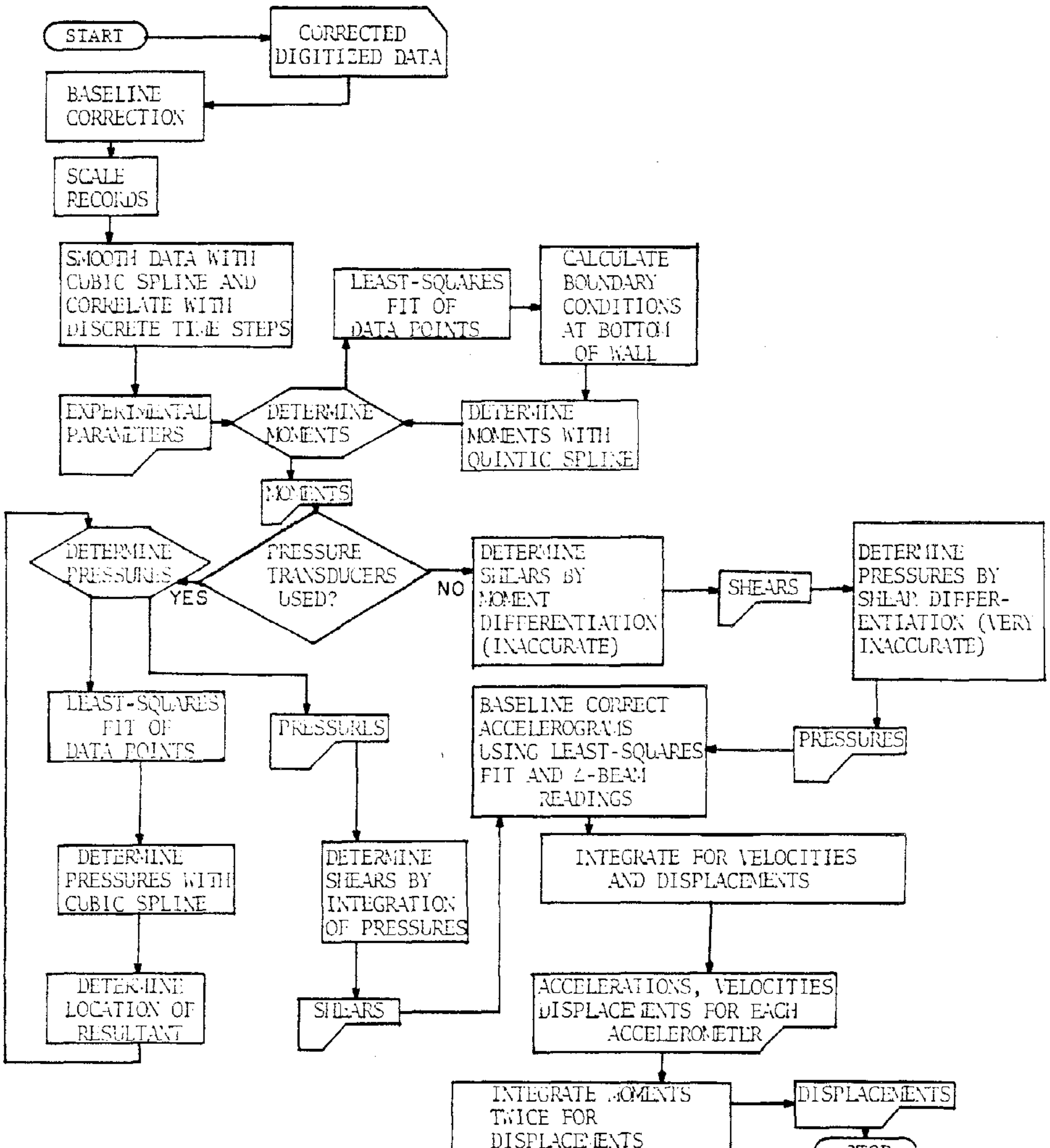

FIGURE 4.7

CHAPTER V

RESULTS

5.1. Dimensionless Groups

Henceforth, for convenience, all parameters will be discussed as dimensionless groups. This will make the discussion indifferent as to model or prototype.

The principles of dimensional analysis (reference [3] and Appendix A) are used to determine the dimensionless groups. From the tests, the following parameters are involved in influencing the results:

TABLE 5.1

Parameters Involved in Tests

x - vertical location
H - height of wall
EI - stiffness of wall*
M - wall moment*
Q - wall shear force*
y - lateral displacement of wall
P - lateral earth pressure
γ - density of soil
ϕ - angle of internal friction of soil
e - soil void ratio
g - gravitational acceleration
a - lateral acceleration
v - lateral velocity
t - time
f_1 - fundamental frequency of system

*per unit width

Parameters like Young's Modulus, Poissons's ratio and wave velocities for the soil were not used since these imply the soil is elastic, and are items that can only be assumed, not measured.

Table 5.1 gives a total number of parameters n of 14. From the Buckingham Π theorem, the total number of independent dimensionless groups k that can be derived is n minus the rank r of the dimensional matrix:

$$k = n - r \tag{5.1}$$

For the parameters listed the dimensional matrix is shown as Table 5.2.

TABLE 5.2

Dimensional Matrix of Test Parameters

Parameter	Force (F)	Length (L)	Time (T)
x	0	1	0
H	0	1	0
EI	1	1	0
M	1	0	0
Q	1	−1	0
y	0	1	0
P	1	−2	0
γ	1	−3	0
ϕ	0	0	0
e	0	0	0
g	0	1	−2
a	0	1	−2
t	0	0	1
f_1	0	0	1
v	0	1	−1

The rank of the above matrix is 3. From equation (5.1), therefore, 12 independent dimensionless groups can be determined. They were chosen as follows:

TABLE 5.3

Dimensionless Parameters

Parameter	Symbol	Dimensionless Group
Location	x	x/H
Time	t	tf_1
Moment (bending)	M	MH/EI
Moment (overturning)	M	$6M/\gamma H^3$
Shear force	Q	$Q/(1/2\gamma H^2)$
Pressure	P	$P/\gamma H$
Displacement	y	y/H
Velocity	v	$v/f_1 H$
Acceleration	a	a/g
Friction angle	ϕ	ϕ
Void ratio	e	e
-	-	v^2/gH

In addition, the ratio of bending to overturning moment gives the non-independent dimensionless grouping $\gamma H^4/6EI$ which can be used as an indication of the relative stiffness of the wall-soil system.

In the following sections, unless otherwise noted, a reference to Pressure (P) will imply its dimensionless group ($P/\gamma H$), reference to time (t) will imply tf_1, and so forth. This will avoid any model/prototype confusion, and will also simplify the discussion.

5.2. The Experimental "Earthquake"

Although the "earthquake generating" mechanism employed in the experiment was quite simple, the recorded motions are such that they are within the realm of strong earthquake ground motions which have been recorded in reality.

The accelerograms recorded at the top and bottom of the wall, as well as the free field (i.e., in the backfill some distance behind the wall) during various experiments, are displayed in Figures 5.1a through 5.40a. Their corresponding velocities and displacements are shown in Figures 5.1b through 5.40b and 5.1c through 5.40c respectively.

The displacement curves include both the initial static displacements due to the backfill load (assuming that no backfill implies no wall deflection) plus those generated by the shaking. The magnitudes of the displacements prior to the earthquake are greater than 1/2% of the wall height which indicates a state of plastic equilibrium behind the wall, and thus the development of full active pressure.

From the accelerograms it can be seen that the general pattern of shaking is such as one would expect from the motion-generating mechanism involved, namely that of a decaying sinusoid. However, due to the inherent complexity of the experimental system, this basic pattern is enhanced by some extra acceleration noise probably generated from reverberations, collisions, nonlinearities, etc., of the

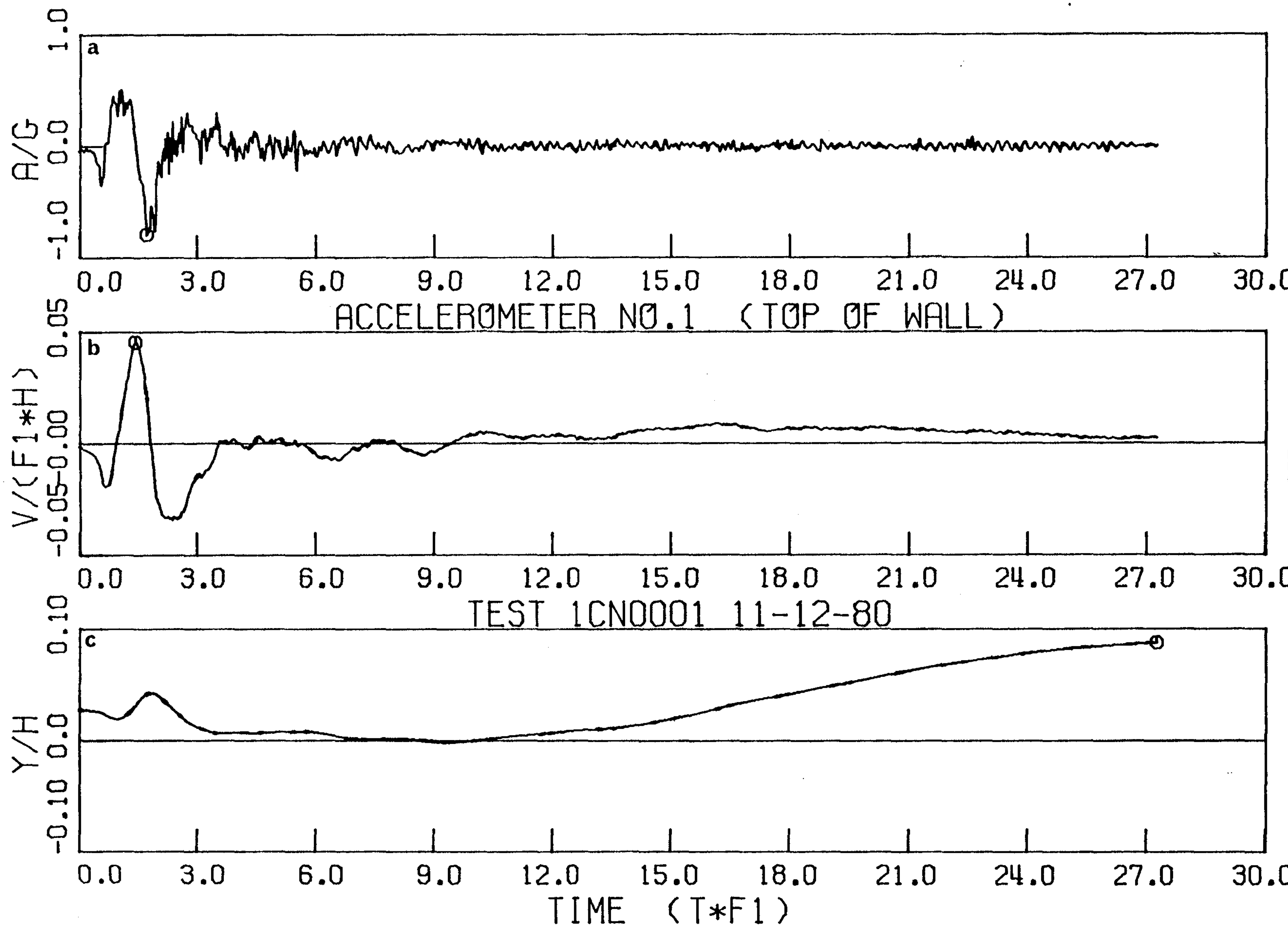
a
A/G
1.0
0.0
-1.0
0.0
3.0
6.0
9.0
12.0
15.0
18.0
21.0
24.0
27.0
30.0
ACCELEROMETER NO.1 (TOP OF WALL)
b
V/(F1*H)
0.05
0.00
-0.05
TEST 1CN0001 11-12-80
c
Y/H
0.10
0.0
-0.10
TIME (T*F1)

FIGURE 5.1

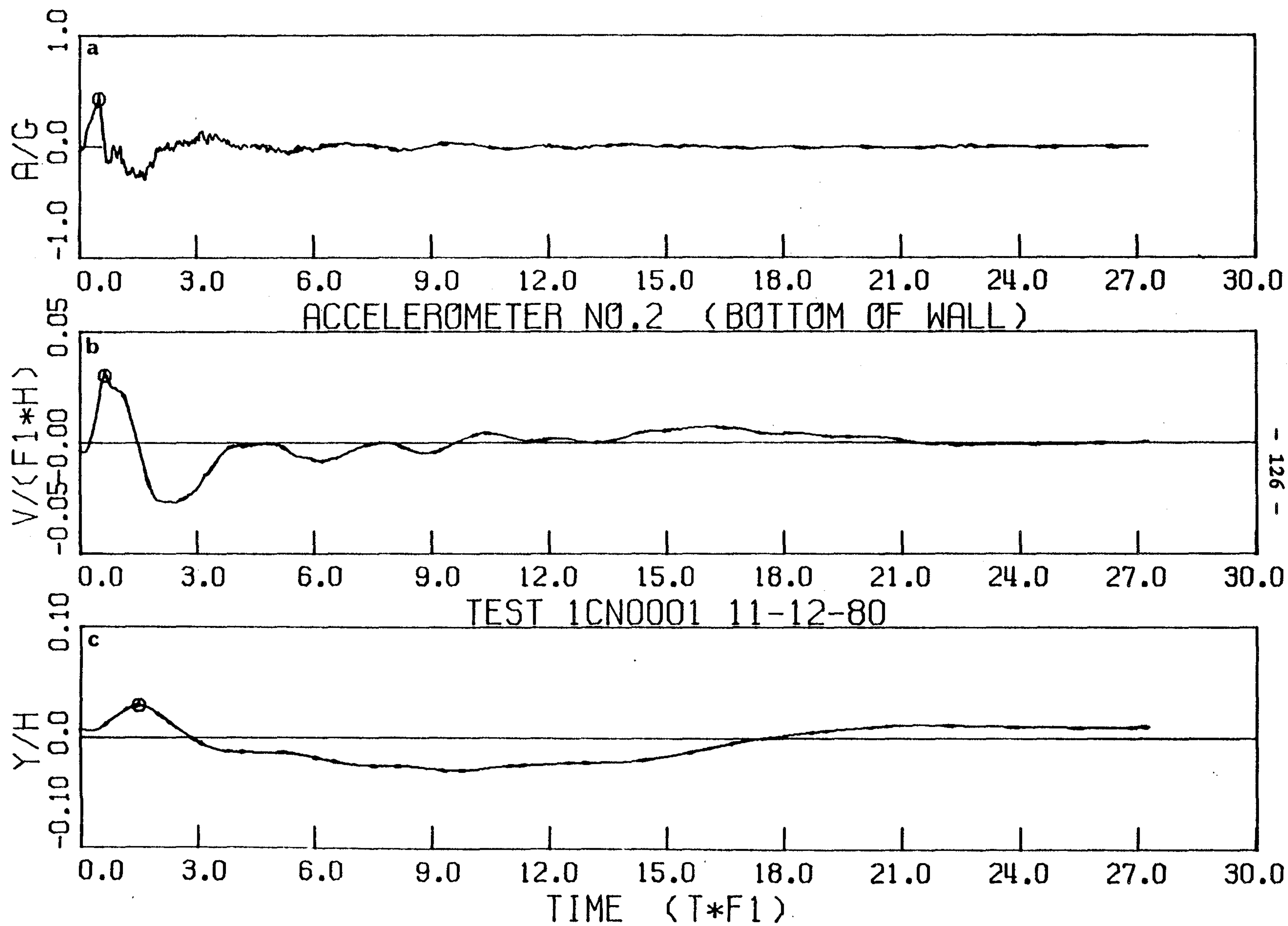
a
b
c
A/G
1.0
0.0
-1.0
V/(F1*H)
0.05
-0.00
-0.05
Y/H
0.10
0.0
-0.10
0.0 3.0 6.0 9.0 12.0 15.0 18.0 21.0 24.0 27.0 30.0
ACCELEROMETER NO.2 (BOTTOM OF WALL)
TEST 1CN0001 11-12-80
TIME (T*F1)

FIGURE 5.2

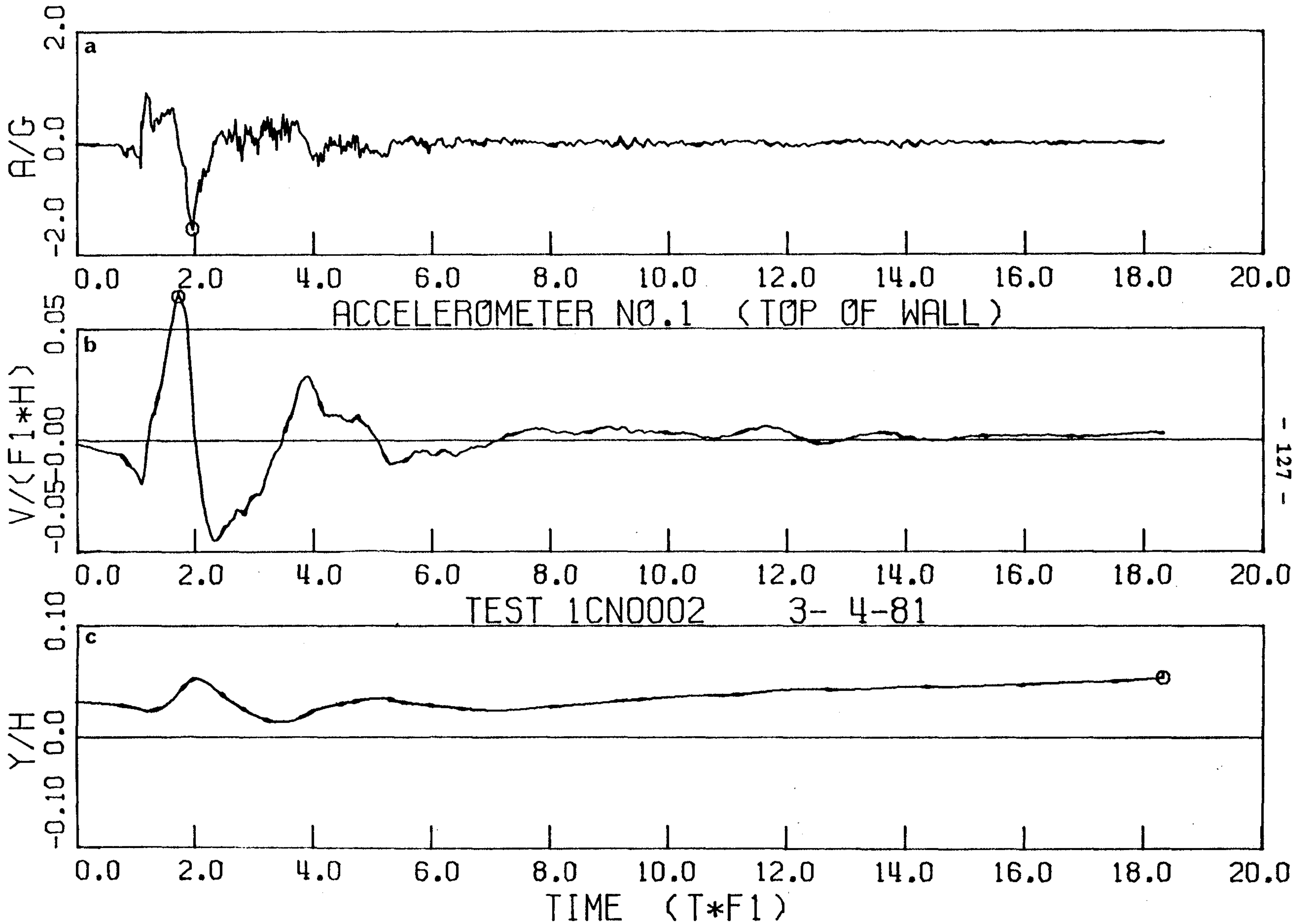
a
A/G
2.0
0.0
-2.0
0.0
2.0
4.0
6.0
8.0
10.0
12.0
14.0
16.0
18.0
20.0
ACCELERØMETER NØ.1 (TØP ØF WALL)
b
V/(F1*H)
0.05
0.00
-0.05
TEST 1CN0002 3- 4-81
c
Y/H
0.10
0.0
-0.10
TIME (T*F1)

FIGURE 5.3

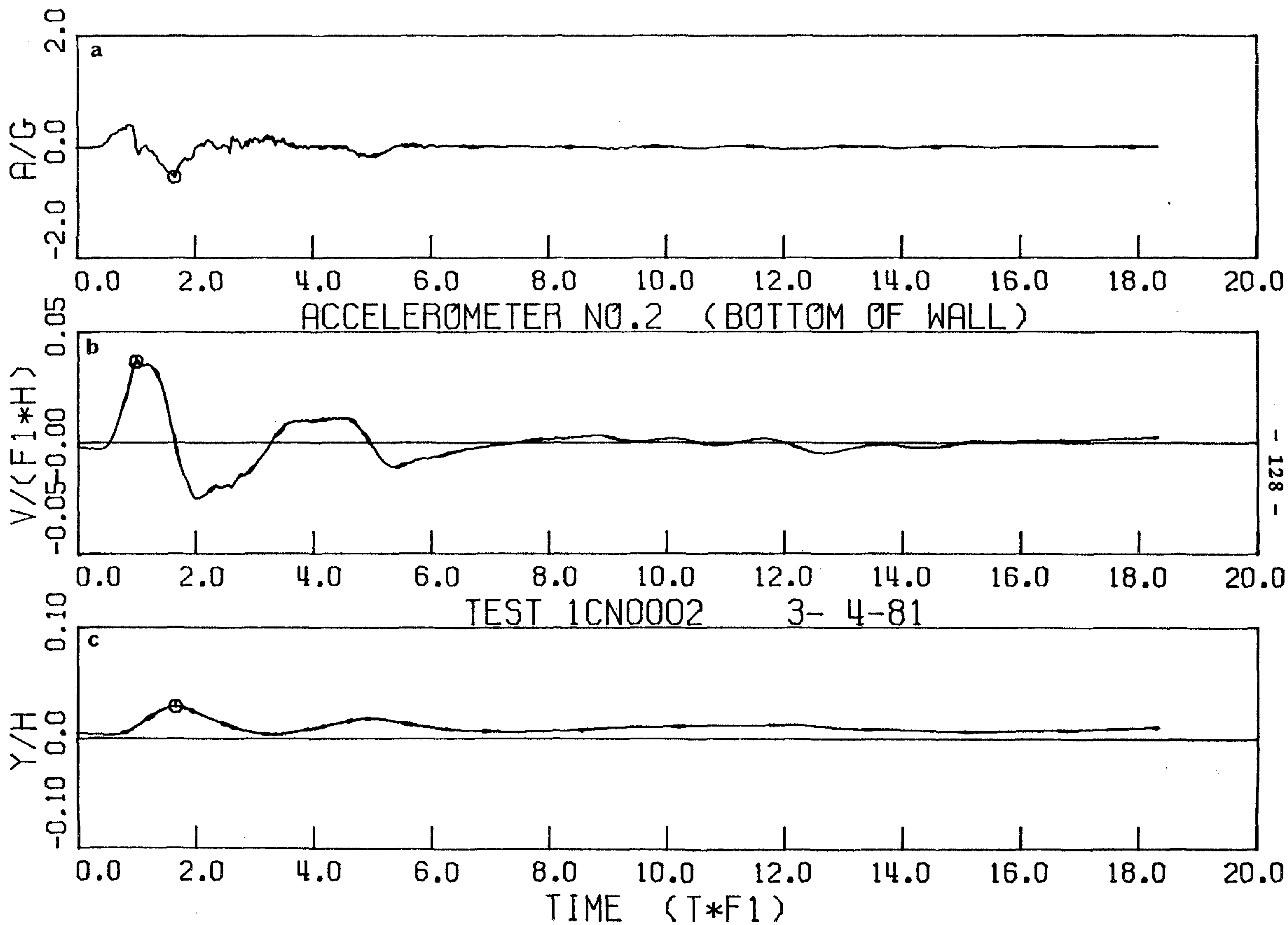

a
A/G
2.0
0.0
-2.0
0.0 2.0 4.0 6.0 8.0 10.0 12.0 14.0 16.0 18.0 20.0
ACCELERØMETER NØ.2 (BØTTØM ØF WALL)
b
V/(F1*H)
0.05
0.00
-0.05
0.0 2.0 4.0 6.0 8.0 10.0 12.0 14.0 16.0 18.0 20.0
TEST 1CN0002 3- 4-81
c
Y/H
0.10
0.0
-0.10
0.0 2.0 4.0 6.0 8.0 10.0 12.0 14.0 16.0 18.0 20.0
TIME (T*F1)

FIGURE 5.4

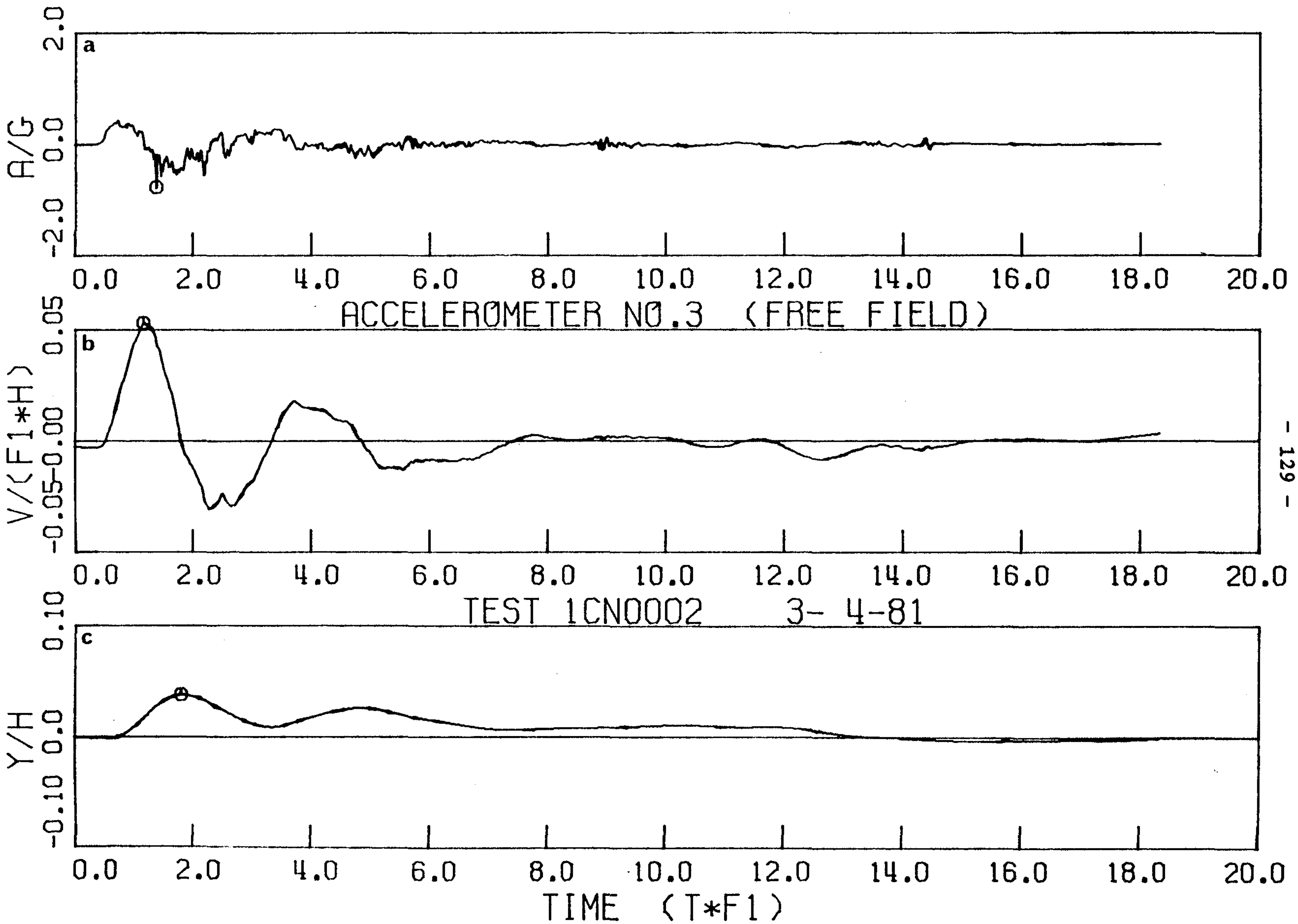
a
A/G
2.0
0.0
-2.0
0.0 2.0 4.0 6.0 8.0 10.0 12.0 14.0 16.0 18.0 20.0
ACCELERØMETER NØ.3 (FREE FIELD)
b
V/(F1*H)
0.05
0.00
-0.05
0.0 2.0 4.0 6.0 8.0 10.0 12.0 14.0 16.0 18.0 20.0
TEST 1CN0002 3- 4-81
c
Y/H
0.10
0.0
-0.10
0.0 2.0 4.0 6.0 8.0 10.0 12.0 14.0 16.0 18.0 20.0
TIME (T*F1)

FIGURE 5.5

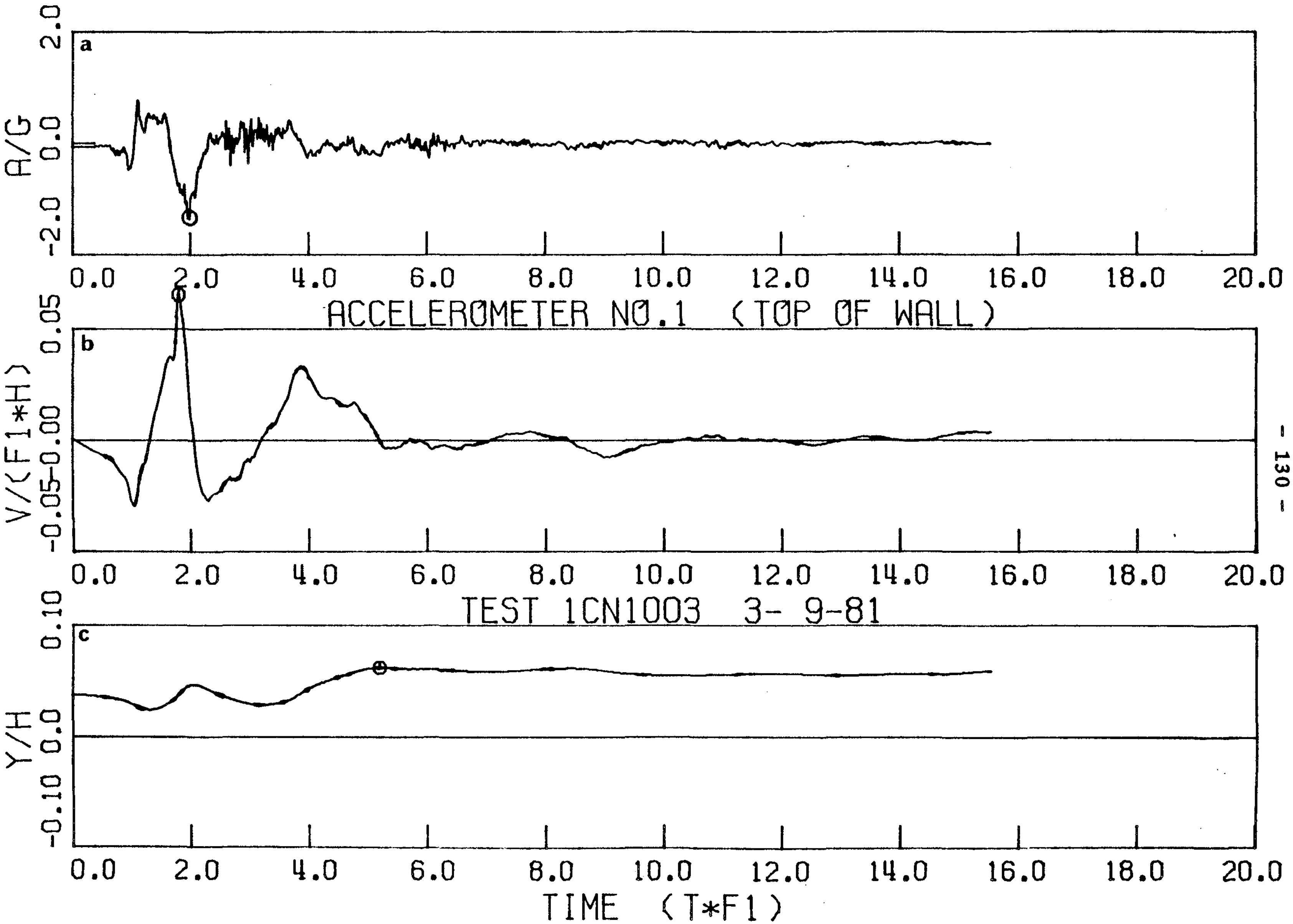

a
b
c
A/G
2.0
0.0
-2.0
ACCELEROMETER NO.1 (TOP OF WALL)
V/(F1*H)
0.05
-0.00
-0.05
TEST 1CN1003 3- 9-81
Y/H
0.10
0.0
-0.10
0.0
2.0
4.0
6.0
8.0
10.0
12.0
14.0
16.0
18.0
20.0
TIME (T*F1)

FIGURE 5.6

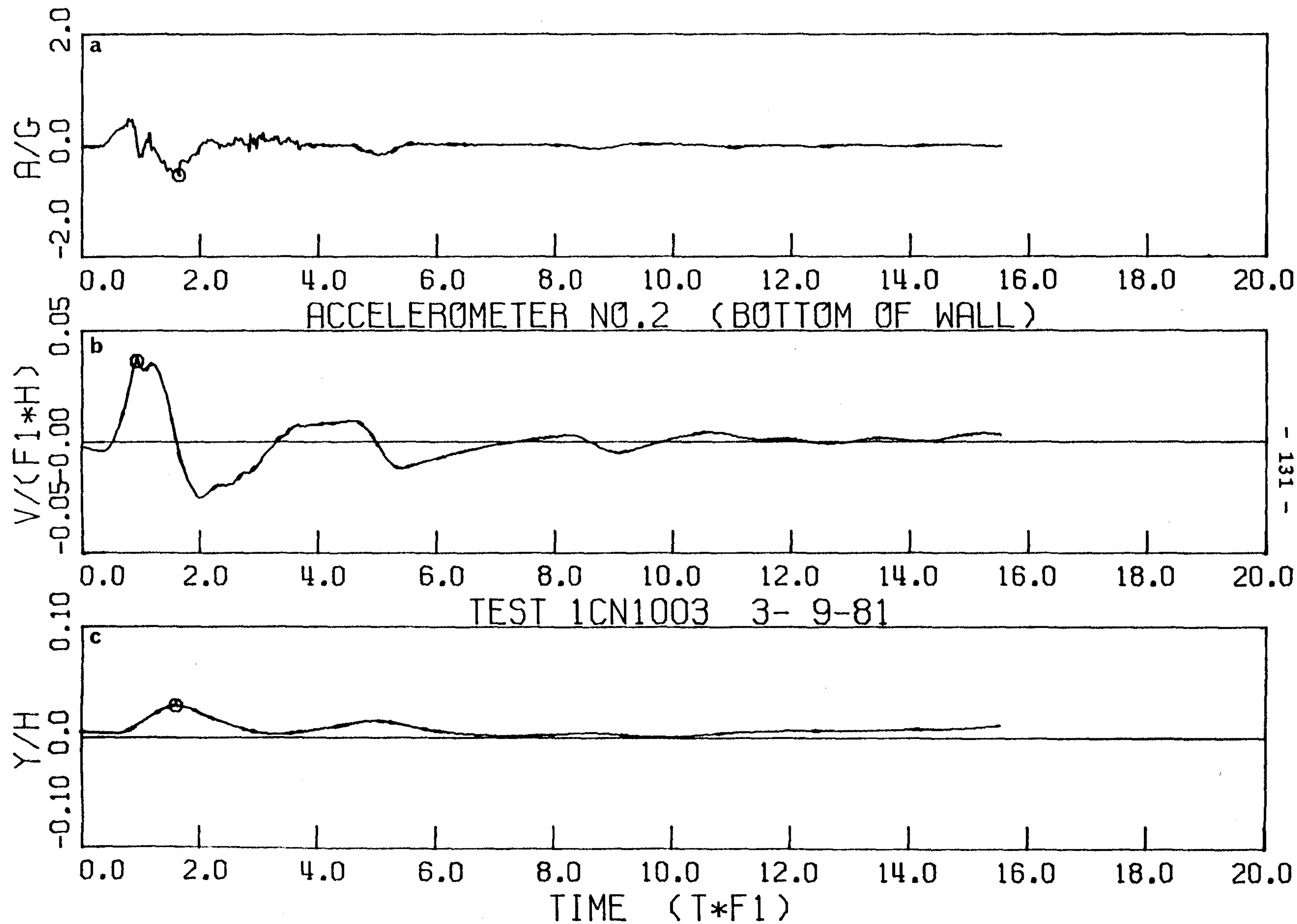
a
A/G
2.0
0.0
-2.0
0.0 2.0 4.0 6.0 8.0 10.0 12.0 14.0 16.0 18.0 20.0
ACCELEROMETER NO.2 (BOTTOM OF WALL)
b
V/(F1*H)
0.05
0.00
-0.05
0.0 2.0 4.0 6.0 8.0 10.0 12.0 14.0 16.0 18.0 20.0
TEST 1CN1003 3- 9-81
c
Y/H
0.10
0.0
-0.10
0.0 2.0 4.0 6.0 8.0 10.0 12.0 14.0 16.0 18.0 20.0
TIME (T*F1)

FIGURE 5.7

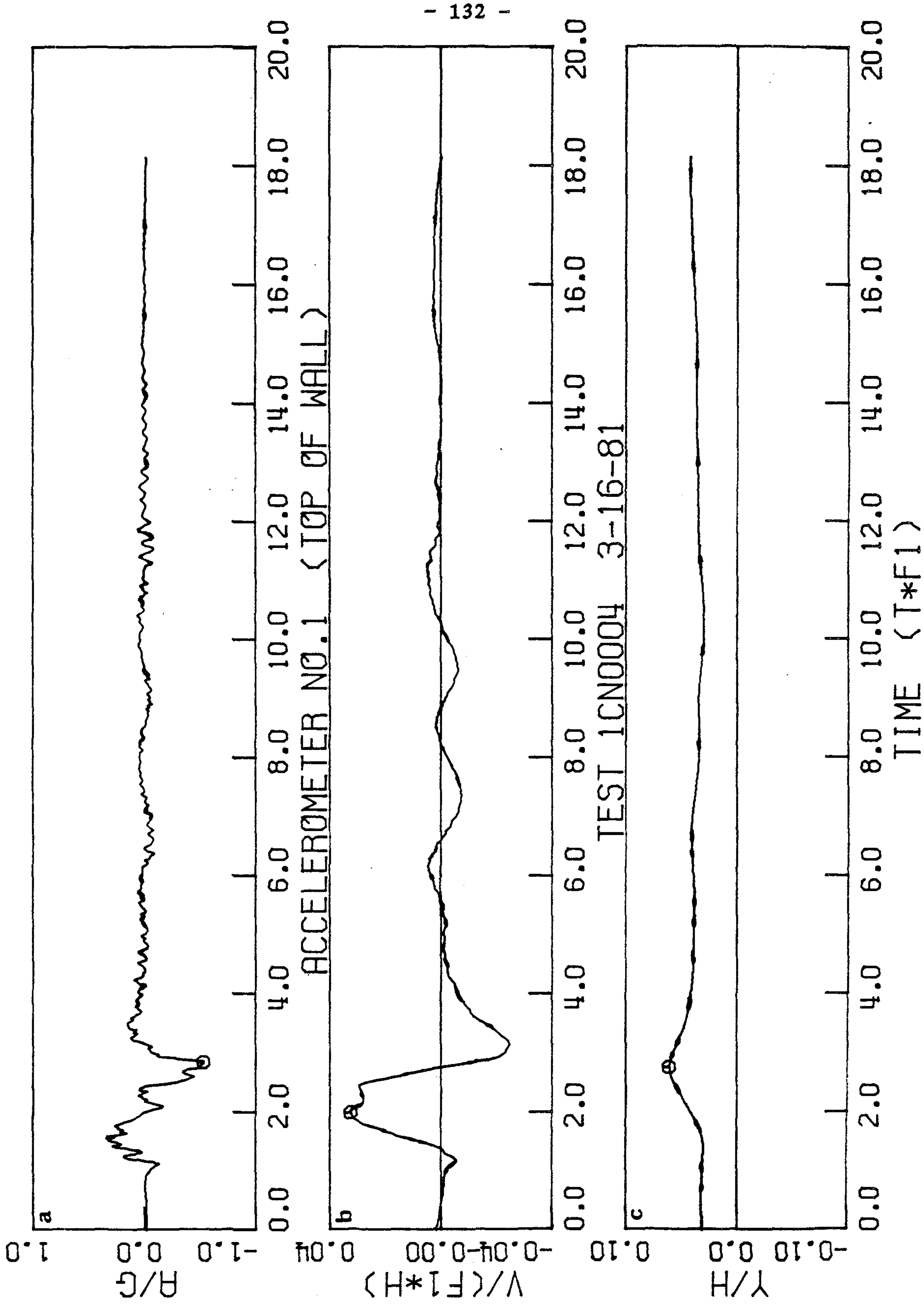
ACCELEROMETER NO.1 (TOP OF WALL)
TEST 1CN0004 3-16-81
A/G
1.0
0.0
-1.0
V/(F1*H)
0.04
0.00
-0.04
Y/H
0.10
0.0
-0.10
a
b
c
0.0
2.0
4.0
6.0
8.0
10.0
12.0
14.0
16.0
18.0
20.0
TIME (T*F1)

FIGURE 5.8

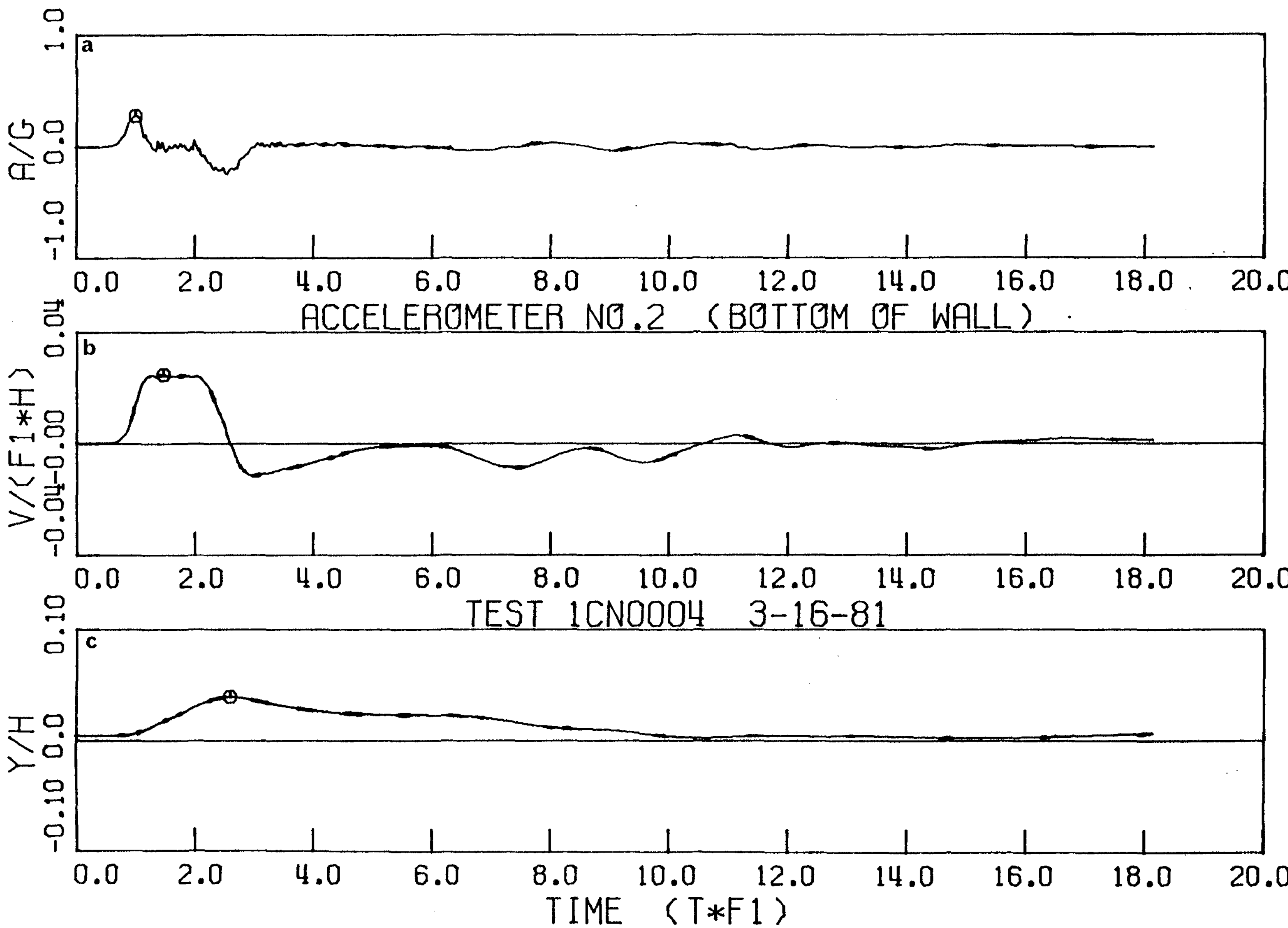
A/G
1.0
0.0
-1.0
a
ACCELEROMETER NO.2 (BOTTOM OF WALL)
V/(F1*H)
0.04
0.00
-0.04
b
TEST 1CN0004 3-16-81
Y/H
0.10
0.0
-0.10
c
0.0 2.0 4.0 6.0 8.0 10.0 12.0 14.0 16.0 18.0 20.0
TIME (T*F1)

FIGURE 5.9

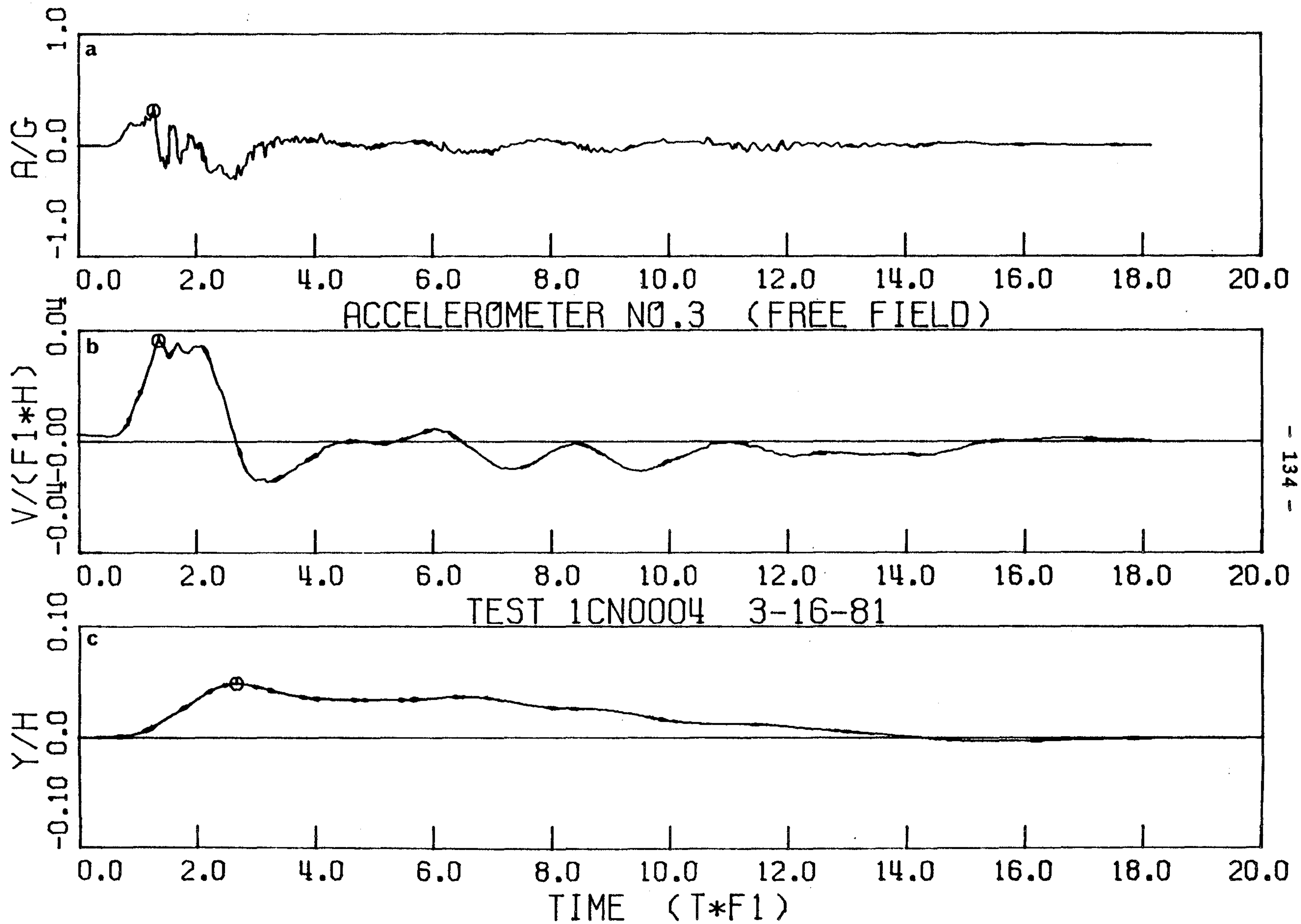
1.0
A/G 0.0
-1.0
a
0.0 2.0 4.0 6.0 8.0 10.0 12.0 14.0 16.0 18.0 20.0
ACCELERØMETER NØ.3 (FREE FIELD)
0.04
V/(F1*H) -0.00
-0.04
b
0.0 2.0 4.0 6.0 8.0 10.0 12.0 14.0 16.0 18.0 20.0
TEST 1CN0004 3-16-81
0.10
Y/H 0.0
-0.10
c
0.0 2.0 4.0 6.0 8.0 10.0 12.0 14.0 16.0 18.0 20.0
TIME (T*F1)

FIGURE 5.10

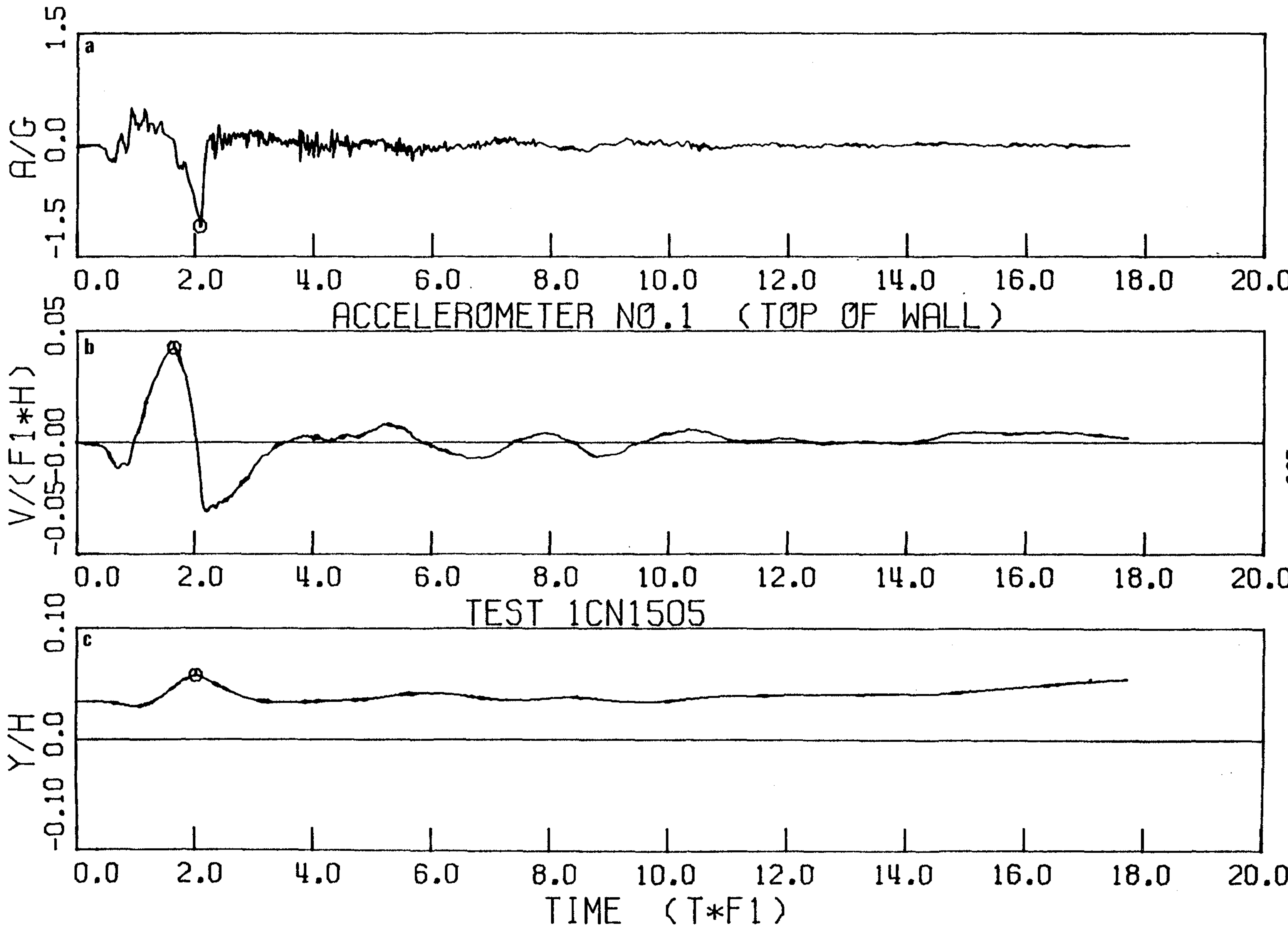
A/G
1.5
0.0
-1.5
a
0.0 2.0 4.0 6.0 8.0 10.0 12.0 14.0 16.0 18.0 20.0
ACCELERØMETER NØ.1 (TØP ØF WALL)
V/(F1*H)
0.05
0.00
-0.05
b
0.0 2.0 4.0 6.0 8.0 10.0 12.0 14.0 16.0 18.0 20.0
TEST 1CN1505
Y/H
0.10
0.0
-0.10
c
0.0 2.0 4.0 6.0 8.0 10.0 12.0 14.0 16.0 18.0 20.0
TIME (T*F1)

FIGURE 5.11

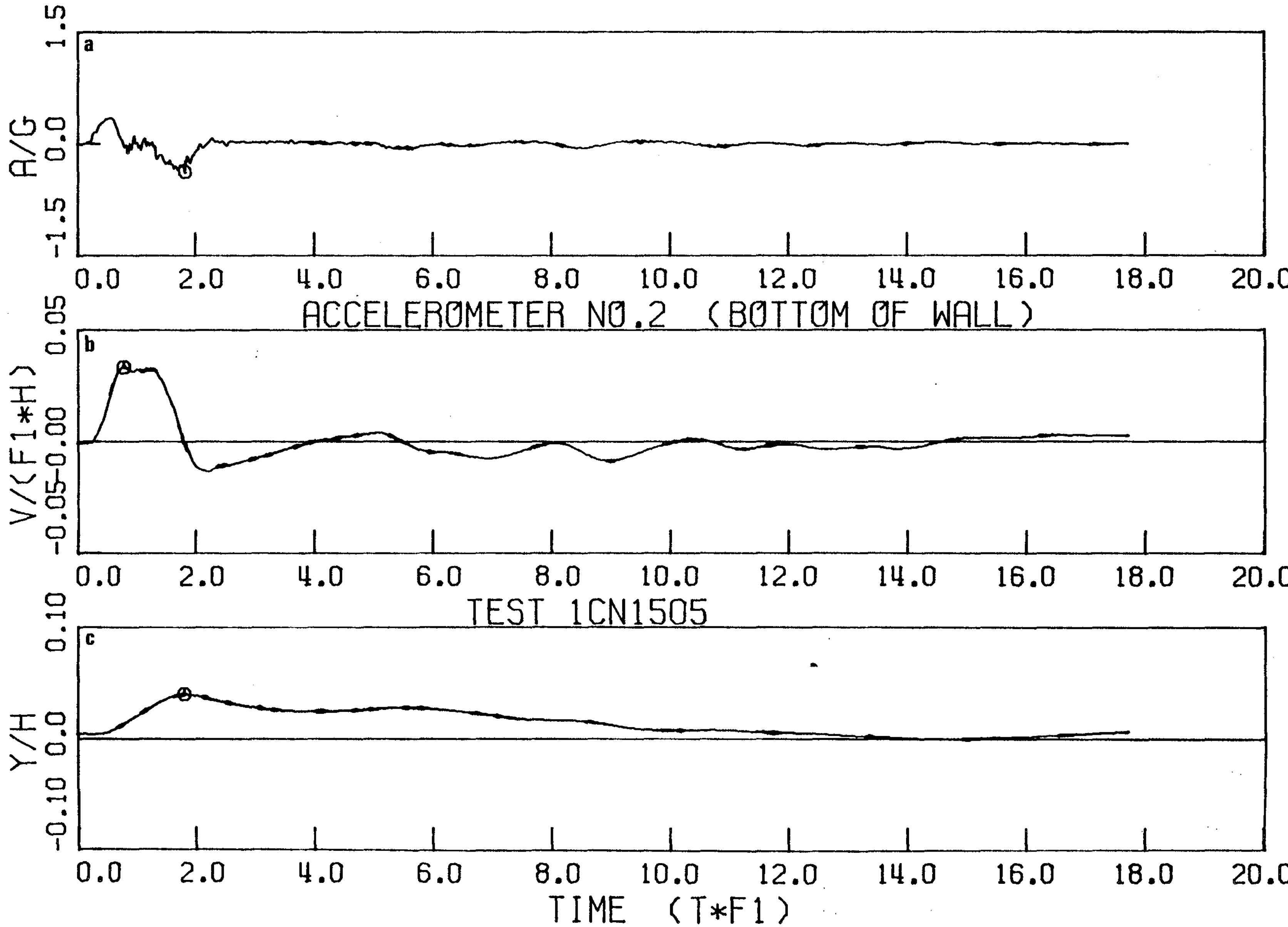

ACCELEROMETER NO.2 (BOTTOM OF WALL)
TEST 1CN1505
A/G
V/(F1*H)
Y/H
a
b
c
1.5
0.0
-1.5
0.05
0.00
-0.05
0.10
0.0
-0.10
0.0
2.0
4.0
6.0
8.0
10.0
12.0
14.0
16.0
18.0
20.0
TIME (T*F1)

FIGURE 5.12

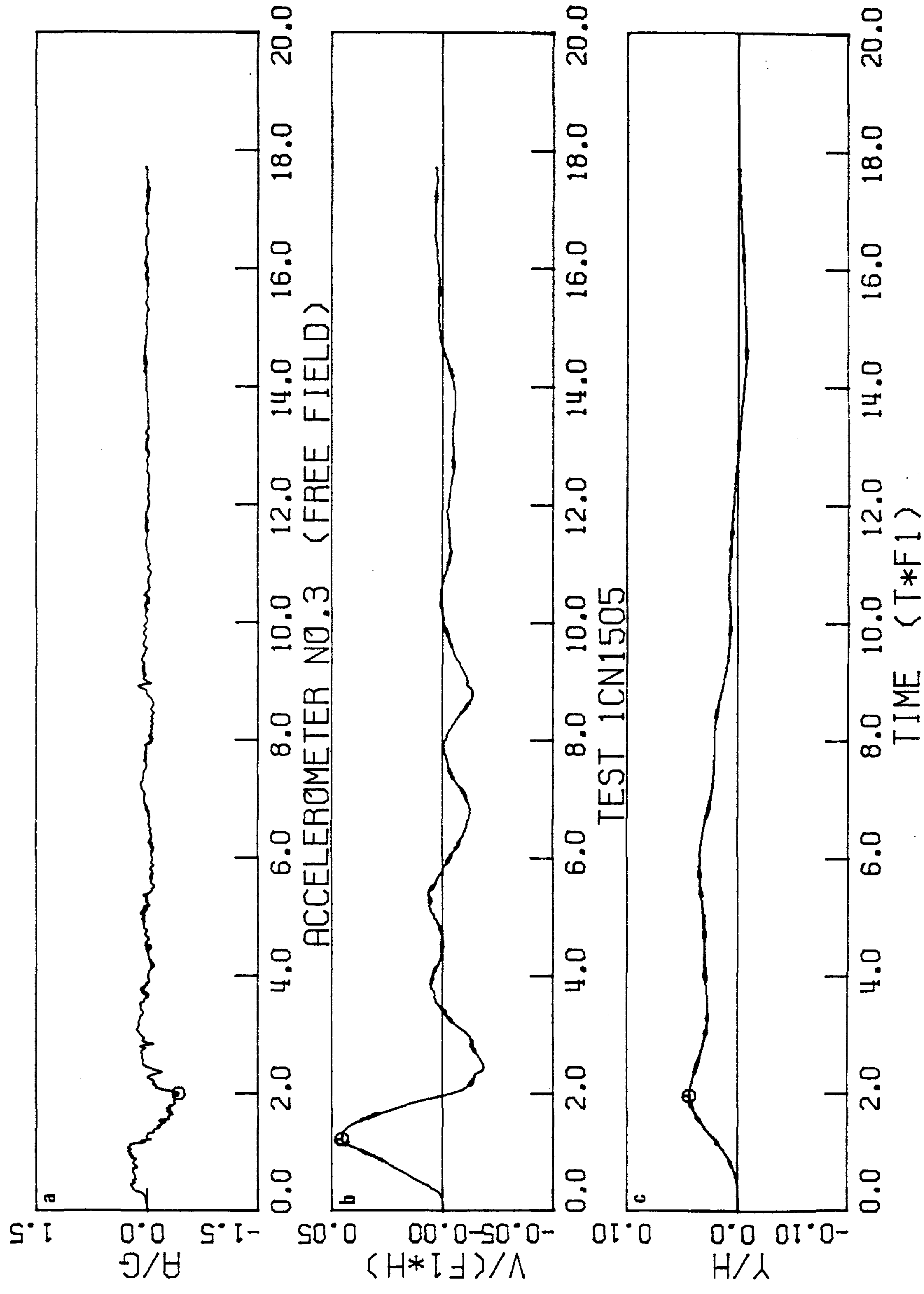
ACCELEROMETER NØ.3 (FREE FIELD)
TEST 1CN1505
TIME (T*F1)
A/G
V/(F1*H)
Y/H
a
b
c
1.5
0.0
-1.5
0.05
0.00
-0.05
0.10
-0.10
0.0
2.0
4.0
6.0
8.0
10.0
12.0
14.0
16.0
18.0
20.0

FIGURE 5.13

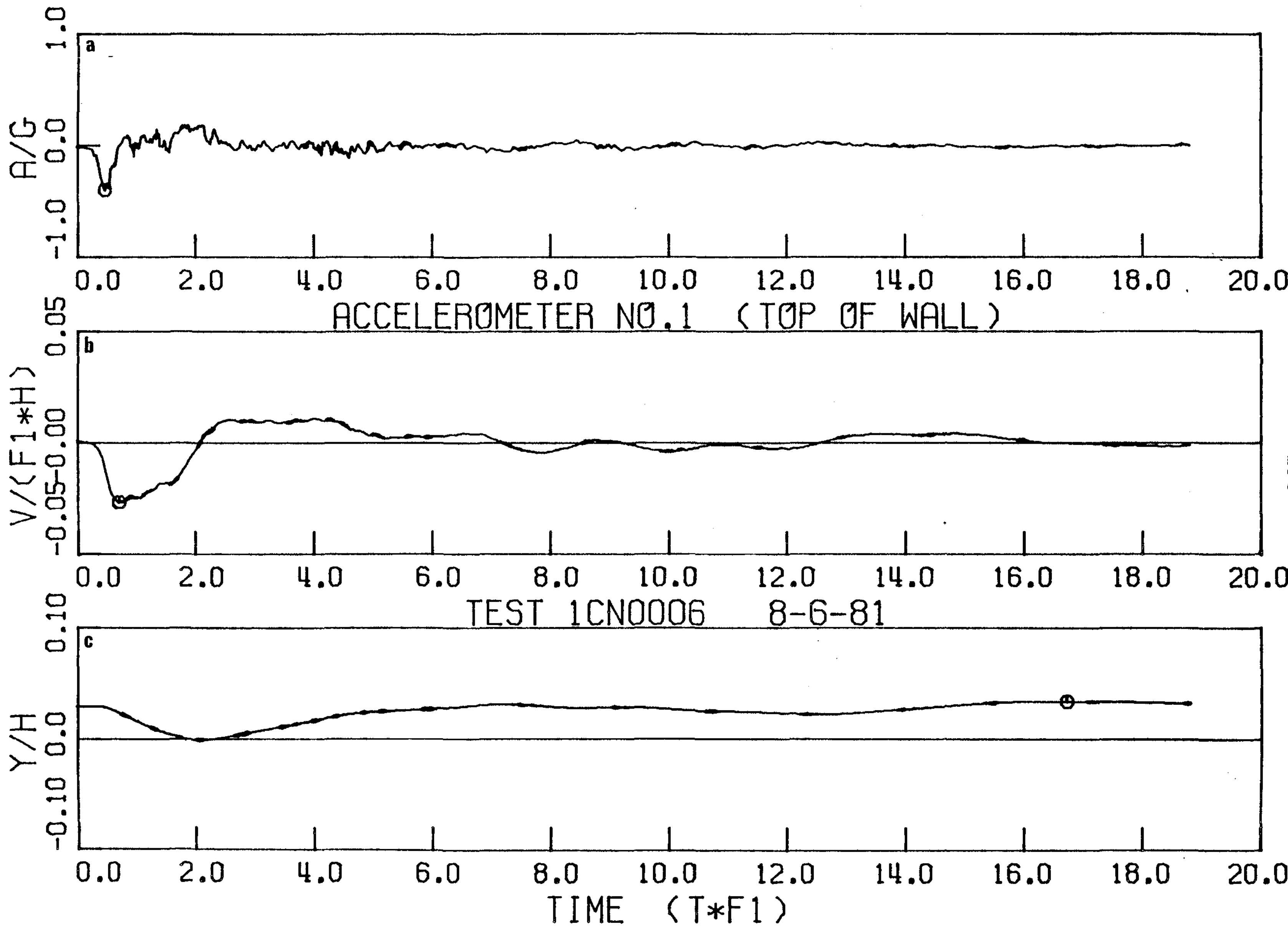
1.0
A/G
0.0
-1.0
a
0.0
2.0
4.0
6.0
8.0
10.0
12.0
14.0
16.0
18.0
20.0
ACCELERØMETER NØ.1 (TØP ØF WALL)
0.05
V/(F1*H)
-0.00
-0.05
b
TEST 1CN0006 8-6-81
0.10
Y/H
0.0
-0.10
c
TIME (T*F1)

FIGURE 5.14

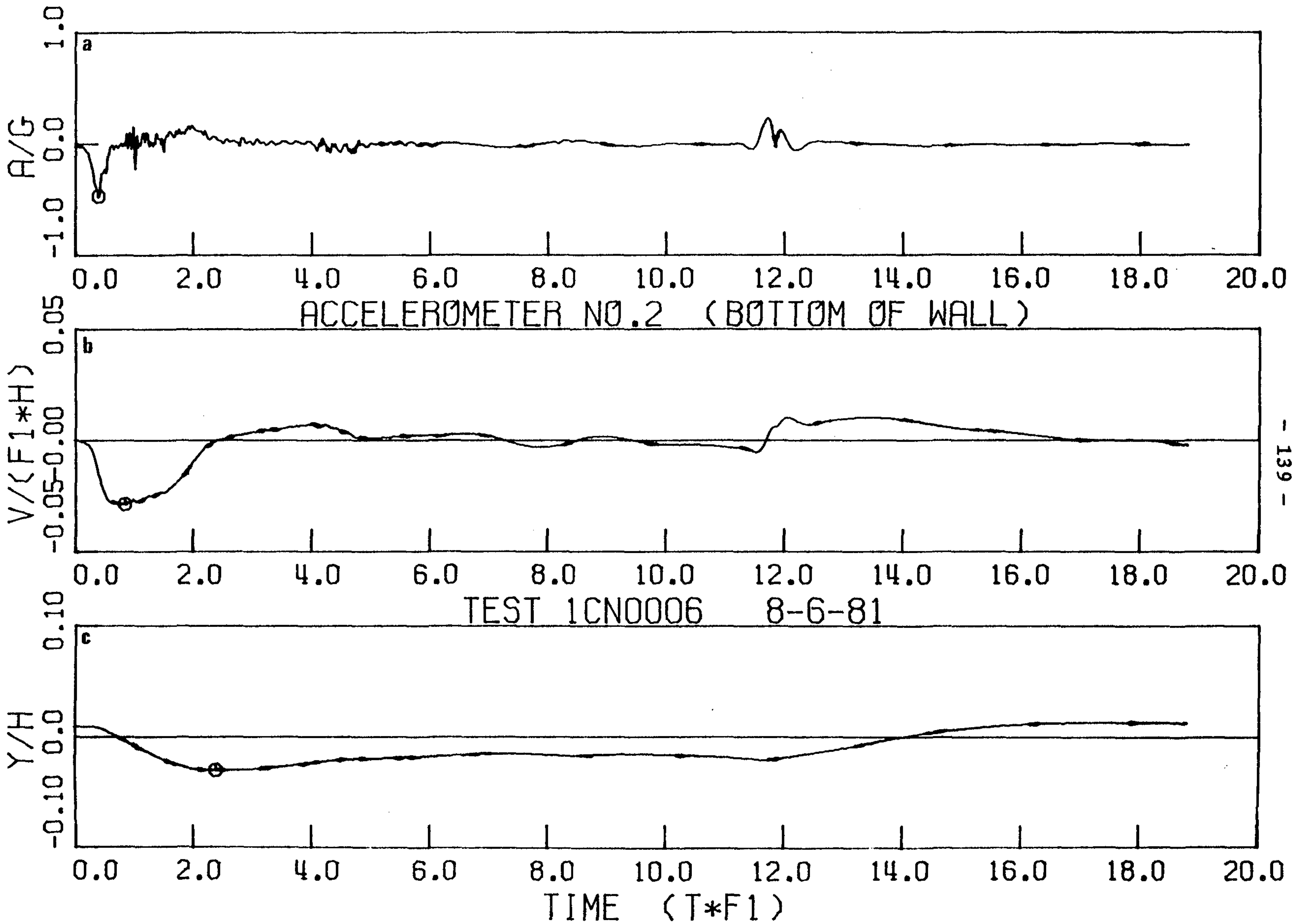
a
A/G
1.0
0.0
-1.0
0.0
2.0
4.0
6.0
8.0
10.0
12.0
14.0
16.0
18.0
20.0
ACCELERØMETER NØ.2 (BØTTØM ØF WALL)
b
V/(F1*H)
0.05
-0.00
-0.05
TEST 1CN0006 8-6-81
c
Y/H
0.10
0.0
-0.10
TIME (T*F1)

FIGURE 5.15

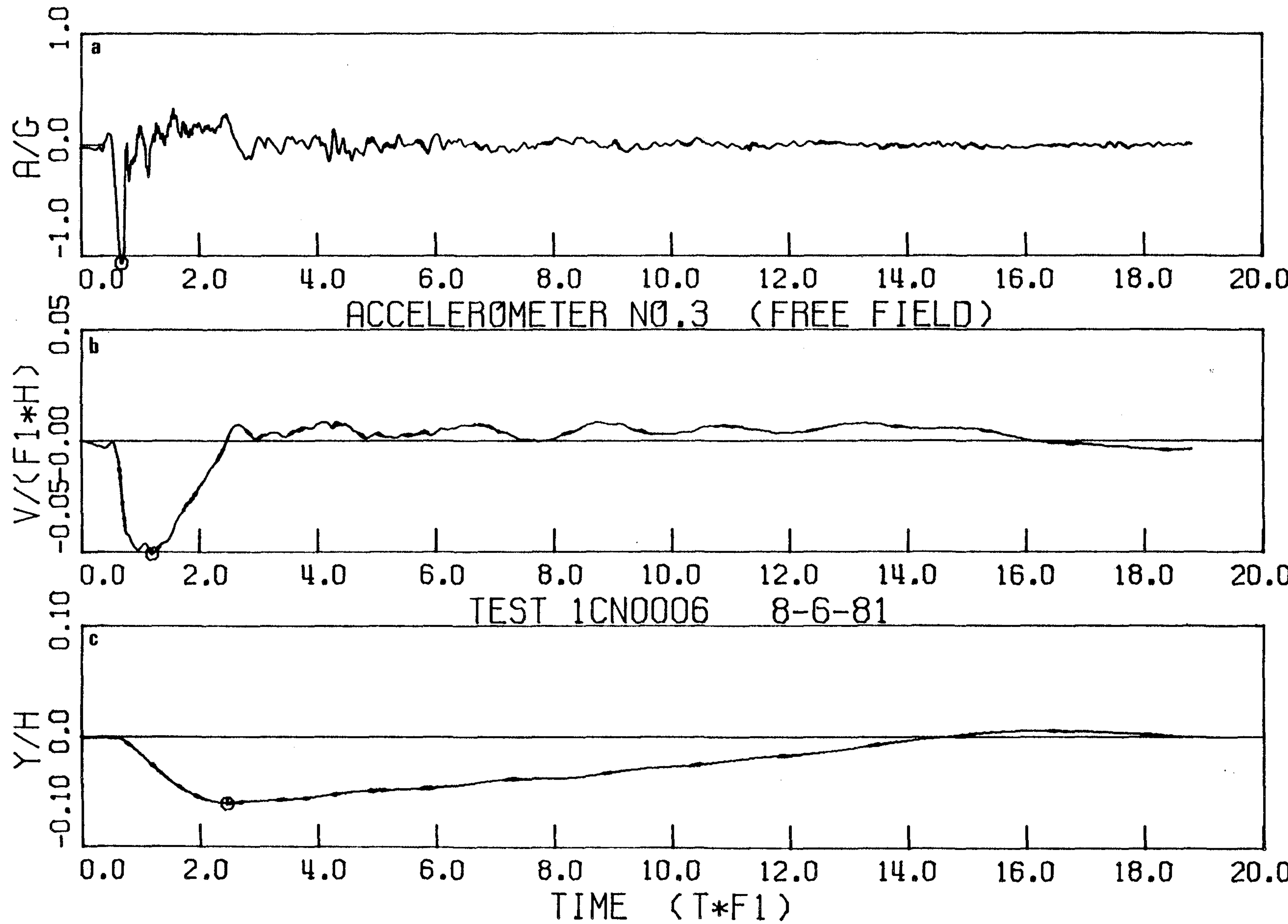
a
A/G
1.0
0.0
-1.0
0.0 2.0 4.0 6.0 8.0 10.0 12.0 14.0 16.0 18.0 20.0
ACCELERØMETER NØ.3 (FREE FIELD)
b
V/(F1*H)
0.05
0.00
-0.05
0.0 2.0 4.0 6.0 8.0 10.0 12.0 14.0 16.0 18.0 20.0
TEST 1CN0006 8-6-81
c
Y/H
0.10
0.0
-0.10
0.0 2.0 4.0 6.0 8.0 10.0 12.0 14.0 16.0 18.0 20.0
TIME (T*F1)

FIGURE 5.16

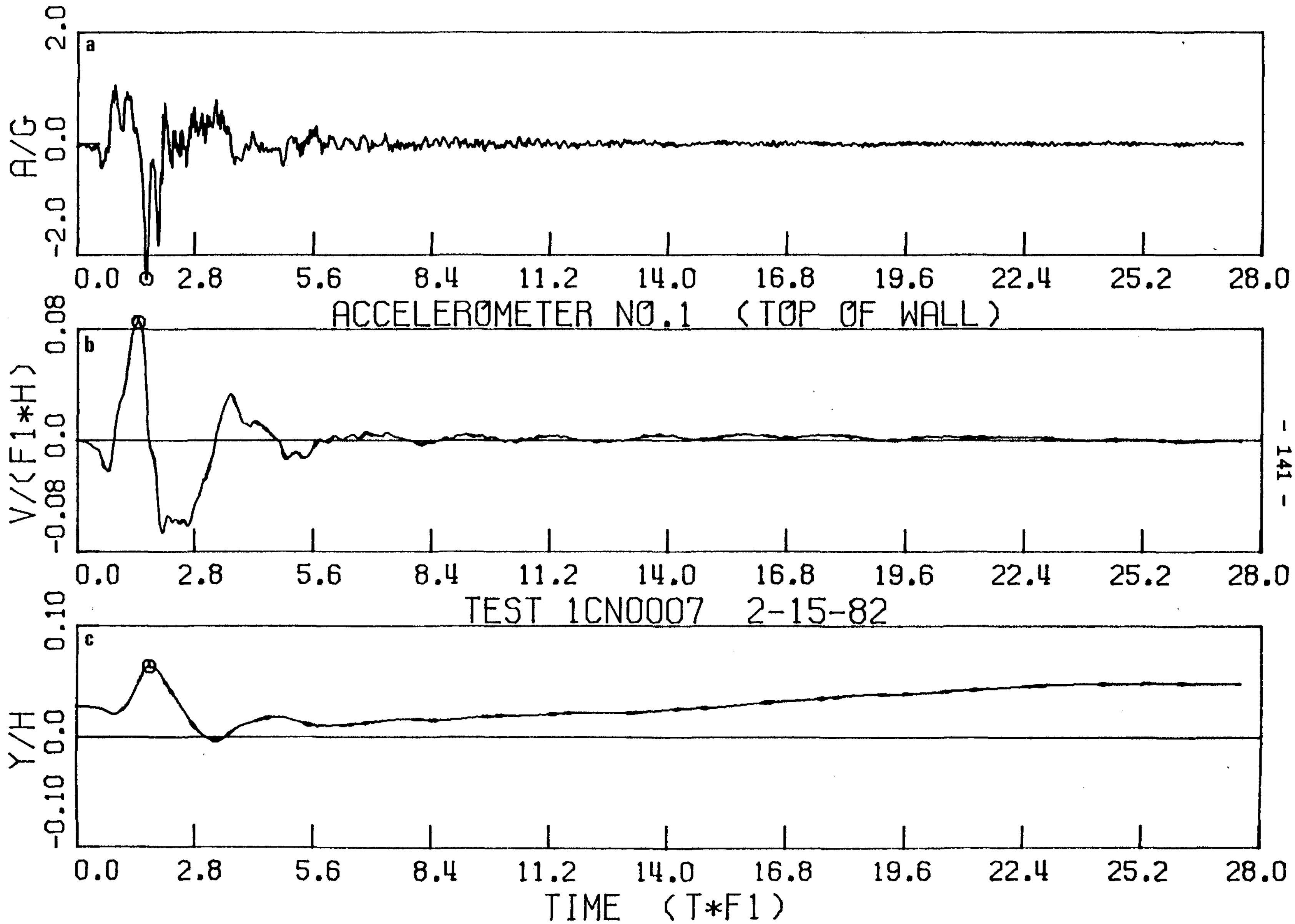
a
A/G
2.0
0.0
-2.0
0.0
2.8
5.6
8.4
11.2
14.0
16.8
19.6
22.4
25.2
28.0
ACCELEROMETER NO.1 (TOP OF WALL)
b
V/(F1*H)
0.08
0.0
-0.08
TEST 1CN0007 2-15-82
c
Y/H
0.10
0.0
-0.10
TIME (T*F1)

FIGURE 5.17

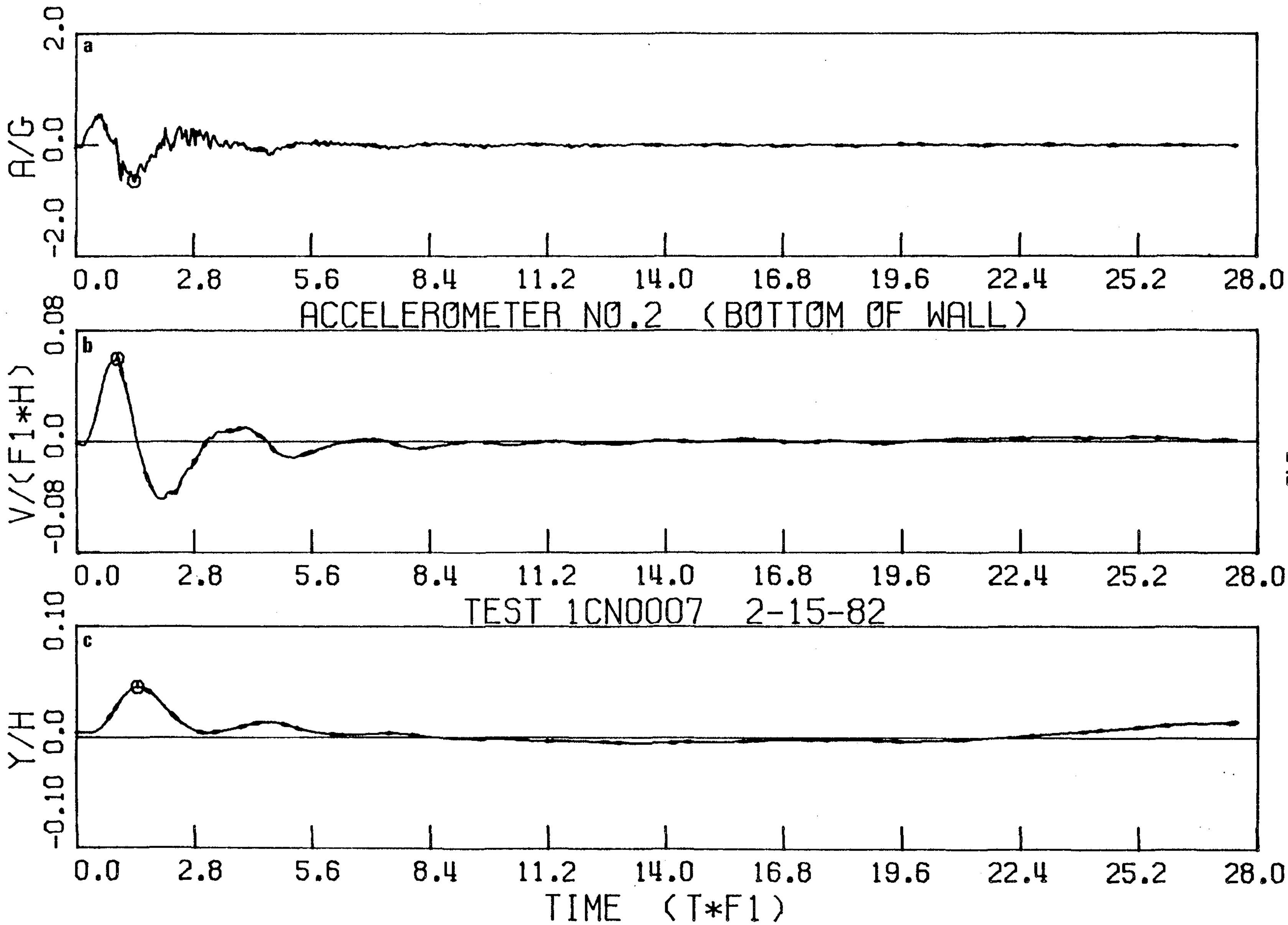
a
A/G
2.0
0.0
-2.0
0.0
2.8
5.6
8.4
11.2
14.0
16.8
19.6
22.4
25.2
28.0
ACCELERØMETER NØ.2 (BØTTØM ØF WALL)
b
V/(F1*H)
0.08
0.0
-0.08
TEST 1CN0007 2-15-82
c
Y/H
0.10
0.0
-0.10
TIME (T*F1)

FIGURE 5.18

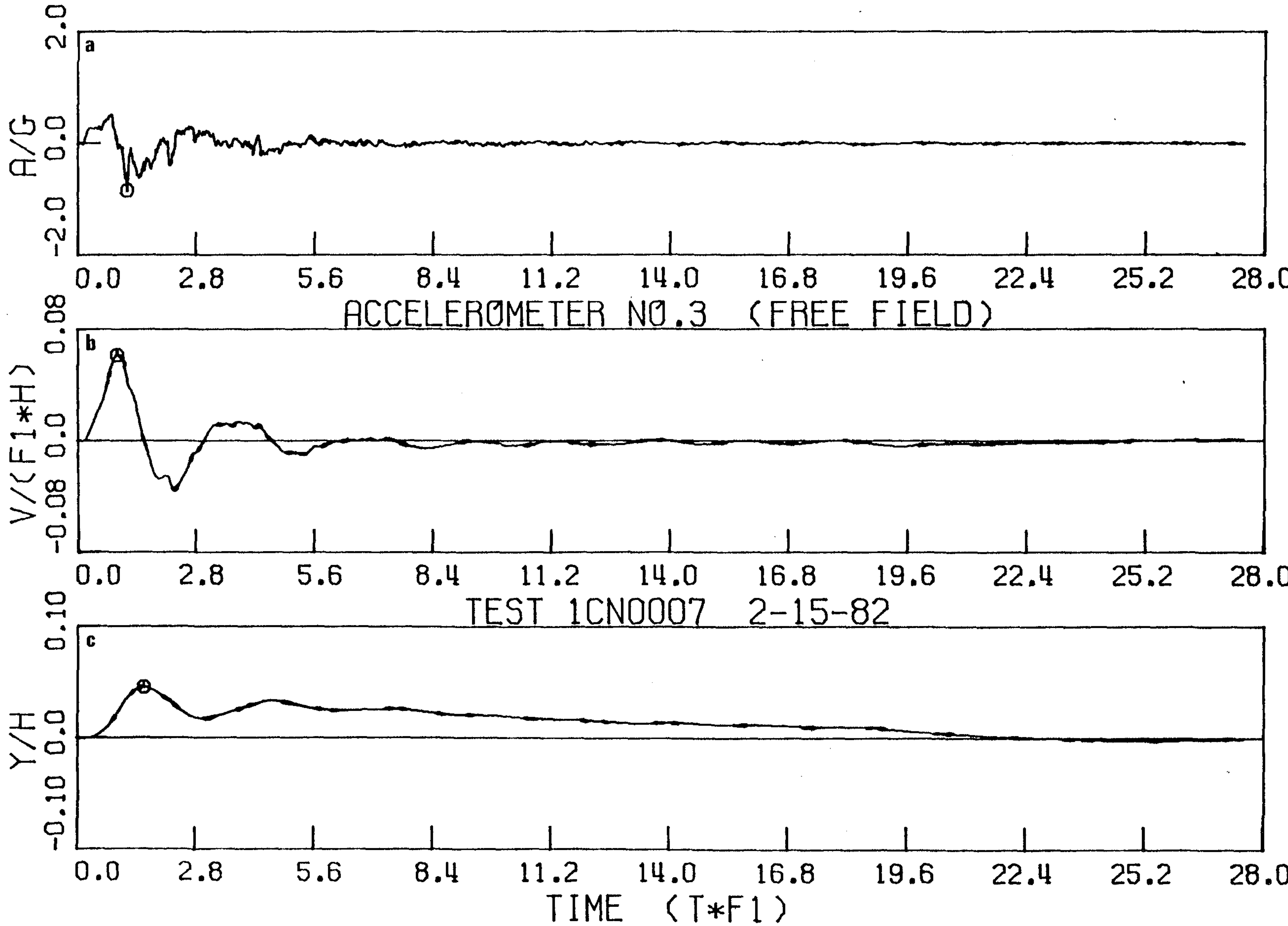
a
b
c
A/G
2.0
0.0
-2.0
V/(F1*H)
0.08
0.0
-0.08
Y/H
0.10
0.0
-0.10
0.0 2.8 5.6 8.4 11.2 14.0 16.8 19.6 22.4 25.2 28.0
ACCELEROMETER NO.3 (FREE FIELD)
TEST 1CN0007 2-15-82
TIME (T*F1)

FIGURE 5.19

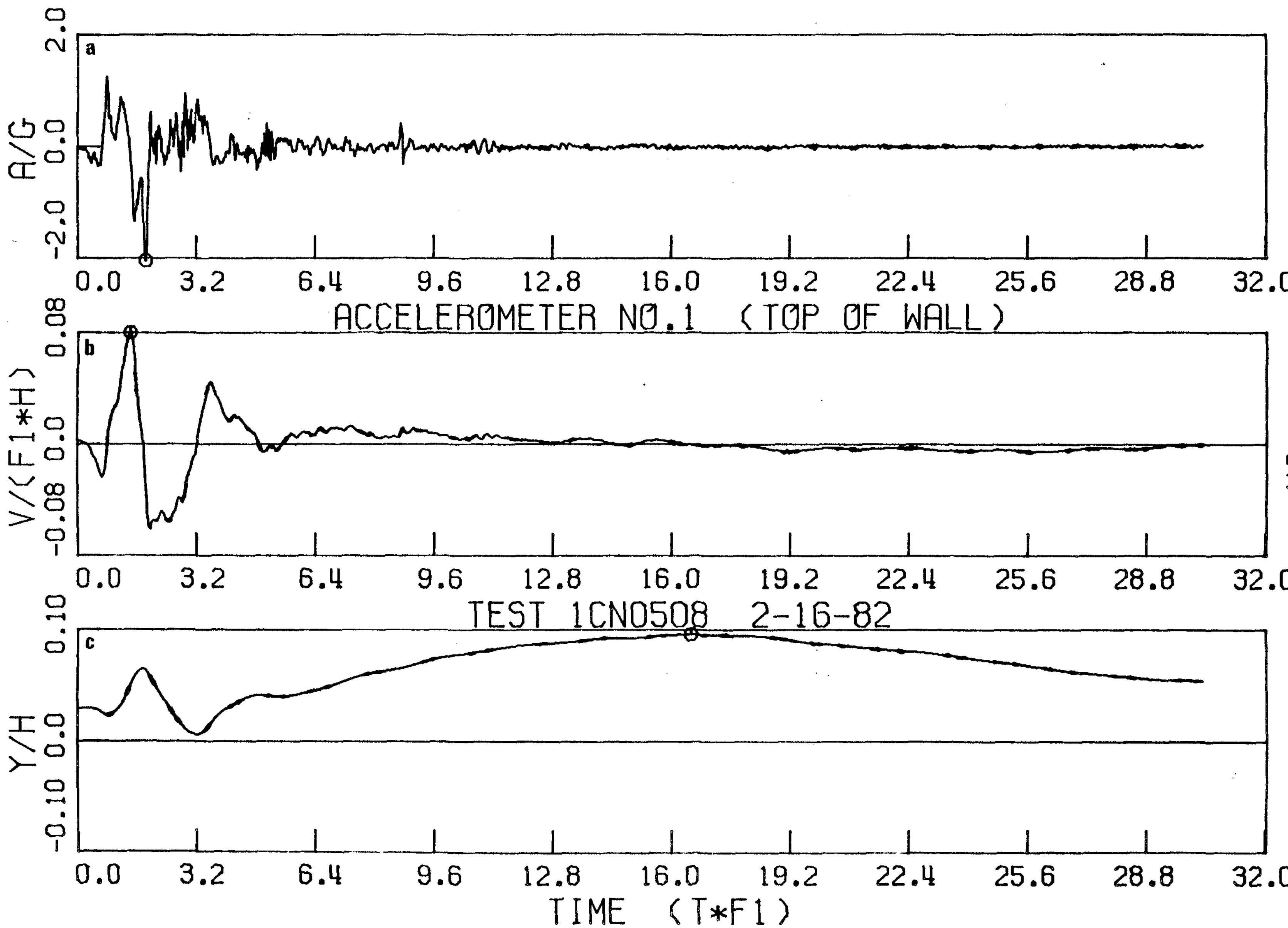
a
A/G
2.0
0.0
-2.0
0.0
3.2
6.4
9.6
12.8
16.0
19.2
22.4
25.6
28.8
32.0
ACCELEROMETER NO.1 (TOP OF WALL)
b
V/(F1*H)
0.08
0.0
-0.08
TEST 1CN0508 2-16-82
c
Y/H
0.10
0.0
-0.10
TIME (T*F1)

FIGURE 5.20

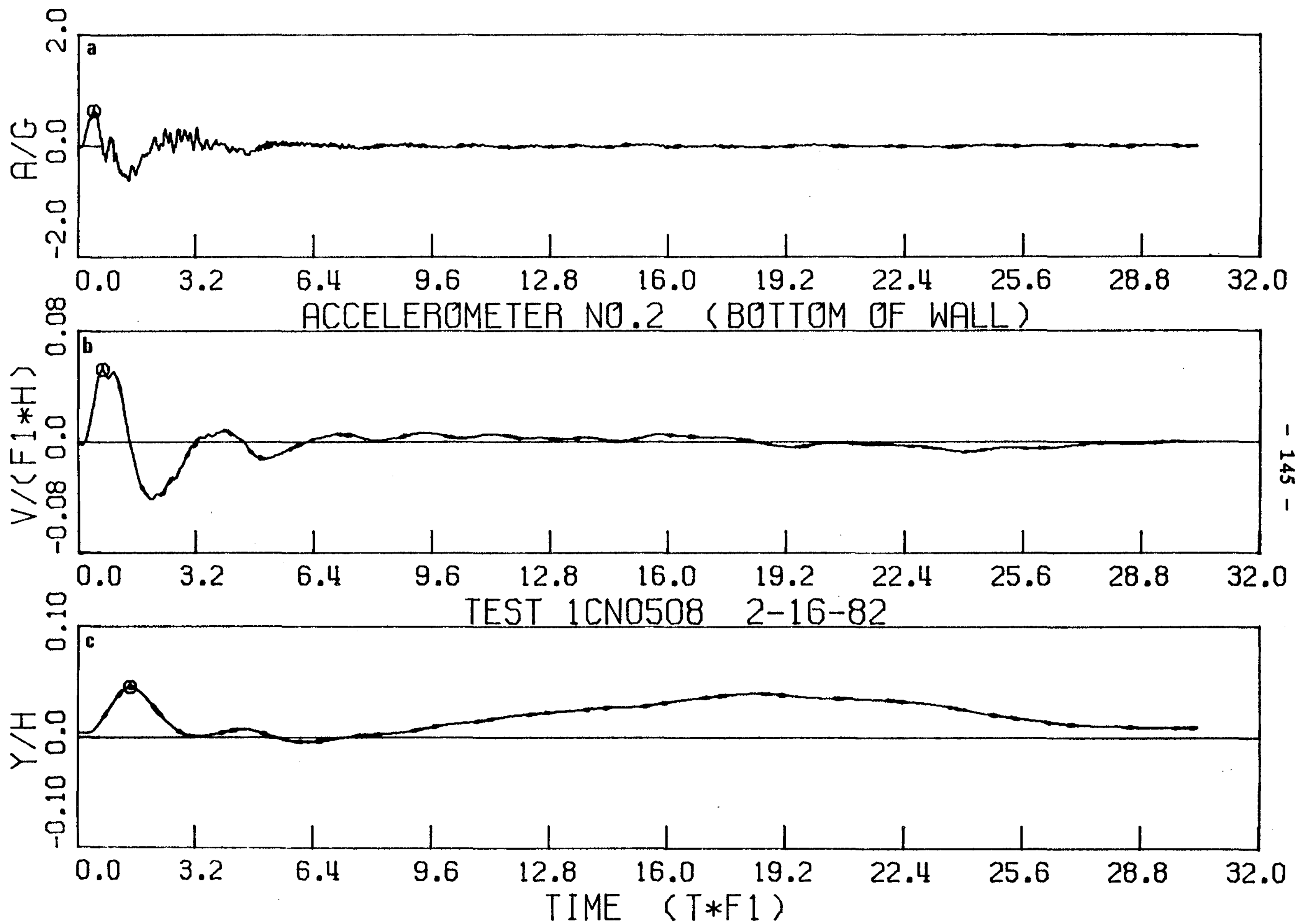
A/G
2.0
0.0
-2.0
a
ACCELEROMETER NO.2 (BOTTOM OF WALL)
V/(F1*H)
0.08
0.0
-0.08
b
TEST 1CN0508 2-16-82
Y/H
0.10
0.0
-0.10
c
0.0
3.2
6.4
9.6
12.8
16.0
19.2
22.4
25.6
28.8
32.0
TIME (T*F1)

FIGURE 5.21

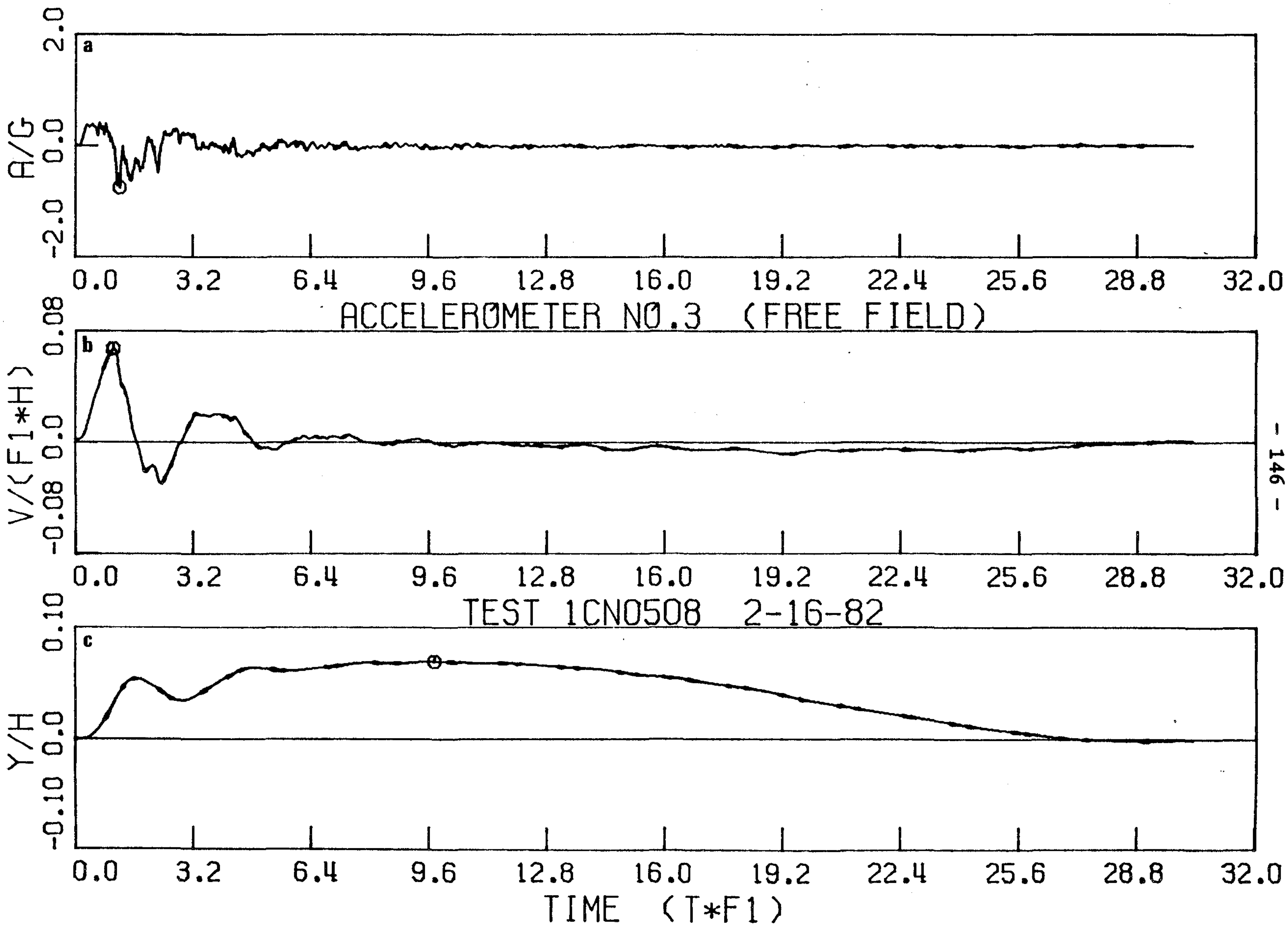

A/G
V/(F1*H)
Y/H
ACCELERØMETER NØ.3 (FREE FIELD)
TEST 1CN0508 2-16-82
TIME (T*F1)
a
b
c
2.0
0.0
-2.0
0.08
0.0
-0.08
0.10
0.0
-0.10
0.0
3.2
6.4
9.6
12.8
16.0
19.2
22.4
25.6
28.8
32.0

FIGURE 5.22

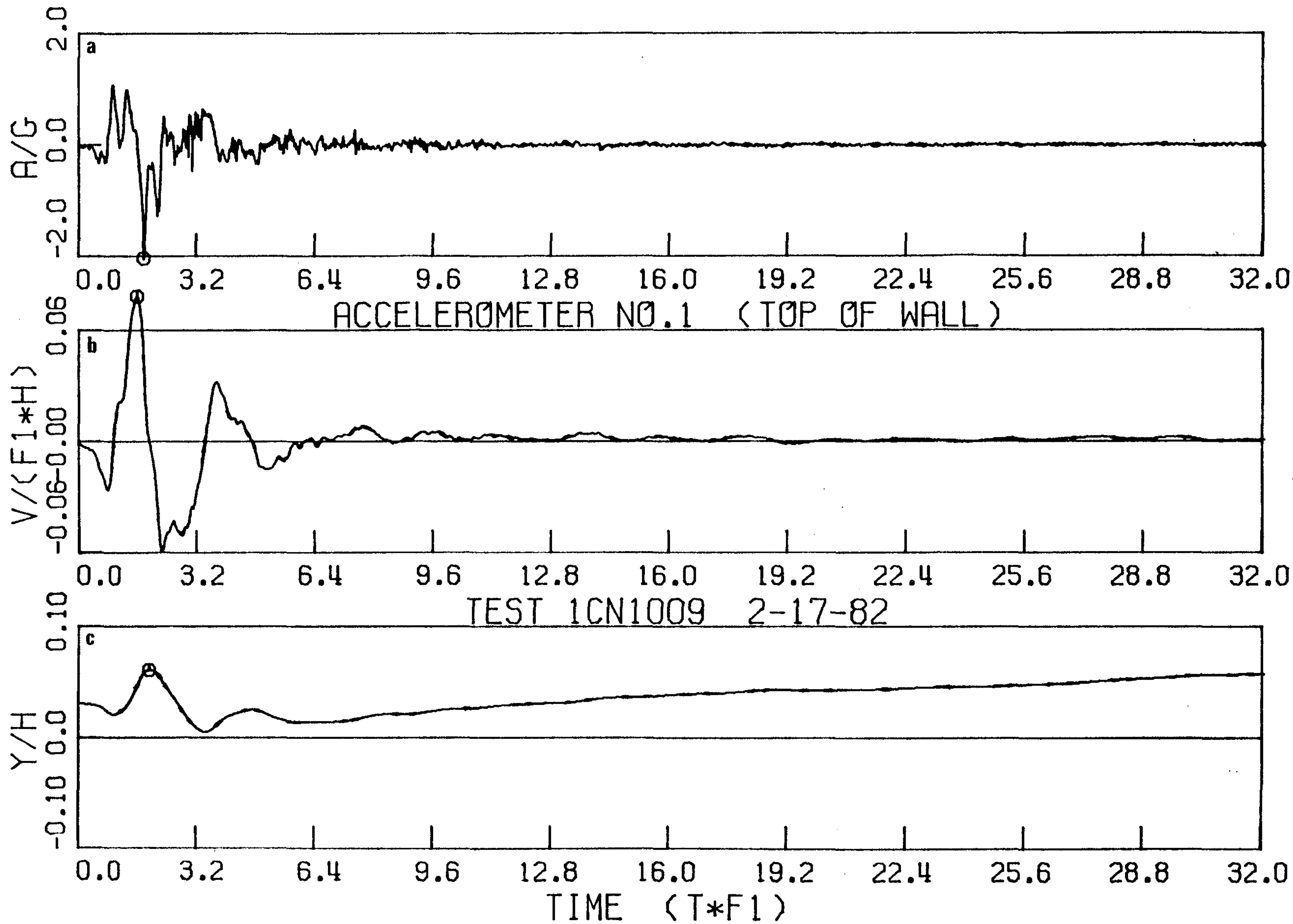
a
A/G
2.0
0.0
-2.0
ACCELERØMETER NO.1 (TØP ØF WALL)
b
V/(F1*H)
0.06
-0.00
-0.06
TEST 1CN1009 2-17-82
c
Y/H
0.10
0.0
-0.10
0.0 3.2 6.4 9.6 12.8 16.0 19.2 22.4 25.6 28.8 32.0
TIME (T*F1)

FIGURE 5.23

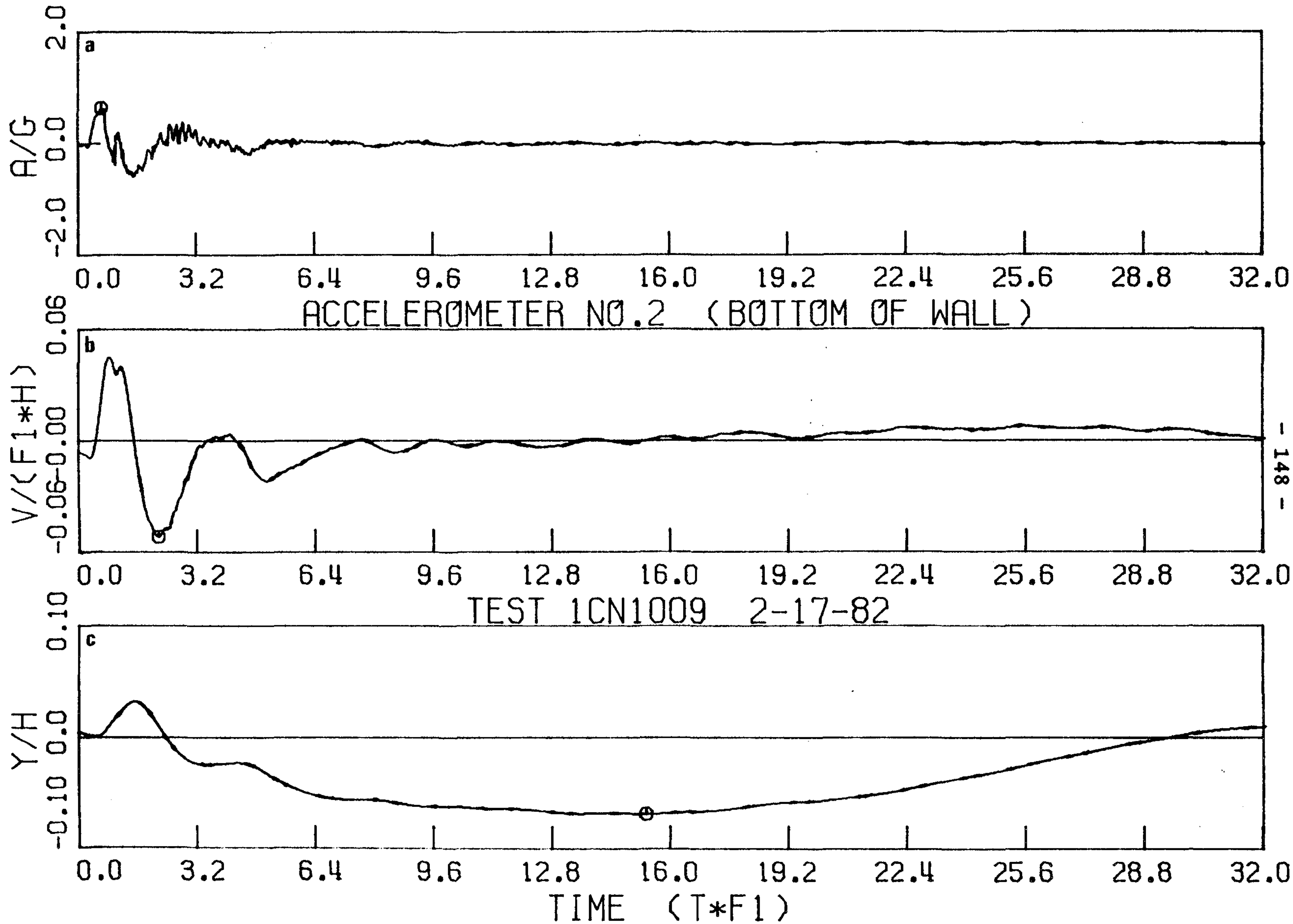
a
A/G
2.0
0.0
-2.0
0.0
3.2
6.4
9.6
12.8
16.0
19.2
22.4
25.6
28.8
32.0
ACCELERØMETER NØ.2 (BØTTØM ØF WALL)
b
V/(F1*H)
0.06
-0.00
-0.06
TEST 1CN1009 2-17-82
c
Y/H
0.10
0.0
-0.10
TIME (T*F1)

FIGURE 5.24

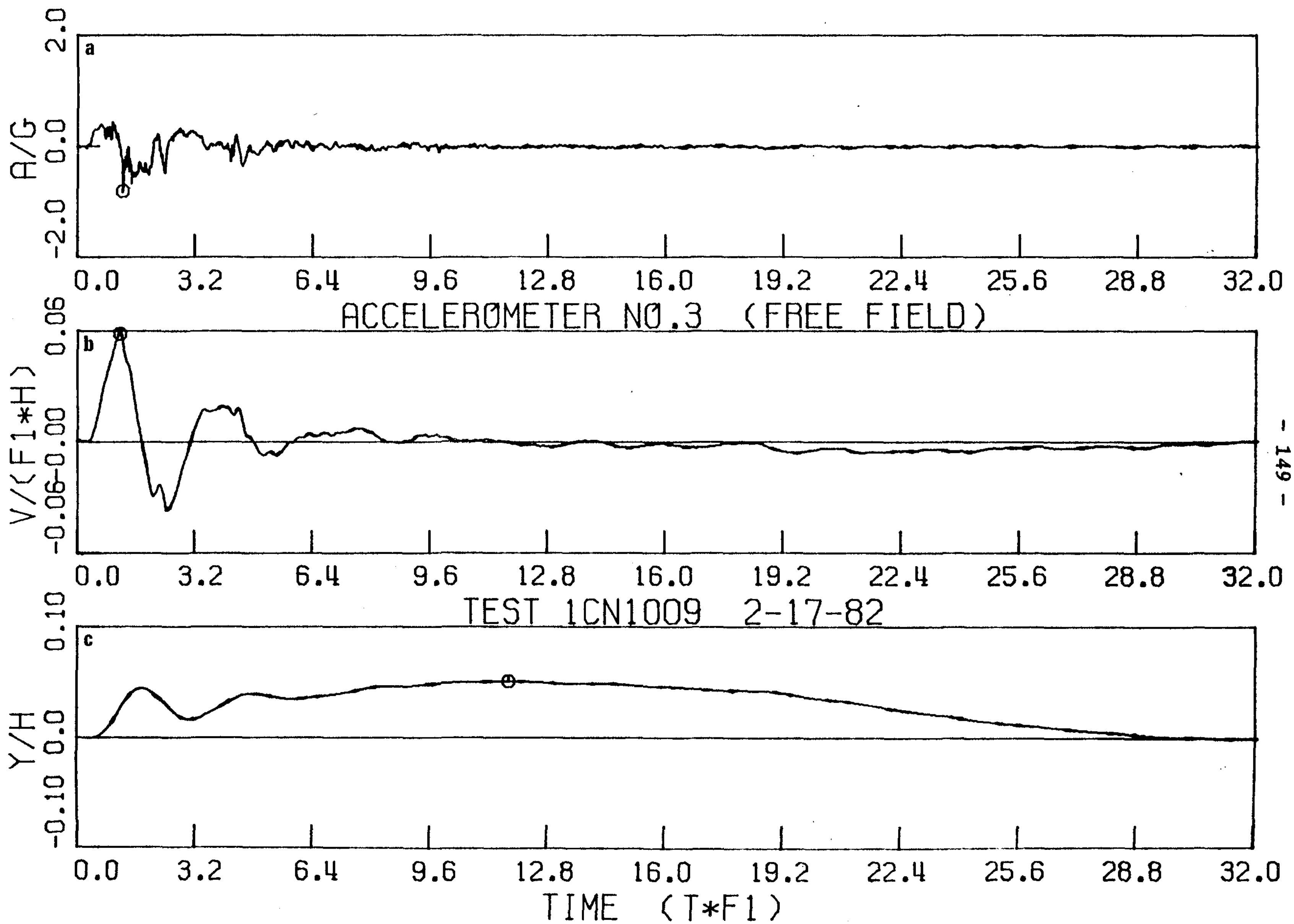
a
b
c
A/G
2.0
0.0
-2.0
V/(F1*H)
0.06
0.00
-0.06
Y/H
0.10
0.0
-0.10
0.0 3.2 6.4 9.6 12.8 16.0 19.2 22.4 25.6 28.8 32.0
ACCELERØMETER NØ.3 (FREE FIELD)
TEST 1CN1009 2-17-82
TIME (T*F1)

FIGURE 5.25

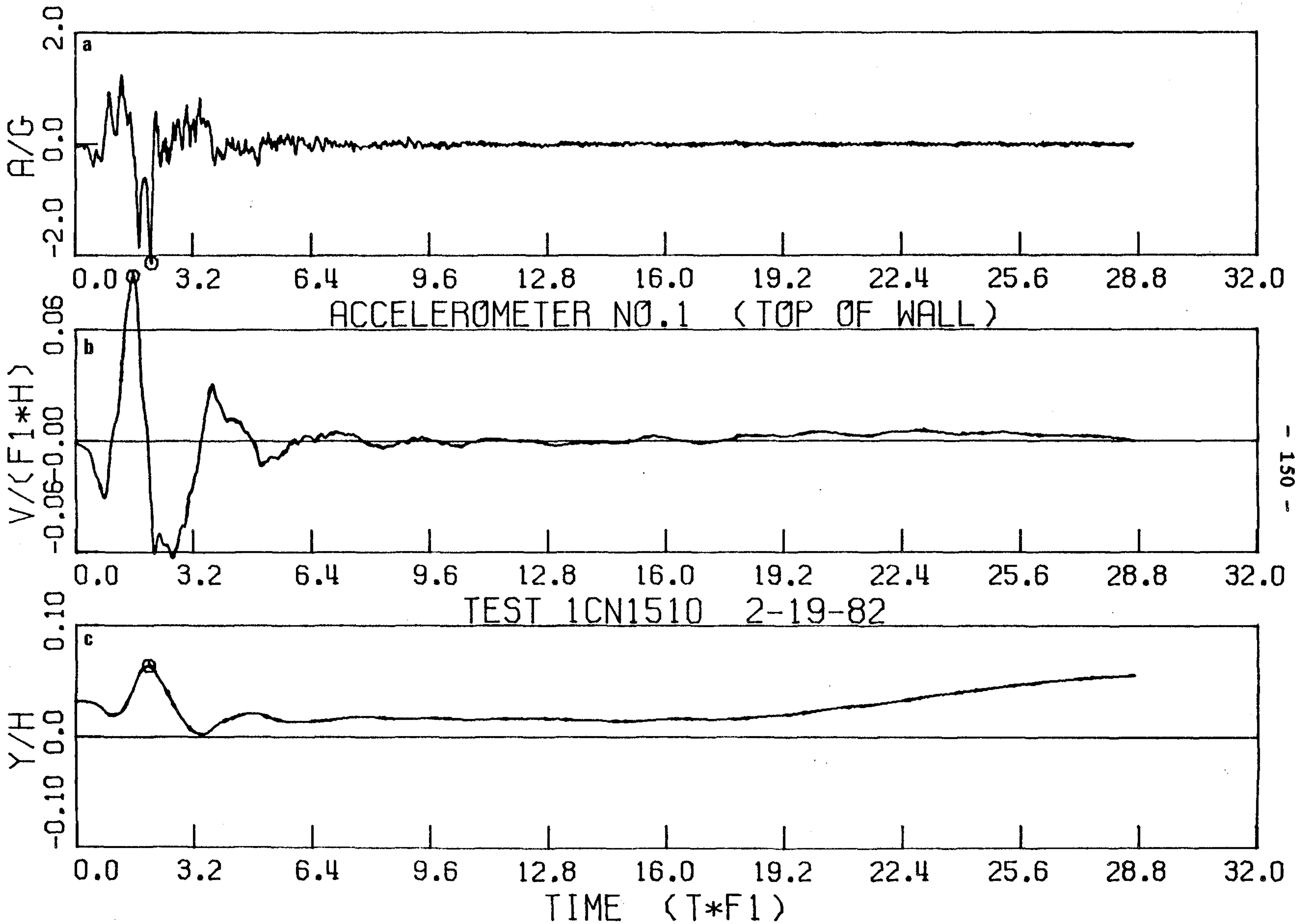
a
b
c
A/G
2.0
0.0
-2.0
V/(F1*H)
0.06
0.00
-0.06
Y/H
0.10
0.0
-0.10
0.0
3.2
6.4
9.6
12.8
16.0
19.2
22.4
25.6
28.8
32.0
ACCELERØMETER NØ.1 (TØP ØF WALL)
TEST 1CN1510 2-19-82
TIME (T*F1)

FIGURE 5.26

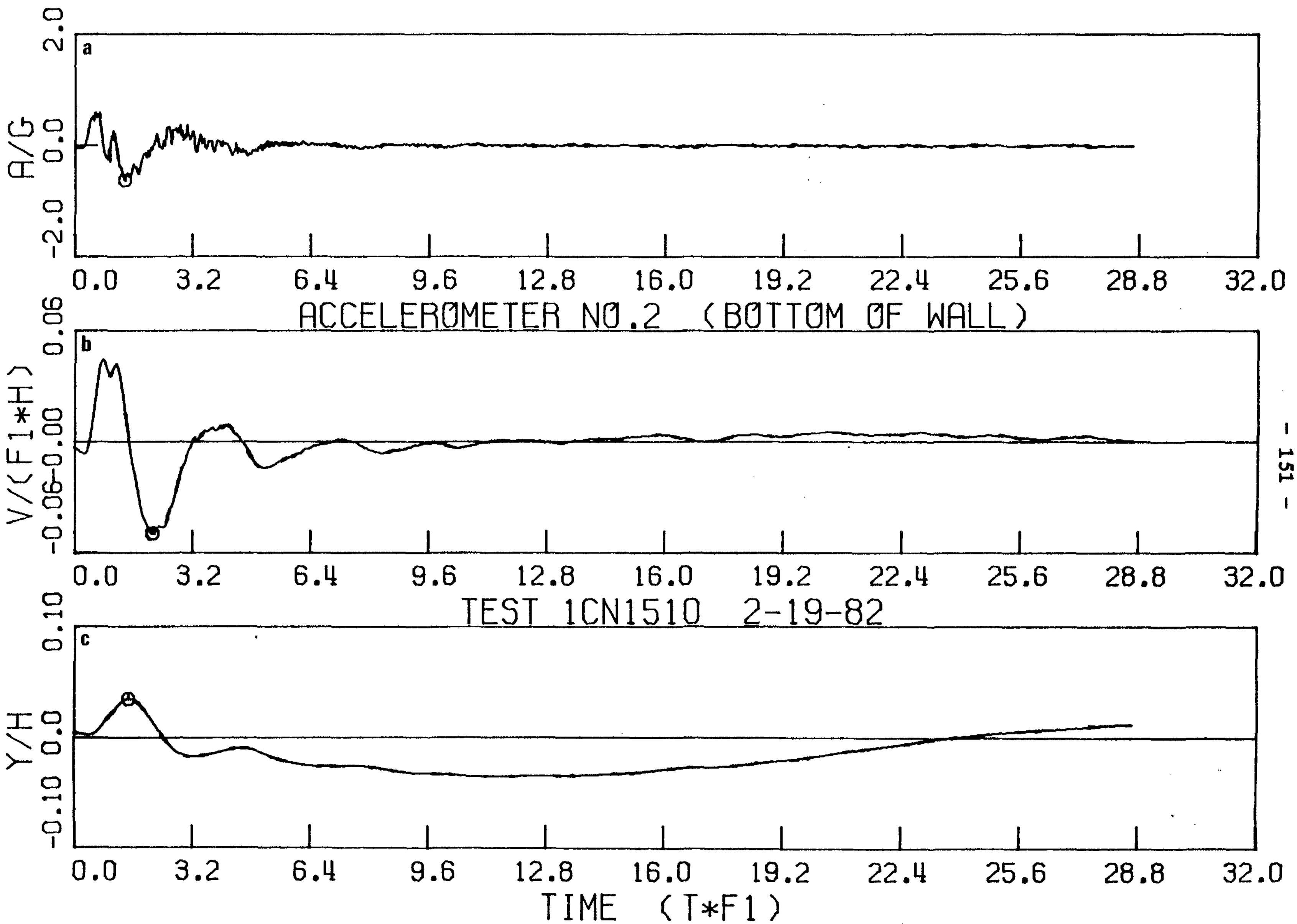
a
A/G
2.0
0.0
-2.0
0.0 3.2 6.4 9.6 12.8 16.0 19.2 22.4 25.6 28.8 32.0
ACCELERØMETER NØ.2 (BØTTØM ØF WALL)
b
V/(F1*H)
0.06
-0.00
-0.06
0.0 3.2 6.4 9.6 12.8 16.0 19.2 22.4 25.6 28.8 32.0
TEST 1CN1510 2-19-82
c
Y/H
0.10
0.0
-0.10
0.0 3.2 6.4 9.6 12.8 16.0 19.2 22.4 25.6 28.8 32.0
TIME (T*F1)

FIGURE 5.27

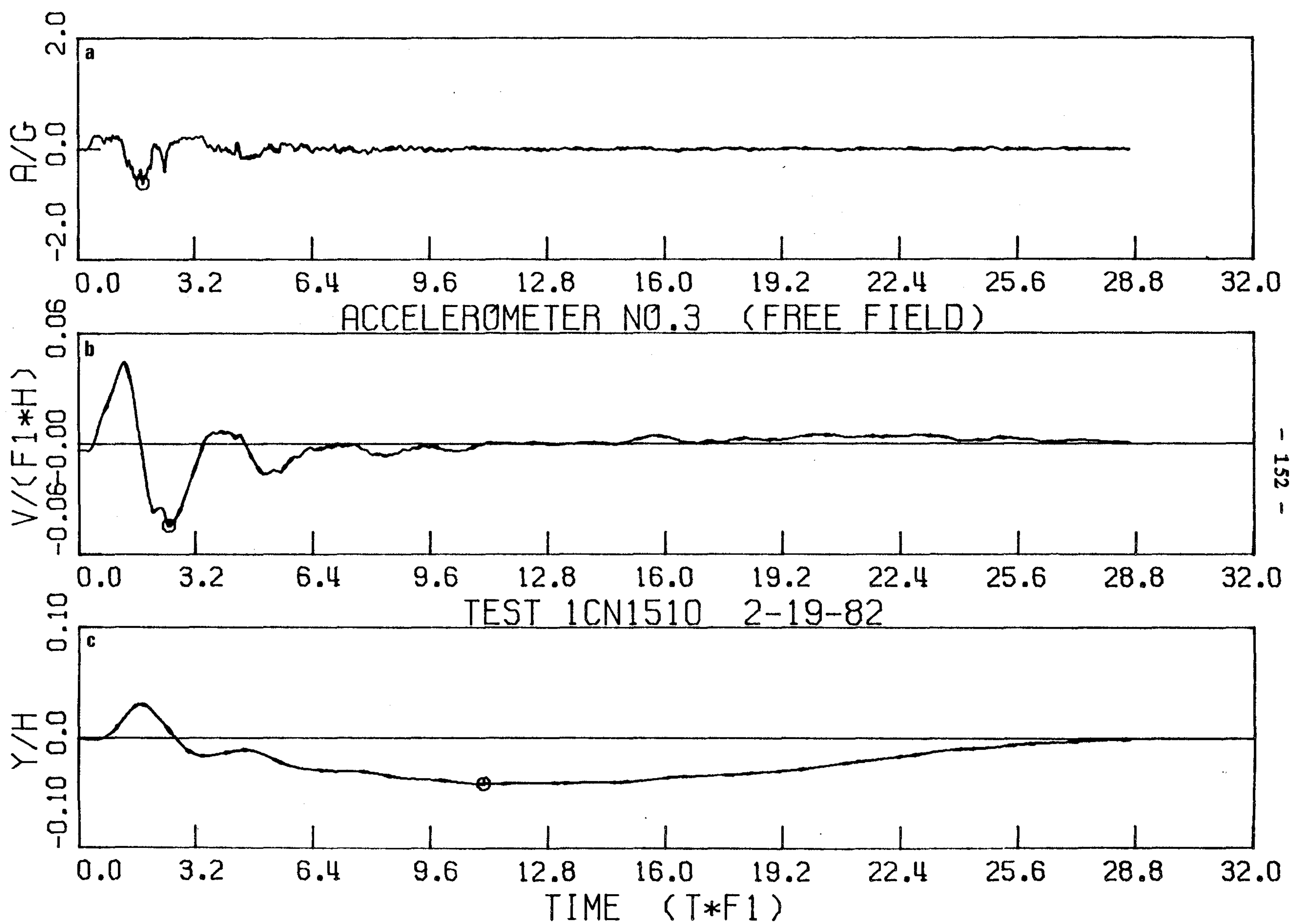
a
A/G
2.0
0.0
-2.0
0.0 3.2 6.4 9.6 12.8 16.0 19.2 22.4 25.6 28.8 32.0
ACCELERØMETER NØ.3 (FREE FIELD)
b
V/(F1*H)
0.06
-0.00
-0.06
0.0 3.2 6.4 9.6 12.8 16.0 19.2 22.4 25.6 28.8 32.0
TEST 1CN1510 2-19-82
c
Y/H
0.10
0.0
-0.10
0.0 3.2 6.4 9.6 12.8 16.0 19.2 22.4 25.6 28.8 32.0
TIME (T*F1)

FIGURE 5.28

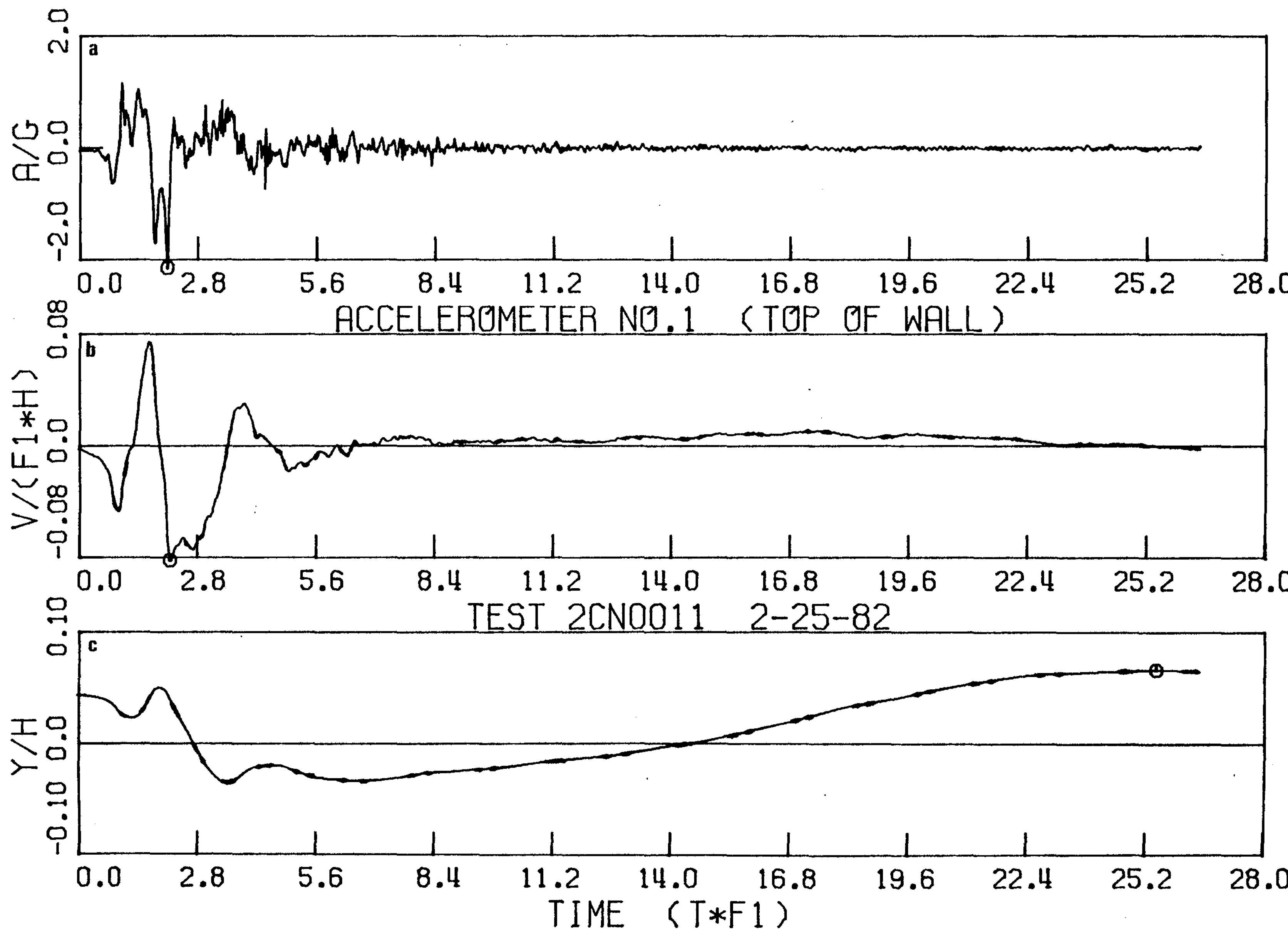
2.0
A/G
0.0
-2.0
a
0.0
2.8
5.6
8.4
11.2
14.0
16.8
19.6
22.4
25.2
28.0
ACCELEROMETER NO.1 (TOP OF WALL)
0.08
V/(F1*H)
0.0
-0.08
b
0.0
2.8
5.6
8.4
11.2
14.0
16.8
19.6
22.4
25.2
28.0
TEST 2CN0011 2-25-82
0.10
Y/H
0.0
-0.10
c
0.0
2.8
5.6
8.4
11.2
14.0
16.8
19.6
22.4
25.2
28.0
TIME (T*F1)

FIGURE 5.29

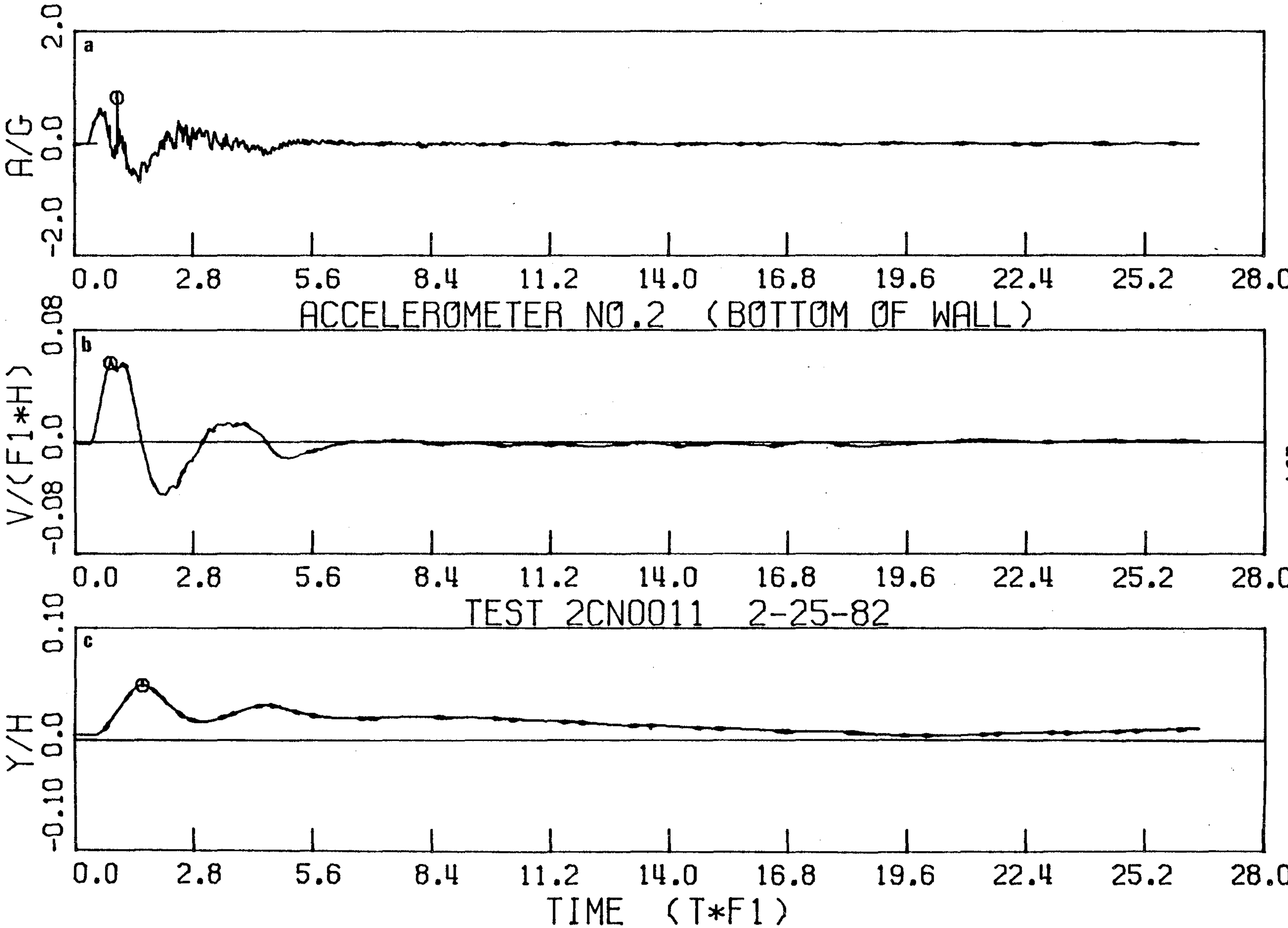
a
A/G
2.0
0.0
-2.0
0.0
2.8
5.6
8.4
11.2
14.0
16.8
19.6
22.4
25.2
28.0
ACCELERØMETER NØ.2 (BØTTØM ØF WALL)
b
V/(F1*H)
0.08
0.0
-0.08
TEST 2CN0011 2-25-82
c
Y/H
0.10
0.0
-0.10
TIME (T*F1)

FIGURE 5.30

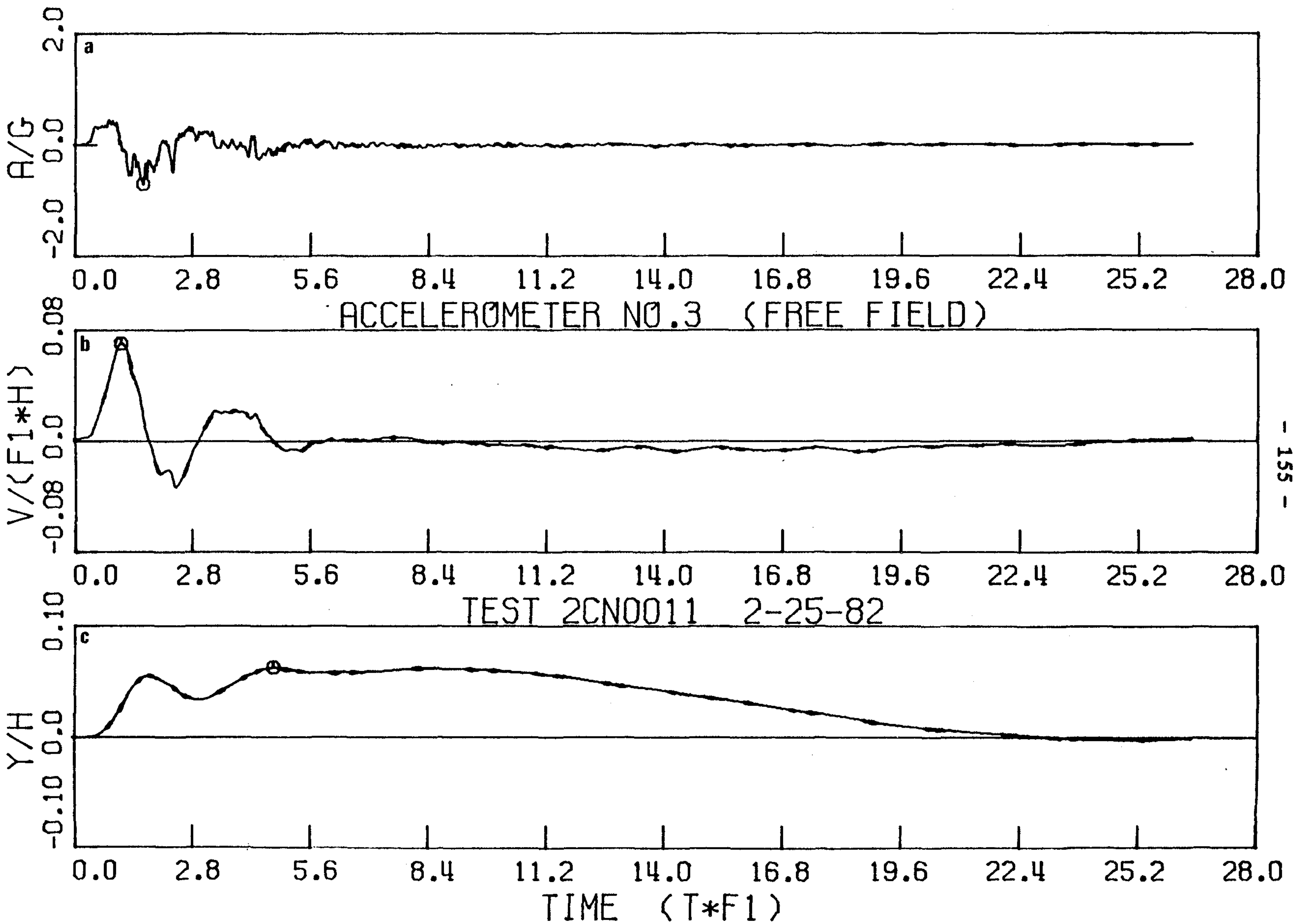
a
A/G
2.0
0.0
-2.0
0.0
2.8
5.6
8.4
11.2
14.0
16.8
19.6
22.4
25.2
28.0
ACCELERØMETER NØ.3 (FREE FIELD)
b
V/(F1*H)
0.08
0.0
-0.08
TEST 2CN0011 2-25-82
c
Y/H
0.10
0.0
-0.10
TIME (T*F1)

FIGURE 5.31

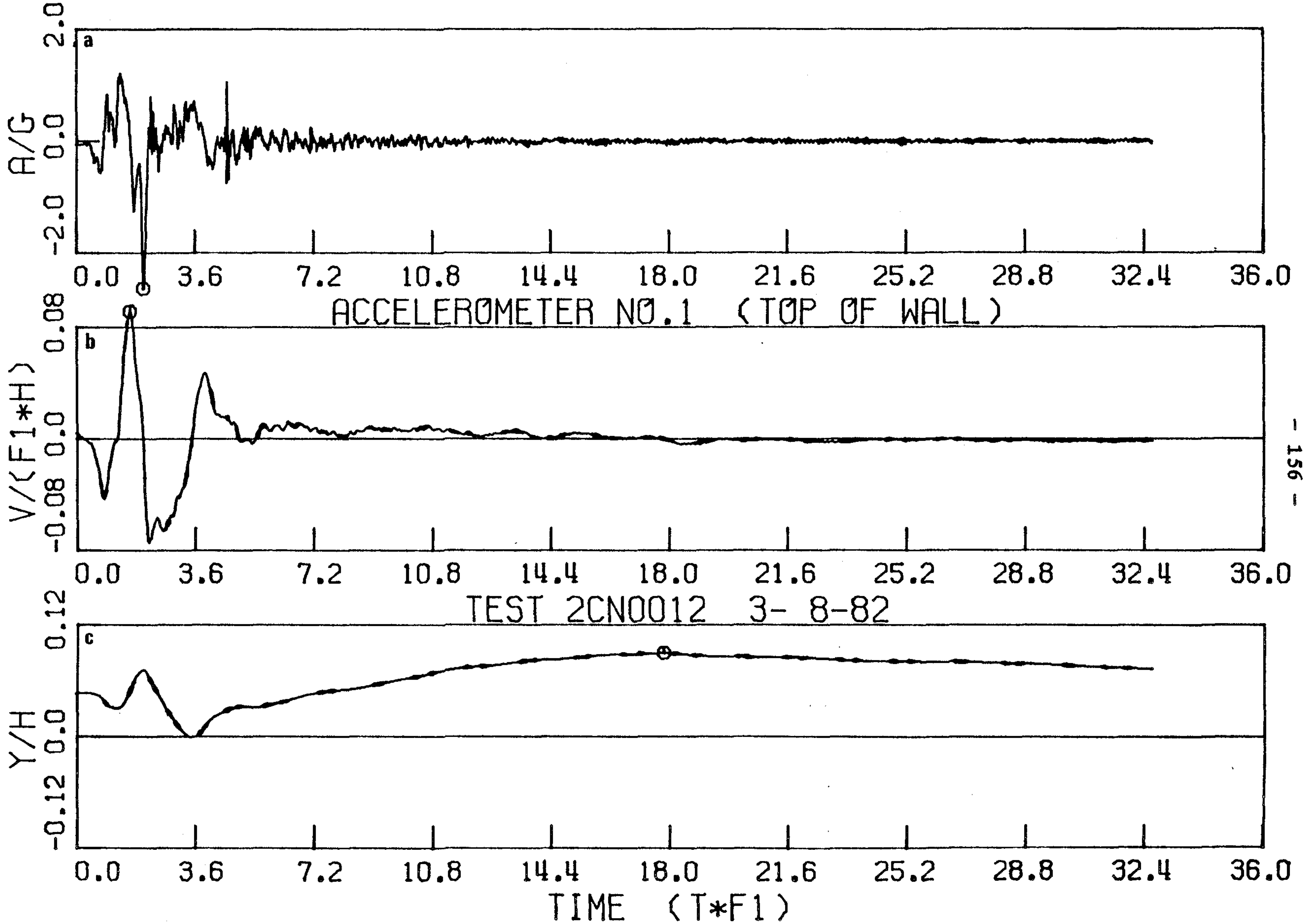
a
b
c
A/G
2.0
0.0
-2.0
V/(F1*H)
0.08
0.0
-0.08
Y/H
0.12
0.0
-0.12
0.0
3.6
7.2
10.8
14.4
18.0
21.6
25.2
28.8
32.4
36.0
ACCELEROMETER NO.1 (TOP OF WALL)
TEST 2CN0012 3- 8-82
TIME (T*F1)

FIGURE 5.32

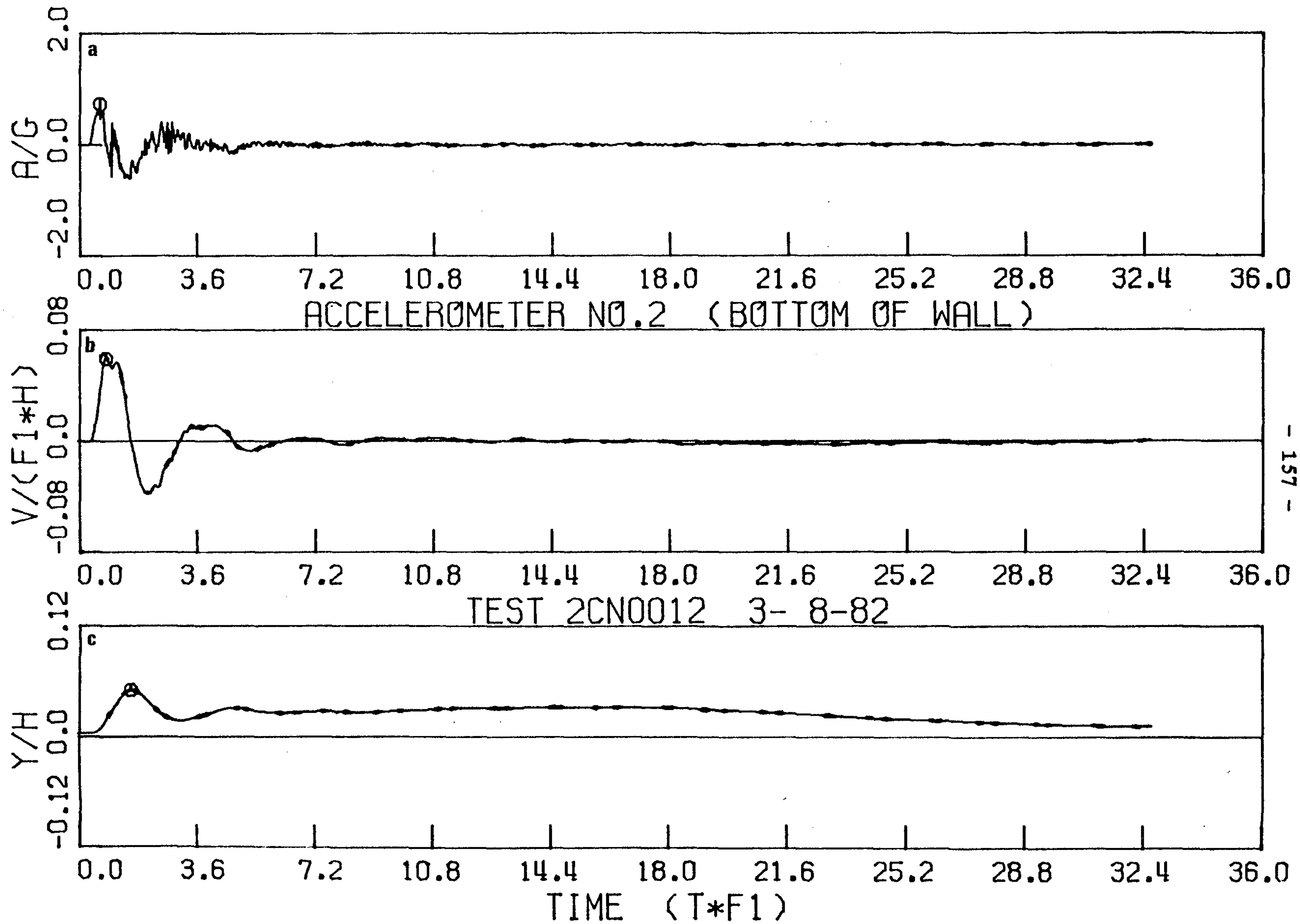
a
b
c
A/G
2.0
0.0
-2.0
V/(F1*H)
0.08
0.0
-0.08
Y/H
0.12
0.0
-0.12
0.0 3.6 7.2 10.8 14.4 18.0 21.6 25.2 28.8 32.4 36.0
ACCELEROMETER NO.2 (BOTTOM OF WALL)
TEST 2CN0012 3- 8-82
TIME (T*F1)

FIGURE 5.33

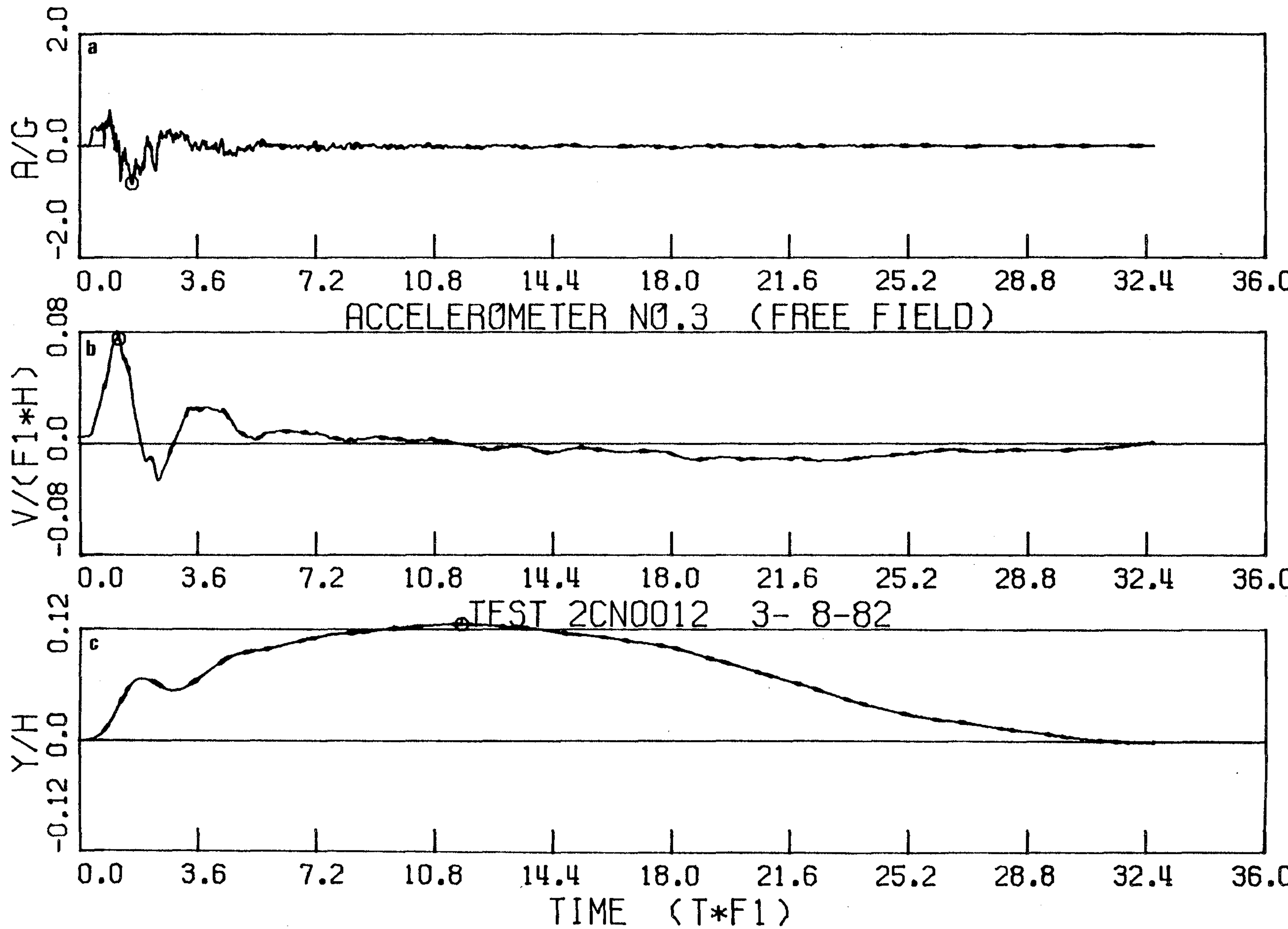

a
b
c
A/G
2.0
0.0
-2.0
V/(F1*H)
0.08
0.0
-0.08
Y/H
0.12
0.0
-0.12
0.0 3.6 7.2 10.8 14.4 18.0 21.6 25.2 28.8 32.4 36.0
ACCELERØMETER NØ.3 (FREE FIELD)
TEST 2CN0012 3- 8-82
TIME (T*F1)

FIGURE 5.34

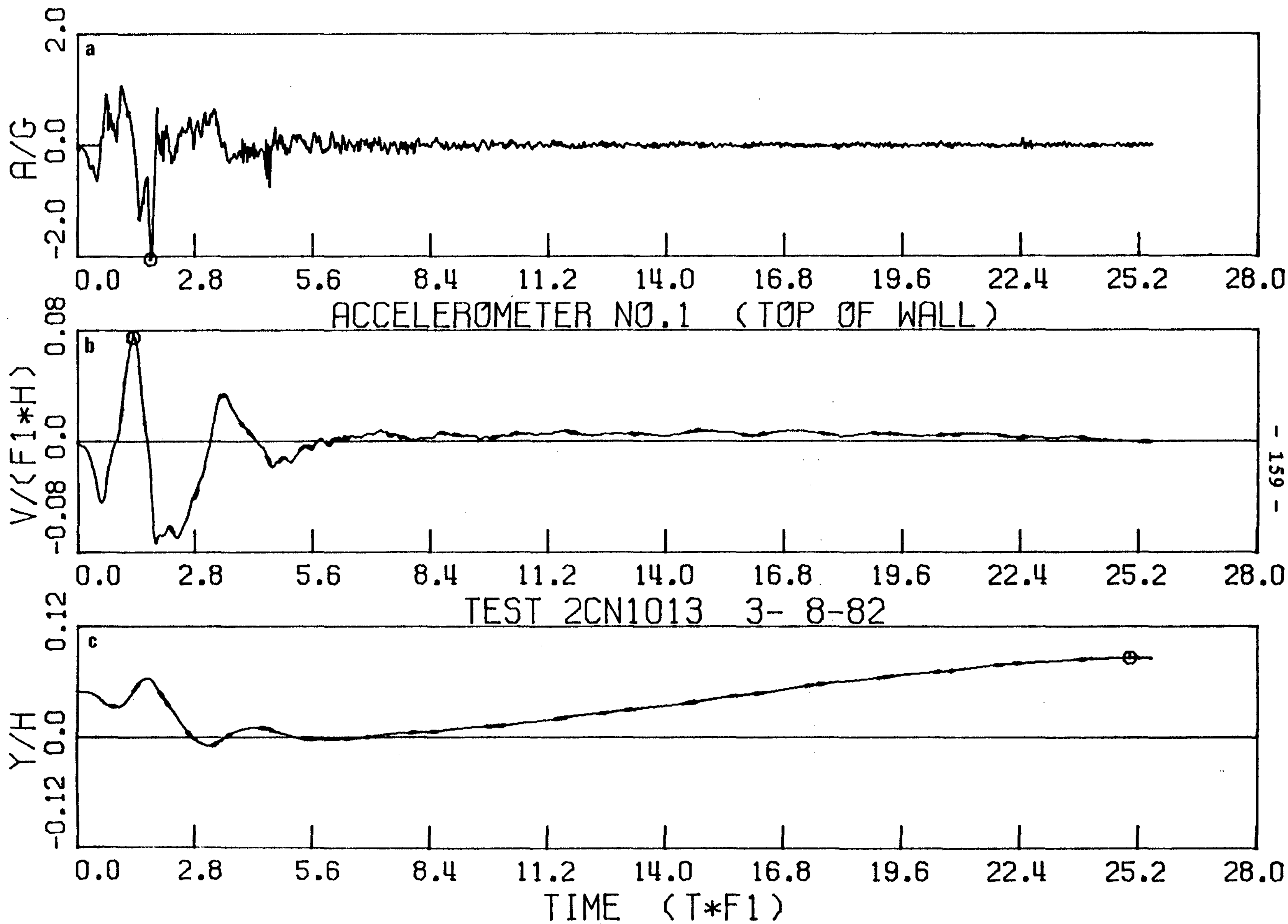
a
A/G
2.0
0.0
-2.0
0.0
2.8
5.6
8.4
11.2
14.0
16.8
19.6
22.4
25.2
28.0
ACCELERØMETER NØ.1 (TØP ØF WALL)
b
V/(F1*H)
0.08
0.0
-0.08
TEST 2CN1013 3- 8-82
c
Y/H
0.12
0.0
-0.12
TIME (T*F1)

FIGURE 5.35

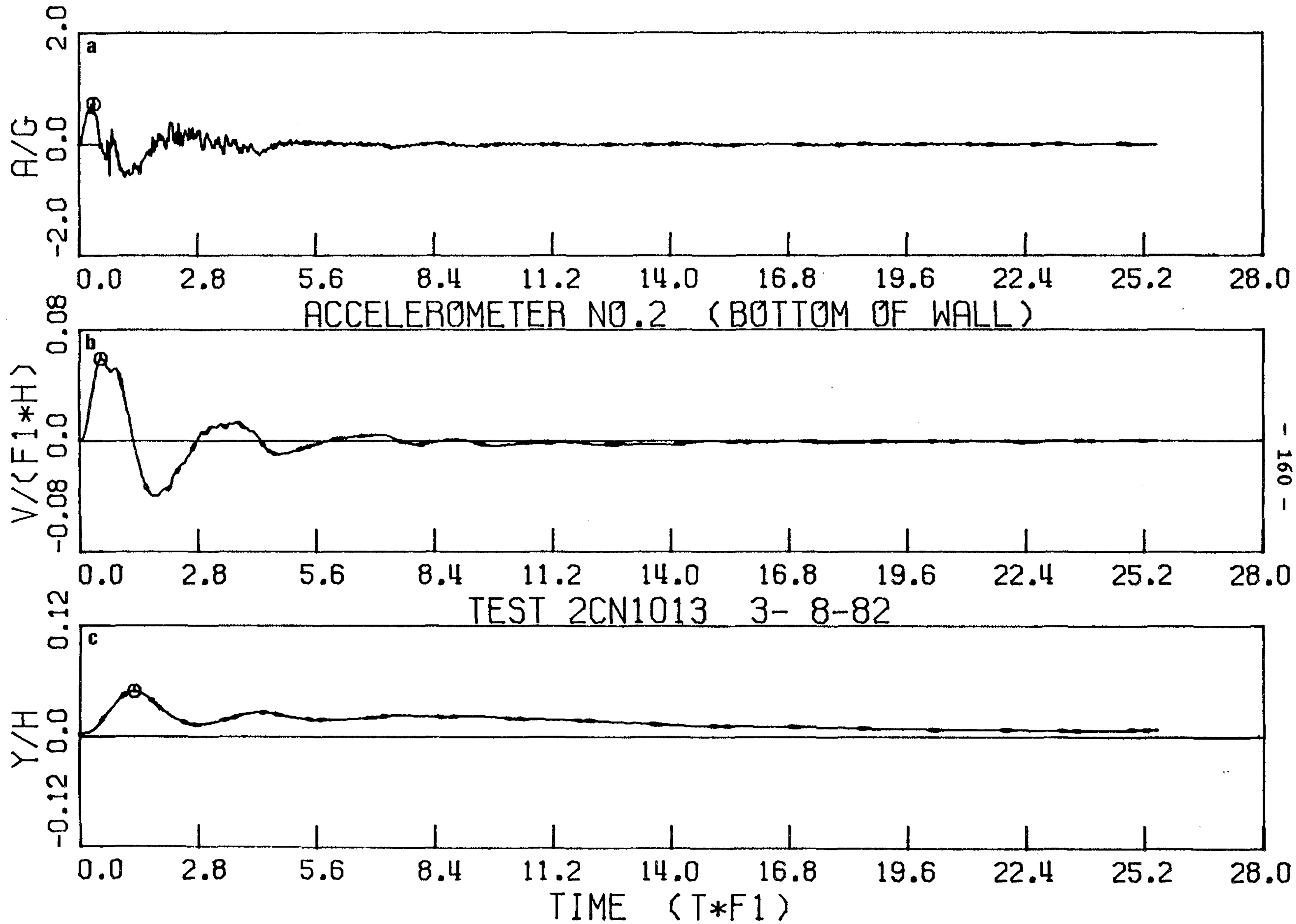

2.0
A/G 0.0
-2.0
a
0.0 2.8 5.6 8.4 11.2 14.0 16.8 19.6 22.4 25.2 28.0
ACCELERØMETER NØ.2 (BØTTØM ØF WALL)
0.08
V/(F1*H) 0.0
-0.08
b
0.0 2.8 5.6 8.4 11.2 14.0 16.8 19.6 22.4 25.2 28.0
TEST 2CN1013 3- 8-82
0.12
Y/H 0.0
-0.12
c
0.0 2.8 5.6 8.4 11.2 14.0 16.8 19.6 22.4 25.2 28.0
TIME (T*F1)

FIGURE 5.36

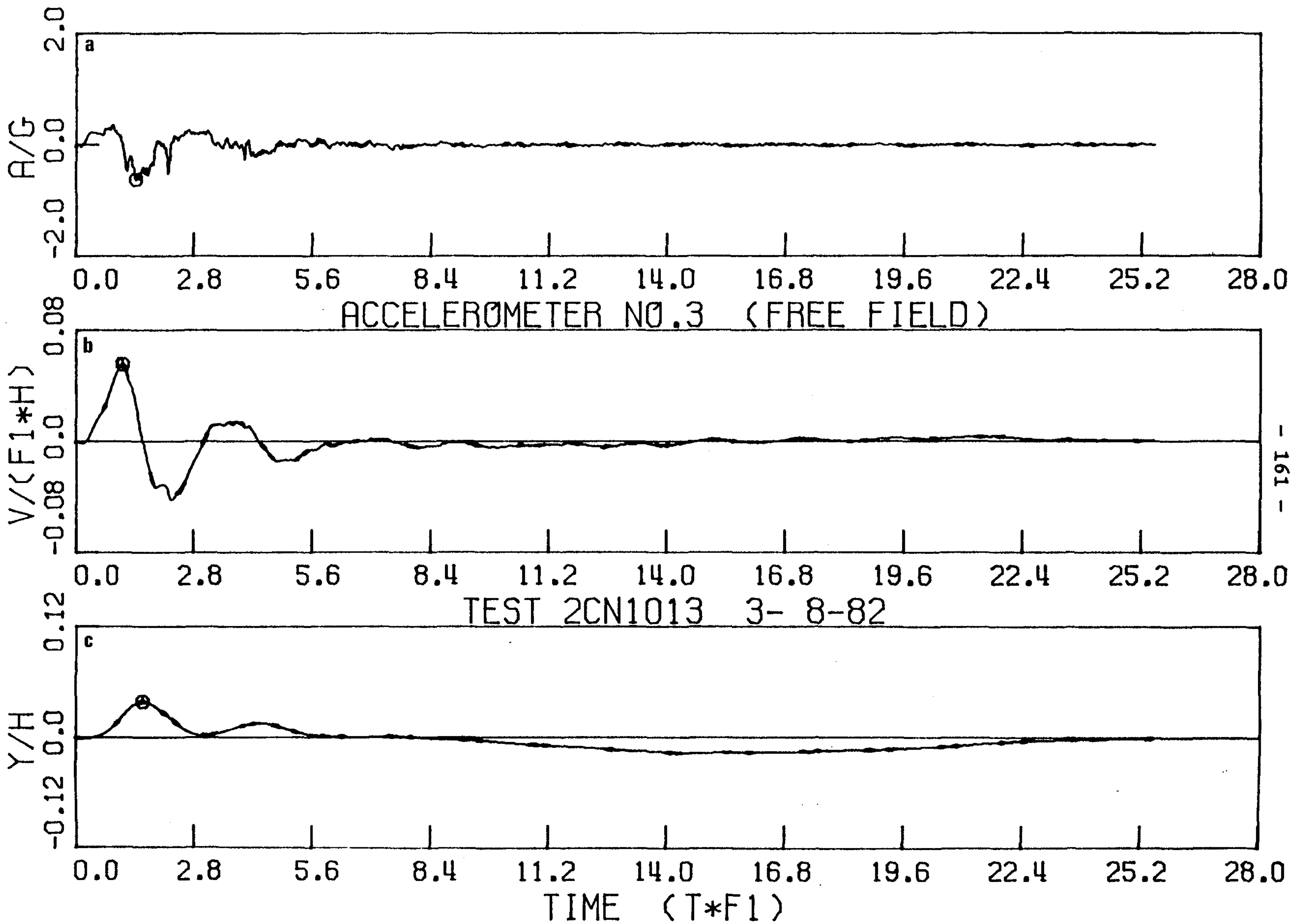
a
A/G
2.0
0.0
-2.0
0.0 2.8 5.6 8.4 11.2 14.0 16.8 19.6 22.4 25.2 28.0
ACCELERØMETER NO.3 (FREE FIELD)
b
V/(F1*H)
0.08
0.0
-0.08
0.0 2.8 5.6 8.4 11.2 14.0 16.8 19.6 22.4 25.2 28.0
TEST 2CN1013 3- 8-82
c
Y/H
0.12
0.0
-0.12
0.0 2.8 5.6 8.4 11.2 14.0 16.8 19.6 22.4 25.2 28.0
TIME (T*F1)

FIGURE 5.37

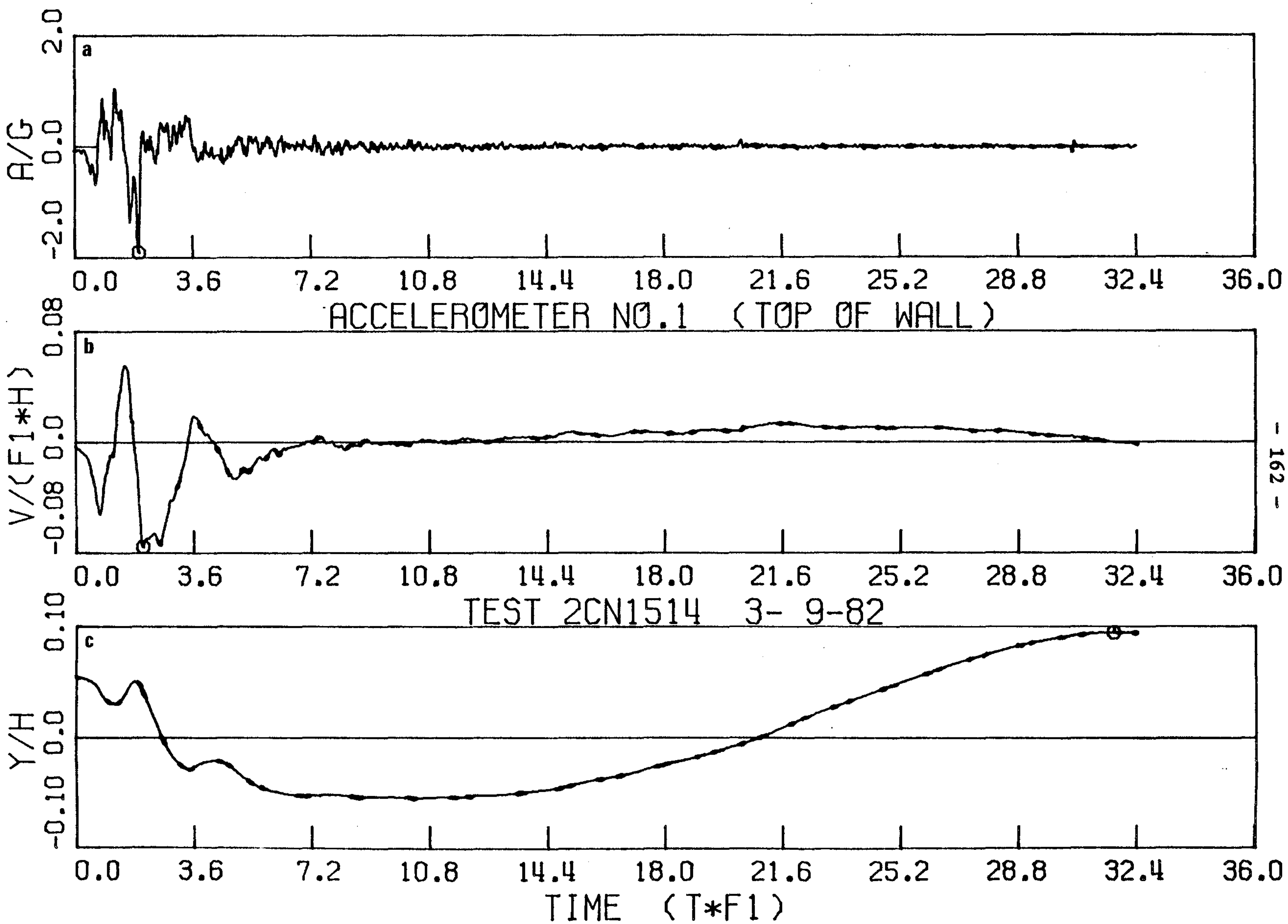
a
b
c
A/G
2.0
0.0
-2.0
V/(F1*H)
0.08
0.0
-0.08
Y/H
0.10
0.0
-0.10
0.0
3.6
7.2
10.8
14.4
18.0
21.6
25.2
28.8
32.4
36.0
ACCELEROMETER NO.1 (TOP OF WALL)
TEST 2CN1514 3- 9-82
TIME (T*F1)

FIGURE 5.38

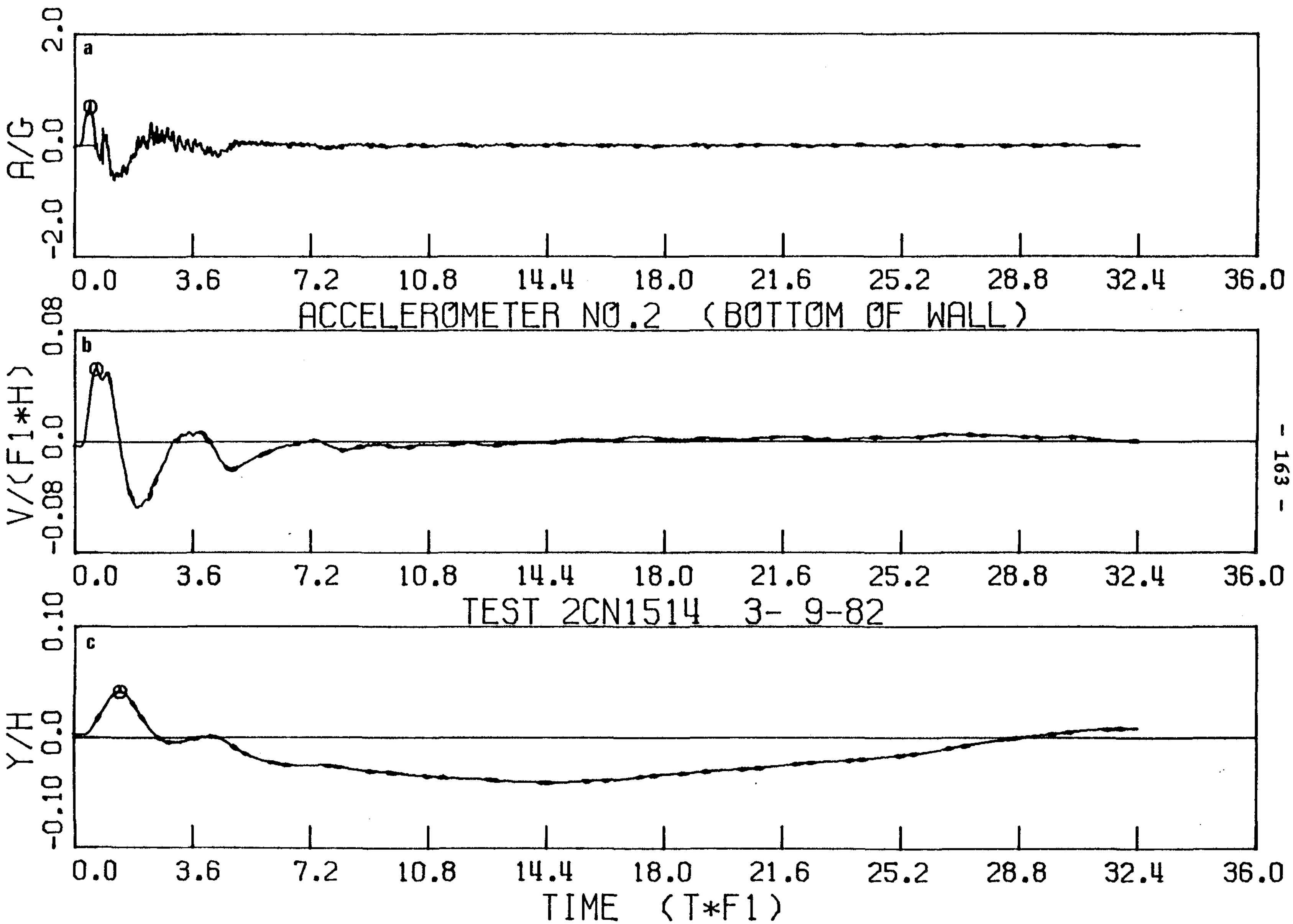

a
b
c
A/G
2.0
0.0
-2.0
ACCELEROMETER NO.2 (BOTTOM OF WALL)
V/(F1*H)
0.08
0.0
-0.08
TEST 2CN1514 3- 9-82
Y/H
0.10
0.0
-0.10
0.0
3.6
7.2
10.8
14.4
18.0
21.6
25.2
28.8
32.4
36.0
TIME (T*F1)

FIGURE 5.39

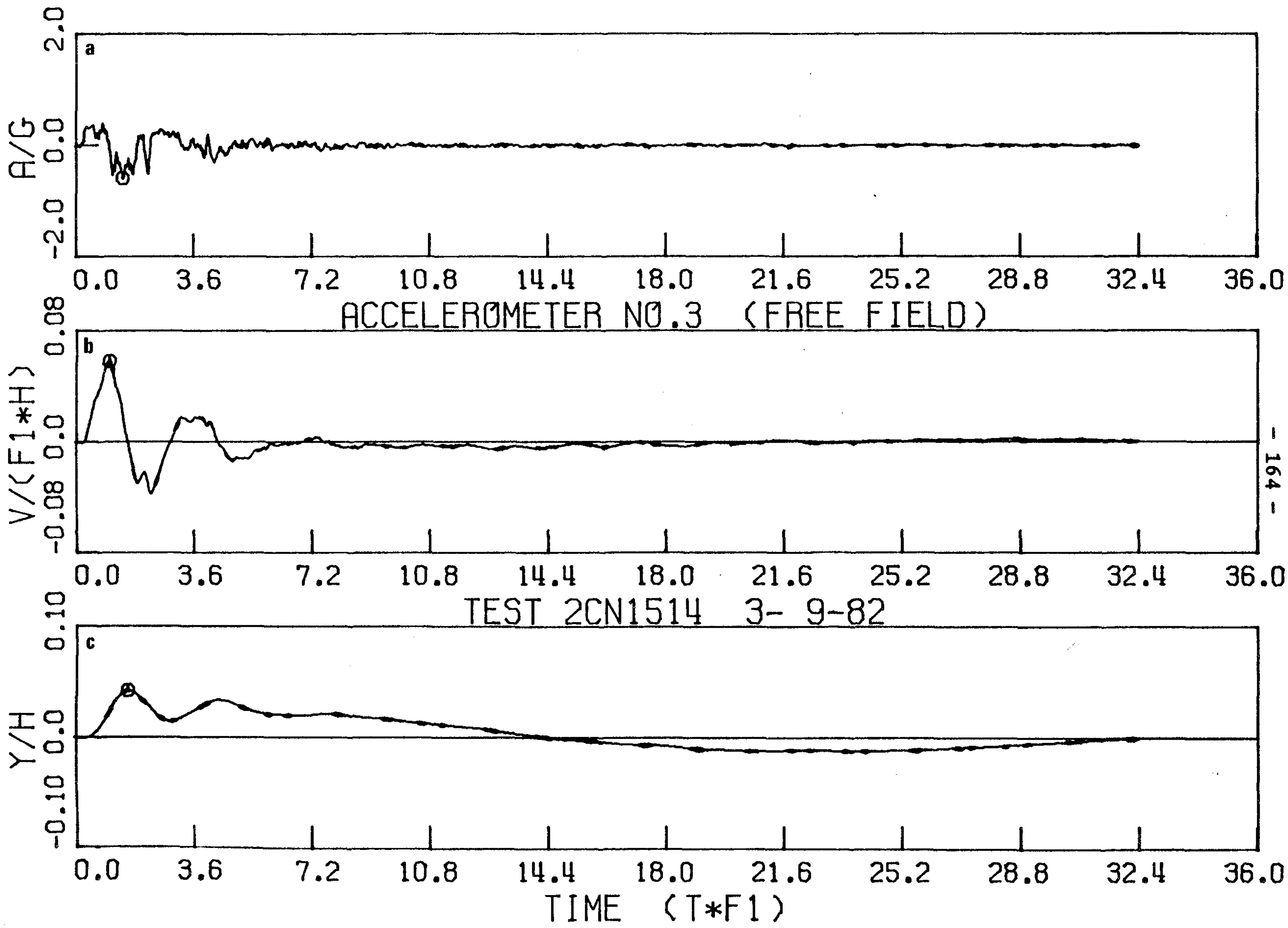
a
b
c
A/G
2.0
0.0
-2.0
V/(F1*H)
0.08
0.0
-0.08
Y/H
0.10
0.0
-0.10
0.0 3.6 7.2 10.8 14.4 18.0 21.6 25.2 28.8 32.4 36.0
ACCELERØMETER NØ.3 (FREE FIELD)
TEST 2CN1514 3- 9-82
TIME (T*F1)

FIGURE 5.40

centrifuge-frame-bucket-toggle-spring-bumper-wall-soil system. The accelerograms recorded in the free-field are very similar to the corresponding ones at the base of the wall (which indicate the input excitation into the wall-soil system), although they are not exactly alike. The peak amplitudes range from about 0.25 to 0.70 depending on the test, and the duration of shaking is from about 18 to about 33 (note the dimensionless variables). The accelerograms recorded at the top of the wall indicate that the motion can be amplified by greater than a factor of 2.0. The "earthquakes" can be generally categorized as short but severe.

The shaking exhibited in the experiments is not unlike that which has been recorded very near a ruptured fault. For example, used for comparison is the accelerogram (Figure 5.41) recorded at Station 2 of the Cholame-Shandon array during the Parkfield, California earthquake of June 27, 1966 ($M_L = 5.6$). The strong motion accelerograph was located just a few yards from the San Andreas fault trace. This record also exhibits sharp pulse-like accelerations which decay quite quickly. Although the maximum recorded ground acceleration was 50% of gravity, there was little damage to nearby structures presumably because of the narrowness of the acceleration spikes (low energy content) and because of the short duration of the severe shaking [8,16].

From an engineering standpoint, the response spectrum is very important since it gives an indication of how the response of a structure to an earthquake will be. Comparing the response spectra of the centrifuge accelerograms of tests 1CN0001, 1CN0002, 1CN0003, and

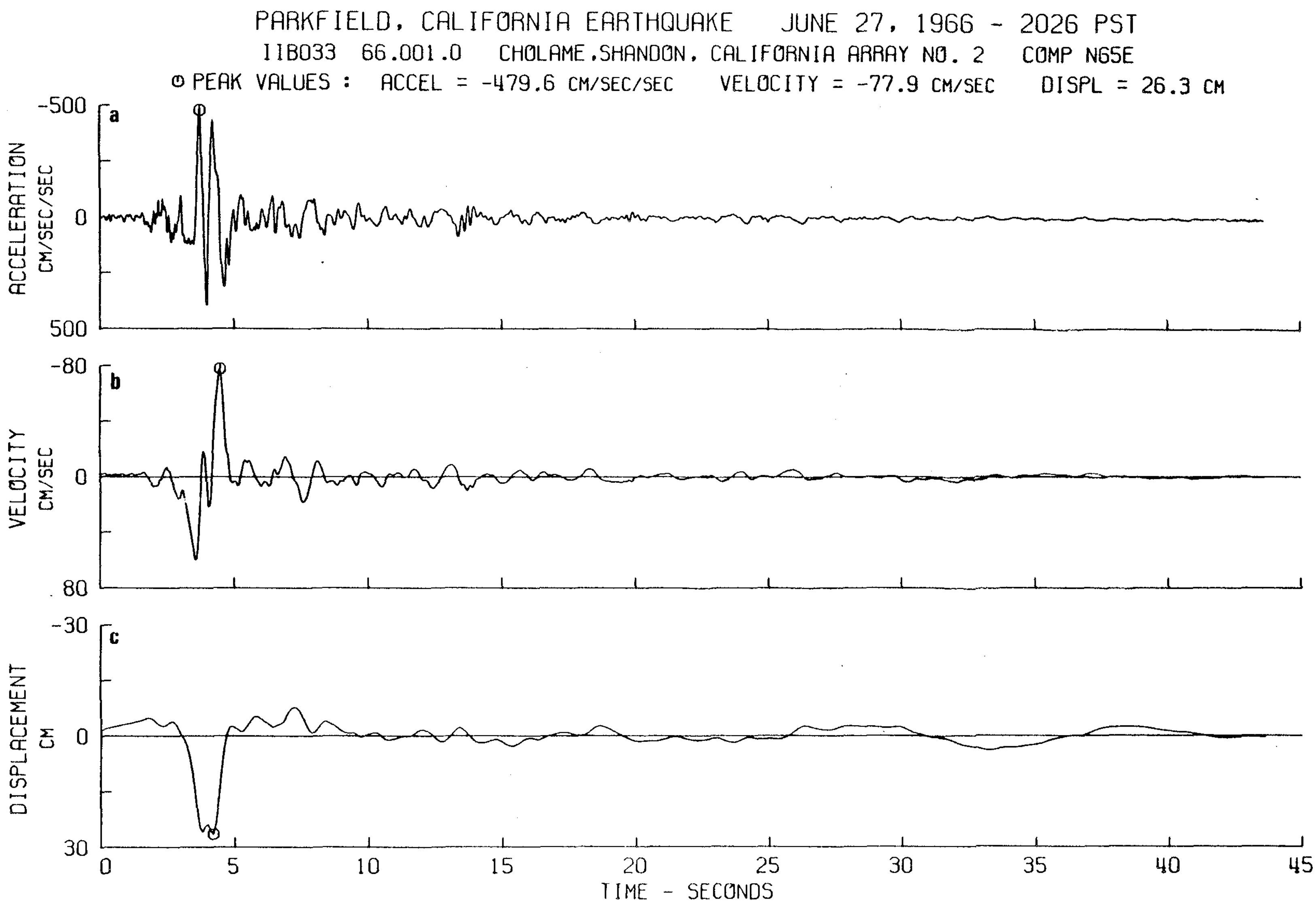
PARKFIELD, CALIFORNIA EARTHQUAKE JUNE 27, 1966 - 2026 PST
IIB033 66.001.0 CHOLAME,SHANDON, CALIFORNIA ARRAY NO. 2 COMP N65E
PEAK VALUES : ACCEL = -479.6 CM/SEC/SEC VELOCITY = -77.9 CM/SEC DISPL = 26.3 CM
a
ACCELERATION CM/SEC/SEC
-500
0
500
b
VELOCITY CM/SEC
-80
0
80
c
DISPLACEMENT CM
-30
0
30
0
5
10
15
20
25
30
35
40
45
TIME - SECONDS

FIGURE 5.41

RESPONSE SPECTRUM

TEST 1CN0001 CENTRIFUGE EARTHQUAKE 11-12-80

IIXX0100 80.001.0 SOIL MECHANICS CENTRIFUGE -- TOP OF WALL ACCELEROMETER COMP HOR

DAMPING VALUES ARE 0, 2, 5, 10 AND 20 PERCENT OF CRITICAL

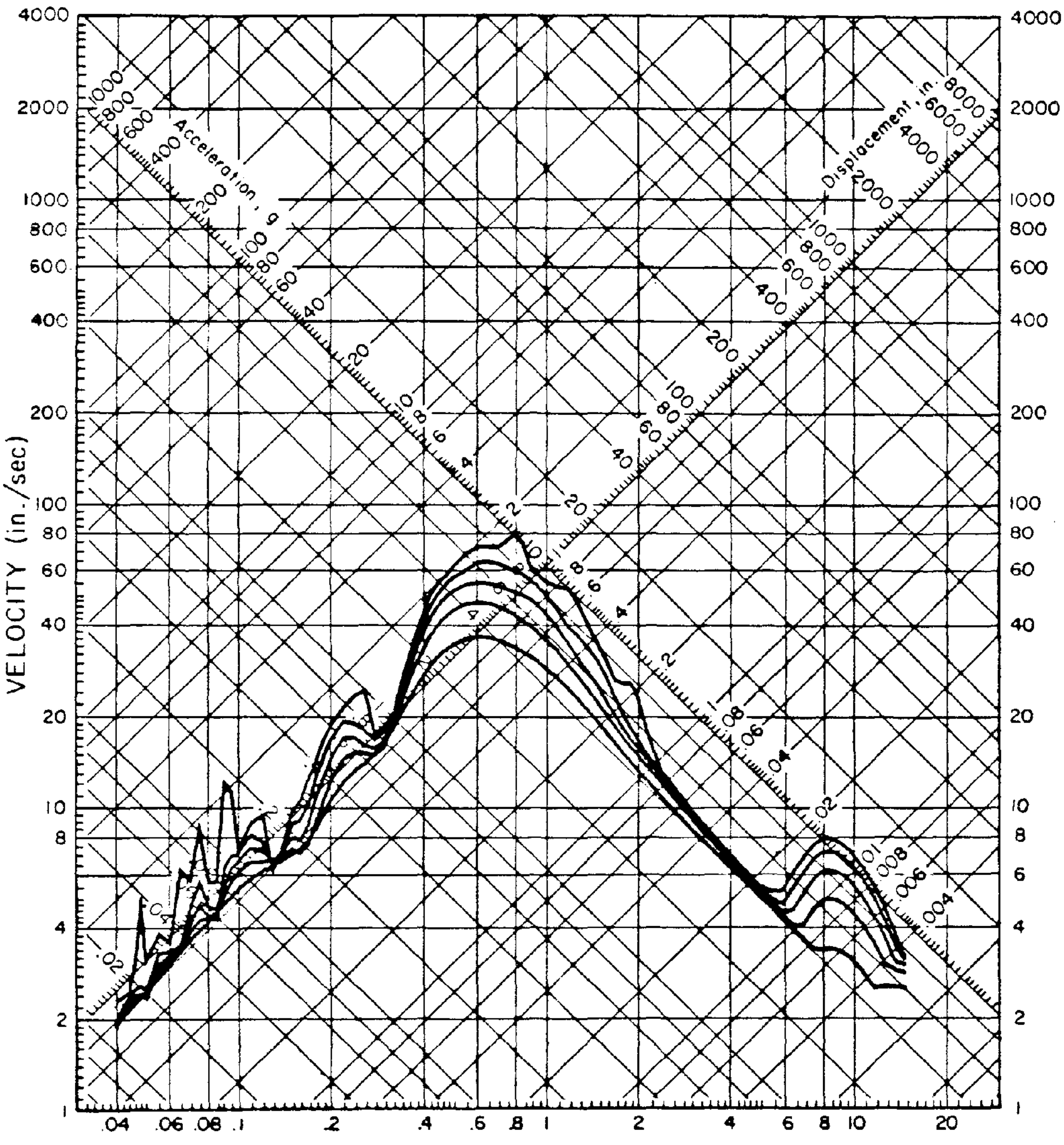

FIGURE 5.42

RESPONSE SPECTRUM

TEST 1CN0001 CENTRIFUGE EARTHQUAKE 11-12-80

IIXX0100 80.001.0 SOIL MECHANICS CENTRIFUGE-BOTTOM OF WALL ACCELEROMETER COMP HOR

DAMPING VALUES ARE 0. 2. 5. 10 AND 20 PERCENT OF CRITICAL

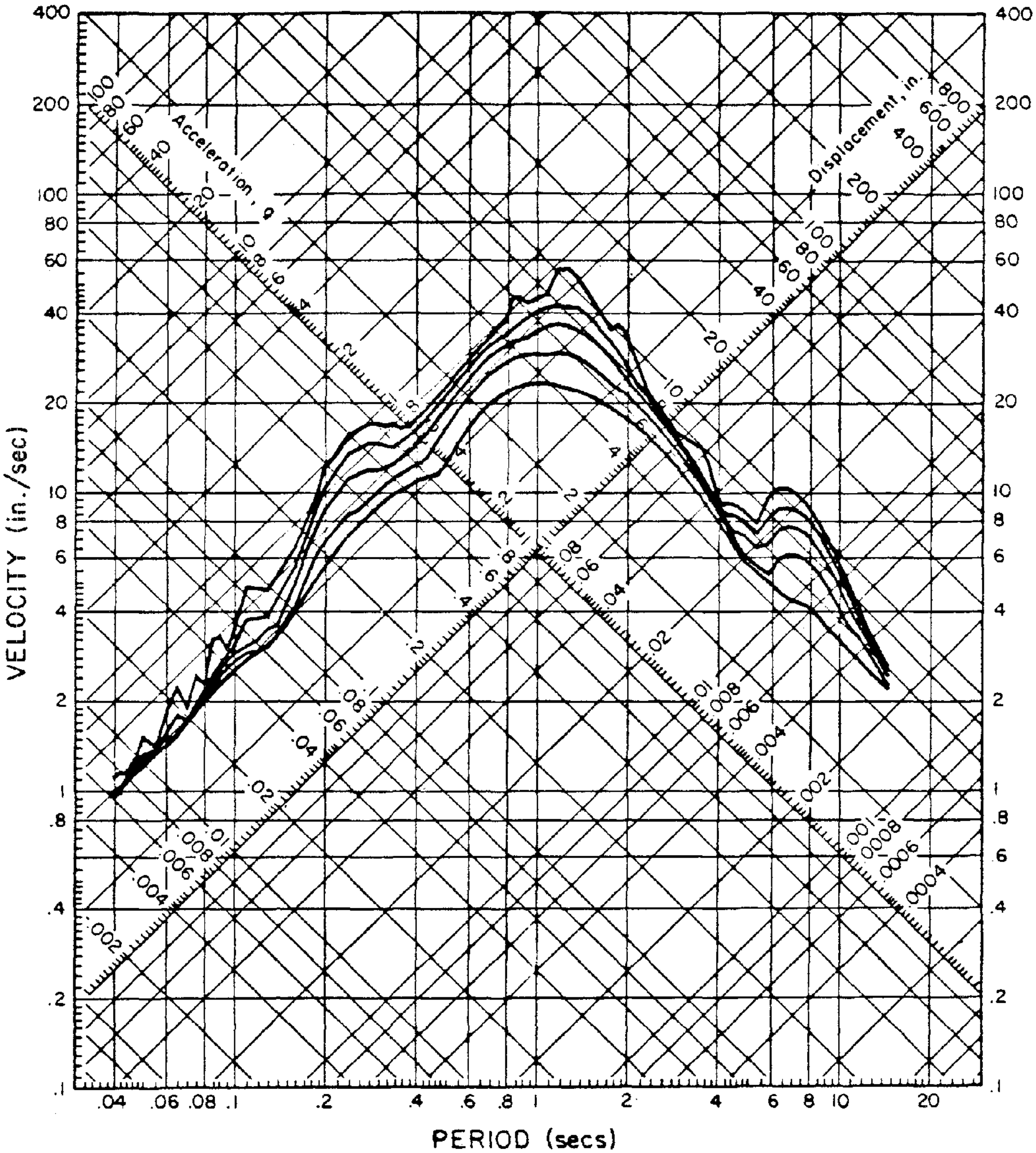

FIGURE 5.43

RESPONSE SPECTRUM

TEST 1CN0002 CENTRIFUGE EARTHQUAKE 3- 4-81

IIXX0200 81.002.0 SOIL MECHANICS CENTRIFUGE -- TOP OF WALL ACCELEROMETER COMP HOR

DAMPING VALUES ARE 0, 2, 5, 10 AND 20 PERCENT OF CRITICAL

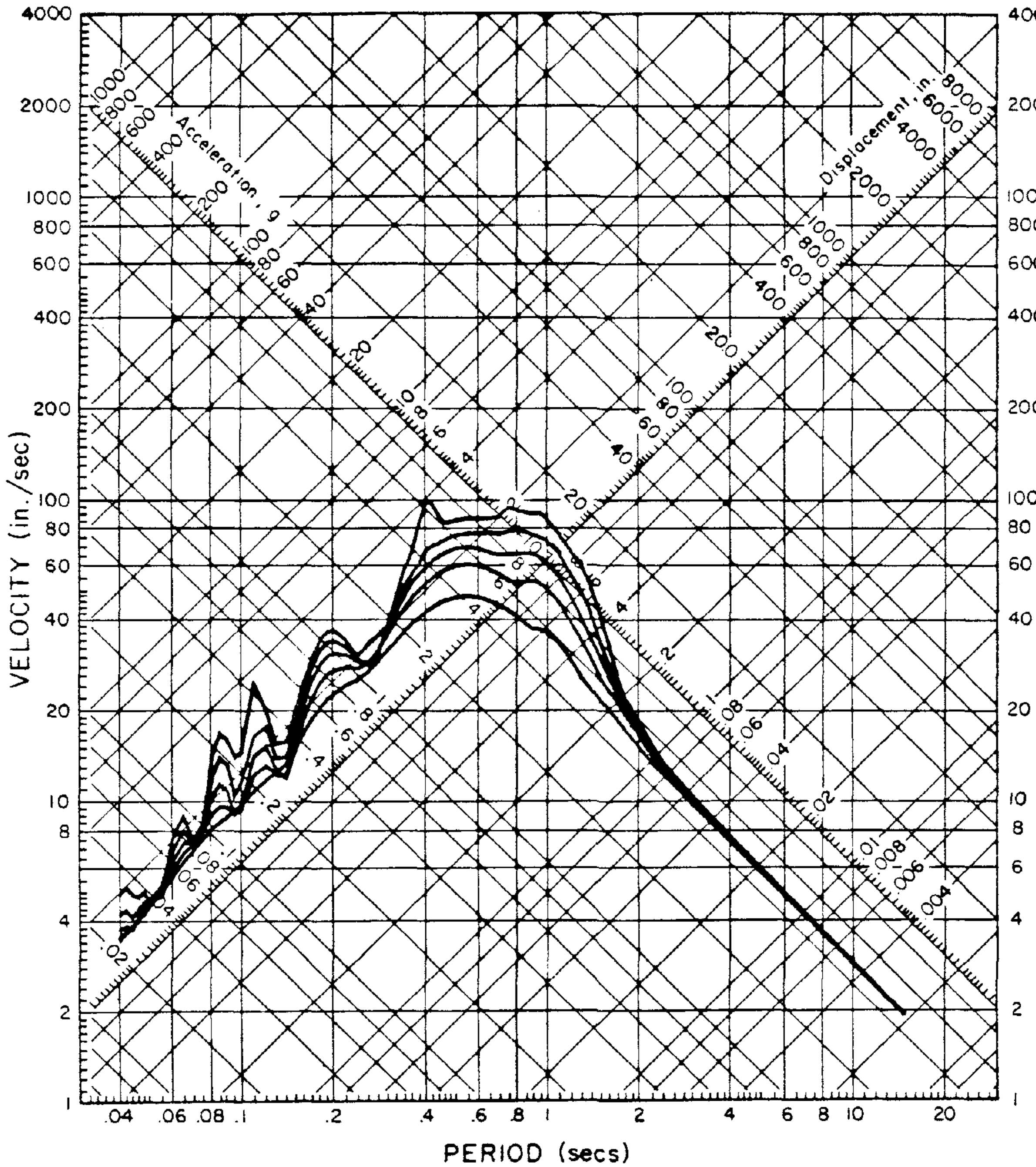

FIGURE 5.44

RESPONSE SPECTRUM

TEST 1CN0002 CENTRIFUGE EARTHQUAKE 3- 4-81

IIXX0200 81.002.0 SOIL MECHANICS CENTRIFUGE-BOTTOM OF WALL ACCELEROMETER COMP HOR

DAMPING VALUES ARE 0, 2, 5, 10 AND 20 PERCENT OF CRITICAL

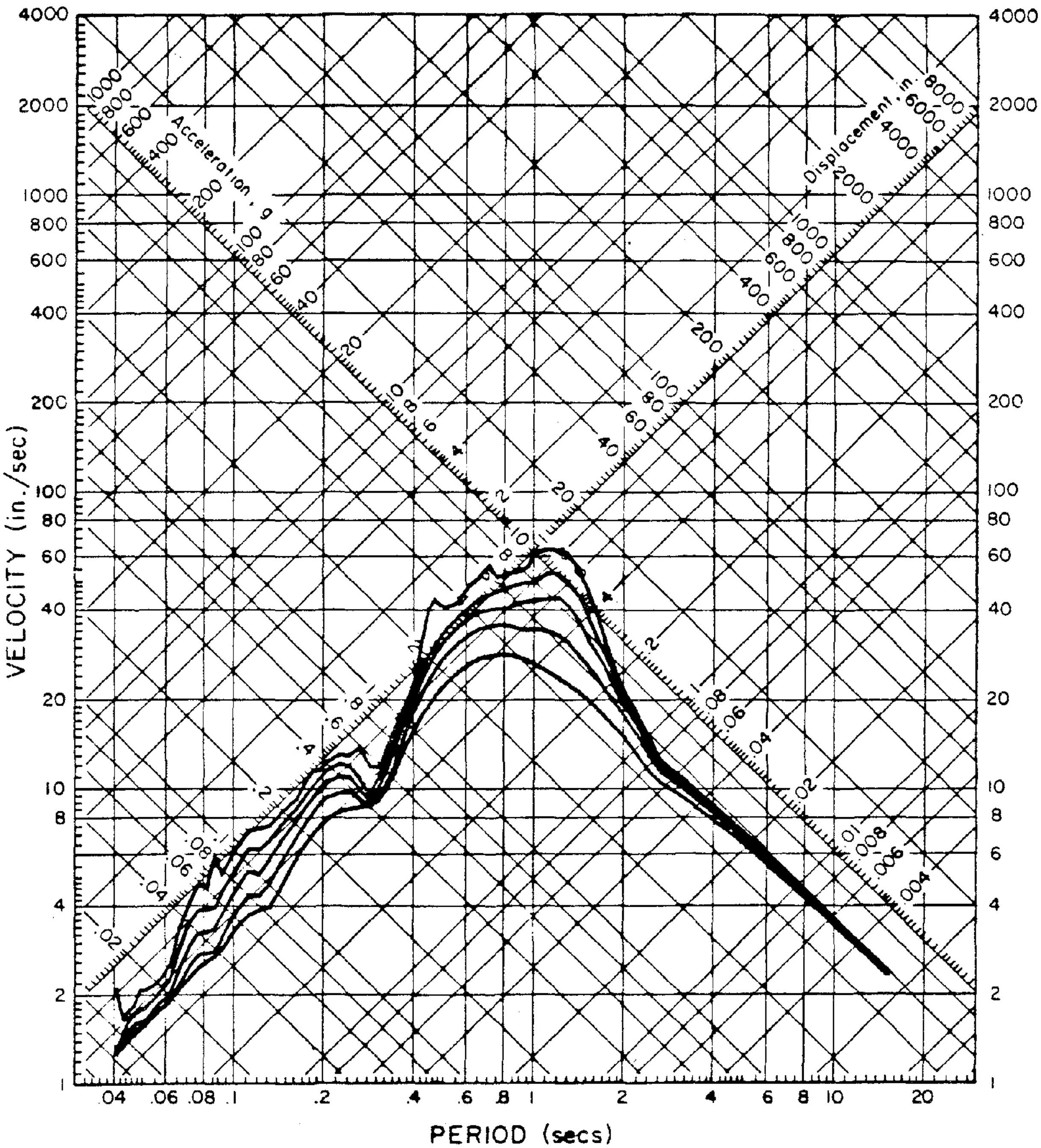

FIGURE 5.45

RESPONSE SPECTRUM

TEST 1CN0002 CENTRIFUGE EARTHQUAKE 3- 4-81

IIXX0200 81.002.0 SOIL MECHANICS CENTRIFUGE - FREE FIELD ACCELEROMETER COMP HOR

DAMPING VALUES ARE 0, 2, 5, 10 AND 20 PERCENT OF CRITICAL

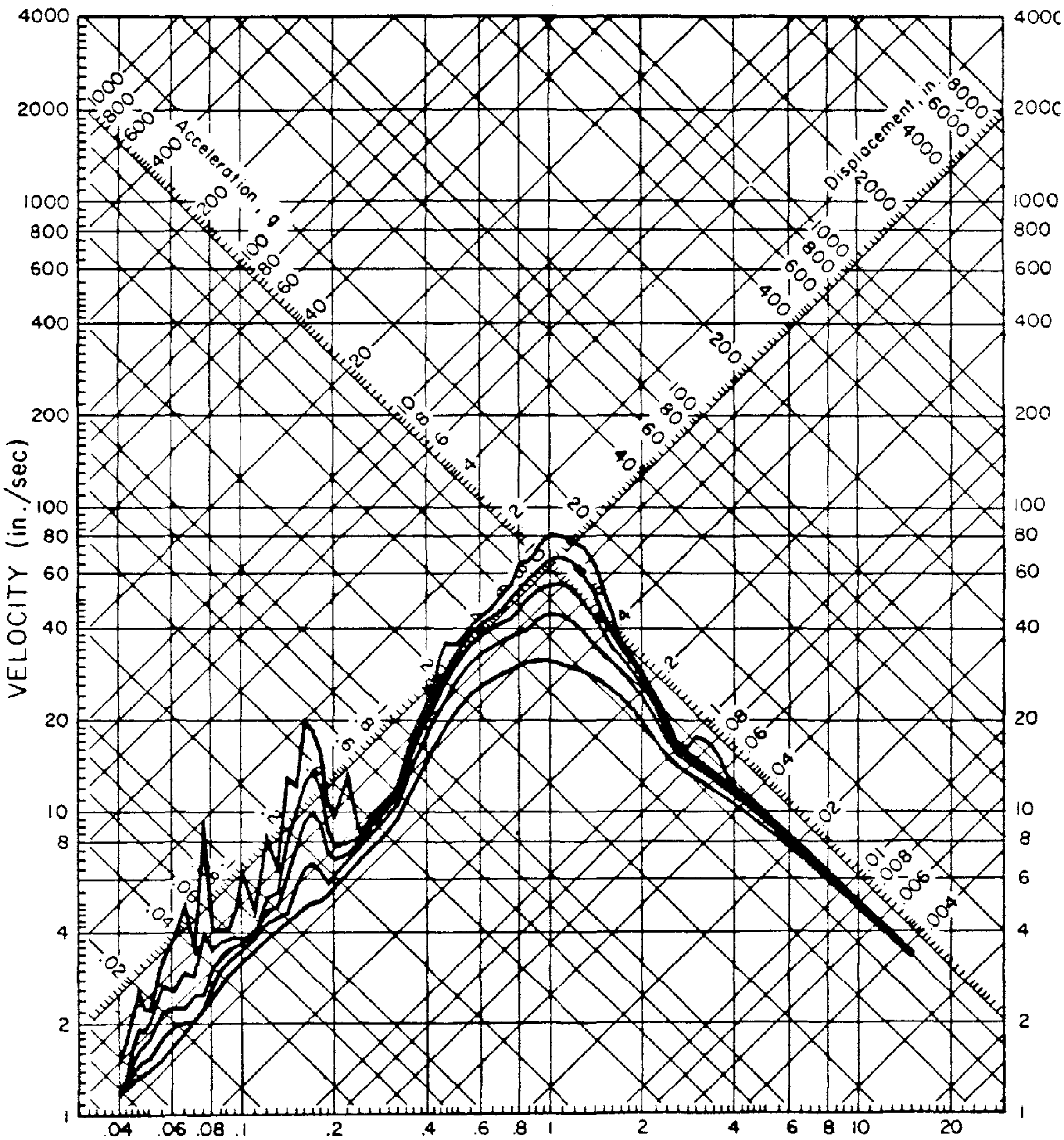

FIGURE 5.46

RESPONSE SPECTRUM

TEST 1CN1003 CENTRIFUGE EARTHQUAKE 3- 9-81

IIXX0300 81.003.0 SOIL MECHANICS CENTRIFUGE — TOP OF WALL ACCELEROMETER COMP HOR

DAMPING VALUES ARE 0, 2, 5, 10 AND 20 PERCENT OF CRITICAL

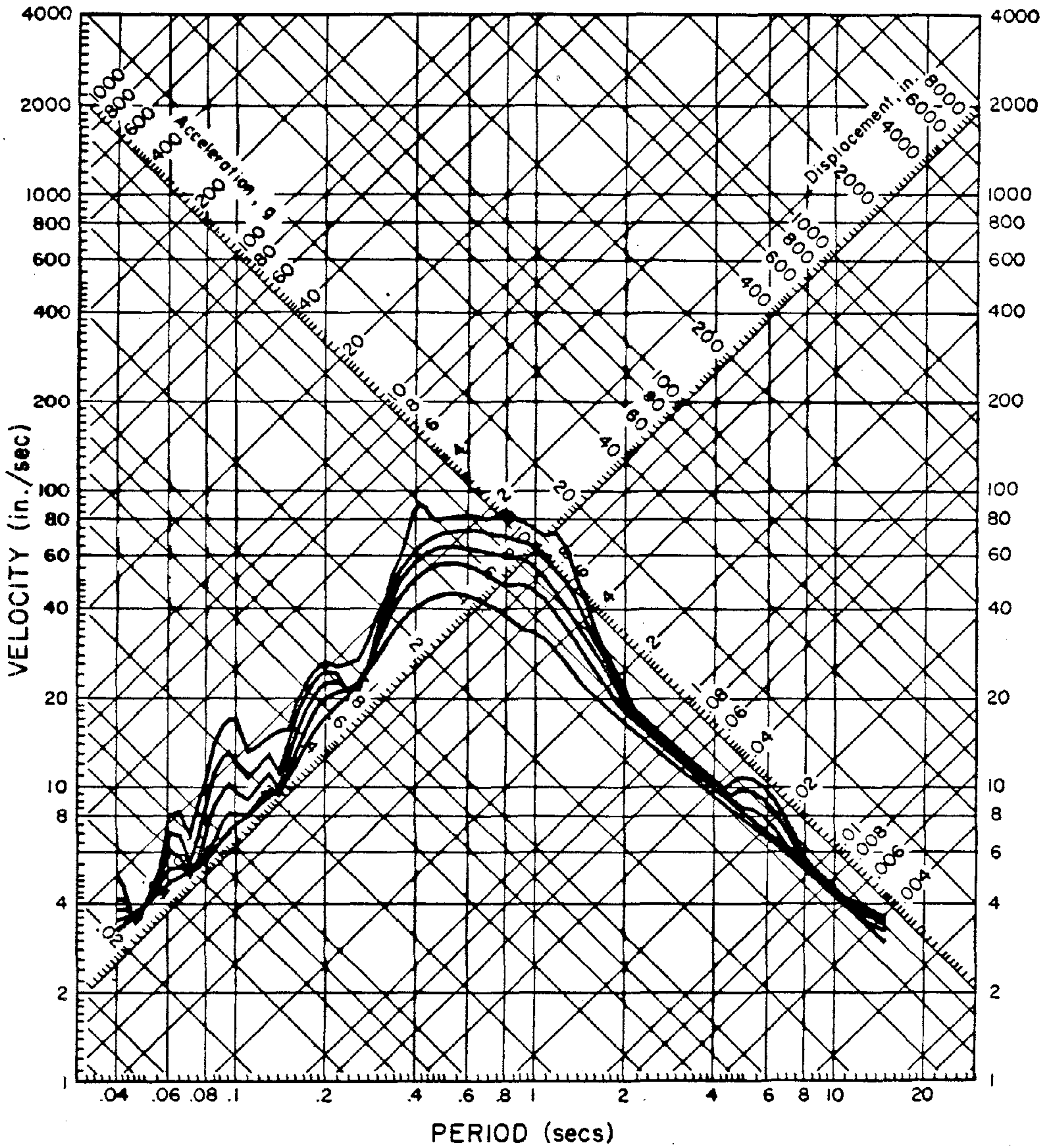

FIGURE 5.47

RESPONSE SPECTRUM

TEST 1CN1003 CENTRIFUGE EARTHQUAKE 3- 9-81

IIXX0300 81.003.0 SOIL MECHANICS CENTRIFUGE-BOTTOM OF WALL ACCELEROMETER COMP HOR

DAMPING VALUES ARE 0, 2, 5, 10 AND 20 PERCENT OF CRITICAL

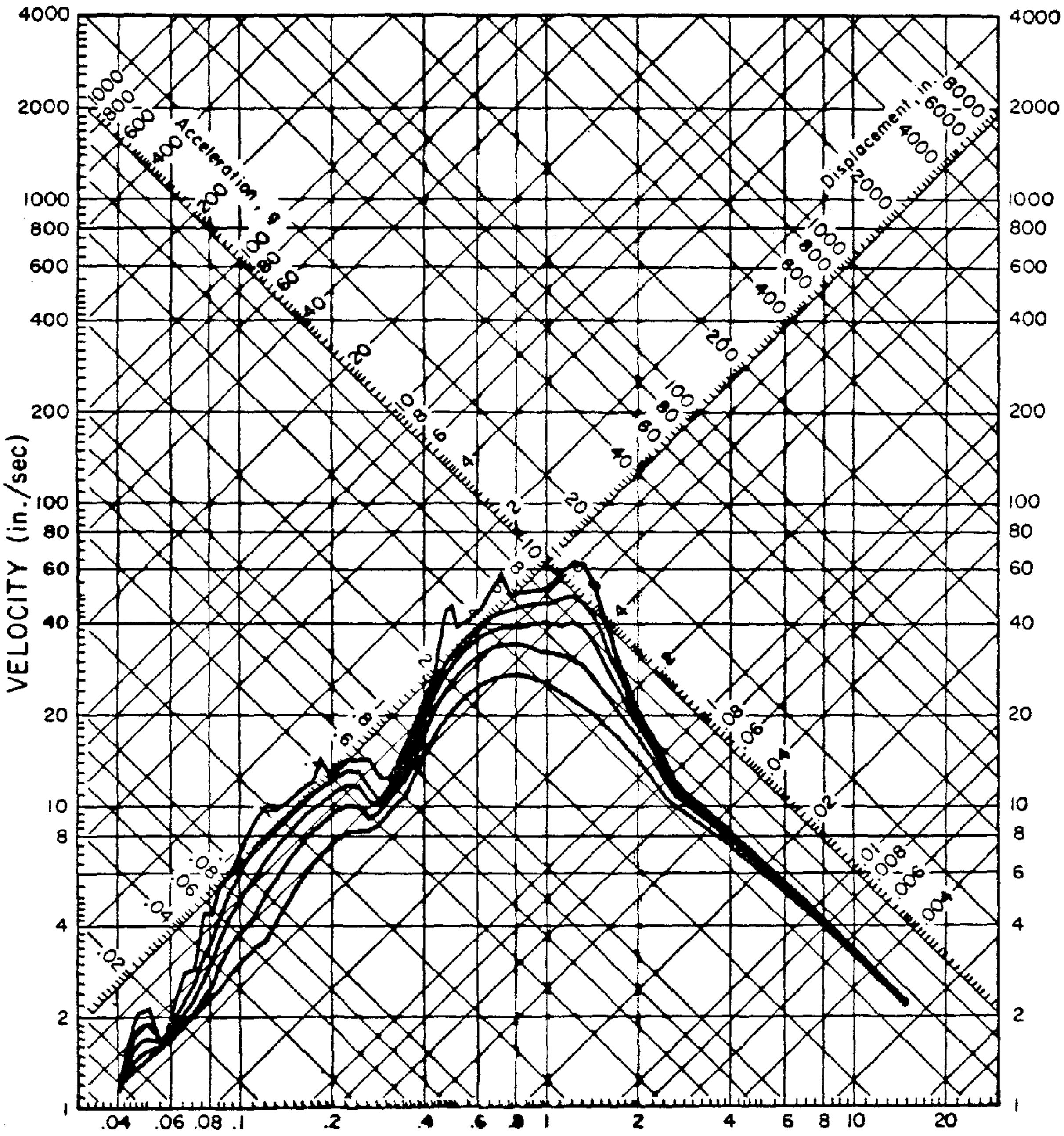

FIGURE 5.48

RESPONSE SPECTRUM

TEST 2CN0011 CENTRIFUGE EARTHQUAKE 2-25-82

IIXX0100 82.011.0 SOIL MECHANICS CENTRIFUGE — TOP OF WALL ACCELEROMETER COMP HOR

DAMPING VALUES ARE 0, 2, 5, 10 AND 20 PERCENT OF CRITICAL

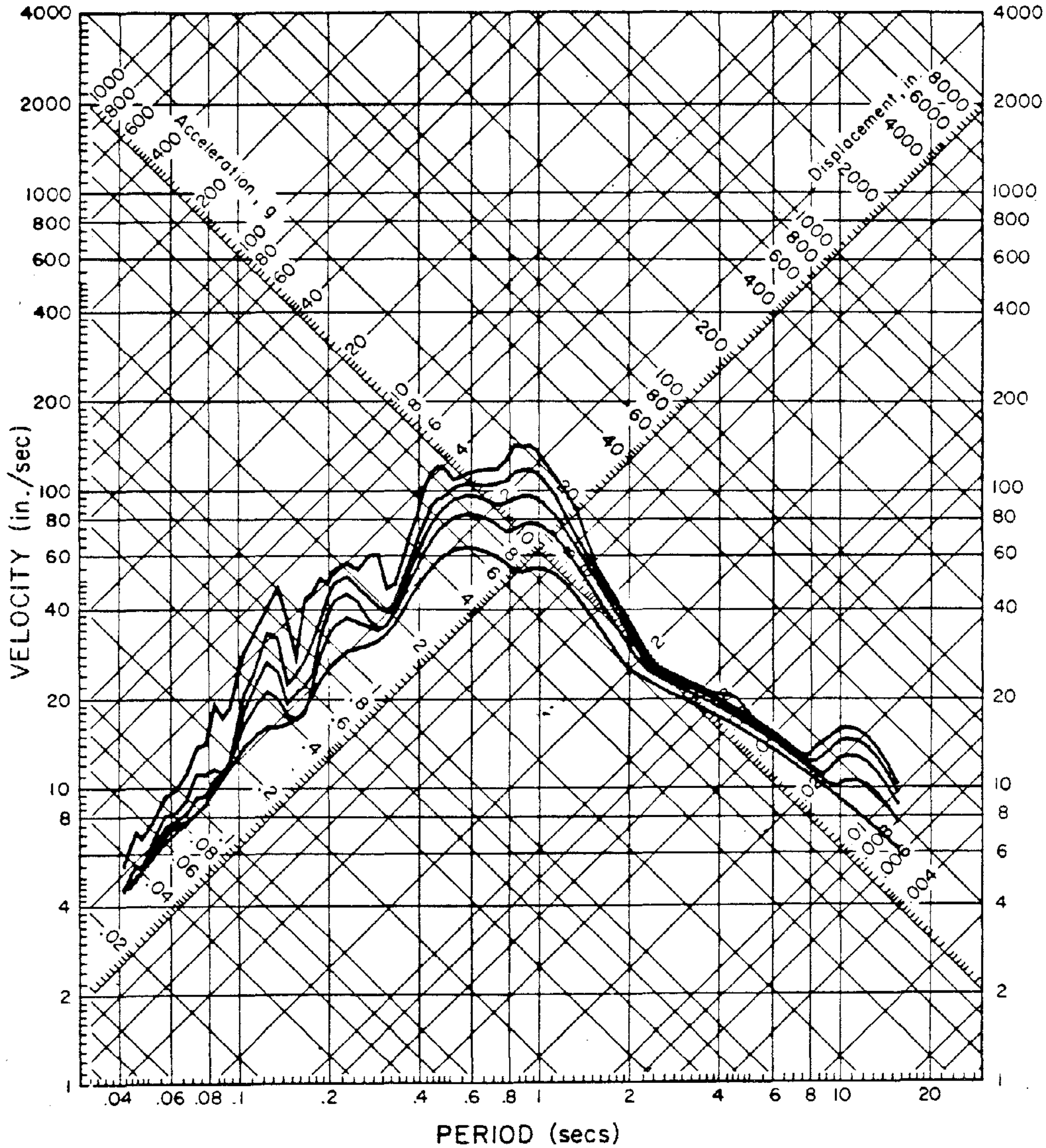

FIGURE 5.49

RESPONSE SPECTRUM

TEST 2CN0011   CENTRIFUGE EARTHQUAKE   2-25-82

IIXX0100 82.011.0 SOIL MECHANICS CENTRIFUGE-BOTTOM OF WALL ACCELEROMETER COMP HOR

DAMPING VALUES ARE 0, 2, 5, 10 AND 20 PERCENT OF CRITICAL

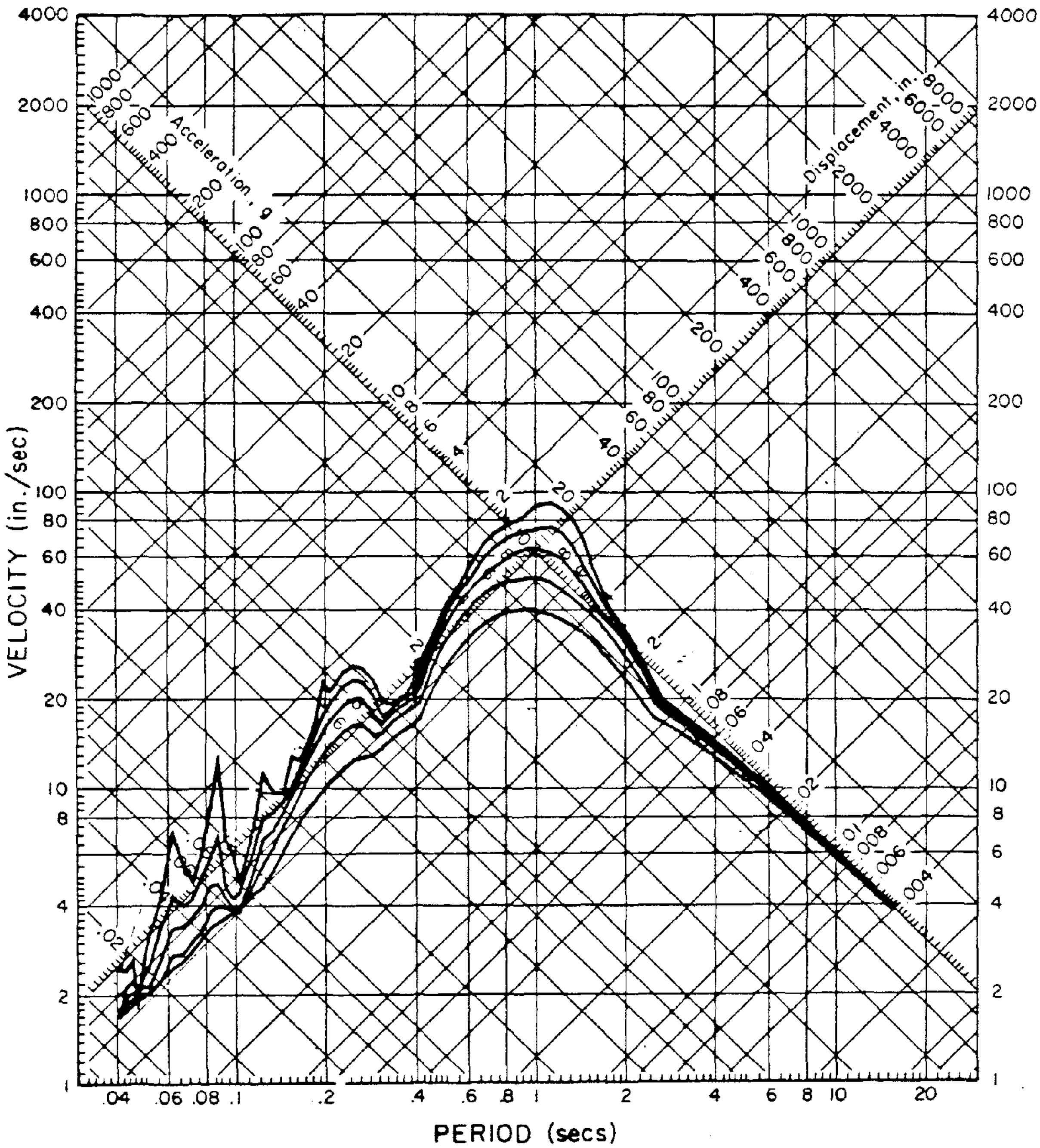

FIGURE 5.50

RESPONSE SPECTRUM

TEST 2CN0011 CENTRIFUGE EARTHQUAKE 2-25-82

IIXX0100 82.011.0 SOIL MECHANICS CENTRIFUGE - FREE FIELD ACCELEROMETER COMP HOR

DAMPING VALUES ARE 0. 2. 5. 10 AND 20 PERCENT OF CRITICAL

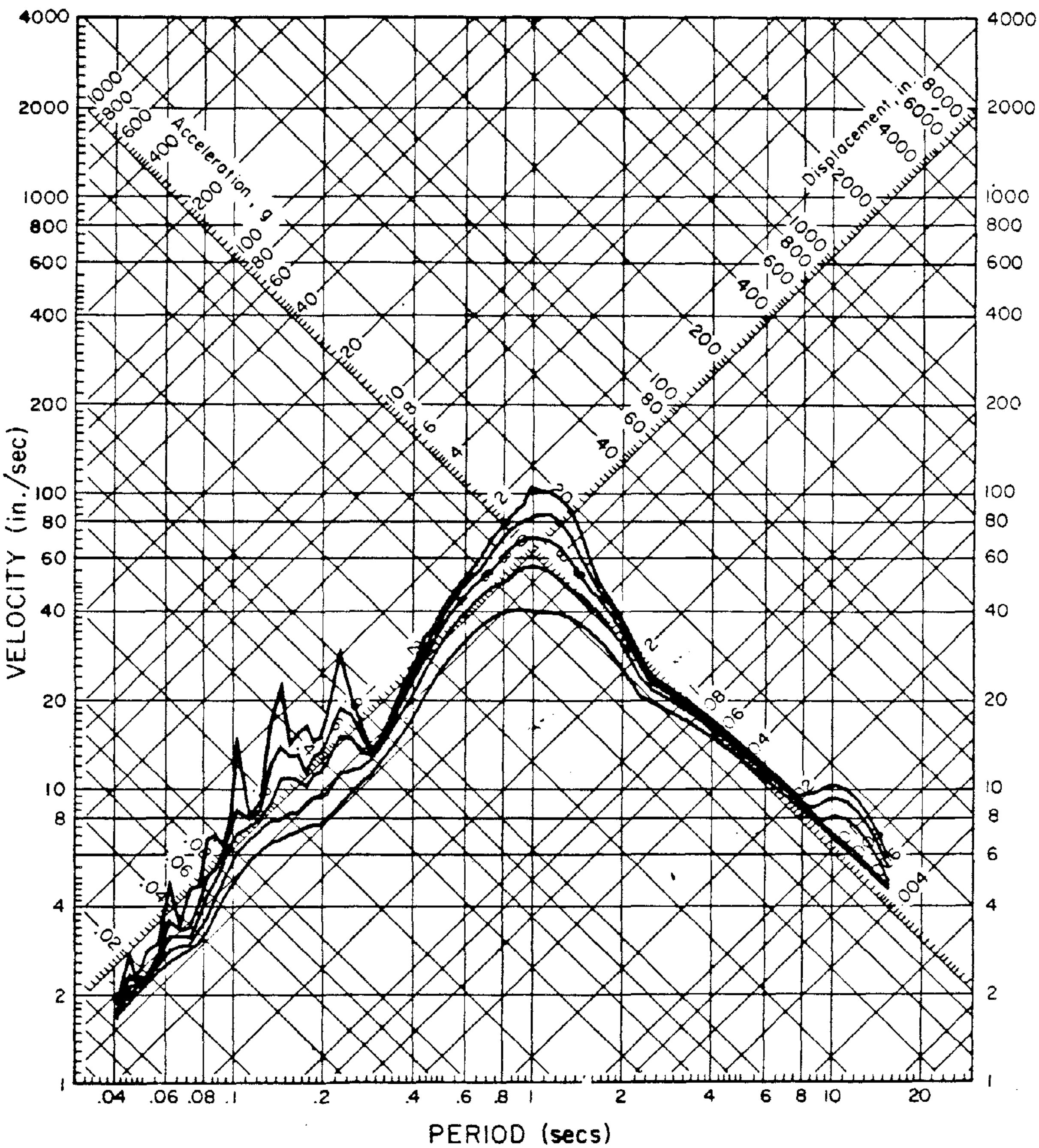

FIGURE 5.51

RESPONSE SPECTRUM

PARKFIELD, CALIFORNIA EARTHQUAKE JUNE 27, 1966 - 2026 PST

IIIB033 66.001.0 CHOLAME.SHANDON. CALIFORNIA ARRAY NO. 2 COMP N65E

DAMPING VALUES ARE 0, 2, 5, 10 AND 20 PERCENT OF CRITICAL

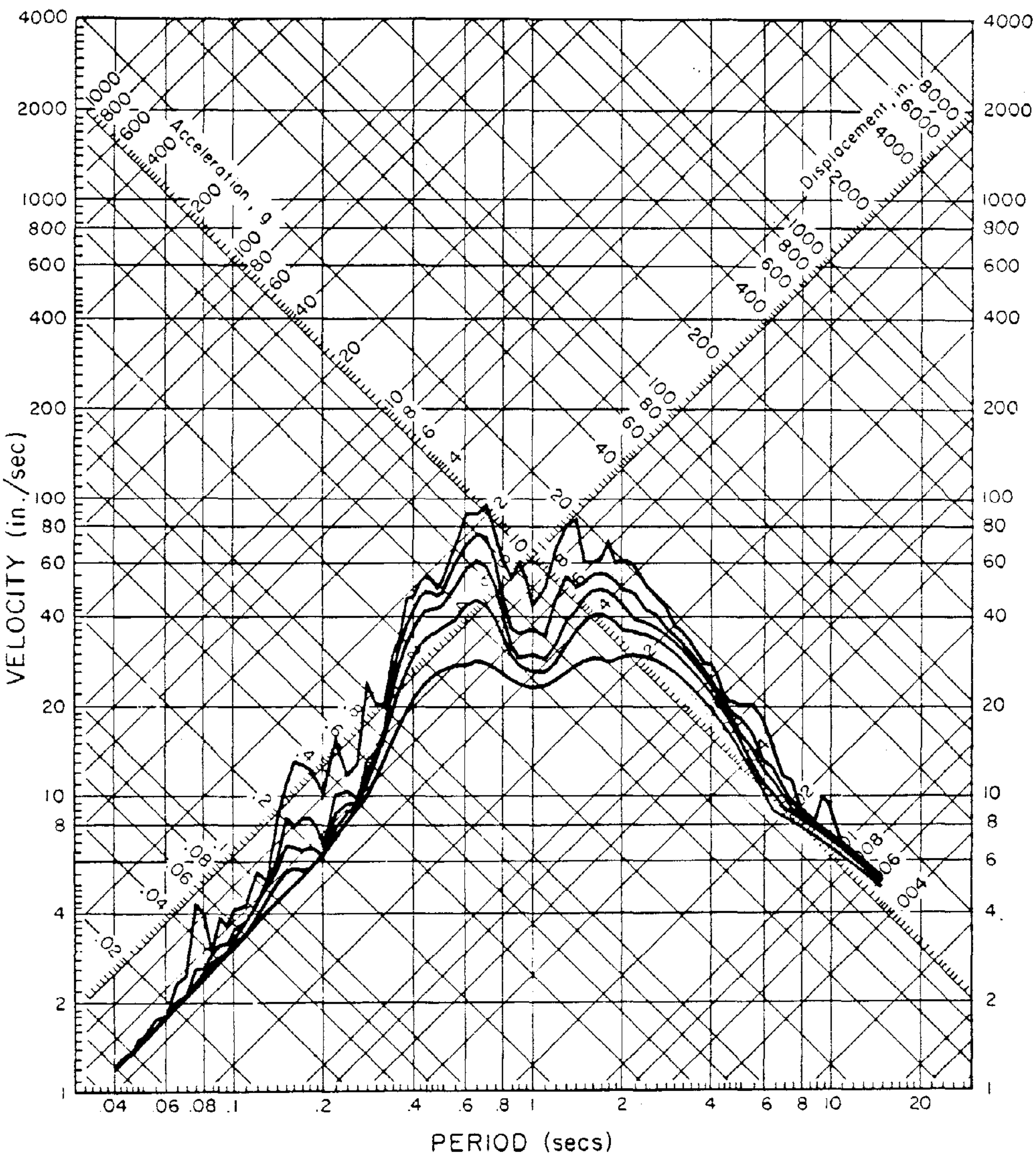

FIGURE 5.52

2CN0011 (Figures 5.42 through 5.51) with that of the stronger horizontal component of Parkfield (Figure 5.52), it can be seen that they are all very similar. They have peaks for periods between 0.4 and 1.5 seconds (prototype) which are at similar levels for similar dampings. The main difference lies in the observation that the centrifuge shaking lacks the longer (> 2.0 sec) period components which the Parkfield motion contains. The above would seem to indicate that the prototype structure of the centrifuge model would have behaved very much like the model during an earthquake similar to Parkfield, had it been close to the rupturing fault.

The comparisons clearly show that, although the shaking mechanism employed in the centrifuge is not sophisticated, it does give motions which have realistic characteristics and thus can be used to provide some real insight into the problem at hand. Longer duration shaking would primarily affect walls retaining saturated backfill in which pore pressure effects might be important.

5.3. Parameter Diagrams

Figures 5.53 through 5.107 show the moment, pressure, shear force, and lateral displacement distributions obtained from the 14 tests performed. As explained in Section 4.2, these figures show the entire response of the system to the particular shaking it was subjected to. Table 5.4 should be used as a key to the interpretation of the figures.

TABLE 5.4
Key To Figures 5.53 Through 5.107

Frame a - Contour map of the parameter distribution with respect to location and time.

Frame b - Parameter distribution with respect to time at location where maximum occurs (Section A-A of contour map).

Frame c - Parameter distribution with respect to location-static, maximum dynamic (section B-B of the contour map), and final static after motion ceases.

+ Location of strain gages

x Location of pressure transducers

O Maximum

Δ Data point

On Frame c of pressure distribution plots, the following symbols appear. [Along (P/ρg H) axis]:

O Location of static resultant

□ Location of maximum resultant

◇ Location of final static resultant

Rankine/Coulomb (static) and Mononobe-Okabe (maximum dynamic) pressure distributions are also shown in this frame.

Except for tests 1CN0001, 1CN0002, 1CN1003, 1CN0004, and 1CN1505, the time (tf_1) scales (on Frames a and b) are set up so that the first 20% of the record is displayed over the first 50% of the graph and the final 80% over the other 50%. This was done to enhance the presentation of the more critical part of the tests.

FIGURE 5.53

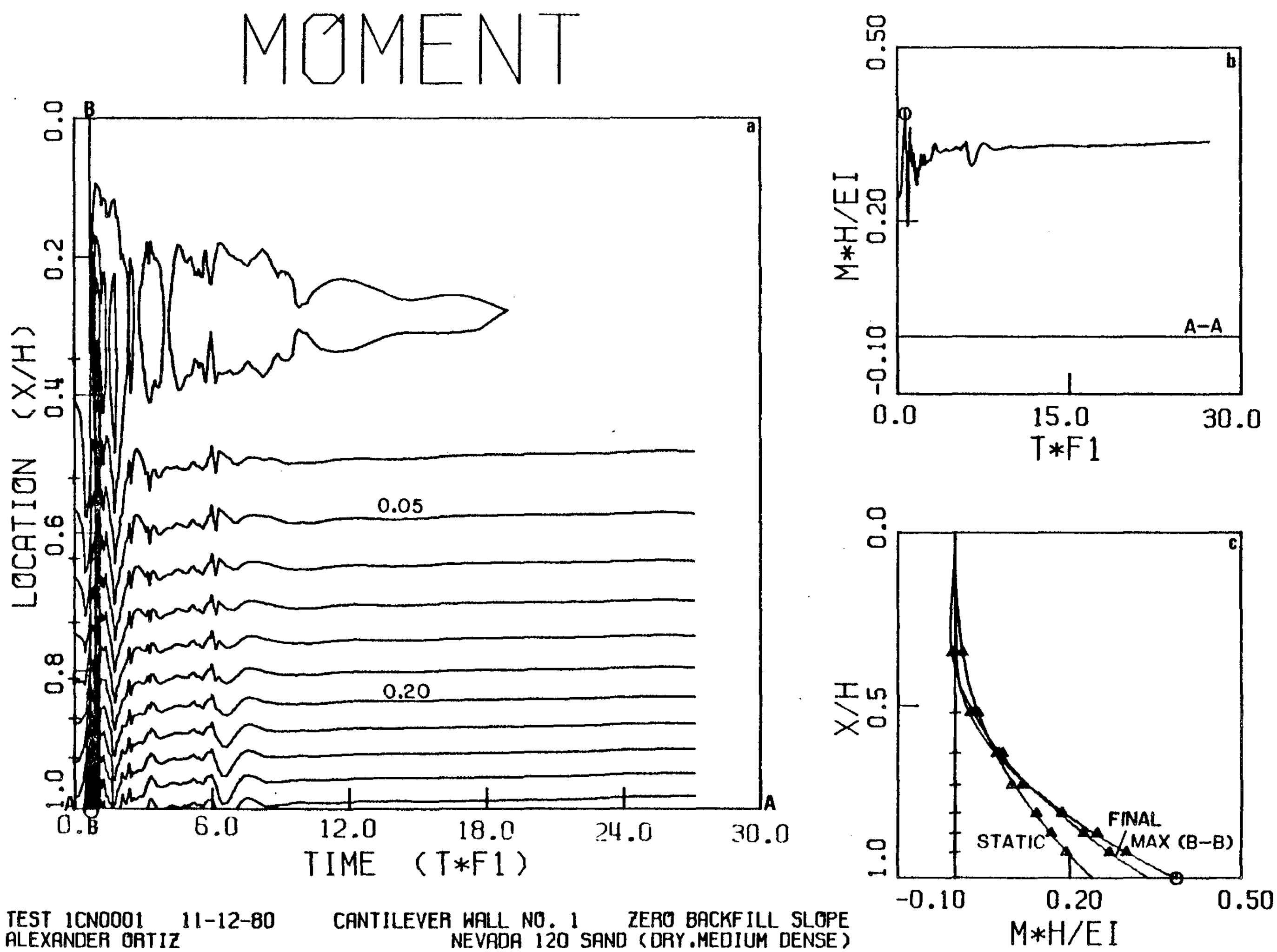
MØMENT
LØCATIØN (X/H)
0.0
0.2
0.4
0.6
0.8
1.0
B
a
A
0.05
0.20
0.0
6.0
12.0
18.0
24.0
30.0
TIME (T*F1)
TEST 1CN0001 11-12-80
ALEXANDER ORTIZ
CANTILEVER WALL NO. 1 ZERO BACKFILL SLOPE
NEVADA 120 SAND (DRY.MEDIUM DENSE)
b
M*H/EI
0.50
0.20
-0.10
A-A
0.0
15.0
30.0
T*F1
c
X/H
0.0
0.5
1.0
FINAL
MAX (B-B)
STATIC
-0.10
0.20
0.50
M*H/EI

FIGURE 5.54

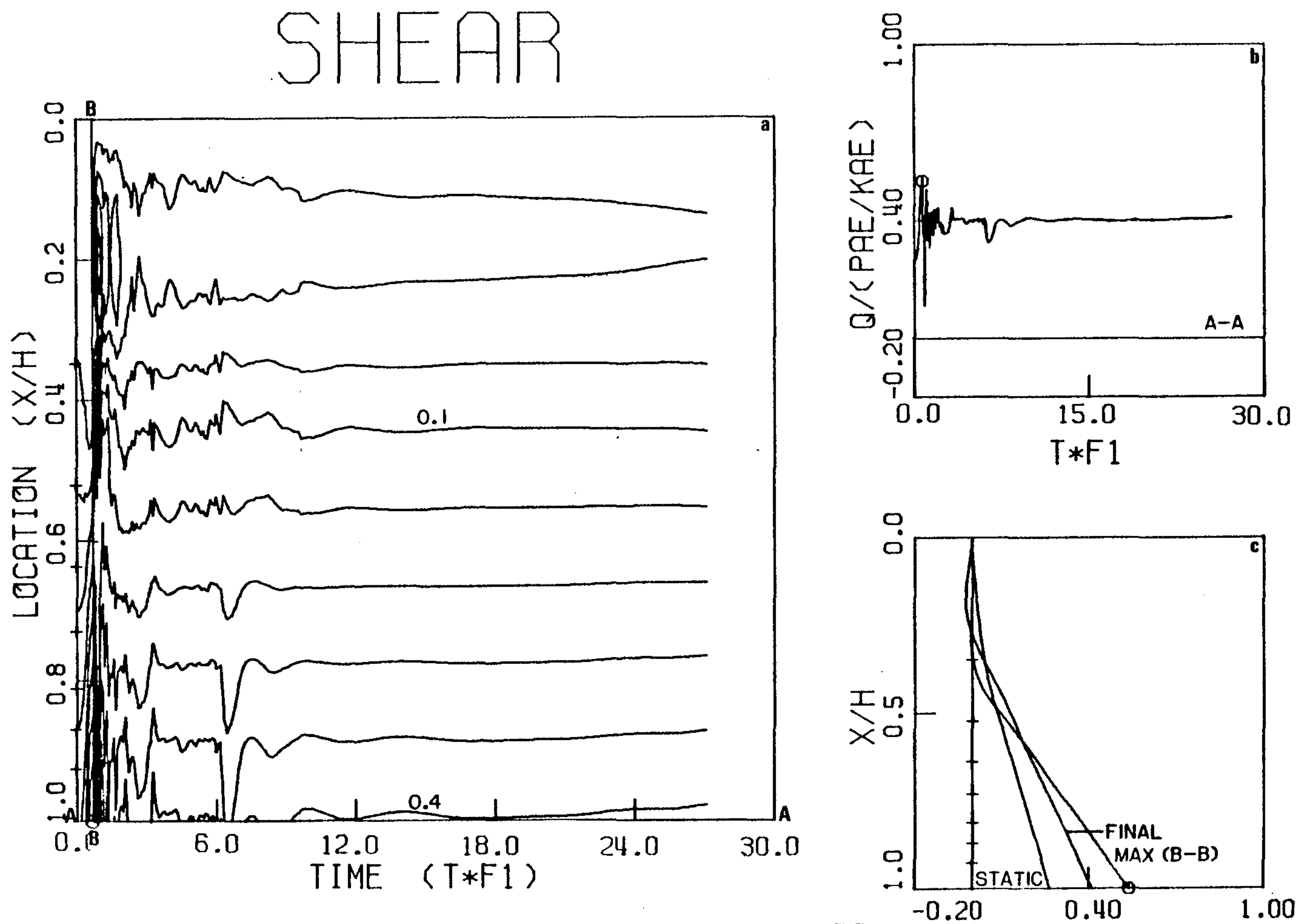

TEST 1CN0001 11-12-80 CANTILEVER WALL NO. 1 ZERO BACKFILL SLOPE
ALEXANDER ORTIZ NEVADA 120 SAND (DRY, MEDIUM DENSE)

FIGURE 5.55

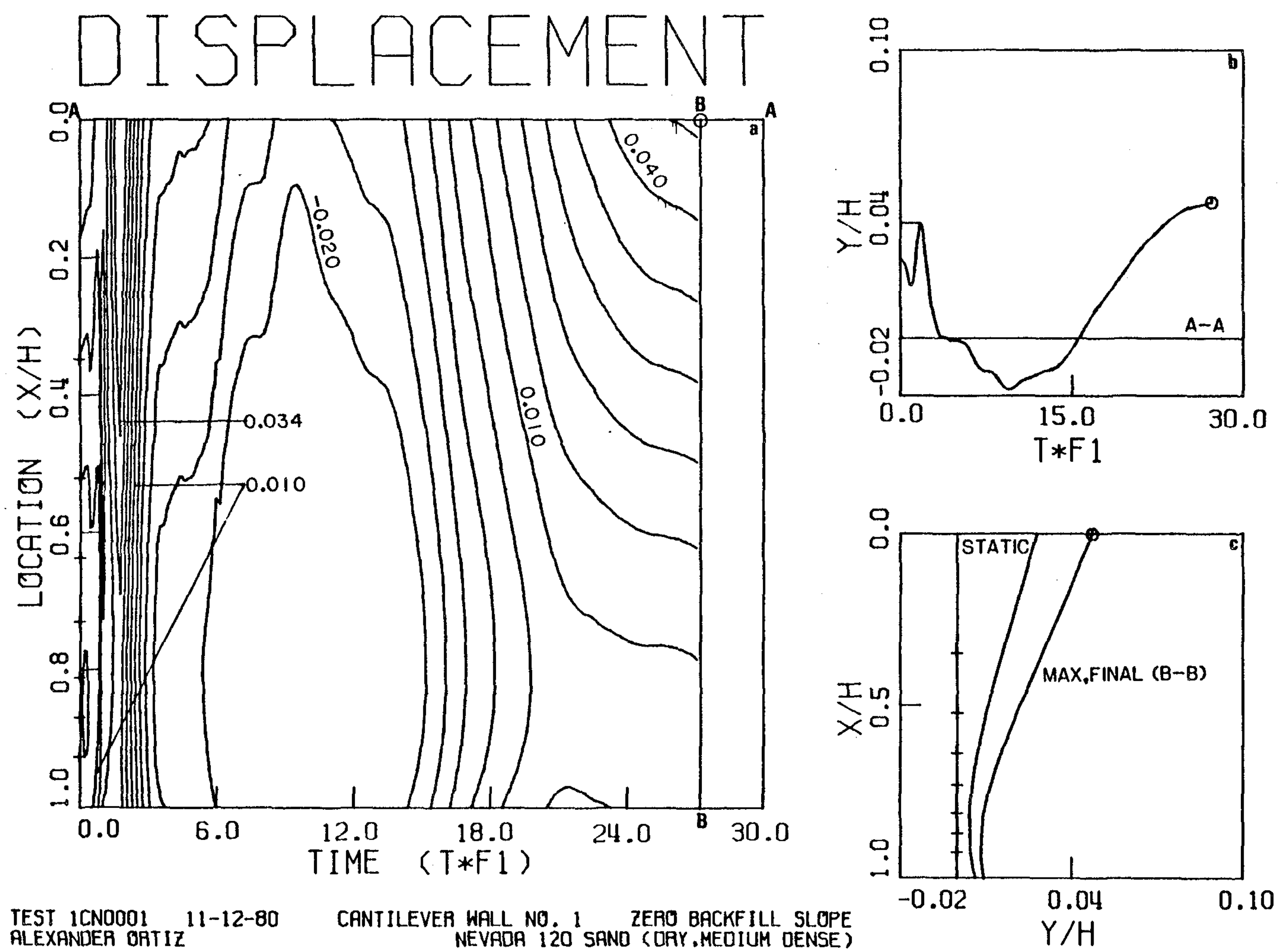
DISPLACEMENT
A
B
a
0.040
-0.020
0.010
0.034
0.010
LOCATION (X/H)
0.0
0.2
0.4
0.6
0.8
1.0
0.0
6.0
12.0
18.0
24.0
30.0
TIME (T*F1)
b
A-A
Y/H
0.10
0.04
-0.02
T*F1
15.0
c
STATIC
MAX,FINAL (B-B)
X/H
0.5
Y/H
TEST 1CN0001 11-12-80
ALEXANDER ORTIZ
CANTILEVER WALL NO. 1 ZERO BACKFILL SLOPE
NEVADA 120 SAND (DRY,MEDIUM DENSE)

FIGURE 5.56

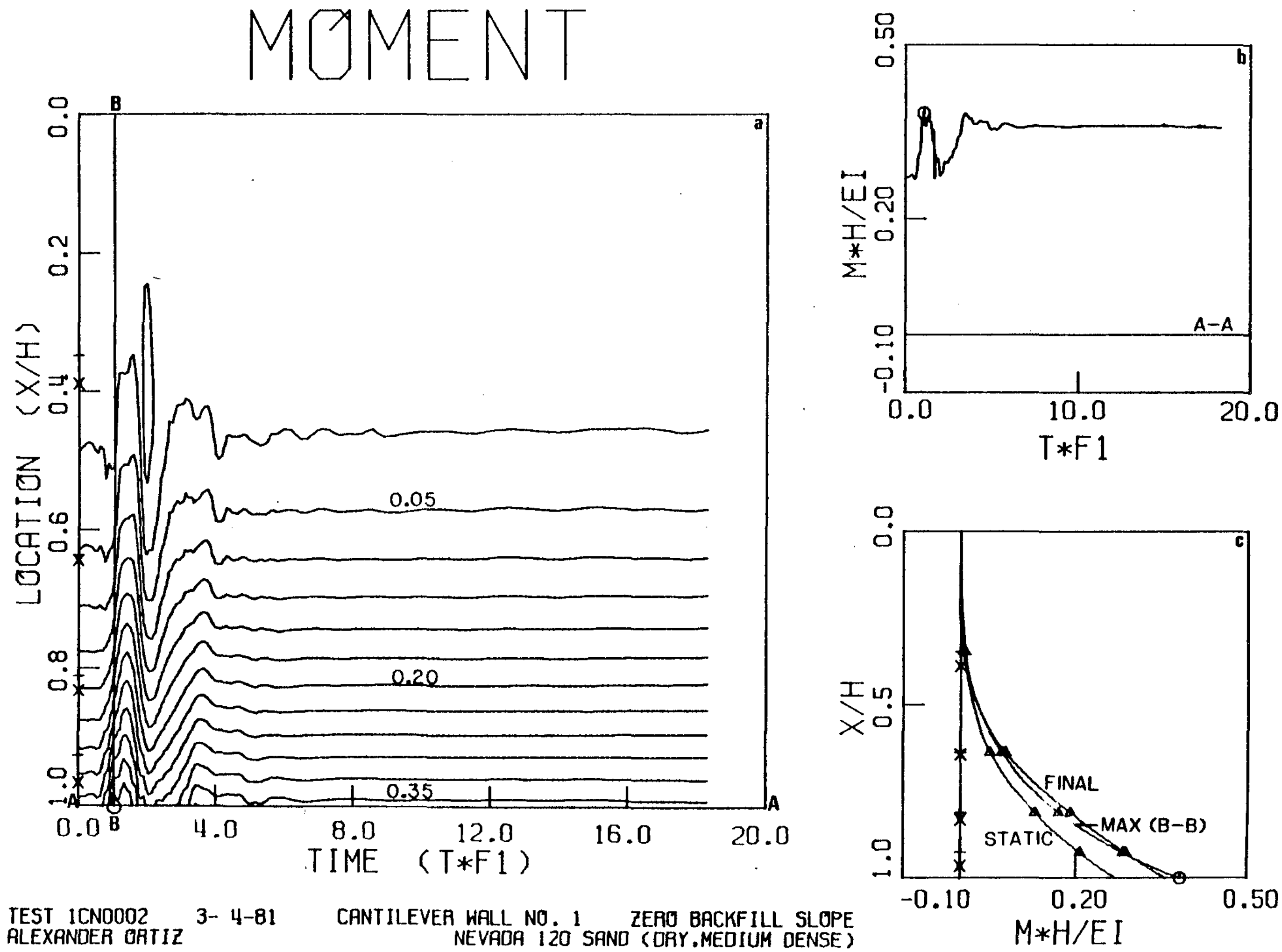
MOMENT
LOCATION (X/H)
TIME (T*F1)
0.05
0.20
0.35
M*H/EI
T*F1
A-A
X/H
FINAL
MAX (B-B)
STATIC
M*H/EI
TEST 1CN0002 3- 4-81 CANTILEVER WALL NO. 1 ZERO BACKFILL SLOPE
ALEXANDER ORTIZ NEVADA 120 SAND (DRY,MEDIUM DENSE)

FIGURE 5.57

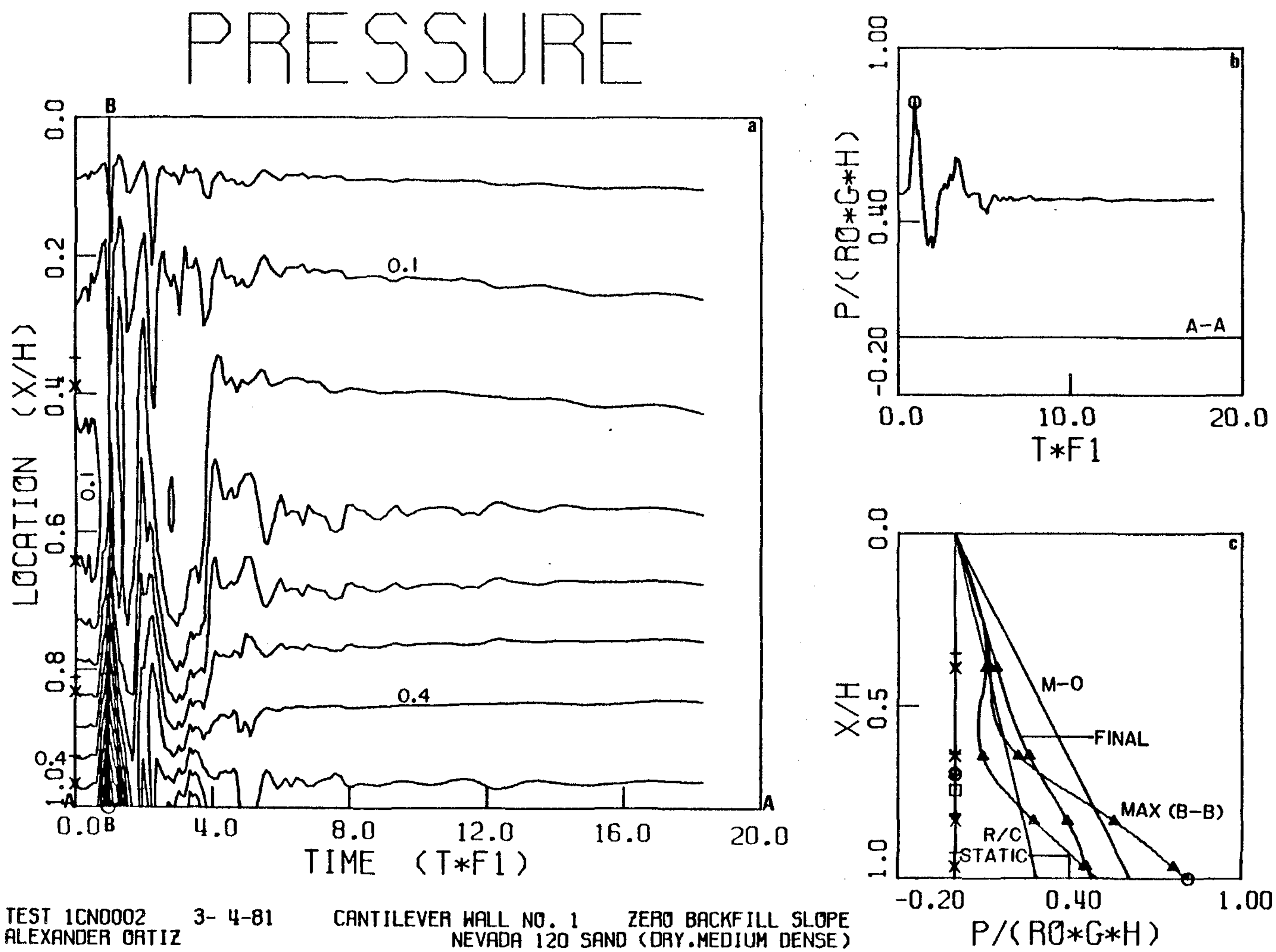

TEST 1CN0002 3- 4-81 CANTILEVER WALL NO. 1 ZERO BACKFILL SLOPE
ALEXANDER ORTIZ NEVADA 120 SAND (DRY.MEDIUM DENSE)

FIGURE 5.58

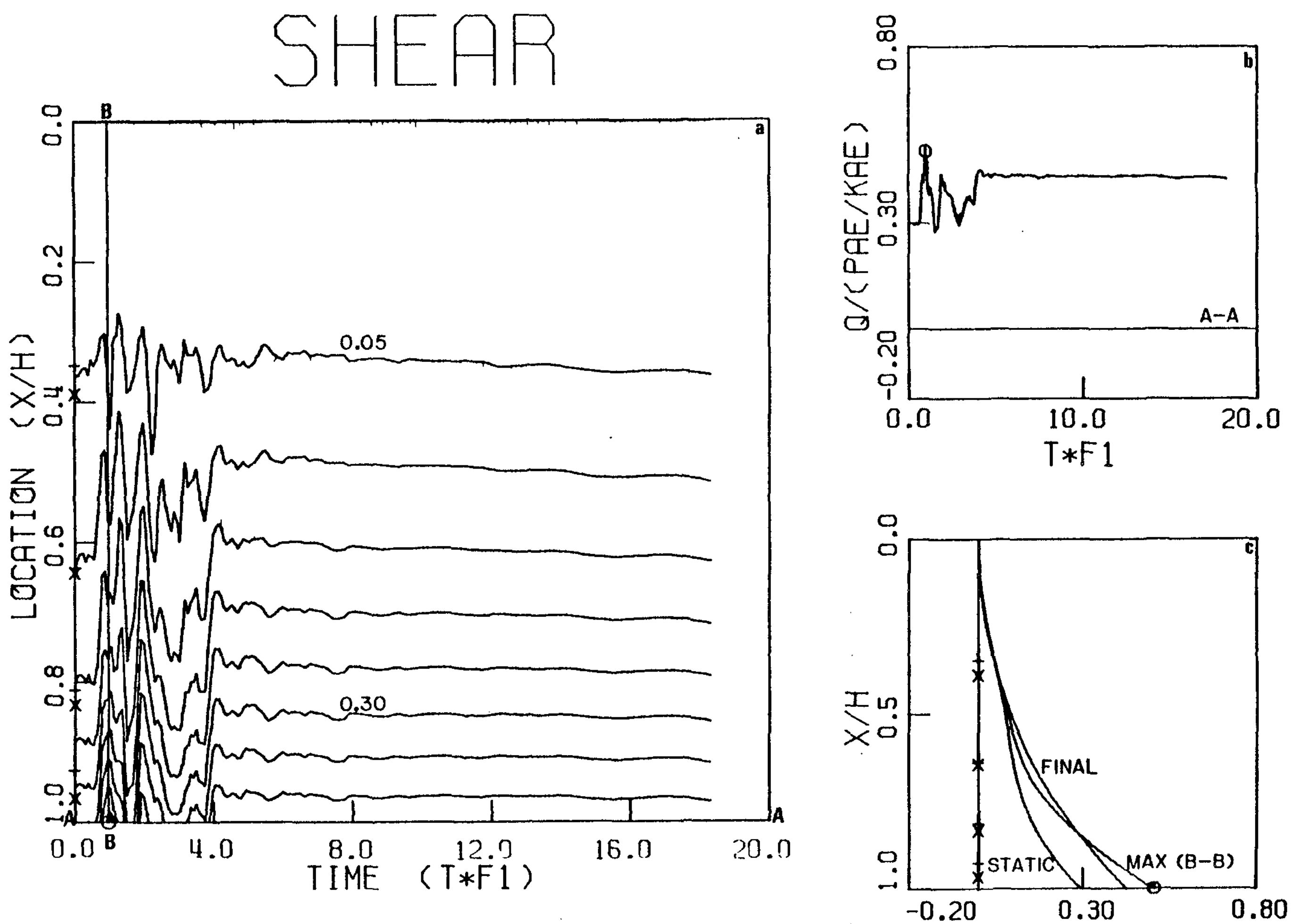

TEST 1CN0002 3- 4-81 CANTILEVER WALL NO. 1 ZERO BACKFILL SLOPE
ALEXANDER ORTIZ NEVADA 120 SAND (DRY.MEDIUM DENSE)

FIGURE 5.59

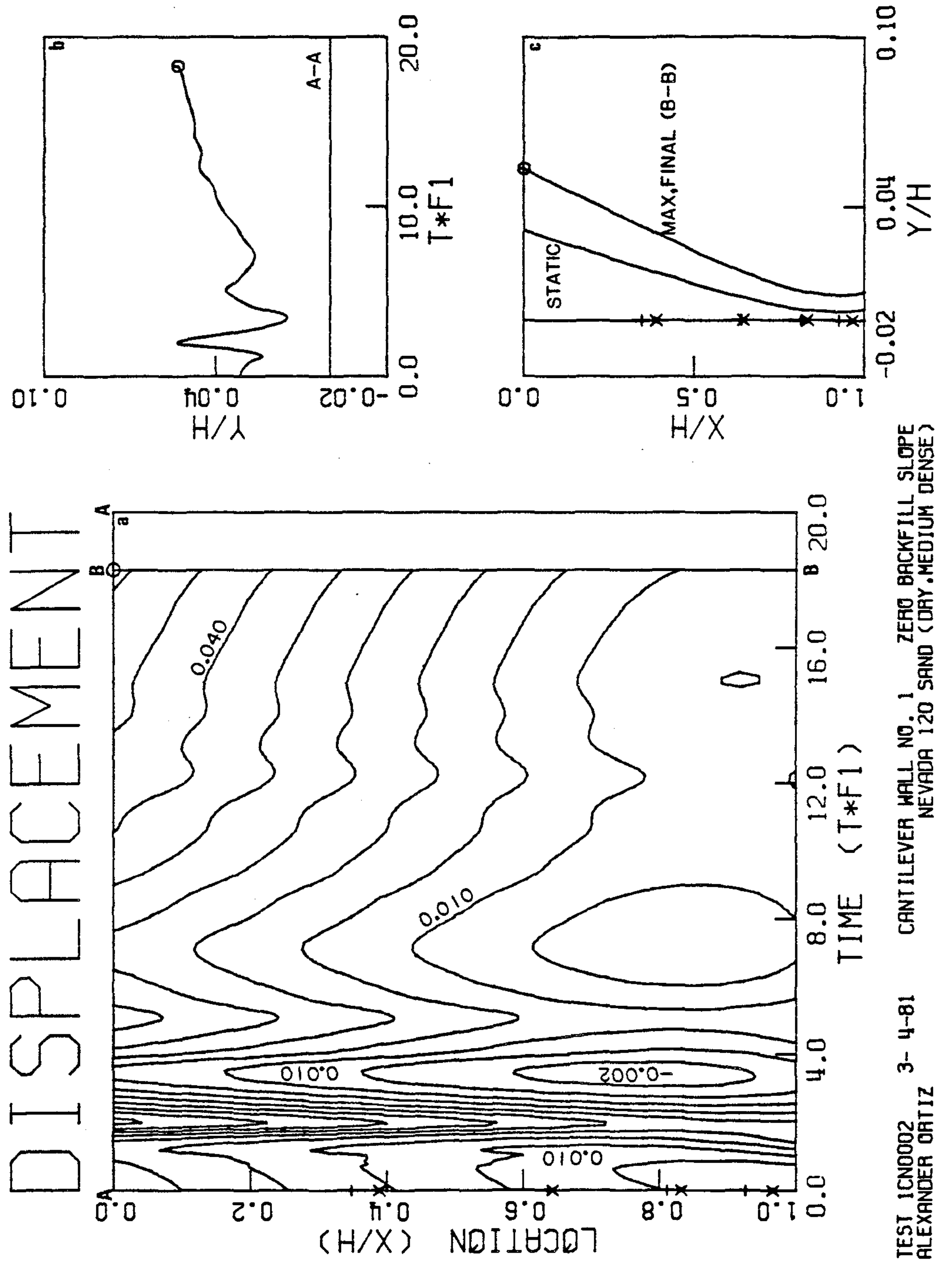
DISPLACEMENT
LOCATION (X/H)
TIME (T*F1)
0.010
0.040
-0.002
Y/H
T*F1
A-A
X/H
STATIC
MAX,FINAL (B-B)
TEST 1CN0002 3- 4-81 CANTILEVER WALL NO. 1 ZERO BACKFILL SLOPE
ALEXANDER ORTIZ NEVADA 120 SAND (DRY,MEDIUM DENSE)

FIGURE 5.60

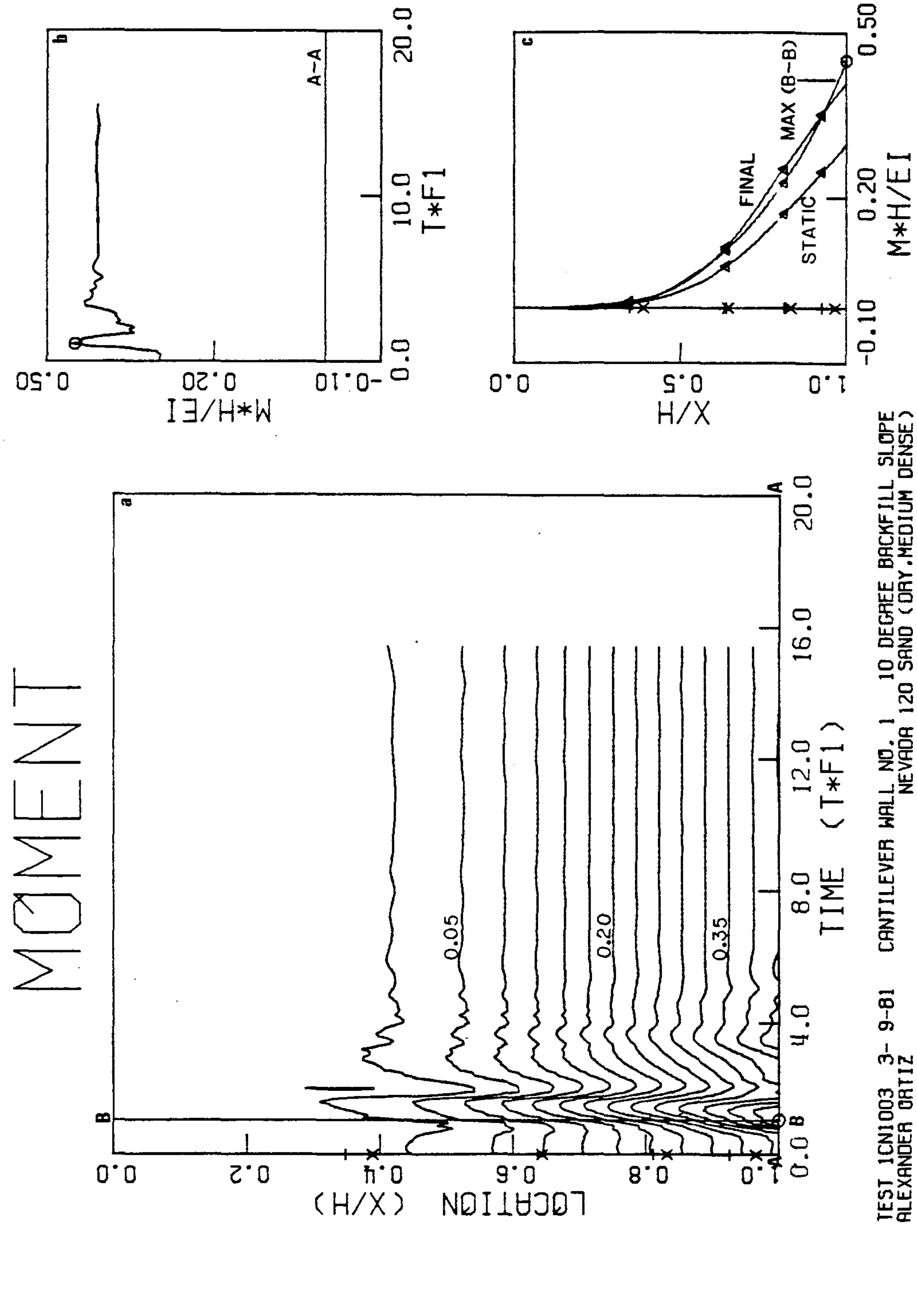
MOMENT
LOCATION (X/H)
TIME (T*F1)
0.05
0.20
0.35
M*H/EI
T*F1
A-A
X/H
FINAL
MAX (B-B)
STATIC
TEST 1CN1003 3- 9-81 CANTILEVER WALL NO. 1 10 DEGREE BACKFILL SLOPE
ALEXANDER ORTIZ NEVADA 120 SAND (DRY, MEDIUM DENSE)

FIGURE 5.61

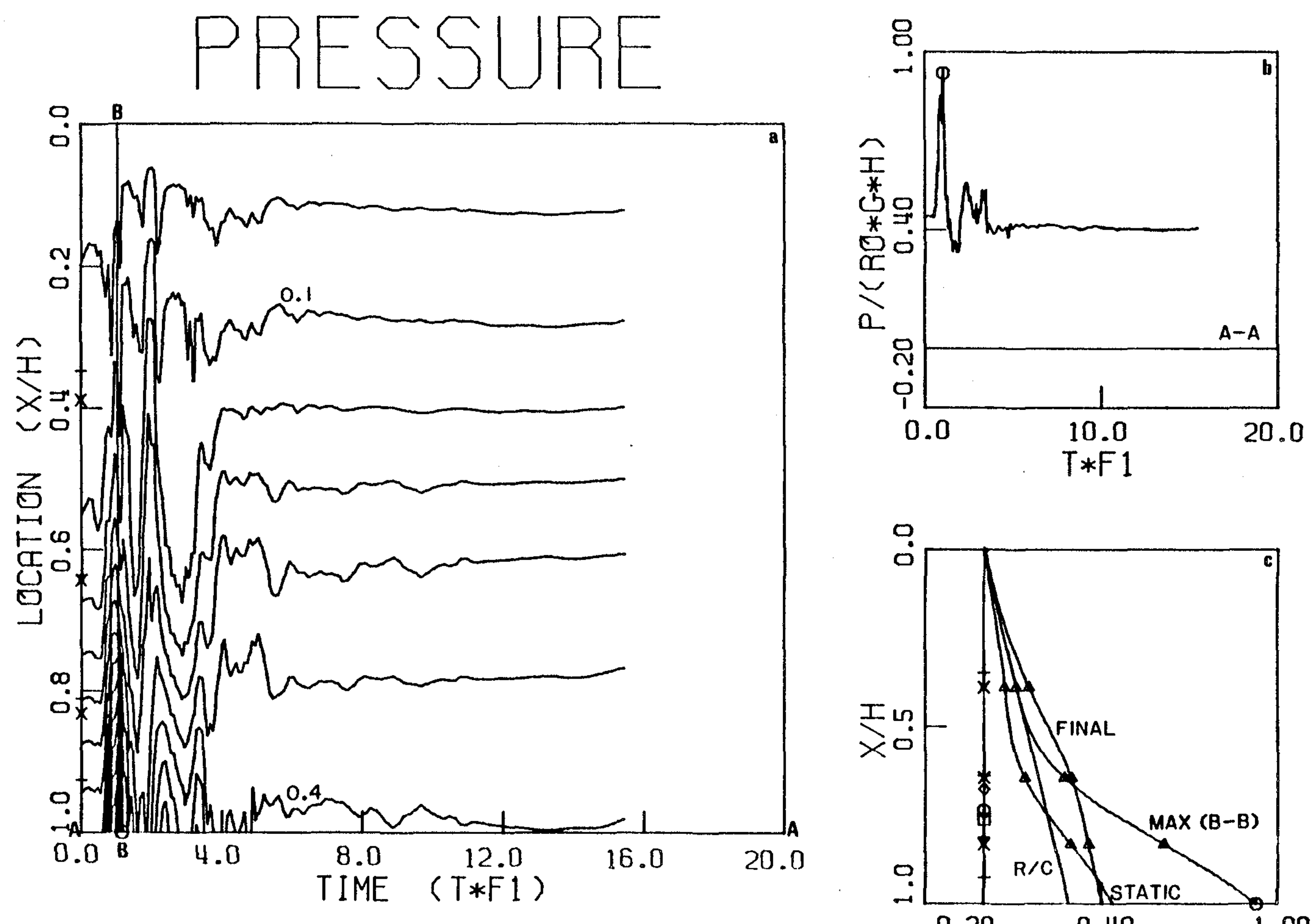

TEST 1CN1003 3- 9-81 CANTILEVER WALL NO. 1 10 DEGREE BACKFILL SLOPE
ALEXANDER ORTIZ NEVADA 120 SAND (DRY,MEDIUM DENSE)

FIGURE 5.62

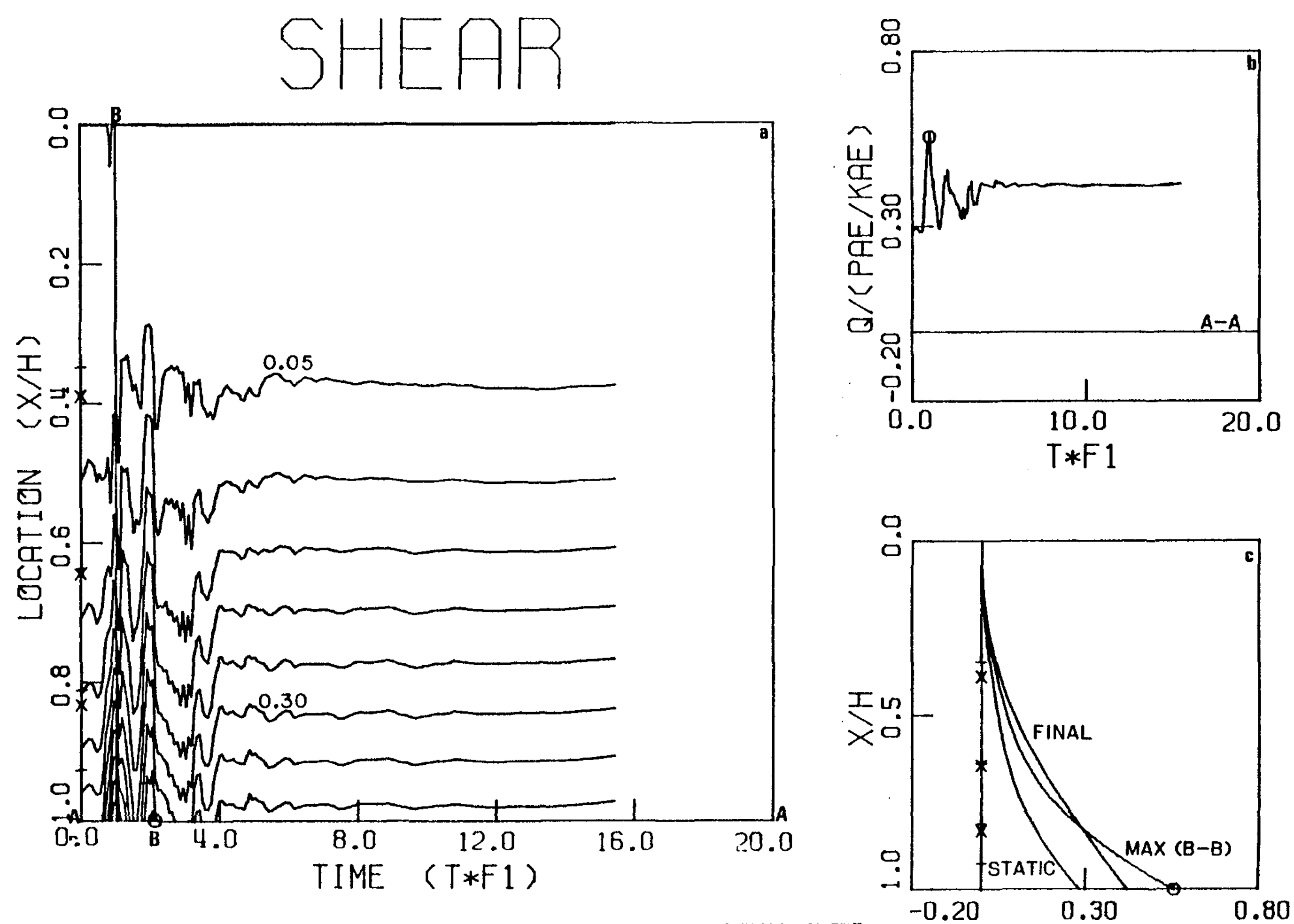

TEST 1CN1003 3- 9-81 CANTILEVER WALL NO. 1 10 DEGREE BACKFILL SLOPE
ALEXANDER ORTIZ NEVADA 120 SAND (DRY.MEDIUM DENSE)

FIGURE 5.63

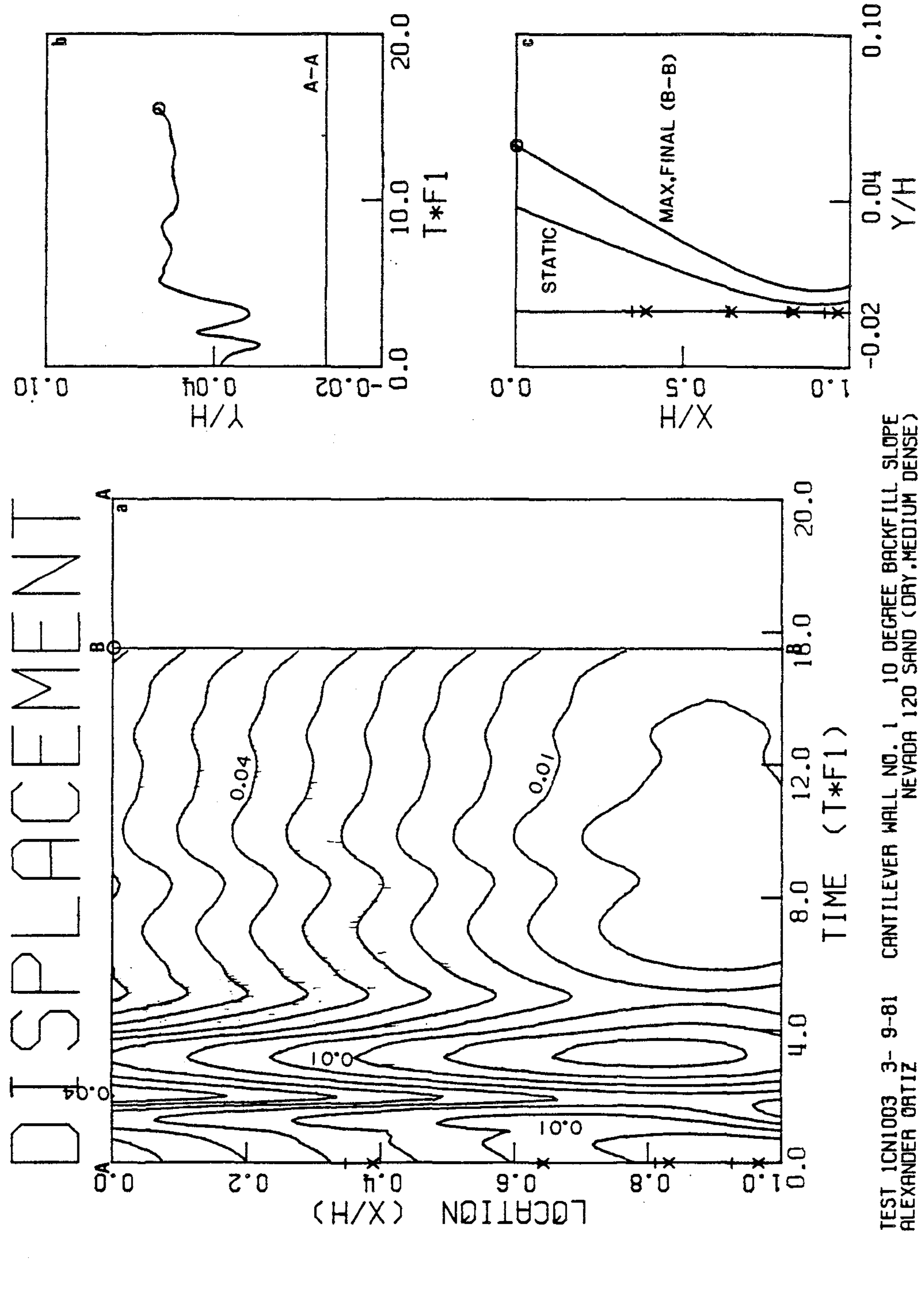
DISPLACEMENT
LOCATION (X/H)
TIME (T*F1)
0.0
0.2
0.4
0.6
0.8
1.0
4.0
8.0
12.0
16.0
20.0
0.04
0.01
A
B
a
b
c
Y/H
T*F1
A-A
X/H
STATIC
MAX,FINAL (B-B)
-0.02
0.04
0.10
0.5
TEST 1CN1003 3- 9-81
ALEXANDER ORTIZ
CANTILEVER WALL NO. 1 10 DEGREE BACKFILL SLOPE
NEVADA 120 SAND (DRY,MEDIUM DENSE)

FIGURE 5.64

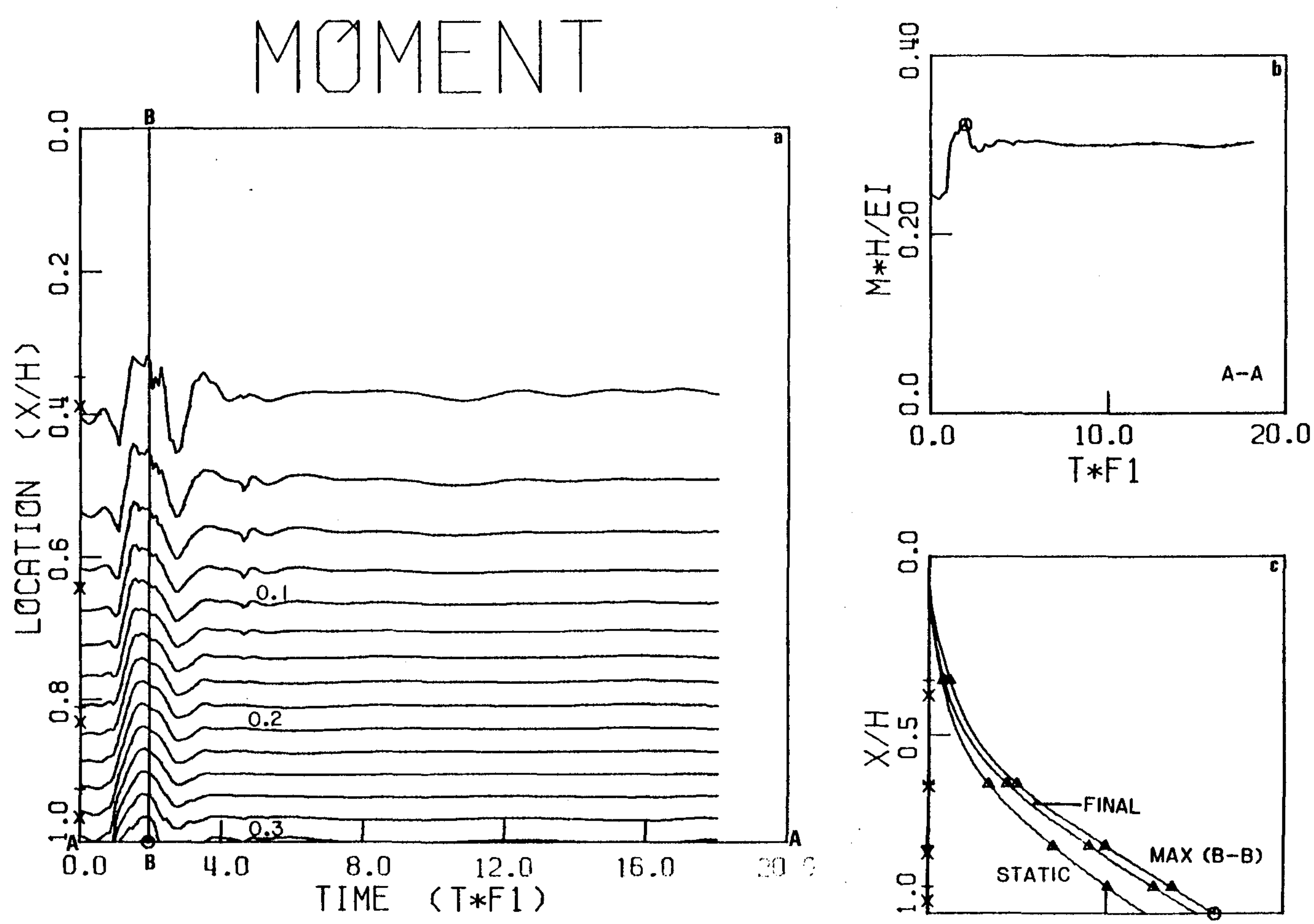

TEST 1CN0004 3-16-81
ALEXANDER ORTIZ

CANTILEVER WALL NO. 1 ZERO BACKFILL SLOPE
NEVADA 120 SAND (DRY.MEDIUM DENSE)

FIGURE 5.65

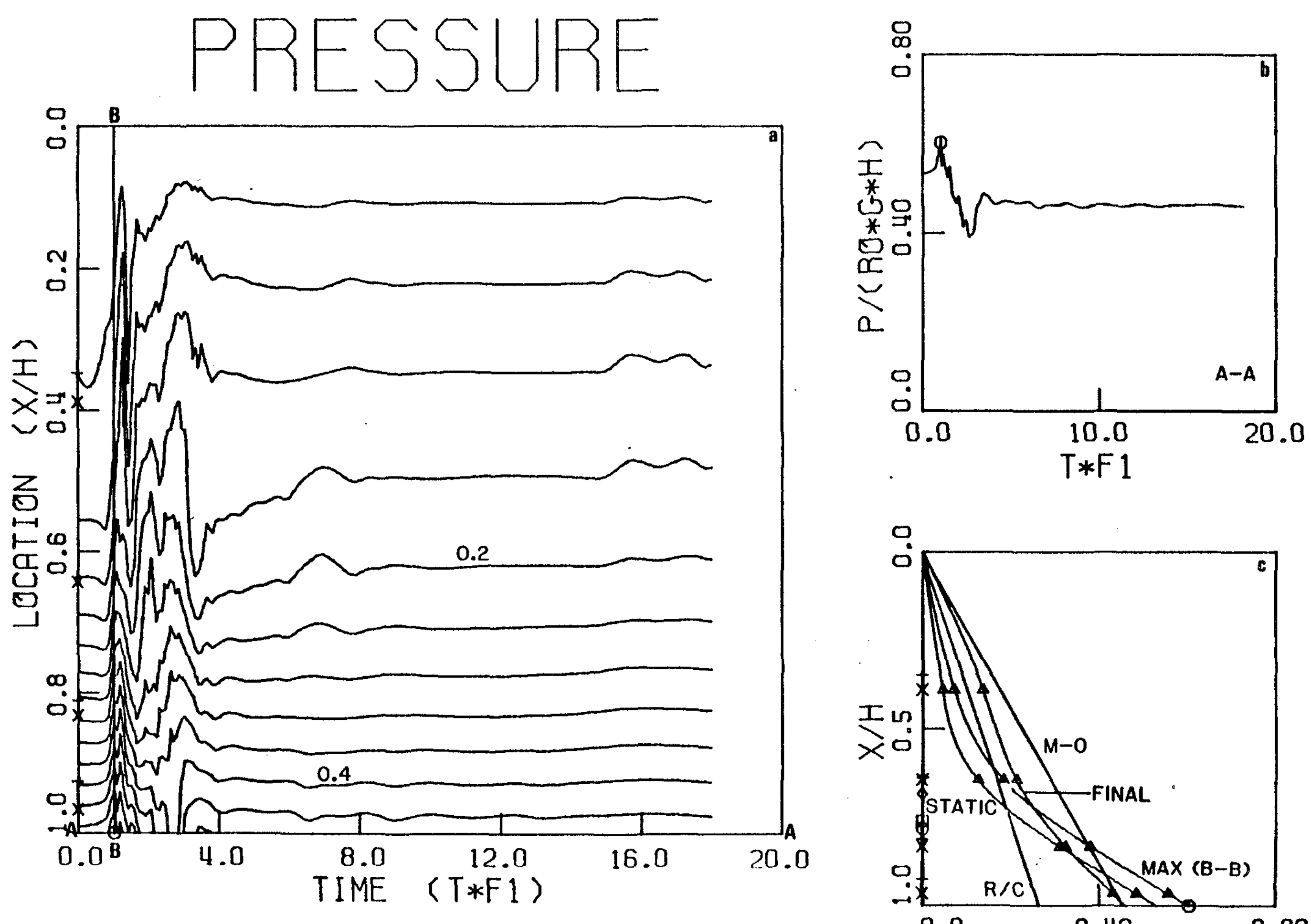

TEST 1CN0004 3-16-81
ALEXANDER ORTIZ

CANTILEVER WALL NO. 1 ZERO BACKFILL SLOPE
NEVADA 120 SAND (DRY,MEDIUM DENSE)

FIGURE 5.66

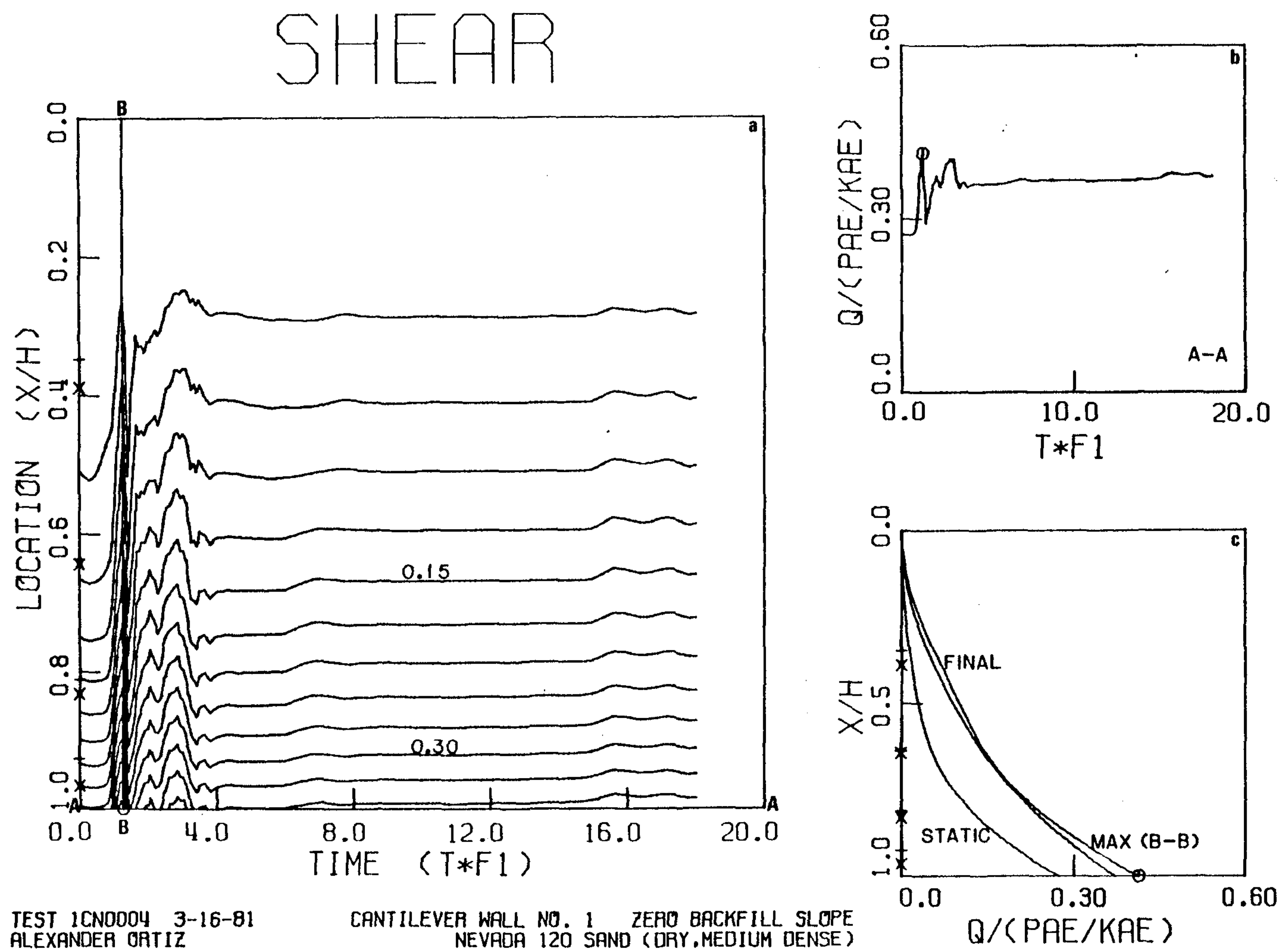
SHEAR
LOCATION (X/H)
0.0
0.2
0.4
0.6
0.8
1.0
B
A
a
0.15
0.30
0.0
4.0
8.0
12.0
16.0
20.0
TIME (T*F1)
b
Q/(PAE/KAE)
0.0
0.30
0.60
A-A
10.0
T*F1
c
X/H
0.5
FINAL
STATIC
MAX (B-B)
Q/(PAE/KAE)
TEST 1CN0004 3-16-81
ALEXANDER ORTIZ
CANTILEVER WALL NO. 1 ZERO BACKFILL SLOPE
NEVADA 120 SAND (DRY,MEDIUM DENSE)

FIGURE 5.67

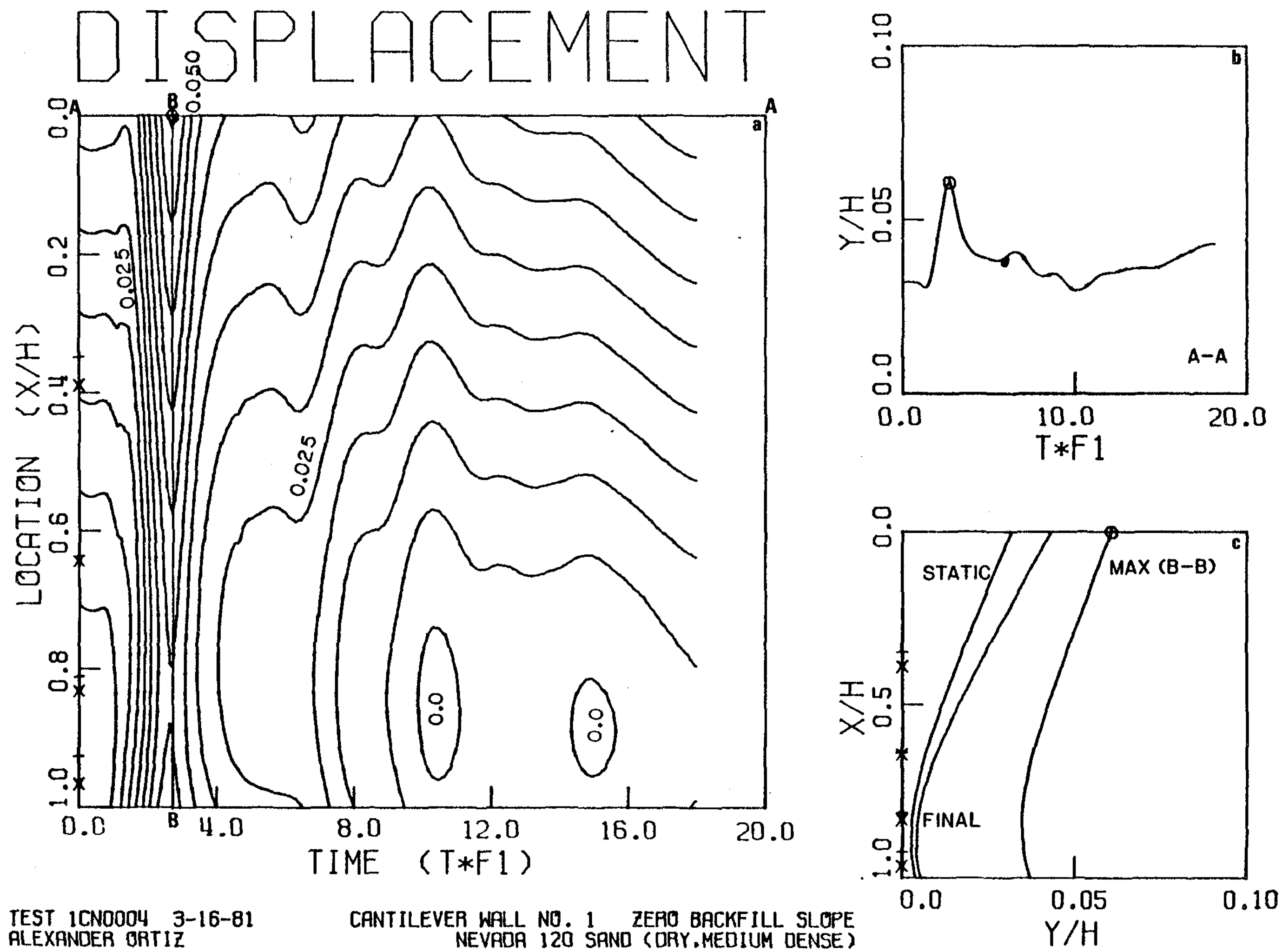
DISPLACEMENT
LOCATION (X/H)
TIME (T*F1)
0.025
0.050
0.0
A-A
MAX (B-B)
STATIC
FINAL
Y/H
X/H
T*F1
TEST 1CN0004 3-16-81
ALEXANDER ORTIZ
CANTILEVER WALL NO. 1 ZERO BACKFILL SLOPE
NEVADA 120 SAND (DRY.MEDIUM DENSE)

FIGURE 5.68

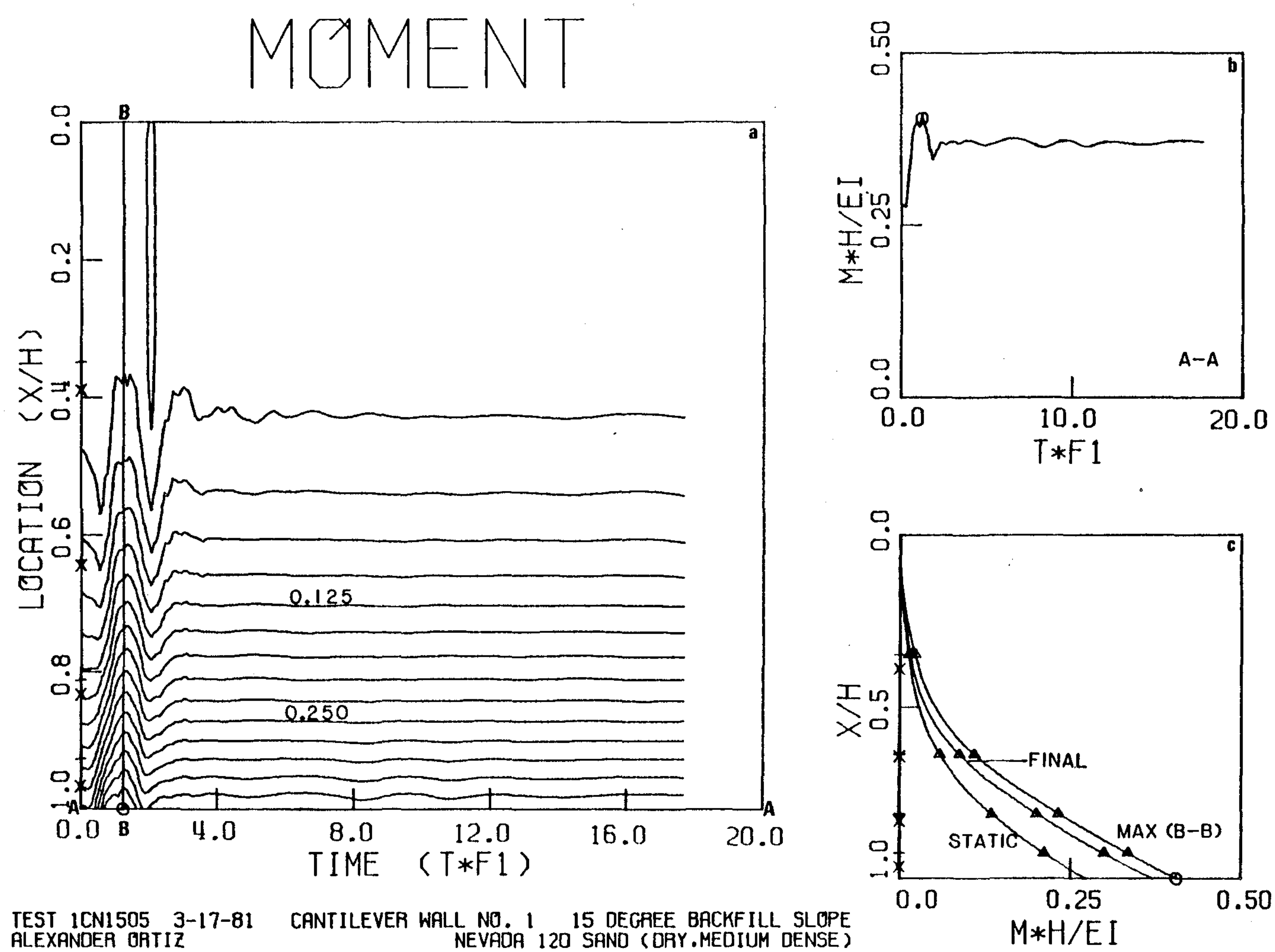
MOMENT
LOCATION (X/H)
TIME (T*F1)
0.125
0.250
A-A
M*H/EI
T*F1
X/H
FINAL
MAX (B-B)
STATIC
TEST 1CN1505 3-17-81 CANTILEVER WALL NO. 1 15 DEGREE BACKFILL SLOPE
ALEXANDER ORTIZ NEVADA 120 SAND (DRY, MEDIUM DENSE)

FIGURE 5.69

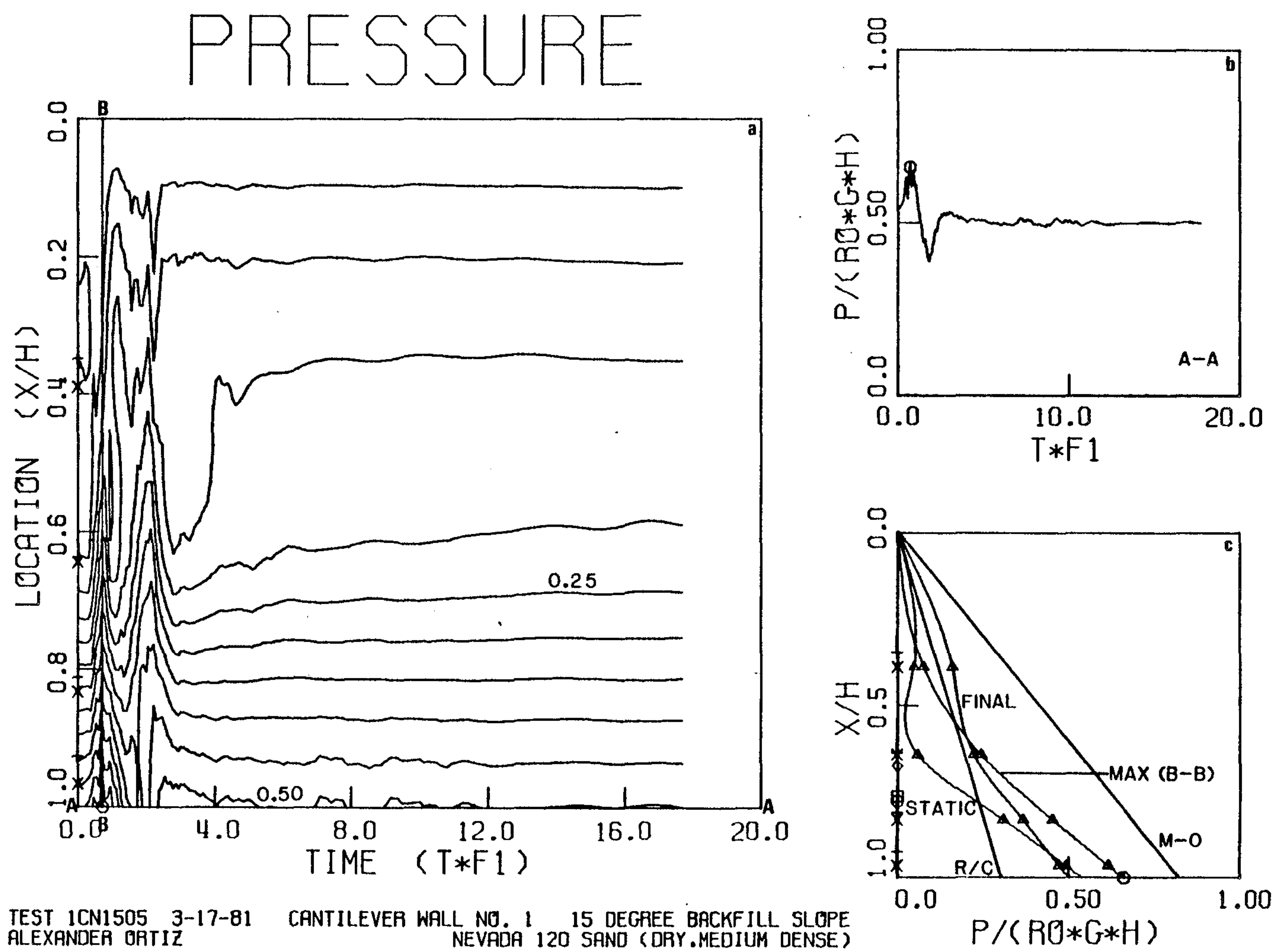

TEST 1CN1505 3-17-81 CANTILEVER WALL NO. 1 15 DEGREE BACKFILL SLOPE
ALEXANDER ORTIZ NEVADA 120 SAND (DRY.MEDIUM DENSE)

FIGURE 5.70

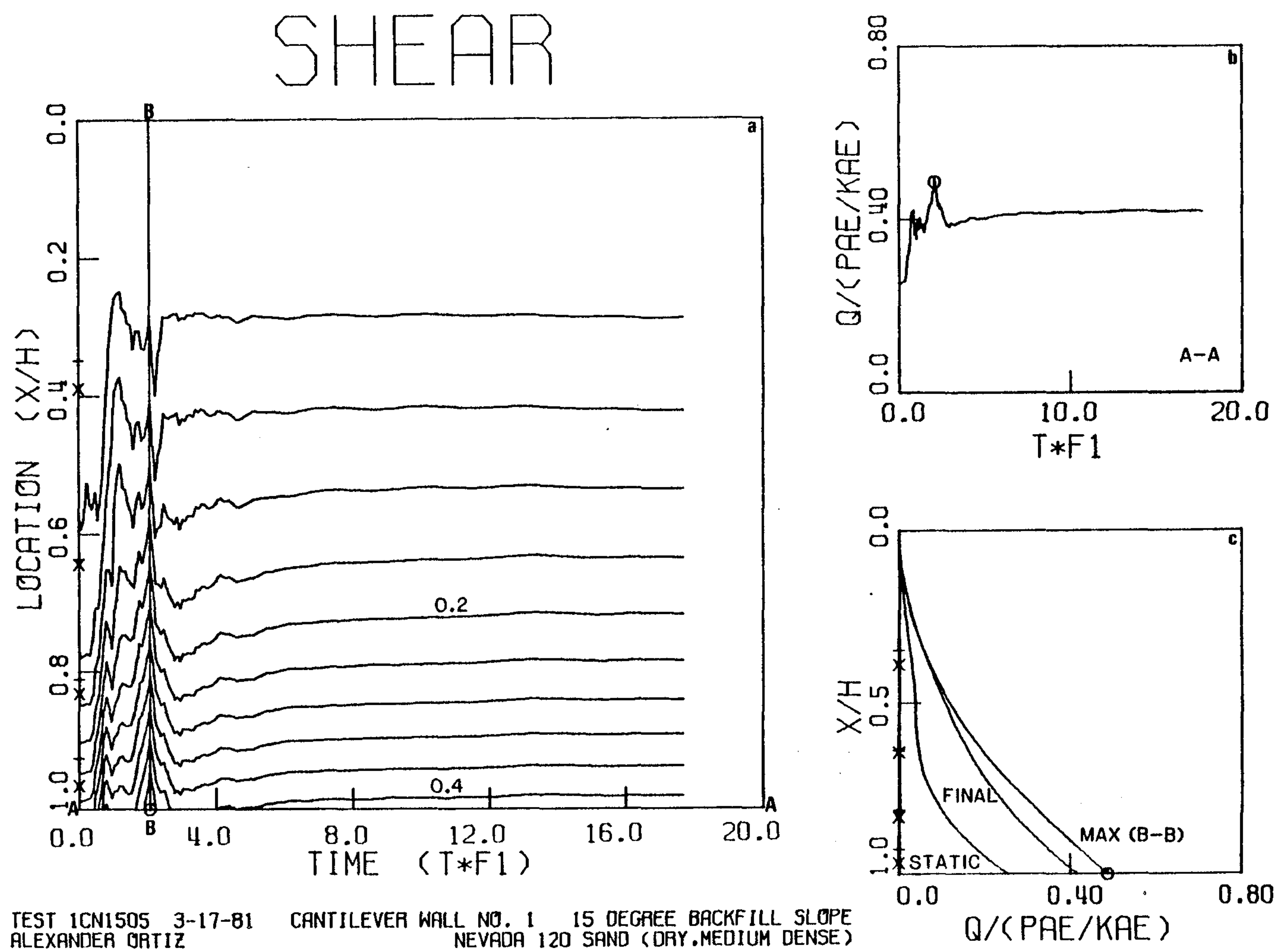
SHEAR
LOCATION (X/H)
TIME (T*F1)
0.2
0.4
Q/(PAE/KAE)
T*F1
A-A
X/H
FINAL
MAX (B-B)
STATIC
TEST 1CN1505 3-17-81 CANTILEVER WALL NO. 1 15 DEGREE BACKFILL SLOPE
ALEXANDER ORTIZ NEVADA 120 SAND (DRY,MEDIUM DENSE)

FIGURE 5.71

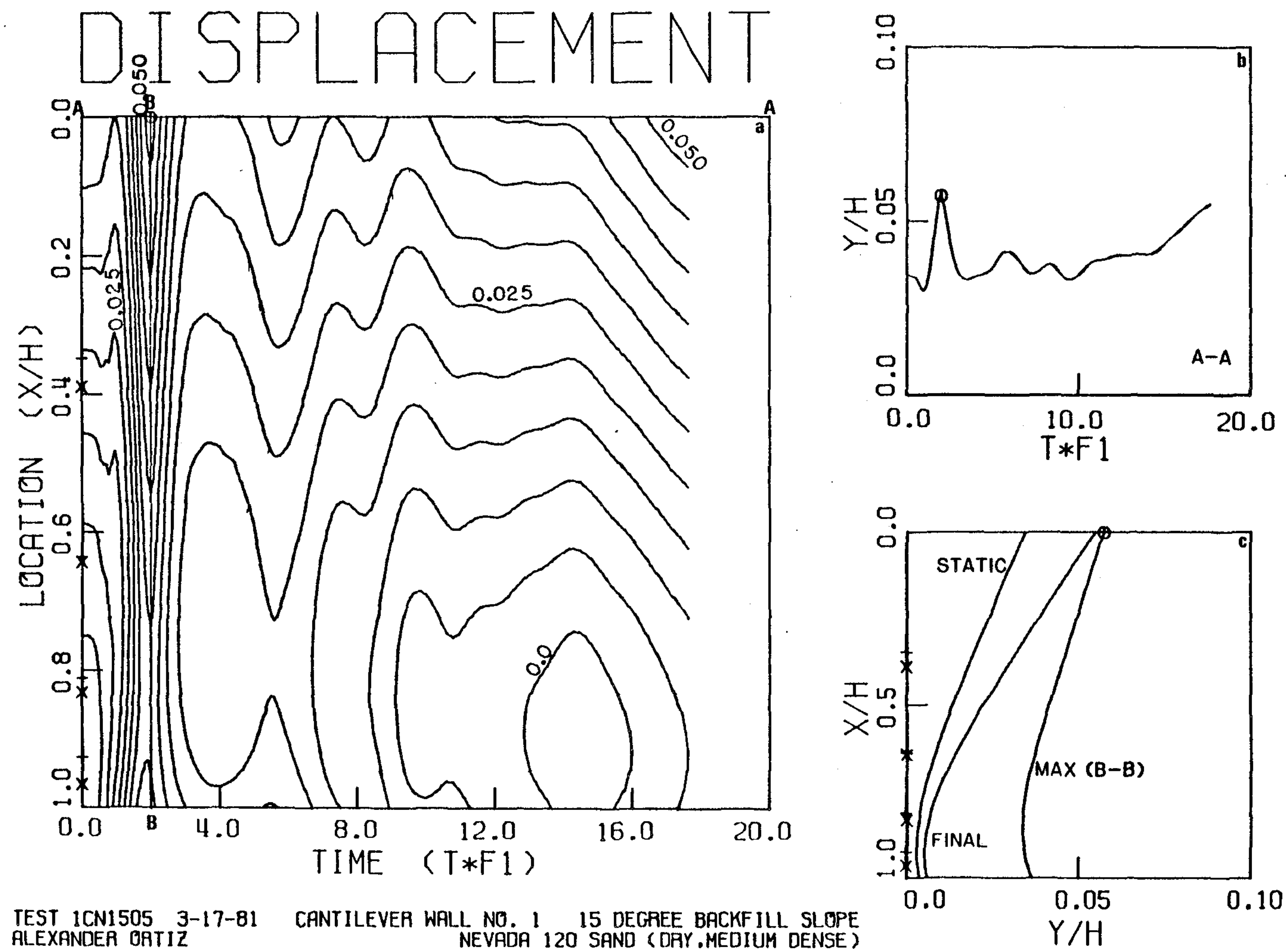
DISPLACEMENT
a
A
B
0.050
0.025
0.0
LOCATION (X/H)
0.0
0.2
0.4
0.6
0.8
1.0
4.0
8.0
12.0
16.0
20.0
TIME (T*F1)
b
A-A
Y/H
0.0
0.05
0.10
10.0
20.0
T*F1
c
STATIC
MAX (B-B)
FINAL
X/H
0.5
Y/H
TEST 1CN1505 3-17-81 CANTILEVER WALL NO. 1 15 DEGREE BACKFILL SLOPE
ALEXANDER ORTIZ NEVADA 120 SAND (DRY, MEDIUM DENSE)

FIGURE 5.72

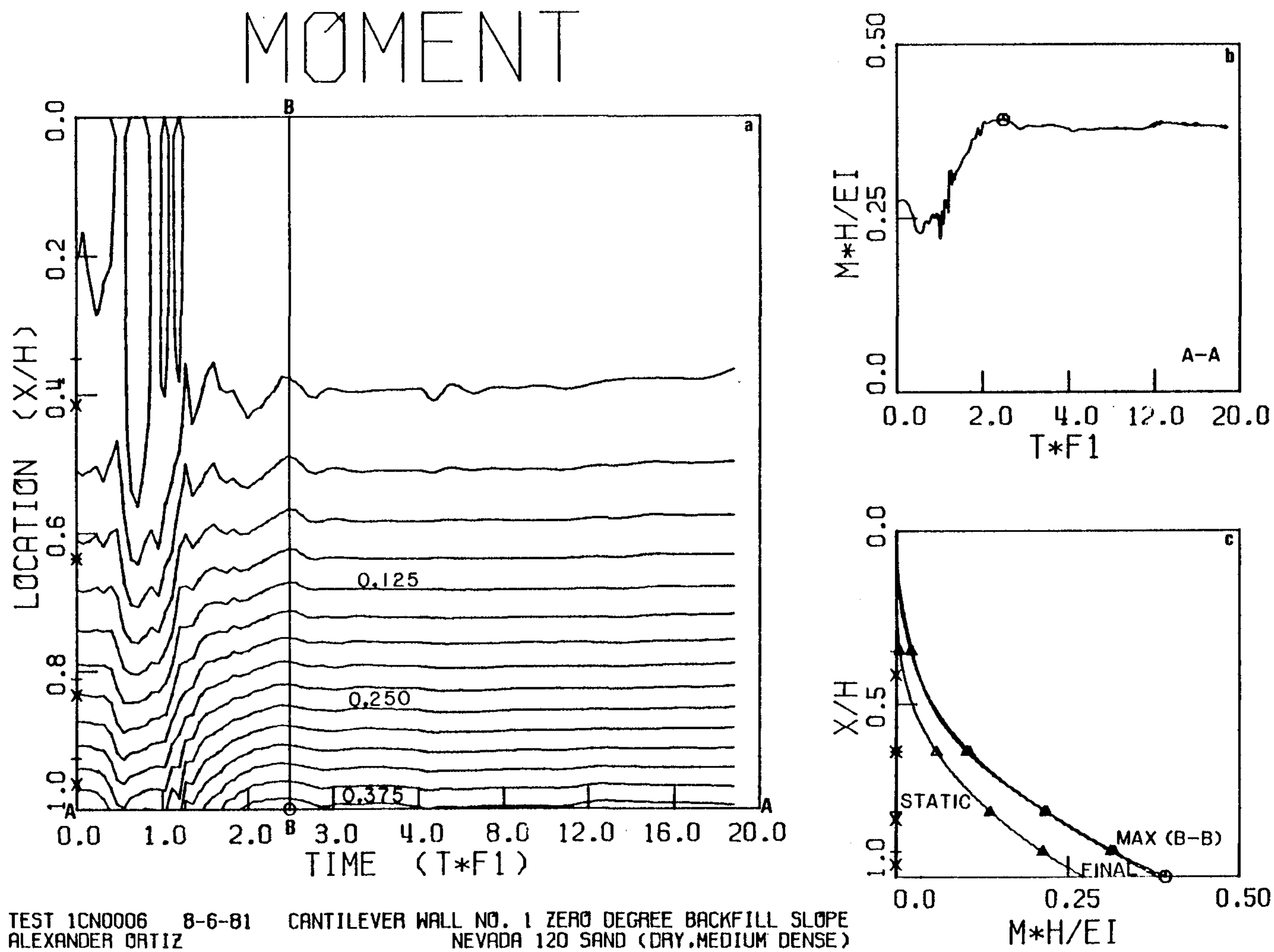
MOMENT
LOCATION (X/H)
TIME (T*F1)
0.125
0.250
0.375
M*H/EI
T*F1
A-A
X/H
STATIC
MAX (B-B)
FINAL
TEST 1CN0006 8-6-81 CANTILEVER WALL NO. 1 ZERO DEGREE BACKFILL SLOPE
ALEXANDER ORTIZ NEVADA 120 SAND (DRY, MEDIUM DENSE)

FIGURE 5.73

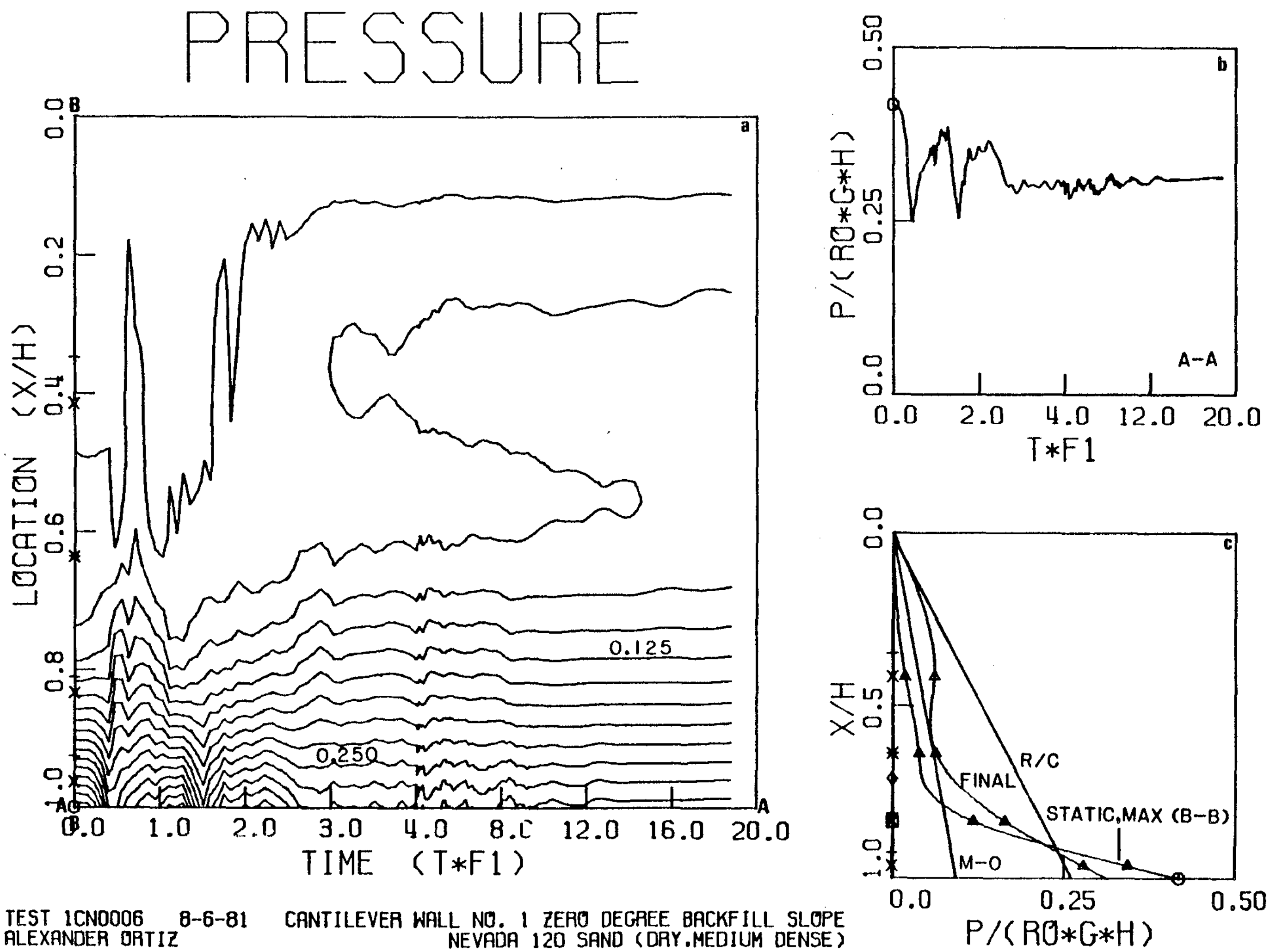

TEST 1CN0006 8-6-81 CANTILEVER WALL NO. 1 ZERO DEGREE BACKFILL SLOPE
ALEXANDER ORTIZ NEVADA 120 SAND (DRY.MEDIUM DENSE)

FIGURE 5.74

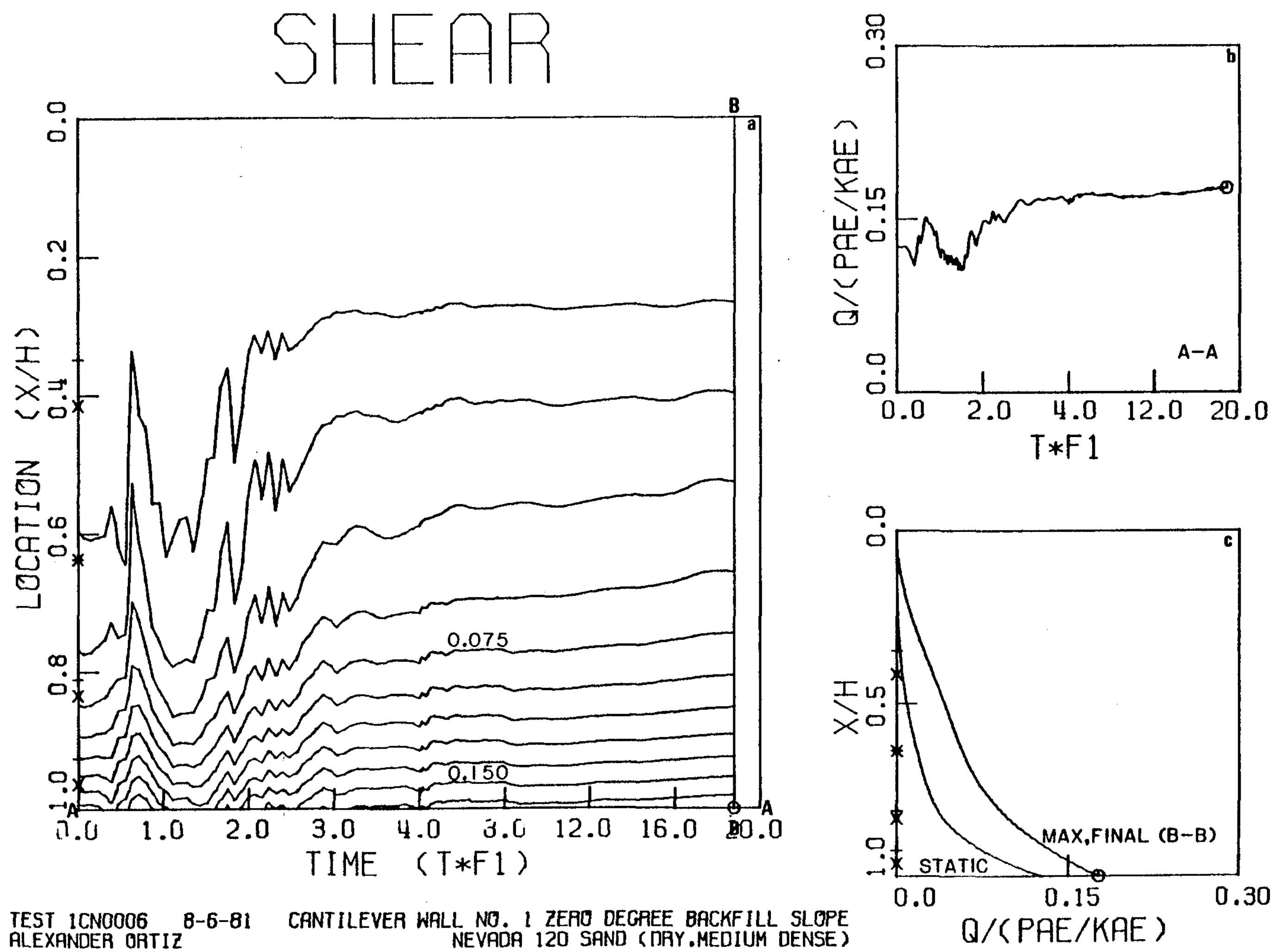
SHEAR
LOCATION (X/H)
0.0
0.2
0.4
0.6
0.8
1.0
TIME (T*F1)
0.0
1.0
2.0
3.0
4.0
8.0
12.0
16.0
20.0
0.075
0.150
A
B
a
b
c
Q/(PAE/KAE)
0.0
0.15
0.30
T*F1
A-A
X/H
0.5
MAX,FINAL (B-B)
STATIC
TEST 1CN0006 8-6-81 CANTILEVER WALL NO. 1 ZERO DEGREE BACKFILL SLOPE
ALEXANDER ORTIZ NEVADA 120 SAND (DRY,MEDIUM DENSE)

FIGURE 5.75

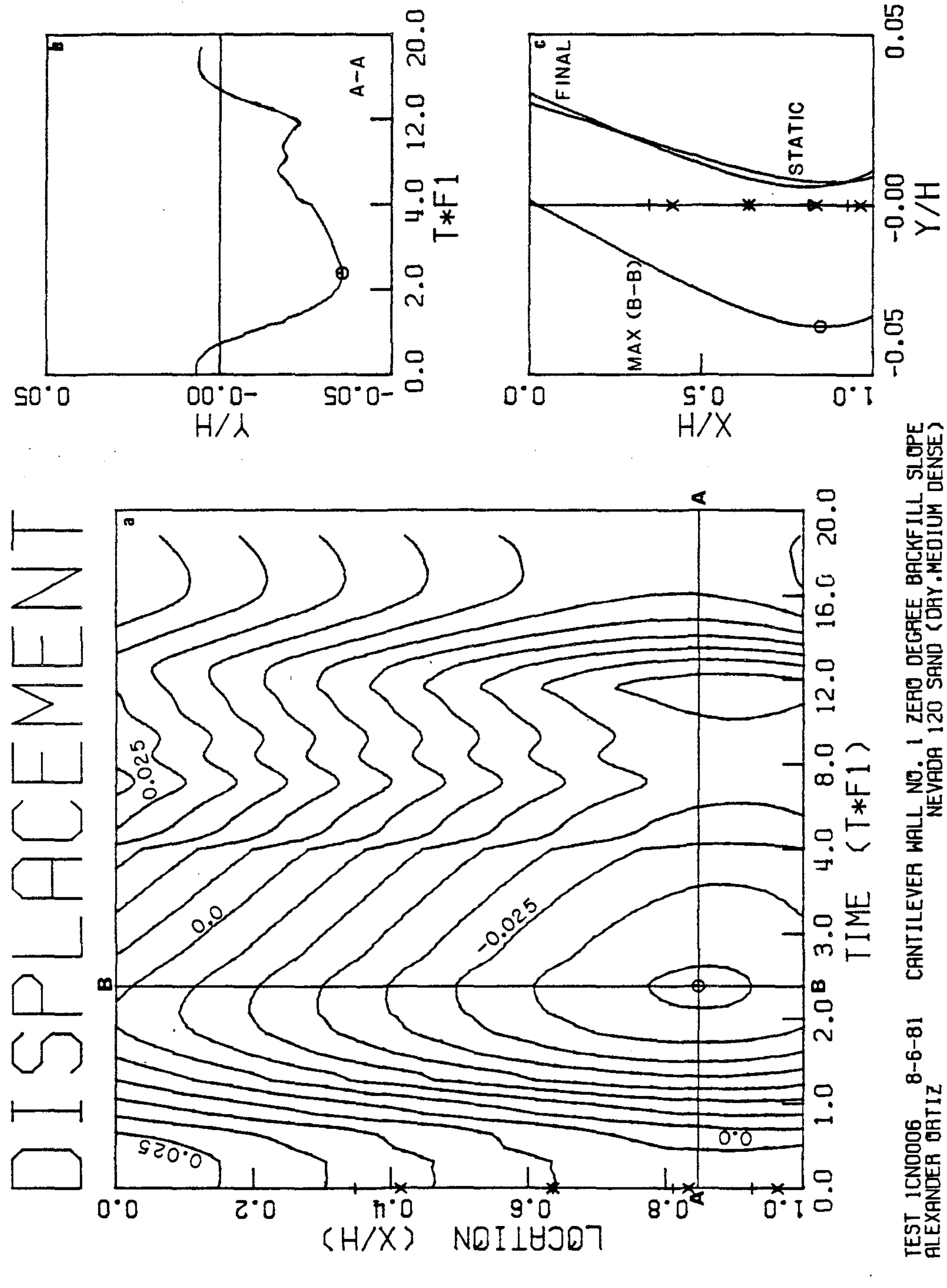

DISPLACEMENT
LOCATION (X/H)
TIME (T*F1)
0.025
0.0
-0.025
A-A
MAX (B-B)
STATIC
FINAL
Y/H
X/H
T*F1
TEST 1CND006 8-6-81 CANTILEVER WALL NO. 1 ZERO DEGREE BACKFILL SLOPE
ALEXANDER ORTIZ NEVADA 120 SAND (DRY.MEDIUM DENSE)

FIGURE 5.76

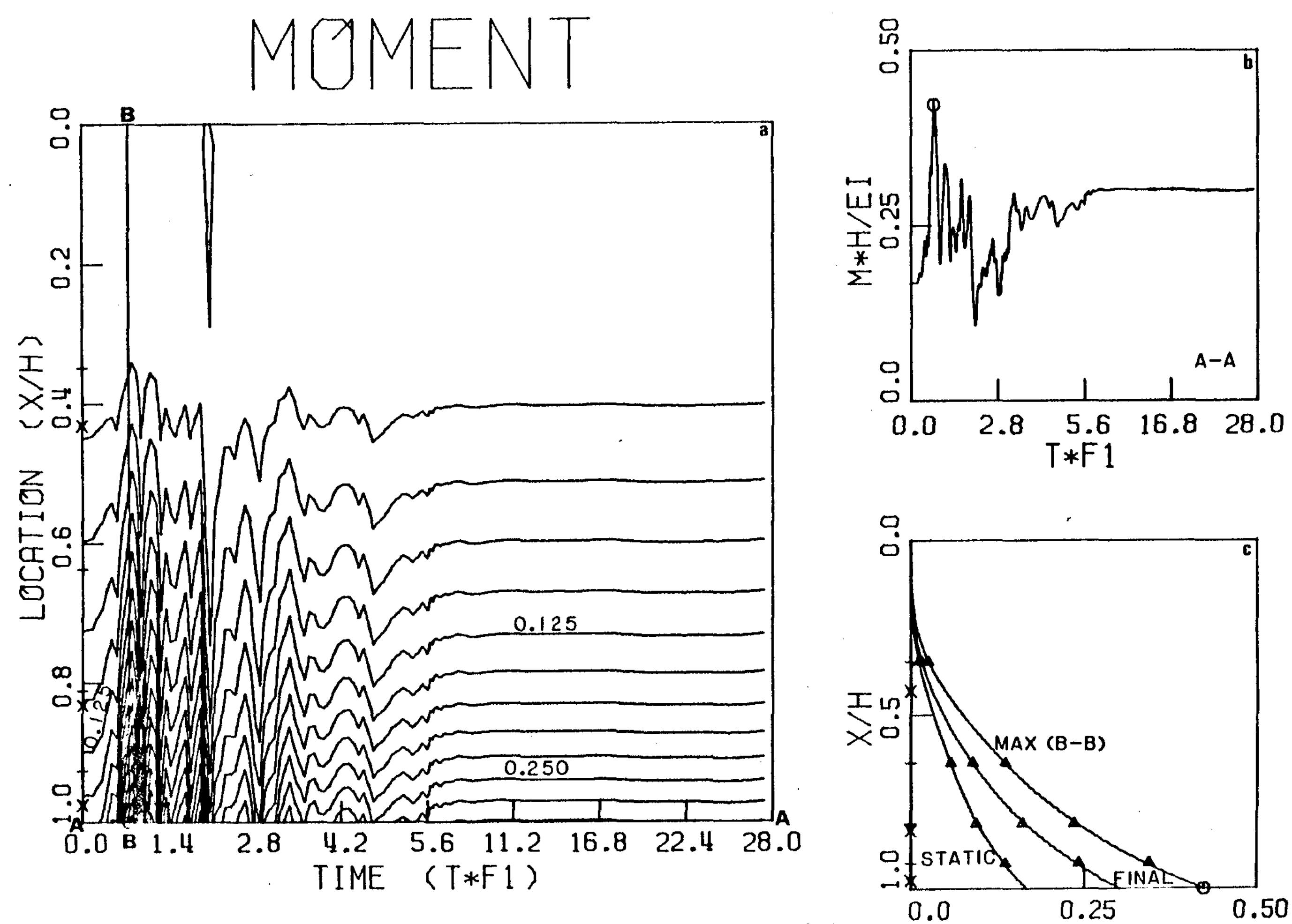

TEST 1CN0007 2-15-82 CANTILEVER WALL NO. 1 ZERO DEGREE BACKFILL SLOPE
ALEXANDER ORTIZ NEVADA 120 SAND (DRY.DENSE)

FIGURE 5.77

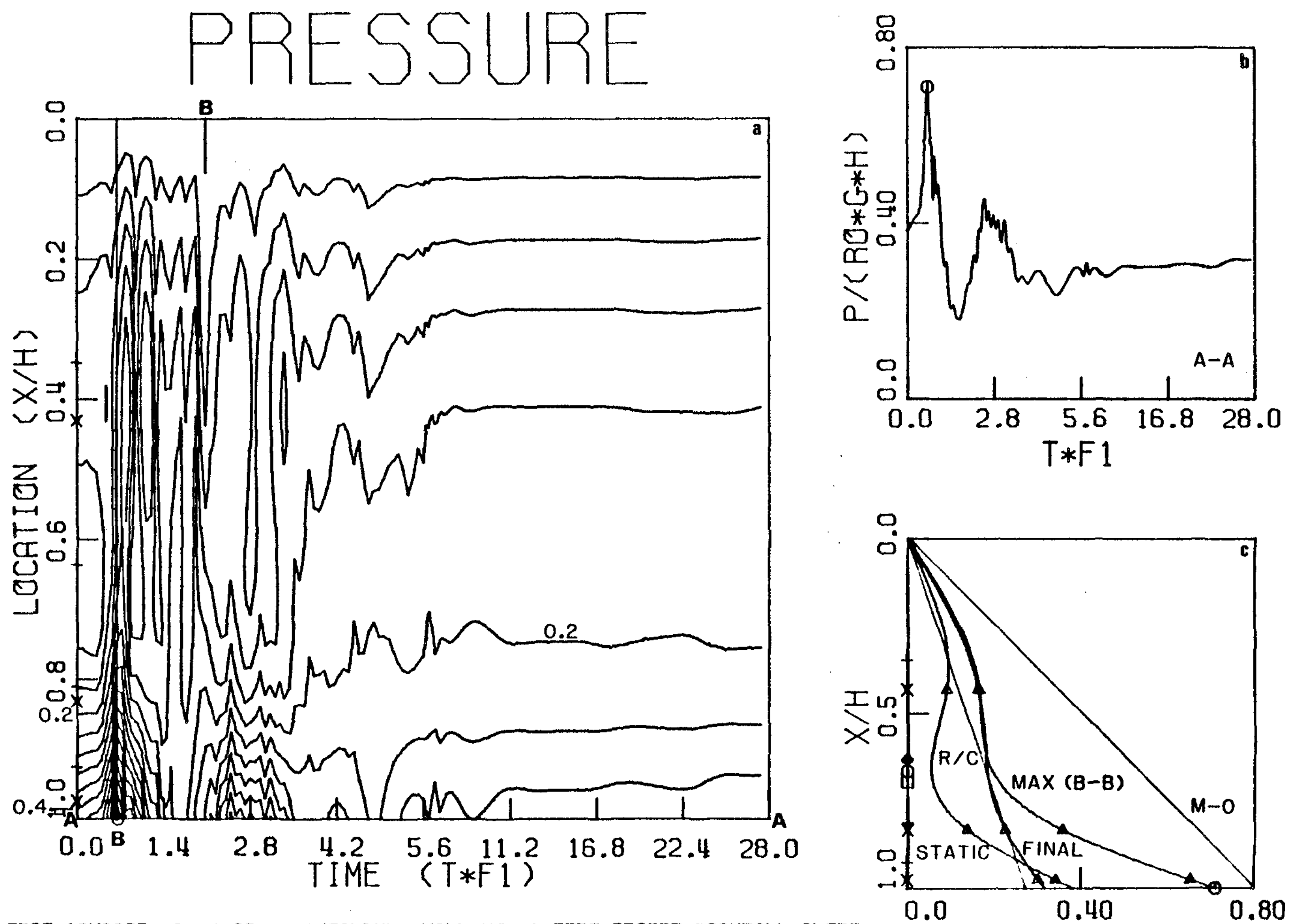

TEST 1CN0007 2-15-82 CANTILEVER WALL NO. 1 ZERO DEGREE BACKFILL SLOPE
ALEXANDER ORTIZ NEVADA 120 SAND (DRY,DENSE)

FIGURE 5.78

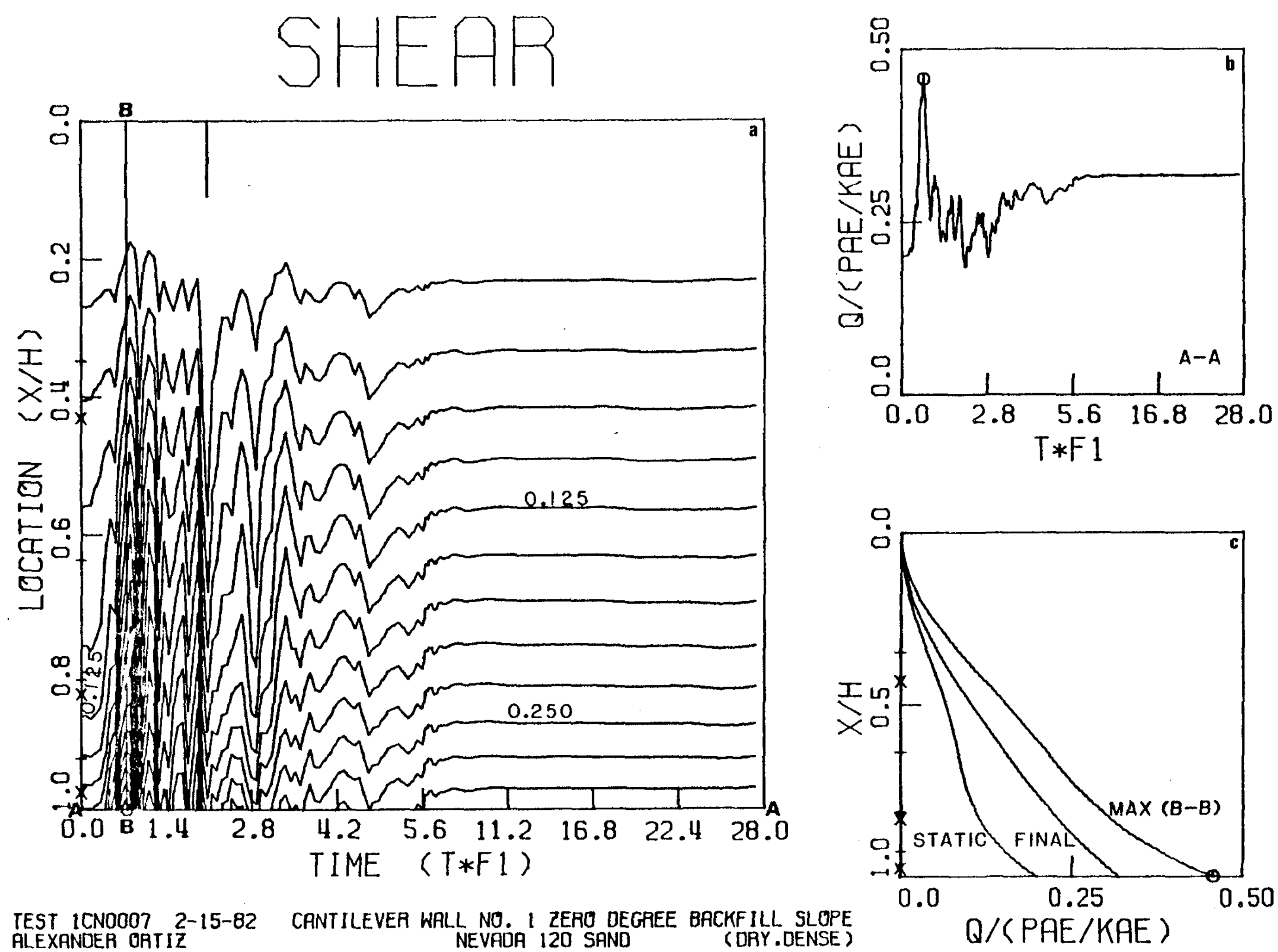

TEST 1CN0007 2-15-82 CANTILEVER WALL NO. 1 ZERO DEGREE BACKFILL SLOPE
ALEXANDER ORTIZ NEVADA 120 SAND (DRY.DENSE)

FIGURE 5.79

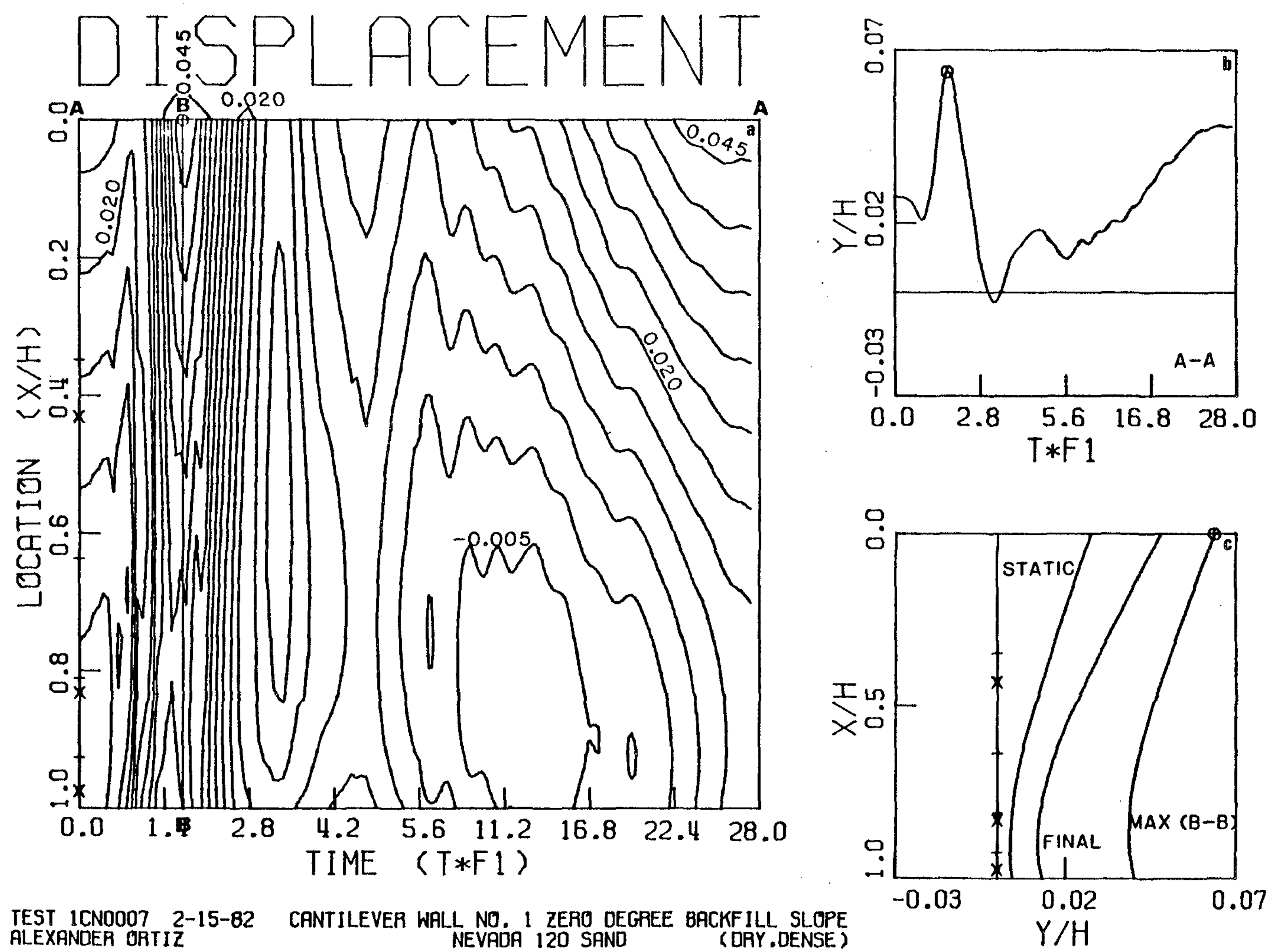
DISPLACEMENT
A
B
A
0.045
0.020
0.020
0.045
0.020
-0.005
a
b
c
LOCATION (X/H)
0.0
0.2
0.4
0.6
0.8
1.0
0.0
1.4
2.8
4.2
5.6
11.2
16.8
22.4
28.0
TIME (T*F1)
Y/H
0.07
0.02
-0.03
A-A
0.0
2.8
5.6
16.8
28.0
T*F1
X/H
0.0
0.5
1.0
STATIC
FINAL
MAX (B-B)
-0.03
0.02
0.07
Y/H
TEST 1CN0007 2-15-82
ALEXANDER ORTIZ
CANTILEVER WALL NO. 1 ZERO DEGREE BACKFILL SLOPE
NEVADA 120 SAND (DRY,DENSE)

FIGURE 5.80

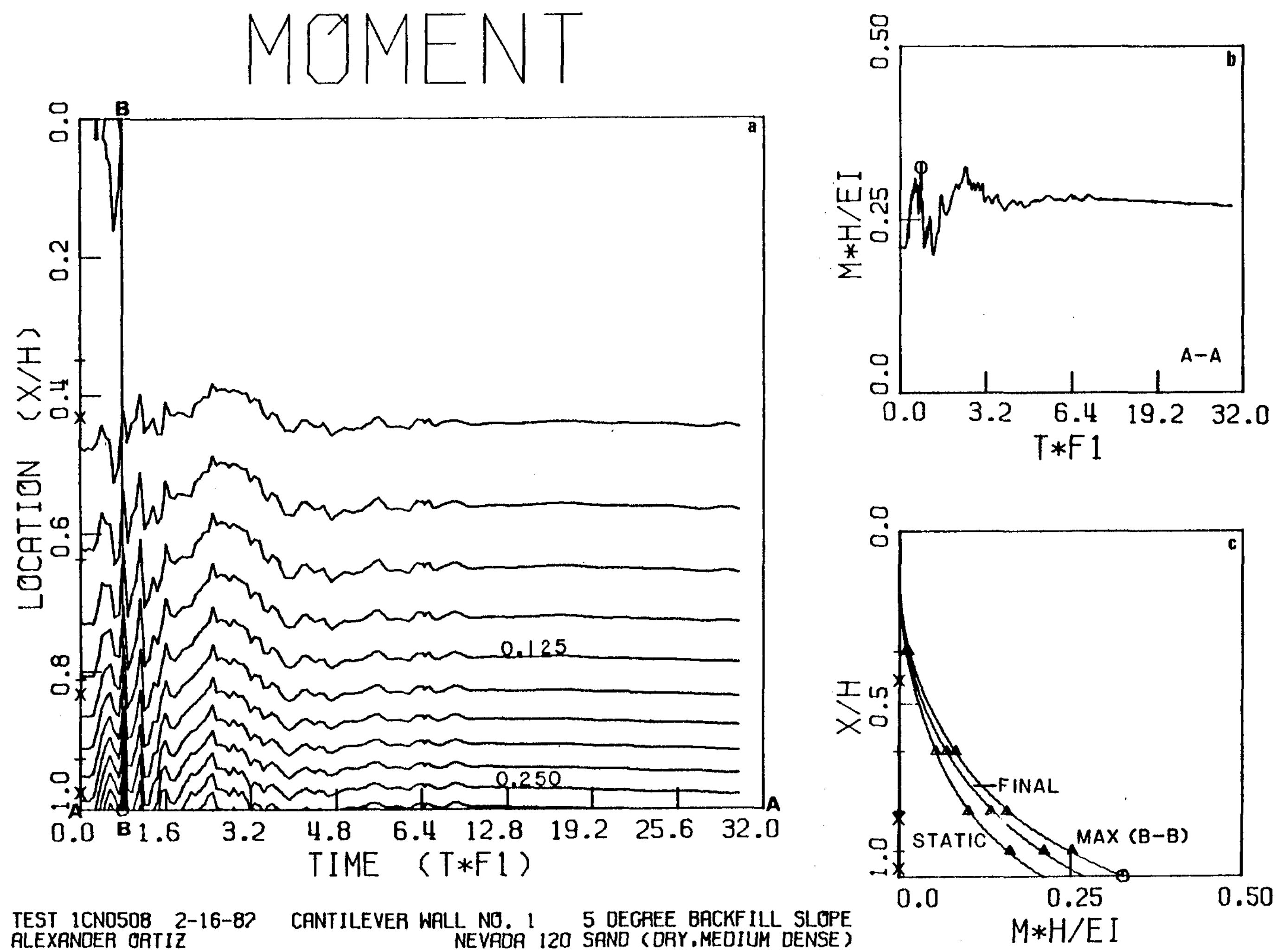
MØMENT
LØCATIØN (X/H)
0.0
0.2
0.4
0.6
0.8
1.0
B
A
a
0.125
0.250
0.0 1.6 3.2 4.8 6.4 12.8 19.2 25.6 32.0
TIME (T*F1)
b
M*H/EI
0.0
0.25
0.50
A-A
0.0 3.2 6.4 19.2 32.0
T*F1
c
X/H
0.0
0.5
1.0
FINAL
STATIC
MAX (B-B)
0.0 0.25 0.50
M*H/EI
TEST 1CN0508 2-16-87 CANTILEVER WALL NO. 1 5 DEGREE BACKFILL SLOPE
ALEXANDER ORTIZ NEVADA 120 SAND (DRY, MEDIUM DENSE)

FIGURE 5.81

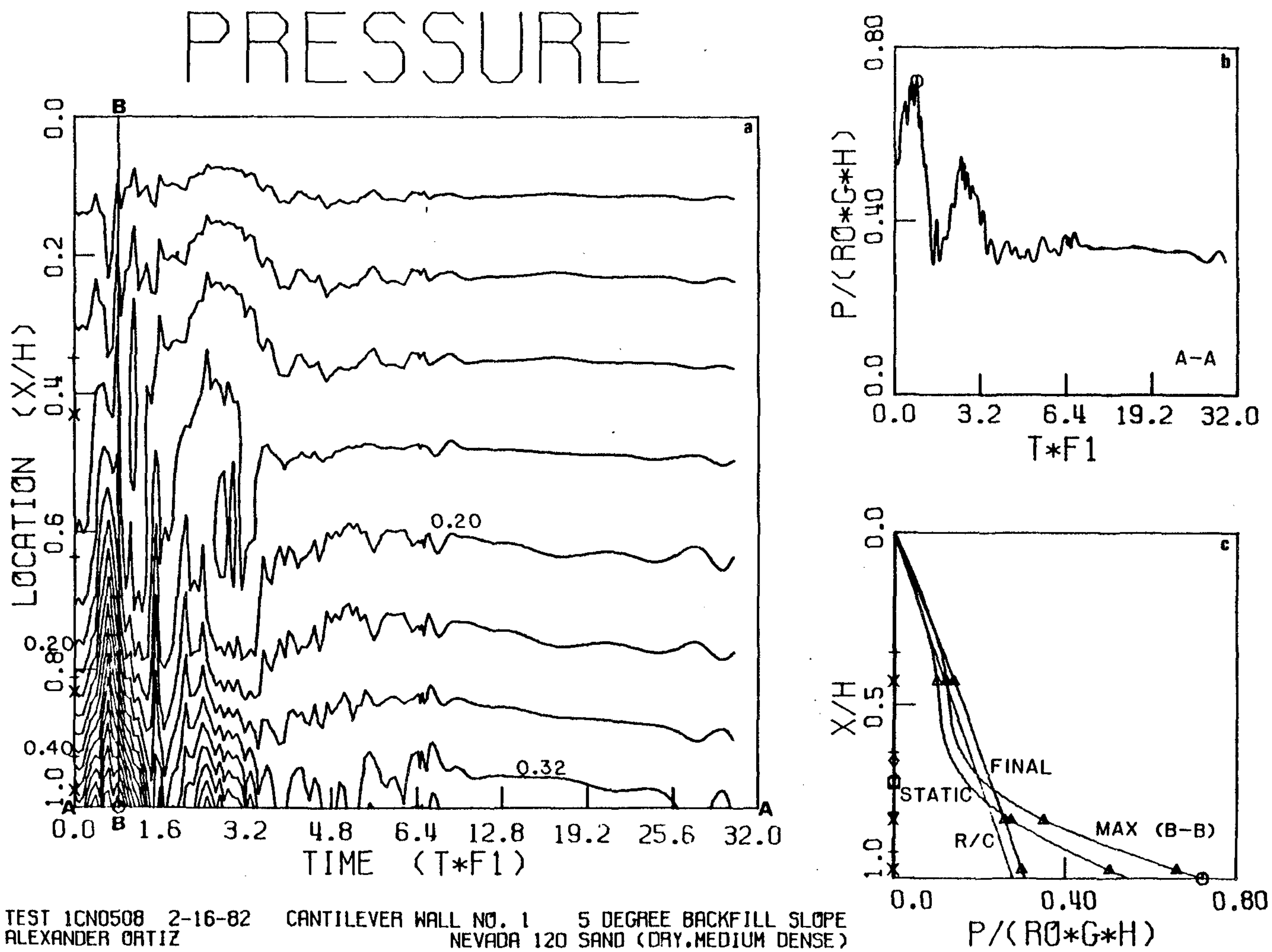

TEST 1CN0508 2-16-82 CANTILEVER WALL NO. 1 5 DEGREE BACKFILL SLOPE
ALEXANDER ORTIZ NEVADA 120 SAND (DRY.MEDIUM DENSE)

FIGURE 5.82

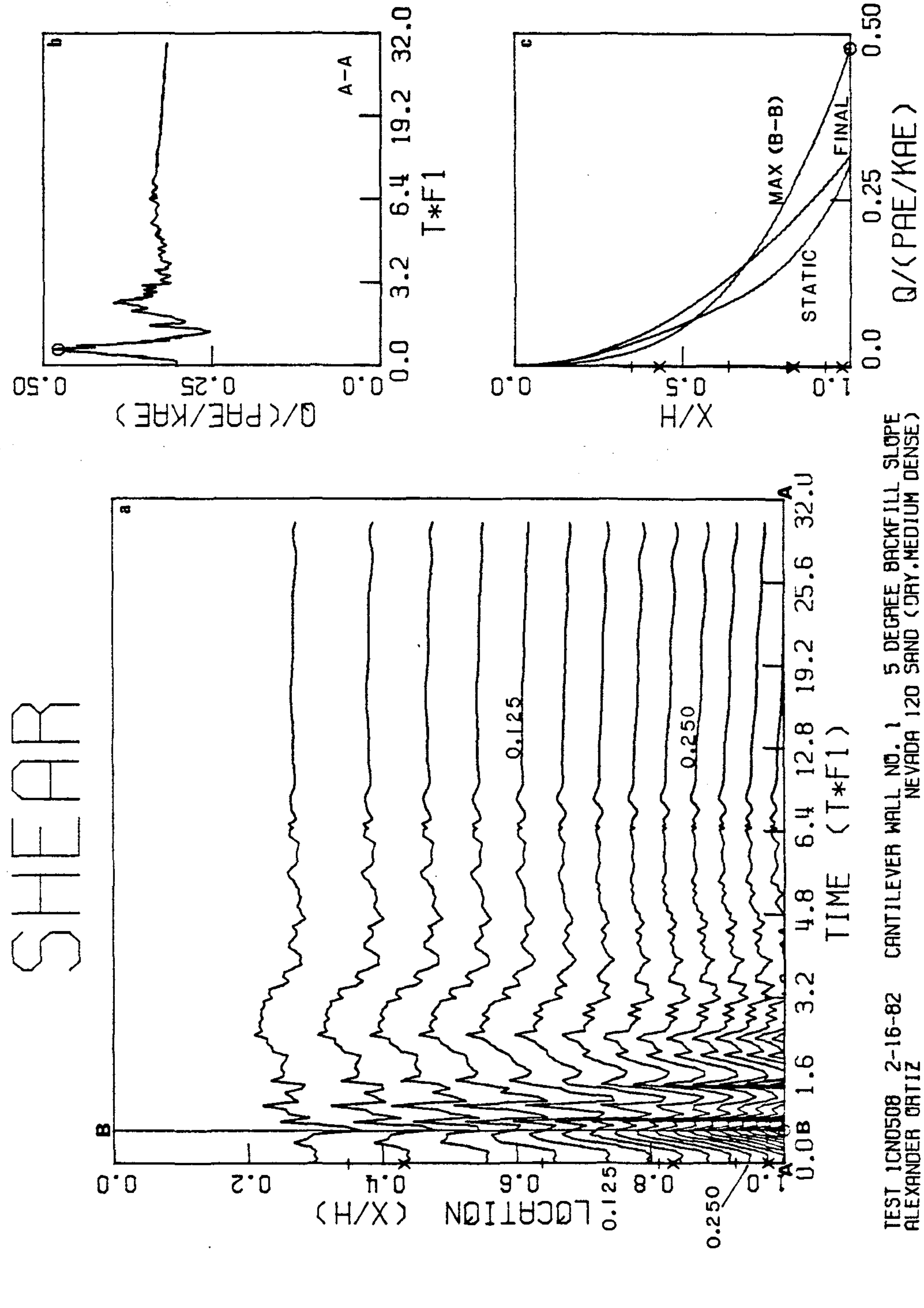
SHEAR
LOCATION (X/H)
TIME (T*F1)
0.125
0.250
Q/(PAE/KAE)
T*F1
A-A
X/H
MAX (B-B)
FINAL
STATIC
TEST 1CN0508 2-16-82 CANTILEVER WALL NO. 1 5 DEGREE BACKFILL SLOPE
ALEXANDER ORTIZ NEVADA 120 SAND (DRY,MEDIUM DENSE)

FIGURE 5.83

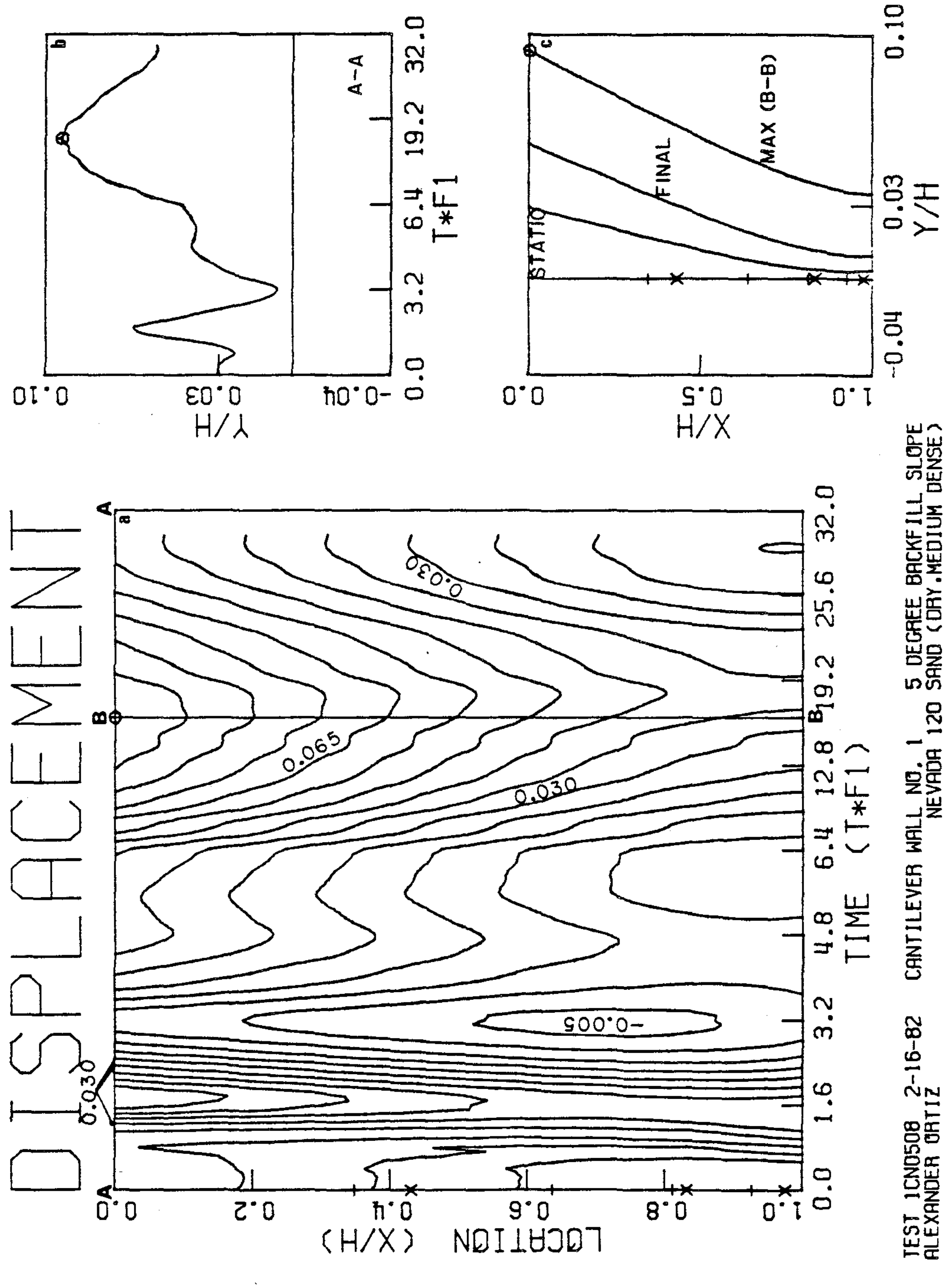
DISPLACEMENT
LOCATION (X/H)
TIME (T*F1)
0.030
0.065
-0.005
Y/H
T*F1
A-A
X/H
Y/H
STATIC
FINAL
MAX (B-B)
TEST 1CN0508 2-16-82 CANTILEVER WALL NO. 1 5 DEGREE BACKFILL SLOPE
ALEXANDER ORTIZ NEVADA 120 SAND (DRY, MEDIUM DENSE)

FIGURE 5.84

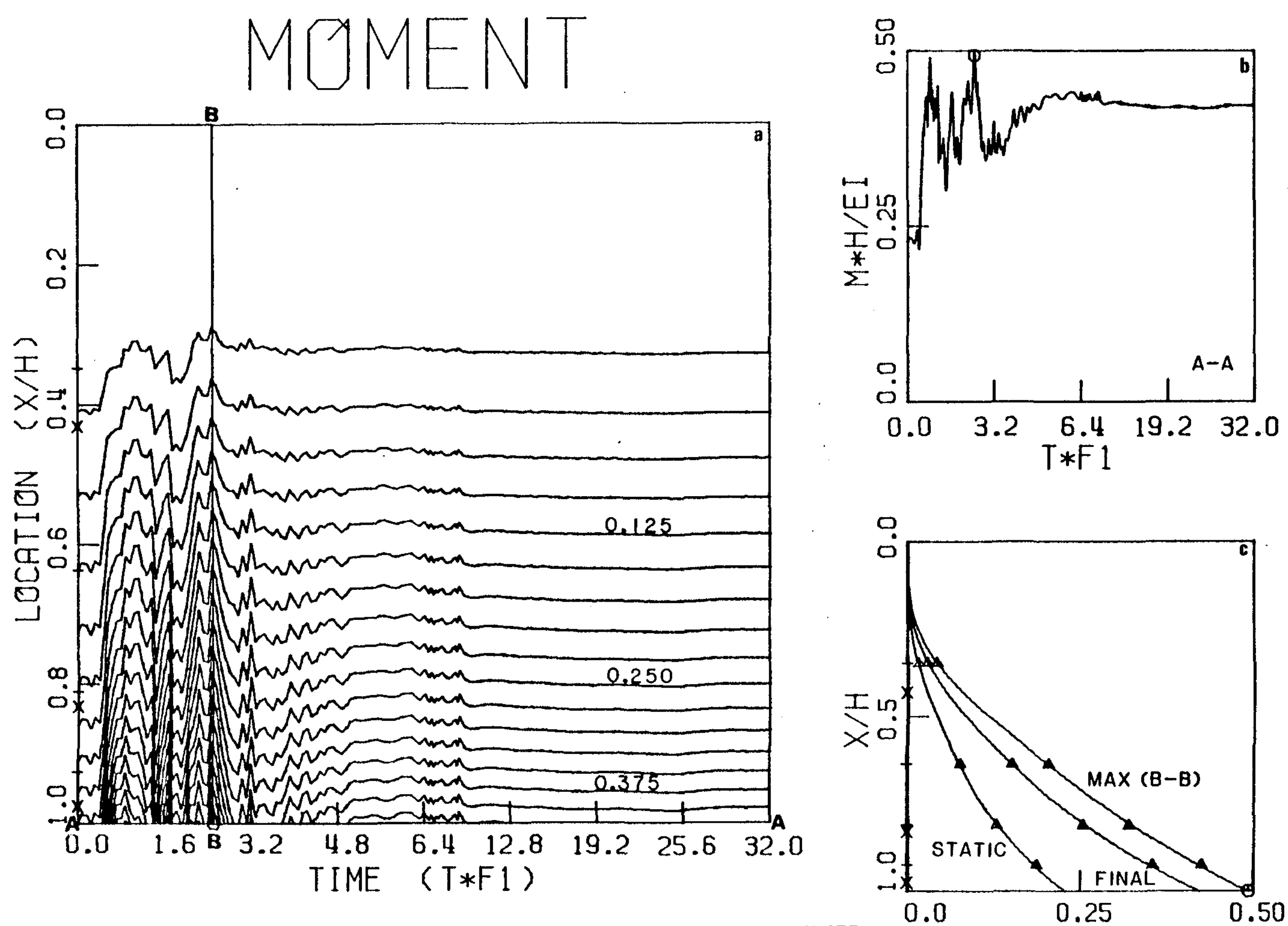

TEST 1CN1009 2-17-82 CANTILEVER WALL NO. 1 10 DEGREE BACKFILL SLOPE
ALEXANDER ORTIZ NEVADA 120 SAND (DRY, DENSE)

FIGURE 5.85

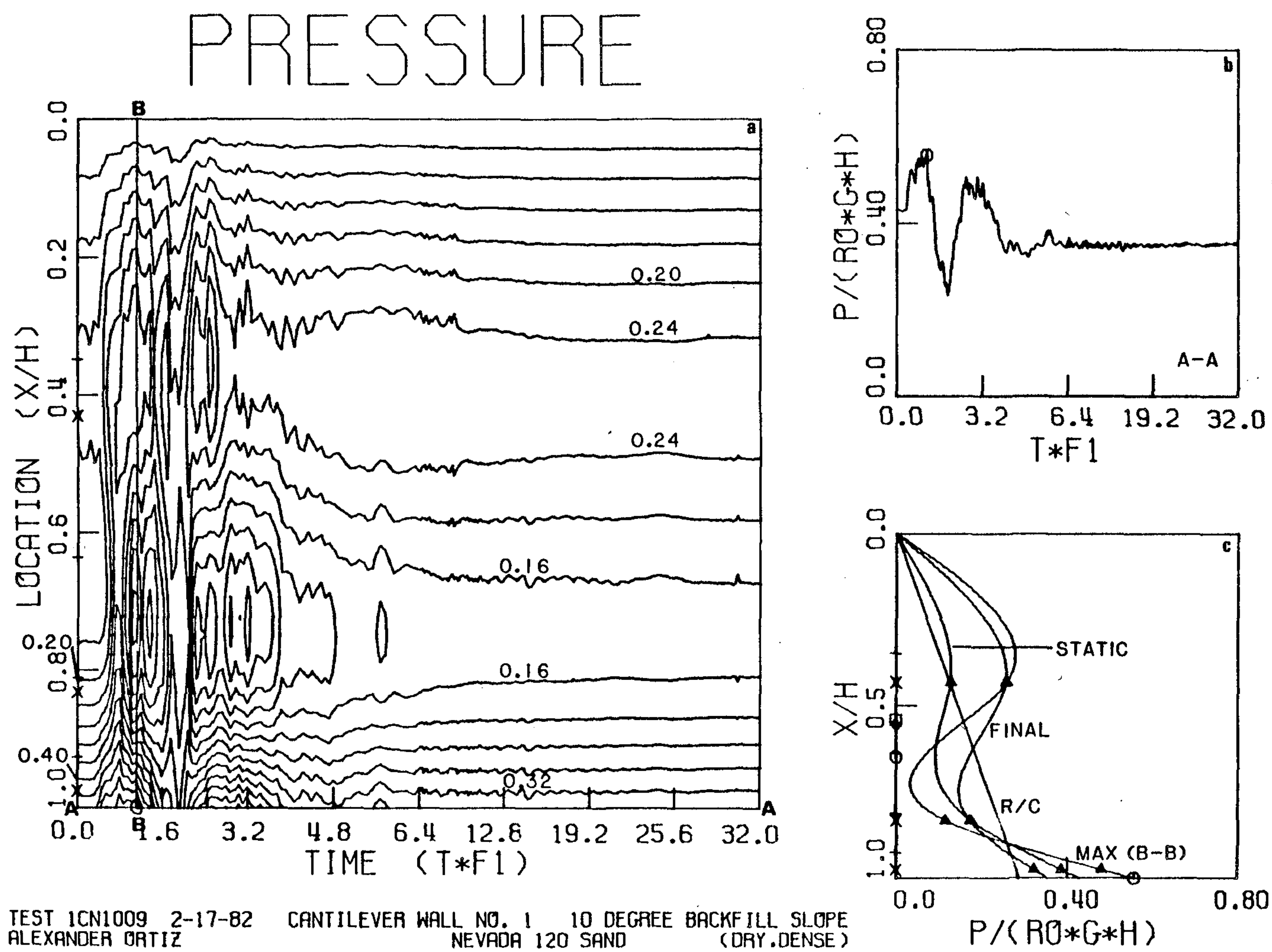
PRESSURE
LOCATION (X/H)
TIME (T*F1)
0.20
0.24
0.16
0.32
0.40
A
B
a
b
A-A
P/(RO*G*H)
T*F1
c
X/H
STATIC
FINAL
R/C
MAX (B-B)
TEST 1CN1009 2-17-82 CANTILEVER WALL NO. 1 10 DEGREE BACKFILL SLOPE
ALEXANDER ORTIZ NEVADA 120 SAND (DRY.DENSE)

FIGURE 5.86

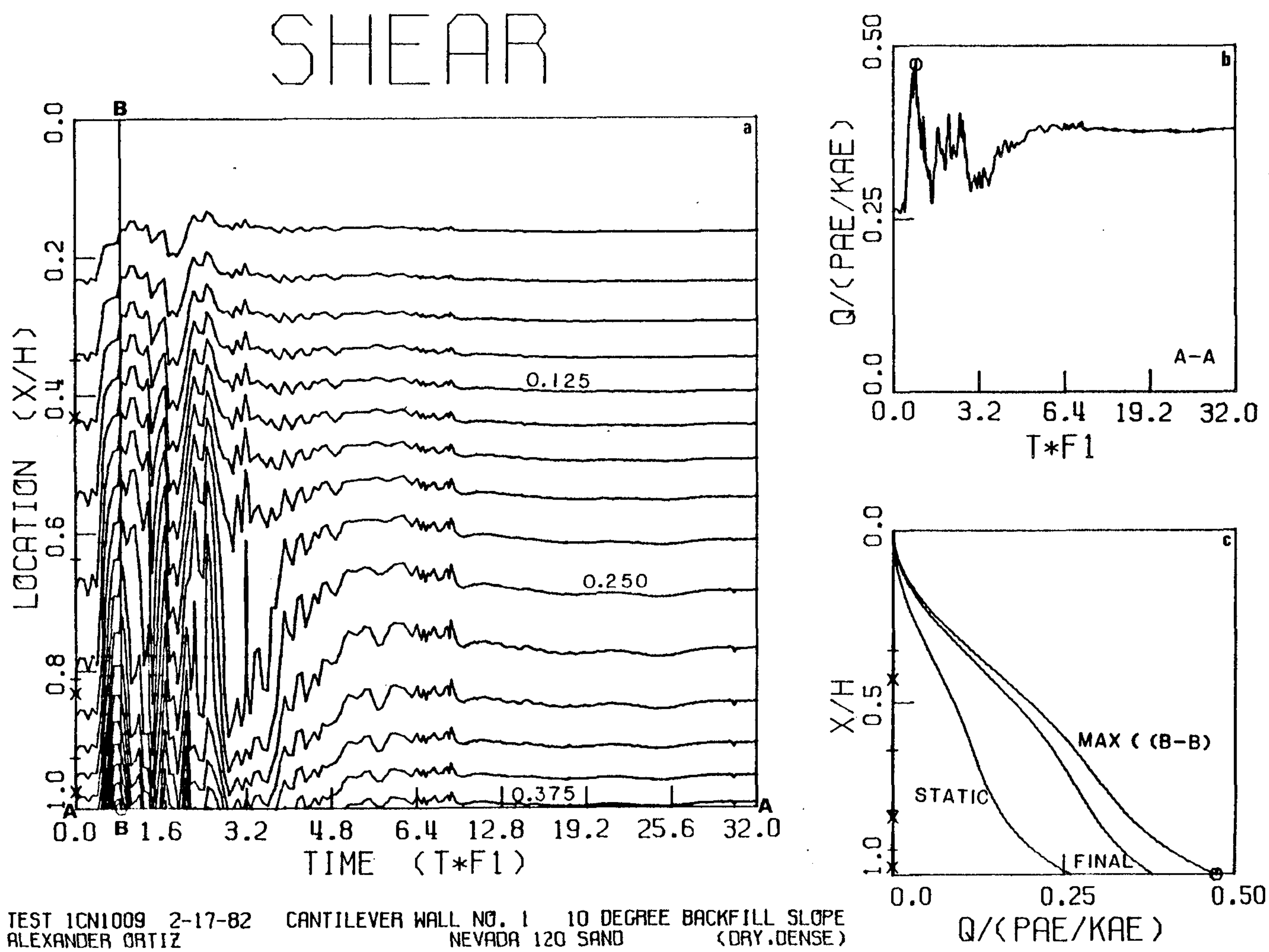
SHEAR
LOCATION (X/H)
0.0
0.2
0.4
0.6
0.8
1.0
TIME (T*F1)
0.0 1.6 3.2 4.8 6.4 12.8 19.2 25.6 32.0
A
B
a
0.125
0.250
0.375
Q/(PAE/KAE)
0.0
0.25
0.50
T*F1
0.0 3.2 6.4 19.2 32.0
b
A-A
c
X/H
0.0
0.5
1.0
Q/(PAE/KAE)
0.0 0.25 0.50
MAX ((B-B)
STATIC
FINAL
TEST 1CN1009 2-17-82 CANTILEVER WALL NO. 1 10 DEGREE BACKFILL SLOPE
ALEXANDER ORTIZ NEVADA 120 SAND (DRY,DENSE)

FIGURE 5.87

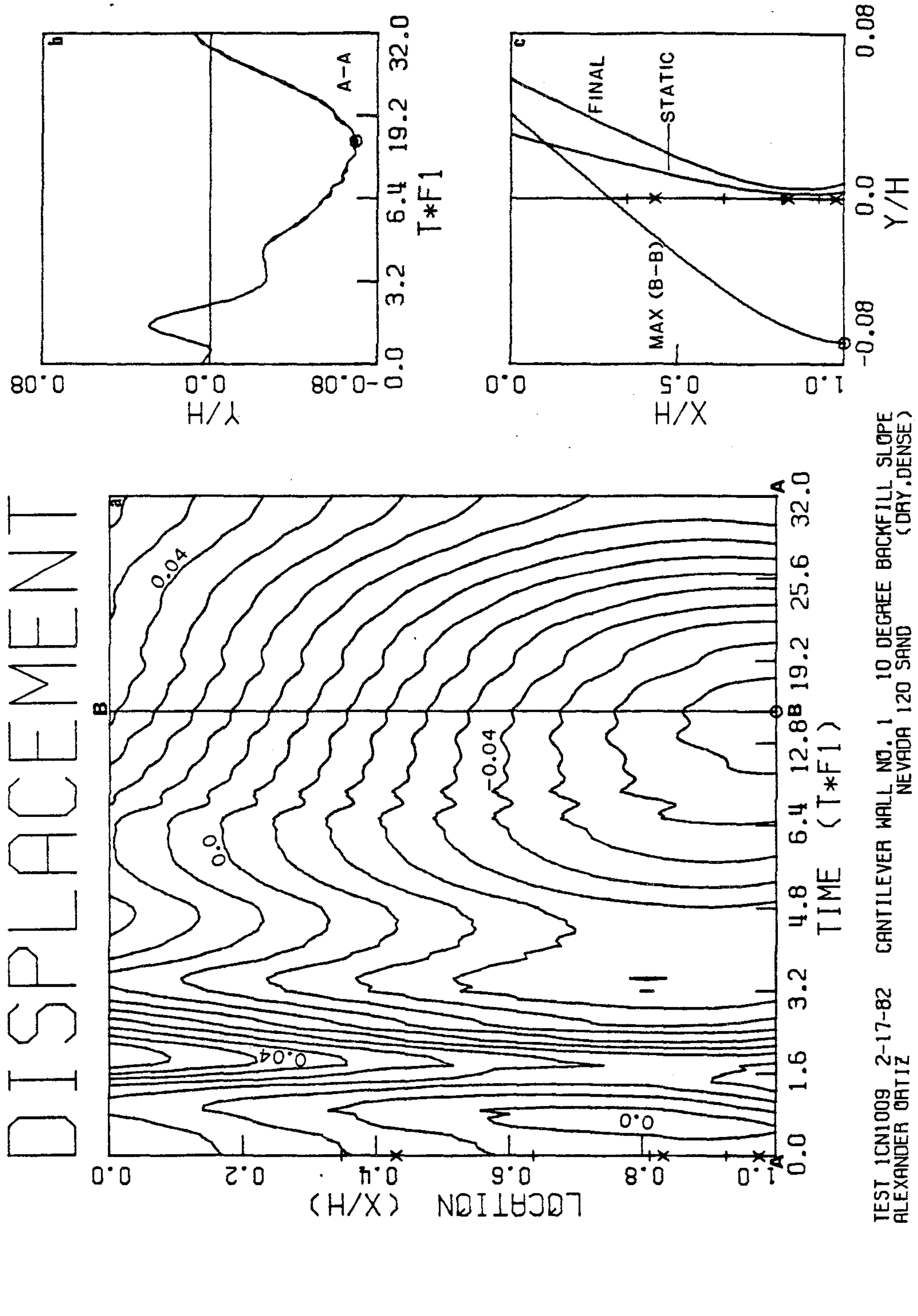
DISPLACEMENT
LOCATION (X/H)
TIME (T*F1)
0.0
0.2
0.4
0.6
0.8
1.0
1.6
3.2
4.8
6.4
12.8
19.2
25.6
32.0
0.04
-0.04
A
B
a
b
c
A-A
T*F1
Y/H
0.08
-0.08
X/H
0.5
FINAL
STATIC
MAX (B-B)
TEST 1CN1009 2-17-82
ALEXANDER ORTIZ
CANTILEVER WALL NO. 1 10 DEGREE BACKFILL SLOPE
NEVADA 120 SAND (DRY,DENSE)

FIGURE 5.88

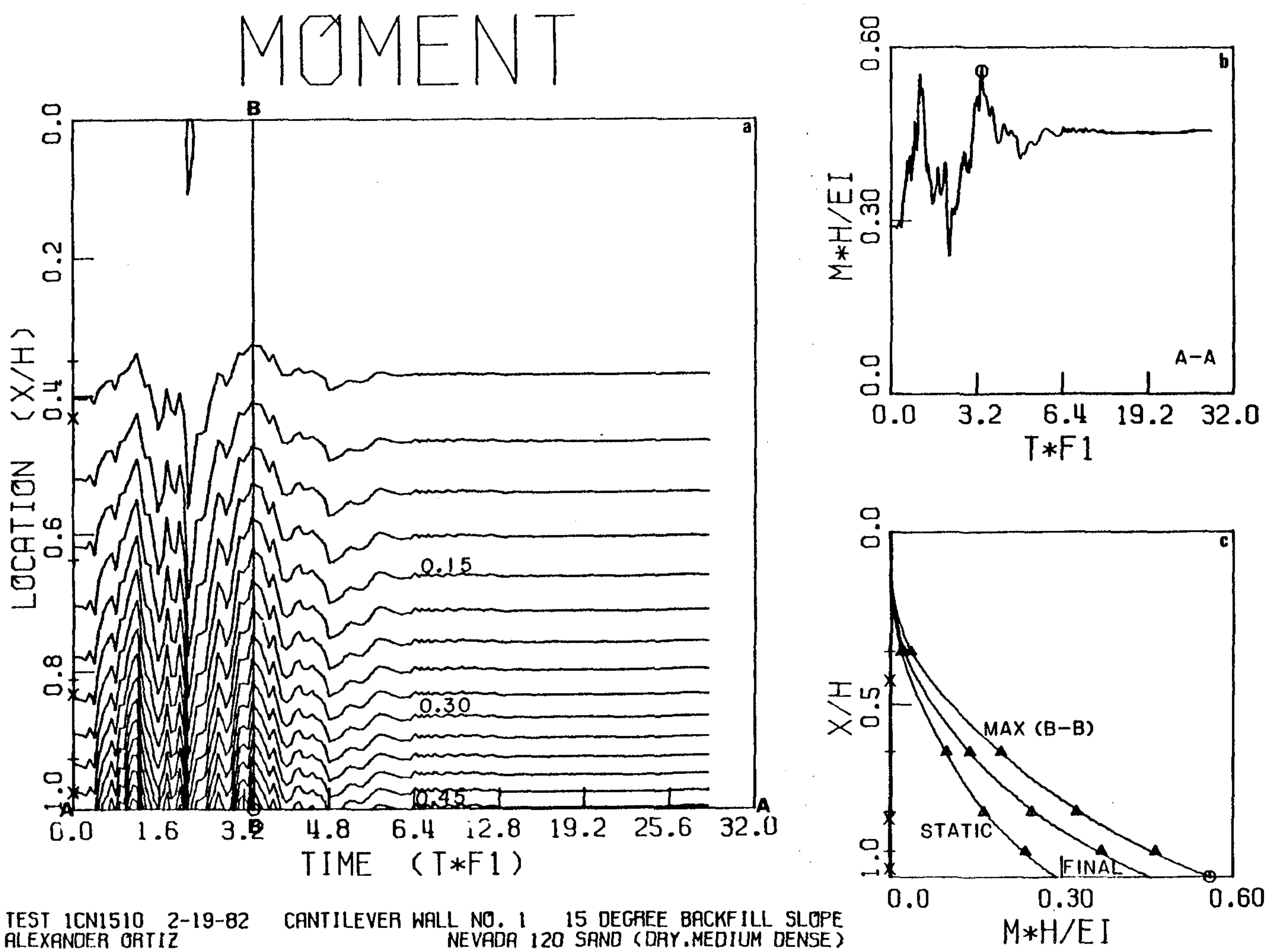
MØMENT
LOCATION (X/H)
TIME (T*F1)
0.15
0.30
0.45
M*H/EI
T*F1
A-A
X/H
MAX (B-B)
STATIC
FINAL
TEST 1CN1510 2-19-82 CANTILEVER WALL NO. 1 15 DEGREE BACKFILL SLOPE
ALEXANDER ORTIZ NEVADA 120 SAND (DRY.MEDIUM DENSE)

FIGURE 5.89

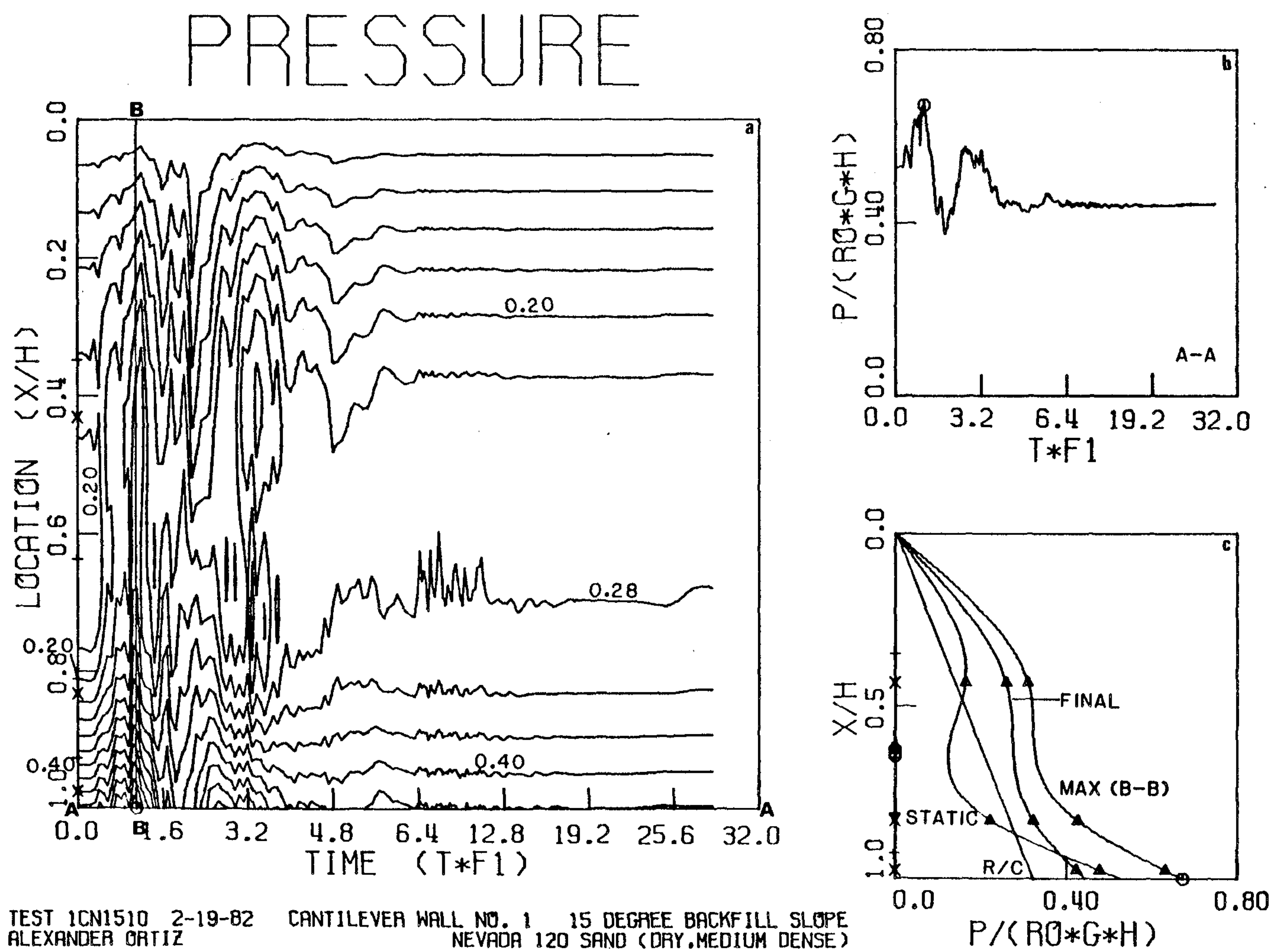
PRESSURE
LOCATION (X/H)
TIME (T*F1)
0.0
0.2
0.4
0.6
0.8
1.0
0.0
1.6
3.2
4.8
6.4
12.8
19.2
25.6
32.0
0.20
0.28
0.40
A
B
a
b
A-A
P/(RO*G*H)
T*F1
0.80
0.40
c
X/H
0.5
FINAL
MAX (B-B)
STATIC
R/C
TEST 1CN1510 2-19-82 CANTILEVER WALL NO. 1 15 DEGREE BACKFILL SLOPE
ALEXANDER ORTIZ NEVADA 120 SAND (DRY,MEDIUM DENSE)

FIGURE 5.90

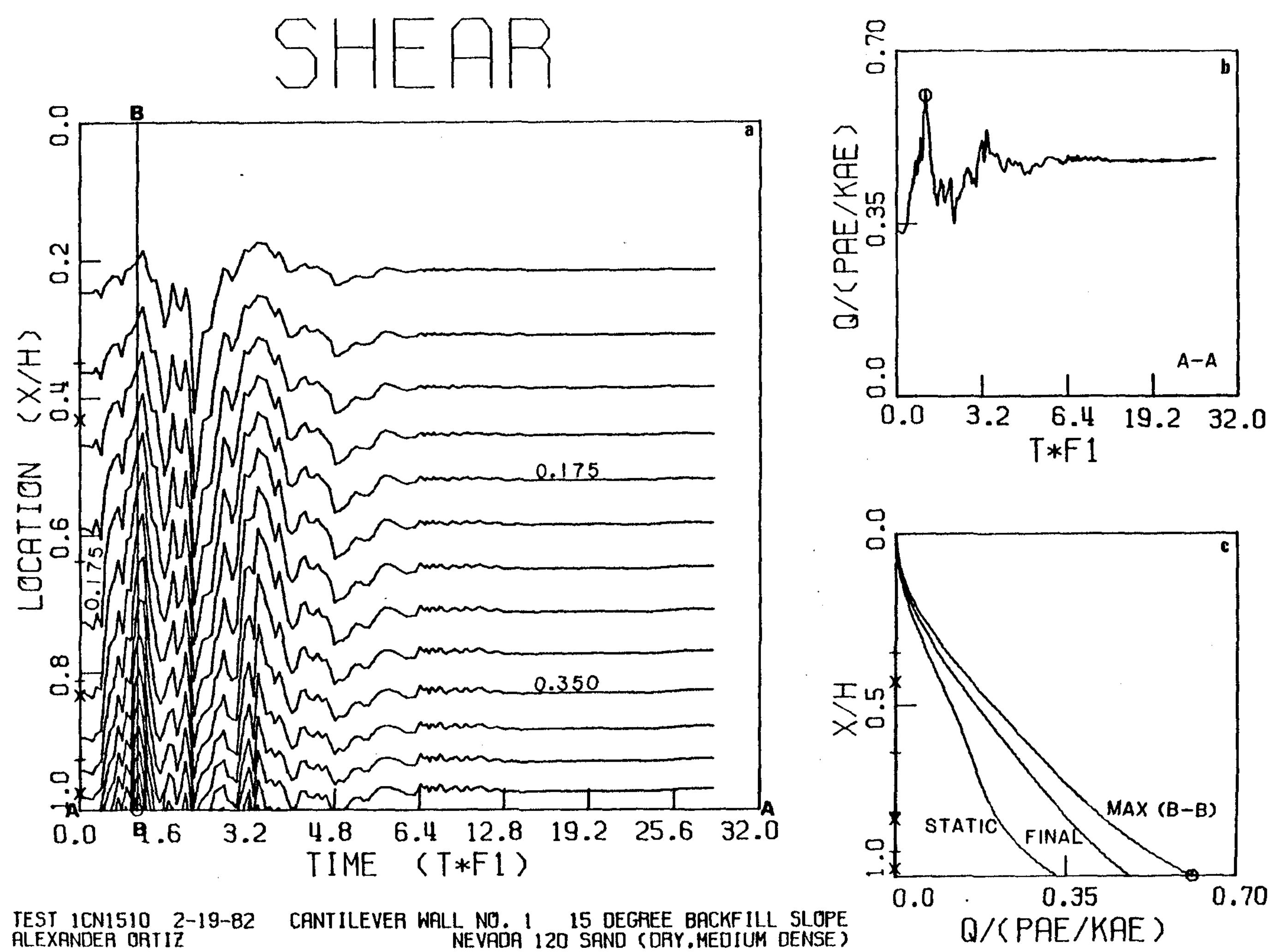
SHEAR
a
B
A
LOCATION (X/H)
0.0
0.2
0.4
0.6
0.8
1.0
0.175
0.350
0.0
1.6
3.2
4.8
6.4
12.8
19.2
25.6
32.0
TIME (T*F1)
b
Q/(PAE/KAE)
0.0
0.35
0.70
A-A
T*F1
c
X/H
0.5
STATIC
FINAL
MAX (B-B)
Q/(PAE/KAE)
TEST 1CN1510 2-19-82 CANTILEVER WALL NO. 1 15 DEGREE BACKFILL SLOPE
ALEXANDER ORTIZ NEVADA 120 SAND (DRY,MEDIUM DENSE)

FIGURE 5.91

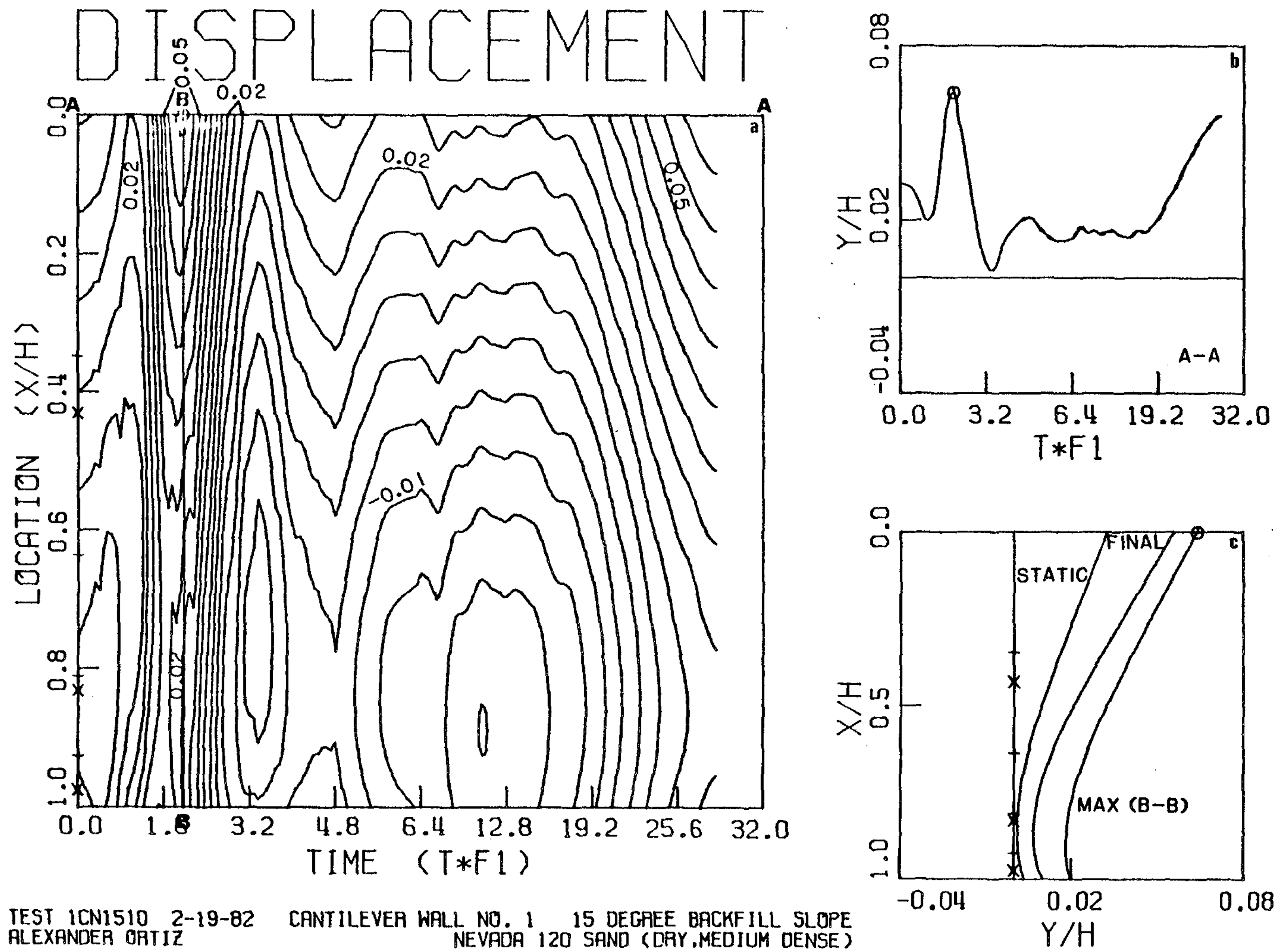
DISPLACEMENT
a
b
c
A
B
0.05
0.02
-0.01
LOCATION (X/H)
TIME (T*F1)
0.0
0.2
0.4
0.6
0.8
1.0
1.6
3.2
4.8
6.4
12.8
19.2
25.6
32.0
Y/H
T*F1
0.08
0.02
-0.04
A-A
X/H
0.5
STATIC
FINAL
MAX (B-B)
TEST 1CN1510 2-19-82 CANTILEVER WALL NO. 1 15 DEGREE BACKFILL SLOPE
ALEXANDER ORTIZ NEVADA 120 SAND (DRY, MEDIUM DENSE)

FIGURE 5.92

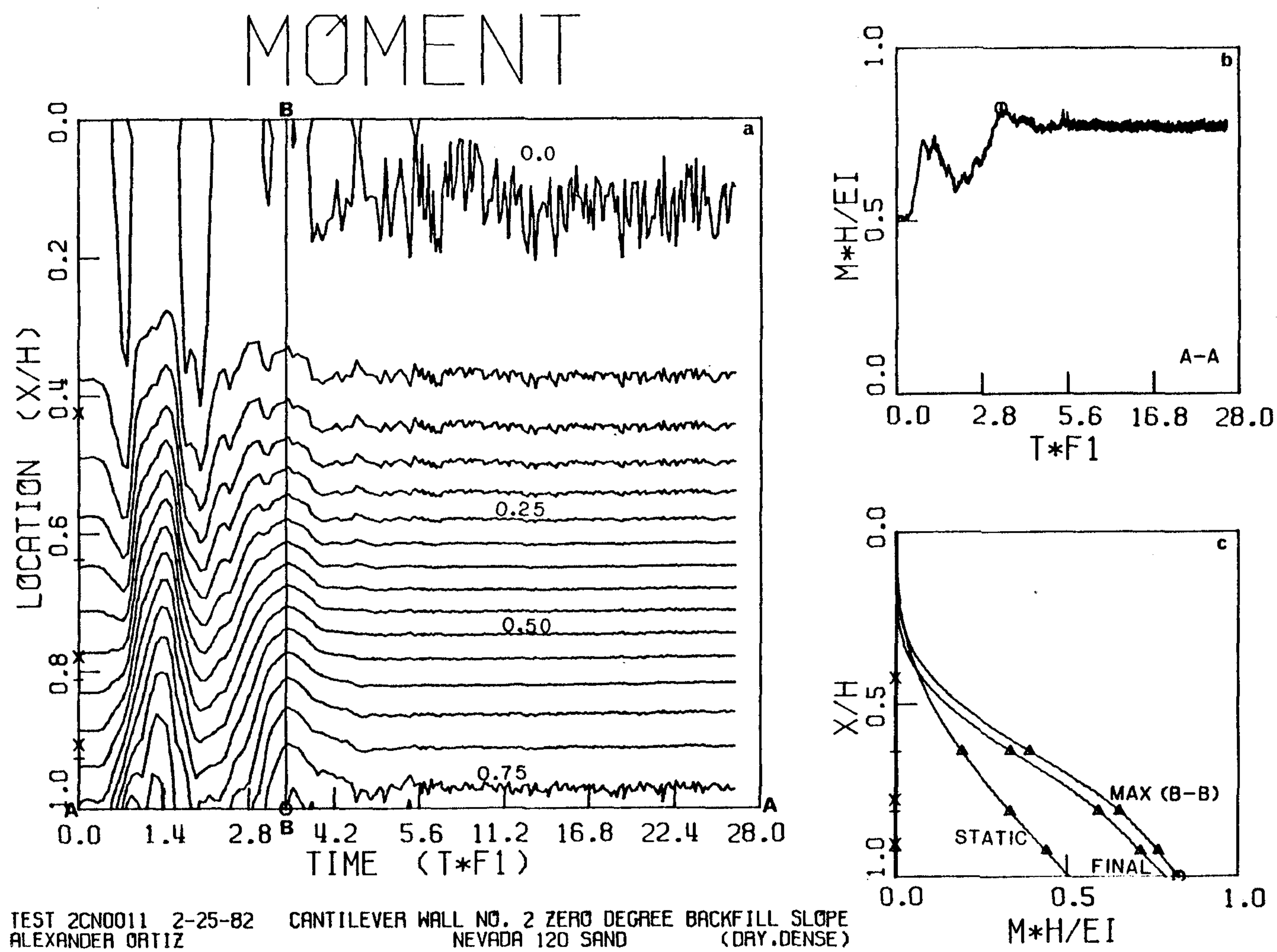
MOMENT
a
b
c
0.0
0.25
0.50
0.75
B
A
LOCATION (X/H)
0.0
0.2
0.4
0.6
0.8
1.0
0.0 1.4 2.8 4.2 5.6 11.2 16.8 22.4 28.0
TIME (T*F1)
TEST 2CN0011 2-25-82 CANTILEVER WALL NO. 2 ZERO DEGREE BACKFILL SLOPE
ALEXANDER ORTIZ NEVADA 120 SAND (DRY.DENSE)
M*H/EI
1.0
0.5
0.0
A-A
0.0 2.8 5.6 16.8 28.0
T*F1
X/H
0.0
0.5
1.0
MAX (B-B)
STATIC
FINAL
0.0 0.5 1.0
M*H/EI

FIGURE 5.93

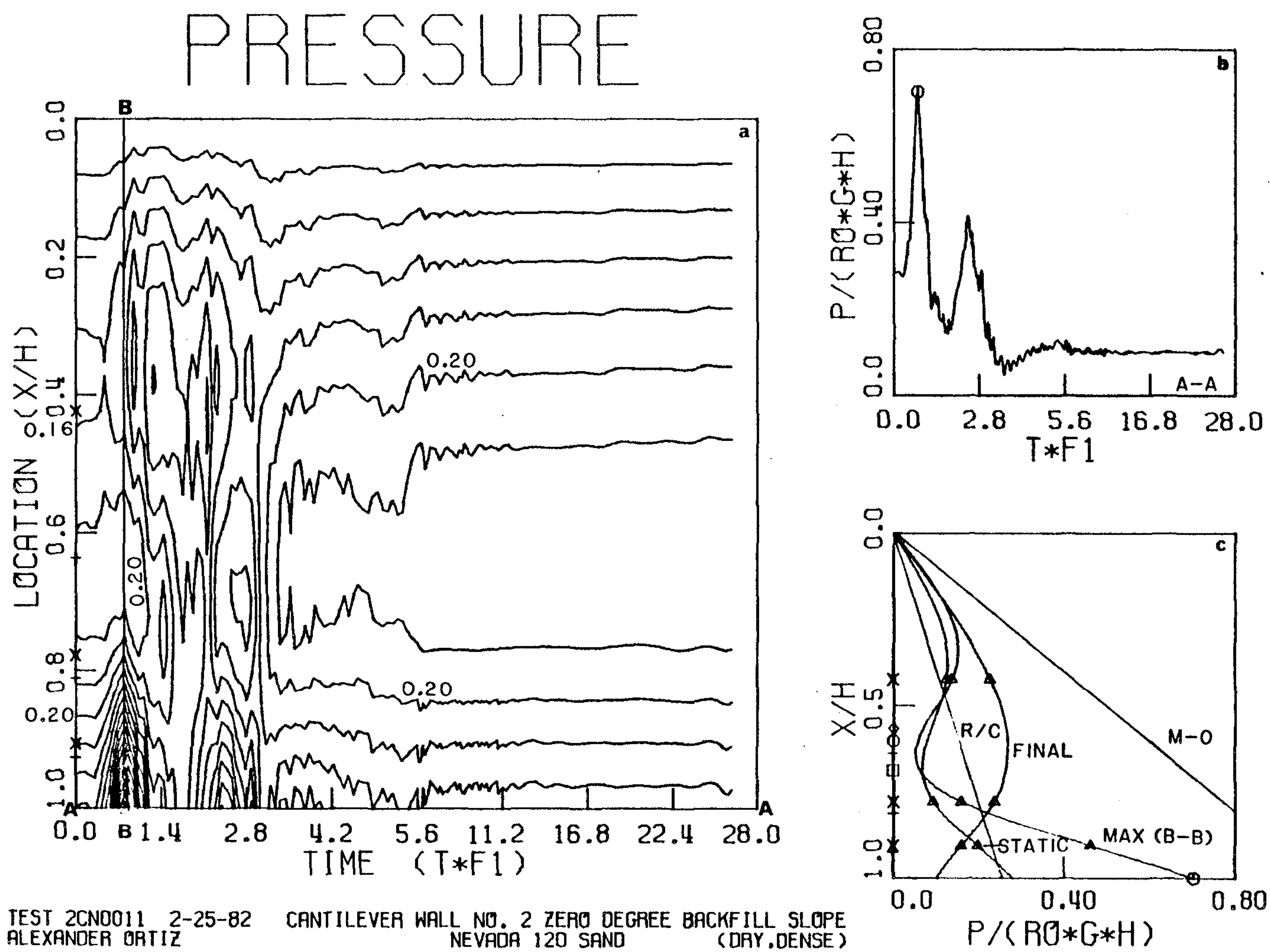

TEST 2CN0011 2-25-82 CANTILEVER WALL NO. 2 ZERO DEGREE BACKFILL SLOPE
ALEXANDER ORTIZ NEVADA 120 SAND (DRY,DENSE)

FIGURE 5.94

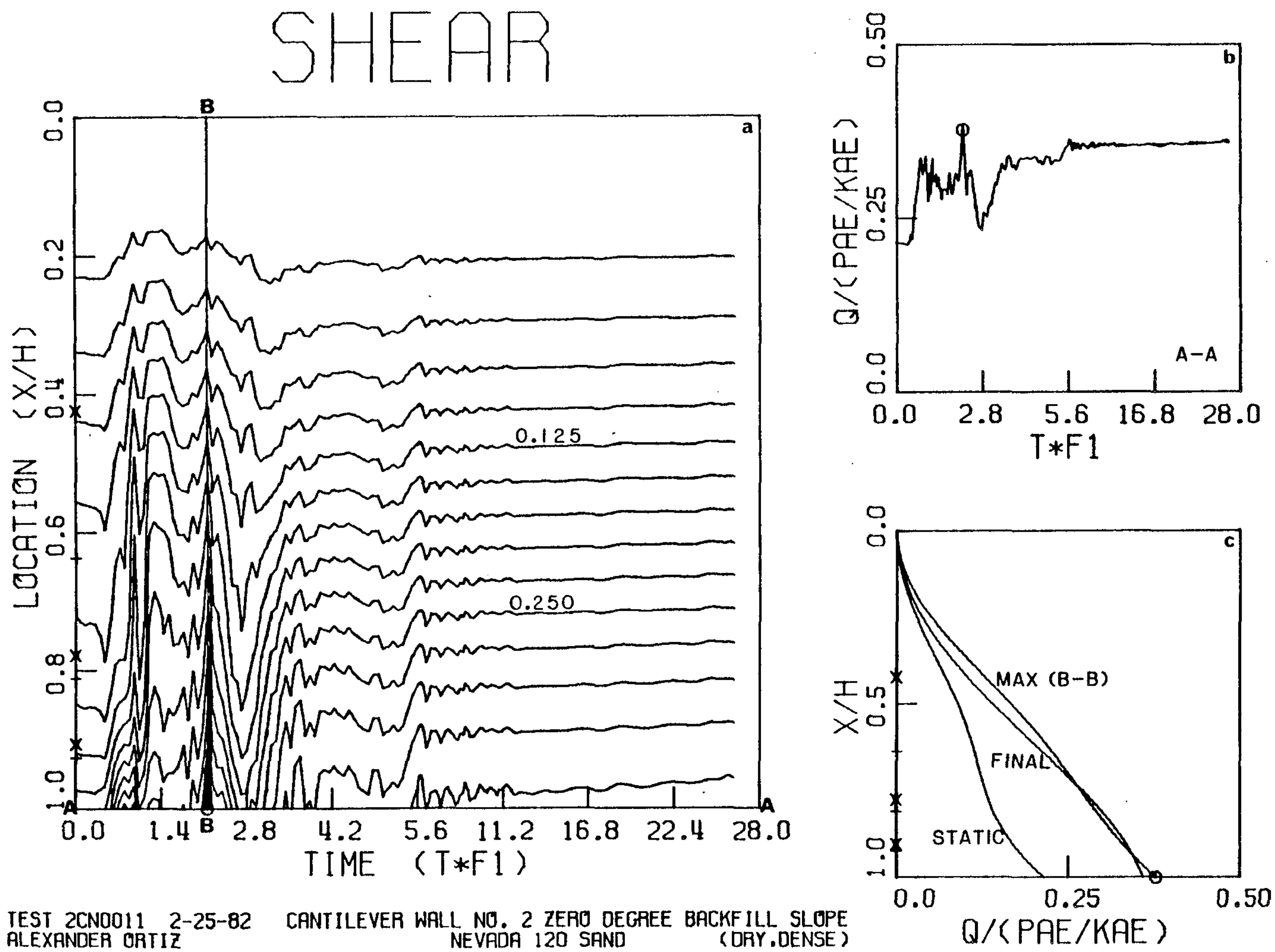
SHEAR
B
a
LOCATION (X/H)
0.0
0.2
0.4
0.6
0.8
1.0
0.125
0.250
A
0.0
1.4
2.8
4.2
5.6
11.2
16.8
22.4
28.0
TIME (T*F1)
b
Q/(PAE/KAE)
0.50
0.25
0.0
A-A
T*F1
c
X/H
0.5
MAX (B-B)
FINAL
STATIC
0.0
0.25
0.50
Q/(PAE/KAE)
TEST 2CN0011 2-25-82
ALEXANDER ORTIZ
CANTILEVER WALL NO. 2 ZERO DEGREE BACKFILL SLOPE
NEVADA 120 SAND (DRY.DENSE)

FIGURE 5.95

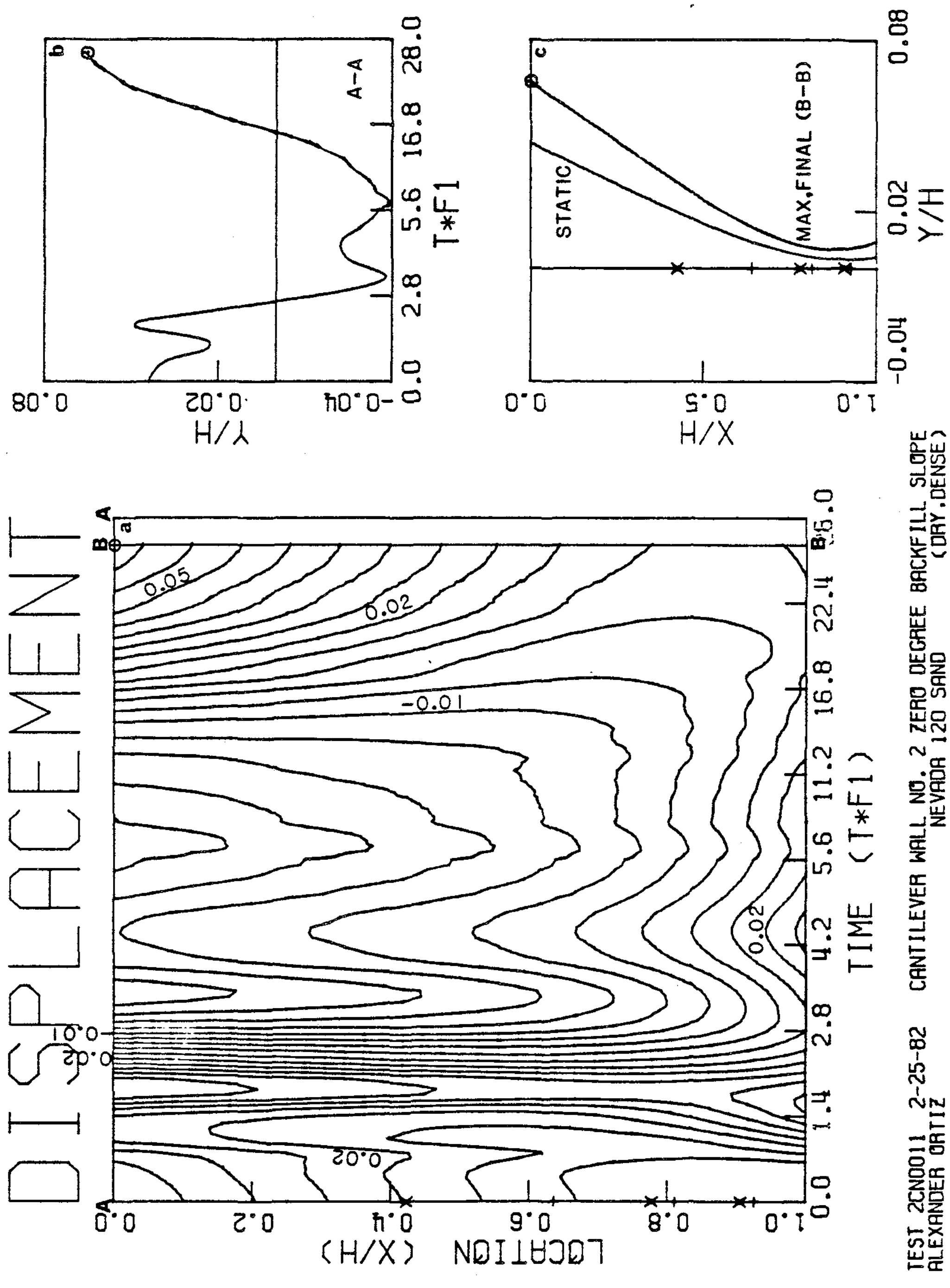
DISPLACEMENT
LOCATION (X/H)
TIME (T*F1)
0.05
0.02
-0.01
Y/H
T*F1
A-A
X/H
Y/H
STATIC
MAX,FINAL (B-B)
TEST 2CN0011 2-25-82 CANTILEVER WALL NO. 2 ZERO DEGREE BACKFILL SLOPE
ALEXANDER ORTIZ NEVADA 120 SAND (DRY,DENSE)

FIGURE 5.96

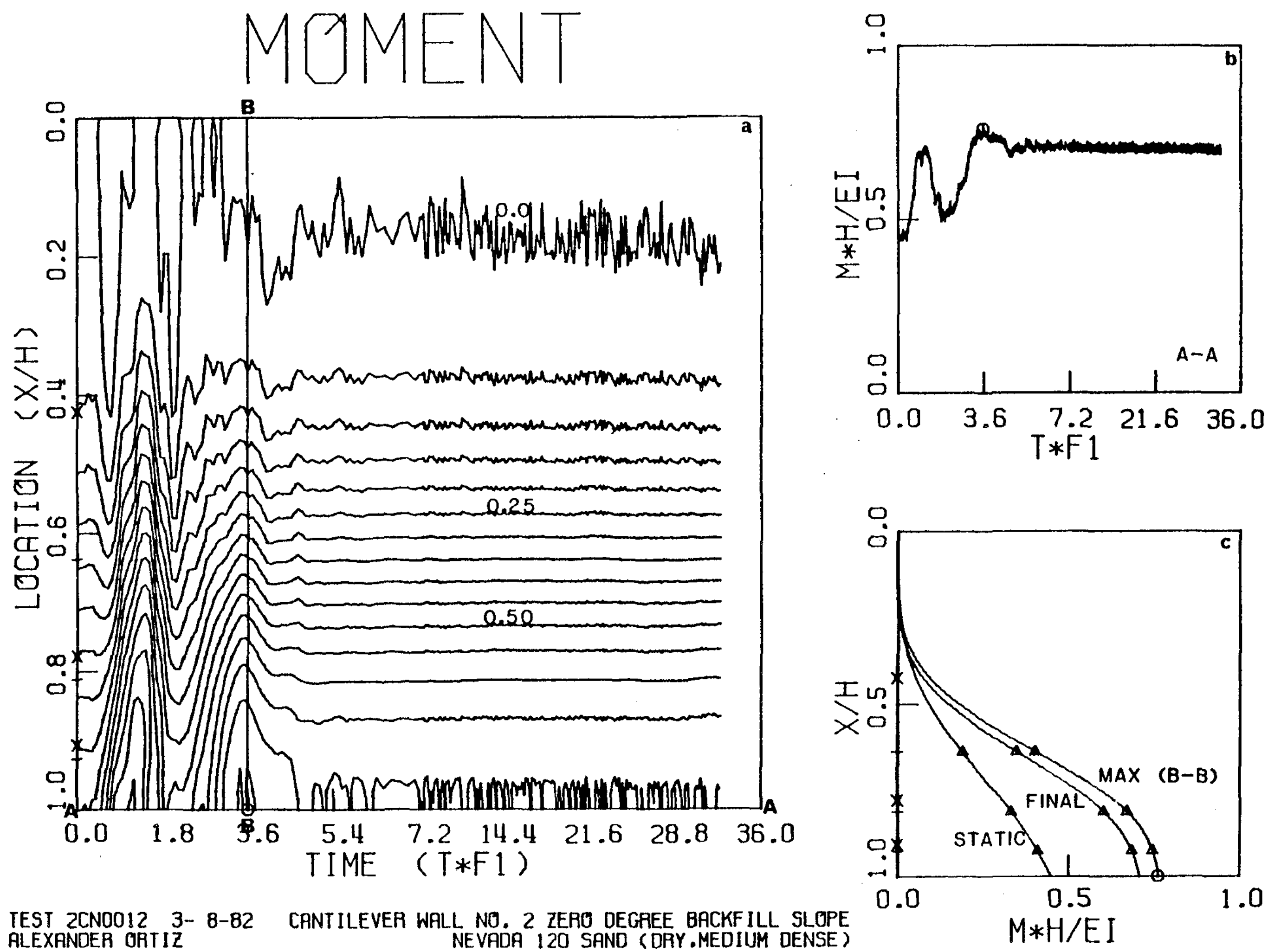
MOMENT
LOCATION (X/H)
TIME (T*F1)
0.0
0.2
0.4
0.6
0.8
1.0
0.0 1.8 3.6 5.4 7.2 14.4 21.6 28.8 36.0
0.0
0.25
0.50
A
B
a
b
c
M*H/EI
T*F1
A-A
0.0 3.6 7.2 21.6 36.0
0.0 0.5 1.0
X/H
MAX (B-B)
FINAL
STATIC
TEST 2CN0012 3- 8-82 CANTILEVER WALL NO. 2 ZERO DEGREE BACKFILL SLOPE
ALEXANDER ORTIZ NEVADA 120 SAND (DRY,MEDIUM DENSE)

FIGURE 5.97

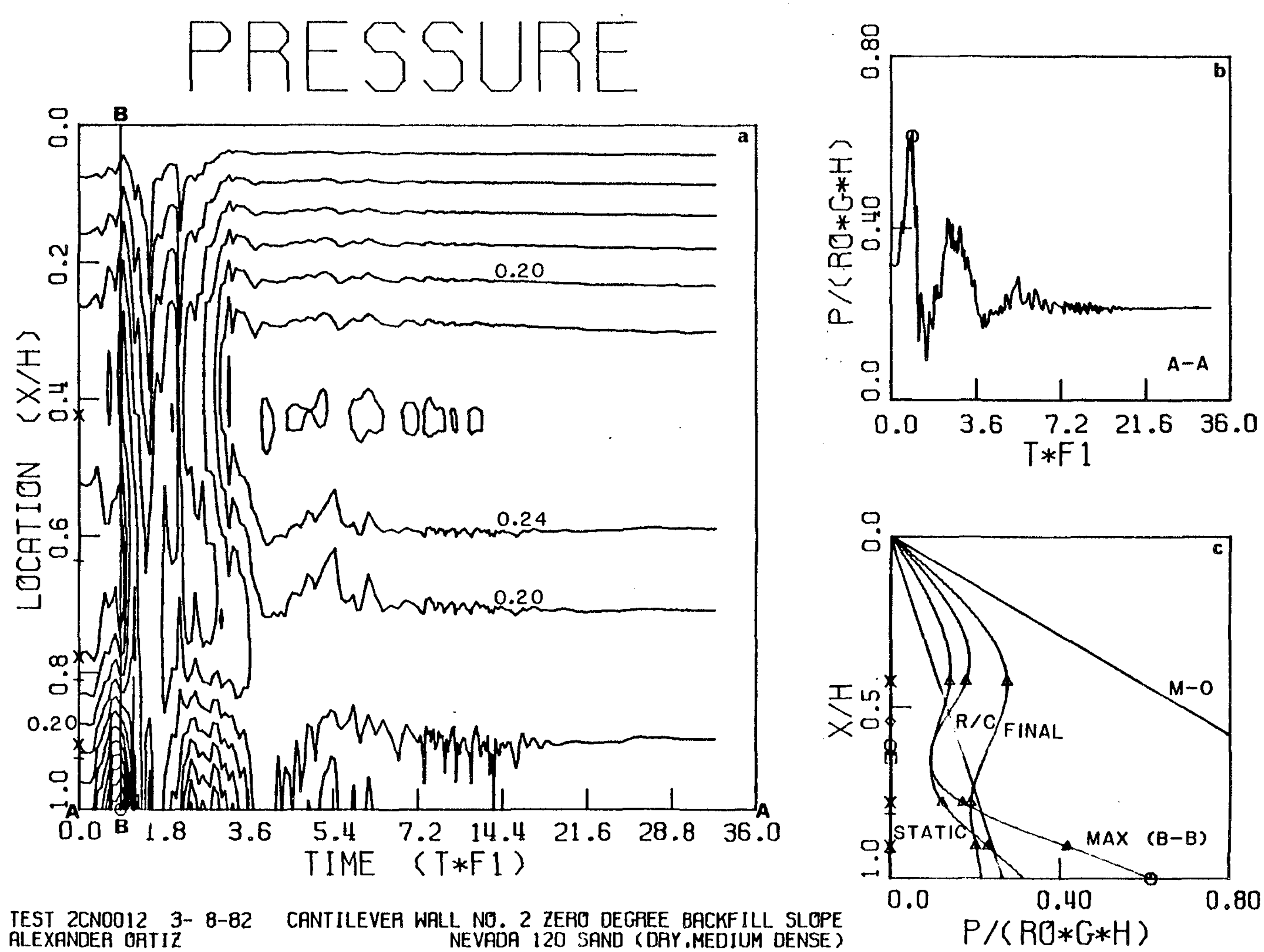

TEST 2CN0012 3- 8-82 CANTILEVER WALL NO. 2 ZERO DEGREE BACKFILL SLOPE
ALEXANDER ORTIZ NEVADA 120 SAND (DRY,MEDIUM DENSE)

FIGURE 5.98

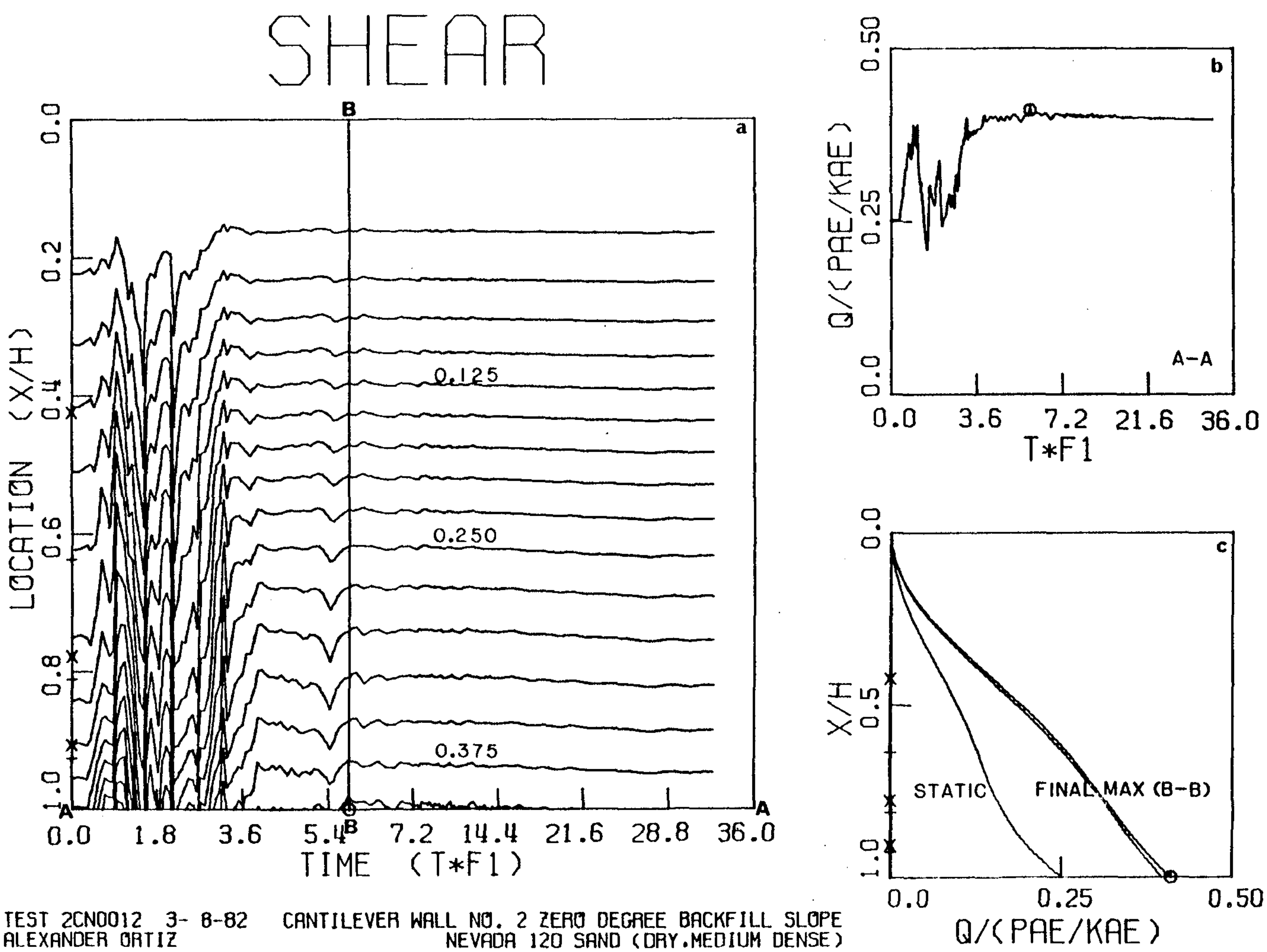

TEST 2CN0012 3- 8-82 CANTILEVER WALL NO. 2 ZERO DEGREE BACKFILL SLOPE
ALEXANDER ORTIZ NEVADA 120 SAND (DRY.MEDIUM DENSE)

FIGURE 5.99

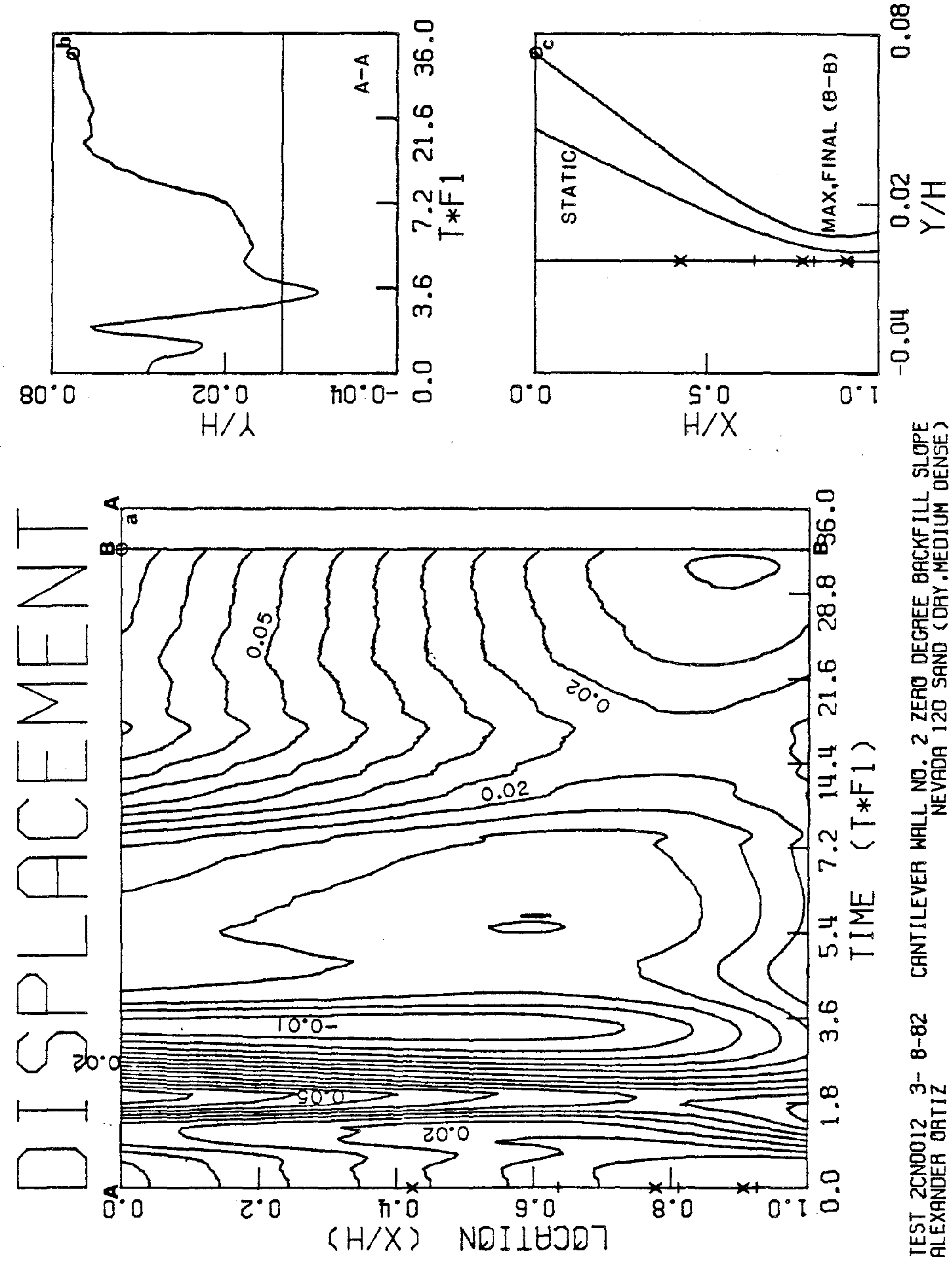

TEST 2CN0012 3- 8-82 CANTILEVER WALL NO. 2 ZERO DEGREE BACKFILL SLOPE
ALEXANDER ORTIZ NEVADA 120 SAND (DRY,MEDIUM DENSE)

FIGURE 5.100

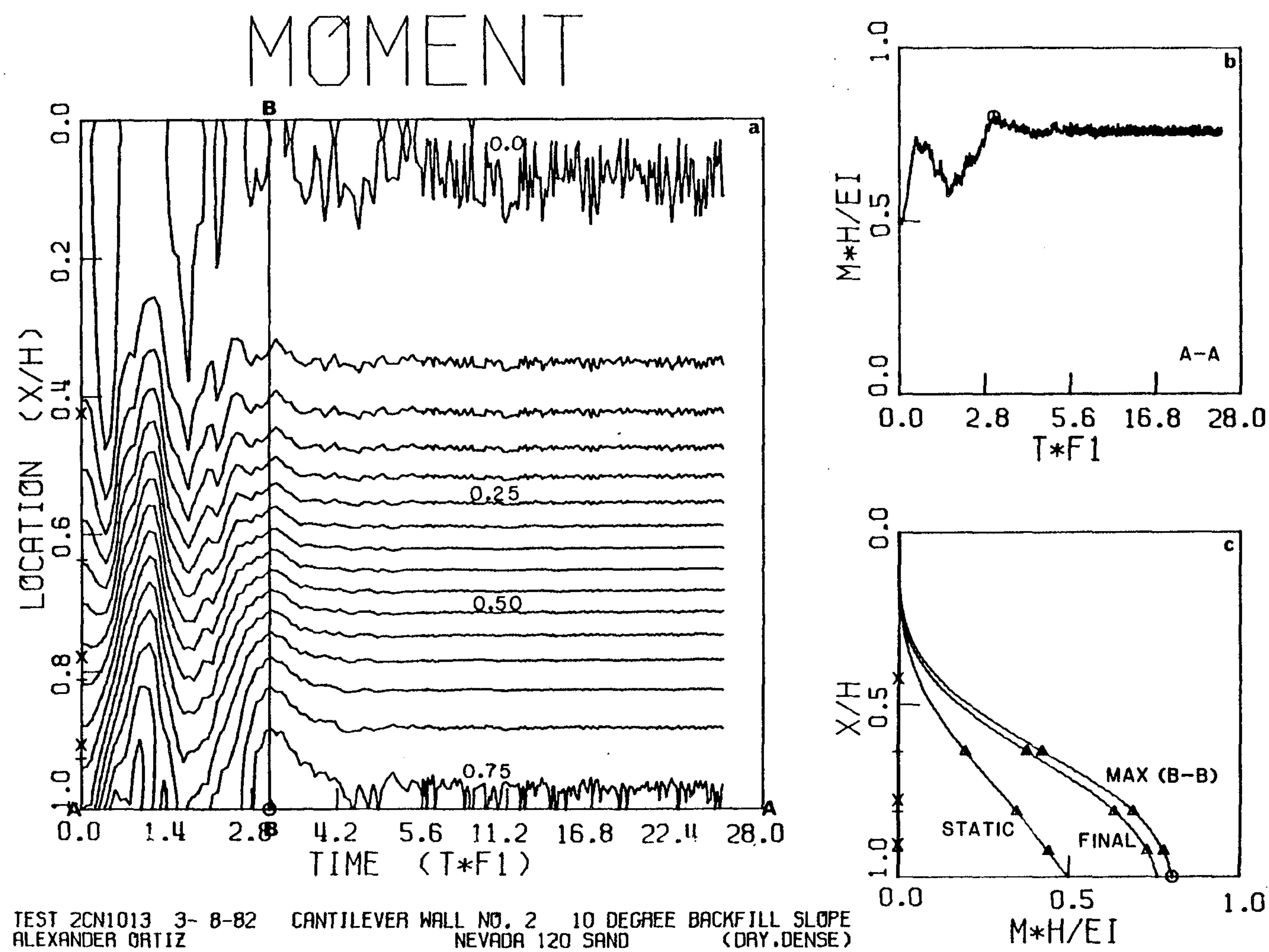
MOMENT
a
b
c
LOCATION (X/H)
TIME (T*F1)
0.0
0.25
0.50
0.75
A
B
M*H/EI
T*F1
A-A
X/H
MAX (B-B)
FINAL
STATIC
TEST 2CN1013 3- 8-82 CANTILEVER WALL NO. 2 10 DEGREE BACKFILL SLOPE
ALEXANDER ORTIZ NEVADA 120 SAND (DRY,DENSE)

FIGURE 5.101

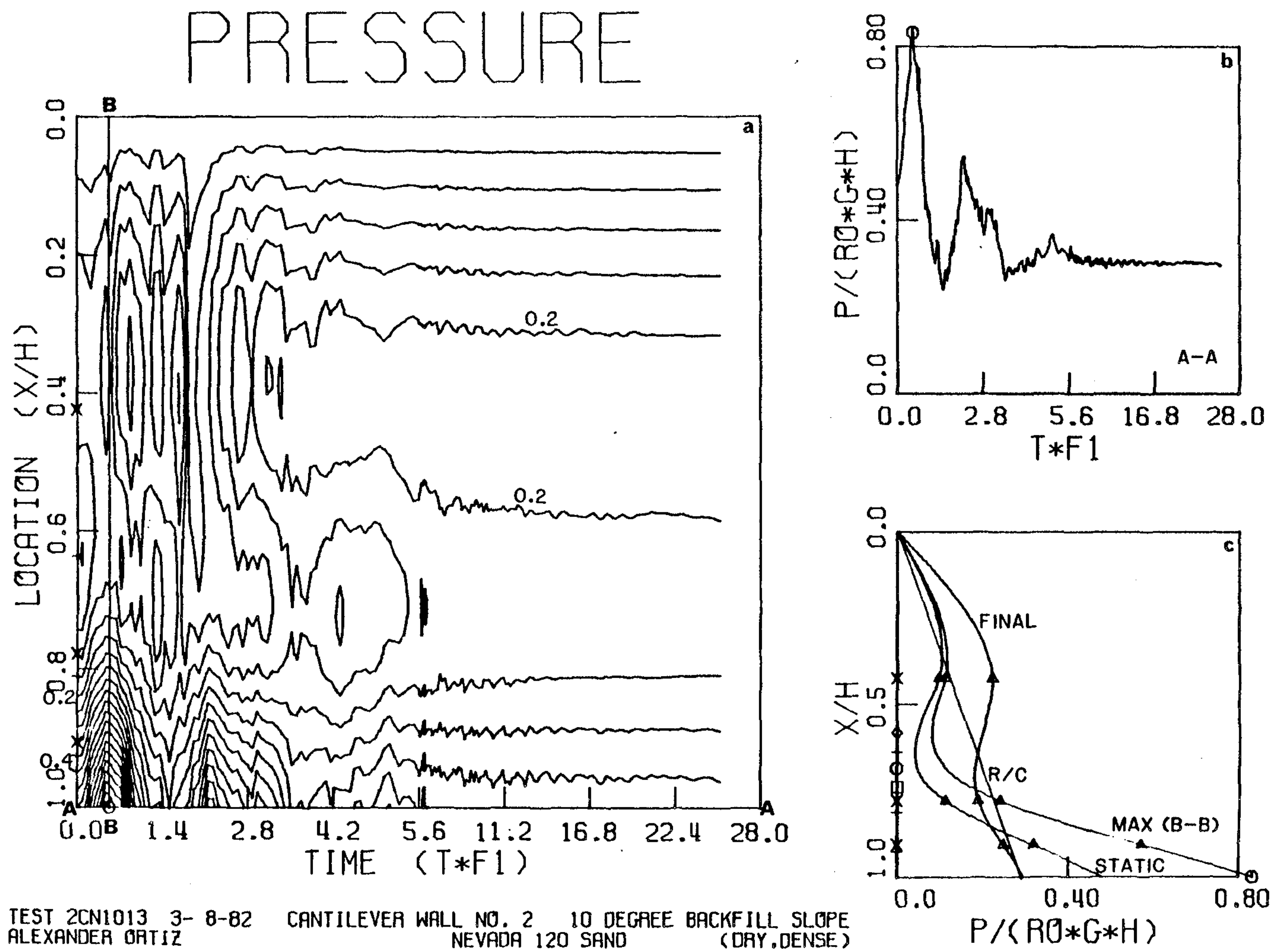
PRESSURE
LOCATION (X/H)
TIME (T*F1)
0.2
0.2
A
B
a
b
A-A
P/(RO*G*H)
T*F1
c
FINAL
R/C
MAX (B-B)
STATIC
X/H
P/(RO*G*H)
TEST 2CN1013 3- 8-82 CANTILEVER WALL NO. 2 10 DEGREE BACKFILL SLOPE
ALEXANDER ORTIZ NEVADA 120 SAND (DRY,DENSE)

FIGURE 5.102

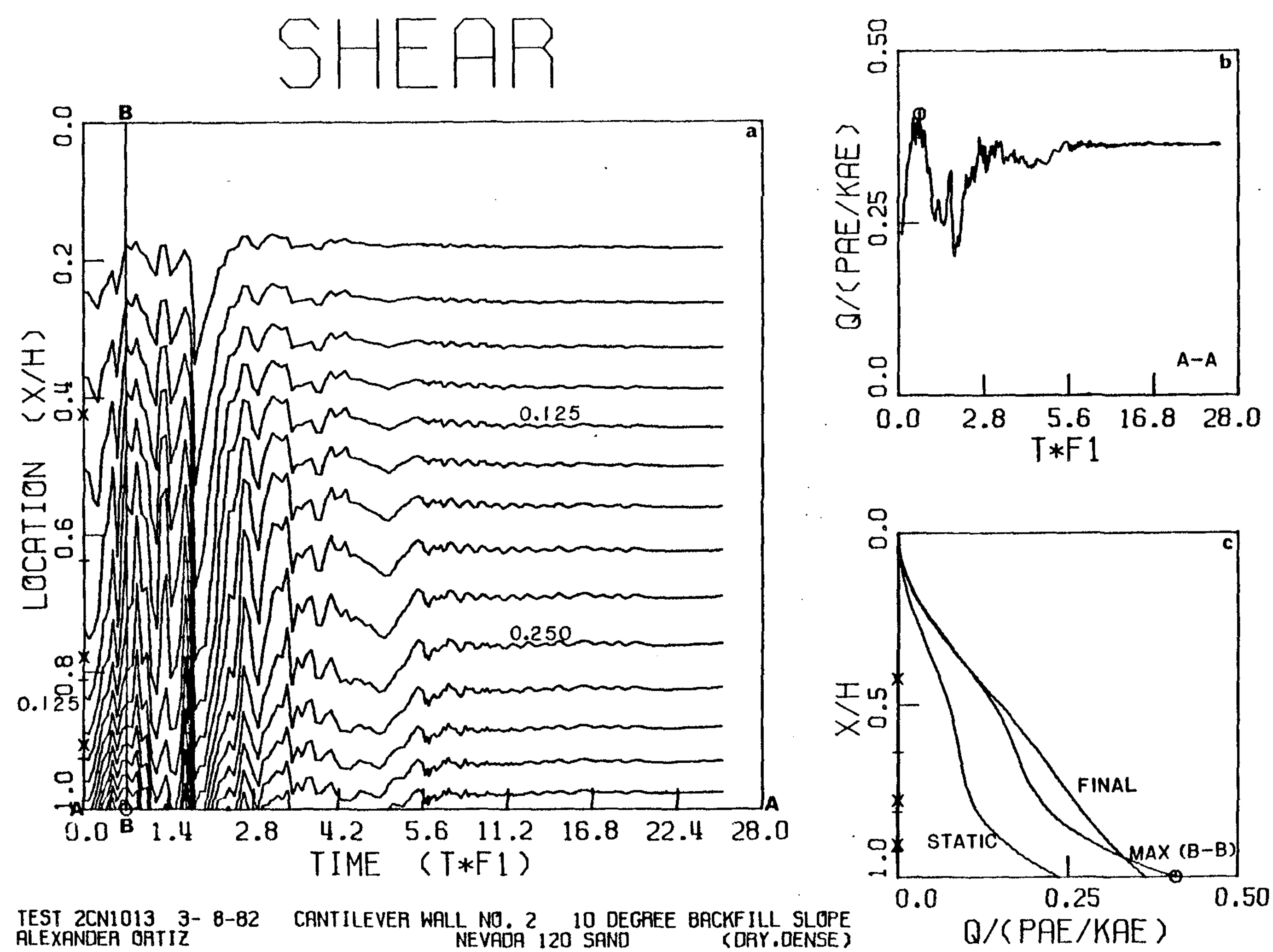

TEST 2CN1013 3- 8-82 CANTILEVER WALL NO. 2 10 DEGREE BACKFILL SLOPE
ALEXANDER ORTIZ NEVADA 120 SAND (DRY,DENSE)

FIGURE 5.103

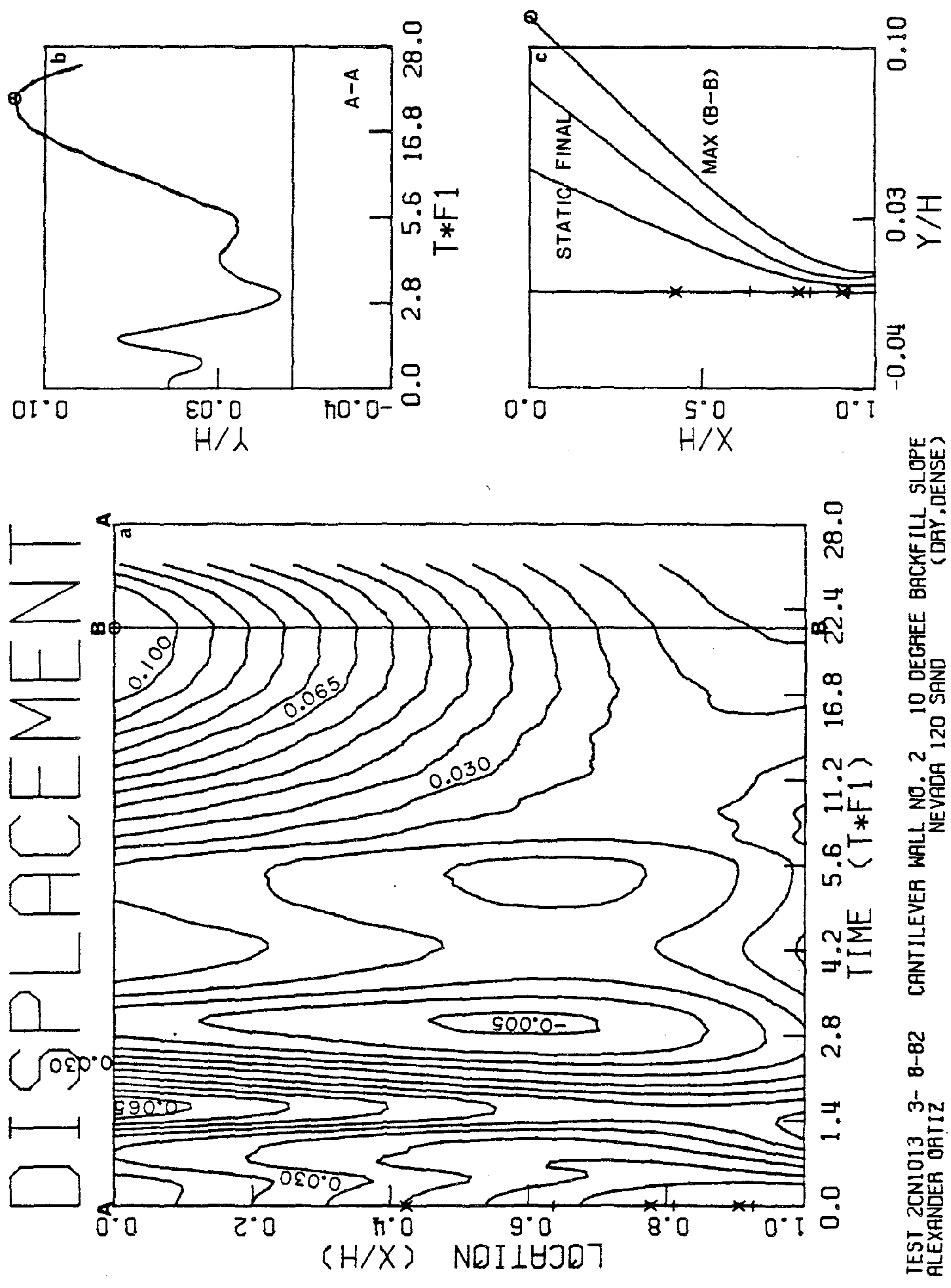
DISPLACEMENT
LOCATION (X/H)
TIME (T*F1)
0.030
0.065
0.100
-0.005
A-A
MAX (B-B)
FINAL
STATIC
Y/H
X/H
T*F1
TEST 2CN1013 3- 8-82 CANTILEVER WALL NO. 2 10 DEGREE BACKFILL SLOPE
ALEXANDER ORTIZ NEVADA 120 SAND (DRY, DENSE)

FIGURE 5.104

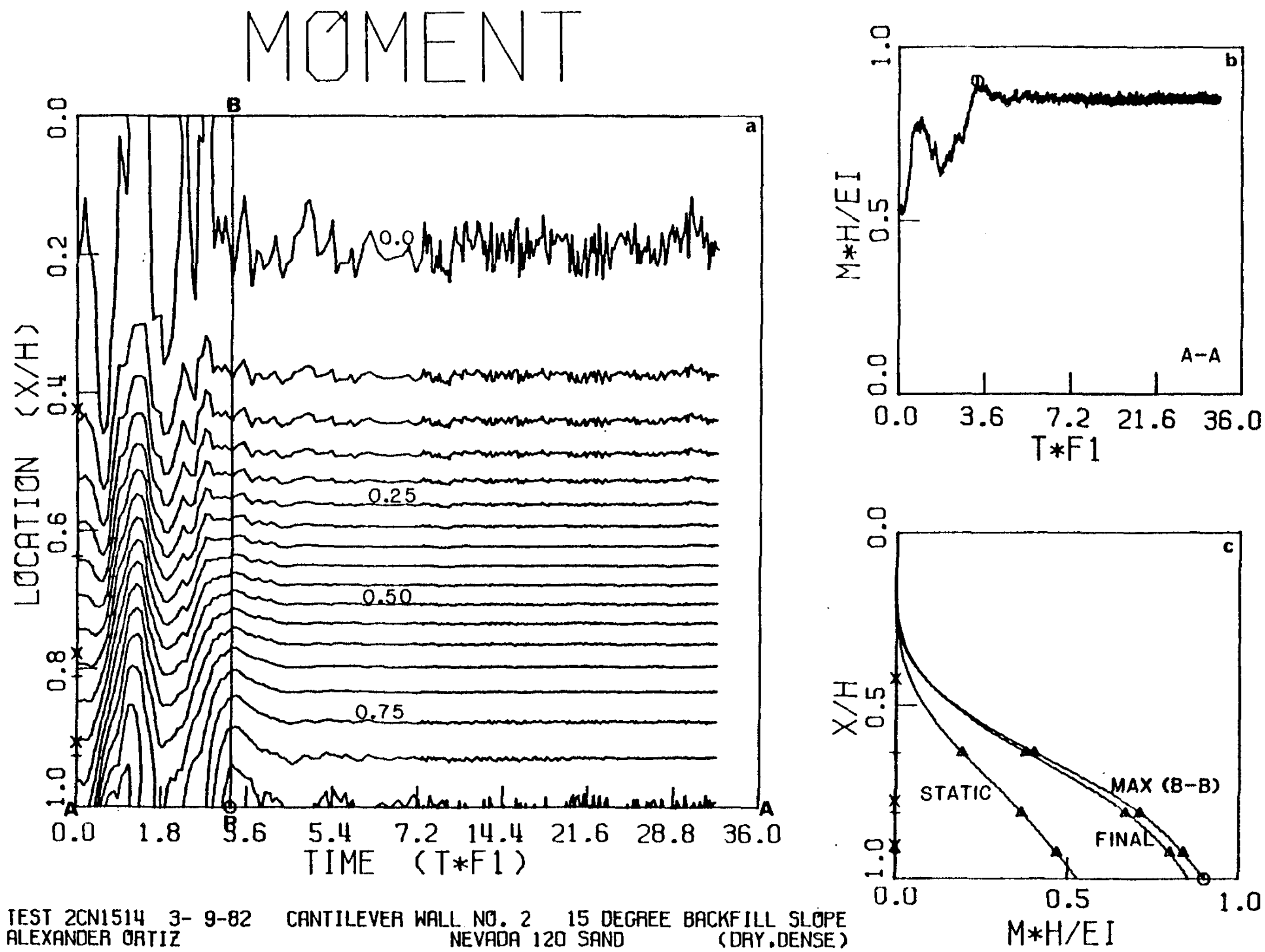

TEST 2CN1514 3- 9-82 CANTILEVER WALL NO. 2 15 DEGREE BACKFILL SLOPE
ALEXANDER ORTIZ NEVADA 120 SAND (DRY,DENSE)

FIGURE 5.105

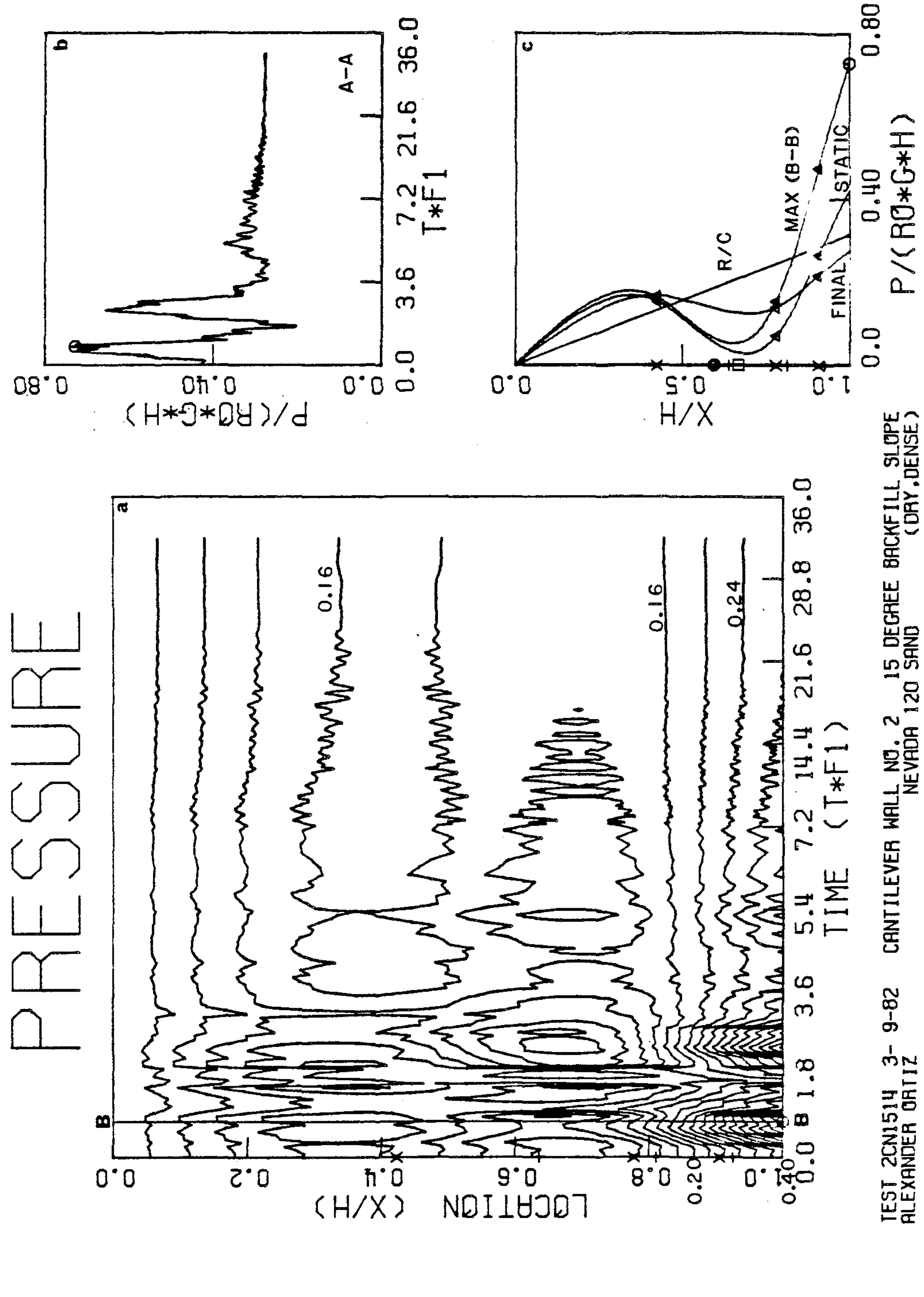

TEST 2CN1514 3- 9-82 CANTILEVER WALL NO. 2 15 DEGREE BACKFILL SLOPE
ALEXANDER ORTIZ NEVADA 120 SAND (DRY, DENSE)

FIGURE 5.106

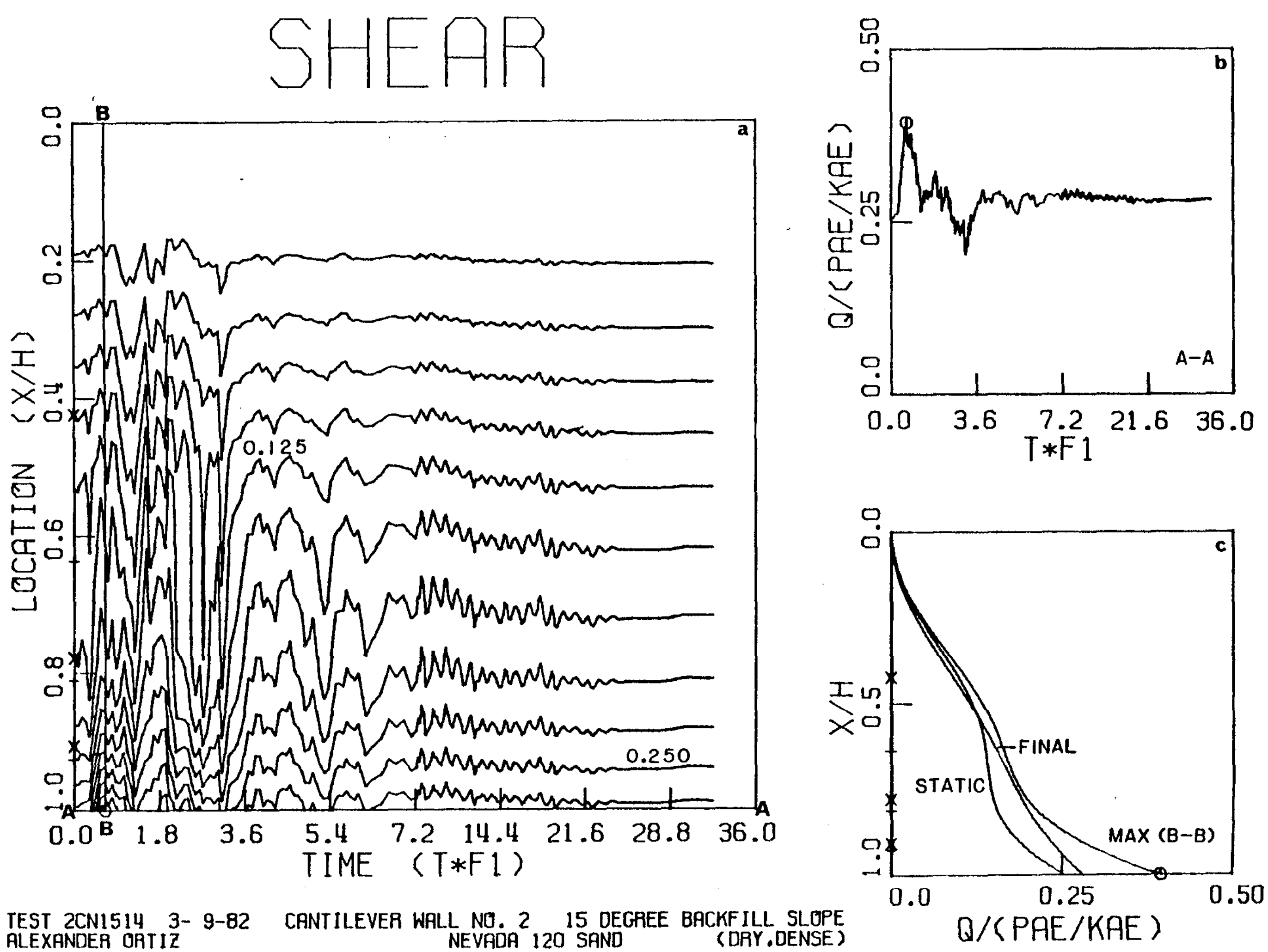

TEST 2CN1514 3- 9-82 CANTILEVER WALL NO. 2 15 DEGREE BACKFILL SLOPE
ALEXANDER ORTIZ NEVADA 120 SAND (DRY,DENSE)

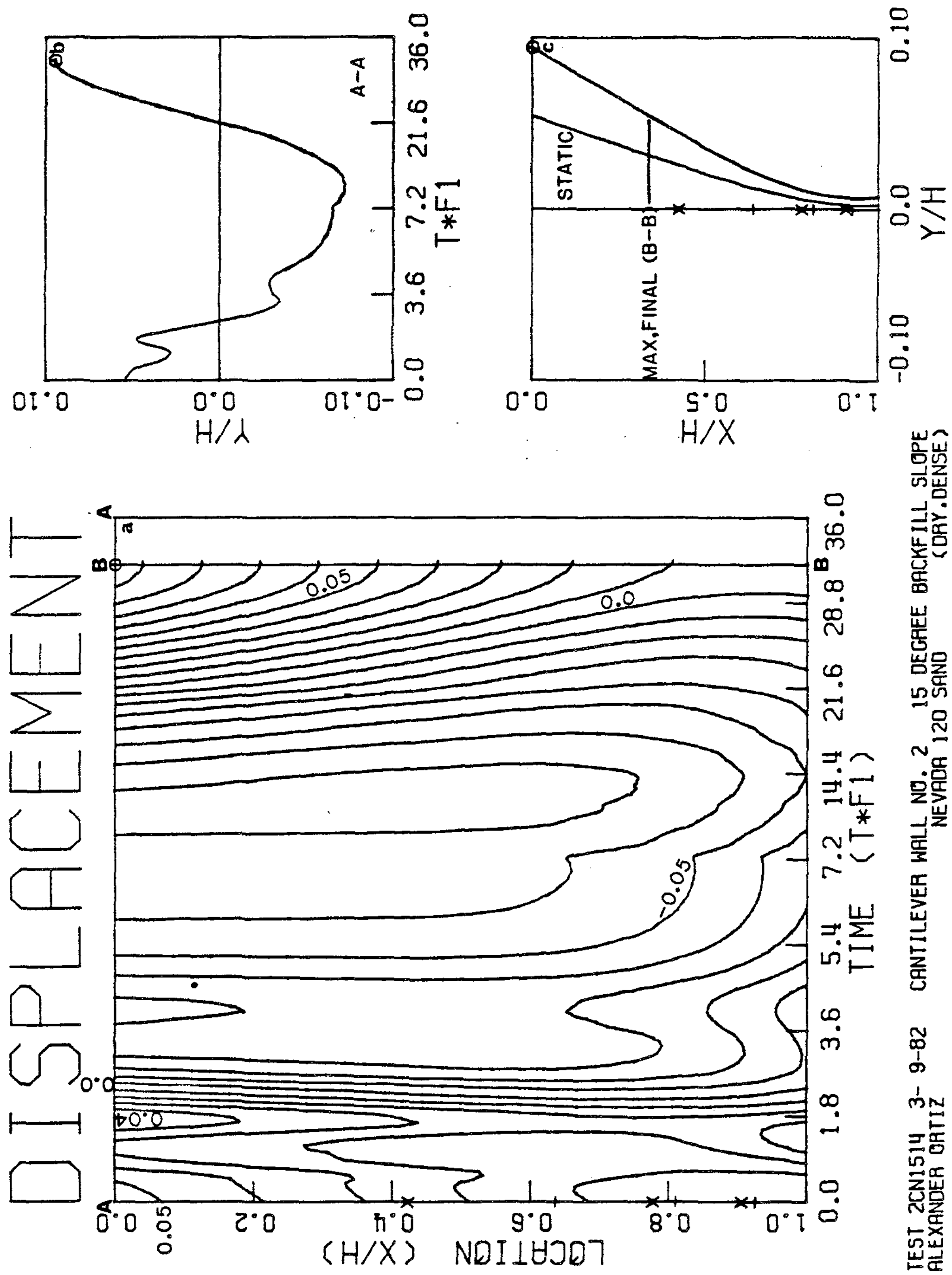
DISPLACEMENT
LOCATION (X/H)
TIME (T*F1)
0.0 1.8 3.6 5.4 7.2 14.4 21.6 28.8 36.0
0.0 0.05 0.2 0.4 0.6 0.8 1.0
0.04
0.0
-0.05
0.05
A
B
a
Y/H
T*F1
0.0 3.6 7.2 21.6 36.0
0.10 0.0 -0.10
A-A
b
X/H
Y/H
-0.10 0.0 0.10
0.0 0.5 1.0
STATIC
MAX,FINAL (B-B)
c
TEST 2CN1514 3- 9-82 CANTILEVER WALL NO. 2 15 DEGREE BACKFILL SLOPE
ALEXANDER ORTIZ NEVADA 120 SAND (DRY.DENSE)

FIGURE 5.107

5.4 <u>Static Results</u>

Although the main emphasis of the research project was the study of the dynamic behavior of retaining walls, some interesting results were obtained from a static point of view as well. An important indication that an accurate model has been used is to examine how it behaves statically and compare the results with the accepted Rankine and Coulomb static lateral earth pressure theories.

The Rankine lateral earth pressure theory gives the resultant active force $P_A/(1/2\gamma H^2)$ acting on the retaining wall as:

$$\frac{P_A}{1/2\gamma H^2} = K_A = \frac{(1 - \sin\phi)}{(1 + \sin\phi)} \tag{5.2}$$

The coefficient K_A is referred to as the active earth pressure coefficient. The assumptions under which this theory is formulated are very approximately fulfilled by the model tests which have a horizontal backfill, namely:

- The wall is rigid and vertical.
- The backfill is horizontal.
- There is no friction between soil and wall.
- There is active pressure (wall displaces more than 1/2% of its height).

The Coulomb lateral earth pressure theory (of which the Rankine is only a special case) follows the same assumptions as the Mononobe-Okabe theory (Section 5.5), with the exception that there are no lateral or vertical acceleration coefficients k_h or k_v (i.e. $\theta = 0^o$). The resultant force acting on the wall is expressed as:

$$\frac{P_A}{1/2\gamma H^2} = K_A = \frac{\cos^2(\phi-\beta)}{\cos^2\beta\,\cos(\delta+\beta)}\left[1+\left(\frac{\sin(\phi+\delta)\,\sin(\phi-i)}{\cos(\delta+\beta)\,\cos(i-\beta)}\right)^{1/2}\right]^{-2} \qquad (5.3)$$

For the previously mentioned assumptions, with the exception that the backfill can be sloping, equation (5.3) can be reduced to:

$$\frac{P_A}{1/2\gamma H^2} = K_A = \cos^2\phi\left[1+\left(\frac{\sin\phi\,\sin(\phi-i)}{\cos i}\right)^{1/2}\right]^{-2} \qquad (5.4)$$

This equation will be used as a comparison basis for the tests with sloping backfills.

In the Rankine and Coulomb theories, under the assumptions listed, the resultant acts at one third of the height above the wall base since the pressure distribution is assumed triangular. Therefore, the overturning moment $6M/\gamma H^3$ from the Rankine/Coulomb theory is:

$$\frac{6M_A}{\gamma H^3} = K_A \qquad (5.5)$$

The maximum bending moment is:

$$\frac{M_A H}{EI} = \frac{\gamma H^4}{6EI} K_A \qquad (5.6)$$

Table 5.5 gives a comparison of the maximum measured static parameters from the tests with the Rankine/Coulomb theories, recalling that the friction angle of the soil used is 35^o.

The lateral earth pressure theories (both static and dynamic) unfortunately only estimate the resultant force and its point of application based on the assumption of a triangular pressure distribution.

TABLE 5.5

Maximum Static Values

		Test 1CN0001	Test 1CN0002	Test 1CN1003	Test 1CN0004	Test 1CN1505	Test 1CN0006	Test 1CN0007	Test 1CN0508	Test 1CN1009	Test 1CN1510	Test 2CN0011	Test 2CN0012	Test 2CN1013	Test 2CN1514
$\frac{MH}{EI}$	Test	0.241	0.272	0.298	0.246	0.274	0.274	0.168	0.210	0.228	0.291	0.506	0.448	0.498	0.532
	R/C	0.209	0.205	0.229	0.211	0.245	0.213	0.221	0.227	0.242	0.252	0.445	0.432	0.485	0.518
$\frac{6M}{\gamma H^3}$	Test	0.313	0.359	0.390	0.315	0.357	0.349	0.206	0.263	0.283	0.367	0.308	0.281	0.308	0.328
	R/C	0.271	0.271	0.300	0.271	0.319	0.271	0.271	0.284	0.300	0.319	0.271	0.271	0.300	0.319
$\frac{P}{\gamma H}$	Test	-	0.499	0.442	0.532	0.539	0.419	0.383	0.550	0.430	0.529	0.281	0.315	0.482	0.421
	R/C	0.271	0.271	0.300	0.271	0.319	0.271	0.271	0.284	0.300	0.319	0.271	0.271	0.300	0.319
$\frac{Q}{1/2\ \gamma\ H^2}$	Test	0.267	0.297	0.285	0.275	0.255	0.127	0.200	0.304	0.261	0.334	0.215	0.252	0.237	0.255
	R/C	0.271	0.271	0.300	0.271	0.319	0.271	0.271	0.284	0.300	0.319	0.271	0.271	0.300	0.319
y/H	Test	0.0279	0.0319	0.0376	0.0317	0.0344	0.0298	0.0276	0.0294	0.0310	0.0327	0.0439	0.0464	0.0497	0.0547

R/C = Rankine/Coulomb

Maximum $\left\{\begin{array}{c}\text{Moment}\\ \text{Shear-Force}\\ \text{Pressure}\end{array}\right\}$ always at base of wall.

Maximum displacement always at top of wall.

Therefore, the most accurate comparison that can be made is that of the resultant forces.

Comparing the Rankine/Coulomb resultant forces with the maximum shear forces (which are an integration of the pressure distribution behind the wall) it can be concluded that there is reasonable agreement between theory and experiment in this respect, the maximum difference being of the order of 25% between the two. The sole exceptions are tests 1CN1505 and especially 1CN0006 where the pressure distributions show a small magnitude in the upper 60% or so of the height and then increase rapidly below that (Figures 5.69c and 5.73c). This then contains a smaller area under the curve, although the maximum pressures (at the bottom of the wall) are comparable to those of similar tests.

From frames c of the pressure distribution figures, it can be observed that the static pressure distributions are not linear, as the Rankine/Coulomb theories assume, although for the most part, the centroid of the distribution (location of the resultant force) is at around 1/3 of the wall height above the base as a triangular distribution would indicate. It should be noted that, for RW2, the more flexible wall, this centroid does generally creep up to about 40% of the wall height above the base. The maximum pressures (at the bottom of the wall) are much greater in all cases, except 2CN0011 (Figure 5.93c), than those predicted by the Rankine/Coulomb assumption. The maximum static pressures recorded are on an average on the order of 60% higher than those than the Rankine/Coulomb theories would give. From these figures it can, however, be seen that the traditional theories do seem to predict a correct average pressure distribution.

Since the traditional lateral earth pressure theories are based on the assumption that the wall holding back the soil is rigid, one can only make a qualitative overturning/ bending moment comparison with the test results which are those of two flexible walls. The Rankine/Coulomb overturning moment is assumed to be the resultant force times the moment arm which is 1/3 of the height above the base. The bending (reaction) moments recorded in the tests are generally greater than the overturning (action) moments given by Rankine/Coulomb. The actual test moments generally vary from just a few percent to about 35% greater than those predicted. Since stems of cantilever walls are designed as bending beams, the actual factor of safety could thus actually be much less than the usual 1.7. For a 35% underestimation, the actual safety factor (static) would then only be 1.25.

Looking at the parameters that do not involve the wall stiffness EI, namely, $6M/\gamma H^3$, $P/\gamma H$, and $Q/(1/2\gamma H^2)$, it can be seen that there is correspondingly virtually no difference in the values for the two walls. This indicates that, for the range of wall stiffnesses tested, the system stiffness has little or no effect on the static response. The stiffness of RW1 is about twice that of RW2, but its moments MH/EI are about half. Thus the dimensional moments would be correspondingly similar also demonstrating the independence of wall flexibility on the response.

As far as is known, nobody has ever measured actual moments, static or otherwise, in a cantilever retaining wall, or has ever considered it to be a flexible bending beam, which it obviously is. Thus the moments shown in frames c of the moment distribution figures provide a first insight into actual moments in cantilever walls due to lateral earth pressures.

The measurement of lateral displacements seems also to be unprecedented. The static displacements for all the tests indicate that the wall has initially displaced laterally at least 1/2% of its height and thus a state of plastic equilibrium in the traditional sense can be assumed to exist behind the wall, and thus comparisons with the traditional theories (which use this assumption) can be considered valid. The maximum static displacements are of the order of 3% to 4% in RW1 and 4% to 6% in the less stiff RW2, and, as expected, always occur at the top of the wall. On some of the displacement curves (frames c), one may note a small outward "curl" near the bottom of the wall. This is probably due to slight faults in the measurements of the boundary conditions and should be considered numerical and not physical. This also applies to the maximum dynamic and final static curves.

5.5. Dynamic Results

One can compare the maximum dynamic parameters obtained from the tests with those which would be estimated from the Mononobe-Okabe Theory (discussed in detail in Section 1.1) for similar circumstances. The envelopes (upper bounds) of the various parameters with respect to the

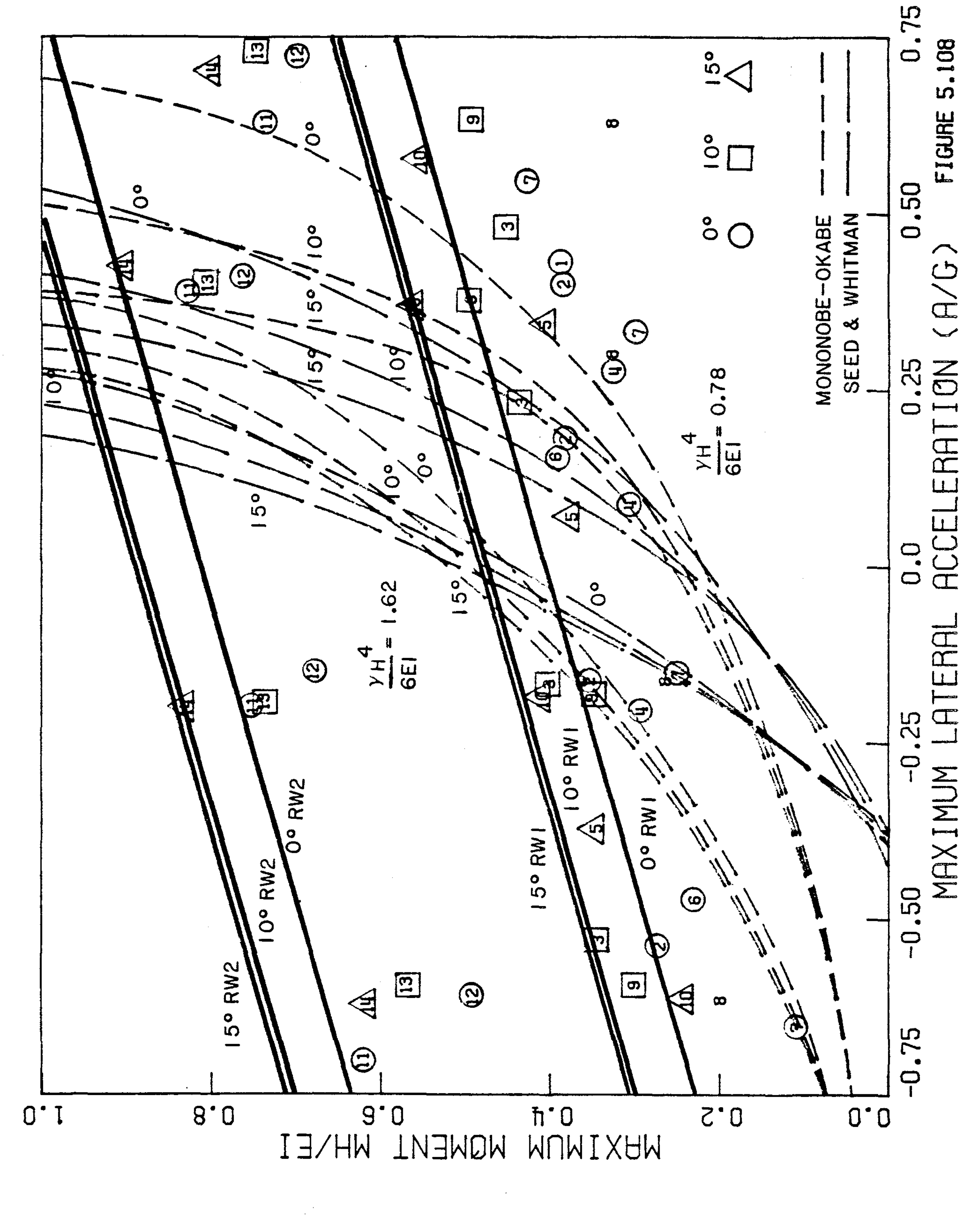
MAXIMUM LATERAL ACCELERATION (A/G)
MAXIMUM MOMENT MH/EI
-0.75
-0.50
-0.25
0.0
0.25
0.50
0.75
0.0
0.2
0.4
0.6
0.8
1.0
MONONOBE-OKABE
SEED & WHITMAN
0°
10°
15°
15° RW2
10° RW2
0° RW2
15° RW1
10° RW1
0° RW1
$\frac{\gamma H^4}{6EI} = 1.62$
$\frac{\gamma H^4}{6EI} = 0.78$

FIGURE 5.108

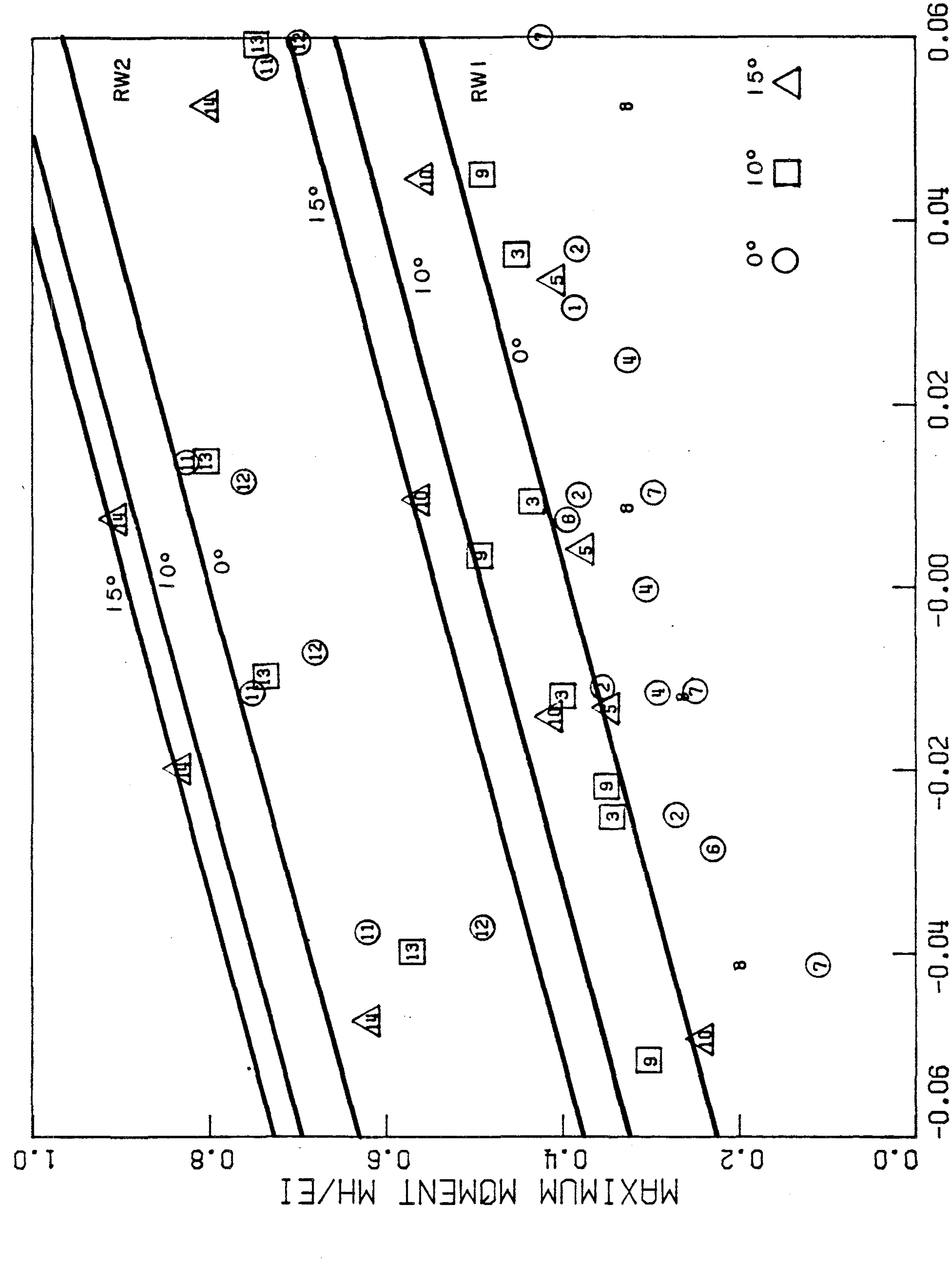
RW2
RW1
15°
10°
0°
0° ○ 10° □ 15° △
MAXIMUM LATERAL VELOCITY V/(F1*H)
MAXIMUM MOMENT MH/EI
-0.06
-0.04
-0.02
-0.00
0.02
0.04
0.06
0.0
0.2
0.4
0.6
0.8
1.0

FIGURE 5.109

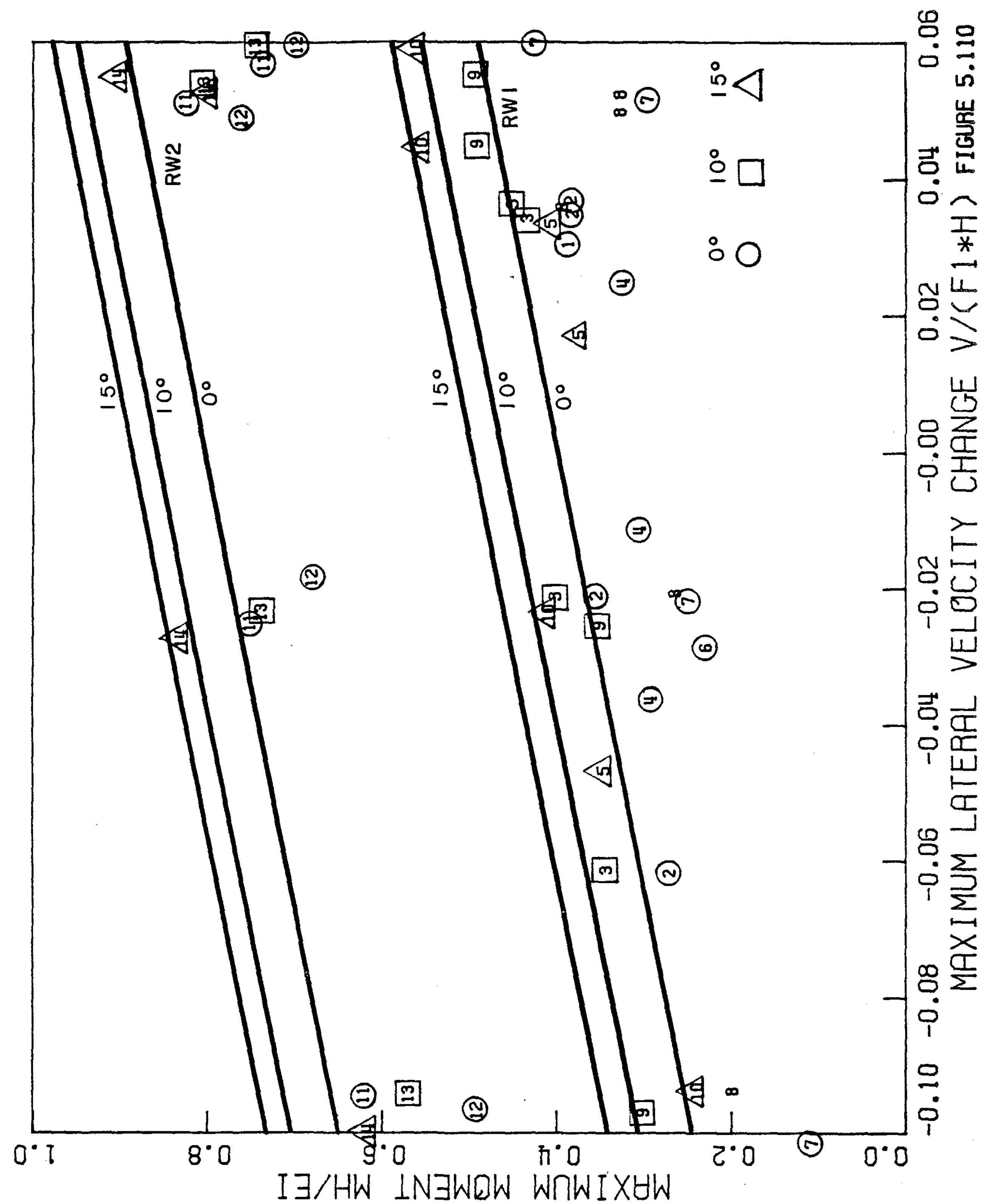
MAXIMUM LATERAL VELOCITY CHANGE V/(F1*H)
MAXIMUM MOMENT MH/EI
-0.10
-0.08
-0.06
-0.04
-0.02
-0.00
0.02
0.04
0.06
0.0
0.2
0.4
0.6
0.8
1.0
RW1
RW2
15°
10°
0°

FIGURE 5.110

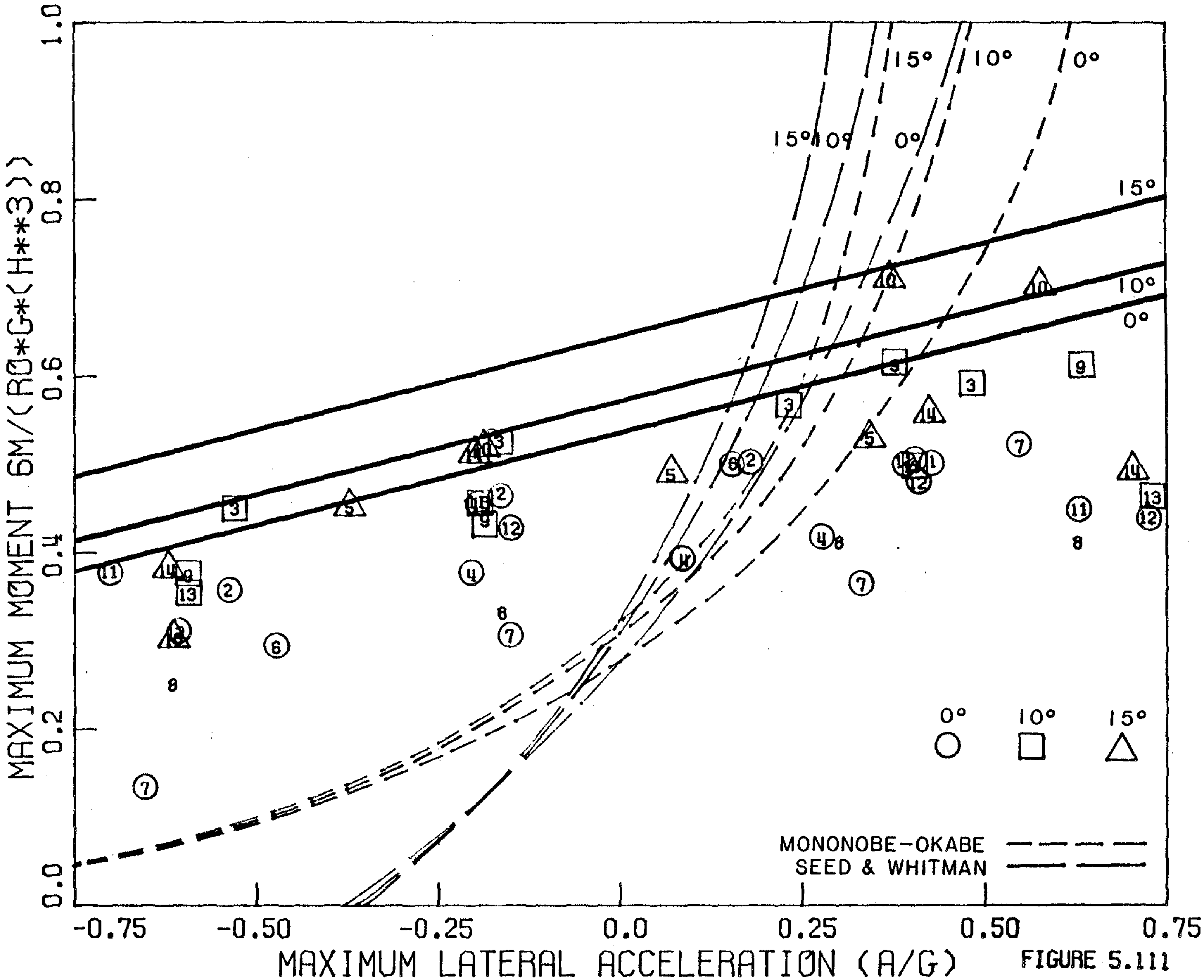
MAXIMUM MOMENT 6M/(RO*G*(H**3))
0.0
0.2
0.4
0.6
0.8
1.0
MAXIMUM LATERAL ACCELERATION (A/G)
-0.75
-0.50
-0.25
0.0
0.25
0.50
0.75
0°
10°
15°
MONONOBE-OKABE
SEED & WHITMAN

FIGURE 5.111

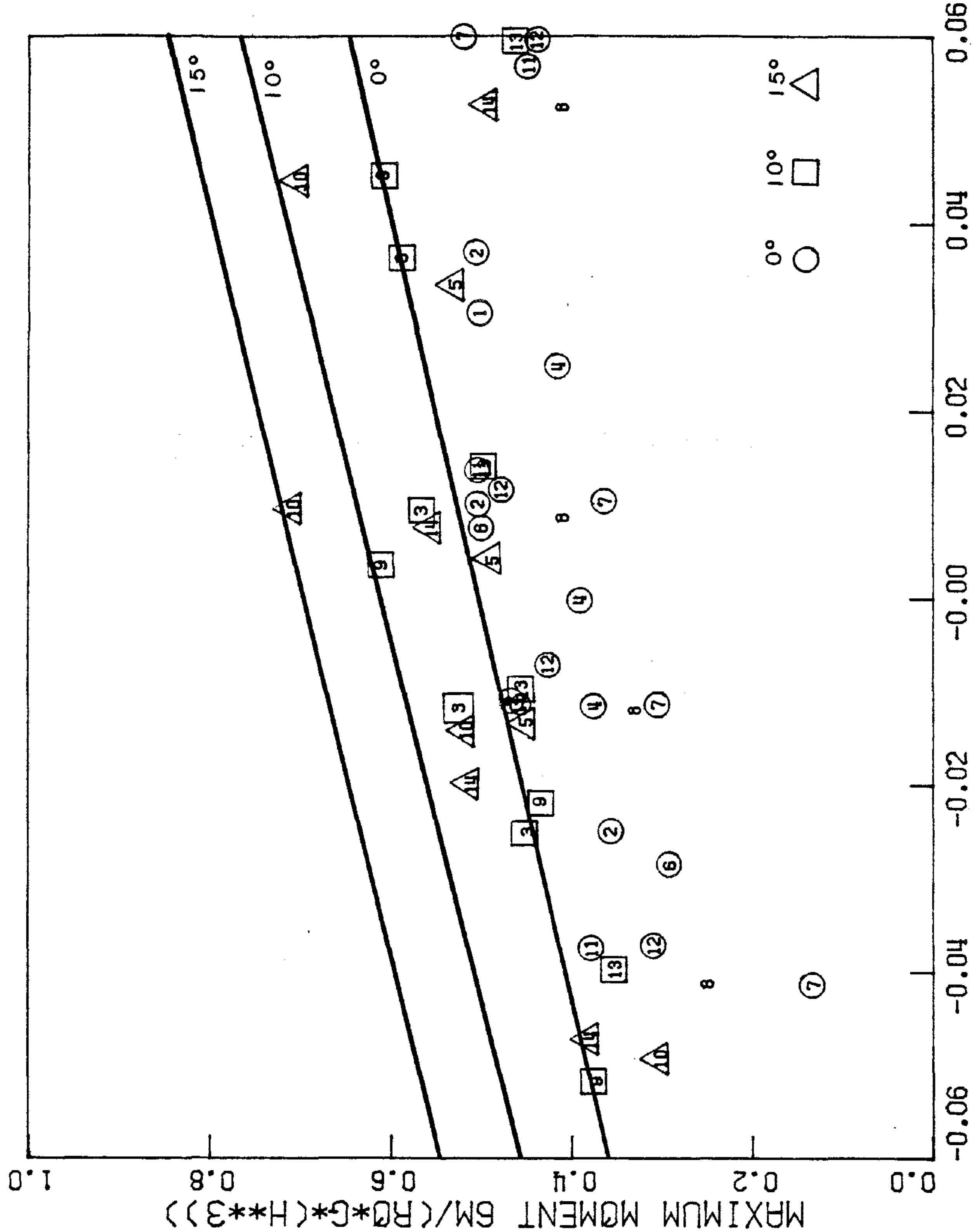
MAXIMUM MOMENT 6M/(RO*G*(H**3))
MAXIMUM LATERAL VELOCITY V/(F1*H)
0.0
0.2
0.4
0.6
0.8
1.0
-0.06
-0.04
-0.02
-0.00
0.02
0.04
0.06
15°
10°
0°

FIGURE 5.112

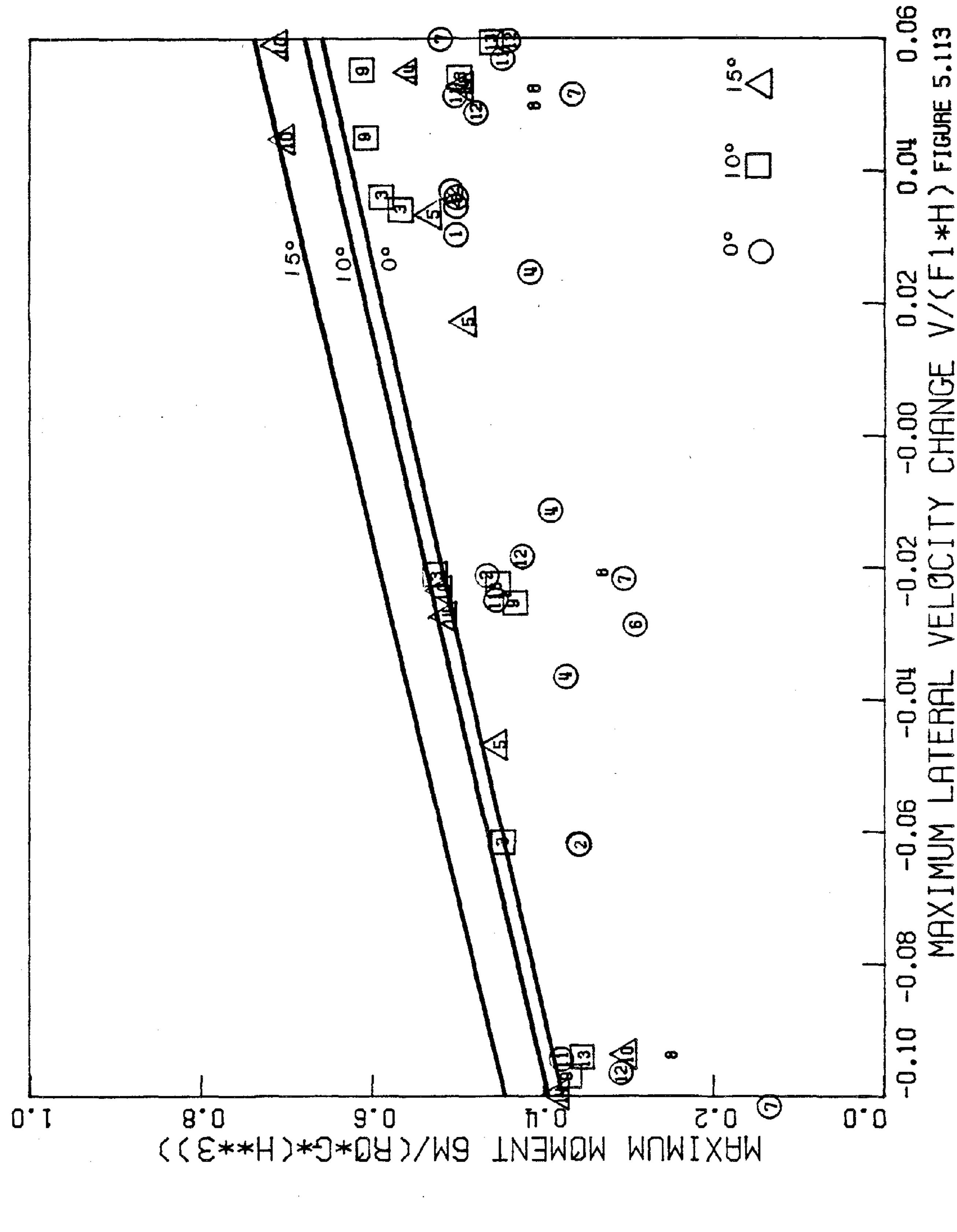
MAXIMUM MOMENT 6M/(RO*G*(H**3))
0.0
0.2
0.4
0.6
0.8
1.0
MAXIMUM LATERAL VELOCITY CHANGE V/(F1*H)
-0.10
-0.08
-0.06
-0.04
-0.02
-0.00
0.02
0.04
0.06
15°
10°
0°

FIGURE 5.113

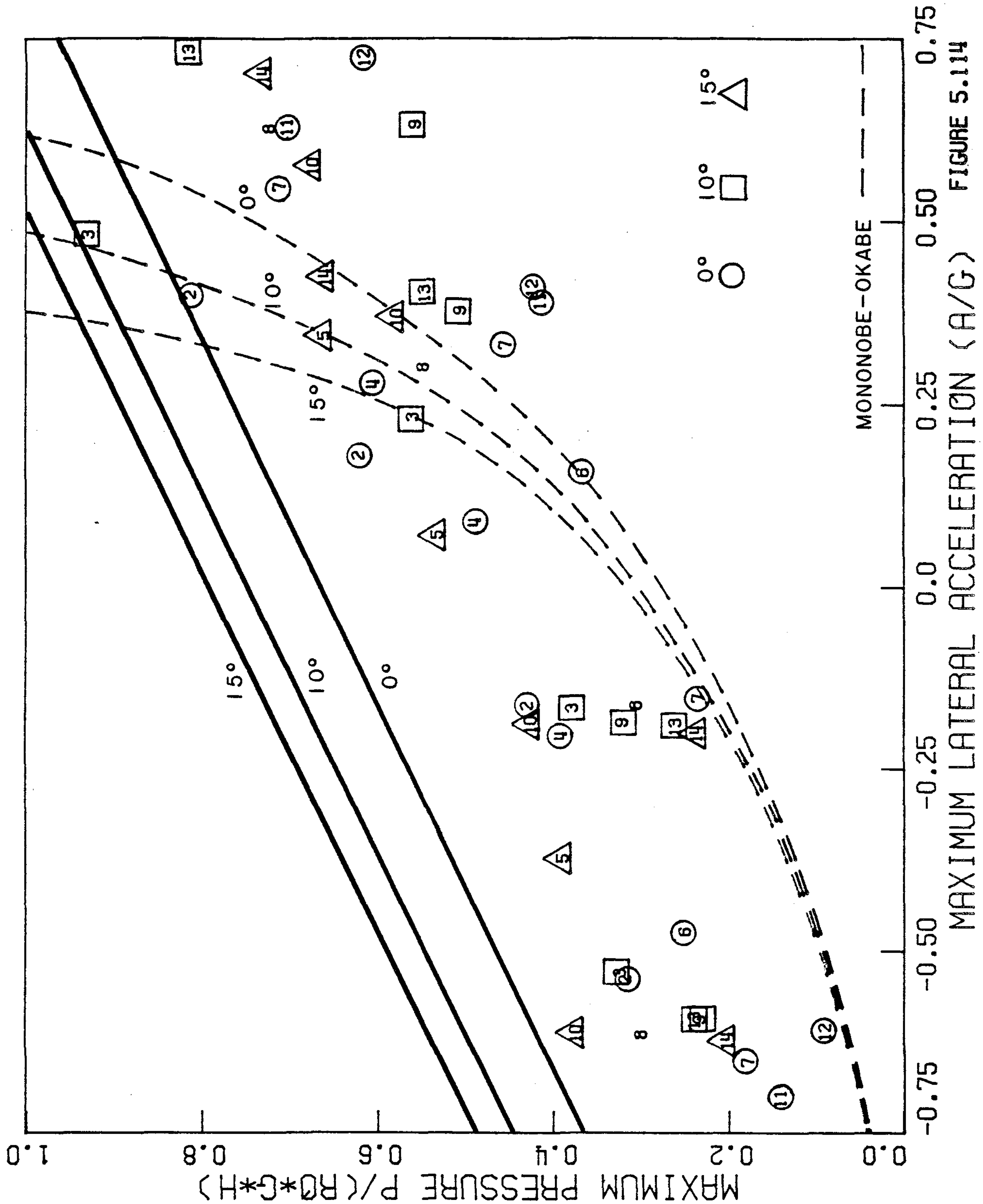
MAXIMUM PRESSURE P/(RO*G*H)
0.0
0.2
0.4
0.6
0.8
1.0
MAXIMUM LATERAL ACCELERATION (A/G)
-0.75
-0.50
-0.25
0.0
0.25
0.50
0.75
MONONOBE-OKABE
0°
10°
15°

FIGURE 5.114

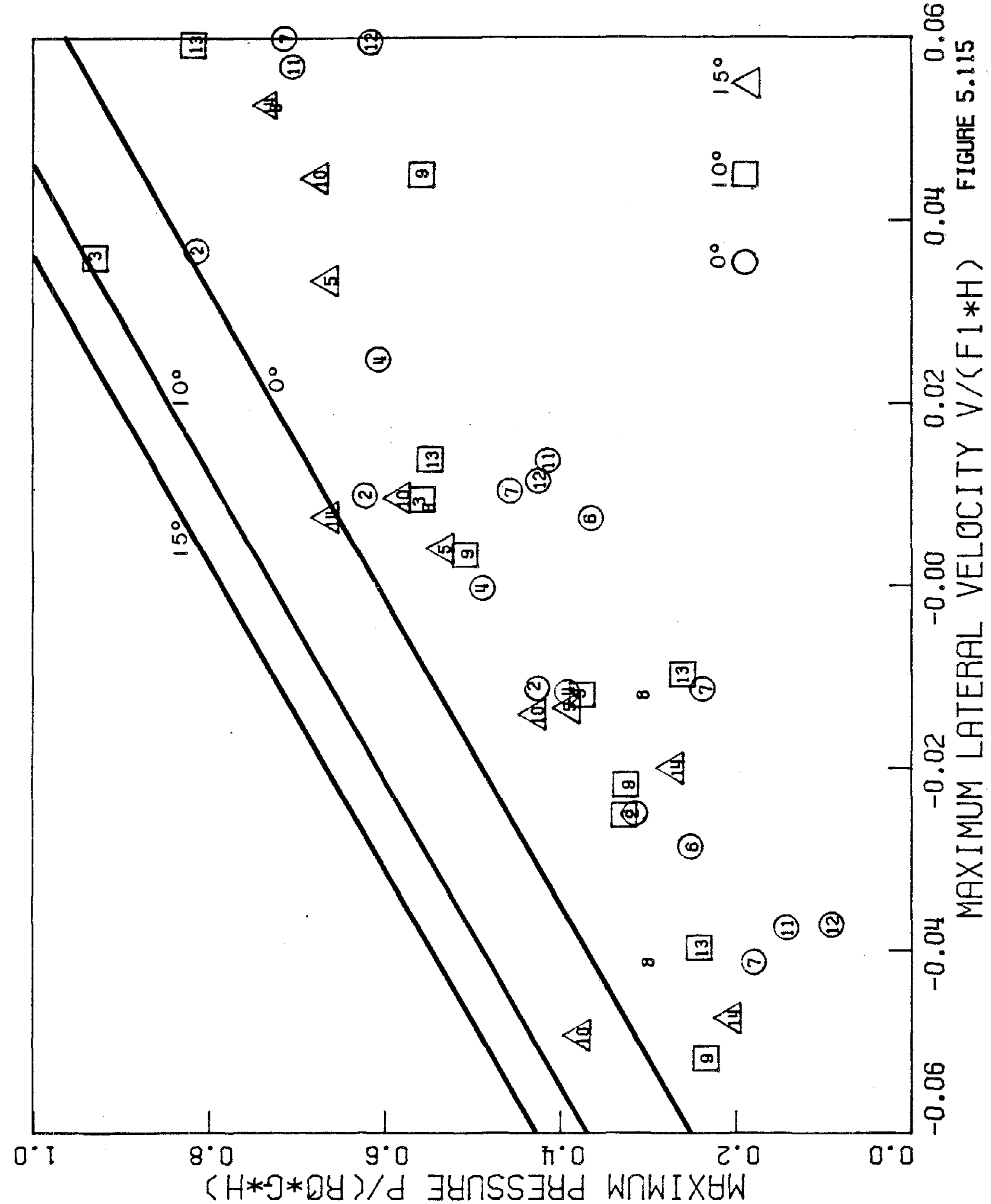
MAXIMUM PRESSURE P/(RO*G*H)
MAXIMUM LATERAL VELOCITY V/(F1*H)
0°
10°
15°

FIGURE 5.115

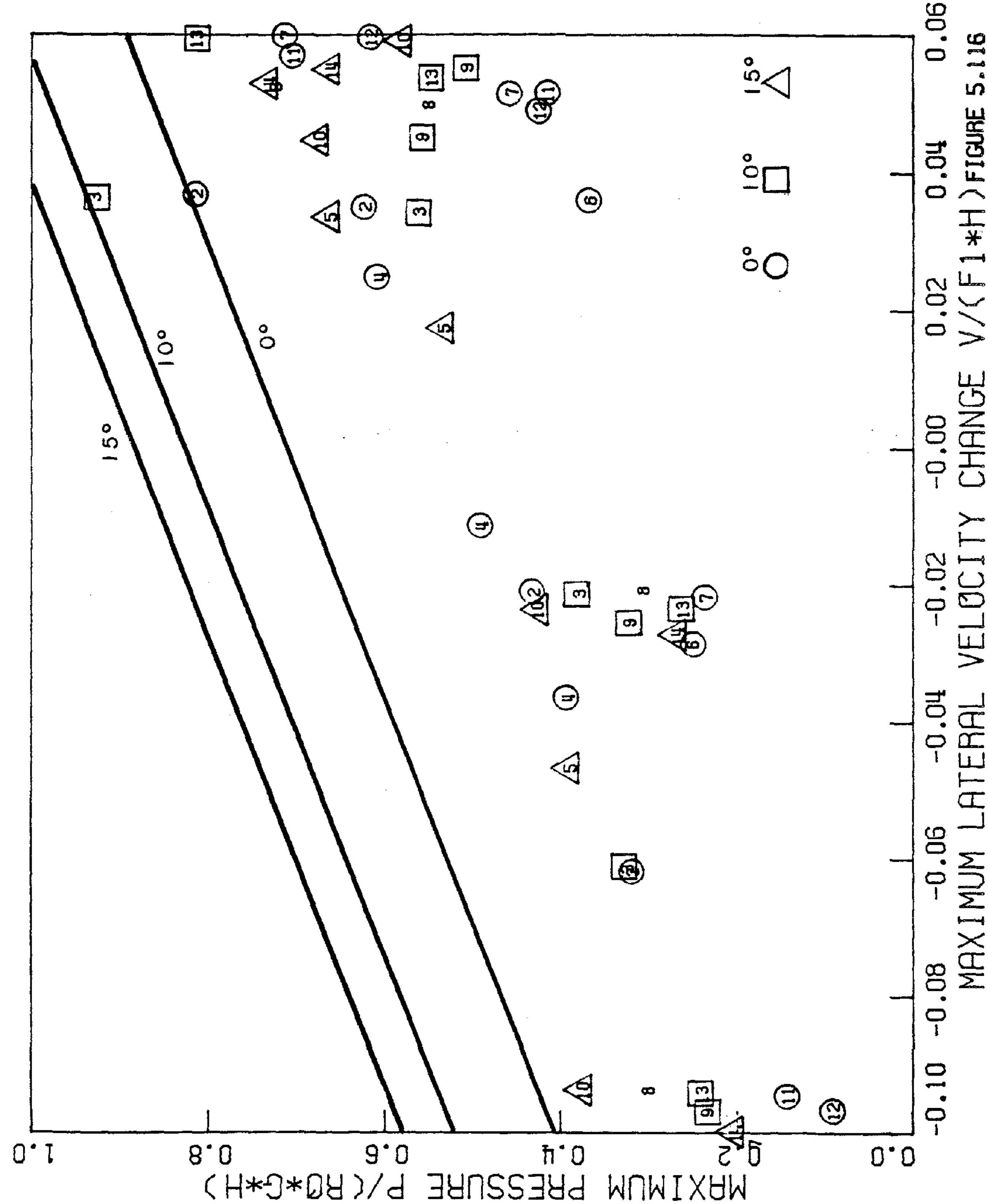
MAXIMUM PRESSURE P/(RO*G*H)
MAXIMUM LATERAL VELOCITY CHANGE V/(F1*H)
0.0
0.2
0.4
0.6
0.8
1.0
-0.10
-0.08
-0.06
-0.04
-0.02
-0.00
0.02
0.04
0.06
0°
10°
15°

FIGURE 5.116

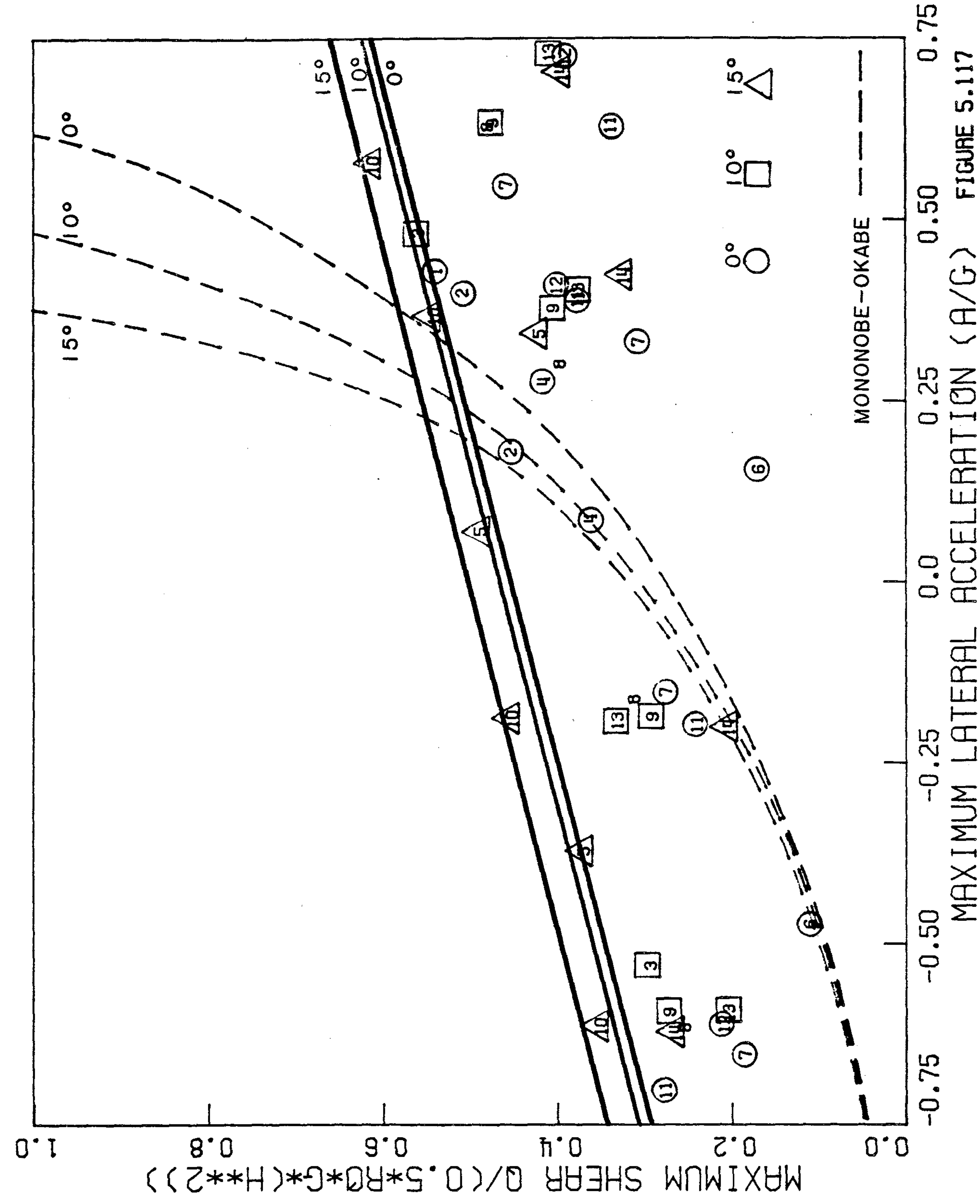
MAXIMUM SHEAR Q/(0.5*RQ*G*(H**2))
MAXIMUM LATERAL ACCELERATION (A/G)
0.0
0.2
0.4
0.6
0.8
1.0
-0.75
-0.50
-0.25
0.0
0.25
0.50
0.75
15°
10°
0°
MONONOBE-OKABE

FIGURE 5.117

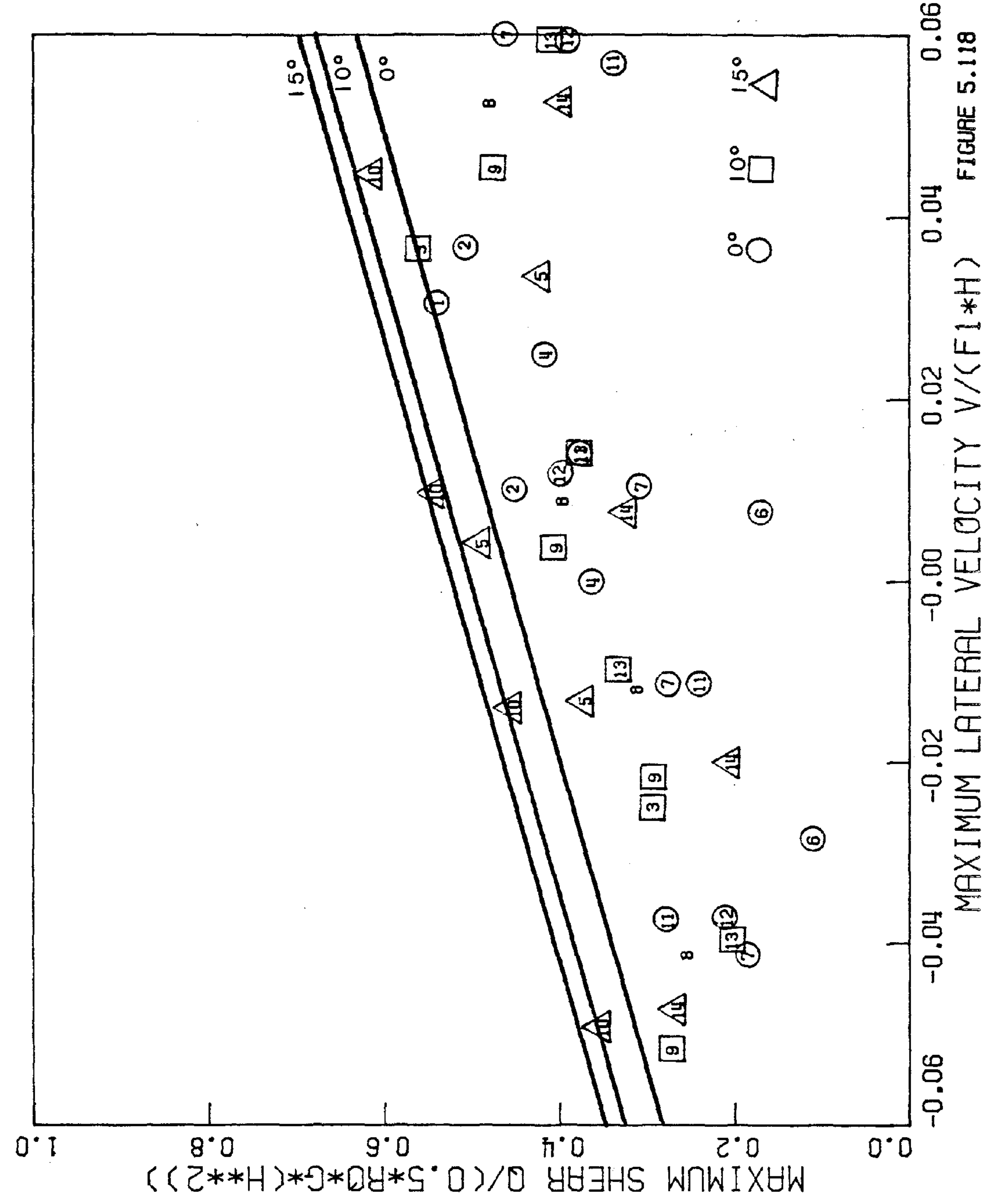
MAXIMUM SHEAR Q/(0.5*RO*G*(H**2))
MAXIMUM LATERAL VELOCITY V/(F1*H)
0.0
0.2
0.4
0.6
0.8
1.0
-0.06
-0.04
-0.02
-0.00
0.02
0.04
0.06
15°
10°
0°

FIGURE 5.118

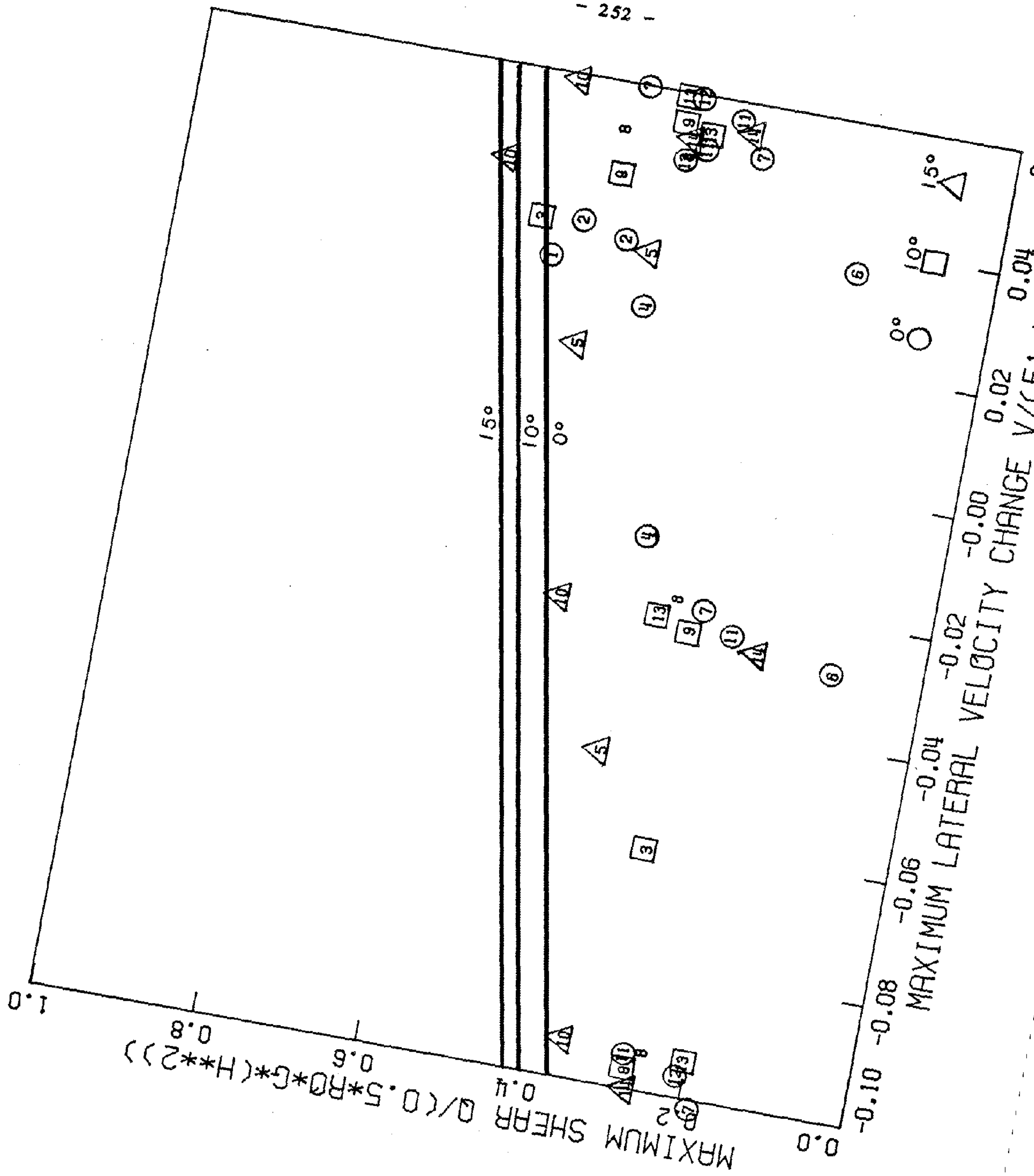
MAXIMUM SHEAR Q/(0.5*RO*G*(H**2))
0.0
0.2
0.4
0.6
0.8
1.0
MAXIMUM LATERAL VELOCITY CHANGE V/(F1*H)
-0.10
-0.08
-0.06
-0.04
-0.02
-0.00
0.02
0.04
0.06
15°
10°
0°

FIGURE 5.119

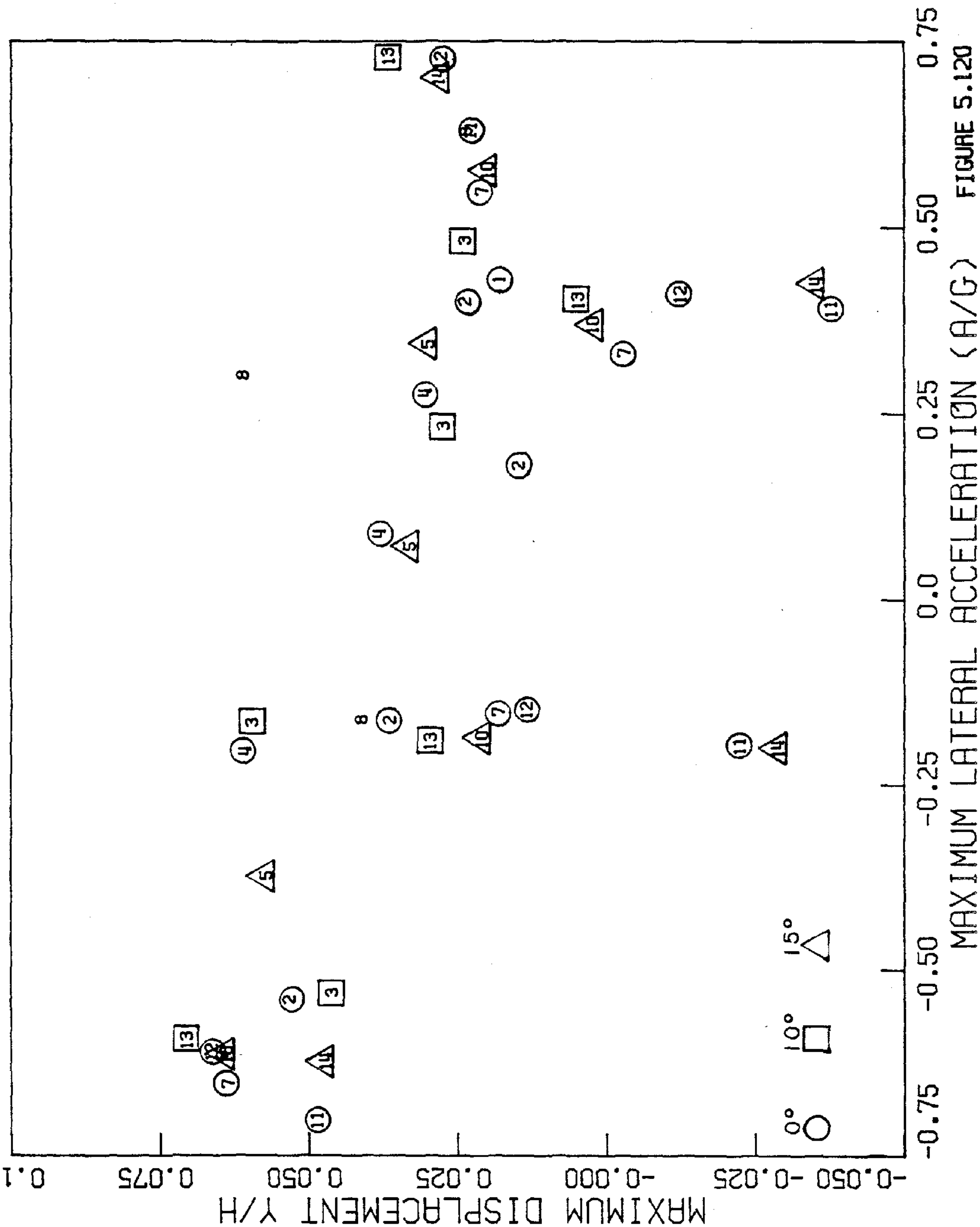
MAXIMUM LATERAL ACCELERATION (A/G)
MAXIMUM DISPLACEMENT Y/H
-0.75
-0.50
-0.25
0.0
0.25
0.50
0.75
-0.050
-0.025
-0.000
0.025
0.050
0.075
0.1
0°
10°
15°

FIGURE 5.120

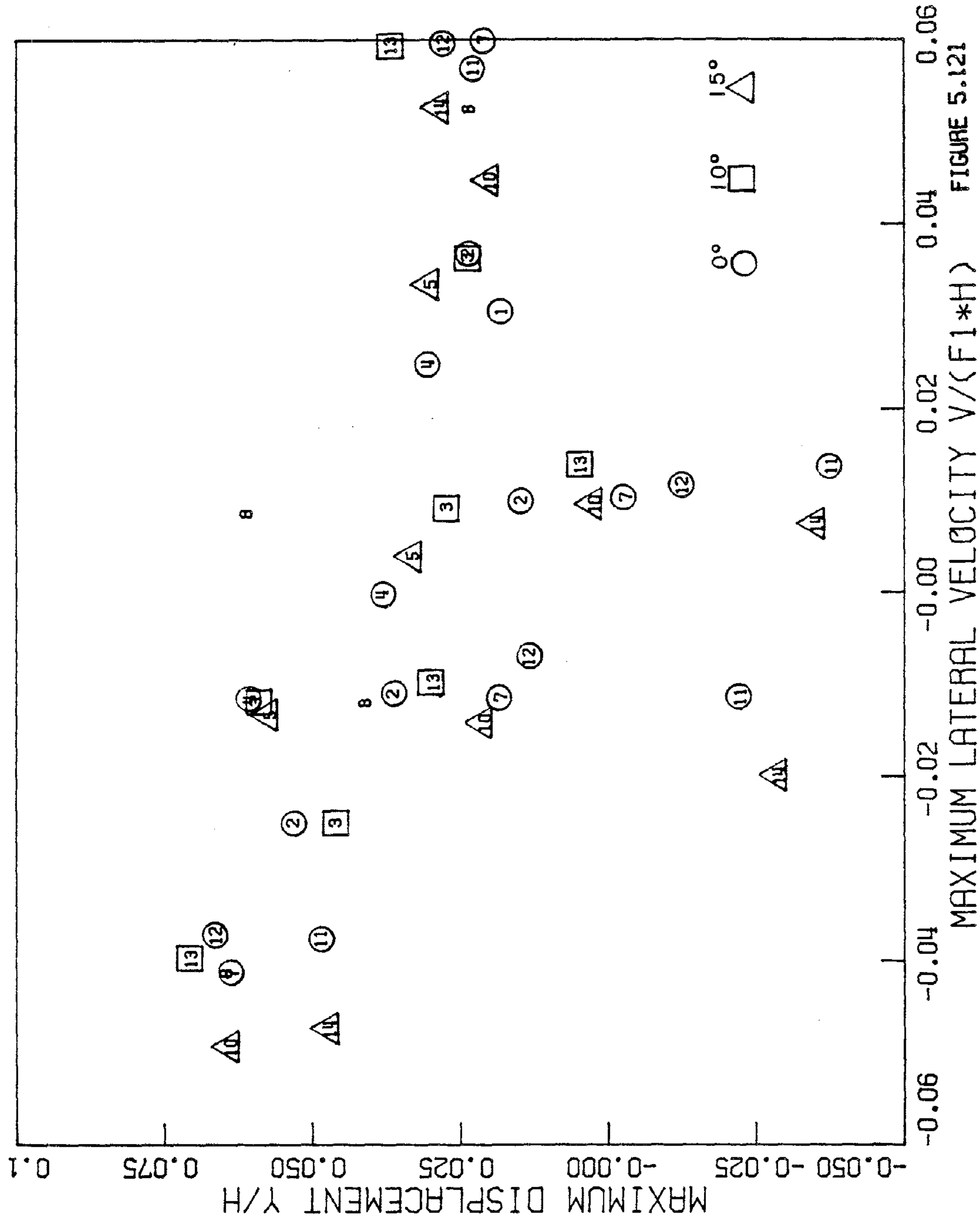
MAXIMUM DISPLACEMENT Y/H
MAXIMUM LATERAL VELOCITY V/(F1*H)
0.1
0.075
0.050
0.025
-0.000
-0.025
-0.050
-0.06
-0.04
-0.02
-0.00
0.02
0.04
0.06
0°
10°
15°

FIGURE 5.121

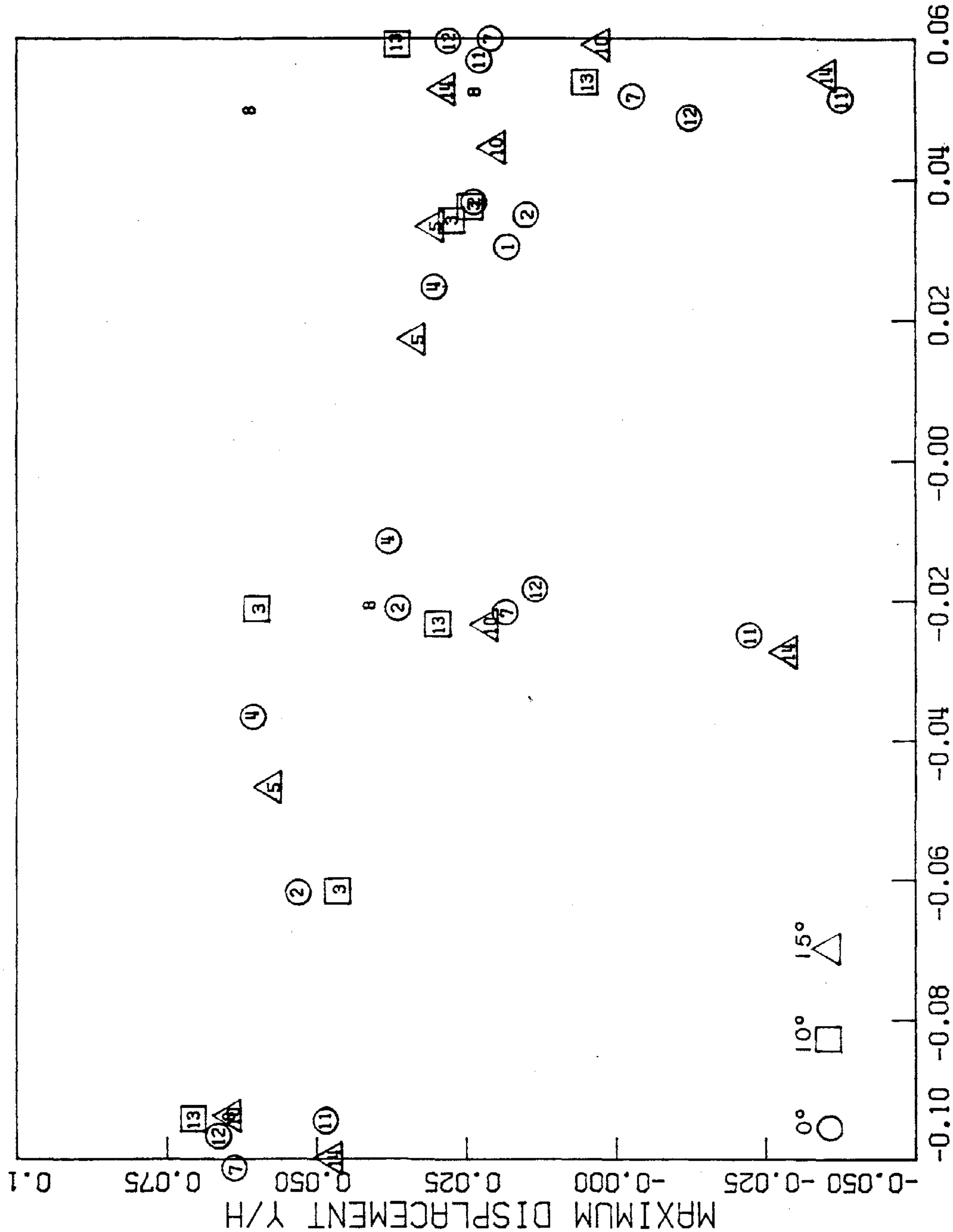
MAXIMUM DISPLACEMENT Y/H
MAXIMUM LATERAL VELOCITY CHANGE V/(F1*H)
0°
10°
15°
-0.10
-0.08
-0.06
-0.04
-0.02
-0.00
0.02
0.04
0.06
0.1
0.075
0.050
0.025
-0.000
-0.025
-0.050

FIGURE 5.122

strong-motion characteristics are illustrated in Figures 5.108 through 5.122. How these envelopes were determined will be explained below. In addition, Mononobe-Okabe distributions with respect to the lateral acceleration coefficients k_h for an average test soil density are shown in Figures 5.108, 5.111, 5.114 and 5.117.

For a flat backfill under the test assumptions (see Section 5.4), the total resultant active force $P_{AE}/(1/2\gamma H^2)$, given by Mononobe-Okabe, reduces from equations (1.1) and (1.2) to:

$$\frac{P_{AE}}{1/2\gamma H^2} = \cos^2 \frac{(\phi-\theta)}{\cos^2 \theta} \left[1 + \left(\frac{\sin \phi \sin (\phi-\theta)}{\cos \theta}\right)^{1/2} \right]^{-2} \tag{5.8}$$

For a sloping backfill of angle i, the resultant force is expressed as:

$$\frac{P_{AE}}{1/2\gamma H^2} = K_{AE} = \frac{\cos^2 (\phi-\theta)}{\cos^2 \theta} \left[1 + \left(\frac{\sin \phi \sin (\phi-\theta-i)}{\cos \theta \cos i}\right)^{1/2} \right]^{-2} \tag{5.9}$$

These equations form the basis for comparison with the maximum dynamic results obtained from the tests.

In the Mononobe-Okabe theory, the resultant force is assumed to act at one third of the height above the base of the wall. Therefore, the overturning moment $6M_{AE}/\gamma H^3$ from the Mononobe-Okabe theory is:

$$\frac{6M_{AE}}{\gamma H^3} = K_{AE} \tag{5.10}$$

The maximum bending moment is:

$$\frac{M_{AE}H}{EI} = \frac{\gamma H^4}{6EI} K_{AE} \tag{5.11}$$

On the basis of previous studies (up to 1970), Seed and Whitman [55] suggest that the dynamic portion of the moment acts at 0.6 of the height above the base of the wall. Therefore the overturning moment is:

$$\frac{6M_{AE}}{\gamma H^3} = K_A + 1.8\Delta K_{AE} = 1.8K_{AE} - 0.8K_A \tag{5.12}$$

where:

$$\Delta K_{AE} = K_{AE} - K_A \tag{5.13}$$

Likewise, the bending moment is:

$$\frac{M_{AE}H}{EI} = \frac{\gamma H^4}{6EI}\left(K_A + 1.8\Delta K_{AE}\right) = \frac{\gamma H^4}{6EI}\left(1.8K_{AE} - 0.8K_A\right) \tag{5.14}$$

This suggestion is also used in the moment comparisons with the experiments, and is shown (for an average test soil density) in Figures 5.108 and 5.111.

The maximum pressure $R_{AE}/\gamma H$ at the base of the wall is:

$$\frac{R_{AE}}{\gamma H} = K_{AE} \tag{5.15}$$

One should keep in mind that the Mononobe-Okabe Theory is based on the assumption that the coefficient of lateral earth pressure k_h is representative of a constant lateral acceleration which provides a constant lateral body-type force to the system. There are no inertia effects. The wall is also assumed to be rigid. In the experiment however, the lateral acceleration was rapidly varying in time, providing for inertia effects, and the retaining walls were flexible.

From equation (5.9) it can be seen that the Mononobe-Okabe equation goes singular when (ϕ - θ-i) is less than zero since the term under the radical goes negative. For $\phi = 35^o$ and a flat backfill ($i = 0^o$) this means that θ has to be less than or equal to 35^o or $k_h \lesssim 0.70$. Likewise, for a 5^o backfill slope $\theta \lesssim 30^o$ or $k_h \lesssim 0.58$, for a 10^o backfill slope $\theta \lesssim 25^o$ or $k_h \lesssim 0.47$ and for a 15^o backfill slope, $\theta \lesssim 20^o$ or $k_h \lesssim 0.36$. From the lateral acceleration values (comparable to k_h) listed in Table 5.6, it can be seen that the upper limits just mentioned are exceeded, or very nearly exceeded, in some of the tests, especially in those where sloping backfills were used. From a Mononobe-Okabe analysis one would then have expected a complete collapse of the walls. In fact, there was never a complete collapse in any of the tests although lateral displacements were in some cases quite high (about 10% of the wall height in tests 1CN0508, 2CN1013, and 2CN1514). Complete collapse would probably have occurred if the lateral acceleration was constant and inertialess as assumed by Mononobe-Okabe. The level of maximum acceleration was only achieved momentarily, however, being followed by changes in acceleration which in time would lead to a restoring force holding the wall back. There might have been a momentary collapse of the system in some cases, which was quickly arrested. It should be noted that in most tests the maximum accelerations recorded (especially at the top of the wall) occur while the wall is being "pushed" back into the backfill (i.e., while the system is being restrained from collapse).

The envelopes of the various parameters with respect to the strong motion characteristics were arrived at in the following manner:

As mentioned in Section 5.2, the ground motion of the centrifuge earthquakes has the shape mainly of a decaying sinusoid with some additional noise added (see the bottom-of-wall accelerograms). In most of the tests there is an initial acceleration spike (positive acceleration) followed by a trough (negative acceleration), then a smaller spike, then a smaller trough, and thereafter low amplitude accelerations. The corresponding velocity diagrams, which, as one would expect, have their extreme values when the acceleration curves cross the zero axis, give the total area under the acceleration curves. The velocity changes from one extreme velocity to the other thus give the area under their respective acceleration spikes. The velocity and velocity changes are important in that they can be used as an indication of the energy content of the acceleration spikes, which is thus an indication of the energy put into the system by the earthquake. Recall that there was little damage from the Parkfield earthquake (Section 5.2), although there were high accelerations, because of the low energy content of the acceleration spikes.

It was observed, from the frames b of the parameter diagrams (Figures 5.53b through 5.107b) that, in almost every experiment, peaks in the maximum moment, pressure and shear distributions at the base of the walls with respect to time were obtained in between the time when the acceleration spikes reached their peaks and the time when they crossed the zero axis (where the corresponding velocities reached their peaks). It was likewise observed that troughs in the maximum moment, pressure and shear distributions were obtained in between the times when accelerations reached troughs (negative maxima) and the times when they recrossed the zero axis (where the corresponding velocities reached their negative maxima). The opposite correlation between acceleration/velocity extremes and the maximum displacements at the top of the walls was also observed.

The peaks and troughs of the parameter distributions were then plotted with respect to their corresponding accelerations, velocities, and velocity changes (which are the areas under individual acceleration spikes) in Figures 5.108 through 5.122. These values are also tabulated in Table 5.6. It should be noted that static values were not included as peaks or troughs in the analysis, as they are probably neither. These values would have been plotted along the axis where acceleration and velocity are zero. However, in dynamic motion, when the acceleration is zero, the velocity might not be, and vice-versa, so the inclusion of static values in the envelope analysis would not have been appropriate to the other dynamic points. Only dynamic values were included.

It should also be noted that the Mononobe-Okabe analysis reduces to the static Rankine/Coulomb analysis for no lateral acceleration which does not seem accurate from a dynamic motion point of view.

TABLE 5.6

Maximum Extreme Dynamic Values (Peaks and Troughs)

	Test 1CN0001	Test 1CN0002				Test 1CN1003				Test 1CN0004			Test 1CN1505		
MH/EI	0.387	0.383	0.271^T	0.382	0.354^T	0.450	0.343^T	0.433	0.401^T	0.323	0.292	0.305^T	0.406	0.346^T	0.314
$6M/\gamma H^3$	0.503	0.505	0.358^T	0.504	0.467^T	0.589	0.489^T	0.566	0.525^T	0.414	0.374^T	0.391	0.529	0.451^T	0.487
$P/\gamma H$	–	0.813	0.318^T	0.622	0.430^T	0.929	0.324^T	0.560	0.378^T	0.605	0.391^T	0.489	0.661	0.389^T	0.532
$Q/(1/2\gamma h^2)$	0.538	0.518	–	0.452	–	0.558	0.293^T	–	–	0.415	–	0.362	0.420	0.370^T	0.488
y/H	0.0181^T	0.0238^T	0.0534	0.0149^T	0.0365	0.0238	0.0462	0.0274	0.0596	0.0305^T	0.0607	0.0383^T	0.0300^T	0.0572	0.0331^T
a/g	0.430	0.401	−0.538	0.181	−0.162	0.483	−0.529	0.234	−0.165	0.279	−0.203	0.090	0.344	−0.371	0.072
v/f_1H	0.0305	0.0369	−0.0249	0.0101	−0.0109	0.0364	−0.0249	0.0094	−0.0117	0.0249	−0.0114	−0.0001	0.0335	−0.0132	0.0041
$\Delta v/f_1H$	0.0305	0.0369	−0.0618	0.0350	−0.0210	0.0364	−0.0613	0.0343	−0.0211	0.0249	−0.0363	0.0113	0.0335	−0.0467	0.0173

	Test 1CN0006		Test 1CN0007				Test 1CN0508				Test 1CN1009				Test 1CN1510
MH/EI	0.229^T	0.393	0.423	0.108^T	0.296	0.249^T	0.327	0.199^T	0.327	0.264^T	0.491	0.301^T	0.493	0.351^T	0.554
$6M/\gamma H^3$	0.292^T	0.500	0.519	0.133^T	0.363	0.305^T	0.410	0.250^T	0.410	0.331^T	0.609	0.373^T	0.611	0.436^T	0.700
$P/\gamma H$	0.250^T	0.366	0.712	0.179^T	0.455	0.235^T	0.723	0.300^T	0.549	0.306^T	0.557	0.233^T	0.506	0.322^T	0.673
$Q/(1/2\gamma H^2)$	0.110^T	0.169	0.458	0.185^T	0.307	0.276^T	0.479	0.254^T	0.397	0.312^T	0.473	0.272^T	0.404	0.291^T	0.611
y/H	–	–	0.0210^T	0.0638	-0.0029^T	0.0182^T	0.0236^T	0.0647	0.0612^T	0.0412^T	–	–	–	–	0.0200^T
a/g	−0.472	0.157	0.549	−0.652	0.332	−0.151	0.629	−0.614	0.302	−0.161	0.634	−0.593	0.379	−0.185	0.575
v/f_1H	−0.0285	0.0075	0.0601	−0.0413	0.0104	−0.0113	0.0525	−0.0412	0.0087	−0.0119	0.0452	−0.0517	0.0036	−0.0217	0.0445
$\Delta v/f_1H$	−0.0285	0.0360	0.0601	−0.1014	0.0517	−0.0217	0.0525	−0.0937	0.0499	−0.0206	0.0452	−0.0969	0.0553	−0.0253	0.0445

	Test 1CN1510(Cont.)			Test 2CN0011				Test 2CN0012				Test 2CN1013			
MH/EI	0.239^T	0.560	0.409^T	0.736	0.622^T	0.826	0.752^T	0.698	0.492^T	0.762	0.680^T	0.746	0.570^T	0.804	0.738^T
$6M/\gamma H^3$	0.302^T	0.707	0.517^T	0.448	0.379^T	0.503	0.458^T	0.438	0.309^T	0.478	0.427^T	0.461	0.352^T	0.497	0.456^T
$P/\gamma H$	0.374^T	0.578	0.426^T	0.703	0.142^T	0.414	–	0.615	0.090^T	0.423	–	0.814	0.239^T	0.456	0.261^T
$Q/(1/2\gamma H^2)$	0.351^T	0.541	0.452^T	0.338	0.277^T	0.377	0.240^T	0.390	0.209^T	0.400	–	0.408	0.203^T	0.375	0.331^T
y/H	0.0640	0.0024^T	0.0210	0.0229^T	0.0488	−0.0376	−0.0222	0.0279^T	0.0666	-0.0124^T	0.0135	0.0368^T	0.0706	0.0048^T	0.0296
a/g	−0.615	0.367	−0.190	0.629	−0.703	0.390	−0.198	0.723	−0.612	0.408	−0.151	0.729	−0.596	0.400	−0.193
v/f_1H	−0.494	0.0095	−0.0142	0.0569	−0.0376	0.0137	−0.0114	0.0595	−0.0373	0.0115	−0.0071	−0.0593	−0.0398	0.0138	−0.0098
$\Delta v/f_1H$	−0.0939	0.0589	−0.0237	0.0569	−0.0945	0.0513	−0.0251	0.0595	−0.0968	0.0488	−0.0186	0.0593	−0.0944	0.0536	−0.0236

	Test 2CN1514			
MH/EI	0.798	0.616^T	0.902	0.830
$6M/\gamma H^3$	0.491	0.379^T	0.555	0.511^T
$P/\gamma H$	0.730	0.202^T	0.659	0.267^T
$Q/(1/2\gamma H^2)$	0.394	0.265^T	0.323	0.203^T
y/H	0.0282^T	0.0472	-0.0351^T	−0.0288
a/g	0.701	−0.624	0.422	−0.202
v/f_1H	0.0526	−0.0474	0.0074	−0.0200
$\Delta v/f_1H$	0.0526	−0.1000	0.0548	−0.0274

^{T} = Trough (local minimum) Peak value otherwise.

$$\text{Maximum} \left\{ \begin{array}{c} \text{Moment} \\ \text{Shear–Force} \\ \text{Pressure} \end{array} \right\} \text{always at bottom of wall.}$$

Maximum displacement always at top of wall.

The extreme points seem to follow, with the exception of the displacement, a general trend; that is, the higher the lateral acceleration, velocity or change in velocity, the higher the extreme. It was decided to fit least-squares straight lines through each of the sets of points one for each backfill slope; 0^o, 10^o, 15^o. The maximum slope from each of the three sets of data was taken as the slope for the envelopes. The envelopes were drawn with these slopes as tangents to the individual sets of points. From the linear correlation coefficients of the least-squares fits, it was determined that the best fits were the maximum moment vs. change in velocity (Figures 5.110 and 5.113), the maximum pressure vs. velocity (Figure 5.115) and, the maximum shear vs. acceleration (Figure 5.117). No conclusions could be drawn from the displacement curves (Figures 5.120 through 5.122).

The best fits would indicate that moment and pressure are more momentum- or energy-governed parameters since they are better related to velocity effects. Similarly, the shear force is more a force-governed parameter (which is logical) since it is better related to acceleration.

The envelopes presented thus provide an upper bound for the various parameters with respect to actual dynamic strong motion characteristics for at least a range of system stiffnesses ($\gamma H^4/6EI$) between about 0.75 and 1.75 which the experiments encompassed (for $\phi \simeq 35^o$).

As in the static case, the various parameters are indicated to be independent of the stiffness of the walls at least for the range of stiffnesses tested. It would be difficult to say if this would hold for rigid walls, or very flexible walls, since the actual walls tested appeared quite flexible as indicated by the deflection shapes.

The only logical comparisons that can be made are those between the envelopes obtained and the corresponding Mononobe-Okabe predictions (which have been simplified for an average of the soil densities encountered). These can be seen in Figures 5.108 and 5.111 for moments, 5.114 for pressures, and 5.117 for shears. In addition, Figures 5.108 and 5.111 show the values for moments suggested by Seed and Whitman which were previously discussed. No comparisons with previous investigators can be made in terms of the envelopes involving the velocity parameters since this does not seem to have been examined before. Having the envelopes with respect to accelerations, velocity and change in velocity should, however, help in better understanding the problem at hand.

Since the Mononobe-Okabe curves and Seed and Whitman curves (in the moment diagrams) generally intersect at one point and at relatively steep angles to each other, it appears that the traditional methods underestimate the actual values of maximum moments below the point of intersection and overestimate them above. It appears that going even a small distance above or below the intersection points leads to large differences between the actual experimental maximum values and those predicted by the theory. For example, from Figure 5.111, for a flat backfill and a lateral acceleration of 0.25g the Mononobe-Okabe method gives a maximum moment around 60% as large as that determined from the envelope. Seed and Whitman indicate one about 80% as large. For 0.50g, however, Mononobe-Okabe predicts a maximum moment about as large as the envelope while Seed and Whitman shows one 1.5 times larger. Similar comparisons can readily be made for the other parameters as well by examining the respective diagrams. The designer would observe, therefore, that the envelopes obtained from the experiments generally give what appear to be conservative values for lateral accelerations less than about 0.50g (which is probably the practical extreme for the use of the Mononobe-Okabe theory in any case). It should also be noted that the envelopes do not seem to be as sensitive to backfill slope as the Mononobe-Okabe theory is.

From the parameter diagrams (Figures 5.53 through 5.107) it can be observed that the maximum moments recorded ranged from about 40% to about 100% higher than the maxima recorded statically (with the exception of test 1CN0007 which had a relatively very low static maximum moment). As mentioned previously, this ratio is more dependent on the energy input into the system (represented by the velocity) than on the peak accelerations. The moment distributions with respect to the location (frames c and vertical cuts of frames a) seem to be smooth curves which could possibly be approximated using low order polynomials, for example, quadratic functions.

The maximum dynamic pressures ranged anywhere from 1 to 2-1/2 times the maximum static ones and like the moments this ratio was more dependent on the velocities recorded. Although the pressure distributions are by no means linear (as assumed by the Mononobe-Okabe theory), their centroids (locations of resultants) generally appear to be at or very near the location of the static centroids, that is, somewhere between 30% to 40% above the wall base. As with the static pressure distributions, this indicates that the distributions are like an "average" of a linear pressure distribution although they are generally difficult to relate to a Mononobe-Okabe distribution. In any case, the dynamic centroid appears to hold steady at around 1/3 the height above the base in contradiction to Seed and Whitman [55] and Prakash and Basavanna [42] (see Section 1.3).

The maximum shear forces recorded in the tests are generally 50% to 100% higher than the maximum recorded statically for the range of maximum test accelerations. It appears that the percentage is more closely associated with the acceleration than the velocity levels. One should keep in mind that shear requirements are usually amply met if a bending design is used unless the beam is short with respect to its thickness (behaving like a shear beam). For reinforced concrete beams, shear is important, however, and some shear reinforcement is usually required by design.

As can be seen from Figures 5.120 through 5.122 no clear trend could be determined between the maximum displacements (at the top of the wall) and the strong motion characteristics.

Richards and Elms [43] performed some tests on a <u>gravity</u> retaining wall on a (1g) shaking table which was subjected to a scaled El Centro, California (1940) earthquake record. They measured the displacements on the wall and noted that the wall always moved outward away from the backfill and continued to move outward until the shaking ceased. By contrast, barring the author's prejudice toward 1g shaking table tests (Section 1.2), in the cantilever retaining wall tests of this investigation, the walls were observed to displace both outwardly and inwardly with respect to the backfill. The maximum displacements were observed to be not necessarily the final ones although in some tests they were. This is as it should be. At 1g, the soil grains are under low stresses and are rigid, so the only displacements are due to grain slipping which is all irreversible. In the centrifuge, the soil behavior is properly elastic/plastic so dynamic to and fro movements are observed. In addition to the sliding and rotation of the base, there is also the flexing of the stem (and base) so the elastic wall can rebound somewhat as well. The maximum deflections ranged from 5% to 9% of the wall height for RW1 and from 7% to 11% for the more flexible RW2. These magnitudes of deflections could lead to some severe cracking in reinforced concrete walls although it should be remembered that part of the deflection is due to a rotation of the base.

From the shape of the deflection curves (frames c and vertical sections through frames a of the parameter diagrams) it can be seen that the wall motion is basically in the first mode with apparently little or no contribution from other modes. This is also confirmed by the Fourier Spectra discussed in Section 3.3.3.

5.6. Final Static (Residual) Results

A visual idea of the results of the earthquake on the retaining walls can be observed from Figures 5.123 (Test 1CN0007), 5.124 (Test

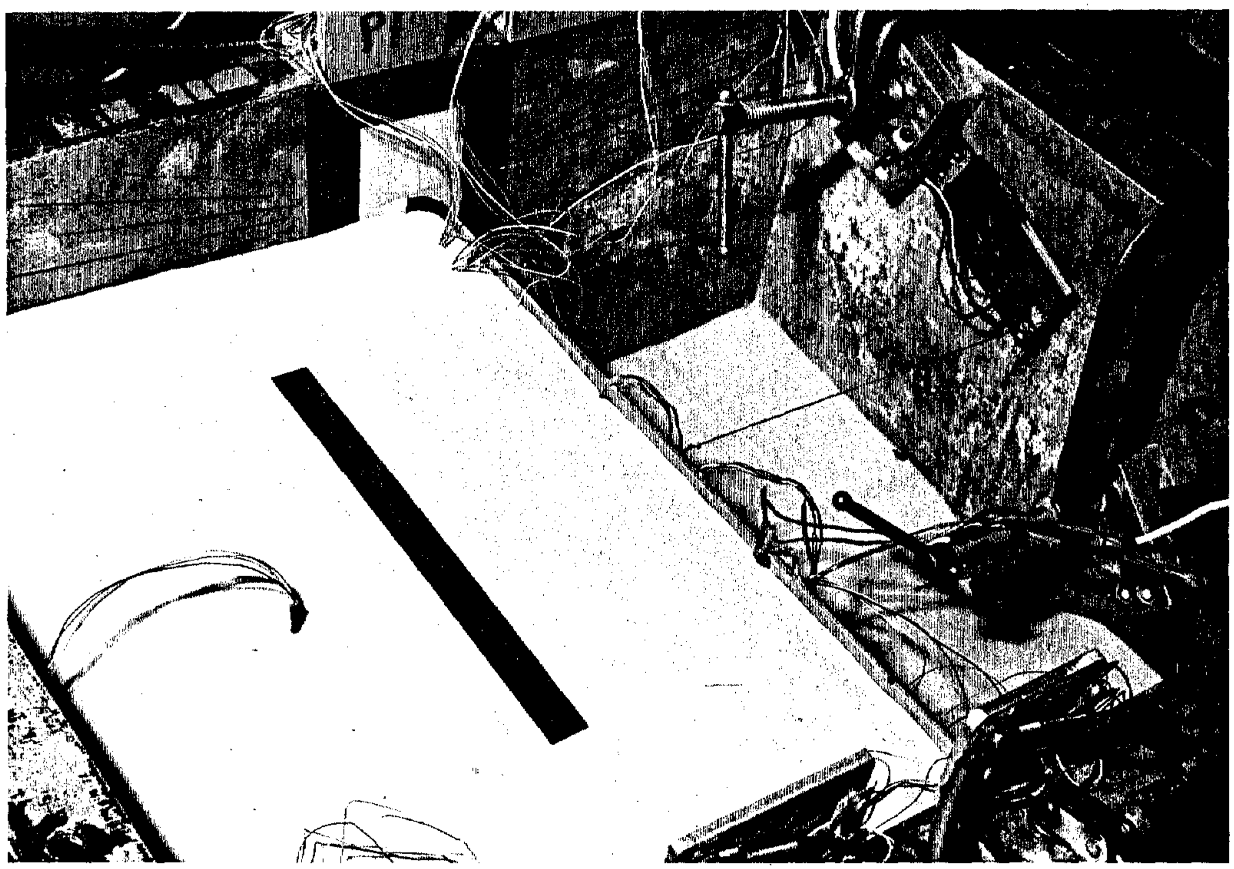

FIGURE 5.123 – TEST 1CN0007,POST TEST VIEW (AT 1G)

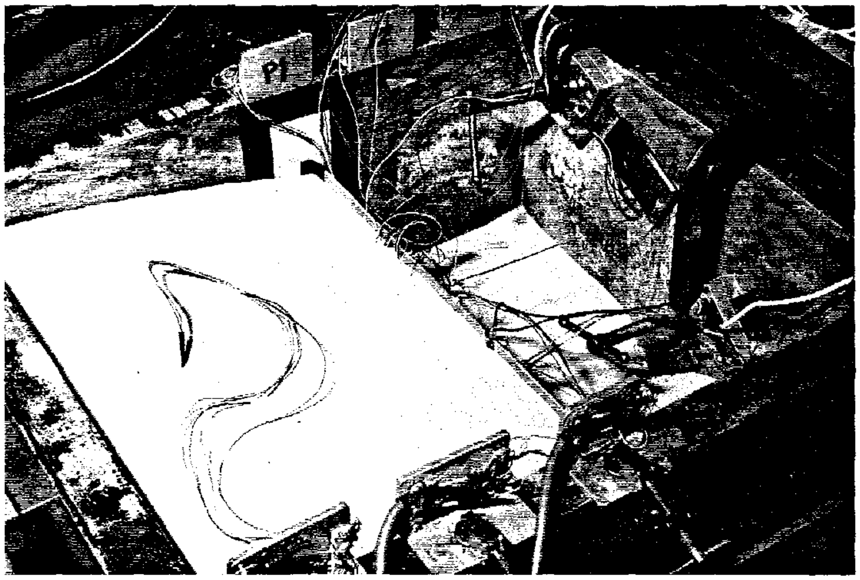

FIGURE 5.124 - TEST 1CN1009,POST TEST VIEW (AT 1G)

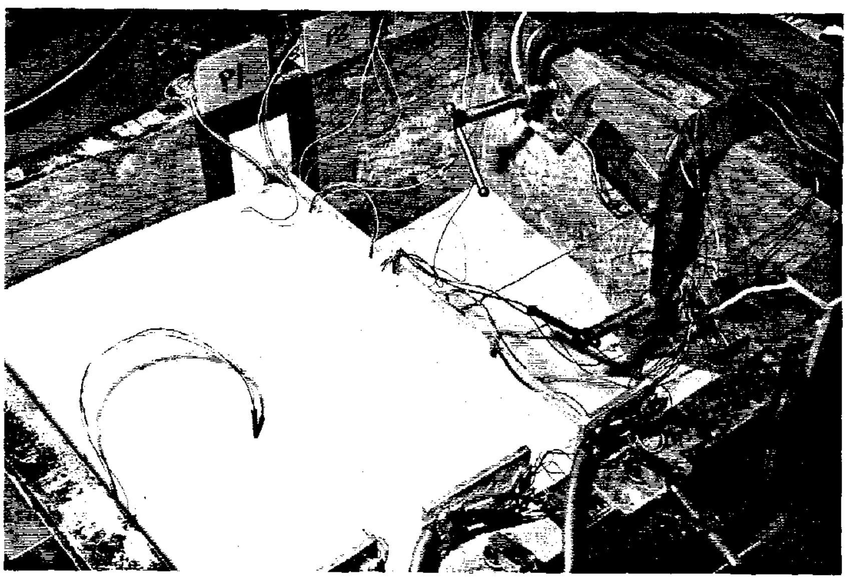

FIGURE 5.125 - TEST 2CN0011,POST TEST VIEW (AT 1G)

1CN1009), and 5.125 (Test 2CN0011). Although the photographs were taken after the centrifuge was brought back down to rest, one can see that there was a large amount of motion of the backfill and wall. There was, of course, an amount of "rebounding" of the system as the artificial gravitational field decreased. One can observe that the backfill, which was originally flush with the lip of the wall, has displaced downward 1/4 to 1/2 of an inch. These kinds of displacements are quite sizeable and it can be safe to speculate that, if colored sand, or slightly moistened sand (with some apparent cohesion) had been used, some cracks in the backfill would have been observed.

Not apparent from the photographs is a "mounding" of the sand observed at the base of the wall. This was obviously produced by the outward movement of the wall during the tests.

An important observation related to the downward sliding of the backfill and the "mounding" at the base is that these features were uniform across the width of the wall and there was no apparent change near the edges. This can be taken as a good indication that the system behaved in a plane strain fashion (as assumed) and that the edge effects (if any) were minimal.

Seed and Whitman [55] mention the fact that after a retaining structure with granular backfill has been subjected to a base excitation, a residual pressure acts on it which is substantially greater than the initial pressure before base excitation. This pressure is also a

TABLE 5.7

Maximum Final (Residual) Static Values From Tests

	Test 1CN0001	Test 1CN0002	Test 1CN1003	Test 1CN0004	Test 1CN1505	Test 1CN0006	Test 1CN0007	Test 1CN0508	Test 1CN1009	Test 1CN1510	Test 2CN0011	Test 2CN0012	Test 2CN1013	Test 2CN1514
Moment MH/EI	0.338	0.358	0.409	0.303	0.371	0.381	0.302	0.270	0.423	0.456	0.790	0.708	0.760	0.856
Moment $6M/\gamma H^3$	0.439	0.472	0.535	0.388	0.483	0.485	0.370	0.379	0.525	0.576	0.481	0.445	0.470	0.527
Pressure $P/\gamma H$	–	0.478	0.408	0.461	0.501	0.314	0.318	0.308	0.354	0.444	0.268*	0.275**	0.297	0.276
Shear $Q/(1/2\ \gamma H^2)$	0.413	0.428	0.423	0.375	0.419	0.177	0.320	0.317	0.381	0.482	0.359	0.398	0.365	0.282
Displacement y/H	0.0474	0.0536	0.0599	0.0433	0.0548	0.0328	0.0481	0.0552	0.0580	0.0561	0.0653	0.0731	0.0856	0.0947

Maximum Moment always at bottom of wall unless otherwise specified.

Maximum Pressure always at bottom of wall unless otherwise specified.

Maximum Shear Force always at bottom of wall unless otherwise specified.

Maximum Displacement always at top of wall.

*. Occurs at $x/H = 0.625$

**. Occurs at $x/H = 0.431$

TABLE 5.8

Ratios of Final Residual to Maximum Static and Maximum Dynamic Values (Test only).

	Test 1CN0001		Test 1CN0002		Test 1CN1003		Test 1CN0004	
	Static	Dynamic	Static	Dynamic	Static	Dynamic	Static	Dynamic
Moment MH/EIΔ6M/ γ H^3	1.40	0.87	1.32	0.93	1.37	0.91	1.23	0.94
Pressure P/ γ H	–	–	0.96	0.59	0.92	0.44	0.87	0.76
Shear Force Q/(1/2 γ H^2	1.55	0.77	1.44	0.84	1.48	0.76	1.36	0.90
Displacement y/H	1.70	1.00*	1.68	1.00*	1.59	1.00*	1.37	0.71

Test 1CN1505		Test 1CN0006		Test 1CN0007		Test 1CN0508		Test 1CN1009	
Static	Dynamic	Static	Dynamic	Static	Dynamic	Static	Dynamic	Static	Dynamic
1.35	0.91	1.39	0.97	1.80	0.71	1.29	0.83	1.86	0.86
0.93	0.76	0.75	0.75	0.83	0.45	0.56	0.43	0.82	0.64
1.64	0.86	1.39	1.00	1.60	0.70	1.04	0.69	1.46	0.81
1.59	0.96	1.10	−0.92	1.61	0.75	1.88	0.59	1.87	−0.83

Test 1CN1510		Test 2CN0011		Test 2CN0012		Test 2CN1013		Test 2CN1514	
Static	Dynamic	Static	Dynamic	Static	Dynamic	Static	Dynamic	Static	Dynamic
1.57	0.81	1.56	0.97	1.58	0.93	1.53	0.95	1.61	0.95
0.84	0.66	0.95	0.38	0.87	0.45	0.62	0.36	0.66	0.38
1.44	0.79	1.07	0.95	1.58	0.97	1.54	0.89	1.11	0.72
1.72	0.88	1.49	1.00	1.58	1.00*	1.72	0.76	1.73	1.00

* Final = Maximum

substantial portion of the maximum pressure developed during the excitation. This statement is quantitatively demonstrated by the experiments.

The maximum residual parameters are listed in Table 5.7 and their ratios to maximum static and maximum dynamic values in Table 5.8.

One can observe that, although the maximum residual pressure is always somewhat lower than the maximum static pressure (5% to 25%), and considerably lower than the maximum dynamic (25% to 60% lower), the resultant (shear) forces (i.e., the areas under the pressure distributions) are in accordance with the Seed and Whitman observation. The residual resultants can be up to 60% higher than the static! This appears to be random with respect to the slope. From frames c of the pressure distribution diagrams, it can also be observed that the final residual resultant is usually located some 20% to 40% above the static and dynamic resultants indicating that a triangular (or "average triangular") pressure distribution no longer exists.

The residual moments are also substantially higher than the static and are only a few percent lower than the maximum. This, again, develops regardless of the magnitude of the shaking the wall was subjected to. This could indicate that a retaining wall which has survived an earthquake intact could be pre-stressed for the following earthquake or aftershock to the point where there is virtually no safety factor and thus fail under an even mild event. It should be noted that in Test 1CN1505 the centrifuge was left running for 3 hours after the shaking occurred. This is the equivalent of 150 hours (over 6 days) in prototype time, and in this period, no rebounding or relaxation was observed in either the strain gage (moment) or pressure transducer readings.

As mentioned in Section 5.5 the walls displaced out and in with respect to the backfill and then generally crept out toward some final displacement which in some tests was the maximum observed. The final displacements were found to be much greater than the static ones in any case. This then gives rise to the question of whether or not such large displacements can be tolerated from a safety or aesthetic point of view although the retaining wall survived the earthquake.

CHAPTER VI

CONCLUSIONS AND RECOMMENDATIONS

The purpose of this investigation was to observe the natural behavior of an 18 ft high cantilever retaining wall when subjected to only a gravity body force with a dynamic lateral earthquake excitation. The retaining walls were properly modelled and were subjected to some earthquake-like motions which were considered to be in a realistic range. Moment, pressure, shear, and displacement distributions (static, dynamic, and residual) were obtained. It was also novel that the retaining walls were considered flexible (as they are in real life) as opposed to rigid, which seems to be the norm in 1g model retaining wall studies and in theoretical analyses. A large amount of data was obtained directly from transducers and indirectly from simple mathematical manipulations of transducer data and was presented in as concise a manner as possible. Some empirical curves for relating the upper bound responses of the retaining walls to strong motion characteristics were also obtained.

From the information acquired from the tests, the following conclusions and recommendations can be made.

6.1. Conclusions

1. The simple "earthquake generating" mechanism employed was found to give realistic characteristics and could thus be employed in the

studies of other earthquake-related problems in geotechnics in the centrifuge.

2. The static earth pressure distributions obtained were not triangular as the Rankine/Coulomb lateral earth pressures assume. The experimental centroids were generally located at about 1/3 the height above the base of the wall. The resultant forces (areas under the pressure curves) were in reasonable agreement with the Rankine/Coulomb theory. This indicates that the Rankine/Coulomb theory estimates an "average" pressure distribution which is taken as triangular.

3. The static moments measured were generally higher than those which would be obtained using a Rankine/Coulomb resultant force with a 1/3 of the height moment arm (by as much as 35%), indicating that the properly designed wall might have a safety factor lower than estimated.

4. Static displacements were sufficiently large to create a state of full active pressure behind the wall.

5. Static and dynamic reaction parameters (moments, pressures, etc.) appear to be independent of wall stiffness, at least for the range of experimental system stiffnesses ($0.75 \lesssim \gamma H^4/6EI \lesssim 1.75$, $\phi \simeq 35^{\circ}$)

6a. The only significant dynamic response of the system is in the fundamental mode.

6b. The two walls had fundamental frequencies of 2.6 Hz and 2.5 Hz with the soils employed.

7. The dynamic response of the system is not only dependent on lateral accelerations, as the Mononobe-Okabe theory assumes, but also on the energy content of the earthquake indicated by the velocities. Maximum moments were found to be more closely associated with the areas under the individual acceleration spikes (changes in velocity), maximum pressures with the velocities, and maximum shear (resultant) forces with the accelerations, although there is a general dependence on all the strong motion characteristics. There is a strong correlation between maximum and minimum (maximum negative) accelerations, velocities, and changes in velocities; and peaks and troughs in the maximum response curves.
8. The experimental envelopes presented in Chapter V provide an upper bound for the various parameters with respect to actual dynamic strong motion characteristics for at least the system stiffness range ($0.75 \leq \gamma H^4/6EI \leq 1.75$, $\phi \simeq 35^o$) which was studied. These envelopes can be used as a design aid (Section 6.2).
9. The Mononobe-Okabe theory underestimates responses (in some cases severely) below certain lateral acceleration levels for each individual case (Figures 5.108, 5.111, 5.114, and 5.117) and overestimates them above that acceleration when compared to the experimental envelopes. This is due to the steep slope of intersection (at only one point) between the recorded parameter envelopes and the Mononobe-Okabe curves. This makes the envelopes appear conservative for k_h values less than 0.5g, but they are not, because they came from tests.

10. The experimental envelopes are not as sensitive to backfill slope as the Mononobe-Okabe theory is.
11. Dynamic moment distributions with respect to wall location are generally smooth, monotonic curves which resemble some low order polynomial, possibly quadratic.
12. As in the static cases, the dynamic pressures were not triangular as the Mononobe-Okabe theory assumes, although the centroids did remain at about 1/3 the height above the base, contradicting other investigators which state that it rises to between 1/2 and 2/3 of the height. The dynamic pressure distributions could thus be considered an "average" of a linear distribution, although they could not generally be related to Mononobe-Okabe.
13. The walls displaced both outwardly and inwardly with respect to the backfills during the severe parts of the shaking and crept outwardly during the milder shaking towards the end. Maximum deflections could be considered excessive in some cases even though the structure survived the event intact. Deflected shapes gave an indication of first mode (only) flexible bending beam behavior.
14. The fact was confirmed that, after a retaining structure with a granular backfill undergoes severe dynamic excitation, a residual pressure acts on it which is substantially greater than the initial pressure before excitation, and is a substantial portion of the maximum pressure developed during the excitation. This also applies to moments, shears, and displacements.

15. No noticeable experimental "edge effects" were observed, and a plane strain condition for the tests could be assumed to hold.
16. Elastic solutions for retaining wall problems should be avoided. This includes the use of elastic finite elements (Appendix D).

6.2. Recommendations

Based on the concluded investigation, it is highly recommended that some type of dynamic analysis in the design of large retaining structures be employed, as the dynamic responses generated can be considerably greater than the static ones. There should be extreme caution in accepting the following quote from Seed and Whitman [55]:

"Thus many walls adequately designed for static earth pressures will automatically have the capacity to withstand earthquake ground motions of substantial magnitudes and in many cases, special seismic earth pressure provisions need not be required".

As an example of how the experimental data from this investigation might be used as a design aid consider the following practical problem:

It is required to design a 20 ft high cantilever retaining wall with a flat, granular backfill with $\phi = 35^{o}$. The wall is to be subjected to a scaled down Parkfield Earthquake (Figure 5.41a) to one half the magnitude shown.

Since the wall/soil description is similar to that of the experiments, the fundamental frequency can be assumed to be about 2.5 Hz. From Figure 5.41, based on test experience, the second acceleration spike (that whose peak is at about 4.1 seconds) should probably generate the critical response. The peak design acceleration is then 215 cm/sec^2, the corresponding velocity 39 cm/sec (which occurs at about 4.6 sec) and the area under the acceleration spike is 49 cm/sec (which is the peak-trough difference on the velocity curve). Based on test experience, the peak response of the wall should then occur sometime between the 4 and 5 second mark.

For a = 215 cm/sec^2, a/g = 0.22. Therefore, from Figure 5.111

$$\frac{6M}{\gamma H^3} = 0.58.$$

For v = 39 cm/sec, (f_1 = 2.5 Hz).

$$\frac{v}{f_1 H} = \frac{39}{(2.5)(20)(30.48)} = 0.026.$$

Therefore, from Figure 5.112,

$$\frac{6M}{\gamma H^3} = 0.55$$

For Δv = 49 cm/sec, (f_1 = 2.5 Hz).

$$\frac{\Delta v}{f_1 H} = 0.032.$$

Therefore, from Figure 5.113,

$$\frac{6M}{\gamma H^3} = 0.57$$

The maximum moment could then be taken as the average of the three values obtained from the envelopes, therefore

$$\left(\frac{6M}{\gamma H^3}\right)_{MAX} = 0.57.$$

Having this value, the stem could then be designed as a regular bending beam using, for example, a quadratic moment distribution for simplicity and having all the design requirements (as was done in Section 3.3.1).

It should be noted that had a Mononobe-Okabe analysis been performed, using the maximum scaled Parkfield acceleration of 240 cm/sec^2 and equation (5.10), the maximum moment would have been:

$$\left(\frac{6M}{\gamma H^3}\right)_{MAX} = 0.42$$

which is 35% below the one obtained from the other analysis. It was based on one dynamic parameter (the peak acceleration) whereas, the other was based on three. If a standard factor of safety of 1.7 is used, it would in actuality only be 1.25 when compared to the previous analysis.

One could also use a similar analysis to investigate the pressures and shears and perhaps refine the design.

Future research could be done using identical types of tests with different wall heights, stiffnesses, different soils and longer earthquake durations.

The data analysis should concentrate more on the highlights (peaks, troughs, etc.) of the dynamic characteristics related to the system responses instead of the detailed, time-consuming, expensive, and tedious data analysis which was performed in this investigation.

Sheetpile walls, channel sections, and other types of bending beam retaining walls should also be studied.

Retaining wall problems with wet or saturated soils should also be examined with the centrifuge, although there could be some problems with retaining the water in the backfill as well as having two time scales (dynamic and consolidation — see Appendix A).

The centrifuge would also be an ideal tool for studying static and dynamic retaining wall behavior with clays.

It would be desirable to develop a better shaker which could be implemented into a centrifuge. There is also a need for some full-scale testing of bending beam retaining structures. Sinusoidal shakers could be used on actual retaining structures to determine some natural frequencies and modes of vibration and perhaps test some to failure.

An actual retaining wall should also be instrumented with two strong motion accelerographs (one at the base and one at the top) and with at least some kind of pressure transducers which could record pressures during an actual earthquake. The recording devices could be triggered by the accelerographs.

BIBLIOGRAPHY

1. K.J. Bathe, E.L. Wilson, F.E. Peterson (1973), "SAPIV - A Structural Analysis Program for Static and Dynamic Response of Linear Systems", Report No. EERC 73-11, College of Engineering, University of California, Berkeley, California, June.

2. Biggs, J.M. (1964), Introduction to Structural Dynamics, McGraw-Hill Book Company, San Francisco.

3. Bridgman, P.W. (1943), Dimensional Analysis, Yale University Press.

4. Bucky, P.B. (1931), "Use of Models for the Study of Mining Problems", American Institute of Mining and Metallurgical Engineers Technical Publication No. 425.

5. Chakrabarti, S., Husak, A.D., Christiano, P.P., Troxell, D.E. (1978), "Seismic Design of Retaining Walls and Cellular Cofferdams", Proceedings of the ASCE Geotechnical Conference, Earthquake Engineering and Soil Dynamics, Pasadena, California.

6. Chang, M.F., Chen, W.F. (1981), "Limit Analysis of Lateral Earth Pressures on Rigid Walls Retaining Cohesionless Soils", Report CE-STR-81-2, School of Civil Engineering, Purdue University, January.

7. Chang, M.F., Chen, W.F. (1981), "Lateral Earth Pressures on Rigid Retaining Walls Subjected to Earthquake Forces", Report CE-STR-81-20, School of Civil Engineering, Purdue University, June.

8. Cloud, W.K. (1967), "Intensity Map and Structural Damage, Parkfield, California Earthquake of June 27, 1966", Bulletin of the Seismological Society of America, Vol. 57, No. 6, December.

9. Cloud, W.K., Perez, V. (1967), "Accelerograms - Parkfield Earthquake", Bulletin of the Seismological Society of America, Vol. 57, No. 6, December.

10. CNEN-ENEL Commission on Seismic Problems Associated with the Installation of Nuclear Power Plants (1976), Contribution to the Study of the Friuli Earthquake of May, 1976.

11. Duke, C.M., Leeds, D.J. (1963), "Response of Soils, Foundations, and Earth Structures to the Chilean Earthquakes of 1960", Bulletin of the Seismological Society of America, Vol. 53, No. 2, February.

12. Ellingwood, B.R., Editor (1980), "An Investigation of the Miyagi-Ken-Oki, Japan Earthquake of June 12, 1978", U.S. Department of Commerce, Bureau of Standards Special Publication 592, October.

13. Greville, T.N.E. (1970), Spline Functions and Applications, National Technical Information Service, Springfield, Virginia.

14. Hayoshi, S., Kubo, K., Nakase, A. (1966), "Damage to Harbor Structures in the Niigata Earthquake", Soils and Foundations, Tokyo.

15. Hoek, E. (1965), "The Design of a Centrifuge for Simulation of Gravitational Force Fields in Mine Models", Journal of the South African Institute of Mining and Metallurgy, Vol. 65, No. 9.

16. Housner, G.W., Trifunac, M.D. (1967), "Analysis of Accelerograms - Parkfield Earthquake", Bulletin of the Seismological Society of America, Vol 57, No. 6, December.

17. International Association for Earthquake Engineering (1970), "Earthquake Engineering Regulations: A World List", November.

18. Ishii, T., Arai, M., Tsuchida, H. (1960), "Lateral Earth Pressures in an Earthquake", Proceedings, Second World Conference on Earthquake Engineering, Tokyo, Japan.

19. Jacobsen, L.S. (1939), Appendix D of "The Kentucky Project", Technical Report No. 13, Tennessee Valley Authority, 1951.

20. Japan Society of Civil Engineers (1980), Earthquake Resistant Design of Civil Engineering Structures and Foundations in Japan.

21. Jennings, P.C., Editor (1971), Engineering Features of the San Fernando Earthquake, Report No. EERL 71-02, Earthquake Engineering Research Laboratory, California Institute of Technology, Pasadena, California.

22. Kawasumi, H. (1968), General Report on the Niigata Earthquake of 1964, Tokyo Electrical Engineering College Press, Tokyo, Japan.

23. Ketter, R.L., Prawel, S.P., Jr. (1969), Modern Methods in Engineering Computation, McGraw-Hill Book Company, New York.

24. Lew, H.S., Leyendecker, E.V., Dikkers, R.D. (1971), "Engineering Aspects of the 1971 San Fernando Earthquake", Building Research Division, Institute for Applied Technology, National Bureau of Standards, Washington, D.C., Building Science Series 40, December.

25. Liu, H-P., Hagman, R.L., Scott, R.F. (1978), "Centrifuge Modeling of Earthquakes", Geophysical Research Letters, Vol. 5, No. 5, May.

26. Matsuo, H. (1941), "Experimental Study on the Distribution of Earth Pressures Acting on a Vertical Wall During Earthquakes", Journal of the Japanese Society of Civil Engineers, Vol. 27, No. 2.

27. Matsuo, M., Ohara, S. (1955), "Seismic Earth Pressure Due to Saturated Soils", Journal of the Japanese Society of Civil Engineers, Vol. 40, No. 6.

28. Matsuo, M., Ohara, S. (1960), "Lateral Earth Pressures and Stability of Quay Walls During Earthquakes", Proceedings, Second World Conference of Earthquake Engineering, Tokyo, Japan.

29. Matsuo, M., Ohara, S. (1965), "Dynamic Pore Water Pressure Acting on Quay Walls During Earthquakes", Proceedings, Third World Conference on Earthquake Engineering, New Zealand.

30. Mononobe, N. (1929), "Earthquake Proof Construction of Masonry Dams", Proceedings, World Engineering Conference, Japan, Vol. 9.

31. Mononobe, N., Matsuo, M. (1929), "On the Determination of Earth Pressures During Earthquakes", Proceedings, World Engineering Conference, Japan, Vol. 9.

32. Murphy, L.M., Scientific coordinator (1973), "Earthquake Damage to Water and Sewerage Facilities: Subcommittee on Water and Sewerage Systems", San Fernando, California, Earthquake of February 9, 1971, U.S. Department of Commerce, National Oceanic and Atmospheric Administration, Environmental Research Laboratories, Washington, D.C.

33. Murphy, V.A. (1960), "The Effect of Ground Characteristics on the Aseismic Design of Structures", Proceedings, Second World Conference on Earthquake Engineering, Tokyo, Japan.

34. Murray, W.M., Stein, P.K. (1958), Strain Gage Techniques, M.I.T. Press.

35. Newmark, N.M. (1965), "Effects of Earthquakes on Dams and Embankments", Geotechnique, Vol. XV, No. 2, June.

36. Niwa, S. (1960), "An Experimental Study of Oscillating Earth Pressures Acting on a Quay Wall", Proceedings, Second World Conference on Earthquake Engineering, Tokyo, Japan.

37. Oberg, E., Jones, F.D., Horton, H. L., Schubert, P.B., Garratt, G., Semioli, W.J., Moltrecht, K.H. (1975) Machinery's Handbook, 20th Edition, Industrial Press, Inc., New York.

38. Ohara, S. (1960), "Experimental Studies of Seismic Active and Seismic Passive Earth Pressure", Proceedings, Third Japanese Earthquake Engineering Symposium, Tokyo, November.

39. Okabe, S. (1926), "General Theory of Earth Pressure", Journal of the Japanese Society of Civil Engineers, Vol. 12, No. 1.

40. Pokrovsky, G.I., Fyodorov, I.S. (1975), "Centrifugal Model Testing in the Construction Industry", Draft translation prepared by Building Research Establishment Library Translation Service, Great Britain, Vols. I and II.

41. Polshin, D.E., Rudnitski, N.Y., Chizhikov, P.G., Yakovleva, T.G. (1973), "Centrifugal Model Testing of Foundation Soils of Building Structures", Proceedings, 8th International Conference of Soil Mechanics and Foundation Engineering, Moscow.

42. Prakash, S., Basavanna, B.M. (1969), "Earth Pressure Distribution Behind Retaining Wall During Earthquake", Proceedings, Fourth World conference on Earthquake Engineering, Santiago, Chile.

43. Richards, R., Jr., Elms, D.G. (1977), "Seismic Behavior of Gravity Retaining Walls", Research Report No. 77-10, University of Delaware, Newark, Delaware, University of Canterbury, Christchurch, New Zealand.

44. Richart, F.E., Jr., Hall, J. R., Jr., Woods, R.D. (1970), Vibration of Soils and Foundations, Prentice Hall.

45. Ross, G.A., Seed, H.B., Migliaccio, R. (1969), "Bridge Foundation Behavior in Alaska Earthquake", Journal of the Soil Mechanics and Foundation Division, American Society of Civil Engineers, July.

46. Rowe, P.W. (1975), "Application of Centrifugal Models to Geotechnical Structures", Proceedings, Symposium on Geotechnical Structures, University of New South Wales, Australia, July.

47. Satake, M. (1979), Investigation of Disasters Caused by the 1978 Miyagi-Ken-Oki Earthquake.

48. Scott, R.F. (1963), Principles of Soil Mechanics, Addison-Wesley Publishing Co., Inc., Reading, Massachusetts.

49. Scott, R.F. (1973), "Earthquake-Induced Earth Pressures on Retaining Walls", Proceedings, Fifth World Conference on Earthquake Engineering, Rome, Italy.

50. Scott, R.F. (1975), "The Centrifugal Technique in Geotechnology-Selected Papers", Soil Mechanics Laboratory, California Institute of Technology, Pasadena, California, November.

51. Scott, R.F., Liu, H-P., Ting, J. (1977), "Dynamic Pile Tests by Centrifuge Modeling", Proceedings, Sixth World Conference on Earthquake Engineering, Paper 4-50, New Delhi, January.

52. Scott, R.F. (1977), "Centrifuge Studies of Cyclic Lateral Load-Displacement Behavior of Single Piles", Soil Mechanics Laboratory, Division of Engineering and Applied Science, California Institute of Technology, Pasadena, California.

53. Scott, R.F. (1979), "Cyclic Static Model Pile Tests in a Centrifuge", Offshore Technology Conference, Paper no. 3492.

54. Seed, H.B., Idriss, I.M. (1970), "Soil Moduli and Damping Factors for Dynamic Response Analyses", Report No. EERC, 70-10, Earthquake Engineering Center, University of California, Berkeley, December.

55. Seed, H.B., Whitman, R.V. (1970), "Design of Earth Retaining Structures for Dynamic Loads", ASCE Specialty Conference, Lateral Stresses in the Ground and the Design of Earth Retaining Structures, Cornell University Ithaca, New York.

56. Sim, L.C. (1979), "Behavior of Retaining Walls Under Seismic Loading", Research Report 79/9, Department of Civil Engineering, University of Canterbury, Christchurch, New Zealand, February.

57. Stratta, J.L., Wyllie, L.A., Jr. (1979), "Reconnaissance Report, Friuli, Italy Earthquakes of 1976", Earthquake Engineering Research Institute, August.

58. Tagaya, K., Scott, R.F., Aboshi, H. (1977), "Fundamental Study on Extraction of Buried Anchors", Proceedings, 12th Conference on Soil Mechanics and Foundation Engineering, Japanese Society of Soil Mechanics and Foundation Engineering, Tokyo.

59. Tajimi, H. (1969), "Dynamic Analysis of a Structure Embedded in an Elastic Stratum", Proceedings, Fourth World Conference on Earthquake Engineering, Santiago, Chile.

60. Tajimi, H. (1970), "Dynamic Earth Pressure on Basement Walls in the Elastic Ground", Proceedings, Third Japanese Earthquake Engineering Symposium, Tokyo, November.

61. Tajimi, H. (1973), "Dynamic Earth Pressures on Basement Wall", Proceedings, Fifth World Conference on Earthquake Engineering, Rome, Italy.

62. Teng, W.C. (1962), Foundation Design, Prentice Hall Inc., Englewood Cliffs, New Jersey.

63. Trifunac, M.D., Lee, V. (1973), "Routine Computer Processing of Strong Motion Accelerograms", Report EERL 73-03, California Institute of Technology, Earthquake Engineering Research Laboratory.

64. Wang, C.K., Salmon, C.G. (1973), Reinforced Concrete Design, Second Edition, Intext Educational Publishers, New York.

65. Winterkorn, H.F., Fang, H.Y. (1975), Foundation Engineering Handbook, Van Nostrand Reinhold, New York.

66. Whitman, R.V. (1979), "Dynamic Behavior of Soil and its Application to Civil Engineering Projects", Proceedings, Sixth Pan- American Conference on Soil Mechanics and Foundation Engineering, Lima, Peru.

67. Wood, J.H. (1973), "Earthquake Induced Soil Pressures on Structures", Report No. EERL 73-05, Earthquake Engineering Research Laboratory California Institute of Technology, Pasadena, California.

68. Wood, J.H. (1975), "Earthquake Induced Pressures on a Rigid Wall Structure", Bulletin of the New Zealand Society for Earthquake Engineering, Vol. 8, No. 3, September.

69. Yanev, P.I., Editor (1978), "Reconnaissance Report, Miyagi-Ken-Oki Japan Earthquake, June 12, 1978", Earthquake Engineering Research Institute, Berkeley, California, December.

70. Yuxian, H. (1979), "Some Engineering Features of the 1976 Tangshan Earthquake", Visit of the Soil Dynamics Delegation of the American Society of Civil Engineers to the People's Republic of China, August 25-September 10, 1979.

APPENDIX A

SCALING RELATIONS (Hoek [15])

Every quantity of physics and mechanics has a dimension which can be expressed as a function of the fundamental dimensions:

M - mass		F - force ($F = MLT^{-2}$)
L - length	or	L - length
T - time		T - time

If a formula is dimensionally correct, it is valid in all systems of units.

By the method of dimensional analysis ([3],[15]) relations between the equations governing the states of the model and prototype can be derived.

The stress and displacement at a point in the structure will depend upon the following factors:

1.) The geometry of the structure. The behavior of a point defined by the coordinates x, y, z can be described by a typical length dimension L and set of dimensionless ratios L_R relating all other lengths to L.

2.) Material properties: For example, for a linearly elastic isotropic material.

ρ = mass density of the material.

E = Young's modulus of the material.

ν = Poisson's ratio of the material (dimensionless).

Other material properties can be related to ρ and E by sets of dimensionless ratios ρ_R, E_R.

3.) Applied stress conditions:

P = externally applied load.

Q = externally applied stress.

u_o = externally induced displacement.

σ_o = internal stress.

g = acceleration of gravity.

a = externally applied acceleration.

Other stress conditions are related to P, Q, u_o, σ_o, a by sets of dimensionless ratios P_R, Q_R, U_{OR}, σ_{OR}, a_R.

The behavior of a point x,y,z in the structure at time t is defined by a resulting stress σ and a resulting displacement u and depend upon the abovementioned parameters and dimensionless ratios.

The quantities σ, u, x, y, z, t, L, ρ, E, ν, P, Q, σ_o, u_o, g, a are all derived from the three fundamental units of force F, length L, and time T. The Poisson's ratio ν is already dimensionless.

The dimensions of the listed parameters are given in Table A.1.

TABLE A.1

	σ	u	x	y	z	t	L	ρ	E	ν	P	Q	σ_o	u_o	g	a
F	1	0	0	0	0	0	0	1	1	0	1	1	1	0	0	0
L	-2	1	1	1	1	0	1	-4	-2	0	0	-2	-2	1	1	1
T	0	0	0	0	0	1	0	2	0	0	0	0	0	0	-2	-2

The table consists of a matrix of rank 3. According to Buckingham's first theorem, one may obtain 16-3 = 13 dimensionless independent groups of parameters from those listed. Hoek chooses the following:

$$\frac{\sigma L^2}{P},\ \frac{u}{L},\ \frac{x}{L},\ \frac{y}{L},\ \frac{z}{L},\ \frac{t^2 a}{L},\ \frac{EL^2}{P},\ \frac{\rho a L^3}{P},\ \nu,\ \frac{a}{g},\ \frac{QL^2}{P},\ \frac{u_o}{L},\ \frac{\sigma_o L^2}{P}$$

It should be noted that other combinations than those listed above are possible. For this particular set, however, all other groups would be combinations of those listed.

Buckingham's second theorem (Buckingham's Π Theorem) states that a dimensionally homogeneous equation (one which does not depend on the units of measurement) can be reduced to a relationship between a complete set of dimensionless products.

From Buckingham's Π Theorem then the displacement u, and the stress σ at a point (x,y,z) can be expressed by the following dimensionless equations

$$\frac{u}{L} = F\left(\frac{x}{L}, \frac{y}{L}, \frac{z}{L}, \frac{t^2 a}{L}, \frac{EL^2}{P}, \frac{\rho a L^3}{P}, \nu, \frac{a}{g}, \frac{QL^2}{P},\right.$$

$$\left.\frac{u_o}{L}, \frac{\sigma_o L^2}{P}, L_R, E_R, P_R, Q_R, u_{OR}, \rho_R, \sigma_{OR}, a_R\right) \qquad (A.1)$$

$$\frac{\sigma L^2}{P} = G\left(\frac{x}{L}, \frac{y}{L}, \ldots\ldots, a_R\right) \qquad (A.2)$$

in which F and G are undetermined functions. The parameter t is the dynamic time scale.

For the two systems, model and prototype to by physically similar, the functions F and G must be the same for each. Therefore, the following conditions of similitude are established.

The subscripts m and p will refer to model and prototype parameters respectively.

1.) Model similitude related to natural properties: Since Poisson's ratio is dimensionless, the model and prototype must have the same Poisson's ratio:

$$\nu_m = \nu_p \qquad (A.3)$$

Combining the remaining natural properties E and ρ by dimensionless grouping:

$$\frac{\rho a L^3}{P} \cdot \frac{g}{a} \cdot \frac{P}{EL^2} = \frac{\rho\, g\, L}{E} \qquad (A.4)$$

Therefore:

$$\frac{\rho_m g_m L_m}{E_m} = \frac{\rho_p g_p L_p}{E_p} \tag{A.5}$$

or

$$\frac{L_p}{L_m} = \frac{E_p}{E_m} \frac{\rho_p}{\rho_m} \frac{g_m}{g_p} \tag{A.6}$$

If the model material is identical to the prototype material ($E_m = E_p$; $\rho_m = \rho_p$; $\nu_m = \nu_p$) and the model is subjected to an artificial acceleration $N \cdot g$ (N is the scale factor) then:

$$\frac{L_p}{L_m} = \frac{g_m}{g_p} = \frac{Ng}{g} = N \tag{A.7}$$

It can be thus seen that by use of the centrifuge, scale models manufactured of the prototype material are suitable.

2.) Model similitude in relation to applied stresses: Applied stresses are defined by the parameters P, Q, σ_o, u_o and a and appear in the dimensionless groups:

$$\frac{t^2 a}{L}, \frac{EL^2}{P}, \frac{\rho a L^3}{P}, \frac{a}{g}, \frac{QL^2}{P}, \frac{u_o}{L}, \frac{\sigma_o L^2}{P}$$

Taking the grouping:

$$\frac{Q}{E} = \frac{QL^2}{P} \cdot \frac{P}{EL^2} \tag{A.8}$$

Therefore:

$$\frac{Q_m}{Q_p} = \frac{E_m}{E_p} \tag{A.9}$$

also:

$$\frac{P_m}{E_m L_m^2} = \frac{P_p}{E_p L_p^2} \quad \text{or} \quad \frac{P_m}{P_p} = \frac{E_m L_m^2}{E_p L_p^2} \tag{A.10}$$

From the grouping:

$$\frac{\sigma_o}{E} = \frac{\sigma_o L^2}{P} \cdot \frac{P}{EL^2} \tag{A.11}$$

Therefore:

$$\frac{\sigma_{om}}{\sigma_{op}} = \frac{E_m}{E_p} \tag{A.12}$$

Displacements are scaled directly by:

$$\frac{u_{om}}{u_{op}} = \frac{L_m}{L_p} \tag{A.13}$$

Inertia and gravity forces in the model and the prototype are characterized by the dimensionless groups $\frac{\rho a L^3}{P}$ and $\frac{a}{g}$ which were already used in deriving expression (A.4).

Finally, dynamic or inertial forces involve a time scale which can be derived from the grouping:

$$\frac{t^2 E}{L^2 \rho} = \frac{t^2 a}{L} \cdot \frac{P}{\rho a L^3} \cdot \frac{EL^2}{P} \tag{A.14}$$

Therefore:

$$\frac{t_m}{t_p} = \left(\frac{\rho_m}{\rho_p}\frac{E_p}{E_m}\right)^{1/2}\frac{L_m}{L_p} \tag{A.15}$$

Using a centrifuge model made of the same material as the prototype ($E_m = E_p$; $\rho_m = \rho_p$; $\nu_m = \nu_p$) and subjecting it to the centrifuge artificial gravitational acceleration $N \cdot g$ (A.7).

(A.9) reduces to: $$Q_m = Q_p \tag{A.16}$$

(A.10) reduces to: $$\frac{P_m}{P_p} = \frac{1}{N^2} \tag{A.17}$$

(A.12) reduces to: $$\sigma_{om} = \sigma_{op} \tag{A.18}$$

(A.13) reduces to: $$\frac{u_{op}}{u_{om}} = N \tag{A.19}$$

(A.15) reduces to: $$\frac{t_p}{t_m} = N \tag{A.20}$$

One can clearly see the convenience of centrifuge modelling. From (A.16), (A.18) and the fact that $E_p = E_m$ can also note that the strains in the model and prototype are identical. In the event that the soil behavior exhibits its usual nonlinearity, the same considerations hold, if prototype and model soils are the same.

In the experiments, it was necessary to model reinforced concrete walls by means of aluminum. The stiffness of the wall EI is modelled as follows. The dimensions of EI are FL (actually FL^2L^{-1}). It has been shown, by equation (A.17) that force scales as N^2, and length of course, scales as N, so that the EI of the model must be equal to $1/N^3$ the EI of the prototype. For a given, but arbitrary design of a prototype reinforced concrete wall, the EI can be calculated. In the model, the E of the aluminum is known, and the wall thickness can therefore be selected to produce the appropriate, scaled value of EI.

The yield characteristics of the wall itself were not modelled. In the prototype, yield would be indicated by the creation of a plastic hinge at the point of maximum moment, i.e., at the base of the stem. In order to model this, a notch or groove would have to be cut along the base of the model to a point so that the stem would fail easily at that point and thus simulate the plastic hinge.

Consolidation time scale (Rowe [46]):

In the study of liquefaction, the time rate of flow of water from the soil is considered in comparison with the rate at which pore pressures are generated. The consolidation process thus requires consolidation time scaling.

The time factor T of consolidation is defined by:

$$T = \frac{C_v \ t_c}{(nH)^2} \tag{A.21}$$

where

c_v is the coefficient of consolidation

t_c is consolidation time

H is the height of the stratum to be drained

n is the number of drainage boundaries (1 or 2)

It is required that $T_m = T_p$. If the soil materials are identical then:

$$\frac{C_v \; t_c m}{n^2 \; H_m^{\;2}} = \frac{C_v \; t_c p}{n^2 \; H_p^{\;2}} \tag{A.22}$$

since

$$\frac{H_m}{H_p} = \frac{1}{N}$$

then

$$\frac{t_c m}{t_c p} = \frac{1}{N^2} \tag{A.23}$$

which establishes the consolidation time scale.

APPENDIX B

WALL PROGRAM LISTING

Following is a listing of the data processing program WALL described in Section 4.2. The following subroutines were developed:

MAIN(program)	DIGIT	PAPRNT
ALGEQN	INTEG	PRESS
APLOT	MAP	QUINT
BASCOR	MAXARR	SHEAR
BIGMAX	MOMENT	SPLINE
CRUNCH	PAGE	SUBU
DERIV	PAPLOT	YDISP

The following called subroutines are system subroutines of the IBM 370/3032 system at the Booth Computing Center of Caltech.

EQSOV - System of equations solving routine.

LSQUAR - Polynomial least-squares fitting routine.

SYSSYM* - Symbol plotting routine.

VLABEL* - Axis/axis label plotting routine.

XYPLOT* - Line plotting routine.

XYPLT* - Point Plotting routine.

*Calcomp plotter.

MAIN

```
C       MAIN PROGRAM
C       ************
C       PROGRAM TO DETERMINE PARAMETERS OF MODEL AND PROTOTYPE
C       RETAINING STRUCTURES BASED ON CENTRIFUGE EXPERIMENTS
C
        COMMON/RED/A(1502,12),T(1502),AX(112),BX(112),CALI(15,2),X(10),
       X          TCALI,ITM,NT,NA,NPOLY,NS2,NINT,R,EIM,HTM,AGS,GAMMAM,
       X          NTYPE,FIM,NC,XP(5)
        COMMON/GREEN/CMAX(2),CMIN(2),IPLTCD
        COMMON/BLACK/DIS(1502,3)
        COMMON/PINK/A1(1502),A2(1502)
        COMMON/ORANGE/TCPI,TCPF,BCTI,BCTF,NC
        COMMON/GRAY/TITLE1(18),TITLE2(18)
        DIMENSION DIS1(2,3)
C
        READ 101,TITLE1,TITLE2
        READ 102,OMEGA,SO,EIM,HTM,FIM,GAMMA,NPOLY,NSR4,NINT,NTYPE
        NS2=NSR4+1
        READ 103,(X(I),I=2,NS2)
        READ 104,NC
        NPR=NC+1
        IF(NPR.EQ.1)NPR=2
        READ 103,(XP(I),I=2,NPR)
C
C       OMEGA  = RPM AT WHICH CENTRIFUGE OPERATES
C       SO     = DISTANCE FROM AXIS OF CENTRIFUGE ROTATION TO TOP OF MODEL
C                WALL (IN)
C       EIM    = EI OF MODEL WALL (LB-IN**2/IN)
C       HTM    = HEIGHT OF MODEL WALL (IN)
C       FIM    = FUNDAMENTAL FREQUENCY OF MODEL WALL (HZ)
C       GAMMA  = UNIT WEIGHT OF PROTOTYPE (AND MODEL) SOIL AT 1G (PCF)
C       NPOLY  = ORDER OF POLYNOMIAL DESIRED FOR LEAST-SQUARES FIT OF DATA
C                MUST BE GE.3 AND LE.(NSR4+1)
C       NSR4   = NUMBER OF STRAIN GAGE LOCATIONS AT THE CENTER OF MODEL
C                WALL (VERTICAL AXIS)
C       NINT   = NUMBER OF DESIRED INTERVALS FOR WHICH RESULTS ARE WANTED
C                ALONG THE WALL
C       NTYPE  = TYPE OF WALL
C                NTYPE=0  CANTILEVER WALL
C                NTYPE=1  SHEET PILE WALL
C       X(I)   = LOCATIONS OF STRAIN GAGES FROM TOP TO BOTTOM
C       NC     = NUMBER OF PRESSURE TRANSDUCERS
C       XP(I)  = LOCATIONS OF PRESSURE TRANSDUCERS FROM TOP TO BOTTOM
C
        NS2=NS2+1
        X(1)=0.0
        X(NS2)=HTM
        NSR4A=NS2
        NPR=NPR+1
        XP(1)=0.0
        XP(NPR)=HTM
C
C       DETERMINE GRAVITATIONAL ACCELERATION (AGS)
C
        R=SO+(HTM/2.0)
        AGS=0.000028394*R*(OMEGA**2)
```

```
C
      ANINT=FLOAT(NINT)
      H=HTM/ANINT
      ANINT=ANINT+1.0
      NINT=NINT+1+3
      AX(1)=0.0
      DO 10 I=2,NINT
   10 AX(I)=AX(I-1)+H
      DO 11 I=1,NINT
   11 EX(I)=-AX(I)/HTM
      EI=EIM*AGS**3
      HT=HTM*AGS
      F1=F1M/AGS
      GAMMAM=GAMMA*AGS
      GAMMA=GAMMA/1728.0
      GAMMAM=GAMMAM/1728.0
C
      CALL DIGIT
C
      NINTT=NINT-3
      GAMMA1=GAMMAM*1728.0
      GAMMA2=GAMMA*1728.0
      PRINT 200
      PRINT 201,TITLE1,TITLE2
      PRINT 202,OMEGA,SG,R,AGS,HTM,HT,EIM,EI,F1M,F1,GAMMA1,GAMMA2,
     XNPCLY,NINTT,NA,NSR4,NQ
      PRINT 214,ITM
C
      IF(NA.EQ.0)GO TO 21
      DO 20 I=1,ITM
      DO 20 J=1,NA
   20 A(I,J)=-A(I,J)*386.22
C
   21 DO 22 I=1,NS2
   22 X(I)=X(I)/HTM
      IF(NA.EQ.0)GO TO 24
      PRINT 203
      DO 23 I=1,NA
   23 PRINT 204,I,(CALI(I,J),J=1,2)
   24 PRINT 205
      DO 25 I=1,NSR4
      K=I+NA
      L=I+1
   25 PRINT 206,I,(CALI(K,J),J=1,2),X(L)
      DO 26 I=1,NSR4A
   26 X(I)=X(I)*HTM
C
      IF(NQ.NE.0)GO TO 61
   27 IF(NC.EQ.0)GO TO 29
      PRINT 207
      DO 28 I=1,NC
      K=NT+I+NC
   28 PRINT 204,I,(CALI(K,J),J=1,2)
   29 PRINT 208,TCALI
C
C     CMIN(I),CMAX(I) / I=1 LOCATION   I=2 TIME
```

MAIN

```
C       IPLTCD = TIME PLOT CODE
C       IPLTCD = 0 FIRST 20% OF TIME PLOT IS AMPLIFIED
C       IPLTCD = 1 REGULAR LINEAR TIME PLOT
C
        READ 105,CMIN(1),CMAX(1),CMIN(2),CMAX(2),IPLTCD
C
C       CALL MOMENT
        IF(NC.NE.0)GO TO 70
        CALL SHEAR
        CALL PRESS
C
     30 IF(NA.EQ.0)GO TO 37
C
C       FIND DISPLACEMENTS BY INTEGRATING ACCELEROMETER RECORDS
C       THERE IS A BASELINE CORRECTION OF THE ACCELEROGRAPHS
C
        DIS1(1,1)=TOPI
        DIS1(2,1)=TOPF
        DIS1(1,2)=BOTI
        DIS1(2,2)=BOTF
        DIS1(1,3)=0.0
        DIS1(2,3)=0.0
        DO 31 J=1,NA
     31 CALL BASCOR(J)
        DO 34 J=1,NA
        DO 32 I=1,ITM
     32 A1(I)=A(I,J)
        CALL INTEG(ITM,T,A1,A2,0)
        CALL INTEG(ITM,T,A2,A1,0)
        CCCC=(DIS1(2,J)-DIS1(1,J)+A1(1)-A1(ITM))/(T(ITM)-T(1))
        DDDD=DIS1(1,J)-A1(1)-CCCC*T(1)
        DO 33 I=1,ITM
     33 DIS(I,J)=A1(I)+CCCC*T(I)+DDDD
     34 CONTINUE
C
        IF(NA.NE.1)GO TO 36
        DO 35 J=2,3
        DO 35 I=1,ITM
     35 DIS(I,J)=0.0
     36 CONTINUE
C
     37 CALL MDISP
C
        IF(NA.EQ.0)GO TO 39
        DO 38 I=1,ITM
        DO 38 J=1,NA
        A(I,J)=A(I,J)/(AGS*386.22)
     38 DIS(I,J)=DIS(I,J)/FTM
     39 DO 40 I=1,ITM
     40 T(I)=T(I)*FIM
C
C       PLOT AND PRINT OUT ACCELEROGRAPH AND DISPLACEMENT RECORDS
C
        IF(NA.EQ.0)GO TO 47
        CALL APLOT
        DO 46 N=1,30
```

```
      PRINT 200
      PRINT 210
      L=N*50
      DO 45 J=1,50
      I=(L-50)+J
      IF(I.GT.ITM)GO TO 47
      IF(NA.EQ.1)GO TO 44
      IF(NA.EQ.2)GO TO 43
      PRINT 211,I,T(I),A(I,1),DIS(I,1),A(I,2),DIS(I,2),A(I,3),DIS(I,3)
      GO TO 45
   43 PRINT 212,I,T(I),A(I,1),DIS(I,1),A(I,2),DIS(I,2)
      GO TO 45
   44 PRINT 213,I,T(I),A(I,1),DIS(I,1)
   45 CONTINUE
   46 CONTINUE
   47 CONTINUE
      GO TO 77
C
   61 DO 64 I=1,NPP
   64 XP(I)=XP(I)/FTM
      PRINT 209
      DO 66 I=1,NG
      K=I+NT
      L=I+1
   66 PRINT 206,I,(CALI(K,J),J=1,2),XP(L)
      DO 67 I=1,NPP
   67 XP(I)=XP(I)*FTM
      GO TO 27
C
   70 CALL PRESS
      CALL SHEAR
      CALL MOMENT
      GO TO 30
C
   77 CONTINUE
C
  101 FORMAT(18A4/18A4)
  102 FORMAT(6F10.0,4I5)
  103 FORMAT(8F10.0)
  104 FORMAT(I5)
  105 FORMAT(4F10.0,I5)
C
  200 FORMAT(1H1)
  201 FORMAT( 9X,18A4,/,9X,18A4,/,9X,'************************************
     X***************************************')
  202 FORMAT(//,1X,'CENTRIFUGE RPM=',31X,F8.2,
     X/,1X,'DISTANCE FROM CENTRIFUGE AXIS TO TOP OF WALL=',F9.2,1X,
     X'INCHES',
     X/,1X,'DISTANCE FROM CENTRIFUGE AXIS TO MIDDLE OF WALL=',F6.2,1X,
     X'INCHES',
     X/,1X,'GRAVITATIONAL ACCELERATION AT MIDDLE OF WALL=',F9.2,1X,
     X'G-S',//,
     X/,1X,'MODEL WALL HEIGHT=',F19.2,1X,'INCHES',15X,'PROTOTYPE WALL HE
     XIGHT=',F19.2,1X,'INCHES',
     X/,1X,'MODEL WALL EI=',F23.2,1X,'LB-IN**2/IN',10X,'PROTOTYPE WALL E
     XI=',F23.2,1X,'LB-IN**2/IN',
```

MAIN

```
                 X/,1X,'MODEL FUNDAMENTAL FREQUENCY=',F9.2,1X,'HERTZ',16X,'PROTOTYPE
                 X FUNDAMENTAL FREQUENCY=',F9.2,1X,'HERTZ',
                 X/,1X,'DENSITY OF MODEL SOIL=',F15.2,1X,'PCF',18X, 'DENSITY OF PROT
                 XOTYPE SOIL=',F15.2,1X,'PCF',//,
                 X/,1X,'ORDER OF POLYNOMIAL IN LEAST-SQUARES FIT=',15X,I2,
                 X/,1X,'NUMBER OF POINTS AT WHICH DATA EVALUATION TAKES PLACE=',I4,
                 X///,1X,'NUMBER OF ACCELEROMETERS=',I3,
                 X/,1X,'NUMBER OF STRAIN GAGES=',I5,
                 X/,1X,'NUMBER OF PRESSURE GAGES=',I3)
0151          203 FORMAT(//,1X,'CALIBRATION FACTORS OF TRANSDUCERS',
                 X/,1X,'**********************************',/,
                 X/,1X,'ACCELEROMETER',11X,'SLOPE',9X,'Y-INTERCEPT',
                 X/,1X,'-------------',11X,'-----',9X,'-----------')
0152          204 FORMAT(6X,I2,2X,2E20.3)
0153          205 FORMAT(/,1X,'STRAIN GAGE',13X,'SLOPE',9X,'Y-INTERCEPT',
                 X12X,'LOCATION',
                 X        /,1X,'-----------',13X,'-----',9X,'-----------',
                 X12X,'--------')
0154          206 FORMAT(6X,I2,2X,2E20.3)
0155          207 FORMAT(/,1X,' DELTA BEAM',13X,'SLOPE',9X,'Y-INTERCEPT',
                 X        /,1X,' ----------',13X,'-----',9X,'-----------')
0156          208 FORMAT(/,1X,'TIME CALIBRATION SCALE=',E10.3)
0157          209 FORMAT(/,1X,'PRESSURE GAGE',11X,'SLOPE',9X,'Y-INTERCEPT',
                 X12X,'LOCATION',
                 X        /,1X,'-------------',11X,'-----',9X,'-----------',
                 X12X,'--------')
0158          210 FORMAT(     21X,'ACCELEROMETER NO.1 (TOP OF WALL)',
                 X              5X,'ACCELEROMETER NO.2 (BASE OF WALL)',
                 X              7X,'ACCELEROMETER NO.3 (FREE FIELD)',/,
                 X             21X,'********************************',
                 X              5X,'*********************************',
                 X              7X,'*******************************',/,
                 X1X,'TIME',    ' DIMENSIONLESS',3X,'DIMENSIONLESS',6X,'DIMENSIONLESS'
                 X           ,6X,'DIMENSIONLESS',6X,'DIMENSIONLESS',6X,'DIMENSIONLESS'
                 X           ,6X,'DIMENSIONLESS',/,1X,'STEP',1X,'TIME (T*F1)',
                 X2X,'ACCELERATION (A/G) DISPLACEMENT (Y/H)',
                 X1X,'ACCELERATION (A/G) DISPLACEMENT (Y/H)',
                 X1X,'ACCELERATION (A/G) DISPLACEMENT (Y/H)',/,
                 X1X,'---- ------------ ----------------- ----------------- ------
                 X------------',1X,    '----------------- ----------------- ------
                 X------------')
0159          211 FORMAT(1X,I4,E13.3,6E19.3)
0160          212 FORMAT(1X,I4,E13.3,4E19.3)
0161          213 FORMAT(1X,I4,E13.3,2E19.3)
0162          214 FORMAT(1X,'NUMBER OF TIME STEPS=',I7,/)
            C
0163              STOP
0164              END
```

ALGEQN

```
      SUBROUTINE ALGEQN(N,A,B,Y)
C
C     SUBROUTINE CALLED IN SPLINE
C
      DIMENSION A(1500,3),U(1500,3),D(1500,3),B(1),Y(1)
C
      U(1,2)=A(1,2)
      U(1,3)=A(1,3)
      Y(1)=B(1)
      DO 23 I=2,N
      I1=I-1
      D(I,2)=1.0
      U(I,3)=A(I,3)
      D(I,1)=A(I,1)/U(I1,2)
      U(I,2)=A(I,2)-D(I,1)*U(I1,3)
      IF(ABS(U(I,2)).LT.1.0E-09)GO TO 35
   20 CONTINUE
   23 Y(I)=B(I)-D(I,1)*Y(I1)
      Y(N)=Y(N)/U(N,2)
      I=N
   25 I1=I-1
      Y(I1)=(Y(I1)-U(I1,3)*Y(I))/U(I1,2)
      I=I-1
      IF(I.EQ.1)GO TO 31
      GO TO 25
   31 RETURN
   35 PRINT 107
C
  107 FORMAT(//5X'A IS A MATRIX WHICH REQUIRE PIVOTING OR IS SINGULAR')
C
      RETURN
      END
```

APLOT

```
      SUBROUTINE APLOT
C
C     SUBROUTINE TO PLOT ACCELEROGRAPHS AND CORRESPONDING DISPLACEMENTS
C
      COMMON/RED/A(1502,12),T(1502),AX(112),BX(112),CALI(15,2),X(10),
     X         TCALI,ITM,NT,NA,NPOLY,NS2,NINT,F,EIM,FTM,AGS,GAMMAM,
     X         NTYPE,F1M,NC,XP(5)
      COMMON/BLACK/DIS(1502,3)
      COMMON/PINK/A1(1502),A2(1502)
      COMMON/GRAY/TITLE1(18),TITLE2(18)
      DIMENSION AA(2),BB(2),CCC(3),AMXX(3),DMXX(3),MAXX(3),MDXX(3),
     X         AAA(1),BBB(1)
C
C     AMIN=-AMAX
C     YMIN=-YMAX
C
      READ 270,TMIN,TMAX,AMIN,AMAX,YMIN,YMAX
C
      DO 105 J=1,NA
      DO 104 I=1,ITM
      A1(I)=A(I,J)
  104 A2(I)=DIS(I,J)
      CALL BIGMAX(A1,ITM,AMXX(J),MAXX(J))
  105 CALL BIGMAX(A2,ITM,DMXX(J),MDXX(J))
C
      CINTT=(ABS(TMAX-TMIN))/8.0
      CINTA=(ABS(AMAX-AMIN))/2.5
      CINTY=(ABS(YMAX-YMIN))/2.5
      TMN=-1.75*CINTT
      TMX=13.25*CINTT
      AMN=-6.25*CINTA
      AMX= 3.75*CINTA
      YMN=-2.75*CINTY
      YMX= 7.25*CINTY
C
      DO 125 I=1,3
  125 CCC(I)=0.0
C
      K=10
      DO 160 I=1,NA
      CALL VLABEL(1.75,1.5,TMIN,TMAX,8.0,K,'TIME   (T*F1)',12,0,'(F4.1)',
     X4)
      CALL SYSSYM(2.75,4.275,0.1,TITLE1,72,0.0)
      CALL SYSSYM(2.75,4.125,0.1,TITLE2,72,0.0)
      IF(I.NE.1)GO TO 131
      CALL VLABEL(1.75,5.0,TMIN,TMAX,8.0,K,'ACCELEROMETER NO.1  (TOP OF
     XWALL)',33,0,'(F4.1)',4)
  131 CONTINUE
      IF(I.NE.2)GO TO 132
      CALL VLABEL(1.75,5.0,TMIN,TMAX,8.0,K,'ACCELEROMETER NO.2  (BOTTOM
     XOF WALL)',36,0,'(F4.1)',4)
  132 CONTINUE
      IF(I.NE.3)GO TO 133
      CALL VLABEL(1.75,5.0,TMIN,TMAX,8.0,K,'ACCELEROMETER NO.3  (FREE FI
     XELD)',32,0,'(F4.1)',4)
  133 CONTINUE
```

APLOT

```
      CALL VLABEL(1.75,1.5,YMIN,YMAX,2.5,2,'DISP  (Y/M)',11,1,
     X'(F5.2)',5)
      CALL VLABEL(1.75,5.0,AMIN,AMAX,2.5,4,'ACCEL  (A/G)',12,1,
     X'(F4.1)',4)
C
      CALL PAGE
      LAB=0
      AA(1)=1.75
      AA(2)=9.75
      BB(1)=2.75
      BB(2)=2.75
      CALL XYPLOT(2,AA,BB,0.0,15.0,0.0,10.0,DDD,LAB)
      BB(1)=4.0
      BB(2)=4.0
      CALL XYPLOT(2,AA,BB,0.0,15.0,0.0,10.0,DDD,LAB)
      BB(1)=6.25
      BB(2)=6.25
      CALL XYPLOT(2,AA,BB,0.0,15.0,0.0,10.0,DDD,LAB)
      BB(1)=7.5
      BB(2)=7.5
      CALL XYPLOT(2,AA,BB,0.0,15.0,0.0,10.0,DDD,LAB)
      AA(1)=9.75
      BB(1)=1.5
      BB(2)=4.0
      CALL XYPLOT(2,AA,BB,0.0,15.0,0.0,10.0,DDD,LAB)
      BB(1)=5.0
      BB(2)=7.5
      CALL XYPLOT(2,AA,BB,0.0,15.0,0.0,10.0,DDD,LAB)
C
      DO 136 J=1,ITM
      A1(J)=A(J,I)
  136 A2(J)=DIS(J,I)
      AAA(1)=AMXX(I)
      BBB(1)=T(MAXX(I))
      CALL XYPLT(1,BBB,AAA,TMN,TMX,AMN,AMX,DDD,LAB,1)
      AAA(1)=DMXX(I)
      BBB(1)=T(MDXX(I))
      CALL XYPLT(1,BBB,AAA,TMN,TMX,YMN,YMX,DDD,LAB,1)
      CALL XYPLOT(ITM,T,A1,TMN,TMX,AMN,AMX,DDD,LAB)
      LAB=-1
      CALL XYPLOT(ITM,T,A2,TMN,TMX,YMN,YMX,DDD,LAB)
  160 CONTINUE
C
  270 FORMAT(6F10.0)
C
      RETURN
      END
```

BASCOR

```
      SUBROUTINE BASCOR(J)
C
C     SUBROUTINE TO CORRECT ACCELEROGRAPHS WITH RESPECT TO THE BASELINE
C
      COMMON/RED/A(1502,12),T(1502),AX(112),BX(112),CALI(15,2),X(10),
     X           TCALI,ITM,NT,NA,NPOLY,NS2,NINT,F,EIM,FTM,AGS,GAMMAM,
     X           NTYPE,FIM,NC,XP(9)
      COMMON/BLACK/DIS(1502,3)
      REAL*8 STOR(2,7)
      DIMENSION DATA(3,1502),C(2)
      EQUIVALENCE (DIS,DATA)
C
      IF(J.GT.1)GO TO 440
      DO 436 I=1,ITM
  436 DATA(3,I)=1.0
  440 DO 444 I=1,ITM
      DATA(1,I)=T(I)
  444 DATA(2,I)=A(I,J)
      CHISQ=0.0
C
      CALL LSQUAR(DATA,ITM,2,C,CHISQ,STOR)
C
      DO 446 I=1,ITM
  446 A(I,J)=A(I,J)-(C(1)+C(2)*T(I))
C
      RETURN
      END
```

BIGMAX

```
      SUBROUTINE BIGMAX(A,K,AMAX,KMAX)
C
C     SUBROUTINE TO PICK OUT LARGEST VALUE OF A ONE DIMENSIONAL ARRAY A(K)
C
      DIMENSION A(1)
C
      AMAX=0.0
      DO 770 I=1,K
      IF(ABS(A(I)).GT.ABS(AMAX))GO TO 765
      GO TO 770
  765 AMAX=A(I)
      KMAX=I
  770 CONTINUE
C
      RETURN
      END
```

CRUNCH

```
      SUBROUTINE CRUNCH
C
C     SUBROUTINE TO SORT OUT PARAMETERS FROM TIME-SPACE ARRAY XX FOR
C     PLOTTING AND OUTPUT
C     PARAMETERS CHOSEN ARE STATIC,MAXIMUM DYNAMIC,AND FINAL STATIC
C
      COMMON/RED/A(1502,12),T(1502),AX(112),BX(112),CALI(15,2),X(10),
     X             TCALI,ITM,NT,NA,NPOLY,NS2,NINT,F,EIM,FTM,AGS,GAMMAM,
     X             NTYPE,FIM,NC,XP(5)
      COMMON/BLUE/X1(112),X2(112),X3(112),TT(1502),XX(1502,112),XM(1),
     X              YM(1),TM(1),ITMAX,IXMAX
C
C     FIND MAXIMUM PARAMETER AND CORRESPONDING TIME AND LOCATION
C
      NINTT=NINT-3
      CALL MAXARR(XX,ITM,NINTT,XXMAX,ITMAX,IXMAX)
C
      DO 140 I=1,NINT
      X1(I)=XX(1,I)
      X2(I)=XX(ITMAX,I)
  140 X3(I)=XX(ITM,I)
      XM(1)=XXMAX
      YM(1)=-AX(IXMAX)/FTM
      TM(1)=T(ITMAX)*FIM
      DO 141 I=1,ITM
  141 TT(I)=XX(I,IXMAX)
C
      RETURN
      END
```

DERIV

```
0001          SUBROUTINE DERIV(N,H,Y,DY)
         C
         C    SUBROUTINE TO NUMERICALLY DIFFERENTIATE A SET OF N POINTS (X,Y)
         C    USING A 4TH ORDER FINITE DIFFERENCE SCHEME
         C
0002          DIMENSION Y(1),DY(1)
         C
0003          N=N-2
0004          DO 2 I=1,2
0005        2 DY(I)=(-50.0*Y(I)+96.0*Y(I+1)-72.0*Y(I+2)+32.0*Y(I+3)-6.0*Y(I+4))/
             X(24.0*H)
0006          DO 4 I=3,N
0007        4 DY(I)=(Y(I-2)-8.0*Y(I-1)+8.0*Y(I+1)-Y(I+2))/(12.0*H)
0008          N=N+2
0009          M=N-1
0010          DO 6 I=M,N
0011        6 DY(I)=(50.0*Y(I)-96.0*Y(I-1)+72.0*Y(I-2)-32.0*Y(I-3)+6.0*Y(I-4))/
             X(24.0*H)
         C
0012          RETURN
0013          END
```

DIGIT

```
      SUBROUTINE DIGIT
C
C     SUBROUTINE TO READ AND SCALE VALUES FROM THE DIGITIZER (FORMAT(10I8))
C
      COMMON/RED/A(1502,12),T(1502),AX(112),BX(112),CALI(15,2),X(10),
     X           TCALI,ITM,NT,NA,NPOLY,NS2,NINT,H,EIM,HTM,AGS,GAMMAM,
     X           NTYPE,FIM,NC,XP(5)
      COMMON/BLUE/X1(112),X2(112),X3(112),TT(1502),XX(1502,112),XM(1),
     X            YM(1),TM(1),ITMAX,IXMAX
      COMMON/PINK/A1(1502),A2(1502)
      COMMON/CRANGE/TCPI,TCPF,PCTI,ECTF,NC
      REAL*8 STOR(2,7)
      DIMENSION IA(1502,12),IT(1502),IXBASE(21),IYBASE(21),XBASE(21),
     X          YBASE(21),DATA(3,21),C(2),TMAX(12),ITMM(12),ICHECK(12)
      EQUIVALENCE (IA,A),(IT,T),(IXBASE,XBASE),(IYBASE,YBASE)
C
C     NA=NUMBER OF ACCELEROMETERS (UP TO 3)
C     NC=NUMBER OF CANTILEVER DISPLACEMENT TRANSDUCERS (UP TO 2)
C     NP=NUMBER OF PRESSURE TRANSDUCERS
C     NT=NUMBER OF TRACES DIGITIZED (UP TO 12)=ACCELEROMETERS + STRAIN GAGES
C                                          + PRESSURE TRANSDUCERS
C     CALI(I,J)=CALIBRATION FACTORS FOR EACH TRACE
C              CALI(I,1)=SLOPE OF CALIBRATION
C              CALI(I,2)=Y-INTERCEPT OF CALIBRATION
C              Y=CALI(I,1)*X+CALI(I,2)
C     A(I,J) IS THE ARRAY OF DIGITIZED POINTS
C     TCALI=TIME CALIBRATION SCALE
C
      READ 501,NA,NS,NP,NC
      NT=NA+NS+NP
      N=NT+NC
      READ 502,((CALI(I,J),J=1,2),I=1,N),TCALI
C
C     SET UP DIGITIZER COORDINATES WITH FIXED TRACE
C
      DO 305 J=1,5
      I1=(5*J)-4
      I2=I1+4
      READ 503,((IXBASE(I),IYBASE(I)),I=I1,I2)
      DO 302 K=I1,I2
      IF(IXBASE(K).EQ.999999)GO TO 306
      XBASE(K)=FLOAT(IXBASE(K))
  302 YBASE(K)=FLOAT(IYBASE(K))
  305 CONTINUE
  306 KK=K-1
      DO 307 I=1,KK
      DATA(1,I)=XBASE(I)
      DATA(2,I)=YBASE(I)
  307 DATA(3,I)=1.0
      CHISQ=0.0
C
      CALL LSQUAR(DATA,KK,2,CHISQ,STOR)
C
      AC=XBASE(1)
      BC=C(1)+(XBASE(1)*C(2))
      CC=XBASE(KK)
```

DIGIT

```
      DC=C(1)+(XBASE(KK)*C(2))
      HYPO=((DC-AC)**2)+((DC-BC)**2)
      HYPO=SQRT(HYPO)
      SINW=(DC-BC)/HYPO
      COSW=(DC-AC)/HYPO
C
C     READ IN DIGITIZED TRACES
C
      DO 380 J=1,NT
      DO 311 K=1,300
      I1=(5*K)-4
      I2=I1+4
      READ 503,((IT(I),IA(I,J)),I=I1,I2)
      DO 310 L=I1,I2
      IF(IT(L).EQ.999999)GO TO 312
      XX(L,J)=FLOAT(IT(L))
  310 A(L,J)=FLOAT(IA(L,J))
  311 CONTINUE
  312 ITM=L-1
C
C     BASELINE CORRECTION
C
      DO 315 I=1,ITM
      XC=XX(I,J)
      YC=A(I,J)
      XX(I,J)=((XC-AC)*COSW)+((YC-BC)*SINW)
  315 A(I,J)=-((XC-AC)*SINW)+((YC-BC)*COSW)
C
C     THE XX(I,J) ARRAY STORES TIME VALUES TEMPORARILY
C
C     * * * * * * * * * * * * * * * * * * * * * * * * * * * * * * * * * *
C     * A(1,J) WILL BE THE SET OF TRACES AT ONE G (STATIC)              *
C     * A(2,J) WILL BE THE SET OF TRACES AT MULTIPLE G (STATIC)         *
C     * FROM A(3,J) ON, THE TRACES WILL BE FROM THE DYNAMIC PORTION      *
C     * * * * * * * * * * * * * * * * * * * * * * * * * * * * * * * * * *
C
      ICHECK(J)=0
      XX(1,J)=0.0
      XX(2,J)=0.0
      IF(ITM.LE.2) GO TO 349
      DO 340 I=4,ITM
  340 XX(I,J)=XX(I,J)-XX(3,J)
      XX(3,J)=0.0
      DO 348 I=4,ITM
      IF(XX(I,J).LE.XX(I-1,J))GO TO 343
      GO TO 348
  343 ICHECK(J)=ICHECK(J)+1
      PRINT 600,J,ICHECK(J),I,XX(I-1,J),XX(I,J)
  348 CONTINUE
  349 CONTINUE
C
      IF(J.GT.NA)GO TO 354
      DO 350 I=3,ITM
  350 A(I,J)=A(I,J)-A(2,J)
      A(1,J)=0.0
      A(2,J)=0.0
```

```
          GO TO 357
      354 CONTINUE
          DO 355 I=2,ITM
      355 A(I,J)=A(I,J)-A(1,J)
          A(1,J)=0.0
      357 CONTINUE
C
C         SCALE RECORDS
C
          DO 360 I=1,ITM
          XX(I,J)=TCALI*XX(I,J)
      360 A(I,J)=A(I,J)*CALI(J,1)+CALI(J,2)
C
C         MODEL PARAMETERS HAVE NOW BEEN SCALED
C
          IF(NA.EQ.0)GO TO 370
          ITM1=ITM-2
          DO 365 I=1,ITM1
          XX(I,J)=XX(I+2,J)
      365 A(I,J)=A(I+2,J)
          ITM=ITM1
          GO TO 375
C
      370 ITM=1
          A(1,J)=A(2,J)
      375 CONTINUE
          TMAX(J)=XX(ITM,J)
          ITMM(J)=ITM
      380 CONTINUE
C
          DO 381 I=1,NT
          IF(ICHECK(I).NE.0)STOP
      381 CONTINUE
C
          CALL BIGMAX(TMAX,NT,TMX,IDUM)
          TMX=TMX*FIM
          IF(TMX.GE.3.0)GO TO 383
          ITM=(TMX*150.0)+1.0
          ITM=ITM+1
          T(1)=0.0
          DO 382 I=2,ITM
      382 T(I)=(FLOAT(I-1)/150.0)/FIM
          GO TO 388
      383 ITM=((TMX-3.0)*75.0)+451.0
          ITM=ITM+1
          T(1)=0.0
          DO 384 I=2,450
      384 T(I)=(FLOAT(I-1)/150.0)/FIM
          DO 385 I=451,ITM
      385 T(I)=(FLOAT(I-226)/75.0)/FIM
          IF(ITM.LE.1500)GO TO 388
          PRINT 601,ITM
          ITM=1500
C
C         SMOOTH CUT DATA WITH CUBIC SPLINE
C
```

DIGIT

```
      388 DO 397 J=1,NT
          ITS=ITMP(J)
          DO 395 I=1,ITS
          A1(I)=XX(I,J)
      395 A2(I)=A(I,J)
          CALL SPLINE(ITS,A1,A2,ITM,T,TT)
          DO 396 I=1,ITM
      396 A(I,J)=TT(I)
      397 CONTINUE
C
C         READ IN INITIAL AND FINAL DIGITIZED DISPLACEMENT VALUES
C         AT TOP AND BOTTOM OF WALL
C
          READ 503,ITOPI,ITOPF,IBOTI,IBOTF
          TOPI=FLOAT(ITOPI)
          TOPF=FLOAT(ITOPF)
          BOTI=FLOAT(IBOTI)
          BOTF=FLOAT(IBOTF)
          M1=NT+1
          M2=NT+2
          IF(NC.EQ.0)GO TO 399
          TOPI=TOPI*CALI(M1,1)+CALI(M1,2)
          TOPF=TOPF*CALI(M1,1)+CALI(M1,2)
          IF(NC.EQ.1)GO TO 399
          BOTI=BOTI*CALI(M2,1)+CALI(M2,2)
          BOTF=BOTF*CALI(M2,1)+CALI(M2,2)
      399 CONTINUE
          NT=NA+NS
C
      501 FORMAT(4I5)
      502 FORMAT(8F10.0)
      503 FORMAT(10I8)
C
      600 FORMAT(1X,'***ERROR*** - TRACE J=',I3,' ICHECK(J)=',I3,' I=',I4,
         X' XX(I-1,J)=',F10.2,' XX(I,J)=',F10.2)
      601 FORMAT(1H1,1X,'ACTUAL NUMBER OF TIME STEPS WAS ',I4,/,1X,
         X'ONLY FIRST 1500 TIME STEPS COULD BE USED DUE TO STORAGE LIMITS')
C
          RETURN
          END
```

INTEG

```
      SUBROUTINE INTEG(N,X,Y,SY,K)
C
C     SUBROUTINE TO NUMERICALLY INTEGRATE A SET OF N DATA POINTS (X,Y)
C     OVER A PRESCRIBED INTERVAL USING THE TRAPEZOIDAL RULE
C     THE INTEGRAL BETWEEN X(1) AND X(I) WILL BE EVALUATED AT EACH STEP I
C     K=0   ORDER OF INTEGRATION MAINTAINED
C     K=1   ORDER OF INTEGRATION REVERSED
C
      DIMENSION Y(1),SY(1),X(1)
C
      IF(K.EQ.1)GO TO 5
      NN=N
      SY(1)=0.0
      DO 1 I=2,NN
    1 SY(I)=SY(I-1)+((X(I)-X(I-1))/2.0)*(Y(I)+Y(I-1))
      GO TO 9
C
    5 NN=N-1
      SY(N)=0.0
      DO 6 J=1,NN
      I=N-J
    6 SY(I)=SY(I+1)+((X(I+1)-X(I))/2.0)*(Y(I)+Y(I+1))
    9 CONTINUE
C
      RETURN
      END
```

MAP

```
      SUBROUTINE MAP(X,Y,Z,XMAX,XMIN,YMAX,YMIN,ZMAX,ZMIN,NXX,NYY,NCTR)
C
C     SUBROUTINE TO MAKE CONTOUR PLOTS OF A RECTANGULAR GRID CONTAINING
C     COORDINATES (X,Y) AND CORRESPONDING FUNCTION Z(X,Y)
C
      DIMENSION X(1),Y(1),DDD(3),CTR(61),XX(4),YY(4),ZZ(4),XC(4),YC(4),
     X          XD(1),YD(1),Z(1502,1)
C
      DO 2 I=1,3
    2 DDD(I)=0.0
C
C     SET UP CONTOURS
C
      NCTRS=NCTR-1
      TRS=FLOAT(NCTRS)
      DZ=(ZMAX-ZMIN)/TRS
      CTR(1)=ZMIN
      DO 3 I=2,NCTR
    3 CTR(I)=CTR(I-1)+DZ
C
      LAM=0
      IOPK=-1
      NX=NXX-6
      NY=NYY-2
      DO 50 I=1,NX,6
      XX(1)=X(I)
      XX(2)=X(I+6)
      XX(3)=X(I+6)
      XX(4)=X(I)
      DO 50 J=1,NY,2
      YY(1)=Y(J)
      YY(2)=Y(J)
      YY(3)=Y(J+2)
      YY(4)=Y(J+2)
      ZZ(1)=Z(I,J)
      ZZ(2)=Z(I+6,J)
      ZZ(3)=Z(I+6,J+2)
      ZZ(4)=Z(I,J+2)
      DO 50 K=1,NCTR
C
C     INTERPOLATE
C
    5 L=0
      DO 17 II=1,4
      JJ=MOD(II,4)+1
      IF(CTR(K).GT.ZZ(II))GO TO 7
      IF(CTR(K).GT.ZZ(JJ))GO TO 10
      GO TO 17
    7 IF(CTR(K).LE.ZZ(JJ))GO TO 10
      GO TO 17
   10 L=L+1
      IF(ZZ(II).EQ.ZZ(JJ))GO TO 12
      ZSL=(CTR(K)-ZZ(II))/(ZZ(JJ)-ZZ(II))
      XC(L)=XX(II)+(XX(JJ)-XX(II))*ZSL
      YC(L)=YY(II)+(YY(JJ)-YY(II))*ZSL
      GO TO 17
```

PAF

```
   12 XC(L)=XX(II)
      YC(L)=YY(II)
   17 CONTINUE
C
C     PLOTTING
C
      IF(L.EQ.0)GO TO 50
      IF(L.GT.2)GO TO 40
      CALL XYPLOT(L,XC,YC,XMIN,XMAX,YMIN,YMAX,DLC,LAB)
   40 CONTINUE
   50 CONTINUE
C
      RETURN
      END
```

MAXARR

```
      SUBROUTINE MAXARR(A,KX,KY,AMAX,KXMAX,KYMAX)
C
C     SUBROUTINE TO PICK OUT THE LARGEST ABSOLUTE VALUE OF A
C     TWO-DIMENSIONAL ARRAY A(KX,KY)
C
      DIMENSION A(1502,1)
C
      AMAX=0.0
      DO 770 I=1,KX
      DO 770 J=1,KY
      IF(ABS(A(I,J)).GT.ABS(AMAX))GO TO 765
      GO TO 770
  765 AMAX=A(I,J)
      KXMAX=I
      KYMAX=J
  770 CONTINUE
C
      RETURN
      END
```

MOMENT

```
      SUBROUTINE MOMENT
C
C     SUBROUTINE TO FIND MOMENTS ALONG THE WALL FOR ALL TIME
C     A LEAST-SQUARES POLYNOMIAL FIT WILL BE MADE ON THE STRAIN GAGE DATA
C     WHICH WILL GENERATE BOUNDARY CONDITIONS AT THE BOTTOM OF THE WALL
C     SO THAT A QUINTIC SPLINE FIT CAN BE MADE
C
      COMMON/RED/A(1502,12),T(1502),AX(112),BX(112),CALI(15,2),X(10),
     X           TCALI,ITM,NT,NA,NPOLY,NS2,NINT,H,EIM,HTM,AGS,GAMMAM,
     X           NTYPE,FIM,NC,XP(5)
      COMMON/GREEN/CMAX(2),CMIN(2),IPLTCD
      COMMON/BLUE/X1(112),X2(112),X3(112),TT(1502),XX(1502,112),XM(1),
     X           YM(1),TM(1),ITMAX,IXMAX
      COMMON/YELLOW/TR(112),TS(112)
      REAL*8 STOR(11,25)
      DIMENSION AM(10),EM(10),DATA(3,10),C(11),BC(6),S1(2),S2(2),LS(2),
     X          CCC(3)
      DATA S1/'MOME','NT'/,S2/'M*H/','EI'/,LS/6,6/
C
      READ 701,CMIN,CMAX
C
      NP=NPOLY+1
      NS1=NS2-1
C     GO TO 6500
      IF(NTYPE.NE.1)GO TO 602
      NPT=NS2
      AM(NS2)=0.0
      GO TO 604
  602 NPT=NS1
  604 AM(1)=0.0
      DO 605 I=1,NPT
  605 DATA(3,I)=1.0
      CHISQ=0.0
      DO 606 I=1,3
  606 BC(I)=0.0
C
      DO 650 I=1,ITM
      DO 6509 J=1,NINT
 6509 TR(J)=XX(I,J)
      CALL INTEG(NINT,AX,TR,TS,0)
      AM(2)=TS(26)
      AM(3)=TS(47)
      AM(4)=TS(59)
      AM(5)=TS(69)
C     DO 607 J=2,NS1
C 607 AM(J)=A(I,J+NA-1)
      DO 610 J=2,NPT
      DATA(1,J-1)=X(J)
  610 DATA(2,J-1)=AM(J)
      NPT=NPT-1
C
      CALL LSQUAR(DATA,NPT,NP,C,CHISQ,STOR)
C
      NPT=NPT+1
      DO 616 J=4,6
  616 BC(J)=0.0
```

MOMENT

```
      DO 617 J=1,NS2
  617 AM(J)=0.0
      DO 618 J=2,NS2
      DO 618 K=1,NF
  618 AM(J)=AM(J)+C(K)*X(J)**(K-1)
      IF(NTYPE.EQ.1)AM(NS2)=0.0
C
C     CALCULATE BOUNDARY CONDITIONS AT BOTTOM OF THE WALL
C
      DO 620 J=1,NF
      BC(4)=BC(4)+C(J)*X(NS2)**(J-1)
      BC(5)=BC(5)+FLOAT(J-1)*C(J)*X(NS2)**(J-2)
  620 BC(6)=BC(6)+FLOAT(J-2)*FLOAT(J-1)*C(J)*X(NS2)**(J-3)
      IF(NTYPE.NE.1)GO TO 624
      BC(4)=0.0
C
C     CALCULATE MOMENTS WITH QUINTIC SPLINE
C
  624 CALL QUINT(NS2,X,AM,NINT,AX,TS,BC)
C
      DO 625 J=1,NINT
  625 XX(I,J)=TS(J)*2.0
  651 CONTINUE
C6500 DO 6025 I=1,ITM CCCCCCCCCCC
C     DO 6005 J=1,NINT          C
C6005 TM(J)=XX(I,J)             C
C     CALL INTEG(NINT,AX,TM,TS,0)C
C     DO 6020 J=1,NINT          C
C6020 XX(I,J)=TS(J)             C
C6025 CONTINUE CCCCCCCCCCCCCCCCCC
C
      WRITE(21)XX
      ENDFILE 21
      REWIND 21
      CALL CRUNCH
C
      DO 652 I=1,ITM
      DO 652 J=1,NINT
  652 XX(I,J)=XX(I,J)*HTM/EIM
      DO 655 I=1,NINT
      X1(I)=X1(I)*HTM/EIM
      X2(I)=X2(I)*HTM/EIM
  655 X3(I)=X3(I)*HTM/EIM
      XM(1)=XM(1)*HTM/EIM
      DO 656 I=1,ITM
  656 TT(I)=TT(I)*HTM/EIM
C
      NS0=NS1-1
      DO 658 I=1,NS0
  658 EM(I)=-X(I+1)/HTM
      DO 660 I=1,3
  660 DCC(I)=0.0
      LAB=0
      CINTX=(ABS(CMAX(1)-CMIN(1)))/2.5
      CINTD=(ABS(DMAX-DMIN))/2.5
      YMIN=-4.0*CINTX
```

MOMENT

```
           YMAX= 6.0*CINTX
           XMIN=-7.5*CINTD+CMIN
           XMAX= 7.5*CINTD+CMIN
C          DO 670 J=1,3
C          GO TO (661,663,665),J
C     661  DO 662 I=1,NSO
C     662  AM(I)=2.0*A(1,I+NA)*HTM/EIM
C          GO TO 667
C     663  DO 664 I=1,NSO
C     664  AM(I)=2.0*A(ITMAX,I+NA)*HTM/EIM
C          GO TO 667
C     665  DO 666 I=1,NSO
C     666  AM(I)=2.0*A(ITM,I+NA)*HTM/EIM
C     667  CALL XYPLT(NSO,AM,BM,XMIN,XMAX,YMIN,YMAX,DDD,LAB,2)
C     670  CONTINUE
C
           DO 670 J=1,3
           GO TO (661,663,665),J
      661  AM(1)=X1(26)
           AM(2)=X1(47)
           AM(3)=X1(59)
           AM(4)=X1(68)
           GO TO 667
      663  AM(1)=X2(26)
           AM(2)=X2(47)
           AM(3)=X2(59)
           AM(4)=X2(68)
           GO TO 667
      665  AM(1)=X3(26)
           AM(2)=X3(47)
           AM(3)=X3(59)
           AM(4)=X3(68)
      667  CALL XYPLT(NSO,AM,BM,XMIN,XMAX,YMIN,YMAX,DDD,LAB,2)
      670  CONTINUE
C
           CALL PAPRNT(1)
           CALL PAPLOT(S1,S2,LS,CMIN,CMAX)
C
           DO 680 I=1,ITM
           DO 680 J=1,NINT
      680  XX(I,J)=XX(I,J)*EIM/HTM
C
      701  FORMAT(2F10.0)
C
           RETURN
           END
```

PAGE

```
      SUBROUTINE PAGE
C
C     SUBROUTINE TO SET UP PLOTTING ON AN 8-1/2 X 11 INCH AREA
C
      DIMENSION A(2),B(2),CCC(3)
C
      DO 120 I=1,3
  120 CCC(I)=0.0
      LAB=0
      A(1)=0.0
      A(2)=11.0
      B(1)=0.0
      B(2)=0.0
      CALL XYPLOT(2,A,B,0.0,15.0,0.0,10.0,CCC,LAB)
      A(1)=11.0
      B(2)=8.5
      CALL XYPLOT(2,A,B,0.0,15.0,0.0,10.0,CCC,LAB)
      A(1)=0.0
      A(2)=0.0
      CALL XYPLOT(2,A,B,0.0,15.0,0.0,10.0,CCC,LAB)
      A(2)=11.0
      B(1)=8.5
      CALL XYPLOT(2,A,B,0.0,15.0,0.0,10.0,CCC,LAB)
C
      RETURN
      END
```

PAPLCT

```
      SUBROUTINE PAPLOT(S1,S2,LS,DMIN,DMAX)
C
C     SUBROUTINE TO PLCT OUT,CN A SINGLE 8-1/2 X 11 PAGE A CONTOUR MAP CF
C     A PARAMETER ALCNG WITH PLOTS OF STATIC INITIAL AND FINAL VALUES AS
C     WELL AS MAXIMUM DYNAMIC VALUES
C
      CCMMON/RED/A(1502,12),T(1502),AX(112),BX(112),CALI(15,2),X(10),
     X           TCALI,ITM,NT,NA,NPOLY,NS2,NINT,H,EIM,HTM,AGS,GAMMAM,
     X           NTYPE,FIM,NG,XP(9)
      COMMON/BLUE/X1(112),X2(112),X3(112),TT(1502),XX(1502,112),XM(1),
     X            YM(1),TM(1),ITMAX,IXMAX
      CCMMCN/GREEN/CMAX(2),CMIN(2),IPLTCD
      CCMMCN/GRAY/TITLE1(18),TITLE2(18)
      DIMENSICN S1(1),S2(1),LS(1),DOC(3),AA(2),BB(2),T1(4),T2(3),T3(1),
     X          LT(4),CX(10),CY(10),CZ(10),PX(1),PY(1),TO(1)
      DATA T1/'LOCA','TION','  (X','/H)'/,T2/'TIME','  (T','*F1)'/,
     X     T3/'X/H'/,T4/'T*F1'/,LT/15,12,3,4/,TO/'    '/
C
      DC 701 I=1,3
  701 DCC(I)=0.0
      DC 702 I=1,ITM
  702 T(I)=T(I)*FIM
      NINT=NINT-3
C
      CALL PAGE
      LAB=0
      CALL VLABEL(1.5,2.0,CMAX(1),CMIN(1),5.0,5,T1,LT(1),1,'(F3.1)',3)
      CALL VLABEL(7.5,1.5,CMAX(1),CMIN(1),2.5,2,T3,LT(3),1,'(F3.1)',3)
      CALL VLABEL(7.5,1.5,DMIN,DMAX,2.5,2,S2,LS(2),0,'(F5.2)',5)
      CALL VLABEL(7.5,5.0,DMIN,DMAX,2.5,2,S2,LS(2),1,'(F5.2)',5)
      START=1.5+((5.0-(FLOAT(LS(1))*5.0/12.0))/2.0)
      CALL SYSSYM(START,7.25,0.5,S1,LS(1),0.0)
      CALL SYSSYM(1.0,1.15,0.1,TITLE1,72,0.0)
      CALL SYSSYM(1.0,1.0,0.1,TITLE2,72,0.0)
      IF(IPLTCD.EC.0)GC TO 703
      CALL VLABEL(1.5,2.0,CMIN(2),CMAX(2),5.0,5,T2,LT(2),0,'(F4.1)',4)
      CALL VLABEL(7.5,5.0,CMIN(2),CMAX(2),2.5,2,T4,LT(4),0,'(F4.1)',4)
      GC TO 704
  703 CALL VLABEL(7.5,5.0,CMIN(2),CMAX(2),2.5,1,T4,LT(4),0,'(F4.1)',4)
      CALL VLABFL(1.5,2.0,CMIN(2),CMAX(2),5.0,1,T2,LT(2),0,'(F4.1)',4)
      CC=CMAX(2)-CMIN(2)
      PA=0.2*CC+CMIN(2)
      PB=0.8*CC+CMIN(2)
      PC=0.05*CC+CMIN(2)
      PD=0.15*CC+CMIN(2)
      PE=0.1*CC+CMIN(2)
      PF=0.6*CC+CMIN(2)
      CALL VLABEL(4.0,2.0,PA,PB,1.875,3,TO,4,0,'(F4.1)',4)
      CALL VLABEL(2.125,2.0,PC,PD,1.25,2,TO,4,0,'(F4.1)',4)
      CALL VLABEL(8.125,5.0,PE,PF,1.25,1,TO,4,0,'(F4.1)',4)
      CALL VLABEL(8.75,5.0,PA,PF,0.625,1,TO,4,0,'(F4.1)',4)
C
  704 AA(1)=1.5
      AA(2)=6.5
      BB(1)=7.0
      BB(2)=7.0
```

PAPLOT

```
      CALL XYPLOT(2,AA,BB,0.0,15.0,0.0,10.0,DOC,LAB)
      AA(1)=6.5
      BB(1)=2.0
      CALL XYPLOT(2,AA,BB,0.0,15.0,0.0,10.0,DOC,LAB)
      AA(1)=7.5
      BB(1)=4.0
      AA(2)=10.0
      BB(2)=4.0
      CALL XYPLOT(2,AA,BB,0.0,15.0,0.0,10.0,DOC,LAB)
      AA(1)=10.0
      BB(1)=1.5
      CALL XYPLOT(2,AA,BB,0.0,15.0,0.0,10.0,DOC,LAB)
      AA(1)=7.5
      BB(1)=7.5
      AA(2)=10.0
      BB(2)=7.5
      CALL XYPLOT(2,AA,BB,0.0,15.0,0.0,10.0,DOC,LAB)
      AA(1)=10.0
      BB(1)=5.0
      CALL XYPLOT(2,AA,BB,0.0,15.0,0.0,10.0,DOC,LAB)
C
      IF(IPLTCD.NE.0)GO TO 712
      CA=CC/(2.0*(PA-CMIN(2)))
      CB=(1.0-CA)*CMIN(2)
      DA=CC/(2.0*(CMAX(2)-PA))
      DB=((CMAX(2)+CMIN(2))/2.0)-(DA*PA)
      DO 710 I=1,ITM
      IF(T(I).LT.PA)GO TO 708
      T(I)=(T(I)*DA)+DB
      GO TO 710
  708 T(I)=(T(I)*CA)+CB
  710 CONTINUE
C
  712 NB=NT-NA
      DO 714 I=1,NB
      CX(I)=-X(I+1)/HTM
  714 CY(I)=0.0
      IF(NC.EQ.0)GO TO 718
      DO 717 I=1,NC
  717 CZ(I)=-XP(I+1)/HTM
C
C     SCALE PARAMETERS FOR CONTOUR PLOTTING
C
  718 CINT=(ABS(CMAX(1)-CMIN(1)))/5.0
      XMIN=-7.0*CINT
      XMAX= 3.0*CINT
      CINT=(ABS(CMAX(2)-CMIN(2)))/5.0
      TMIN=-1.5*CINT
      TMAX=13.5*CINT
C
C     PLOT CONTOURS
C
      IF(NC.EQ.0)GO TO 720
      CALL XYPLT(NC,CY,CZ,TMIN,TMAX,XMIN,XMAX,DOC,LAB,4)
  720 CALL XYPLT(NB,CY,CX,TMIN,TMAX,XMIN,XMAX,DOC,LAB,3)
      AA(1)=CMIN(2)
```

PAPLOT

```
      BB(1)=BX(IXMAX)
      AA(2)=CMAX(2)
      BB(2)=BX(IXMAX)
      CALL XYPLOT(2,AA,BB,TMIN,TMAX,XMIN,XMAX,DOC,LAB)
      AA(1)=T(ITMAX)
      BB(1)=-CMIN(1)
      AA(2)=T(ITMAX)
      BB(2)=-CMAX(1)
      CALL XYPLOT(2,AA,BB,TMIN,TMAX,XMIN,XMAX,DOC,LAB)
      PX(1)=T(ITMAX)
      PY(1)=BX(IXMAX)
      CALL XYPLT(1,PX,PY,TMIN,TMAX,XMIN,XMAX,DOC,LAB,1)
      CALL MAP(T,BX,XX,TMAX,TMIN,XMAX,XMIN,DMAX,DMIN,ITM,NINT,21)
C
C     PLOT INITIAL AND FINAL STATIC PARAMETERS AS WELL AS MAXIMUM DYNAMIC ONES
C
      CINTX=(ABS(CMAX(1)-CMIN(1)))/2.5
      CINTT=(ABS(CMAX(2)-CMIN(2)))/2.5
      CINTD=(ABS(DMAX-DMIN))/2.5
      YMIN=-4.0*CINTX
      YMAX= 6.0*CINTX
      XMIN=-7.5*CINTD+DMIN
      XMAX= 7.5*CINTD+DMIN
      CALL XYPLT(1,XM,YM,XMIN,XMAX,YMIN,YMAX,DOC,LAB,1)
      IF(NC.EQ.0)GO TO 722
      CALL XYPLT(NC,CY,CZ,XMIN,XMAX,YMIN,YMAX,DOC,LAB,4)
  722 CALL XYPLT(NB,CY,CX,XMIN,XMAX,YMIN,YMAX,DOC,LAB,3)
      AA(1)=0.0
      AA(2)=0.0
      BB(1)=-CMAX(1)
      BB(2)=-CMIN(1)
      CALL XYPLOT(2,AA,BB,XMIN,XMAX,YMIN,YMAX,DOC,LAB)
      CALL XYPLOT(NINT,X1,BX,XMIN,XMAX,YMIN,YMAX,DOC,LAB)
      CALL XYPLOT(NINT,X2,BX,XMIN,XMAX,YMIN,YMAX,DOC,LAB)
      CALL XYPLOT(NINT,X3,BX,XMIN,XMAX,YMIN,YMAX,DOC,LAB)
      YMIN=-5.0*CINTD+DMIN
      YMAX= 5.0*CINTD+DMIN
      XMIN=-7.5*CINTT
      XMAX= 7.5*CINTT
      IF(IPLTCD.NE.0)GO TO 726
      IF(TM(1).LT.PA)GO TO 725
      TM(1)=(TM(1)*DA)+DB
      GO TO 726
  725 TM(1)=(TM(1)*CA)+CB
  726 CALL XYPLT(1,TM,XM,XMIN,XMAX,YMIN,YMAX,DOC,LAB,1)
      BB(1)=0.0
      BB(2)=0.0
      AA(1)=CMIN(2)
      AA(2)=CMAX(2)
      CALL XYPLOT(2,AA,BB,XMIN,XMAX,YMIN,YMAX,DOC,LAB)
      LAB=-1
      CALL XYPLOT(ITM,T,TT,XMIN,XMAX,YMIN,YMAX,DOC,LAB)
C
      IF(IPLTCD.NE.0)GO TO 734
      PG=(CMAX(2)+CMIN(2))/2.0
      DO 729 I=1,ITM
```

```
      IF(T(I).LT.PG)GO TO 728
      T(I)=(T(I)-CB)/DA
      GC TO 729
  728 T(I)=(T(I)-CB)/CA
  729 CCNTINUE
      IF(TM(I).LT.PG)GC TO 732
      TM(I)=(TM(I)-DB)/DA
      GC TC 734
  732 TM(I)=(TM(I)-CB)/CA
C
  734 DC 735 I=1,ITM
  735 T(I)=T(I)/FIM
      NINT=NINT+3
C
      RETURN
      END
```

PAPRNT

```
      SUBROUTINE PAPRNT(IPARM)
C
C     SUBROUTINE TO PRINT CUT PARAMETERS
C
      COMMON/RED/A(1502,12),T(1502),AX(112),BX(112),CALI(15,2),X(10),
     X          TCALI,ITM,NT,NA,NPOLY,NS2,NINT,H,EIM,HTM,AGS,GAMMAM,
     X          NTYPE,F1M,NC,XP(9)
      COMMON/BLUE/X1(112),X2(112),X3(112),TT(1502),XX(1502,112),XM(1),
     X          YM(1),TM(1),ITMAX,IXMAX
C
      NINT=NINT-3
      TA=T(1)*F1M
      TB=T(ITMAX)*F1M
      TC=T(ITM)*F1M
      DO 61 N=1,3
      PRINT 200
      GO TO(51,52,53,54),IPARM
   51 PRINT 201
      GO TO 57
   52 PRINT 202
      GO TO 57
   53 PRINT 203
      GO TO 57
   54 PRINT 204
   57 PRINT 220,TA,TB,TC
      L=N*50
      DO 60 J=1,50
      I=(L-50)+J
      IF(I.GT.NINT)GO TO 62
      TX=-BX(I)
   60 PRINT 221,I,X1(I),X2(I),X3(I),TX
   61 CONTINUE
   62 CONTINUE
C
      DO 81 N=1,15
      PRINT 200
      GO TO(71,72,73,74),IPARM
   71 PRINT 201
      GO TO 77
   72 PRINT 202
      GO TO 77
   73 PRINT 203
      GO TO 77
   74 PRINT 204
   77 TX=-BX(IXMAX)
      PRINT 222,TX,TX
      L=N*50
      DO 80 J=1,50
      I=(L-50)+J
      K=I+(N-1)*50
      KK=K+50
      IF(KK.GT.ITM)GO TO 82
      TY=T(K)*F1M
      TZ=T(KK)*F1M
   80 PRINT 223,K,TT(K),TY,KK,TT(KK),TZ
   81 CONTINUE
```

PAPRNT

```
   82 CONTINUE
      NS=(2*N-1)*50
      IF(K.EQ.NS)GO TO 86
      DO 85 I=K,NS
      TY=T(I)*FIM
      IF(I.GT.ITM)GO TO 86
   85 PRINT 224,I,TT(I),TY
   86 CONTINUE
      NINT=NINT+3
C
  200 FORMAT(1H1)
  201 FORMAT(31X,'* * * * * * * * * * * *',
     X      /,31X,'* MOMENT (M*H/EI) *',
     X      /,31X,'* * * * * * * * * * * *')
  202 FORMAT(25X,'* * * * * * * * * * * * * * * * * * *',
     X      /,25X,'* SHEAR (Q/(0.5*RO*G*(H**2))) *'
     X      /,25X,'* * * * * * * * * * * * * * * * * * *')
  203 FORMAT(25X,'* * * * * * * * * * * * * * * * * * *',
     X      /,25X,'* EARTH PRESSURE (P/(RO*G*H)) *',
     X      /,25X,'* * * * * * * * * * * * * * * * * * *')
  204 FORMAT(29X,'* * * * * * * * * * * * * *',
     X      /,29X,'* DISPLACEMENT  (Y/H) *',
     X      /,29X,'* * * * * * * * * * * * * *')
  220 FORMAT(17X,'STATIC',10X,'MAXIMUM DYNAMIC',6X,'FINAL STATIC',6X,
     X'LOCATION',/,12X,'(T*FI)=',E10.3,3X,'(T*FI)=',E10.3,3X,'(T*FI)=',
     XE10.3,5X,'(X/H)',/,12X,'________________   ________________   __
     X________________   ________')
  221 FORMAT(6X,I4,E19.3,2E20.3,F10.3)
  222 FORMAT(10X,'MAXIMUM DYNAMIC',8X,'TIME',14X,'MAXIMUM DYNAMIC',8X,
     X'TIME',/,12X,'(X/H)=',F5.3,9X,'(T*FI)',15X,'(X/H)=',F5.3,9X,
     X'(T*FI)',/,10X,'________________   __________   __________
     X______   ____________')
  223 FORMAT(6X,I4,2E15.3,7X,I4,2E15.3)
  224 FORMAT(6X,I4,2E15.3)
C
      RETURN
      END
```

PRESS

```
      SUBROUTINE PRESS
C
C     SUBROUTINE TO DERIVE EARTH PRESSURES BY SHEAR DIFFERENTIATION
C     OR BY QUINTIC SPLINE FITS OF PRESSURE TRANSDUCER DATA AS DONE
C     IN SUBROUTINE MOMENT
C
      COMMON/RED/A(1502,12),T(1502),AX(112),BX(112),CALI(15,2),X(10),
     X          TCALI,ITM,NT,NA,NPOLY,NS2,NINT,H,EIM,HTM,AGS,GAMMAM,
     X          NTYPE,FIM,NC,XP(9)
      COMMON/BLUE/X1(112),X2(112),X3(112),TT(1502),XX(1502,112),XM(1),
     X            YM(1),TM(1),ITMAX,IXMAX
      COMMON/GREEN/CMAX(2),CMIN(2),IPLTCD
      COMMON/YELLOW/TR(112),TS(112)
      REAL*8 STOR(11,25)
      DIMENSION S1(2),S2(3),LS(2),RE(1502),DOC(3),AA(1),BB(1),AM(10),
     X         BM(10),DATA(3,10),C(11),XP1(10),AM1(10)
      DATA S1/'PRES','SURF'/,S2/'P/(R','O*G*','H)'/,LS/8,10/
C
      READ 991,DMIN,DMAX
C
      NI=NINT-4
      IF(NC.NE.0)GO TO 900
      DO 825 I=1,ITM
      DO 809 J=1,NINT
  809 TR(J)=XX(I,J)
      CALL DERIV(NINT,H,TR,TS)
C
C     FIND LOCATION OF PRESSURE RESULTANT (RE(I))
C
      AR=0.0
      YA=0.0
      DO 815 J=1,NI
      DA=0.5*(AX(J+1)-AX(J))*(TS(J+1)+TS(J))
      Y=(AX(J+1)+AX(J))/2.0
      AR=AR+DA
  815 YA=YA+Y*DA
      RE(I)=YA/AR
      DO 820 J=1,NINT
  820 XX(I,J)=TS(J)
  825 CONTINUE
C
  827 CALL CRUNCH
C
      DO 830 I=1,ITM
      DO 830 J=1,NINT
  830 XX(I,J)=XX(I,J)/(GAMMAM*HTM)
      DO 835 I=1,NINT
      X1(I)=X1(I)/(GAMMAM*HTM)
      X2(I)=X2(I)/(GAMMAM*HTM)
  835 X3(I)=X3(I)/(GAMMAM*HTM)
      XM(1)=XM(1)/(GAMMAM*HTM)
      DO 836 I=1,ITM
      RE(I)=-(RE(I)/HTM)
  836 TT(I)=TT(I)/(GAMMAM*HTM)
C
      DO 840 I=1,3
```

PRESS

```
  840 DCC(I)=0.0
      LAB=0
      CINTX=(ABS(CMAX(1)-CMIN(1)))/2.5
      CINTD=(ABS(DMAX-DMIN))/2.5
      YMIN=-4.0*CINTX
      YMAX= 6.0*CINTX
      XMIN=-7.5*CINTD+DMIN
      XMAX= 7.5*CINTD+DMIN
      AA(1)=0.0
      BB(1)=RE(1)
      CALL XYPLT(1,AA,BB,XMIN,XMAX,YMIN,YMAX,DOC,LAB,1)
      BB(1)=RE(ITMAX)
      CALL XYPLT(1,AA,BB,XMIN,XMAX,YMIN,YMAX,DOC,LAB,0)
      BB(1)=RE(ITM)
      CALL XYPLT(1,AA,BB,XMIN,XMAX,YMIN,YMAX,DOC,LAB,5)
C
      IF(NC.EQ.0)GO TO 940
      NSO=NW-2
      DO 858 I=1,NSO
  858 BM(I)=-XP(I+1)/HTM
      DO 860 I=1,3
  860 DCC(I)=0.0
      LAB=0
      CINTX=(ABS(CMAX(1)-CMIN(1)))/2.5
      CINTD=(ABS(DMAX-DMIN))/2.5
      YMIN=-4.0*CINTX
      YMAX= 6.0*CINTX
      XMIN=-7.5*CINTD+DMIN
      XMAX= 7.5*CINTD+DMIN
      DO 870 J=1,3
      GO TO (861,863,865),J
  861 DO 862 I=1,NSO
  862 AM(I)=A(1,I+NT)/(GAMMAM*HTM)
      GO TO 867
  863 DO 864 I=1,NSO
  864 AM(I)=A(ITMAX,I+NT)/(GAMMAM*HTM)
      GO TO 867
  865 DO 866 I=1,NSO
  866 AM(I)=A(ITM,I+NT)/(GAMMAM*HTM)
  867 CALL XYPLT(NSO,AM,BM,XMIN,XMAX,YMIN,YMAX,DOC,LAB,2)
  870 CONTINUE
      GO TO 940
C
  900 NPP=NPCLY+1
      NPT=NC+1
      NW=NPT+1
      AM(1)=0.0
      DO 905 I=1,NPT
  905 DATA(3,I)=1.0
      CHISQ=0.0
C
      DO 930 I=1,ITM
      DO 907 J=2,NPT
  907 AM(J)=A(I,J+NT-1)
      DO 910 J=2,NPT
      DATA(1,J-1)=XP(J)
```

```
      910 DATA(2,J-1)=AM(J)
          NPT=NPT-1
C
          CALL LSQUAR(DATA,NPT,NPP,C,CHISQ,STOR)
C
          NPT=NPT+1
          DO 917 J=1,NW
      917 AM(J)=0.0
          DO 918 J=2,NW
          DO 918 K=1,NPP
      918 AM(J)=AM(J)+C(K)*XP(J)**(K-1)
          NW1=NW-1
          DO 922 J=1,NW1
          XP1(J)=XP(J)
      922 AM1(J)=AM(J)
C
C         CALCULATE PRESSURES WITH CUBIC SPLINE
C
          CALL SPLINE(NW1,XP1,AM1,NINT,AX,TS)
C
C         FIND LOCATION OF PRESSURE RESULTANT (RE(I))
C
          AR=0.0
          YA=0.0
          DO 925 J=1,NI
          DA=0.5*(AX(J+1)-AX(J))*(TS(J+1)+TS(J))
          Y=(AX(J+1)+AX(J))/2.0
          AR=AR+DA
      925 YA=YA+Y*DA
          RE(I)=YA/AR
          DO 927 J=1,NINT
      927 XX(I,J)=TS(J)
      930 CONTINUE
          GO TO 827
C
      940 CALL PAPRNT(3)
          CALL PAPLOT(S1,S2,LS,DMIN,DMAX)
C
          DO 943 I=1,ITM
          DO 943 J=1,NINT
      943 XX(I,J)=XX(I,J)*(GAMMAM*HTM)
C
      991 FORMAT(2F10.0)
C
          RETURN
          END
```

QUINT

```
      SUBROUTINE QUINT(NN,X,Y,M,S,T,BC)
C
C ....SUBROUTINE TO FIT A QUINTIC SPLINE TO A SET OF DATA POINTS (X,Y)
C     BC ARE BOUNDARY CONDITIONS
C     BC(1)=Y(1);BC(2)=Y'(1);BC(3)=Y''(1);
C     BC(4)=Y(NN);BC(5)=Y'(NN);BC(6)=Y''(NN)
C
      DIMENSION BC(6)
      DIMENSION X(1),Y(1),S(1),T(1),H(500),A(50,50),B(50),U(6,6),C(6,7)
      COMMON/PURPLE/JWANT,FIR(500),SEC(500)
C
      IF(NN.GT.501)GO TO 99
      N=NN-1
      NM1=N-1
      DO 5 I=1,N
      H(I)=X(I+1)-X(I)
    5 CONTINUE
      N6=N*6
      DO 15 I=1,N6
      B(I)=0
      DO 15 J=1,N6
   15 A(J,I)=0.0
      DO 25 I=1,3
   25 A(I,I)=1.0
C
      B(1)=BC(1)
      B(2)=BC(2)
      B(3)=BC(3)
      B(N6-2)=BC(4)
      B(N6-1)=BC(5)
      B(N6)=BC(6)
C
      DO 40 I=1,NM1
      B(4+(I-1)*6)=Y(I+1)
      IR=4+(I-1)*6
      IC=6*I+1
      A(IR,IC)=1.0
      IC=IC-1
      DO 35 J=1,5
   35 A(IR+J,IC+J)=-1.0
      ARG=H(I)
      IR=3+(I-1)*6
      IC=(I-1)*6
      CALL SUBU(ARG,U)
      DO 37 JC=1,6
      DO 37 JR=1,6
   37 A(IR+JR,IC+JC)=U(JR,JC)
   40 CONTINUE
C
      CALL SUBU(H(N),U)
      IR=N6-3
      IC=N6-6
      DO 50 JC=1,6
      DO 50 JR=1,6
   50 A(IR+JR,IC+JC)=U(JR+1,JC)
C
```

CUINT

```
C ....ECSOV IS A SYSTEM SUBROUTINE
C
          CALL ECSOV(N6,A,B,10,1.0E-4,C,IT,0)
          DC 60 I=1,M
          IF(S(I).LT.X(1)) GC TO 53
          DC 52 J=1,N
          IF(S(I).LE.X(J+1)) GO TO 55
.     52 CONTINUE
CCCCCCCCCCCCCCCCCCCC
.         GC TC 55
CCCCCCCCCCCCCCCCCCCC
     53 PRINT 106,I
          GC TG 60
     55 CCNTINUE
          SX=S(I)-X(J)
          T(I)=C(1,J)+SX*(C(2,J)+(SX/2.)*(C(3,J)+(SX/3.)*(C(4,J)+(SX/4.)*
         X(C(5,J)+(SX/5.)*C(6,J)))))
          IF(JWANT.EC.0) GC TC 60
          SEC(I)=C(3,J)+SX*(C(4,J)+(SX/2.)*(C(5,J)+(SX/3.)*C(6,J)))
     60 CCNTINUE
          RETURN
C
     99 PRINT 107
C
    106 FCRMAT(/,' THE',I5,'TH ELEMENT OF THE ARRAY S IS OUT OF RANGE',/,
         X' ERROR MESSAGE FROM QUINT',/)
    107 FCRMAT(/,' N IS LARGER THAN 501',/,
         X' ERROR MESSAGE FROM CUINT',/)
C
          RETURN
          END
```

SHEAR

```
      SUBROUTINE SHEAR
C
C     SUBROUTINE TO DERIVE SHEARS BY MOMENT DIFFERENTIATION OR
C     PRESSURE DISTRIBUTION INTEGRATION
C
      COMMON/RED/A(1502,12),T(1502),AX(112),BX(112),CALI(15,2),X(10),
     X           TCALI,ITM,NT,NA,NPOLY,NS2,NINT,H,EIM,HTM,AGS,GAMMAM,
     X           NTYPE,FIM,NC,XP(9)
      COMMON/BLUE/X1(112),X2(112),X3(112),TT(1502),XX(1502,112),XM(1),
     X            YM(1),TM(1),ITMAX,IXMAX
      COMMON/YELLOW/TR(112),TS(112)
      DIMENSION S1(2),S2(3),LS(2)
      DATA S1/'SHEA','R'/,S2/'C/(P','AE/K','AE)'/,LS/5,11/
C
      READ 801,DMIN,DMAX
C
      DO 725 I=1,ITM
      DO 709 J=1,NINT
  709 TR(J)=XX(I,J)
      IF(NC.NE.0)GO TO 712
      CALL DERIV(NINT,H,TR,TS)
      GO TO 714
  712 CALL INTEG(NINT,AX,TR,TS,0)
  714 DO 720 J=1,NINT
  720 XX(I,J)=TS(J)
  725 CONTINUE
C
      CALL CRUNCH
C
C     PAE/KAE=0.5*RO*G*(H**2) - FROM M-O ANALYSIS
C
      DO 727 I=1,ITM
      DO 727 J=1,NINT
  727 XX(I,J)=XX(I,J)/(0.5*GAMMAM*(HTM**2))
      DO 735 I=1,NINT
      X1(I)=X1(I)/(0.5*GAMMAM*(HTM**2))
      X2(I)=X2(I)/(0.5*GAMMAM*(HTM**2))
  735 X3(I)=X3(I)/(0.5*GAMMAM*(HTM**2))
      XM(1)=XM(1)/(0.5*GAMMAM*(HTM**2))
      DO 736 I=1,ITM
  736 TT(I)=TT(I)/(0.5*GAMMAM*(HTM**2))
C
      CALL PAPRNT(2)
      CALL PAPLOT(S1,S2,LS,DMIN,DMAX)
C
      DO 744 I=1,ITM
      DO 744 J=1,NINT
  744 XX(I,J)=XX(I,J)*(0.5*GAMMAM*(HTM**2))
C
  801 FORMAT(2F10.0)
C
      RETURN
      END
```

SPLINE

```
      SUBROUTINE SPLINE(NN,X,Y,M,S,T)
C
C     SUBROUTINE TO FIT A CUBIC SPLINE TO A SET OF NN POINTS (X,Y)
C
      COMMON/WHITE/IWANT,DER(1500)
      DIMENSION X(1),Y(1),S(1),T(1),A(1500,3),B(1500),P(1500),H(1500)
C
      IF(NN.GT.1501)GO TO 90
      N=NN-1
      NM1=N-1
      DO 5 I=1,N
    5 H(I)=X(I+1)-X(I)
      DO 15 I=1,NM1
      A(I,1)=H(I)/H(I+1)
      A(I,2)=2.0*(H(I+1)+H(I))/H(I+1)
      A(I,3)=1.0
   15 B(I)=6.0*((Y(I+2)-Y(I+1))/H(I+1)-(Y(I+1)-Y(I))/H(I))/H(I+1)
      A(1,1)=0
      A(NM1,3)=0
      CALL ALGECN(NM1,A,B,P)
      DO 45 I=1,M
      IF(S(I).LT.X(1))GO TO 26
      DO 25 J=1,N
      IF(S(I).LE.X(J+1))GO TO 28
   25 CONTINUE
C     CCCCCCCC
      GO TO 28
C     CCCCCCCC
   26 PRINT 106,I
      GO TO 45
   28 IF(J.EQ.1)GO TO 30
      IF(J.EQ.N)GO TO 40
      T(I)=(P(J-1)*(X(J+1)-S(I))**3+
     XP(J)*(S(I)-X(J))**3+(6.0*Y(J+1)-H(J)**2*P(J))*(S(I)-X(J))+
     X(6.0*Y(J)-H(J)**2*P(J-1))*(X(J+1)-S(I)))/(6.0*H(J))
      GO TO 45
   30 T(I)=(P(J)*(S(I)-X(J))**3+(6.0*Y(J+1)-H(J)**2*P(J))*(S(I)-X(J))+
     X6.0*Y(J)*(X(J+1)-S(I)))/(6.0*H(J))
      GO TO 45
   40 T(I)=(P(J-1)*(X(J+1)-S(I))**3+6.0*Y(J+1)*(S(I)-X(J))+
     X(6.0*Y(J)-H(J)**2*P(J-1))*(X(J+1)-S(I)))/(6.0*H(J))
   45 CONTINUE
      IF(IWANT.EQ.0)RETURN
      DO 80 I=1,M
      IF(S(I).LT.X(1))GO TO 52
      DO 50 J=1,N
      IF(S(I).LE.X(J+1))GO TO 54
   50 CONTINUE
   52 PRINT 106,I
      GO TO 80
   54 IF(J.EQ.1)GO TO 60
      IF(J.EQ.N)GO TO 70
      DER(I)=(3.0*(P(J)*(S(I)-X(J))**2-P(J-1)*(X(J+1)-S(I))**2)+
     X6.0*(Y(J+1)-Y(J))-H(J)**2*(P(J)-P(J-1)))/(6.0*H(J))
      GO TO 80
   60 DER(I)=(3.0*P(J)*(S(I)-X(J))**2+6.0*(Y(J+1)-Y(J))-H(J)**2*P(J))/
```

SPLINE

```
                 X(6.0*H(J))
0046               GC TO 80
0047            70 DER(I)=(-3.0*P(J-1)*(X(J+1)-S(I))**2+6.0*(Y(J+1)-Y(J))+
                 XH(J)**2*P(J-1))/(6.0*H(J))
0048            80 CCNTINUE
0049               RETURN
0050            90 PRINT 107
             C
0051           106 FCRMAT('0   THE ',I5,'TH ELEMENT OF ARRAY S IS OUT OF RANGE -----
                 XERROR MESSAGE FROM SPLINE')
0052           107 FCRMAT ('0  N IS LARGER THAN 1501, SCRRY')
             C
0053               RETURN
0054               END
```

SUBU

```
      SUBROUTINE SUBU(X,U)
C
C ....SUBROUTINE CALLED IN QUINT
C
      DIMENSION U(6,6)
      DO 5 I=1,6
      DO 5 J=1,6
    5 U(I,J)=0.0
      DO 15 I=2,6
   15 U(I,I)=X
      DO 25 I=1,5
   25 U(I+1,I)=1.0
      U(2,3)=0.5*X*X
      U(3,4)=U(2,3)
      U(4,5)=U(2,3)
      U(5,6)=U(2,3)
      U(2,4)=U(2,3)*X/3.0
      U(3,5)=U(2,4)
      U(4,6)=U(2,4)
      U(2,5)=U(2,4)*X/4.0
      U(3,6)=U(2,5)
      U(2,6)=U(2,5)*X/5.0
C
      RETURN
      END
```

YDISP

```
      SUBROUTINE YDISP
C
C     SUBROUTINE TO DETERMINE DISPLACEMENTS BY DOUBLE INTEGRATION OF MOMENTS
C
      COMMON/RED/A(1502,12),T(1502),AX(112),BX(112),CALI(15,2),X(10),
     X          TCALI,ITM,NT,NA,NPOLY,NS2,NINT,H,EIM,HTM,AGS,GAMMAM,
     X          NTYPE,FIM,NC,XP(5)
      COMMON/BLUE/X1(112),X2(112),X3(112),TT(1502),XX(1502,112),XM(1),
     X          YM(1),TM(1),ITMAX,IXMAX
      COMMON/YELLOW/TR(112),TS(112)
      COMMON/BLACK/DIS(1502,3)
      DIMENSION S1(3),S2(1),LS(2)
      DATA S1/'DISP','LACE','MENT'/,S2/'Y/H'/,LS/12,3/
C
      READ(21)XX
      READ 381,DMIN,DMAX
      DO 201 I=1,ITM
      DO 201 J=1,2
  201 DIS(I,J)=DIS(I,J)*EIM
C
C     DETERMINE DISPLACEMENTS
C
      DO 250 I=1,ITM
      DO 212 J=1,NINT
  212 TR(J)=XX(I,J)
      CALL INTEG(NINT,AX,TR,TS,1)
      CALL INTEG(NINT,AX,TS,TR,1)
      EE=(TR(1)-TR(NINT)+DIS(I,2)-DIS(I,1))/(AX(NINT)-AX(1))
      FF=DIS(I,1)-(EE*AX(1))-TR(1)
      DO 237 J=1,NINT
  237 XX(I,J)=(TR(J)+(EE*AX(J))+FF)/EIM
  250 CONTINUE
C
      CALL CRUNCH
C
      DO 274 I=1,ITM
      DO 274 J=1,NINT
  274 XX(I,J)=XX(I,J)/HTM
      DO 277 I=1,NINT
      X1(I)=X1(I)/HTM
      X2(I)=X2(I)/HTM
  277 X3(I)=X3(I)/HTM
      XM(1)=XM(1)/HTM
      DO 278 I=1,ITM
  278 TT(I)=TT(I)/HTM
C
      CALL PAPRNT(4)
      CALL PAPLOT(S1,S2,LS,DMIN,DMAX)
C
      DO 280 I=1,ITM
      DO 280 J=1,NINT
  280 XX(I,J)=XX(I,J)*HTM
      DO 288 I=1,ITM
      DO 288 J=1,2
  288 DIS(I,J)=DIS(I,J)/EIM
C
```

```
      381 FORMAT(2F10.0)
C
          RETURN
          END
```

BLK DATA

```
BLOCK DATA
COMMON/WHITE/IWANT,DER(1500)
COMMON/PURPLE/JWANT,FIR(500),SEC(500)
DATA IWANT/0/,JWANT/0/
END
```

APPENDIX C

LIST OF SYMBOLS

Symbols are defined where they first appear in the text. A summary of the symbols employed and their dimensions is given in this appendix.

LOWER CASE SYMBOLS

Symbol	Definition	Dimensions
a	externally applied acceleration	LT^{-2}
a_R	set of dimensionless external acceleration ratios	-
d	thickness	L
du	digitizer unit	-
e	void ratio	-
f_a	elastic strength of aluminum	FL^{-2}
$f_m f_p$	frequency of vibration of model, prototype	T^{-1}
f_1	fundamental frequency	T^{-1}
g	gravitational acceleration	LT^{-2}
$g_m g_p$	gravitational acceleration of model, prototype	LT^{-2}
h	height	L
i	angle of backfill slope	o
k	number of dimensionless groups	-
l	length of beam	L

Symbol	Definition	Dimensions
n	number of drainage boundaries	-
n	number of parameters	-
t	time	T
t_c	consolidation time	T
$t_{cm}t_{cp}$	consolidation time of model, prototype	T
$t_m t_p$	model, prototype time	T
u_o	externally induced displacement	L
$u_{om}u_{op}$	externally induced displacement of model, prototype	L
u_{oR}	set of dimensionless externally induced displacement ratios	L
v	lateral velocity	LT^{-1}
x,y,z	length and distance in coordinate directions	L
y	wall displacement	L

UPPER CASE SYMBOLS

Symbol	Definition	Dimensions
A	constant of integration	-
B	constant of integration	L
C_a	expression dependent on Mononobe-Okabe parameters	-
C_v	coefficient of consolidation	L^2T^{-1}
E	Young's modulus	FL^{-2}
E_A	Young's modulus of aluminum	FL^{-2}
E_mE_p	Young's modulus of model, prototype	FL^{-2}
E_R	set of dimensionless Young's modulus ratios	-
EI	stiffness per unit width of wall	FL^2L^{-1}
F	typical force dimension	F
F()	function of	-
F.S.	factor of safety	-
G	shear modulus	FL^{-2}
G_mG_p	shear modulus of model, prototype	FL^{-2}
G()	function of	-
G.S.	Ground surface	-
H	height	L
H_A	height at which resultant force acts	L
H_f	depth of frost cover in front of wall	L
H_mH_p	height of model, prototype	L
I	moment of inertia per unit width of wall	L^4L^{-1}

Symbol	Definition	Dimensions
K_A	coefficient of static active lateral earth pressure	-
K_{AE}	coefficient of total active lateral earth pressure	-
K_{PE}	coefficient of total passive lateral earth pressure	-
L	typical length dimension	L
$L_m L_p$	length scale of model, prototype	L
L_R	set of dimensionless length ratios	-
M	typical mass dimension	M
M	moment	FLL^{-1}
M_A	active static moment	FLL^{-1}
M_{AE}	active total (static + dynamic) moment	FLL^{-1}
M_D	design moment	FLL^{-1}
M_o	overturning moment	FLL^{-1}
M_R	resisting moment	FLL^{-1}
MMI	Modified Mercalli Intensity	-
N	centrifuge gravitational acceleration scale factor	-
N	ratio of prototype to model length scales	-
P	pressure	FL^{-2}
P	externally applied load	F
P_A	active static resultant wall force	FL^{-1}
$P_m P_p$	externally applied load of model, prototype	F
P_{AE}	total (static + dynamic) active wall force	FL^{-1}

Symbol	Definition	Dimensions
P_{PE}	total (static + dynamic) passive wall force	FL^{-1}
P_R	set of dimensionless external load ratios	-
Q	shear force	FL^{-1}
Q	externally applied stress	FL^{-2}
$Q_m Q_p$	externally applied stress of model, prototype	FL^{-2}
Q_R	set of dimensionless externally applied stress ratios	-
R_A	maximum static active pressure	FL^{-2}
R_{AE}	maximum total (static + dynamic) active pressure	FL^{-2}
RW1	Retaining Wall #1	-
RW2	Retaining Wall #2	-
S	unit section modulus of cross section	$L^3 L^{-1}$
T	typical time dimension	T
T	time factor of consolidation	-
$T_m T_p$	time factor of consolidation of model, prototype	-
W	weight of soil wedge behind wall	FL^{-1}
W	weight of backfill	FL^{-1}

GREEK SYMBOLS

Symbol	Definition	Dimensions
β	angle of wall back slope	^{o}
γ	unit weight of soil	FL^{-3}
δ	angle of wall-soil friction	^{o}
θ	$\tan^{-1}[k_h/(1-k_v)]$	
ν	Poisson's ratio	-
$\nu_m \nu_p$	Poisson's ratio of model, prototype	-
ρ	mass density	ML^{-3}
$\rho_m \rho_p$	mass density of model, prototype	ML^{-3}
σ_o	internal stress	FL^{-2}
$\sigma_{om} \sigma_{op}$	internal stress of model, prototype	FL^{-2}
σ_{oR}	set of dimensionless internal stress ratios	-
ϕ	angle of internal friction of soil	^{o}
ΔP_{AE}	active wall force increment due to earthquake load	FL^{-1}

APPENDIX D

FINITE ELEMENT COMPARISON

For an analytical comparison, it was decided to perform a finite element analysis on the wall-soil system of test 1CN0002 using the linearly elastic structural analysis program SAPIV (Bathe, et. al. [1]).

The finite element grid was first drawn up as shown in Figure D.1 with the retaining wall (shown with speckles) embedded in the soil. Prototype dimensions were used (i.e., wall height was 18 ft) and the boundaries were determined to be those existing in a postulated prototype centrifuge bucket (i.e., 50 times larger than their actual size). The wall illustrated is much thicker than that which would be the prototype (1 ft thick vs. 3.15" thick if it were aluminum), but its Young's Modulus was chosen much less so that the stiffnesses EI would be the same. This was done in order to get a more suitable aspect ratio for the elements which form the wall and base. Incompatible modes were used in the wall and base quads in order to have better bending behavior in these elements, especially since the wall was modelled with only one layer of elements.

Unfortunately, the soil elements had to be attached to the beam (wall) elements as there was no provision in the code to have sliding between elements. This would have been more desirable.

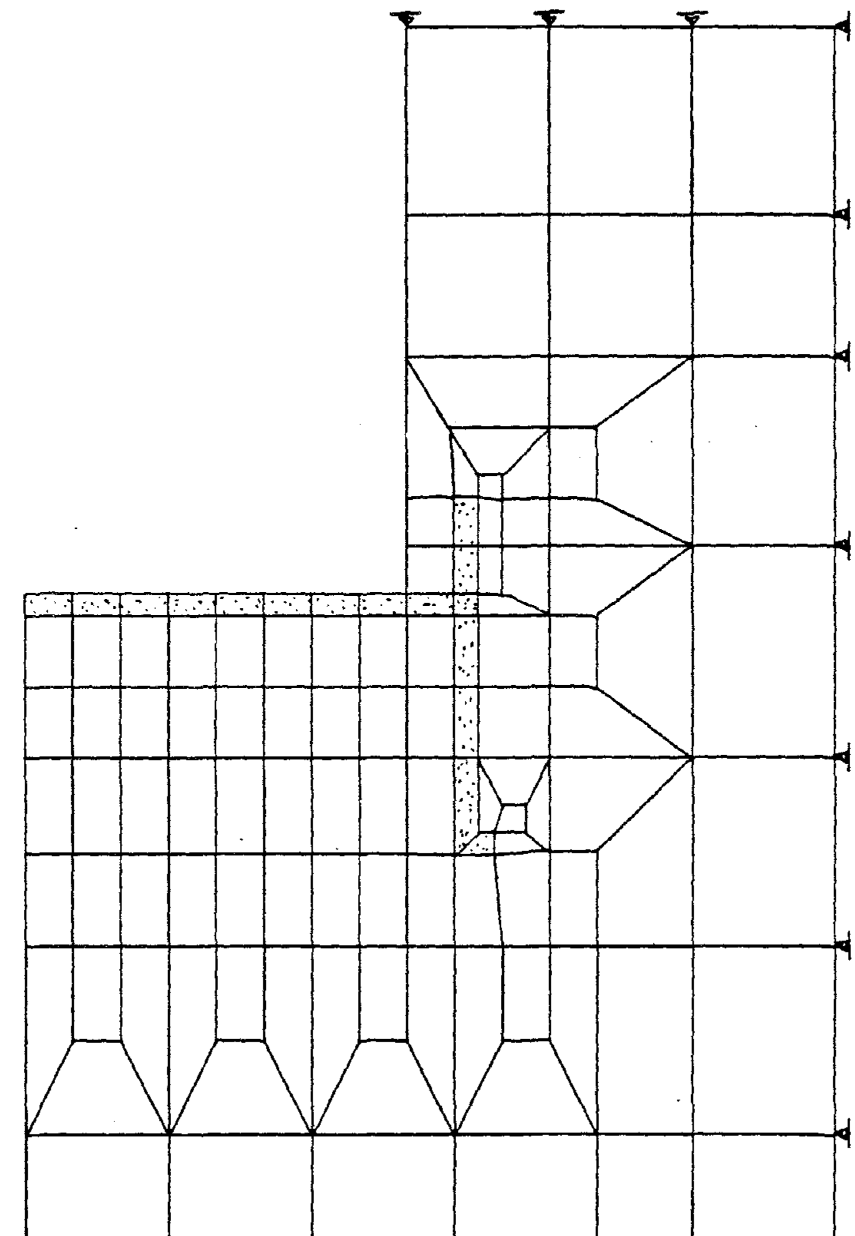

FIGURE D.1 - FINITE ELEMENT GRID (SCALE 7.8 FT. PER IN.)

The soil shear moduli were determined from the relationship given by Seed and Idriss [54] between the shear modulus and the confining pressure:

$$G = 1000K_2(\sigma'_m)^{1/2} \tag{D.1}$$

in which

G = shear modulus of soil

σ'_m = mean principal effective stress.

K_2 = a parameter which is primarily a function of void ratio and strain amplitude

Because of the high strain range involved in a retaining wall problem, K_2 was chosen from the extreme right of Figure D.2 to be 4. The soil moduli were then calculated from equation (D.1) for the various depths, making some adjustments for the soil in the vicinity of the toe of the wall for the fact that the soil level in front of the wall is lower than that in back.

First of all, the problem was run for a static gravity body load in the negative vertical direction. The problem was then run dynamically as a forced response problem using modal superposition and the free-field acceleration record (prototype) of test 1CN0002 (Figure 5.5a) in the horizontal direction. The damping used was assumed 10% of critical. The total dynamic response was then obtained by superposition of the static response and the lateral dynamic one.

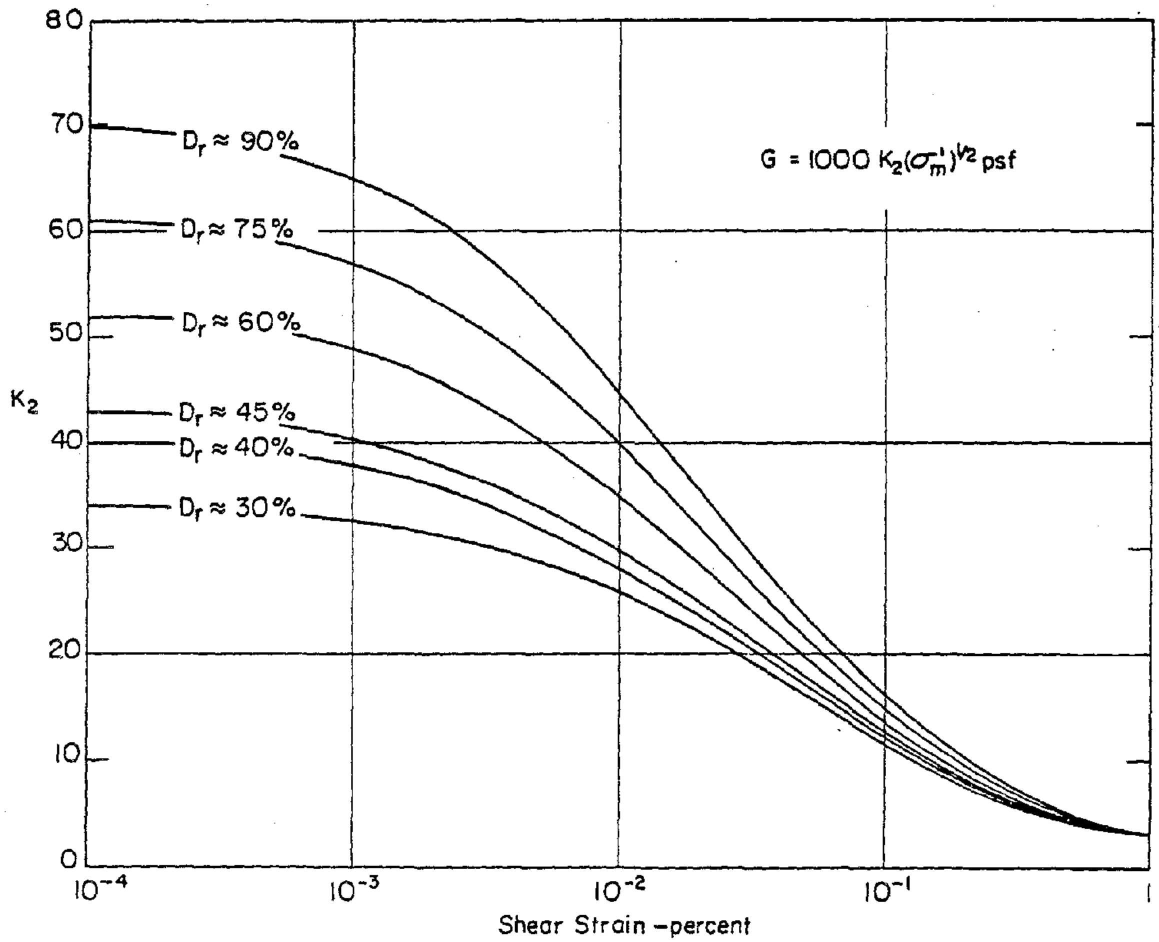

SHEAR MODULI OF SANDS AT DIFFERENT RELATIVE DENSITIES.

FIGURE D.2 – FROM (54)

The first six natural frequencies of the finite element system were found to be 1.188 Hz, 1.388 Hz, 1.45 Hz, 1.987 Hz, 2.449 Hz, and 2.536 Hz. Only the 6th frequency of 2.536 Hz even resembled the actual fundamental frequency of 2.57 Hz and its mode shape is most likely very different.

Figures D.3, D.4, and D.5 illustrate the static and maximum dynamic displacement, pressure, and moment distributions along the wall for both the centrifuge model test and the finite element problem. As can be seen from these figures there is virtually no correlation between the two in any of the cases.

From this illustration one can see the perils in using elastic theories (which are the basis for the finite element program used) in trying to model the retaining wall problem which after all is the classic most simple plasticity example. Elastic solutions for retaining wall problems should be avoided.

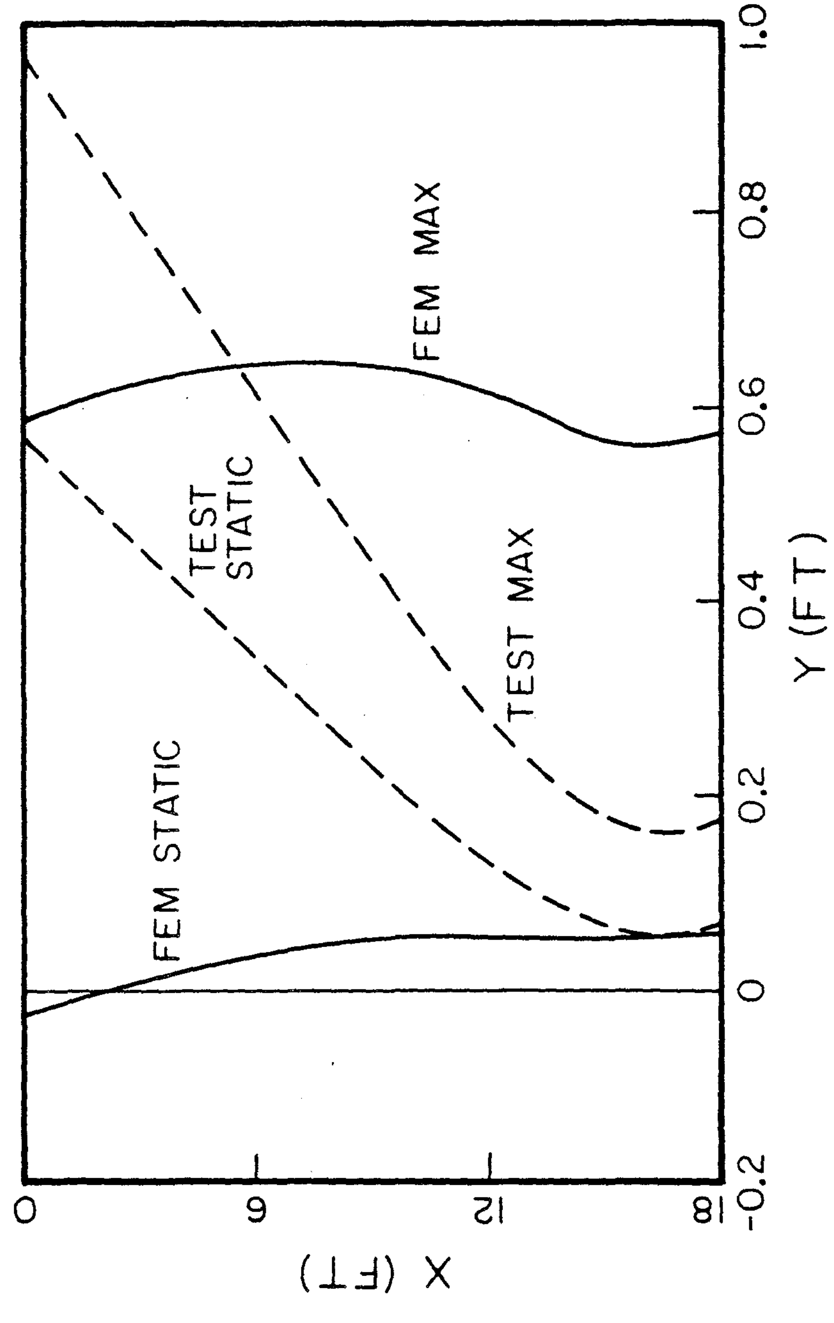
FEM MAX
TEST STATIC
TEST MAX
FEM STATIC
Y (FT)
X (FT)
1.0
0.8
0.6
0.4
0.2
0
-0.2
0
6
12
18

FIGURE D.3

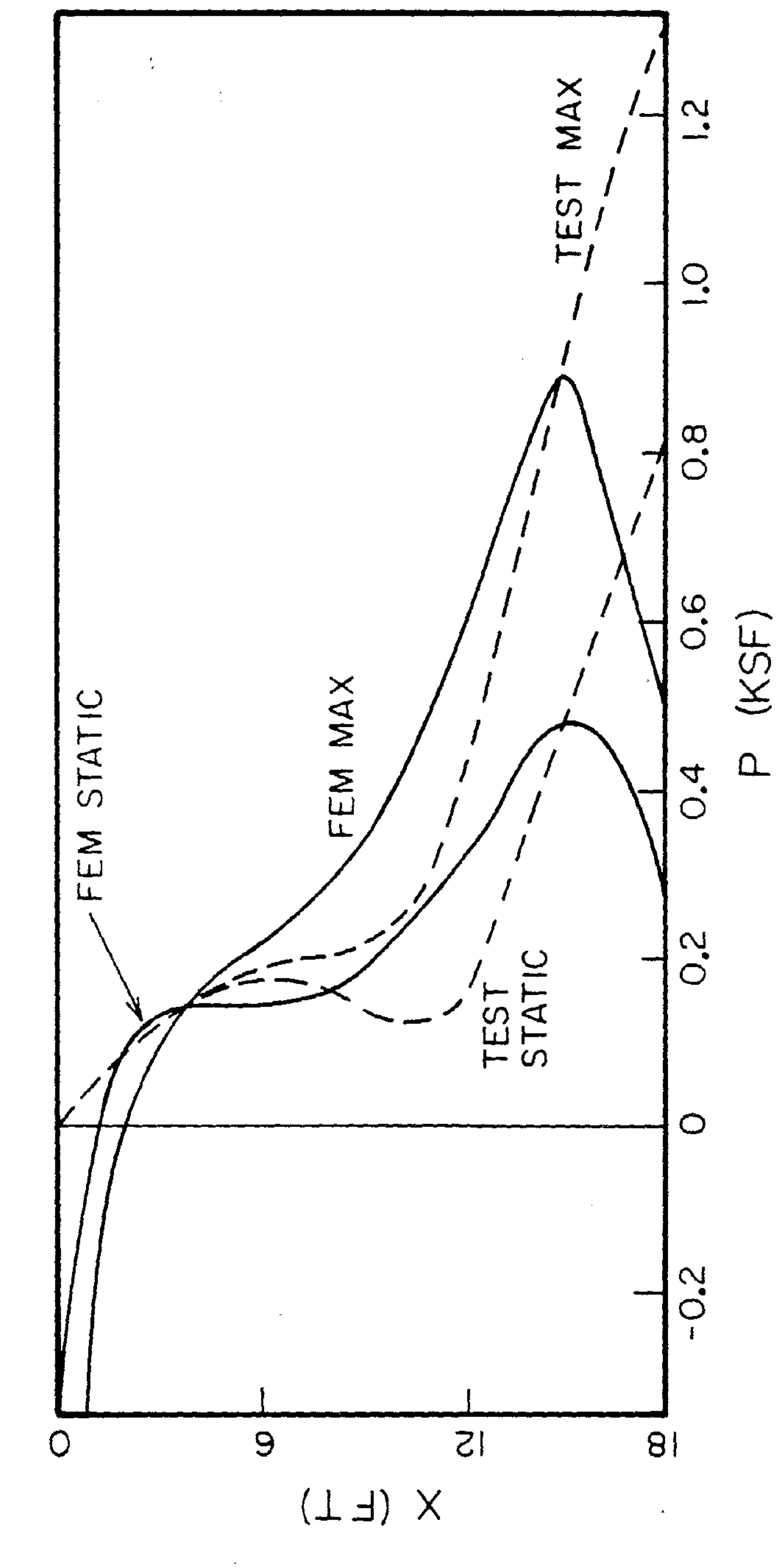
FEM STATIC
FEM MAX
TEST MAX
TEST STATIC
P (KSF)
X (FT)
-0.2
0
0.2
0.4
0.6
0.8
1.0
1.2
0
6
12
18

FIGURE D.4

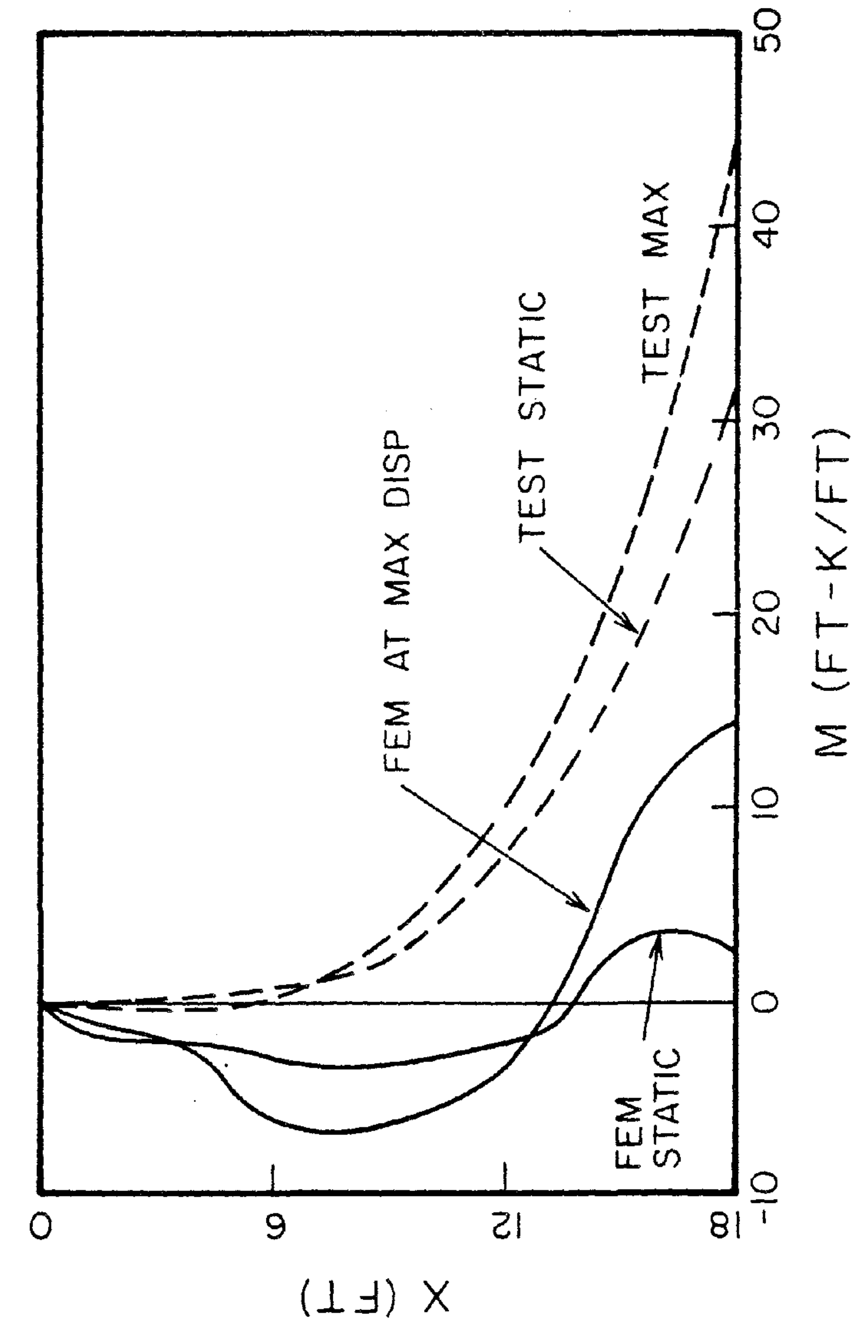
FEM AT MAX DISP
TEST STATIC
TEST MAX
FEM STATIC
M (FT-K/FT)
X (FT)
-10
0
10
20
30
40
50
0
6
12
18

FIGURE D.5